SPECTROCHIMICA ACTA

Founder Editor

A. GATTERER S.J. +

Editors

U.S.A.

V. A. FASSEL *Ames, Iowa*

F. A. MILLER *Pittsburgh*

UNITED KINGDOM

H. W. THOMPSON *Oxford*

EDITORIAL ADVISORY BOARD

B. Bak, *Copenhagen*
N. S. Bayliss, *Perth, W. Aust.*
L. J. Bellamy, *Waltham Abbey*
Wallace R. Brode, *Washington, D.C.*
C. G. Cannon, *Pontypool*
C. G. Carlsson, *Stockholm*
B. L. Crawford, *Minneapolis*
G. Duyckaerts, *Liège*
C. Feldman, *Oak Ridge*
H. Friedman, *Washington*
W. Gordy, *Durham, N.C.*
D. Hadzi, *Ljubljana*
D. F. Hornig, *Princeton, N.J.*
R. N. Jones, *Ottawa*
H. Kaiser, *Dortmund*
M. Kasha, *Tallahassee*
J. A. A. Ketelaar, *Amsterdam*
J. Lecomte, *Paris*
E. Loeuille, *Paris*
R. C. Lord, *Cambridge, Mass.*
S. L. Mandelstam, *Moscow*
A. Mangini, *Bologna*
J. R. McNally, *Oak Ridge*
R. Mecke, *Freiburg*
A. C. Menzies, *London*
S. Mizushima, *Tokyo*
R. L. Mitchell, *Aberdeen*
G. Porter, *Sheffield*
W. C. Price, *London*
R. E. Richards, *Oxford*
H. Schüler, *Hechingen-Hohenzollern*
B. F. Scribner, *Washington, D.C.*
N. Sheppard, *Cambridge*
H. Shull, *Bloomington, Indiana*
D. M. Smith, *Wembley*
E. H. S. van Someren, *Broxbourne*
H. Stammreich, *São Paulo*
B. Vodar, *Bellevue, S. et O.*
A. Walsh, *Melbourne*
H. L. Welsh, *Toronto*
M. Kent Wilson, *Medford, Mass.*
N. Wright, *Midland (Mich.)*

VOLUME X

1957

PERGAMON PRESS

NEW YORK · LONDON · PARIS · LOS ANGELES

VOL. 10 957/58

Spectrochim. Acta

SPECTROCHIMICA ACTA

CONTENTS OF VOLUME X

No. 1

MICHIRO HAYASHI, ISAO ICHISIMA, TAKEHIKO SHIMANOUCHI and SAN-ICHIRO MIZUSHIMA: Internal rotation in 1:2-dichloro-2-methylpropane . . . 1

WILLIAM G. FATELEY and ELLIS R. LIPPINCOTT: Normal co-ordinate analysis of the vibrational spectrum of iron pentacarbonyl . . . 8

P. J. STONE and H. W. THOMPSON: Vibrational band intensity of the hydroxyl group in phenols . 17

M. ST. C. FLETT: Studies of the band near 3 μ in some hydroxy compounds . . . 21

D. HADŽI and D. PREVORŠEK: Infra-red absorption bands associated with the NH group—III. Hydroxamic acids and derivatives . . . 38

J. GAUNT and J. B. AINSCOUGH: The molecular structure of niobium pentachloride . . . 52

J. GAUNT and J. B. AINSCOUGH: The molecular structure of antimony pentafluoride . . . 57

H. SCHÜLER und E. LUTZ: Organische Moleküle in der Glimmentladung—III. Spektroskopische Untersuchungen über das Verhalten von Benzol, Toluol, Chlorbenzol, Diphenyl und Benzylchlorid[1] . . . 61

URNER LIDDEL and EDWIN D. BECKER: Infra-red spectroscopic studies of hydrogen bonding in methanol, ethanol and *t*-butanol . . . 76

A. FIORENZA et M. LACHIN: La mésure de la "largeur effective" des raies dans l'analysis des substances en poudre . . . 85

K. D. MIELENZ: Zur Ausleuchtung von Spektrographen durch Zwischenabbildung der Lichtquelle 99

J. G. HAWKINS, E. R. WARD and D. H. WHIFFEN: Characteristic infra-red absorption frequencies of substituted naphthalenes . . . 105

J. ARTAUD, J. BLAISE et S. GERSTENKORN: Analyse isotopique du lithium par spectroscopie optique—I. Utilisation de la raie $\lambda = 4603$ Å . . . 110

Research Notes:

H. J. PHILCOX: A slide rule for calculating blackening curve separations . . . 119

E. E. FERGUSON: Infra-red spectra of solutions of iodine in alkyl benzenes . . . 123

D. M. SHAW: Some aspects of the determination of barium in silicate rocks . . . 125

Book Reviews:

F. WEVER, W. KOCH und S. ECKHARD: Erfahrungen mit der spektrochemischen Analyse von Gefügebestandteilen des Stahles (Reviewed by E. VAN SOMEREN) . . . 128

PAUL W. MERRILL: Lines of the Elements in Astronomical Spectra (Reviewed by VELMER A. FASSEL) . . . 128

W. WEST (edited by): Chemical Applications of Spectroscopy, Vol. IX (Reviewed by FOIL A. MILLER) . . . 129

HERBERT M. HERSHENSON: Ultra-violet and Visible Absorption Spectra: Index for 1930–1954 (Reviewed by R. A. FRIEDEL) . . . 131

A. BEER (edited by): Vistas in Astronomy (Reviewed by P. B. FELLGETT) . . . 132

Erratum . . . 132

No. 2

K. BUNGE: Materialabbau in Funkenentladungen. Experimentelle Untersuchungen an Zinkkathoden . . . 133

THEODORE L. BROWN: The solvent effect in infra-red intensities . . . 149

J. B. LEANE and R. E. RICHARDS: Proton resonance spectra of some crystals containing nitrogen and fluorine . . . 154

D. C. MCKEAN: Infra-red spectrum of tetramethylhydrazine . . . 161

A. YAMAGUCHI, T. MIYAZAWA, T. SHIMANOUCHI and S. MIZUSHIMA: Normal vibrations of urea and urea-d_4 . . . 170

O. S. HEAVENS, J. RING and S. D. SMITH: Interference filters for the infra-red . . . 179

WILLIAM F. MEGGERS: The spectrochemistry of actinium . . . 195

F. ROSENDAHL: Untersuchung der statistischen Streuung der Restgehaltsbestimmung nach dem spektrochemischen Zugabeverfahren . . . 201

Reports of Meetings:

The Annual Symposium on Molecular Structures and Spectroscopy . . . 213

The Symposium on Spectrochemical Analysis for Trace Elements . . . 238

Research Note

R. MOCCIA and H. W. THOMPSON: Vibrational band intensity of the NH group in substituted acetanilides . . . 240

Meetings and News Items . . . 242

Papers to be published in future issues . . . 243

VOL. 10 1957/5

No. 3

J. R. Barceló: The infra-red spectrum of some metallic chelate compounds—I. Rubeanates . 245
E. Lieber, C. N. R. Rao and T. S. Chao: The ultra-violet absorption spectra of substituted phenyl amino-1,2,3-triazoles 250
Gilbert Michel et Georges Duyckaerts: Contribution à la spectrométrie Raman—II. Intensité de la raie du carbonyle aliphatique 259
P. Krumholz: Spectroscopic studies on rare-earth compounds—I. Instrumentation . . 269
P. Krumholz: Spectroscopic studies on rare-earth compounds—II. A comparative study of the absorption spectra of neodymium ion in aqueous solution and in crystalline salts . . . 274
R. M. Hexter: High-resolution, temperature-dependent spectra of calcite 281
R. M. Hexter: Infrared spectroscopic investigation of anion rotational disorder in sodium nitrate 291
H. Richard Linton and Eugene R. Nixon: Infrared spectra of silyl and silyl-d_3 cyanides . 299
Ellis R. Lippincott and Richard D. Nelson: The vibrational spectra of ferrocene and ruthenocene 307
Reports of Meetings
Symposium on Applied Spectroscopy 330
Conference on Industrial Applications of X-ray Analysis 335
Papers to be published in future issues 340

No. 4

C. G. Cannon: The nature of hydrogen bonding. A review of published work and discussion . . 341
A. N. Zaidel: Spectral-isotopic method for the determination of hydrogen in metals . . 369
G. A. Crosby and M. Kasha: Intramolecular energy transfer in ytterbium organic chelates . . 377
L. Bovey: Emission and absorption spectra of plutonium excited in a King furnace . . 383
Llewellyn H. Jones: Systematics in the vibrational spectra of uranyl complexes . . . 395
A. K. Rusanov and V. G. Khitrov: Spectrographic analysis of ores by introducing the powder into the arc in a stream of air 404
R. C. Taylor and A. R. Emery: The Raman spectra of four isotopic varieties of diborane in the gas phase 419
Research Notes
E. L. Eliel, C. C. Price, R. J. Convery and T. J. Prosser: Infrared spectra of some deuterated carboxylic acids and alcohols 423
C. G. Cannon: The infra-red spectrum of NH_2 in carbon tetrachloride 425
C. G. Cannon: The interaction of NH_2 and $CHCl_3$ molecules in CCl_4 solution from infra-red spectra 429
Letters to the Editors
R. A. Spurr and T. A. Chubb: Absorption coefficients of four organic fluorine compounds in the vacuum ultraviolet 431
L. Bovey: A tuneable microwave cavity for excitation at 2425 Mc/s of an optical spectroscopic source 432
Report of Meeting 434
Book Review
"Instrumental Analysis" by Paul Delahay (reviewed by G. Porter) 435
Editorial Note 435
Papers to be published in future issues 436

AIMS AND SCOPE

This international journal is designed for the rapid publication of original work dealing with atomic and molecular spectroscopy, with particular reference to problems in chemistry.

Emission and absorption spectroscopy over the entire "optical" and X-ray wavelength range will be accepted, and spectroscopy in the microwave region insofar as it has a direct physico-chemical interest. Raman and fluorescence spectroscopy will also, for example, be included. The main applications will include qualitative and quantitative analysis, the determination of molecular structure and of fundamental atomic or molecular data, as well as the design of equipment, description of new experimental methods or the elucidation of general spectral theory and matters relating thereto.

The journal will also include reports of spectroscopic meetings and symposia, general information on spectroscopic matters of international interest, reviews of books, and from time to time review articles on selected topics.

It is hoped to issue numbers of the journal at monthly intervals, and to make provision for the immediate publication of a limited number of short communications or notes if these are held to be of sufficient and urgent general interest.

NOTES FOR CONTRIBUTORS

I. General

1. Manuscripts should be submitted to one of the main editors or to one of the following regional Editors for the appropriate country or language:

DR. H. KAISER, *Institut für Spektrochemia und Angewandte Spektroskopie, Dortmund—Aplerbeck Marsbruchstrasse* 186, *Bau* 1, *Germany*.

PROF. J. LECOMTE, *Laboratoire des Recherches Physiques*, 1 *Rue Victor Cousin, Paris* 5, *France*.

PROF. S. L. MANDELSTAM, *Academy of Sciences of the U.S.S.R., Moscow, U.S.S.R.*

PROF. R. MECKE, *Institut für Physikalische Chemie der Universität, Hebelstrasse* 38, *Freiburg im Breisgau, Germany*.

PROF. S. MIZUSHIMA, *Faculty of Science, Tokyo University, Hongo, Tokyo, Japan*.

DR. A. WALSH, *Chemical Physics Section, Division of Industrial Chemistry, C.S.I.R.O., Melbourne, Australia*.

2. Papers should have clear scientific value, and either report new experimental data or bring together existing data for new theoretical consideration. Essential technical details can be presented as brief notes, if desirable.

3. Papers which have been published elsewhere will not, in general, be accepted and authors must agree not to communicate to another journal any article accepted for publication in *Spectrochimica Acta*.

4. Special review articles will as a rule be prepared by invitation, but authors may submit such papers or make suggestions to the regional editor concerned for consideration by the Editors.

5. Fifty free reprints of each paper will be provided, and there will be no page charge. Additional copies of reprints can be ordered with return of galley proofs. A reprint order form will accompany proofs.

II. Script Requirements

1. Papers must be written in one of three languages, namely English, French or German.

2. Authors are requested to submit an original typed copy with one (or two) carbons. The text must be ready for printing, and any changes in proof other than typographical errors may be charged to the authors.

3. Half-tone illustrations should be restricted to the minimum necessary, and the photographs should be enlarged sufficiently to permit their clear reproduction in half-tone. These must accompany the manuscript, preferably mounted on separate sheets. Illustrations of photographed spectra should in general be negatives, i.e. emission lines should be reproduced in black. Whilst it is recommended that longer wavelengths should in general be on the right-hand side, the procedure should, where relevant, follow any agreed international custom. If words or numbers appear on photographs, two copies are requested, one clearly printed and the other without inscription. If line drawings are already well drawn, it may be possible to reproduce them direct from the original, but in this case it is essential that the original drawings or good photo-prints should be provided. It is not possible to reproduce from "dyeline" prints, or from prints with weak lines, and illustrations for reproduction should normally be about twice the final size required. All illustrations and tables should be provided with descriptive legends and illustrations should accompany the manuscript separately, with legends typed on a separate sheet.

4. Only such references to literature should be given as are referred to in the text. References should be listed together by number at the end of the paper, using standard abbreviations for the journal, followed by year, volume, and first page number. Author's initials should be given.

5. Papers must be concise without unnecessary historical introduction. An abstract must be provided and, where they consider it appropriate, authors may provide abstracts in English, French, and German; but, in any case, where possible, authors should provide an English abstract in addition to that in the language of the paper. Authors may indicate which parts of the paper (e.g. details of experimental method, tables of results) may be printed in smaller type.

VOL.
10
1957/5

SUBJECT INDEX TO VOLUME X

Absorption spectra:
of rare earth salts 274
of organic fluorine compounds . . 431
Actinium, spectrochemistry of . . 195
Antimony pentafluoride, infrared and Raman spectra of 57
Barium, determination in silicate rocks 125
Book Reviews:
Chemical Applications of Spectroscopy, Edited by W. West . . . 129
Instrumental Analysis by P. Delahay 435
Lines of Elements in Astronomical Spectra by P. W. Merrill . 128
Spectrochemical Analysis of Inclusions in Steel by F. Wever, W. Koch and S. Eckhardt 128
Ultraviolet and Visual Absorption Spectra Index for 1930–1954 by H. M. Henderson . . . 131
Vistas in Astronomy, Edited by A. Beer 132
Calcite, high resolution temperature-dependent spectra of . . 281
Emission spectrographic analysis:
additive method of 201
an improved method for powders . 85
determination of hydrogen in metals 369
of actinium 195
of plutonium 383
of powdered ores in arc . . . 404
Ferrocene, infrared and Raman spectra of 307
Filters, interference for use in infrared 179
Glow discharge, in benzene and derivatives 61
Hydrogen bonding:
in hydroxy compounds . . . 21
in hydroxamic acids . . . 38
in methanol, ethanol and butanol . 70
a review 341
Hydroxamine acids, infrared spectra of 38
Infrared absorption spectra of:
ammonia in carbon tetrachloride . 425
antimony pentafluoride . . . 57
calcite 281
deuterated carboxylic acids and alcohols 423
1:2-dichloro-2-methyl propane . 1
ferrocene and ruthenocene . . 307
hydroxamic acids 38
metallic chelates, rubeanates . . 245
methanol, ethanol and butanol . 70
mixtures of NH_3 and $CHCl_3$ in CCl_4 . 429
niobium pentachloride . . . 52
silyl and silyl-d_3 cyanides . . 299
sodium nitrate crystals . . . 291
solutions of iodine in alkyl benzenes . 123
substituted napthalenes . . . 105
tetramethyl hydrazine . . . 161
urea and urea-d_4 170
Infrared intensity measurements on:
hydroxy compounds . . . 21
hydroxyl group in alcohols . . 70
NH group in acetanilides . . 240
phenols 17
solvent effect on CN, OH and CH nitrations 149
Instrumentation:
grating spectrometer . . . 269
interference filters, for infrared . 179
slide rule, for blackening curve separation 119
tunable microwave cavity for excitation of optical source . . 432
Internal rotation, of 1:2-dichloro-2-methyl phenones . . . 1
Iron pentacarbonyl, normal co-ordinate analysis of 8
Light source, technical improvements in focusing of 99
Lithium, interferometric assay of . 110
Luminescence emission of ytterbium chelates 377
Napthalenes, infrared spectra of . . 105
Niobium pentachloride, infrared and Raman spectra of . . . 52
Meetings, Reports of:
Society of Applied Spectroscopy, 12th Annual 434
Symposium of Applied Spectroscopy, 4th Canadian 330
Symposium of Spectrochemical Analysis for Trace Elements . . 238
Symposium on Molecular Structure and Spectroscopy, Columbus, Ohio 213
X-ray-fluorescence Spectroscopy and Industrial Applications, Denver, Colorado 335
Plutonium, emission and absorption spectra of 383
Proton resonance spectra in crystals containing nitrogen and fluorine . 154

Raman spectra of:
1:2-dichloro-2-methyl propane . . 1
antimony pentafluoride . . . 57
carbonyl groups 259
diborane 419
niobium tetrachloride . . . 52
ferrocene and ruthenocene . . 307
urea 170
Silyl cyanides, infrared spectra of . 299
Slide rule, for use in calculating blackening curve separations . . 119
Solvent, effect on vibrational band intensities 149
Sparks (zinc), material transfer in . . 133
Tetramethyl hydrazine, infrared spectra of 161
Ultraviolet spectra:
glow discharge in aromatic substances 61
substituted phenyl amino 1,2,3-triazoles 250
Urea, infrared and Raman spectra of . 170
Vacuum ultraviolet spectra of organic fluorine compounds . . . 431
Vibrational frequency assignments in:
diborane 419
ferrocene and ruthenocene . . 307
substituted napthalenes . . . 105
uranyl complexes 395
urea and urea-d_4 170

VOL.
10
1957/5

AUTHOR INDEX TO VOLUME X

AINSCOUGH, J. B.: *see* GAUNT, J.

ARTAUD, J., BLAISE, J. and GERSTENKORN, S.: Isotopic analysis of lithium 110

BARCELO, J. B.: Infra-red spectrum of rubeanates 245

BECKER, E. D.: *see* LIDDEL, U.

BEER, A. (Edit.): Vistas in astronomy, (reviewed by P. B. FELLGETT) . . 132

BLAISE, J.: *see* ARTAUD, J.

BOVEY, L.: Emission and absorption spectra of plutonium 383

BOVEY, L.: (Note) A tuneable microwave cavity for a source . . . 432

BUNGE, K.: Material transfer in spark discharges; tests on zinc cathodes . 133

BROWN, T. L.: Solvent effect in infra-red intensities 149

CANNON, C. G.: The nature of hydrogen bonding 341

CANNON, C. G.: (Note) Spectrum of ammonia in carbon tetrachloride . 425

CANNON, C. G.: (Note) Interactions of molecular spectra 429

CHAO, T. S.: *see* LIEBER, E.

CHUBB, T. A.: *see* SPURR, R. A.

CONVERY, R. J.: *see* ELIEL, E. L.

CROSBY, G. A. and KASHA, M.: Intramolecular energy transfer in ytterbium organic chelates 377

DELAHAY, P.: Instrumental analysis, (reviewed by G. PORTER) . . . 435

DUYCKAERTS, G.: *see* MICHEL, G.

ECKHARD, S.: *see* WEVER, F.

ELIEL, E. L., PRICE, C. C., CONVERY, R. J. and PROSSER, T. J.: (Note) Infra-red spectra of some deuterated carboxylic acids 423

EMERY, A. R.: *see* TAYLOR, R. C.

FATELEY, W. G. and LIPPINCOTT, E. R.: Analysis of the spectrum of iron pentacarbonyl 8

FERGUSON, E. E.: (Note) Infra-red spectra of iodine in alkyl benzenes . 123

FIORENZA, A. and LACHIN, M.: The measurement of line-breadth in the analysis of powders 85

FLETT, M. ST. C.: Studies of the band near 3 μ in some hydroxy compounds 21

GAUNT, J. and AINSCOUGH, J. B.: Molecular structure of antimony pentafluoride 57

GAUNT, J. and AINSCOUGH, J. B.: Molecular structure of niobium pentachloride 52

GERSTENKORN, S.: *see* ARTAUD, J.

HADŽI, D. and PREVORŠEK, D.: Infra-red absorption bands of hydroxamic acids and derivatives 38

HAWKINS, J. G., WARD, F. R. and WHIFFEN, D. H.: Infra-red absorption of substituted naphthalenes . . 105

HAYASHI, M., ICHISHIMA, I., SHIMANOUCHI, T. and MIZUSHIMA, S.: Internal rotation in 1,2-dichloro-2-methylpropane 1

HEAVENS, O. S., RING, J. and SMITH, S. D.: Interference filters for the infra-red 179

HERSHENSON, H. M.: Ultra-violet and visual absorption spectra. Index for 1930–54 131

HEXTER, R. M.: Spectra of sodium nitrate 291

HEXTER, R. M.: High resolution, temperature-dependent spectra of calcite 281

ICHISHIMA, I.: *see* HAYASHI, M.

JONES, LL. H.: Vibrational spectra of uranyl complexes 395

KASHA, M.: *see* CROSBY, G. A.

KHITROV, V. G.: *see* RUSANOV, A. R.

KOCH, W.: *see* WEVER, F.

KRUMHOLZ, P.: Spectroscopic studies on rare earth compounds—I. Instrumentation 269

KRUMHOLZ, P.: Spectroscopic studies on rare earth compounds—II. Neodymium salts 274

LACHIN, M.: *see* FIORENZA, A.

LEANE, J. B. and RICHARDS, R. E.: Proton resonance spectra of some crystals containing nitrogen and fluorine 154

LIDDEL, U. and BECKER, E. D.: Infra-red spectroscopic studies of hydrogen bonding in some alcohols 70

LIEBER, E., RAO, C. N. R. and CHAO, T. S.: The ultra-violet spectra of substituted phenylamino-triazoles . 250

LINTON, H. R. and NIXON, E. R.: Infra-red spectra of silyl and cyanides . 299

LIPPINCOTT, E. R. and NELSON, R. D.: Vibrational spectra of ferrocene and ruthenocene 307

LIPPINCOTT, E. R.: *see* FATELEY, W. G.
LUTZ, E.: *see* SCHULER, H.
McKEAN, D. C.: Infra-red spectrum of tetramethylhydrazine . . . 161
MEGGERS, W. F.: Spectrochemistry of actinium 195
MERRILL, P. W.: Lines of elements in astronomical spectra, (reviewed by V. A. FASSELL) 128
MICHEL, G. and DUYCKAERTS, G.: Contributions to Raman spectroscopy —II. Intensity of the aliphatic carbonyl band 259
MIELENZ, K. D.: The illumination of a spectrograph by intermediate focusing of the source 99
MIYAZAWA, T.: *see* YAMAGUCHI, A.
MIZUSHIMA, S.: *see* ICHISHIMA, I.; HAYASHI, M.; YAMAGUCHI, A.
THOMPSON, H. W. and MOCCIA, R.: Vibrational band intensity in substituted acetanilides . . . 240
NELSON, R. D.: *see* LIPPINCOTT, E. R.
NIXON, E. R.: *see* LINTON, H. R.
PHILCOX, H. J.: (Note) Slide-rule for calculating blackening curve separations 119
PREVORŠEK, D.: *see* HADŽI, D.
PRICE, C. O.: *see* ELIEL, E. L.
RAO, C. N. R.: *see* LIEBER, E.
RICHARDS, R. E.: *see* LEANE, J. B.
RING, J.: *see* HEAVENS, O. S.
ROSENDAHL, F.: Statistical scatter of results in analysis by the addition method 201
RUSANOV, A. K. and KHITROV, V. G.: Spectrographic analysis of ores in the arc 404
SCHULER, H. and LUTZ, E.: Organic molecules in glow discharges . . 61
SHAW, D. M.: (Note) Silicate rocks, estimation of barium 125
SHIMANOUCHI, T.: *see* HAYASHI, M. and YAMAGUCHI, A.
SMITH, S. D.: *see* HEAVENS, O. S.
SPURR, R. A. and CHUBB, T. A.: Ultraviolet absorption coefficients of fluorine compounds in the vacuum ultraviolet 431
STONE, P. J. and THOMPSON, H. W.: Vibrational band intensity of the hydroxyl group in phenols . . 17
TAYLOR, R. C. and EMERY, A. R.: Raman spectra of diborane . . 419
THOMPSON, H. W.: *see* MOCCIA, R. and STONE, P. J.
WARD, E. R.: *see* HAWKINS, J. G.
WEST, W. (Ed.): Chemical applications of spectroscopy, (reviewed by F. A. MILLER). 129
WEVER, F., KOCH, W. and ECKHARD, S.: Spectrochemical analysis of inclusions in steel, (reviewed by E. VAN SOMEREN) 128
WHIFFEN, D. H.: *see* HAWKINS, J. G.
YAMAGUCHI, A., MIYAZAWA, T., SHIMANOUCHI, T. and MIZUSHIMA, S.: Normal vibrations of urea 170
ZAIDEL, A. N.: Spectral-isotopic method for the determination of hydrogen in metals 369

VOL.
10
1957/5

Spectrochimica Acta, 1957, Vol. 10, pp. 1 to 7. Pergamon Press Ltd., London

Internal rotation in 1:2-dichloro-2-methylpropane

Michiro Hayashi, Isao Ichishima, Takehiko Shimanouchi,
and San-ichiro Mizushima
Faculty of Science, Tokyo University, Hongo, Tokyo, Japan

(*Received* 28 *March* 1957)

Abstract—Infra-red spectra of 1:2-dichloro-2-methylpropane have been measured in the gaseous, liquid, and solid states and in various solutions. Raman spectra of this substance have been measured in the liquid and solid states, and in solutions. The normal vibrations of the skeleton of the molecule have been calculated, using a potential function of the Urey-Bradley type. From these results the equilibrium molecular forms of rotational isomers have been determined and their stability in different states has been discussed. The observed infra-red and Raman frequencies have been assigned.

Introduction

In a series of researches, the internal rotation in many substances has been studied in our laboratory [1]. As a continuation of these researches, the spectroscopic investigation on 1:2-dichloro-2-methylpropane $(CH_3)_2ClC—CH_2Cl$ has been made, and the result will be reported in the present note.

The Raman spectrum of this substance in the liquid state was measured by Kohlrausch and Kahovec [2] and the dipole moment was determined by Miyagawa [3] with the result that the molecule of this substance exists in two forms with the energy difference of 0·90 kcal/mole. However, the experimental data so far obtained are not sufficient to determine the actual molecular forms and assign the observed frequencies to different modes of vibration. For this purpose the infra-red spectra have been taken in the gaseous, liquid, and solid states and in various solutions and the Raman spectra in the liquid and solid states and in solutions. Furthermore, the normal vibrations of the skeleton of this molecule has been calculated, using a potential function of the Urey-Bradley type.

Experimental

The sample of 1:2-dichloro-2-methylpropane was prepared as follows [4]: Tertiary butyl alcohol was treated by concentrated hydrochloric acid to obtain tertiary butyl chloride. This was then treated with sulphuryl chloride in chlorobenzene solution, using benzoyl peroxide as catalyst. The product was fractionally distilled with a column of thirty-five theoretical plates and a fraction boiling at 107°C was used in the measurement.

A sample kindly given us by Dr. I. Miyagawa was also used in the measurement. This was prepared from *iso*butyl alcohol, and should contain no trace of chlorobenzene. Both samples showed the same spectra.

1-(20pp.)

Table 1. Infra-red and Raman spectra of 1:2-dichloro-2-methylpropane

Raman		Infra-red				Assignment
Liquid	Solid	Gas	Liquid	Solid		
111(5)					G	Torsion?
191(5)	193(0)				T,G	δ(CCCl) out of phase (T), δ(CCCl) in phase (G)
275(8)	286(8)				T	δ(CCCl) in phase
299(3)					G	CH_3—C—CH_3 twisting
315(3)	312(5b)				T,G	CH_3—C—CH_3 twisting (T) CH_3—C—CH_3 bending (G)
356(8)	364(8)				T	CH_3—C—CH_3 bending
379(3)					G	CH_3—C—CH_3 wagging
393(2)					G	CH_3—C—CH_3 rocking
420(8)	417(7)				T,T	CH_3—C—CH_3 wagging CH_3—C—CH_3 rocking
468(5)			469 m		G	δ(CCCl) out of phase
572(9b)		575 w	572 m		G	ν(C—Cl) in [$(CH_3)_2CCl$—]
621(9b)	627(9)	628 vs	624 s		T	ν(C—Cl) in [$(CH_3)_2CCl$—]
724(10b)	724(10)	737 s	726 s	714 vs	T	ν(C—Cl) in [—CCH_2Cl]
749(7)		767 m	750 s		G	ν(C—Cl) in [—CCH_2Cl]
813(9b)	817(9)	824 m	815 m	813 s	T	ν(C—C)
821(6)			827 s		G	ν(C—C)
			854 w	856 vw		$2 \times 417 = 834$
889(4)		890 m	891 m	893 w	T	$\delta(CH_2)$, rocking
936(4)			937 w		G	$\delta(CH_2)$, rocking
966(4)			967 m		G	ν(C—C)
987(3)		982 s	985 s	984 s	T	ν(C—C)
			1021 w	1015 w		$286 + 724 = 1010$
1114(5)	1116(5)	1123 vs	1118 vs	1099 vs	T	$\delta(CH_3)$, rocking
1168(2)		1167 w	1168 s		G	$\delta(CH_3)$, rocking
1211(2)		1223 m	1218 s		G	$\delta(CH_2)$, wagging
1230(1)			1234 m	1237 s	T	$\delta(CH_2)$, wagging
1252(2)			1252 m			$420 + 813 = 1233$
1280(6)	1275(6)	1290 m	1281 s	1278 vs	T	ν(C—C)
1298(3)			1297 s		G	ν(C—C)
1366(0)		1387 vs	1373 vs	1372 vs	T	$\delta(CH_3)$, symmetric deformation
1386(1)			1391 vs		G	$\delta(CH_3)$, symmetric deformation
1432(6)	1435(2)	1450 vs	1447 sh	1443 vs	T,G	$\delta(CH_2)$, bending
1459(5)	1457(3)		1456 vs	1460 vs	T,G	$\delta(CH_3)$, degenerate deformation
2902(3)	2902(3)					
2916(3)						
2944(6b)	2944(2)					
	2952(6)					
2966(3)	2970(3)					ν(C—H)
2986(6b)	2992(3)					
3019(3)	3018(2)					

VOL. 10 1957/5

The measurement of Raman spectra was made with high luminosity spectrographs of our own construction [1]. Infra-red spectra were recorded by means of a Baird spectrophotometer with NaCl optics in the region of 3000 to 650 cm^{-1}, and a Perkin-Elmer instrument, model 21, with KBr optics in the region of 700 to 400 cm^{-1}.

Result

The Raman and infra-red spectra of 1:2-dichloro-2-methylpropane observed in different states are listed in Table 1. The figures in parentheses following Raman frequencies (in cm^{-1}) refer to visually estimated intensities.

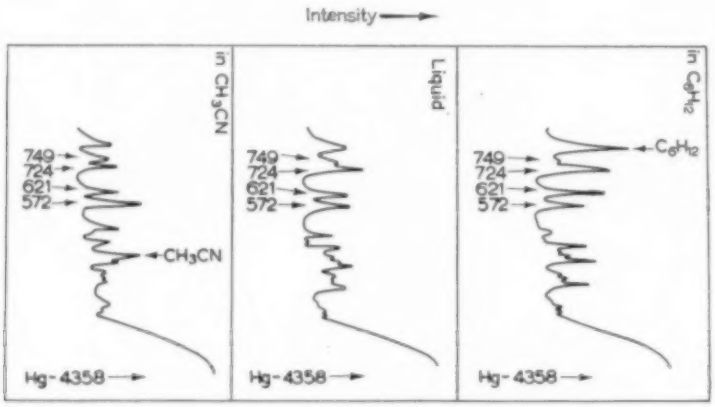

Fig. 1.

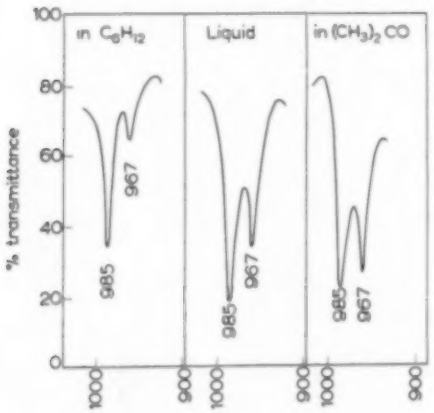

Fig. 2.

More accurate intensity measurement of Raman lines has been made by microphotometer tracing. In Fig. 1 is shown a part of the Raman-spectrum tracing of 1:2-dichloro-2-methylpropane in the liquid state and in solutions. It is

seen that the line at 621 cm^{-1} is weaker than the line at 572 cm^{-1} in CH_3CN, a polar solvent, whereas both of them have almost the same intensity in the pure liquid state and the former becomes stronger than the latter in C_6H_{12}, a non-polar solvent.

A great change of relative intensity of two lines at 749 and 724 cm^{-1} has also been observed. The intensity ratio $I(749)/I(724)$ increases considerably in the order, C_6H_{12} solution, pure liquid, and CH_3CN solution. In other words, this intensity ratio decreases considerably in a non-polar solvent.

Similar intensity change with solvent has also been found by the infra-red measurement. We have chosen a pair of lines at 967 and 985 cm^{-1} and have

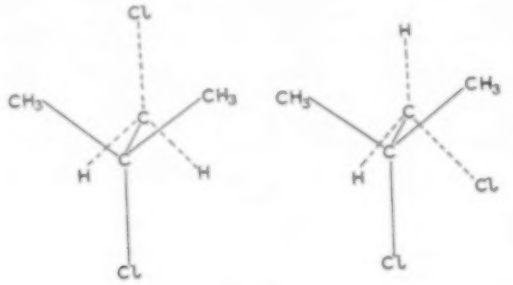

Fig. 3.

observed the ratio of optical density in the liquid state and in C_6H_{12}, CS_2, $CHCl_3$, $(CH_3)_2CO$, and CH_3CN solutions. The dielectric constant of solvent changes from 2·0 to 37·5. It has been shown that the intensity ratio $I(967)/I(985)$ decreases as the solvent becomes more non-polar. In Fig. 2 is shown the recorded absorption in the liquid state and in C_6H_{12} and $(CH_3)_2CO$ solutions.

It is to be noted that all the lines which considerably decrease in intensity in non-polar solvent are those which disappear completely in the solid state.

Discussion

The number of Raman lines and infra-red absorption bands observed in the liquid state is too large to be accounted for as arising from a single molecular form. In the solid state, however, the observed frequencies are materially reduced in number and the spectra can be explained as arising from a single molecular form.

For example, in the frequency region below 500 cm^{-1}, ten frequencies have been observed in the liquid state and five in the solid state. Normal vibration calculation (to be explained below) shows that in this region we have only the skeletal deformation vibrations, which amount to six in number per form. Therefore, it can be concluded that there exist two forms in the liquid state and only one form in the solid state. The fact that the five solid frequencies 193, 286, 312, 364, and 417 cm^{-1} remain practically unchanged in the liquid state shows that these frequencies can be assigned to the molecular form which exists in both the liquid and solid states.

Of these five frequencies, the lowest one (in cm^{-1}) is explained to arise from both forms in the liquid state. This is the reason why the Raman line of this

VOL.
10
1957/5

frequency behaves quite differently in intensity from those of other frequencies on going from the solid to liquid state.

Similar consideration can be made for the C—Cl stretching frequencies observed in the frequency region, 500–700 cm^{-1}. The solid frequencies, 627 and 724 cm^{-1}, which have also been observed in the liquid state can be assigned to the form existing in both these two states, whereas the two frequencies, 572 and 749 cm^{-1}, to the form which disappears in the solid state. The assignment of these frequencies is based on our previous result [5] as well as the normal vibration calculation.

Table 2. Force constants of 1:2-dichloro-2-methylpropane in 10^5 dyn/cm

K(C—Cl) = 1·75	H(CH_3—C—Cl) = 0·17	F(CH_3...(C)...Cl) = 0·49
K(C—CH_3) = 3·44	H(CH_3—C—CH_3) = 0·20	F(CH_3...(C)...CH_3) = 0·33
K(C—CH_2) = 3·04	H(CH_3—C—CH_2) = 0·20	F(CH_2...(C)...CH_3) = 0·33
K(CH_2—Cl) = 2·90	H(CH_2—C—Cl) = 0·17	F(CH_2...(C)...Cl) = 0·49
	H(C—CH_2—Cl) = 0·17	F(C...(CH_2)...Cl) = 0·49

κ (intramolecular tension) = 0·1 × 10^{-11} dyn/cm [8].

In the skeletal frequency region above 750 cm^{-1} we expect the C—C stretching frequencies which will be coupled with CH_2 and CH_3 deformation frequencies. In this case the assignment of the C—C frequencies of $(CH_3)_3CCl$ to 812 cm^{-1} (A_1) and 1234 cm^{-1} (E) helps us in making the assignment of the frequencies of $(CH_3)_2ClC$ CH_2Cl [6]. We consider that the 812 cm^{-1} frequency corresponds to the 813 and 821 cm^{-1} frequencies of Table 1 and the 1234 cm^{-1} (E), which will be observed as two frequencies per form, correspond to 1298, 1280, 966, and 987 cm^{-1}. Of these the frequencies, 813, 987, and 1280 cm^{-1} are assigned to the molecular form persisting in the solid state.

From the vector addition of bond moments, it is easily seen that the dipole moment of 1:2-dichloro-2-methylpropane change considerably with azimuthal angle of internal rotation about the C—C axis. In other words, the two rotational isomers referred to above will be quite different in the moment value. This results in a great change in population ratio of the two isomers between polar and non-polar solutions, and the more polar isomer will become more stable in a more polar solution. Therefore, the Raman lines and infra-red absorption bands which increase in intensity in a less polar solvent can be assigned to a less polar isomer and those increase in intensity in a more polar solvent to a more polar isomer.

As we have shown in the section of experimental result, the Raman lines and infra-red absorption bands, which considerably increase in intensity in a non-polar solvent, also persist in the solid state. Therefore, the rotational isomer which persists in the solid state corresponds to the less polar form and that which exists only in the gaseous and liquid states to the more polar form.

Calculation of normal vibrations

In a previous paper [7] it was shown that the calculation of skeletal vibrations serves to determine the configuration of rotational isomers. For this purpose, the skeletal vibrations of 1:2-dichloro-2-methylpropane have been calculated as a six-body problem, regarding CH_2 and CH_3 groups as dynamical units. A potential function of the Urey-Bradley type [1, 8] has been used with stretching (K), bending (H), and repulsive (F) force constants shown in Table 2. Of these force constants, those concerning the part of the molecule, $(CH_3)_2CClCH_2$—, have been taken from the corresponding constants of $(CH_3)_3CCl$ and others from those of $ClH_2C—CH_2Cl$ [7].

The secular equation $|GF - E\lambda| = 0$ is of eleventh order. This is factored into one of eighth order and the other of third order for the two extreme forms, *trans* and *cis*, where the *trans* form (with respect to the two chlorine atoms) has practically

Table 3. Observed and calculated frequencies of 1:2-dichloro-2-methylpropane in cm^{-1}

Vibrational mode	*Trans* form		*Gauche* form	
	Observed	Calculated	Observed	Calculated
ν(C—C)	1280	1091 (A'')	1298	1113
ν(C—C)	987	1076 (A')	966	1080
ν(C—C)	813	951 (A')	821	923
ν(C—Cl) in [—CH_2Cl]	724	744 (A')	749	767
ν(C—Cl) in [$(CH_3)_2$Cl—]	621	675 (A')	572	612
CH_3—C—CH_3 wagging	420	422 (A')	379	363
CH_3—C—CH_3 rocking	420	414 (A'')	393	394
CH_3—C—CH_3 bending	356	360 (A')	315	319
CH_3—C—CH_3 twisting	315	314 (A'')	299	290
δ(CCCl) in phase	275	272 (A')	191	189
δ(CCCl) out of phase	191	192 (A')	468	469

no moment. Therefore, the normal vibrations of these two forms can be calculated more easily than those of the intermediate forms, for which the secular equation is not factored [9]. It has been shown by this calculation that the computed frequencies for the *trans* and *gauche* forms agree well with those observed for the less polar and more polar forms, respectively (Table 3). Here the *gauche* form is the one obtainable from the *trans* form by an internal rotation of ca. 120°. The stability of the *trans* and *gauche* forms is quite reasonable, as can be seen from the result of many investigations on rotational isomerism made in this laboratory [1].

It is to be noted that the skeletal deformation frequencies δ(CCCl) are very sensitive to the change of the angle of internal rotation and their computed and observed values are in excellent agreement with each other. This shows the azimuthal angles determined above for the *trans* and *gauche* forms are reasonable. The discrepancies between the computed and observed values for the C—C stretching frequencies are considered to be due to the neglect of the coupling of the CH_3 and CH_2 deformation vibrations with the C—C stretching vibrations.

VOL. 10 1957/5

The internal symmetry co-ordinates, S, are related linearly to the normal co-ordinates, Q, through the matrix expression:

$$S = LQ$$

If, therefore, we calculate the elements of the L-matrix for a given normal vibration we can determine the relative amplitude for each symmetry co-ordinate [1]. The result of such calculations is shown qualitatively, in Tables 1 and 3, from which we have a rough idea of the nature of vibrations of the two molecular forms. Of course, the representations are only approximate, since none of the vibrations is restricted in a single symmetry co-ordinate.

Thus from the result of the present experiment, together with that of the normal vibration calculations, we can conclude that the two stable molecular forms of 1:2-dichloro-2-methylpropane are the *trans* and *gauche* forms. The *trans* form corresponds to almost non-polar form which persists in the solid state and the *gauche* form corresponds to the polar form which exists only in the liquid and gaseous states and disappears in the solid state.

The intensity ratio of the two infra-red bands at 572 cm^{-1} (*gauche* form) and 624 cm^{-1} (*trans* form) has been measured at different temperatures in the gaseous state. The result (to be reported in detail elsewhere) could be explained by assigning a value of about 1 kcal/mole to the energy difference between the *trans* and *gauche* forms. This value agrees with that obtained from the dipole measurement [3].

However, the intensity ratio of these two bands remains almost constant at different temperatures in the liquid state. This shows that the two forms have almost the same energy in this state. This is due to the fact that in the liquid state the *gauche* form with large moment is subjected to energy change much larger than the *trans* form with almost no moment. In consequence, the *gauche* form, which is less stable in the gaseous state, becomes as stable as the *trans* form in the liquid state.

The molecule of 1:2-dichloro-2-methylpropane is the one obtainable from 1:2-dichloroethane by substituting the two hydrogen atoms by methyl groups. The result obtained above for the internal rotation of 1:2-dichloro-2-methylpropane (including the energy difference between the rotational isomers) is quite similar to that of 1:2-dichloroethane [1]. This gives us further information about the nature of hindering potential to internal rotation [10].

References

[1] Mizushima S. *Structure of Molecules and Internal Rotation*. Academic Press, New York, 1954.

[2] Kahovec L. and Kohlrausch K. W. F. *Z. Phys. Chem.* B1940 **48** 7.

[3] Miyagawa I. *J. Chem. Soc. Japan* 1954 **75** 1162.

[4] McBride J. J. and Beachell H. C. *J. Amer. Chem. Soc.* 1948 **71** 2532.

[5] Mizushima S., Shimanouchi T., Nakamura K., Hayashi M., and Tsuchiya S. *J. Chem. Phys.* 1957 **26** 970.

[6] Nakagawa I. Private communication.

[7] Mizushima S., Shimanouchi T., Nakagawa I., and Miyake A. *J. Chem. Phys.* 1953 **21** 215.

[8] Shimanouchi T. *J. Chem. Phys.* 1949 **17** 245, 734.

[9] Shimanouchi T. *J. Chem. Phys.* 1955 **23** 2465.

[10] Mizushima S., Morino Y., and Shimanouchi T. *J. Phys. Chem.* 1952 **56** 324.

Spectrochimica Acta, 1957, Vol. 10, pp. 8 to 16. Pergamon Press Ltd., London

Normal co-ordinate analysis of the vibrational spectrum of iron pentacarbonyl

WILLIAM G. FATELEY and ELLIS R. LIPPINCOTT
Department of Chemistry, University of Maryland, College Park, Maryland

(*Received* 6 *May* 1957)

Abstract—Results of a normal co-ordinate analysis of the vibrational spectrum of iron pentacarbonyl are presented. The Wilson FG matrix technique was used to obtain valence force symmetry constants (VFSC) from the assignment of frequencies. The VFSC were used to obtain valence force constants (VFC). A comparison of the Fe–C stretching VFC with the corresponding Ni–C stretching VFC indicates that the Fe–C bonds in iron pentacarbonyl are stronger than the Ni–C in nickel carbonyl.

Introduction

THE infra-red spectrum of iron pentacarbonyl, $Fe(CO)_5$, has been investigated previously, but only recently has the Raman spectrum of the compound been obtained and a complete assignment of frequencies been made [1–3]. It is now desirable to carry out a normal co-ordinate analyses of the vibrational spectrum

Table 1. Symmetry co-ordinates

Species A_1'	$S_s = (1/3)^{1/2}(s_1 + s_2 + s_3)$
	$S_t = (1/3)^{1/2}(t_1 + t_2 + t_3)$
	$S_x = (1/2)^{1/2}(x_1 + x_3)$
	$S_y = (1/2)^{1/2}(y_1 + y_2)$
Species A_2'	$S = (1/3)^{1/2}(\beta_1 + \beta_2 + \beta_3)$
Species A_2''	$S_x = (1/2)^{1/2}(x_1 - x_2)$
	$S_y = (1/2)^{1/2}(y_1 - y_2)$
	$S = (1/3)^{1/2}(\gamma_1 + \gamma_2 + \gamma_3)$
	$S = (1/6)^{1/2}(\varepsilon_1 + \varepsilon_2 + \varepsilon_3 - \varepsilon_4 - \varepsilon_5 - \varepsilon_6)$
Species E''	$S^{e''} = (1/6)^{1/2}(2\gamma_1 - \gamma_2 - \gamma_3)$
	$S^{e''} = (1/12)^{1/2}(2\omega_1 - \omega_2 - \omega_3 - 2\omega_4 + \omega_5 + \omega_6)$
	$S^{f''} = (1/12)^{1/2}(2\varepsilon_1 - \varepsilon_2 - \varepsilon_3 - 2\varepsilon_4 + \varepsilon_5 + \varepsilon_6)$
Species E'	$S_s = (1/6)^{1/2}(2s_1 - s_2 - s_3)$
	$S_t = (1/6)^{1/2}(2t_1 - t_2 - t_3)$
	$S = (1/6)^{1/2}(\alpha_1 - 2\alpha_2 + \alpha_3)$
	$S = (1/2)^{1/2}(\beta_2 - \beta_3)$
	$S = (1/12)^{1/2}(2\varepsilon_1 - \varepsilon_2 - \varepsilon_3 + 2\varepsilon_4 - \varepsilon_5 - \varepsilon_6)$
	$S = (1/12)^{1/2}(2\omega_1 - \omega_2 - \omega_3 + 2\omega_4 - \omega_5 - \omega_6)$

of this trigonal bipyramid molecule to see if the assignment is consistent with the calculated valence force constants. The internal co-ordinates were constructed for a D_{3h} symmetry molecule. This symmetry point group has been verified by electron diffraction studies [4], and is consistent with the spectroscopic studies.

The calculation of the valence force constants will enable us to make a comparison with similar quantities for other compounds.

Normal co-ordinate analysis

The Wilson FG technique [5] was used to obtain the secular equation for the different species. The internal co-ordinates constructed for the molecule are shown

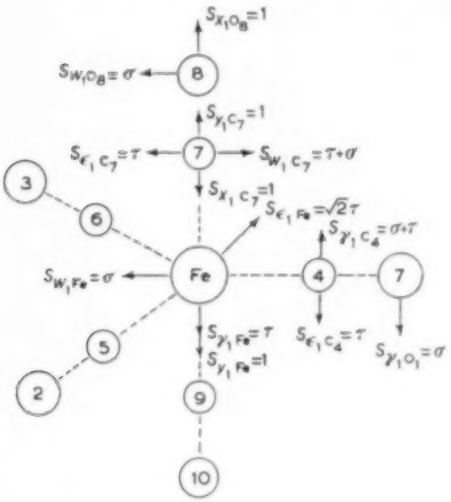

Fig. 1(a). Internal co-ordinates and S vectors

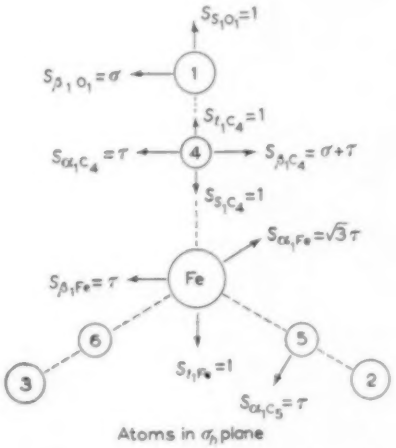

Fig. 1(b). Internal co-ordinates and S vectors.

in Fig. 1. The irreducible representations were used to obtain the symmetry co-ordinates by application of the following equation:

$$S^{(\nu)} = N \sum_R \chi_R{}^{(\nu)} RS_1$$

where N is the normalization factor, $\chi_R{}^{(\nu)}$ is the character of the given species (ν), and RS_1 stands for the co-ordinate to which the displacement S_1 is transferred by operation R. The sum of R is taken over the elements E, $C_3{}^1$, σ_h, $S_3{}^1$, $S_3{}^2$, since these were sufficient to generate the symmetry co-ordinates. In the degenerate species the co-ordinates for α and β are obtained by taking linear combinations of α and β, i.e. $(\alpha_3 + \alpha_1)$ and $(\beta_2 - \beta_3)$ because these combinations will transfer under E, $C_3{}^1$, $C_3{}^2$ in the same way as s_1 and t_1. The symmetry co-ordinates are tabulated in Table 1.

The kinetic energy matrix elements, g_{ij}, were constructed by application of the equation:

$$g_{ij} = \sum_{a=1}^{N} \mu_a S_{ia} \cdot S_{ja}$$

where S_{ia} and S_{ja} are defined in Fig. 1 and $\mu_a = 1/m_a$.

Table 2. Kinetic energy matrix elements G_{kl}

Species A_1'	$G_{xx} = G_{ss} = \mu_0 + \mu_c = 0{\cdot}1457$
	$G_{yy} = G_{tt} = \mu_c = 0{\cdot}0833$
	$G_{xy} = G_{st} = -\mu_c = -0{\cdot}0833$
Species A_2'	$G_{\beta\beta} = \mu_0\sigma^2 + (\sigma+\tau)^2\mu_c = 0{\cdot}2136$
Species A_2''	$G_{zz} = \mu_0 + \mu_c = 0{\cdot}1458$
	$G_{zw} = -\mu_c = -0{\cdot}0833$
	$G_{ww} = \mu_0 + 2\mu_{Fe} = 0{\cdot}1191$
	$G_{\gamma\gamma'} = \sigma^2\mu_0 + (\sigma+\tau)^2\mu_c + 3\tau^2\mu_{Fe} = 0{\cdot}2294$
	$G_{\gamma x} = 0$
	$G_{\gamma y} = -\sqrt{6}\tau\mu_{Fe} = -0{\cdot}0238$
	$G_{xx} = 2\tau^2\mu_c + 8\tau^2\mu_{Fe} = 0{\cdot}0915$
	$G_{x\gamma'} = \sqrt{2}[3\tau^2\mu_{Fe} + (\sigma+\tau)\tau\mu_c] = 0{\cdot}1128$
	$G_{xy} = -2\sqrt{3}\tau^2\mu_{Fe} = -0{\cdot}0183$
	$G_{xz} = 0$
Species E''	$G_{xx} = \frac{7}{2}\mu_c\tau^2 = 0{\cdot}0861$
	$G_{x\gamma'} = \sqrt{2}(\sigma+\tau)\tau\mu_c = 0{\cdot}0904$
	$G_{xw} = (3/4)\tau(\sigma+\tau)\mu_c = 0{\cdot}0479$
	$G_{\gamma\gamma'} = \sigma^2\mu_0 + (\sigma+\tau)^2\mu_c = 0{\cdot}2135$
	$G_{\gamma w} = 0$
	$G_{ww} = \frac{3}{2}(\sigma^2\mu_0 + (\sigma+\tau)^2\mu_c) = 0{\cdot}3202$
Species E'	$G_{xx} = \mu_0 + \mu_c = 0{\cdot}1458$
	$G_{xt} = -\mu_c = -0{\cdot}0834$
	$G_{tt} = \mu_0 + \frac{3}{2}\mu_{Fe} = 0{\cdot}1101$
	$G_{x\chi} = G_{x\beta} = G_{x\sigma} = G_{y\sigma} = 0$
	$G_{t\chi} = -\frac{3}{2}\sqrt{3}\tau\mu_{Fe} = -0{\cdot}0253$
	$G_{t\beta} = \frac{3}{2}\tau\mu_{Fe} = 0{\cdot}0146$
	$G_{t\sigma} = -\dfrac{3}{\sqrt{2}}\tau\mu_{Fe} = -0{\cdot}0206$
	$G_{tw} = -\dfrac{3}{\sqrt{2}}\tau\mu_{Fe} = -0{\cdot}0206$
	$G_{\chi\chi} = 3\tau^2\mu_c + (9/2)\tau^2\mu_{Fe} = 0{\cdot}0976$
	$G_{\chi\beta} = \sqrt{3}[-(3/2)\tau^2\mu_{Fe} - \tau(\sigma+\tau)\mu_c] = -0{\cdot}0680$
	$G_{\chi\sigma} = 3\dfrac{\sqrt{3}}{\sqrt{2}}\tau^2\mu_{Fe} = 0{\cdot}01943$
	$G_{\chi w} = -\dfrac{3\sqrt{3}}{\sqrt{2}}\tau^2\mu_{Fe} = -0{\cdot}01943$
	$G_{\beta\beta} = \sigma^2\mu_0 + (\sigma+\tau)^2\mu_c + \frac{3}{2}\tau^2\mu_{Fe} = 0{\cdot}2214$
	$G_{\beta\sigma} = -\dfrac{3}{\sqrt{2}}\tau^2\mu_{Fe} = -0{\cdot}0112$
	$G_{\beta w} = -\dfrac{3}{2\sqrt{2}}\tau^2\mu_{Fe} = -0{\cdot}0055$
	$G_{\sigma\sigma} = 6\tau^2\mu_{Fe} + 3\tau^2\mu_c = 0{\cdot}0527$
	$G_{\sigma w} = \frac{3}{2}\tau^2\mu_{Fe} + \frac{3}{4}\tau(\sigma+\tau)\mu_c = 0{\cdot}0560$
	$G_{ww} = \frac{3}{2}[\sigma^2\mu_0 + (\sigma+\tau)^2\mu_c + 2\tau^2\mu_{Fe}] = 0{\cdot}3301$

$\mu_0 = 1/m_0$; $\mu_c = 1/m_c$, $\mu_{Fe} = 1/m_{Fe}$; $\sigma = 1/r_{CO}$; $\tau = 1/r_{FeC}$
Masses are in atomic weight units and distances are in Å units.

VOL. 10 1957/5

The kinetic energy matrix elements $G_{K'K}$ are obtained by application of the following equation:

$$G_{K'K} = \left(\frac{1}{U_{K'i}}\right) \sum_j U_{Kj} g_{ij}$$

while the potental energy matrix elements $F_{K'K}$ are obtained from the equation:

$$F_{K'K} = \left(\frac{1}{U_{Ki}}\right) \sum_j U_{Kj} f_{ij}$$

where $F_{K'K}$ is the valence force symmetry constant (VFSC), f is the valence force constant, and U_{Kj} are the coefficients of the symmetry co-ordinates given in Table 1. The secular equations for each species were solved for the force constants by conventional methods. The interaction force constants were set equal to zero in all species, so that independent equations could be obtained which were solvable for the VFC for each species. The assignment of frequencies used in the analysis is given in Table 3.

Table 3. Frequency assignments for $Fe(CO)_5$

Number	Class	cm^{-1}	Description	Symmetry co-ordinate
1	A_1'	1995	CO stretching	s
2	A_1'	1995	CO stretching	x
3	A_1'	410	Fe–C stretching	t
4	A_1'	410	Fe–C stretching	y
5	A_2'	450	CO bending	β
6	A_2''	2028	CO stretching	s
7	A_2''	350	CO bending	γ
8	A_2''	639	Fe–C stretching	y
9	A_2''	100	Fe–C bending	ε
10	E'	1994	CO stretching	s
11	E'	400	CO bending	ω
12	E'	472	CO bending	β
13	E'	614	Fe–C stretching	t
14	E'	110	Fe–C bending	α
15	E'	100	Fe–C bending	ε
16	E''	400	CO bending	γ
17	E''	425	CO bending	ω
18	E''	110	Fe–C bending	ε

Totally symmetrical A_1' species

The symmetrical stretching modes of vibration are found in this Raman active species. The carbon–oxygen in-plane stretching is designated as t in terms of the internal co-ordinates as shown in Fig. 1. The stretching modes of the axial vibrations are x and y which are the oxygen–carbon and carbon–iron stretching modes respectively.

Since the planar modes are perpendicular to the axial modes, the kinetic energy matrix immediately reduced from 4×4 to two 2×2 matrices. The G elements are given in Table 2 and the potential constants in Table 4.

Table 4. $Fe(CO)_5$ VFSC[a]

Species	F_s	F_x	F_t	F_y	F_γ	F_ε	$F_\varkappa$	F_β	F_ω
A_1'	15·07	15·07	2·96	2·96	—	—	—	—	—
A_2'	—	—	—	—	—	—	—	0·55	—
A_2''	—	16·60[b]	—	3·23	0·455	0·183	—	—	—
E'	16·07[b]	—	3·43	—	—	0·17	0·104	0·44	0·39
E''	—	—	—	—	0·40	0·16	—	—	0·35

[a] Stretching and bending VFSC are in units of 10^{-5} dyn/cm and 10^{11} dyn/cm respectively.
[b] These constants were obtained by factoring the high frequencies.

Infra-red active A_2'' species

This species contains an axial carbon–oxygen and carbon–iron stretching, and the out-of-plane carbon–oxygen and carbon–iron bending modes. The carbon–oxygen stretching was factored out of the matrix so that the secular equation could be described in terms of 3×3 matrices. The kinetic energy elements are given in Table 2 while the solution to the secular equations is given in Table 4.

The infra-red and Raman active E' species

This species contains the in-plane carbon–oxygen (s) and carbon–iron (t) stretching modes; carbon–oxygen (β) and carbon–iron–carbon ($\varkappa$) in-plane bending modes; and the axial carbon–oxygen (ω) and carbon–iron–carbon (ε) bending modes. The kinetic energy elements are given in Table 2 and the potential constants in Table 4.

Raman active E'' species

The axial carbon–oxygen bending (ω) perpendicular to plane carbon–oxygen (ν) bending and the carbon (axial) –iron–carbon (in-plane) (ε) bending modes are included in this species. The kinetic energy elements are listed in Table 2 and the calculated VFSC in Table 4.

Valence force constants

The VFSC can be used to calculate the VFC, which in turn can be compared with similar VFC of corresponding bonds of related molecules. The equations for the VFC of the axial (x) and planar (t) Fe–C bond stretching co-ordinates are respectively.

$$F_x = f^a_{\text{Fe-C}} + f^a \qquad \text{species } A_1'$$
$$F_x = f^a_{\text{Fe-C}} - f^a \qquad \text{species } A_2''$$

and

$$F_t = f^p_{\text{Fe-C}} + 2f^p \qquad \text{species } A_1'$$
$$F_t = f^p_{\text{Fe-C}} - f^p \qquad \text{species } E'$$

Here f^a_{Fe-C} and f^p_{Fe-C} are the axial and planar Fe–C bond stretching VFC respectively while f_a and f_p are the corresponding interaction constants. A similar set of equations relates the f^a_{CO} and f^p_{CO} CO bond stretching constants. The calculated Fe–C and CO bond stretching constants are given in Table 5.

Table 5. Axial and planar bond stretching VFC

	Axial	planar
$f_{Fe-C} \times 10^{-5}$ dyn/cm	3·09	3·27
$f_{CO} \times 10^{-5}$ dyn/cm	15·83	15·73

Discussion

The only other metal carbonyl for which a detailed normal co-ordinate analysis has been made is nickel carbonyl, $Ni(CO)_4$ [6]. A comparison of the VFC of $Fe(CO)_5$ with those of $Ni(CO)_4$ is desirable for the information it will furnish concerning their relative bond properties.* There has been considerable discussion as to whether the metal–carbon bonds in $Fe(CO)_5$ are stronger or weaker than those of $Ni(CO)_4$ [7–12]. If the linkage is better represented as a single bond then the theory of directed valence predicts that the Fe–C bond is the stronger since from Pauling's scale the relative bond strength for sp^3 hybridization is less than that for $sp^{1+2n}d^{3-2n}$ hybridization where $0 \leq n \leq 1$. On the other hand, if the metal-carbon linkages are best described in terms of multiple bonds the strengths of the Ni–C bonds should be greater than Fe–C [1, 3, 9].

Infra-red studies by Sheline and Pitzer [1] and Edgell and Wilson [12] and a complete assignment of the vibrational spectrum of $Fe(CO)_5$ indicate that the Fe–C bond is stronger than Ni–C [3]. Cable and Sheline [9], Nyholm [8], Coulson [10], Pauling [11] and Long and Walsh [7] have indicated that the Ni–C bond is the stronger of the two.

The normal co-ordinate analysis of the vibrational spectrum of $Fe(CO)_5$ presented here furnishes further evidence that the Fe–C bond strength is greater than that of the Ni–C bond. The calculated values for the axial and equatorial Fe–C bond stretching VFC are $3{\cdot}09 \times 10^5$ dyn/cm and $3{\cdot}27 \times 10^5$ dyn/cm respectively. The Ni–C bond stretching VFC was found by Crawford and Cross [6] to be $2{\cdot}52 \times 10^5$ dyn/cm. The major part of the difference between these values is certainly associated with a larger Fe–C bond energy. The C–Fe–C bending VFC are also higher than those calculated for $Ni(CO)_4$ which indicates that $Fe(CO)_5$ has a tighter skeletal structure than $Ni(CO)_4$ which is consistent with this order for the relative strengths of the Ni–C and Fe–C bonds. In the case of $Fe(CO)_5$ it is difficult to compare accurately the axial bending to the in-plane bending VFC.

* Recently, L. H. Jones has examined the infra-red spectrum of $Ni(CO)_4$ in a region below 450 cm^{-1}. It appears that the assignment used by Crawford and Cross [6] must be altered to account for the intense infra-red band at 422 cm^{-1}. This might cause a slight change in the calculated VFC for $Ni(CO)_4$. *J. Chem. Phys.* 1955 **23** 2448.

Since the Fe–C bond stretching VFC are greater than the corresponding Ni–C VFC, one would expect that the CO bond stretching VFC in $Fe(CO)_5$ would be somewhat less than that in $Ni(CO)_4$. This is indeed the case since in $Fe(CO)_5$ the axial and equatorial CO bond stretching VFC are $15{\cdot}83 \times 10^5$ dyn/cm and $15{\cdot}73 \times 10^5$ dyn/cm respectively while the CO stretching VFC in $Ni(CO)_4$ is 15·89 dyn/cm.

The $Fe(CO)_5$ the axial Fe–C stretching VFC is smaller than the equatorial Fe–C stretching VFC. This implies that the axial CO stretching VFC in $Fe(CO)_5$ should be slightly greater than the equatorial CO stretching VFC. This is verified by the calculations where values of $15{\cdot}84 \times 10^5$ dyn/cm and 15·73 dyn/cm are obtained respectively.

The CO bending VFC was found to be approximately the same for the axial bending (ω) and the perpendicular to plane bending (ν). This was anticipated since there should be little interaction with other modes for those bending vibrations. It was impossible to solve for in in-plane FeCO bending VFC since there was one equation and two unknowns, but the VFSC has about the same value as those for the axial and perpendicular to plane bending VFSC.

Since the Fe–C stretching VFC have been calculated, it is now possible to compare our force constants with the bond strengths expected from different types of *spd* hybridization. DUFFEY [13] has made calculations of the relative bond strengths for the different $sp^{1+2n}d^{3-2n}$ $(0 \leq n \leq 1)$ configurations of D_{3h} symmetry. He was able to construct a table of bond strengths of planar and axial bonds for different n's. Part of that table is as follows:

n	Strength of equatorial bond	Strength of axial bond
1·000	2·244	2·937
0·444	2·963	2·928
0·000	2·418	2·935

The value of $n = 0{\cdot}444$ corresponds to the maximum relative strength of an equatorial bond. In $Fe(CO)_5$ the axial Fe–C stretching VFC was $3{\cdot}09 \times 10^5$ dyn/cm as compared to $3{\cdot}27 \times 10^5$ dyn/cm for the planar stretching VFC. This would correspond to a $n = 0{\cdot}44$ and a configuration near sp^2d^2.

There always exists the possibility of using a different assignment to calculate the force constants with the result that the VFSC may differ accordingly. First consider the possibility of interchanging an assignment in a given symmetry species. This interchanged assignment cannot affect the calculation of the VFSC in this species since solutions of the secular determinant involves the taking of sums of products of frequencies. The order with which these sums are taken is independent of the solution of the secular determinent. For example, in species A_2'' there has been considerable discussion as to whether the 639 cm^{-1} infra-red band would be assigned as a Fe–C stretching (ω_8) or CO bending frequency (ω_7). We have

VOL.
10
1957/5

assigned it as ω_8. If it is assigned as a CO bending frequency the resulting change in assignment is essentially an interchange of ω_8 with ω_7. The calculated VFSC will remain unchanged for the reason given above. Insofar as the normal co-ordinate analysis is concerned the 639 cm^{-1} infra-red peak can be either a Fe–C stretching or a CO bending frequency. We feel that it is a stretching frequency since a comparison with analogous molecules shows that stretching frequencies are usually higher than the corresponding bending frequency.

If one uses a different set of frequencies for a given species one will obtain different values for the calculated VFSC. The number of alternative sets for a given species is limited by the nature of the infra-red and Raman spectra and our knowledge of characteristic group frequencies. The ideal situation is where only one set of frequencies is reasonable for a given species.

Recently Edgell and Wilson have given as assignment of frequencies for $Fe(CO)_5$ which differs from the one proposed in this paper [12] (species A_1'; $\omega_1 = 2120$, $\omega_2 = 1995$, $\omega_3 = 410$, $\omega_4 = 492$: species A_2'; $\omega_5 = 500$; species A_2''; $\omega_6 = 2014$, $\omega_7 = 619$, $\omega_8 = 472$, $\omega_9 = 115$; species E'; $\omega_{10} = 2034$, $\omega_{11} = 645$, $\omega_{12} = 552$, $\omega_{13} = 426$, $\omega_{14} = 92$, $\omega_{15} = 102$, species E''; $\omega_{16} = 275$, $\omega_{17} = 377$ and $\omega_{18} = 110$). We have recalculated the Fe–C and CO bond stretching VFC using their proposed assignment and our equations. Values of $2{\cdot}97 \times 10^5$ dyn/cm and $16{\cdot}58 \times 10^5$ dyn/cm are calculated for the axial Fe–C and CO bond stretching VFC respectively while values of $3{\cdot}91 \times 10^5$ dyn/cm and $15{\cdot}88 \times 10^5$ dyn/cm are calculated for the planar Fe–C and CO bond stretching VFC respectively. The calculated values for the axial and planar Fe–C stretching VFC from their assignment differ greatly. It seems unlikely that the stretching force constants for two such similar bonds would differ by such a large amount (32 per cent). The value calculated for the planar Fe–C stretching VFC is much larger than similar metal–carbon bond stretching constants in other metal organic compounds [2]. The main reason for this high value of the planar Fe–C stretching frequency lies in their assignment of species A_1', which was based on the estimation of ω_1 and ω_4 at positions in the spectrum where no Raman lines have been observed. Because of this and the fact that totally symmetric frequencies of a given type bond for an odd number of atoms on an axis are usually observed at the lower cm^{-1} values rather than at the higher cm^{-1} values, we feel that their assignment of the A_1' species must be modified. The remaining difficulty with their assignment in terms of relative VFSC is the fact that the calculated CO bending constants for species E^3 are much lower than the corresponding constants calculated from their assignment of species E', whereas it is expected that these VFSC should have approximately the same values. It would appear that some of their assigned frequencies in species E' have been estimated too high or that some of the frequencies in species E'' were estimated too low.

References

[1] Sheline R. K. and Pitzer K. S. *J. Amer. Chem. Soc.* 1950 **72** 1107.
[2] Sheline R. K. *J. Chem. Phys.* 1950 **18** 602–606.
[3] King F. T. and Lippincott E. R. *J. Amer. Chem. Soc.* 1956 **78** 4192.
[4] Ewens R. V. G. and Lister M. W. *Trans. Faraday Soc.* 1949 **35** 681.

[5] Wilson E. B., jr., Decius J. C., and Cross P. C. *Molecular Vibrations.* McGraw-Hill New York, 1955.
[6] Crawford B. L., jr. and Cross P. C. *J. Chem. Phys.* 1938 **6** 525.
[7] Long L. H. and Walsh A. D. *Trans. Faraday Soc.* 1947 **43** 342.
[8] Nyholm R. S. and Short L. N. *J. Chem. Soc.* 1953 2670.
[9] Cable J. W. and Sheline R. K. *Chem. Revs.* 1956 **1** 1.
[10] Coulson L. A. *Valence* p. 216. Clarenden Press, Oxford, 1952.
[11] Pauling L. *Nature of the Chemical Bond* p. 251. Cornell University Press, Ithaca, N.Y. 1944.
[12] Edgell W. F. and Wilson Wm. E. Private communication.
[13] Duffey C. H. *J. Chem. Phys.* 1949 **17** 196.

VOL.
10
1957/5

Spectrochimica Acta, 1957, Vol. 10, pp. 17 to 20. Pergamon Press Ltd., London

Vibrational band intensity of the hydroxyl group in phenols

P. J. Stone and H. W. Thompson
The Physical Chemistry Laboratory, Oxford

(*Received* 15 *May* 1957)

Abstract—The effect of the aromatic ring substituents upon the vibrational frequency, band intensity and half-band width of the hydroxyl group in a number of phenols has been measured. The vibration frequency diminishes as the electron attracting power of the substituent increases, whereas the converse applies in the case of substituted anilines. The band intensities appear to comply with the linear relation between log (intensity) and Hammett factor σ, previously noticed with other similar series; and the slope of this plot is positive. The apparent half-band width of the hydroxyl group increases somewhat with increasing σ value of the substituent.

It is now generally recognized that many of the "characteristic" vibration frequencies of key groups used in infra-red structural diagnosis are affected to a greater or less extent by the remainder of the molecule in which they occur. In many cases the variations in magnitude of these frequencies are not the result of nuclear "mass" effects, but are due to differences in electronic structure arising from inductive or mesomeric factors. As yet, relatively few data are available about the intrinsic intensities of such key absorption bands, but this aspect has been explored in some recent papers from this laboratory. One series of particular interest includes molecules of the type X—Ar—Y, in which substituent groups around an aromatic ring affect the vibration frequencies of a vibrational chromophoric group Y. Systematic variations of this kind have been found with nitrobenzenes, anilines, phenols and other classes of benzene derivatives, but although results are available for the frequency shifts, little information has been recorded about the band intensities. Some measurements were described recently on phenyl cyanides [1], anilines [2], benzoic esters, benzaldehydes and aryl ketones [3] which revealed interesting effects of ring substituents upon the frequency, absorption band intensity, and half-band width of vibrations of the group attached to the aromatic nucleus. If sufficient data of this kind can be assembled, it should be useful not only in relation to structural diagnosis, but also as a means of disentangling the inductive and mesomeric influences which affect the whole molecular structure. Also, comparison of the band intensities in different solvents are especially significant in connexion with quantitative analysis, and in order to clarify current ideas about the influence of solvent medium upon the vibrations of a solute.

This paper summarizes results obtained on the effect of aromatic ring substituents upon the behaviour of the hydroxyl group in a series of phenols, dissolved in carbon tetrachloride. Systematic frequency shifts in this class of compound have been noted previously by Goulden [4], and by Ingraham, Corse, Bailey, and Stitt [5]. Califano and Moccia [6] have recently made intensity measure-

ments on a few phenols which agree closely with our own and Tsubomura [7] has also reported several approximate values for the band intensities.

Experimental method

The measurements were made with a Perkin Elmer 12 C spectrometer, using lithium fluoride prism. The effective slit width was about 10 cm^{-1}. The physical constants of the phenols, after repurification by recrystallization or redistillation, indicated satisfactory purity. Carbon tetrachloride was dried and redistilled. Absorption cells 2 cm and 5 cm in length were used, with concentrations in the range 0·003–0·005 M. At these high dilutions there is no appreciable hydrogen bonding between solute molecules, and this is borne out by the linearity of the Beer's law plot of absorbance against concentration over the range employed.

Values for the true band intensities were determined by extrapolating the plots of

$$B = \frac{1}{ce}\int \ln\left(\frac{T_0}{T}\right)_\nu . d\nu \quad \text{against} \quad \log\left(\frac{T_0}{T}\right)_{max}$$

to zero absorbance in the usual way. The band areas required in determining B were obtained by graphical integration.

Results

The results are given in Table 1 and shown graphically in Fig. 1.

Table 1. OH group in phenols. A in absolute units, natural logarithms

Substituent	σ	ν (cm^{-1})	$A \times 10^7$	$\Delta\nu^{\sigma}_{1/2}$ (cm^{-1})
p-benzyloxy	−0·41	3613	5·3	19
p-hydroxy	−0·36	3617	4·9	18
3:4-dimethyl	−0·30	3615	6·3	20
p-methoxy	−0·27	3614	5·6	20
p-methyl	−0·17	3612	5·8	19
none	0·00	3608	5·8	20
p-phenyl	0·01	3612	7·6	21
m-methoxy	0·11	3612	5·9	21
p-chloro	0·23	3610	6·6	22
m-aldehydo	0·35	3604	6·6	22
m-chloro	0·37	3607	6·7	23
p-carbomethoxy	0·64	3603	8·0	23
p-phenylazo	0·64	3602	9·2	23
p-carboethoxy	0·68	3600	8·1	22
m-nitro	0·71	3600	8·7	25
p-cyano	1·00	3594	8·6	23
p-aldehydo	1·13	3592	7·9	22
p-nitro	1·27	3593	8·5	24

Our values for the frequencies of the hydroxyl group vibration with different ring substituents agree well with the earlier data of Goulden, and of Ingraham *et al.* As the electron attracting power of the substituent increases, the vibrational

VOL. 10 1957/5

frequency of the OH group is lowered. This shift is in the reverse direction to that found for substituted anilines, and the contrast between the O—H and N—H links in the respect is noteworthy.

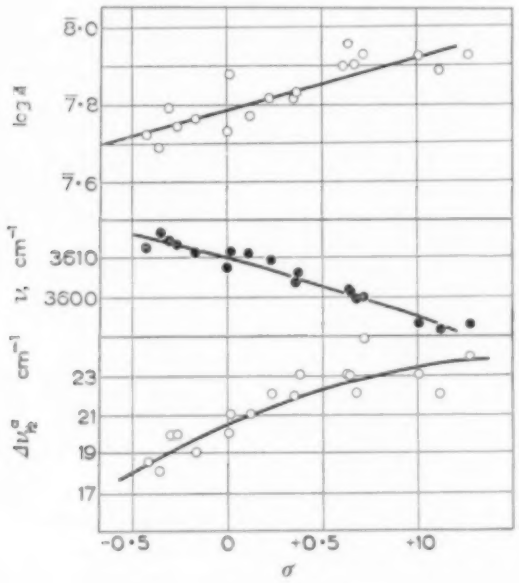

Fig. 1.

The intensity of the OH vibration band is increased by the introduction of electron attracting substituents, and this trend is in the same sense as that found with the substituted anilines. Previous results with substituted phenyl cyanides [1] suggested that there is a linear relation between the logarithm of the band intensity of the chromophoric group and the Hammett sigma factor of the substituent, and this relation has a formal similarity with the well-known Hammett relation concerning reactivity constants. The present results with phenols are consistent with this, and give an essentially linear plot of log A against σ, the positive slope of which is somewhat smaller than the corresponding value for substituted anilines or N-methylanilines. It is perhaps worth noting that the values for the intensity of the OH band in the cases of p-phenyl and p-phenylazo groups as substituent appear rather anomalous since a similar discrepancy was found with these two groups as substituents in the anilines [2]. It is possible that the additional conjugation in these structures has some bearing upon this.

The apparent half-band width of the hydroxyl group shows a definite increase as the electron attracting power of the substituent increases, and the conditions of measurement are such that the true half-band widths will not be much smaller than the apparent widths, and they will show the same trend. In this respect the OH link differs from the NH link in anilines, where the effect of σ upon $\Delta\nu^a_{1/2}$ is in the converse sense.

It now becomes clear from all our results with the various series of substituted benzenes that the influence of σ upon the values of ν, A and $\Delta\nu^a_{1/2}$ for the attached chromophoric group follows a complex pattern. The variation of ν with σ is not always in the same sense, as might indeed be expected, but it is surprising to find that even with vibrational chromophoric groups which might be expected to behave similarly the direction of frequency displacement is different. The effect of σ upon the band intensity in a given pair of series does not always follow the same trends as its effect upon the vibration frequency. Also, the variation of $\Delta\nu^a_{1/2}$ with structural factors seems to bear no immediate relation with the variation upon ν or A. It is hoped in a later paper to consider all the data together and to suggest a general framework into which each type will fit.

As regards the determinations of band intensity, Ramsay [8] suggested a simple procedure for computing the true intensity A in terms of the observed peak absorbance and apparent half-band width, using the relation

$$A = K \,.\, \frac{1}{cl} \,.\, \ln\left(\frac{T_0}{T}\right)_{\max} \,.\, \Delta\nu^a_{1/2}$$

Tables of values of K were calculated, on the assumption of a Lorentz band shape, for different values of $s/\Delta\nu^i_{1/2}$, the ratio of effective slit width to true half-band width. For the average working conditions, K will have a value of about 1·5. We should draw attention to the fact that the values of K determined from our data directly, using the measured integrated band areas, are all about 1·2, a value much lower than that given by Ramsay. This peculiarity has been noted previously, and may arise from the fact that the band contour does not have a strictly Lorentz form. It seems unlikely that it can arise from the neglect of wing corrections in our measurements. Whatever the true cause may be, it should be noted that several authors have recently followed this quick procedure for obtaining the true band intensities, and it may be desirable to regard the values thus obtained as higher than those which would be found by a more complete measurement.

This work was supported by a grant from the Hydrocarbon Research Group of the Institute of Petroleum, to which we again express our thanks.

References

[1] Thompson H. W. and Steel G. *Trans. Faraday Soc.* 1956 **52** 1451.
[2] Krueger P. J. and Thompson H. W. *Proc. Roy. Soc.* In press.
[3] Thompson H. W., Needham R. W., and Jameson D. *Spectrochim. Acta* 1957 **9** 208.
[4] Goulden J. D. S. *Spectrochim. Acta* 1954 **6** 129.
[5] Ingraham L. L., Corse J., Bailey G. F., and Stitt F. *J. Amer. Chem. Soc.* 1952 **74** 2297.
[6] Califano S. and Moccia R. Private communication.
[7] Tsubomura H. *J. Chem. Soc.* 1956 **24** 927.
[8] Ramsay D. A. *J. Amer. Chem. Soc.* 1954 **76** 2526.

VOL.
10
1957/5

Spectrochimica Acta, 1957, Vol. 10, pp. 21 to 37. Pergamon Press Ltd. London

Studies of the band near 3 μ in some hydroxy compounds

M. St. C. Flett
Imperial Chemical Industries Ltd.
Dyestuffs Div., Hexagon House,
Blackley, Manchester 9

(*Received* 30 *April* 1957)

Abstract—The hydroxyl absorption band of a number of compounds has been measured in dilute carbon tetrachloride solution, and attempts made to relate its wavelength, intensity, and shape to structural features of the molecule. Small differences have been observed between the values for primary, secondary, and tertiary alcohols, phenols, and derivatives of polycyclic aromatics. Cases where internal hydrogen bonding is possible have also been considered. It proved possible to distinguish between molecules where quantum mechanical hydrogen bonds are formed, and those where the band is shifted rather by electrostatic effects than by true hydrogen bonding. Some data on cyanhydrins and oximes are also included. The results obtained will be useful in yielding information about the structures of unknowns containing hydroxyl groups.

Introduction

Almost since infra-red spectroscopic measurements began, it has been known that the hydroxyl group gives rise to a band near 3300 cm^{-1} due to its stretching vibration. A great deal of work on this band has been described, and is excellently summarized in Bellamy's book [1]. In the course of diagnostic work it is clearly desirable not merely to use the band as a means of determining whether or not the unknown contains hydroxyl groups, but also to use its strength, shape and precise frequency to find out the type of hydroxylic compound involved. A difficulty arises here, since these compounds in the solid and liquid states normally form polymeric aggregates through hydrogen bonding. The resulting band is usually too wide for precise measurements to be made on it. The extent of this intermolecular bonding is determined partly by the size of the groups surrounding the hydroxyl in the molecule, so in suitable cases some information about the compound can be obtained from the hydroxyl frequency [2, 3]. In general, however, it proves more satisfactory to study the compound in dilute solution where, with increasing dilution, the polymers break up first to dimers and then monomers. For example in the case of carbon tetrachloride, which being virtually transparent in the 3 μ region is perhaps the most suitable solvent for the purpose, most hydroxylic compounds at concentrations less than about 0·005 M are monomeric. This paper describes measurements of band frequencies and intensities under these conditions. Attempts are made to correlate them with the effect of electronic shifts within the molecule, and internal hydrogen bonding. It is believed that, conversely these results will be useful in structural diagnosis.

Experimental

(a) *Materials.* The samples used were either commercially available materials which were purified by recrystallization or distillation, or samples prepared by

colleagues in the course of their researches. Melting or boiling points were checked. "Analar" grade carbon tetrachloride was used as solvent without further purification. It was dried immediately before a solution was made up, by passage of air dried by phosphorus pentoxide.

(b) *Spectroscopic measurements.* In all cases where there were possibilities of internal hydrogen bonding, the spectrum was measured at two different dilutions (usually 0·003 and 0·009 M). If the spectrum was independent of dilution, it was concluded that intermolecular bonding was absent. In addition a few experiments with mixed solutions of alcohols with amines, esters and ketones were carried out to check the above conclusion. The measurements were made with a Grubb-Parsons S4 double-beam spectrometer, using a calcium fluoride prism. An equal path length of carbon tetrachloride was used in the blank beam. The wavelength scale of the spectrometer was checked daily by running a solution of benzyl alcohol or phenol, whose bands have been accurately measured using a grating [4]. All the values reported (except in the case of shoulders and very broad bands) are thought to be accurate to ± 3 cm^{-1}. In some spectra there was a weak band at about 2·70 μ due to a small amount of water in the solute or picked up by the solution. A calculation based on data connecting the strengths of the water band in carbon tetrachloride with its concentration [5] showed that its concentration was far too small for it to associate appreciably with the solute. The band intensities were also measured, except where bands fell so close together that their separate strengths could not be measured. Various methods of measuring the intensity of an infra-red band have been suggested, using both the peak optical density and the area under the band. On the whole, the areas seem better, except in the case of severe overlapping, and have been used during the present work. A rapid and fairly accurate method of determining band areas was described by Ramsey [6] using the peak density ($\log_e I_0/I$) and the width of the band at half density. The absolute intensity is then given by

$$A = \frac{K}{cl} \log_e (I_0/I)_{\max} \Delta\nu_{\frac{1}{2}}$$

where c is the concentration and l the path length in centimetres. If, as is now customary [7] A is expressed in absolute units (cm^{-1} mole^{-1} sec^{-1} $\log_e$) $\Delta\nu_{\frac{1}{2}}$ must be in c/s and c in mole/cm^3. K is a correction factor for instrumental effects on the band shape. These result from the use of finite slits, and the finite resolution of a prism. It has been tabulated by Ramsey for various values of $\log_e (I_0/I)$ and $S/\Delta\nu_{\frac{1}{2}}$, where S is the effective slit width of the spectrometer. For our instrument a figure for S of about 9 cm^{-1} was obtained, and values of K were deduced on this basis. Its value was normally about 1·54 but with the sharpest bands fell to 1·50. Owing to the various uncertainties in the measurement, the values of A are possibly not accurate to better than about ± 5 per cent.

Results

The tables summarize the data on all the compounds examined. They refer to carbon tetrachloride solutions of the stated molality in a 3 cm cell. For each band the wave number, peak optical density, width at half height and the quantity

VOL. 10 1957/5

A described above are recorded. Also some of the spectra are reproduced on a small scale in the figures.

Discussion

We shall first consider compounds where there is no possibility of internal hydrogen bonding. Frequency shifts must then arise from inductive or mesomeric shifts in the molecule. RICHARDS [8] and BARROW [9] have previously considered

Table 1. Hydroxyl bands in some alcohols

Compound	Molality	Wave number of peak (cm^{-1})	Peak optical density ($\log_{10} I_0/I$)	$\Delta\nu_{\frac{1}{2}}$ (cm^{-1})	$A \times 10^7$
Methanol	0·00324	3640	0·459	28	2·32
Ethyl alcohol	0·00322	3632	0·351	39	2·47
n-Propyl alcohol	0·00319	3634	0·387	40	2·74
*Iso*propyl alcohol	0·00300	3620	0·318	36	2·25
n-Butyl alcohol	0·00325	3631	0·430	34	2·65
*Iso*butyl alcohol	0·00292	3636	0·357	39	2·80
Sec.-butyl alcohol†	—	3623	—	—	—
Tert.-butyl alcohol	—	3616	—	—	—
Stearyl alcohol*	—	3636	—	—	—
*Cyclo*hexanol	0·00327	3615	0·430	25	1·93
Allyl alcohol	0·00309	3620	0·395	40	3·07
Benzyl alcohol*	—	3618	—	—	—
Diphenyl carbinol*	—	3616	—	—	—
Triphenyl carbinol*	—	3612	—	—	—

* See reference [8].
† See reference [9].

this topic. The —OH frequency of methanol is less than that of water, which has been attributed to contributions from $H^- CH_2{=}O^+{-}H$ and $H^+ CH_2{=}O\ H^-$ to the resonance hybrid which weaken the O—H bond. The frequency falls farther on passing to secondary alcohols (ca. 3620 cm^{-1}) and tertiary alcohols (ca. 3615 cm^{-1}), because of the increasing numbers of methyl groups available to take part in the effect (Table 1). Hydroxyl frequencies seem thus to decrease with increasing positive charge on the oxygen atom. The values for allyl alcohol, benzyl alcohol, diphenyl and triphenyl carbinols are respectively 3620, 3618, 3616 and 3612 cm^{-1} indicating that electron transfer to the ring or double bond, leaving the oxygen more positive, is possible. The low value for phenol (3610 cm^{-1}) may also be ascribed to electronic shifts involving participation of forms such as

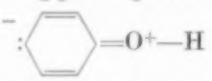

Hydroxyl frequencies for several substituted phenols were reported by INGRAHAM *et al.* [10], and some of these were checked and intensities also measured during the

present work (Table 2). Clearly the frequencies parallel the Hammett σ factors of the substituents. As might be expected electron-attracting substituents lower the frequency, as a result of the increased positive charge on the oxygen atom. This is in contrast to what was found [11] with substituted anilines, where electron-attracting substituents raise the N—H frequency. Cannon [12], from measurements of the effect of N-alkyl substitution on the change of the N—H frequency of amides with change of dielectric constant of the medium, concluded that as positive charge on the N atom increases, the polarity of the N—H link *decreases*. If the same is true of anilines we have an explanation of the above difference between N—H and —OH links, since making oxygen more positive *increases* the polarity of the OH link, as proved by the stronger inter-molecular hydrogen bands formed by phenols than by alcohols [13].

From Table 2 we see that a further lowering of the frequency occurs when a —OH group is attached to a polycyclic hydrocarbon residue. Some calculations on this topic have been made by Lester [14] in connection with his work on antioxidant efficiency. He concludes that the electron in the non-bonding molecular orbital of a phenol will be localized to a lesser extent on the oxygen atom (making it more +), (a) the more extensive the skeleton and (b) the nearer the hydroxyl group to a point of attachment of 2 rings. The present results agree with this insofar as the hydroxyl frequency is definitely lower for polycyclics than phenols. There is, however, no apparent variation in accordance with the second prediction. Also Lester concluded that the frequency should be higher in α-naphthol than in β-naphthol, as observed, though the ratio he predicts is higher than the observed one of 1·001.

There is a striking difference between the shapes and intensities of the phenolic bands described in Table 2 and those of the alcohols. As measured by A, the phenolic bands are about three times as intense, and are much sharper. The increased sharpness may arise because phenols have fairly rigid molecules where the —OH unit vibrates in a constant potential field, whereas the alcohol molecules are flexible so there will be a variety of fields according to the precise configuration of the molecule at a given instant. Some support is given to this hypothesis by the narrowness of the bands in methanol and *cyclo*hexanol compared to the other aliphatic alcohols. Within the phenol series the band intensities are increased by electron-attracting substituents and vice-versa.

We shall now consider molecules in which internal hydrogen bonding is possible. Before this is done, the nature of the hydrogen bond must be briefly considered. The phenomenon of hydrogen bonding has been ascribed both to purely electrostatic effects and to quantum mechanical interaction. In point of fact both of these seem to be shown by hydroxy compounds, and many hydrogen bonds can definitely be assigned to one or other of these types. Fyfe [15] suggests that a quantum mechanical hydrogen bond X—H . . . Y involves overlap of the 1s atomic orbital by an asymmetric non-bonding (lone pair) orbital of the Y atom. Cannon [12] postulates that in addition, for strong hydrogen bonding, the X—H link must be partially ionic, with the 1s orbital partially unfilled to facilitate overlap by the non-bonding orbital. Where these conditions are not satisfied, electrostatic interactions may nevertheless lead to frequency shifts, but it is only

VOL.
10
1957/5

Table 2. Hydroxyl bands in some phenols

Compound	Molality	Wave number	Peak density ($\log_{10} I_0/I$)	$\Delta\nu_{\frac{1}{2}}$ (cm^{-1})	$A \times 10^7$
Phenol	0·000895	3610	0·510	22	7·25
p-Cresol	0·001095	3610 [3612]†	0·610	21	6·74
p-Cl phenol	0·000975	3605 [3608]†	0·582	22	7·65
p-NO_2 phenol	0·001040	3590 [3594]†	0·771	25	10·82
p-Methoxy phenol	0·000920	3610 [3614]†	0·476	22	6·61
β-Naphthol	0·00101	3599	0·630	22	7·78
α-Naphthol	0·00100	3602	0·576	22	7·32
2-OH anthracene*	—	3600	—	—	—
1-OH phenanthrene*	—	3602	—	—	—
2-OH phenanthrene	0·000990	3603	0·616	22	7·92
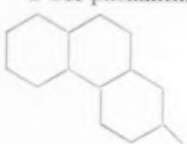 3-OH phenanthrene	0·000940	3600	0·575	22	7·40
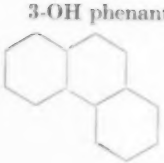					

* No intensity data given because of uncertainty about purity of the compounds.
† See reference [10].

Table 3. Hydroxyl absorption of some strongly internally hydrogen bonded molecules

Compound	Structure	Molality	Absorption range (cm^{-1})
2-(3-chloro-2-hydroxy-phenyl) oxazoline	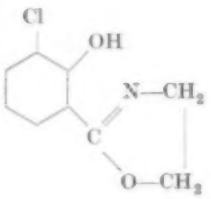	0·00304	3450–2400 max. ca. 2950
Salicyl dimethylamide	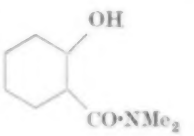	0·00303	3550–2550 max. doubtful
1-Dimethylamino-methyl-2-Naphthol	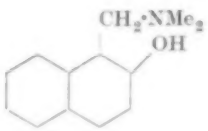	0·00298	3450–2300 max. ca. 2850
Disalisal hydrazone	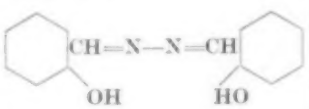	0·00300	3450–2500 max. ca. 3050
o-Hydroxy aceto-phenone	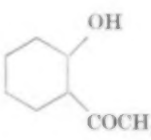	0·00309	3550–2770 max. ca. 3000
2-Acetyl-1-naphthol	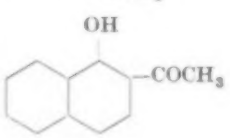	0·00300	3400–2400 max. ca. 2700
Salicyl aldehyde*	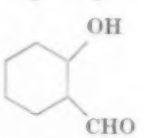	—	3600–3100 max. ca. 3300

* See reference [21].

VOL. 10 1957/5

Table 4. Hydroxyl bands of molecules with internal hydrogen bands

Compound	Structure	Molality	Wave number (cm^{-1})	Peak density $\log_{10} I_0/I$	$\Delta\nu_{\frac{1}{2}}$ (cm^{-1})	$A \times 10^7$
2-Diethylamino ethanol	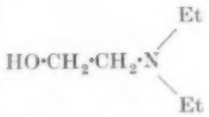	0·00428	3630 3472	0·037 0·281	?30 166	0·151 6·57
1-Diethylamino propan-2-ol	$CH_3{\cdot}CHOH{\cdot}CH_2{\cdot}NEt_2$	0·00402	? 3600 3468	v. weak 0·316	— 156	— 7·37
2-Di-*n*-propyl-amino ethanol	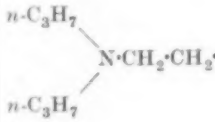	0·00282	3629 3497	v. weak 0·211	— 132	— 5·95
2-Di-*n*-butyl-amino ethanol	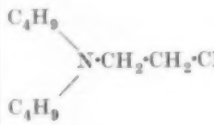	0·00289	? 3631 3497	— 0·1776	— 141	— 5·25
N-(2-hydroxy ethyl) piperidine	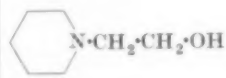	0·00298	3631 3499	— 0·197	— 156	— 6·23
2-morpholino ethanol	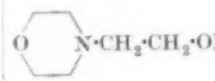	0·00308	3528	0·189	121	4·52
3-Diethylamino propan-1-ol	$HO{\cdot}CH_2{\cdot}CH_2{\cdot}CH_2{\cdot}NEt_2$	0·00296	3628 3288	0·103 0·515	ca.30 240	0·66 25·2
3-Di-*n*-propyl-amino propan-1-ol	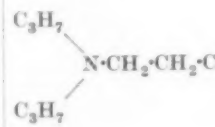	0·00297	3632 3304	0·066 0·446	?35 218	0·48 19·8
2-(Methylanilino) ethanol	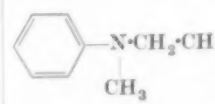	0·00310	3632 ? 3573	0·274 weak	52 —	2·69 —
Ethylene glycol monoacetate	$HO{\cdot}CH_2{\cdot}CH_2{\cdot}O{\cdot}COCH_3$	0·00623	ca.3630 3616 3519 3486	— 0·482 — —	— ?43 — —	— 2·01 — —

Table 4—*continued*

Compound	Structure	Molality	Wave number (cm^{-1})	Peak density $\log_{10} I_0/I$	$\Delta\nu_{\frac{1}{2}}$ (cm^{-1})	$A \times 10^7$
Glycol mono-formate	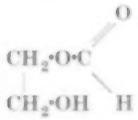	0·00323	3615 3534 3478	0·328 weak weak	46 — —	2·74 — —
Diethylene glycol monoethyl ether	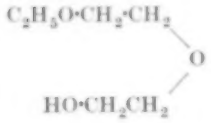	0·00492	ca.3635 3605 3484	— 0·565 0·329	— 36 ? 102	— 2·42 4·05
Ethyl lactate	$CH_3{\cdot}CHOH{\cdot}COOEt$	0·00365	3600 3541 3487	0·072 0·621 v. weak	? 20 35 —	0·30 3·55 —
Diacetone alcohol		0·00388	3612 3532 ? 3412	0·088 0·628 v. weak	? 25 56 —	0·34 5·42 —
Benzoin	$\phi{\cdot}CHOH{\cdot}CO\phi$	0·00378	3623 3480	0·031 0·664	? 30 56	0·14 5·87
8-Hydroxy-quinoline	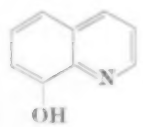	0·00420	3431	0·987	57	7·92
Ethyl mandelate	$C_6H_5{\cdot}CHOH{\cdot}COOEt$	0·00345	3602 3534	0·057 0·772	? 20 39	0·19 4·85
Hydracetyl acetone	$CH_3{\cdot}CHOH{\cdot}CH_2{\cdot}COCH_3$	0·00393	ca.3600 3557	v.weak 0·3404	— 90	 4·64
Ethyl 2-OH propionate	$HOCH_2{\cdot}CH_2{\cdot}COOEt$	0·00293	3635 3598	v. weak 0·334	— 90	 6·11
2-Nitroethyl alcohol	$NO_2{\cdot}CH_2{\cdot}CH_2{\cdot}OH$	0·00304	3588	0·252	64	3·15
o-Nitro-phenol	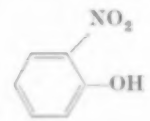	0·001040	3243	0·185	89	9·51

VOL. 10 1957/5

with bonding of the first type that large increases in the width and intensity of the band occur. Whether the term "hydrogen bond" should be used in both cases is a matter of opinion.

The strongest internal hydrogen bonds occur in aromatic systems with hydroxyl groups adjacent to N or O atoms. Several such compounds were studied in the region of hydroxyl frequency second harmonics (near 7000 cm^{-1}) by LIDDELL,

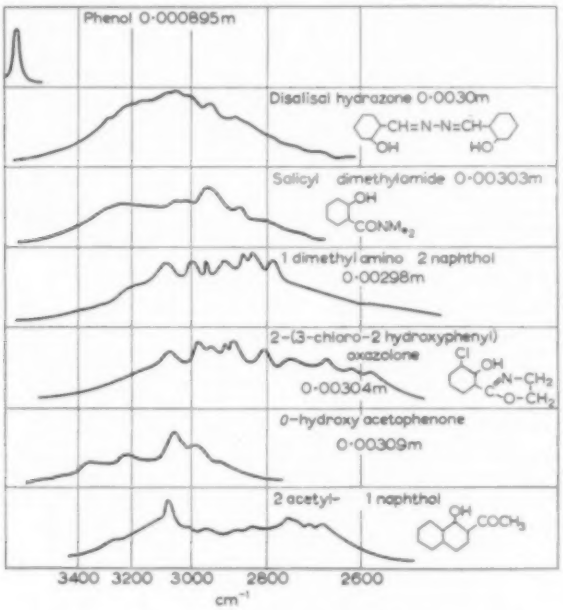

Fig. 1. Spectra illustrating strong internal hydrogen bonding.

WULF, HENDRICKS and HIBBERT [16–19] between 1935 and 1938. The work is summarized in PAULING's book [20]. They found the normal hydroxyl absorption near 7000 cm^{-1} to be completely absent in such cases. Various examples of this phenomenon in the 3 μ region have been reported [21, 22, 23, 24] and also in the region of the third harmonic [25]. In these cases essentially all the molecules are in the internally bonded form. Table 3 and Fig. 1 give some examples, observed during the present work. Frequently since the band is very broad and overlies the C—H absorption region, it is not possible to make an intensity measurement.

Secondly, we consider a class of compounds (mostly aliphatic) in which the bonds are weaker than in the first class, although from the broadening and strengthening of the hydroxyl band, hydrogen bonding clearly occurs. Table 4 gives the data on these compounds, some of whose spectra are shown in Fig. 2. KHUN [26] has described somewhat similar results in the case of glycols, where the 2 hydroxyl groups can interact. Usually a weak band near 3620 cm^{-1} indicates a small proportion of unbonded molecules. Several molecules with the structure

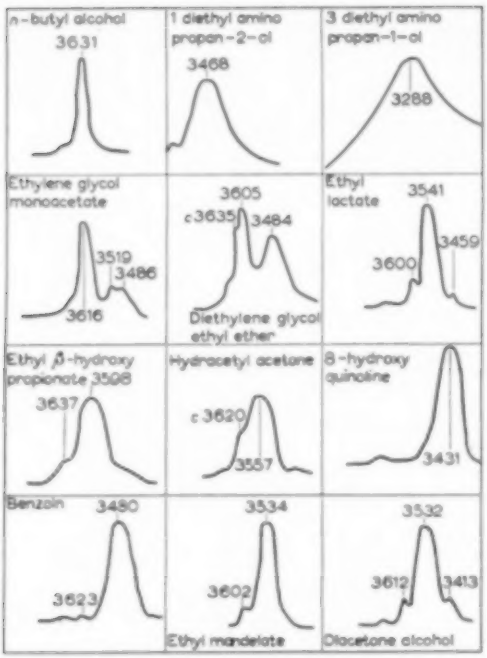

Fig. 2. Hydroxyl bands in some compounds with internal hydrogen bonds.

$R_2 \cdot N \cdot CH_2 \cdot CH_2 \cdot OH$ showed very strong bands. Apparently the ring

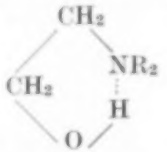

though 5-membered is very stable. The average wave numbers and $A \times 10^7$ factors for this system are 3495 cm^{-1} and 5·9. The corresponding 6-membered ring

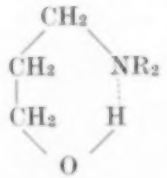

is even more stable ($\nu = 3295$, $A \times 10^7 = 22{\cdot}5$). The importance of the lone pair in hydrogen bonding is illustrated by the virtual absence of internal bonding in the compound

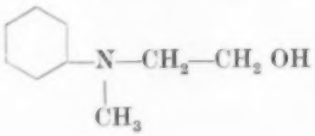

VOL. 10 1957/5

where the pair is partially transferred to the ring

e.g. 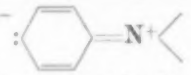

It was also observed that in compounds with the $—NR_2$ group there is a C—H stretching band in the unusual position of 2820 cm^{-1}. This has obvious diagnostic

Table 5. Hydroxyl bands of some *o*-substituted phenols

Compound	Structure	Molality	Wave number	Peak density $\log_{10} I_0/I$	$\Delta\nu_{\frac{1}{2}}$ (cm^{-1})	$A \times 10^7$
Phenol		0·000895	3610	0·510	22	7·25
o-Ethoxyphenol	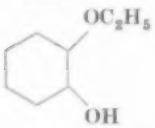	0·00128	3555	0·659	22	6·53
Vanillin	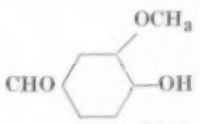	0·000685	3542	0·413	25	8·72
Vanillonitrile	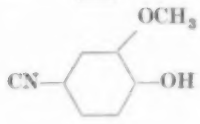	0·000995	3549	0·598	24	8·32
o-Phenoxyphenol	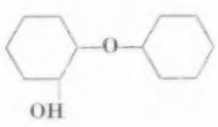	0·00110	3566	0·467	26	6·43
o-Chlorophenol	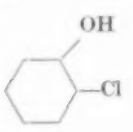	0·00100	3550	0·481	23	6·78
o-Cyanophenol	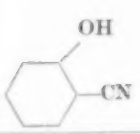	0·00104	3600 3559	weak 0·332	— 23	— 4·47

applications. Ethylene glycol monoacetate and glycol monoformate have their strongest bands respectively at 3616 and 3580 cm^{-1} and are therefore probably mostly in the unbonded form, although the bands at 3519 and 3486 cm^{-1} indicate

some ring formation. Seven-membered rings do not thus appear to be favoured. Most of the molecules are again unbonded in diethylene glycol monoethyl ether, where the 3484 cm^{-1} band indicates a few 8-membered rings. With all the other compounds where internal bonds involving C=O and —OH groups are possible,

Table 6. Hydroxyl frequencies of some compounds of the type $RO{\cdot}CH_2{\cdot}CH_2{\cdot}OH$

Compound	Structure	Molality	Wave number (cm^{-1})	Peak density $\log_{10} I_0/I$	$\Delta\nu_{\frac{1}{2}}$ (cm^{-1})	$A \times 10^7$
2-Ethoxy-ethanol	$C_2H_5O{\cdot}CH_2{\cdot}CH_2{\cdot}OH$	0·00622	3593	0·824	32	2·52
2-Methoxy-ethanol	$CH_3O{\cdot}CH_2{\cdot}CH_2{\cdot}OH$	0·00315	3632 3600	weak 0·450	32	2·67
2-Butoxy-ethanol	$C_4H_9{\cdot}O{\cdot}CH_2{\cdot}CH_2OH$	0·00360	3632 3601	— —	— —	— —
Ethylene glycol monoacetate	$HO{\cdot}CH_2{\cdot}CH_2{\cdot}O{\cdot}COCH_3$	0·00623	ca.3630 3616 3519 3486	v. weak 0·482 — —	— ? 43 — —	— 2·01 — —
Tetra-hydro-furfuryl alcohol	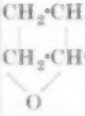	0·00478	3625 3590	— 0·658	— 36	— 2·93
Furfuryl alcohol	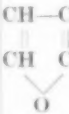	0·00488	3614	0·920	25	2·80
2(2-Hydroxy-ethoxy) naph-thalene	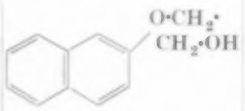	0·00300	? 3634 3616	v. weak 0·474	— 29	— 2·67
1:3 Dimethoxy-propan-2-ol	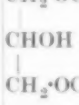	0·00300	3594	0·446	42	3·72

the main band is stronger and wider than in simple alcohols, and at a lower frequency proving that bonding in fact occurs. This applies to ethyl lactate, diacetone alcohol [$(CH_3)_2{\cdot}C(OH){\cdot}CH_2{\cdot}COCH_3$)], benzoin, 8-hydroxyquinoline, ethyl mandelate ($C_6H_5{\cdot}CHOH{\cdot}COOEt$), hydracetyl acetone ($CH_3{\cdot}CHOH{\cdot}CH_2{\cdot}COCH_3$), and ethyl 2-hydroxypropionate. There is no evidence from this set that 5 rings are more or

VOL. 10 1957/5

less stable than 6 rings. Ethyl 2-hydroxypropionate is anomalous in that, although the strength and width of the band clearly indicate an internal bond, its frequency is unexpectedly high. 2-Nitroethyl alcohol probably provides a similar example.

Table 7. Hydroxyl frequencies of some halogenated compounds

Compound	Structure	Molality	Wave number
2:3-Dibromopropan-1-ol	CH_2·Br | CH_2·Br | CH_2·OH	0·00304	3632 (weak) 3596 (strong)
1:3-Dibromopropan-2-ol	CH_2Br | CH_2OH | CH_2Br	0·00315	3578 (weak) 3565 (strong)
2:3-Dichloropropan-1-ol	CH_2Cl | CH_2Cl | CH_2OH	0·00310	3630 (weak) 3595 (strong) 3581 (weak)
3:Chloropropan-1-ol	CH_2OH | CH_2 | CH_2Cl	0·00282	3636
2:Cyanoethanol	CN·CH_2·CH_2·OH	0·00164	3625 3610

We now pass to examples of compounds where for reasons explained below, the —OH frequency shift is not due to internal hydrogen bonding but rather to the electrostatic influence of an adjacent polar group. Table 5 gives data on some *o*-substituted phenols. The significant feature is that in no case is the band greatly widened or strengthened relative to phenol, as found with the hydrogen bonds described in the previous sections. It seems, therefore, more reasonable to attribute the frequency shifts simply to electrostatic interactions, and not to postulate any overlap of the hydrogen orbital by lone pair electrons. The absence of any secondary weak band in these spectra shows that there is only one stable molecular configuration. Some confirmation of this interpretation is provided by the very low values (3550 and 3559 cm^{-1}) found for *o*-chlorophenol and *o*-cyanophenol. It is known that —CN groups do not readily form hydrogen bonds.

An interesting situation arises with the molecules in Table 6, most of which contain the R—O—CH_2—CH_2—OH unit. Frequently we find a sharp strong peak near 3600 cm^{-1} and a weak but definite shoulder near 3630 cm^{-1}. The high value is close to that of simple alcohols and indicates a small proportion of a

Table 8. Hydroxyl bands in some cyanhydrins and oximes

Compound	Structure	Molality	Wave number (cm^{-1})	Peak density ($\log_{10} I_0/I$)	$\Delta\nu_{\frac{1}{2}}$ (cm^{-1})	$A \times 10^7$
*Cyclo*hexanone cyanhydrin	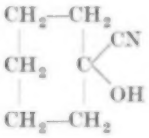	0·00304	3594	0·641	21	2·58
Acetaldehyde cyanhydrin	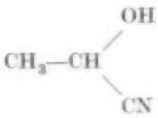	0·00301	3604	0·608	29	3·45
Acetophenone oxime	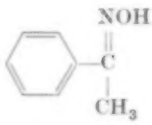	0·00151	3605	0·782	24	7·22
α-Benzaldoxime	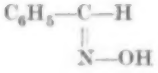	0·00104	3596	0·557	22	6·80
α-Benzil monoxime	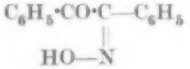	0·00182	3571	0·908	26	7·58
n-Heptaldehyde oxime	$C_6H_{13}CH{=}NOH$	0·000987	3603	0·470	25	6·91
Acetoxime	$(CH_3)_2{\cdot}C{=}NOH$	0·00110	3605	0·478	25	6·34

rotational isomer where the oxygen atom is sufficiently removed from the hydroxyl group to have little effect on its frequency. 3600 cm^{-1} could be due to internal bonding

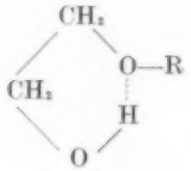

VOL. 10 1957/5

Table 9. Summary of data obtained

Class of compound	Wave number range	$A \times 10^7$ (carbon tetrachloride)	Remarks
Primary alcohols	3630–3636	2·47–2·74	
Secondary alcohols	ca. 3620	ca. 2·0	
Tertiary alcohols	ca. 3615	—	
Alkyl-aryl alcohols	3610–3620	—	
Phenols*	3605–3615	6·6–7·6	much sharper band than in alcohols
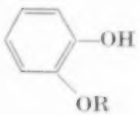	3540–3570	6·4–8·7	sharp bands
Compounds with v. strong internal hydrogen bands	3400–2400	—	very broad bands
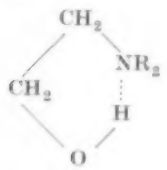	3470–3520	4·5–7·4	v. broad
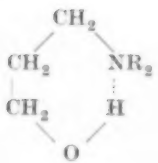	3280–3320	20–25	v. broad
X is 1 or 2 saturated carbon atoms	3450–3600	3·5–6·1	fairly broad bands compared with alcohols
Cyanhydrins	3593–3605	2·5–3·5	sharp bands
Oximes	3595–3605	6·3–7·2	sharp bands

* Nitrophenols fall outside this range.

but for various reasons this is unlikely. The band is sharper and probably no stronger than that in simple alcohols, though the presence of the shoulder makes the intensity estimate uncertain. This contra-indicates hydrogen bonding. Also similar doubling has been reported by Fox and Martin [27] for benzyl alcohol whose hydroxyl band is double with the main peak at 3618 cm^{-1} and a shoulder at about 3630 cm^{-1}. In this case there is no chance of the conventional kind of hydrogen bonding so, as the authors conclude, one can only say that there are 2 molecular configurations in which the hydroxyl group vibrates in slightly different force fields. A similar effect has been reported [28] in the case of certain substituted vinyl alcohols which show a band at 3525 cm^{-1} which can only be due to a hydroxyl group in an unusual force field. Even in simple primary alcohols in the gas phase Badger and Bauer [29] report splitting due to this cause. We, therefore, conclude that the band positions shown in Table 6 are due to rotational isomerism. In the case of 2-methoxy ethanol Lüttke and Mecke reached a similar conclusion from studies of the third harmonic [25].

Somewhat similar effects are shown by halogenated compounds. Table 7 gives a few examples, and others have been described in the literature [30, 25]. Two or more sharp bands are often found, and the question arises whether they correspond to rotational isomers where the halogens have different electrostatic effects on the hydroxyl group, or whether hydrogen bonded rings such as —CH—Cl are formed.

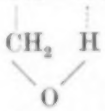

The compound 3-chloropropan-1-ol makes the latter unlikely. Although the conditions seem ideal for a 6-membered ring, a single peak is observed close to that for simple alcohols, suggesting that in other cases the frequency shifts are electrostatic in origin.

Table 8 gives data on a few cyanhydrins and oximes. An internal hydrogen bond in the former would involve a 4-membered ring and is most unlikely. The data support this, the relatively low wave number being no doubt due to the electrostatic influence of the nitrile group. Both wave number and intensity are fairly constant in the oxime case, except for the rather low wave number of α-benzil monoxime. The values of about 3600 cm^{-1} and 7×10^{-7} for A seem typical of a hydroxyl group attached to a nitrogen atom. The structure of the molecule beyond the nitrogen atom has little effect. Rather surprisingly α-benzil monoxime does not seem to form an internal hydrogen bond, though the steric conditions appear quite suitable.

Finally, in Table 9 data on the various kinds of compound studied are summarized.

Acknowledgements—I am grateful to Mr. D. A. Crooks for helpful discussions and to Mr. G. F. Scrimshaw for experimental assistance.

References

[1] Bellamy J. L. *The Infra-red Spectra of Complex Molecules*. Methuen, 1954.
[2] Smith F. A. and Creitz E. C. *J. Res. Nat. Bur. Stand.* 1951 **46** 145.

VOL. 10 1957/5

[3] Freidel R. A. *J. Amer. Chem. Soc.* 1951 **73** 2881.
[4] Fox J. J. and Martin A. E. *Proc. Roy. Soc.* A1937 **162** 419.
[5] Fox J. J. and Martin A. E. *Proc. Roy. Soc.* A1940 **174** 234.
[6] Ramsey D. A. *J. Amer. Chem. Soc.* 1952 **74** 72.
[7] Thompson H. W. *Institute of Petroleum Conference on Molecular Spectroscopy October*, 1954.
[8] Richards R. E. *Trans. Faraday Soc.* 1948 **44** 40.
[9] Barrow G. M. *J. Phys. Chem.* 1955 **59** 1129.
[10] Ingraham L. I., Corse J., Bailey G. F., and Stitt F. *J. Amer. Chem. Soc.* 1952 **74** 2297.
[11] Flett M. St. C. *Trans. Faraday Soc.* 1948 **44** 767.
[12] Cannon G. G. *Mikrochemie* 1955 555.
[13] Flett M. St. C. *J. Soc. Dy. Col.* 1952 **68** 59.
[14] Lester G. R. Private Communication.
[15] Fyfe W. S. *J. Chem. Phys.* 1953 **21** 2.
[16] Liddel U. and Wulf O. R. *J. Amer. Chem. Soc.* 1933 **55** 3574.
[17] Liddel U. and Wulf O. R. *J. Amer. Chem. Soc.* 1935 **57** 1464.
[18] Hilbert G. E., Wulf O. R., Hendricks S. B., and Liddel U. *J. Amer. Chem. Soc.* 1936 **58** 548 and 1991.
[19] Wulf O. R., Liddel U., and Hendricks S. B. *J. Amer. Chem. Soc.* 1936 **58** 2287.
[20] Pauling L. *The Nature of the Chemical Bond*. Oxford University Press, 1940.
[21] Martin A. E. *Nature, Lond.* 1950 **166** 474.
[22] Rasmussen R. S., Tunnicliffe D. D., and Brittain R. R. *J. Amer. Chem. Soc.* 1949 **71** 1068.
[23] Hoyer H. *Chem. Ber.* 1956 **89** (1) 146.
[24] Bergemann E. D., Gil-Av. E., and Pinchas S. *J. Amer. Chem. Soc.* 1953 **75** 68.
[25] Luttke W. and Mecke R. *Z. Phys. Chem.* 1950 **196** 56.
[26] Kuhn L. P. *J. Amer. Chem. Soc.* 1952 **74** 2492.
[27] Fox J. J. and Martin A. E. *Trans. Faraday Soc.* 1940 **56** 897.
[28] Buswell A. M., Rodebush W. H., and Whitney R. McL. *J. Amer. Chem. Soc.* 1947 **69** 770.
[29] Badger R. M. and Bauer S. H. *J. Chem. Phys.* 1936 **4** 711.
[30] Haszeldine R. N. *J. Chem. Soc.* 1953 1757.

Spectrochimica Acta, 1957, Vol. 10, pp. 38 to 51. Pergamon Press Ltd., London

Infra-red absorption bands associated with the NH group—III*

Hydroxamic acids and derivatives

D. Hadži and D. Prevoršek
University Chemical Laboratory, Ljubljana, Yugoslavia

(*Received* 21 *May* 1957)

Abstract—The hydroxamic acids R·C = O·(NH·OH) have been investigated, in which R is H; CH_3; CH_2Cl; $CH_3(CH_2)_{10}$; $CH_3(CH_2)_{14}$ and C_6H_5, respectively. Included in this work are some O- and N-derivatives of hydroxamic acids, and of methyl benzimidate. The spectra of the hydroxamic compounds are interpreted by analogy with the amide spectra, but with deuterated acids an important difference with respect to the amide spectra has been noted: a band in the region 1360–1430 cm^{-1} analogous to the amide III band, believed to be due mainly to the C—N stretching, does not move after deuteration. The hydrogen bonding of hydroxamic acids has been studied in the solid state and in solution, particularly with laurinohydroxamic acid. Monomeric molecules are intramolecularly bridged to 5-membered rings, which seem to be replaced by intermolecular bonds under conditions more favourable for association. The structure of hydroxamic acids and those derivatives which are capable of tautomeric changes is discussed.

Hydroxamic acids may be formulated as

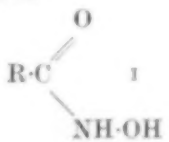

I

or

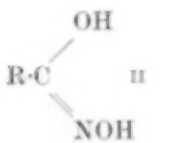

II

Form I, which was shown by Mathis [1] to be the more probable one, is structurally related to the secondary amides. It was therefore expected that the study of the spectra of the hydroxamic acids would contribute to a better understanding of the spectra of the latter. To avoid any ambiguity as to the structure of the former, the present study includes for reference the spectra of some compounds with fixed structure, such as methyl benzimidate and its derivatives, themselves not without interest. It was hoped that the interpretation of the changes on deuterating the hydroxamic acids could be made easier by including the spectra of some of their derivatives in which one of the exchangeable hydrogen atoms was replaced by alkyl or acyl groups. Most of the spectra presented are of solid substances. The very low solubility in appropriate solvents of most of these substances permitted the recording only in limited spectral regions. The study of the association via hydrogen bonds could be done also in a qualitative manner only.

*Part II. *J. Chem. Soc.* 1957 843.

In the following the spectra of the compounds having certain structures will be presented first and followed by the O-derivatives of the hydroxamic acids, the acids proper concluding the series.

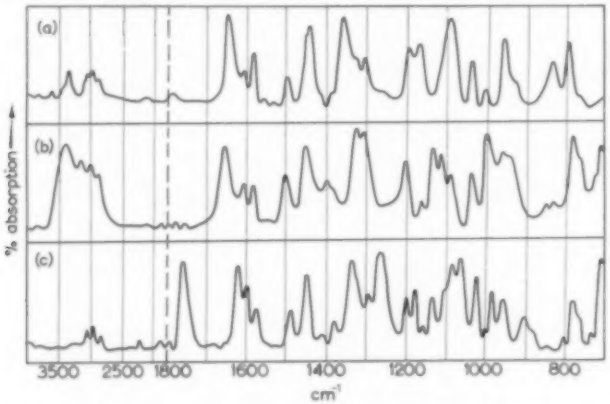

Fig. 1. Infra-red spectra of methyl benzimidate (a, pure liquid), N-hydroxymethylbenzimidate (b, solid), and of N-benzoyloxymethylbenzimidate (c, solid).

Compounds containing the C=N *bond.* The stretching of the C=N bond appears in absorption [2] near 1650 cm^{-1}. We find a strong band at 1639 cm^{-1} in the spectrum of methyl benzimidate,

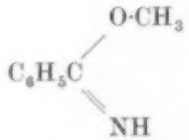

at 1630 cm^{-1} in its N-hydroxy derivative, and at 1620 cm^{-1} with its N-benzoyloxy derivative (Fig. 1). It is important to note that these bands show but very little change in position if the compound is dissolved. Another interesting feature of these three spectra appears between 1320 and 1340 cm^{-1} in the form of a strong band. Similarly strong bands at about 1300 cm^{-1} may be found [3] in the spectra of two related compounds, methyl phenaceturimidate and methyl N-phenylbenzimidate. These bands do not appear to be related with the C=N link itself, because nothing like them can be found in the spectra of the oximes or other compounds containing this group. The band near 1300 cm^{-1} in the spectra of imidates may be tentatively assigned to a stretching of the C—O link, which has acquired some double-bond character from the adjacent C=N group. This assignment is in analogy with the carboxylic acids [4] in which the C—O stretching vibration absorbs also near 1300 cm^{-1}. All three compounds have also strong bands near 1100 cm^{-1} which are to be associated with a skeletal mode, involving the νC_{aliph}—O vibration. The N—O stretching band cannot be picked out with any certainty. It is probably between 900 and 1000 cm^{-1}, but several strong bands appear here in the spectrum of methyl N-hydroxybenzimidate and its benzoyl derivative. Not without interest are the νNH and νOH bands. The νNH band of the methyl benzimidate appears at 3311 cm^{-1} (pure liquid) or at 3356 cm^{-1}

(diluted solution) in carbon tetrachloride. The νOH band of the pure methyl N-hydroxybenzimidate is at 3322 cm^{-1} (broad and very strong) and at 3623 cm^{-1} in a diluted solution in carbon tetrachloride.

N-phenylhydroxamic acids. Two such acids were prepared along with their deuterated analogs. They derive from laurino- and from benzo-hydroxamic acid respectively. An additional complication has been experienced with N-phenyl benzohydroxamic acid because of its two crystalline modifications which have rather different spectra. This point will be discussed later in the paragraph. Characteristic common features of the spectra of the two N-phenylhydroxamic acids are the strong νOH bands near 3000 cm^{-1}, the very strong νC=O band near 1630 cm^{-1}, and a strong band near 1380 cm^{-1}. The low frequency of the carbonyl band indicates both conjugation and hydrogen bonding. The frequency of the free carbonyl could not be observed, since even in diluted solutions hydrogen bonding persists, evidently of the intramolecular type. This is confirmed also by the frequency of the νOH band in N-phenylbenzohydroxamic acid, which is at 3240 cm^{-1} in dilute solution in carbon tetrachloride. Particularly interesting is the band near 1380 cm^{-1}, since it originates probably in a C—N stretching vibration. There should be actually two νC—N bands due to coupled stretchings of the two C—N links, but the other band may be weaker and therefore not observable. The frequency 1380 cm^{-1} is considerably higher than that found with aromatic amines [5], so it may be concluded that it is strongly influenced by the conjugated carbonyl group and approaches the range where the analogous vibrations of (deuterated) primary and secondary amides [6] absorb. The comparison of the spectrum of N-phenyllaurinohydroxamic acid with its deuterated analog shows the apparent shift of a band from 1440 cm^{-1} to 1049 cm^{-1}. This pair of bands may be assigned to the OH and OD in-plane deformation vibration. There is no band with comparable intensity to be assigned to this vibration in the spectra of both modifications of the N-phenylbenzohydroxamic acid. However, possible candidates are a shoulder near 1430 cm^{-1} and a medium, broad band near 1230 cm^{-1}, both being sensitive to deuteration.

The differences between the spectra of the two modifications of N-phenylbenzohydroxamic acid are unusually strong (Fig. 2). A particularly interesting characteristic of one of them, which will be called modification *a* (m.p. 121°) is the doubling of the νC=O and νOH bands; the respective peaks are at 1646, 1637, 2875 and 3100 cm^{-1}. The corresponding single maxima of the form *b* (m.p.123°) are at 1630 and 3190 cm^{-1}. The spectra of carbon tetrachloride solutions of each modification are identical, the νC=O band being at 1636 cm^{-1} and the νOH band 3242 cm^{-1}. No higher frequency band appears in more diluted and even in heated solutions, suggesting a hydrogen bonding of the intramolecular type:

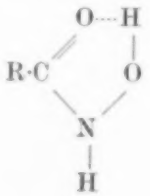

VOL. 10 1957/5

The positions of the assumed νCN bands are also different for each modification. In the spectrum of *a*, this band is at 1390 cm^{-1}, whereas it is at 1376 cm^{-1} with the modification *b*, and at 1360 cm^{-1} in solution. Marked differences in the position and even in the number if bands are observed also in the low frequency part of

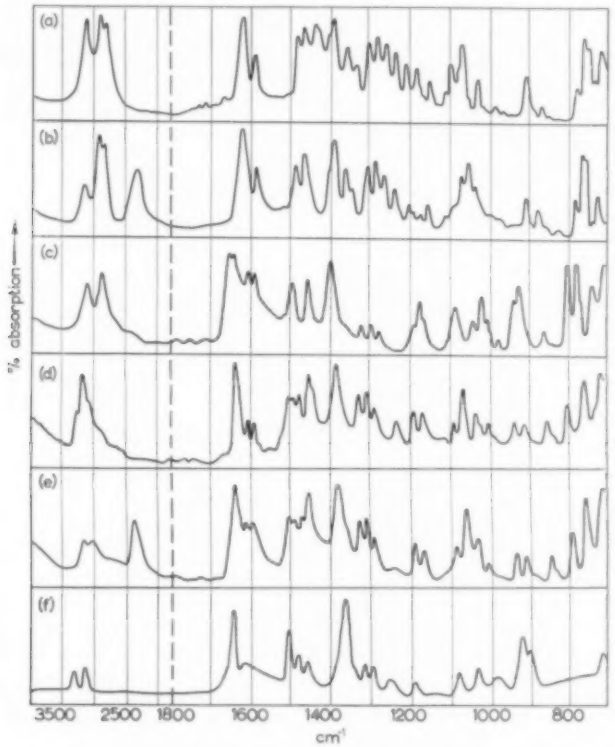

Fig. 2. Infra-red spectra of N-phenyl laurinohydroxamic acid (a, simple; b, deuterated), and N-phenyl benzohydroxamic acid (c, form a; d, form b; e, form b deuterated (all solid); f, solution in carbon tetrachloride).

the spectrum. It may be assumed that the two modifications are due actually to two molecular forms, geometrical isomerism being possible in view of the partial double bond character of the C—N link [7]. One isomer would be *cis* with respect to the carbonyl group, favouring intramolecular bonding and being thus the stabler one in solution. The form *a* may be a mixture of both *cis* and *trans* isomers which would explain the appearance of two each νC=O and νOH bands. However, this is not the only possible explanation for this doubling; another which will be discussed later in connection with similar doubling observed in the spectra of the hydroxamic acids themselves, may be advanced here too.

The acyl and alkyl hydroxamates. In this type of compounds prototropy is possible, hence the question of the true structure should be solved first. The similarity of the spectral features of benzoylbenzohydroxamate, acetylaceto-

hydroxamate, and methyl benzohydroxamate and of the secondary amides, which is reflected in the presence, and behaviour on deuteration of the amide [6] bands I and II, suggests strongly that structure I is the correct one. Thus the

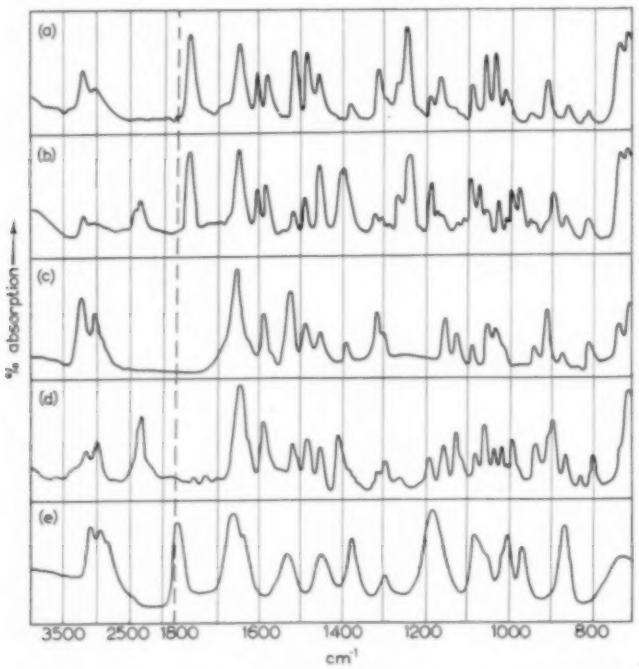

Fig. 3. Infra-red spectra of benzoylbenzohydroxamate (a, simple; b, deuterated), methylbenzohydroxamate (c, simple; d, deuterated), and of acetylacetohydroxamate (e, all solid).

amide I band in these compounds is near 1640 cm^{-1} and shifts to near 1700 cm^{-1} in solution (Fig. 3). It is easily discernible from the ester-carbonyl band of the acylhydroxamates, which is near 1760 cm^{-1}. The amide II band is near 1550 cm^{-1}, and is sensitive to deuteration. As a result of the latter, the band near 1310 cm^{-1} also disappears from the spectra of the benzohydroxamates. Thus it is analogous to the amide III band [6]. New bands appear near 1400 cm^{-1} and at 1180 cm^{-1}, which may be assigned to the C—N stretching and the ND bending vibrations, in analogy with the secondary amide spectra. Besides these groups of bands, a strong feature between 850 and 900 cm^{-1} should be noted, which shifts slightly to lower frequencies on deuteration. It may be attributed to the N—O stretching vibration, in agreement with analogous assignments in the spectra of oximes [8, 9]. Although this band should appear also in the spectra of the N-substituted hydroxamic acids, it could not be clearly assigned, since no particularly strong bands have been observed in this region.

The solid compounds have their νNH bands between 3180 and 3200 cm^{-1}. In diluted solution in carbon tetrachloride, this band is found at 3330 cm^{-1} with benzoylbenzohydroxamate. This is rather a low frequency for a free NH group,

VOL. 10 1957/5

and it is probable that there exists a hydrogen bond of the intramolecular type:

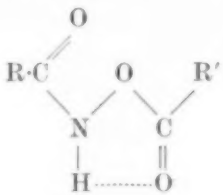

The spectrum of ethyl benzohydroxamate in carbon tetrachloride solution shows two bands in the 3μ region, at 3410 and 3470 cm^{-1}, whereas in chloroform solution only one band is observed (3413 cm^{-1}). Also, in the 6 μ region of the

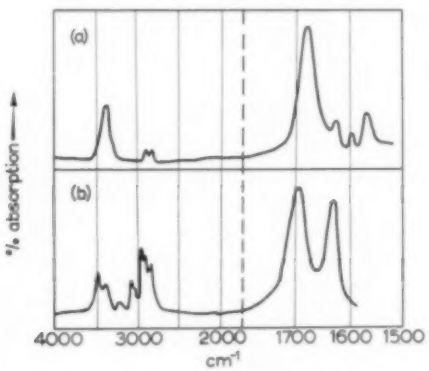

Fig. 4. Infra-red spectra of methylbenzohydroxamate in solution (a, in chloroform; b, in carbon tetrachloride. 2 mm cell, concentration about 4·5 p.p.m.).

spectrum in the latter solvent one carbonyl band only appears (1690 cm^{-1}), whereas the spectrum of the solution in carbon tetrachloride shows two bands, at 1705 and 1633 cm^{-1} (Fig. 4). These facts may be explained by assuming the presence of two tautomeric forms in the latter solution, one of them being the imido-form. Thus the band at 1633 cm^{-1} would represent the C=N stretching vibration with a lower frequency than the (bonded) carbonyl group. Similarly, the band at 3470 cm^{-1} whose frequency appears to be too high for a NH stretching vibration is assigned to the stretching of the intramolecularly bonded OH group.

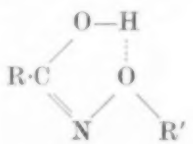

The assumption that the imido form is present in larger amounts in the carbon tetrachloride solution, is in agreement with the well-known fact [10] that solvents of low polarity favour the enolic form, particularly if this is connected with the intramolecular hydrogen bonding.

Hydroxamic acids. Characteristic features (Fig. 5) of the spectra of solid hydroxamic acids appear between 2800 and 3300 cm^{-1} (three strong bands, one of which may be obscured by the strong CH bands in the long-chain compounds), a band near 1640 cm^{-1} (a doublet in most of the spectra investigated), a medium

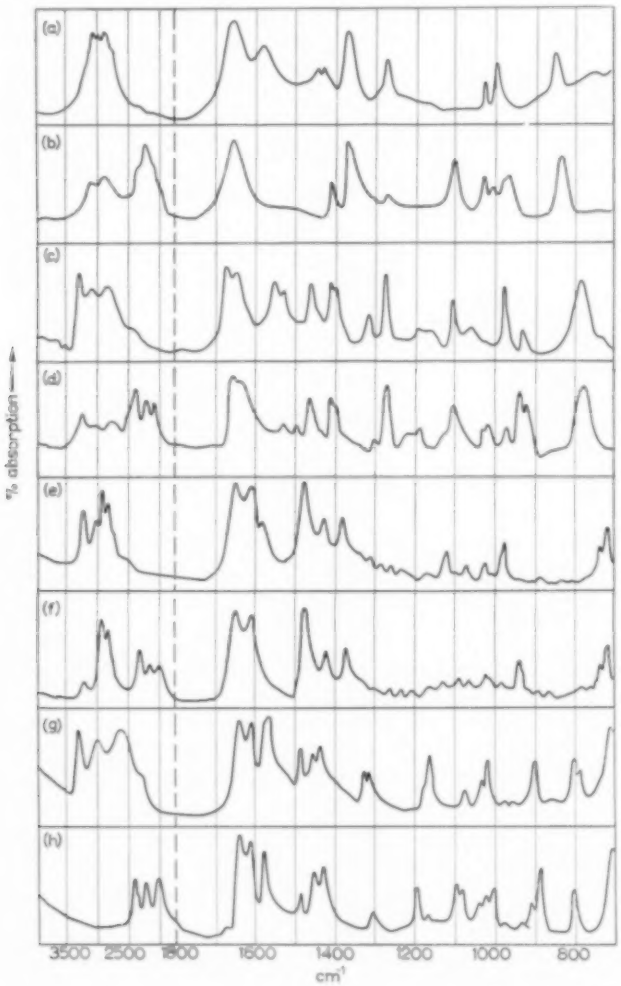

Fig. 5. Infra-red spectra of formohydroxamic acid (a, simple; b, deuterated), chloroacetohydroxamic acid (c, simple; d, deuterated), laurinohydroxamic acid (e, simple; f, deuterated), and of benzohydroxamic acid (g, simple; h, deuterated; all solid).

band near 1550 cm^{-1}, a band of variable intensity between 1360 and 1440 cm^{-1}, and finally a strong band near 900 cm^{-1}. The shifts in solution could be observed only with the bands in the high-frequency region, and with the band near 1640 cm^{-1} because the other regions were obscured by the solvent. The lower molecular weight acids were practically insoluble.

VOL. 10 1957/5

The assignment of the bands due to the vibrations of the hydroxamic acid group will be done on the example of the lowest member of the series, the formohydroxamic acid. The monomeric molecule has 7 atoms, hence it can execute 15 normal vibrations, all of which should be active in infra-red absorption. Most of these vibrations will appear in the rock-salt region. In particular, the OH and NH stretching vibrations are represented by the strong maxima near 2900 cm^{-1}, which cover probably also the weaker νCH band. Since formohydroxamic acid is insoluble in suitable solvents, this interesting region will be discussed later on hand of the absorption of laurinohydroxamic acid. The strong and broad band near 1650 cm^{-1} is assigned as an amide I band. This is by analogy with the higher members of the series, in which the shift of this band in solution could be observed. It is characteristic of the C=O bands as compared with the C=N bands. The band at 1536 cm^{-1} is removed by deuteration and may be thus related to the amide II band. One of the most prominent bands in the spectrum is that at 1362 cm^{-1}. Its position is very similar to the δCH band of formic acid [11], but is much stronger than the latter and makes this assignment improbable. Alternatively, the band at 1362 cm^{-1} could be considered as an analogue of the amide III band but, in contrast to the behaviour of this band in secondary amides, it does not move on deuteration. However, this is not the only unexpected feature of the deuterated formohydroxamic acid spectrum. Although the band at 1536 cm^{-1} disappears on deuteration, no new band appears between 1400 and 1500 cm^{-1} as would be expected in analogy with secondary amides and also with benzohydroxamates. The only change in this region is the shift of a weak band from 1420 to 1405 cm^{-1}. Although something of this order of magnitude would be expected for a C—N stretching vibration on the ground of mass increase of the substituent, it would not contradict the assignment of the pair of bands to the C—H bending vibration, not independent of the NH or OH vibrations. The band at 1258 cm^{-1} is removed by deuteration, and may be thus attributed to the OH in-plane bending. There are two new bands to appear with deuteration, i.e. at 985 and 1095 cm^{-1} respectively. By analogy with the amide spectra, the latter might be assigned to the ND deformation [12]. The band at 1563 cm^{-1} is not simply its light analogue, for the frequency ratio is 1·43 which is more than the theoretically predicted one. The other new band at 985 cm^{-1} is probably due to the δOD vibration. The weak and sharp band at 1010 cm^{-1} may be assigned to the CH out-of-plane vibration, its frequency being similar as found with formic acid [11]. The band at 965 cm^{-1}, which shifts on deuteration to 955 cm^{-1}, is best assigned to the N—O stretching. Its position is in a satisfactory agreement with those found for similar bands in oximes [8, 9], and so is the shift on deuteration. The frequency of the band at 837 cm^{-1} suggests that it might be due to the out-of-plane vibration of either OH or NH groups, or to a skeletal deformation. The small shift on deuteration eliminates the first possibility, hence the band is believed to be due to the OCN angle deformation. The corresponding band in secondary amides [13] has a lower frequency, but the difference is not too great. The very broad and ill-defined absorption extending from about 800 to 680 cm^{-1} with an indication of two maxima disappears on deuteration, hence it is suitable for assignment to OH and NH out-of-plane vibrations.

At this stage, it might be interesting to compare (Table 1) the characteristic bands of the various hydroxamic acids between them, the bands in the high frequency region being discussed later. The carbonyl bands of the solid acids are double, except for formohydroxamic and acetohydroxamic acids. It is possible that even in these two cases the bands are double, but owing to the broadness of

Table 1. Some infra-red absorption bands of hydroxamic acids and derivatives

Compound/state	νOH solid	νOD solid	νOH soln.	νNH solid	νND solid	νNH soln.	amide I solid	amide I soln.	amide II solid	amide III solid
Formohydroxamic ac.	2985 2874	2252 2150	n.i.†	3100	2380	n.i.†	1650	n.i.†	1563	1362
Acetohydroxamic ac.	3080 2800	n.i.†	n.i.†	3250	n.i.†	n.i.†	1665	n.i.†	1570	1380
Chloroacetohydroxamic ac.	3050 2850	2257 2113	n.i.†	3280	2418	n.i.†	1669 1637	n.i.†	1550	1460 (?)
Laurinohydroxamic ac.	3050 28??	2210 2050	3215 3160 3317	3250	2380	3430	1653 1612	1660	1560	1427
Palmitohydroxamic ac.	3050 28??	2210 2050		3250	n.i.†	n.i.†	1655 1605	n.i.†	1560	1425
Stearohydroxamic ac.	3050 28??	2210 2050	n.i.†	3250		n.i.†	1654 1613	n.i.†	1560	1429
Benzohydroxamic ac.	3058 2762	2250 2080	3300 (hot sol.)	3320	2370	3420	1640 1610	1660	1555	1439
O-acetylacetohydroxamate	—	—	—	3175	n.i.†	n.i.†	1658	n.i.†	1527	1295 (?)
O-benzoylbenzohydroxamate	—	—	—	1386	2326	3330	1641	1706	1515	1309
O-methylbenzohydroxamate	—	—	(3484)	3200	2350	3413	1645	1704	1523	1312
N-phenyllaurinohydroxamic ac.	3125		3242	—	—	—	1628	n.i.†	—	1385
N-phenylbenzohydroxamic ac. (form *a*)	3096 2857	n.i.†	3240	—	—	—	1646 1637	1636	—	1397
(form *b*)	3190	2380	3240	—	—	—	1630	1636	—	1376

† n.i. = not investigated.

the components they remain unresolved. The doublet structure seems to be connected with the crystalline state, the carbonyl bands being single in solution, even in such concentrations where the molecules are strongly associated. It may be mentioned here that the νOH bands in the spectra of the solid hydroxamic acids are also double. The frequency of the (associated) carbonyl bands is of the same order as found with the amides [6]. The difference of the frequencies of the carbonyl bands of solid hydroxamic acids and of those in solution is of the order of 10–30 cm^{-1}. However, the νC=O frequencies of the acids in solution, although higher, do not correspond yet to the free carbonyl frequencies, which should be over 1700 cm^{-1}, as observed with methyl benzohydroxamate. This is due to intramolecular hydrogen bonding which persists also in solution, as demonstrated also by the low frequency of the νOH vibration.

The amide II band is of medium intensity or rather weak in the spectra of the long-chain aliphatic acids. Unfortunately, its frequency in solution could not be observed due to the strong absorption of the solvents in thick layers, which

VOL. 10 1957/5

could not be avoided. The disappearance of this band after deuteration was clearly observed in all cases, even with benzohydroxamic acid where it coincides nearly with the aromatic band near 1500 cm^{-1}.

The amide III band is of particular interest. Rather strong in acetohydroxamic and formohydroxamic acids, it appears much weaker with the longer-chain acids and also with the benzohydroxamic acid. It is also of higher frequency in the latter (near 1430 cm^{-1}). The comparison with the spectra of several related compound (aldehydes, alcohols and similar) have revealed no band with a similar frequency. In the analogous carboxylic acids, there is a strong band near 1420 cm^{-1} but this is due to the δOH vibration of the dimers [4]. However, the primary amides (stearic and palmitic) have a band of similar intensity at 1420 cm^{-1}, and in benzamide a stronger band is at 1400 cm^{-1}. This supports the above assignment, although there seems to be a significant difference in the behaviour on deuteration. The amide III bands of hydroxamic acids keep their position practically unchanged, whereas the mentioned band of benzamide shifts slightly to higher frequencies on deuteration [14]. The position of the amide III band in the spectrum of chloroacetohydroxamic acid is not quite clear. The band at 1406 cm^{-1} appears with about the same intensity in the spectrum of the chloroacetic acid too, whereas the band at 1464 cm^{-1} does not occur in the latter. However, 1464 cm^{-1} seems to be rather high a frequency for the νC—N band in relation to other hydroxamic acids.

Bands due to the δOH vibration are not easy to pick out in all spectra of hydroxamic acids. With benzohydroxamic acid, suitable candidates are the bands of medium intensity at 1312 and 1325 cm^{-1} (doublet), which disappear on deuteration. A medium band at 1303 cm^{-1} in the spectrum of chloracetohydroxamic acid is strongly reduced on deuteration and so is a weak band in this region in the spectrum of laurinohydroxamic acid (1311 cm^{-1}), and a medium intensity one with benzohydroxamic acid. These bands are best associated with the OH in-plane deformation vibration. The frequencies are in good agreement with those observed by Palm and Verbin in the spectra of oximes [8], and also with our own observation [14]. We have found bands at 1302 and 1312 cm^{-1} to disappear on deuteration from the spectra of acetophenonoxime and benzaldoxime, respectively. The corresponding δOD bands appeared near 1070 cm^{-1}. However, this region undergoes rather complicated changes on deuteration in the case of hydroxamic acids because of the δND band appearing there. The vibrations of the OH and OD groups seem to couple with other vibrations of similar frequencies, causing thus a number of shifts, which are too difficult to be interpreted in details.

The N—O stretching band is rather easily observable in all spectra investigated. It appears rather regularly near 890 cm^{-1} and shifts slightly to lower frequencies on deuteration.

The vOH *and* vNH *bands and the hydrogen bonding in hydroxamic acids.* This paragraph is based mainly on the results obtained with laurinohydroxamic acid, the lower acids being unsuitable for a study of the spectra of solutions. The cold saturated solution of laurinohydroxamic acid in carbon tetrachloride (20 mm cell), has a broad band at 3215 cm^{-1} with a weak shoulder at the high frequency slope

and a sharp bend at 3436 cm^{-1} besides the very strong νCH bands at 2850 and 2920 cm^{-1}. The sharp band at 3436 cm^{-1} does not show any change of relative intensity or position on diluting further or heating the solutions (Fig. 6). Its sharpness and position suggest the assignment to the stretching of the free NH

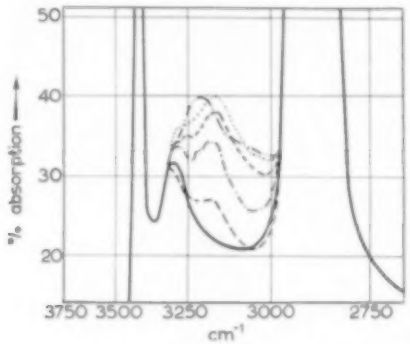

Fig. 6. The νOH bands of laurinohydroxamic acid in carbon tetrachloride solution at various temperatures.

— — — —
— · — ·—
· · · · · · · ·
· · · · · · · ·
— · — · · —
20 mm cell, concentration 0·4 p.p.m., Temperature intervals from 75° to room temperature

50 mm cell, concentration 0·16 p.p.m., 75°C.

group. The other band (3215 cm^{-1}) is reduced in hot carbon tetrachloride (75°) and is superceded by a higher-frequency band at 3317 cm^{-1} of considerable breadth. Since no new band above 3450 cm^{-1} attributable to free OH groups appears under these conditions, it is concluded that monomeric molecules of laurinohydroxamic acid form intramolecular hydrogen bonds:

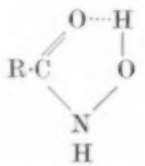

The NH group is excluded from similar bonding on steric reasons, and its stretching frequency corresponds to a free group.

If a hot solution of laurinohydroxamic acid is allowed to cool off slowly, and the absorption recorded at various temperatures (Fig. 6), a gradual increase of the intensity of the band at 3175 cm^{-1} is observed. On further cooling, the maximum shifts gradually back to 3215 cm^{-1}. This may be best explained by assuming that the intramolecular bond in monomeric molecules is replaced by stronger intermolecular bonds in associated molecules. The changes of the position of the peak of the broad association band suggest that various types of associates are simultaneously present in solution, their relative concentrations being dependent on temperature. The molecules associate probably to chains or to rings with different numbers of inks, each type being characterized by a different νOH

VOL. 10 1957/5

frequency or frequencies. No quantitative study of this interesting association behaviour could be made because of two main difficulties: the various types of OH bands were overlapping hence their intensities not obtainable with sufficient accuracy, and the solubility of the compound was low so that the intensities were too low for reliable measuring.

The solid hydroxamic acids show three bands (Table 1) in the spectral region of the hydrogen stretching region if free of interference with CH bands. The highest frequency one is much sharper and may be assigned to the NH stretching vibration. The other two bands are considerably broader and must be due to bonded OH groups. One of them is obscured by the CH bands in the long-chain aliphatic hydroxamic acids, but may be clearly observed with the deuterated acids. Both OH bands are at lower frequencies with respect to solution.

The already mentioned doubling of the νC=O and that of the νOH bands in the solid and the differences in frequencies with respect to solution demonstrate that the type of association in the solid state is different from that in solution. In the former, even the νNH band has a lower frequency; apparently this group undergoes some type of hydrogen bonding too. It should be noted that double νOH bands have been observed previously, amongst other, also with oximes [9, 15]. This observation remained, however, without a satisfactory explanation. Since the doubling of the νC=O and the νOH bands in the spectra of hydroxamic acids and their N-phenyl derivatives appears only in the solid state, the most plausible explanation would be the one involving vibrational coupling between the molecules in a unit cell, probably through the strong hydrogen bonds. A better understanding of this interesting phenomenon could be reached after more experimental work has been done.

Discussion. Although the primary interest in this work was in the spectroscopic results, the question of the true structure of hydroxamic acids should be briefly discussed. One of the most striking differences between structures I and II is, on the formal side, the presence of C=O and C=N links, respectively. However, the difference in frequencies between the C=N stretching vibration in benzoimidates and the C=O stretching vibration of the N-phenylhydroxamic acids, is not large and would be insufficient for the differentiation between both types of structures. More significant is the shift of the νC=O band on dissolving the N-phenylhydroxamic acids. As it is observed also with the band near 1650 cm^{-1} of the hydroxamic acids, and as the νC=N bands do not shift under these circumstances, this may serve as a proof for the assignment to the carbonyl group and hence of structure I. A strong piece of evidence in favour of structure I may be found also in the presence of the νNH band, but this can be brought out beyond doubt only in solution. Structure II with a C—O link would require the presence of a strong band in the range between 1050 cm^{-1} (alcohols [16]) and 1300 cm^{-1} (carboxylic acids [4]) which would shift more or less on deuteration. No such band is found in the spectra of hydroxamic acids. On the other hand, structure II cannot provide a simple explanation for the band near 1550 cm^{-1}, no case of OH deformation with such a high frequency being known. Other arguments, such as the fact that O-derivatives of hydroxamic acids in the solid state are in the amide-form and also that simple amides as well as lectams appear predominantly in this form, are of an indirect nature.

Johns and Werner have observed [17] the chloracethydroxamic acid to appear in two modifications having m.p. 89° and 109°, respectively, and have supposed them to be the two tautomeric forms. However, the spectra of the two forms which we have prepared were practically identical, although their melting points were as given by Johns and Werner [17].

The pair of bands near 1550 cm^{-1} and between 1350 and 1430 cm^{-1}, respectively seems to merit a particular attention in connection with the problem of the spectra of secondary amides. By analogy with the latter, it might be expected that both bands would disappear from the spectra of deuterated hydroxamic acids to yield a new band between 1400 cm^{-1} and 1500 cm^{-1} and another near 1000 or 1200 cm^{-1}. This has been indeed observed with the acyl and alkyl hydroxamates, but not with the acids themselves. Here the band near 1550 cm^{-1} disappears on deuteration whereas the other band, assigned to the C—N stretching vibration, stays firm. This is an exception amongst the compounds with a CNH group, the C—N vibration being usually coupled to the NH (or ND) bending vibration. As a result of this, both corresponding bands shift after the isotopic substitution of the light atom. The frequency range of the νC—N bands in hydroxamic acids is rather wide, its high frequency end extending considerably towards the region of double bonds, but compares well with the frequencies of analogous bands found with other compounds [5].

According to the preceding paragraph, the band near 1550 cm^{-1} in the spectra of hydroxamic acids has not much connection with the C—N stretching. It seems rather straightforward to assign it to the NH bending, although the ratio of frequencies of this band and the one replacing it in the spectrum of the deuterated compounds is larger then theoretically predicted. This may be due to some interference of the ND and OD bending vibrations. That the role of the latter is not negligible is clearly shown by the different behaviour of the amide III band on deuteration in the spectra of the hydroxamic acids and the hydroxamates, respectively.

Experimental part. The compounds were prepared accordingly to standard procedures, and purified until they showed the required melting points. Deuteration has been performed either by recrystallization from heavy water, or by adding the latter to the solution of the substance in dry dioxane. All solvents were carefully dried. For solutions in hot carbon tetrachloride thick-walled brass cells were used, with windows of sapphire. Boiling solutions were poured into preheated cells. As these had a rather large thermal capacity, the solution cooled off but very little during the time of the recording of the small spectral interval between 2·5 and 3·5 μ. For records at lower temperatures, the solution was allowed to cool off in the cell. The formation of crystals in the oversaturated solutions took place usually shortly after cooling. The spectra of solids were recorded with the compounds mulled in Nujol and hexachlorobutadiene, respectively. The instrument used was a Perkin-Elmer Mod. 21, equipped with NaCl and LiF prism, respectively.

Acknowledgements—The spectroscopic work has been executed at the Institute Boris Kidrič, Academy. The authors are grateful to its Director, Prof. M. Samec,

VOL. 10 1957/5

for the kind permission to use the facilities. Thanks are due also to Prof. PERPAR for her interest in this work and for her advice in the preparation of the compounds.

References

[1] MATHIS M. F. *C. R. Acad. Sci., Paris* 1951 **232** 505.
[2] FABIAN J., LEGRAND M., and POIRIER P. *Bull. Soc. Chim. Fr.* 1956 1499.
[3] RANDALL H. M., FOWLER R. G., FUSON N., and DANGL J. R. *Infra-red Determination of Organic Structures* pp. 181–2. New York, 1949.
[4] HADŽI D. and SHEPPARD N. *Proc. Roy. Soc.* A1953 **216** 247.
[5] HADŽI D. and ŠKRBLJAK M. *J. Chem. Soc.* 1957 843.
[6] BELLAMY L. J. *The Infra-red Spectra of Complex Molecules.* Methuen, London, 1954.
[7] RUSSELL R. A. and THOMPSON H. W. *Spectrochim. Acta* 1956 **8** 138.
[8] PALM A. and WERBIN H. *Canad. J. Chem.* 1954 **32** 854.
[9] HADŽI D. *J. Chem. Soc.* 1956 2725.
[10] WHELAND G. W. *Advanced Organic Chemistry* p. 607. John Wiley, New York, 1951.
[11] ORVILLE-THOMAS W. J. *Disc. Faraday Soc.* 1950 **9** 339.
[12] FRAZER R. D. B. and PRICE W. C. *Nature, Lond.* 1952 **170** 490.
[13] MIYAZAWA T., SHIMANOUCHI T., and MIZUSHIMA S.-I. *J. Chem. Phys.* 1956 **24** 408.
[14] Unpublished work from this laboratory.
[15] CALIFANO S. and LÜTTKE W. *Z. Phys. Chem.* 1955 **5** 240.
[16] COLTHUP N. B. *J. Opt. Soc. Amer.* 1950 **40** 397.
[17] JOHNS L. W. and WERNER L. F. *J. Amer. Chem. Soc.* 1917 **39** 413.

OL.
10
7/58

Spectrochimica Acta, 1957, Vol. 10, pp. 52 to 56. Pergamon Press Ltd., London

The molecular structure of niobium pentachloride

J. Gaunt and J. B. Ainscough
United Kingdom Atomic Energy Authority, Atomic Energy Research Establishment, Harwell Didcot, Berks; and Research and Development Branch, United Kingdom Atomic Energy Authority, Industrial Group, Springfields Works, Salwick, Preston, Lancs

(*Received* 6 *June* 1957)

Abstract—The infra-red and Raman spectra of niobium pentachloride have been measured. An interpretation of the spectra has been made in a manner consistent with the rigid selection rules for the trigonal bipyramid structure (D_{3h}) and the thermodynamic properties have been calculated on the simple harmonic oscillator approximation.

An unsuccessful attempt has also been made to examine the infra-red and Raman spectra of niobium trichloride and tetrachloride.

Introduction

Investigations of the vibrational spectrum of niobium pentachloride have been reported in two papers [1, 2] on the Raman spectra of various compounds of the type MX_5. An incomplete spectrum of niobium pentachloride was obtained, from a study of both the solid and its solution in carbon disulphide, from which an interpretation of the structure was not possible. Skinner and Sutton have, however, carried out an electron diffraction study of niobium pentachloride [3] and concluded that the most probable structure for the molecule was the trigonal bipyramid in which all the bonds were of equal length.

In an attempt to obtain more complete spectral data, the Raman spectrum of niobium pentachloride has been re-examined. The infra-red spectrum has also been investigated and an attempt has been made to interpret the results.

Experimental

Preparation of niobium pentachloride. The pentachloride was prepared by chlorination of the metal and purified by vacuum sublimation at 90–100°C. Debye-Scherrer photographs failed to show any trichloride or tetrachloride present as impurity.

Raman apparatus. The technique used for studying the Raman spectra of the solid was similar to that described by Brandmüller [4]. As the apparatus has not been described previously it is convenient to give a brief description here. Raman lines scattered from a solid are usually of very low intensity and consequently long exposures become necessary, so that if the lines are to be distinguishable from the background the continuum produced by the source must be reduced. To achieve this a Toronto type arc was used and the light from it passed through a filter to isolate the exciting line, before falling on the sample. Since the 5461 Å line of mercury was used, this filter consisted of a 1 cm layer of a mixture of cupric chloride and calcium chloride solutions followed by a similar layer of neodymium nitrate solution [5]. The sample was orientated so that the major reflections from it were

VOL.
10
1957/5

directed back along the path of the incident beam, only that radiation scattered at 45° to the incident beam being collected. Under these conditions the much weaker beam which follows the optical path is made up of light of both the incident and the Raman frequencies. This beam was collimated on to an interference filter set at 45° to the normal and adjusted to transmit as large a fraction of the light of the incident frequency as possible, whilst reflecting the Raman frequencies. The reflected beam was then focused by means of a cylindrical lens, on to the slit of the spectrograph.

Three spectrographs, fitted with glass optics, were used. Most of the measure-

Table 1. Raman spectra of niobium and tantalum pentachlorides

Niobium pentachloride			Tantalum pentachloride	
This work	Moureu, Magat, and Süe		Moureu, Magat, and Süe	
Solid (cm^{-1})	Solid (cm^{-1})	Solution in CS_2 (cm^{-1})	Solid (cm^{-1})	Liquid (cm^{-1})
106 *w.*			90	
153 *v.w.* (diffuse)	170		170	180
355 *m.*	353		370	365
396 *v.w.*	400	400	410	420
412 *s.*	425		460	
497 *v.w.* (diffuse)		500	490	

ments were made on a Hilger F/4 instrument but in order to search for lines closer to the exciting line than about 200 cm^{-1} some measurements were made on a Hilger medium and a Hilger large Littrow spectrograph. Exposure times ranged from about 3 hr with the F/4 to 190 hr with the Littrow. Spectra were calibrated by superimposing an iron arc on the Raman lines. The plates were examined under a travelling microscope.

Apart from the inherent complications of Raman spectroscopy of the solid state, there are other difficulties peculiar to niobium pentachloride. The first of these is the great ease with which it is hydrolysed in moist air and this necessitated care in the mounting of the sample, which was loaded in a dry box into a glass tube fitted with a plane-glass window. The sample was melted under nitrogen to form a thin layer on the inside of this window and then allowed to cool and the tube sealed off. The other difficulty is that the pentachloride, which is yellow, absorbs in the region of the 4358 Å mercury line. However, the absorption is much less in the green region of the spectrum [1, 2] and the 5461 Å mercury line was used throughout the present work. The Raman lines obtained are recorded in Table 1, together with those obtained by Moureu, Magat, and Süe for this compound and for tantalum pentachloride [2].

Infra-red apparatus. The infra-red spectrum was observed on a Hilger H 800 double beam, recording prism spectrophotometer over the range 5000–310 cm^{-1}

using rock-salt, potassium bromide, and caesium bromide prisms. At the lower end of the caesium bromide region an additively coloured caesium bromide filter of the type described by BURNS and GAUNT [6] was used to cut down the effect of stray light. The pentachloride was examined as a solution in carbon disulphide with a

Table 2. Symmetries and activities of the fundamental vibrations of a D_{3h} molecule of the type MX_5

Assignment	Symmetry	Degeneracy	Activity
ν_1	A_1'	1	R
ν_2	A_1''	1	R
ν_3	A_2''	1	IR
ν_4	A_2''	1	IR
ν_5	E'	2	R and IR
ν_6	E'	2	R and IR
ν_7	E'	2	R and IR
ν_8	E''	2	R

compensating cell of solvent placed in the second beam of the spectrophotometer. Solutions were made up as required in a dry box under nitrogen. Nujol mulls were also examined but without success. The observed absorption bands are recorded, together with their assignments, in Table 4.

Discussion

The three most likely structures for the $NbCl_5$ molecule are the plane pentagon, point group D_{5h}, the square pyramid, C_{4v}, and the trigonal bipyramid, D_{3h}. The observation of more than three Raman lines excludes the first of these structures but the present evidence, from the Raman spectrum alone, is insufficient to decide between the square pyramid and the trigonal bipyramid. There is however other evidence for the structure of niobium pentachloride. Electron diffraction work [3] has shown the trigonal bipyramid to be a more probable structure than the square pyramid and at least one other MX_5 molecule, phosphorus pentachloride, has been shown to be a trigonal bipyramid. The selection rules for a trigonal bipyramid allow eight vibrational modes [7]; six of these are Raman active and five infra-red active. The symmetries and activities of the vibrational modes are shown above [8] (Table 2).

The observation of six Raman lines (Table 1) is consistent with the selection rules for a trigonal bipyramid. The strong sharp line at 412 cm^{-1} can probably be assigned as ν_1, the symmetrical stretching frequency; and the next strongest, at 355 cm^{-1}, is probably ν_2. No infra-red lines which might be considered as fundamentals have been observed. An attempt has been made to assign the Raman frequencies as fundamentals and to interpret the observed infra-red absorption bands in terms of overtone and combination bands in a manner consistent with the rigid selection rules for molecules of D_{3h} symmetry.

VOL. 10 1957/5

In order to make a complete assignment of the observed bands it has been necessary to postulate an infra-red fundamental at 315 cm^{-1}. This was not observed but it is at the limit of detection of the infra-red spectrophotometer in its present form and, after modifications to the instrument, a re-investigation of this part of the spectrum and an extension of the investigation to 250 cm^{-1} will be made. Some

Table 3. Assignment of fundamental frequencies in $NbCl_5$

Assignment	Frequency (cm^{-1})	Assignment	Frequency (cm^{-1})
ν_1	412 observed	ν_5	497 observed
ν_2	355 observed	ν_6	396 observed
ν_3	315 derived	ν_7	153 observed
ν_4	260 derived	ν_8	106 observed

Table 4. Intepretation of the infra-red spectrum of $NbCl_5$

Observed frequency (cm^{-1})	Calculated frequency (cm^{-1})	Assignment
897 *m.*	893	$\nu_5 + \nu_6$
846 *m.*	852	$\nu_2 + \nu_5$
729 *w.*	727	$\nu_1 + \nu_3$
672 *w.*	672	$\nu_1 + \nu_4$
616 *w.*	615	$\nu_2 + \nu_4$
421 *m.*	421	$\nu_3 + \nu_8$
415, 412 *m.*	412	$2\nu_7 + \nu_8$

Table 5. Calculated thermodynamic properties of $NbCl_5$ gas

T(°K)	S° (cal/deg. mole)	C_p (cal/deg. mole)	$-(G - E_0)/T$ (cal/deg. mole)
100	66·05	16·21	54·83
150	73·53	20·74	59·85
200	79·95	23·99	64·09
250	85·56	26·15	67·83
273·1	87·90	26·88	69·54
298·1	90·29	27·53	71·09
350	94·79	28·55	74·27
400	98·74	29·23	77·18
500	105·27	30·09	82·08

assistance to this interpretation has also been given by a parallel interpretation of the infra-red and Raman spectra of antimony pentafluoride, details of which are reported in the following paper [9]. The success achieved in this present interpretation provides strong supporting evidence for the assumption of the trigonal bipyramidal structure for this molecule. The results are recorded in Tables 3 and 4.

It is also of interest that an additional infra-red absorption was observed at 770 cm^{-1}. This band, the intensity of which was found to increase with time, appears to be due to some decomposition product of niobium pentachloride.

On the basis of a D_{3h} symmetry and using the fundamental frequencies given in Table 3 and taking the Nb–Cl distance as 2·29 Å [3] the thermodynamic properties of niobium pentachloride have been calculated on the simple harmonic oscillator approximation and are shown in Table 5.

Acknowledgements—The authors wish to thank Mr. A. M. DEANE for his assistance throughout this work and also Dr. R. W. M. D'EYE and Mr. I. F. FERGUSON who took and interpreted the Debye-Scherrer photographs of the niobium chlorides.

Appendix

During the course of this work an attempt has been made to observe the infra-red and Raman spectra of solid niobium trichloride and tetrachloride. Both these compounds are very dark in colour and absorb strongly over practically the whole spectral range. All attempts to observe the Raman spectra of these compounds, using the 4358 Å and 5461 Å mercury lines, have been unsuccessful. The infra-red spectra of the solids, as pressed discs and nujol mulls, were also examined over the same range as niobium pentachloride. No absorption bands were observed for the trichloride and only two, at 926 cm^{-1} and 742 cm^{-1}, for the tetrachloride. It was not possible to make an assignment of these bands.

VOL.
10
1957/5

References

[1] MOUREU H., MAGAT M., and WETROFF P. *Proc. Indian Acad. Sci.* A1938 **8** 356.
[2] MOUREU H., MAGAT M., and SÜE P. *Contributions à l'Étude de la Structure Moléculaire, Victor Henri Commemorative Vol.* p. 125. Desoer, Liege, 1947–1948.
[3] SKINNER H. A. and SUTTON L. E. *Trans. Faraday Soc.* 1940 **36** 668.
[4] BRANDMÜLLER J. *Z. Angew. Phys.* 1953 **5** 95.
[5] BOWEN E. J. *Chemical Aspects of Light* (Second Edition). Clarendon Press, Oxford, 1946.
[6] BURNS W. G. and GAUNT J. *Institute of Petroleum—Conference on Molecular Spectroscopy* p. 66. 1954.
[7] WILSON E. B. *J. Chem. Phys.* 1934 **2** 432.
[8] HERZBERG G. *Infra-red and Raman Spectra of Polyatomic Molecules.* Van Nostrand, New York, 1945.
[9] GAUNT J. and AINSCOUGH J. B. *Spectrochim. Acta* 1957 **10** 57–60.

Spectrochimica Acta, 1957, Vol. 10, pp. 57 to 60. Pergamon Press Ltd., London

The molecular structure of antimony pentafluoride

J. Gaunt and J. B. Ainscough
United Kingdom Atomic Energy Authority, Atomic Energy Research Establishment
Harwell, Didcot, Berks, and Research and Development Branch
United Kingdom Atomic Energy Authority, Industrial Group
Springfields Works, Salwick, Preston, Lancs.

(*Received* 6 *June* 1957)

Abstract—The infra-red and Raman spectra of antimony pentafluoride have been investigated. Five Raman lines were observed and have been assigned as fundamentals. An interpretation of the infra-red spectrum has been made in a manner consistent with the rigid selection rules for the trigonal bipyramid structure (D_{3h}).

The thermodynamic properties have been calculated on the simple harmonic oscillator approximation.

Introduction

In the previous paper [1] the results of an examination of the infra-red and Raman spectra of niobium pentachloride have been reported. During the course of that work it was decided that, to provide a comparison and in order to facilitate interpretation of the niobium pentachloride spectra, the infra-red and Raman spectra of antimony pentafluoride should be investigated. This, to the best of our knowledge, had not previously been examined and it seemed probable that niobium pentachloride and antimony pentafluoride might have the same structure.

Experimental

The antimony pentafluoride was supplied by Dr. P. L. Robinson of King's College, Newcastle. It was a colourless, viscous liquid which fumed violently in moist air, and so was handled in an all-glass vacuum system. Since antimony pentafluoride attacks hydrocarbon tap grease, all taps and joints which were likely to come into contact with the vapour were lubricated with a fluorocarbon grease. The vapour pressure of the pentafluoride is quite low, about 4 mm at 20°C [2], but was sufficient to give a satisfactory infra-red sprectrum in a 35 cm gas cell. The vapour attacked the windows of this cell forming a greenish-yellow deposit on them.

The infra-red spectrum of the vapour was observed on a Hilger H 800 recording, double beam, prism spectrophotometer over the range 5000–310 cm^{-1}, using the same prisms and filter as in the work on niobium pentachloride. The absorption cell was of glass with windows of both potassium bromide and caesium bromide attached by fluorocarbon grease. The infra-red spectrum of liquid antimony pentafluoride was also observed using a 0·1 mm cell fitted with caesium bromide windows.

The apparatus used to excite the Raman spectrum was fairly conventional and has been described elsewhere [3]. The liquid sample was contained in a tube surrounded by three concentric vessels containing cooling water, a 0·5 cm layer

of saturated sodium nitrite solution, and a 0·5 cm layer of saturated rhodamine G solution to isolate the 4358 Å mercury line which was used for excitation. The spectra were photograhed on two spectrographs, a Hilger F/4 and a Hilger medium, using glass optics; exposure times ranged from a few hours to a week. Spectra were calibrated by superimposing an iron arc on the Raman lines. The plates were examined under a travelling microscope and on a recording microphotometer.

Discussion

So far as we are aware no work has previously been carried out to elucidate the molecular structure of antimony pentafluoride. However, like niobium pentachloride, the molecule is probably either a plane pentagon, a square pyramid, or a trigonal bipyramid. The observation of five Raman lines immediately excludes the first of these but is not sufficient evidence to distinguish between the square pyramid and the trigonal bipyramid as the former has seven and the latter six Raman active frequencies [4]. The more probable structure seems to be a trigonal bipyramid and an attempt has been made to interpret the spectra on this assumption. The strong, sharp line observed in the Raman spectrum at 667 cm^{-1} can probably be assigned as ν_1, the symmetrical stretching frequency; and the infra-red absorption at 710 cm^{-1}, which is also observed in the Raman spectrum at 716 cm^{-1}, can probably be assigned as ν_3. An attempt has been made to assign the other observed Raman frequencies as fundamentals and then to interpret the observed infra-red absorption bands in a way consistent with the rigid selection rules for a molecule of D_{3h} symmetry.

In order to make a complete assignment of the fundamental bands, a Raman line at 498 cm^{-1}, which was not in fact observed, has been postulated, though an adsorption band at 491 cm^{-1} was observed in the infra-red spectrum. The assignment also requires an infra-red fundamental at 294 cm^{-1}. No definite peak could be observed here as this is outside the present instrumental range but the spectrophotometer trace shows that a very strong absorption occurs below 315 cm^{-1} and this is strong evidence for a fundamental absorption band in this region. Weak absorption bands at 1195, 1130 and 1076 cm^{-1} were also observed but as these were found in the spectrum of an empty cell after the antimony pentafluoride had been pumped out, they were attributed to absorption by the deposit formed on the cell windows. An absorption at 1030 cm^{-1} was attributed to silicon tetrafluoride.

Some supporting evidence for the assumption of the D_{3h} structure, in the case of the niobium compound, has been cited previously [1] and as there are quite marked similarities in the order of the assignments of the fundamental frequencies of the two molecules we feel that this provides strong evidence for assuming that antimony pentafluoride molecule is also a trigonal bipyramid. The fundamental frequencies with their respective symmetries, degeneracies and activities are given in Table 1, while the interpretation of the infra-red spectrum is given in Table 2.

In order to calculate the thermodynamic properties of antimony pentafluoride it has been necessary to estimate the Sb—F bond length. The As—F distance in arsenic trifluoride is 1·71 Å while the As—Cl and Sb—Cl distances in the trichlorides are 2·16 Å and 2·37 Å respectively. Assuming that the difference between

VOL. 10 1957/5

the bond lengths in the two fluorides is the same as in the chlorides a Sb—F bond length of 1·92 Å is obtained for antimony trifluoride. There is probably some increase in bond length in going from the trifluoride to the pentafluoride as there

Table 1. Fundamental vibrations of antimony pentafluoride

Assignment	Symmetry	Degeneracy	Activity	Frequency (cm^{-1}) calculated	Frequency (cm^{-1})
ν_1	A_1'	1	R	667	667 *s.*
ν_2	A_1'	1	R	264	264 *m.* (diffuse)
ν_3	A_2''	1	IR	294	Not observed
ν_4	A_2''	1	IR	212	Not observed
ν_5	E′	2	R and IR	713	710 (IR) *s.* 716 (R) *s.* (diffuse)
ν_6	E′	2	R and IR	498	491 (IR only)*m.*
ν_7	E′	2	R and IR	107	ca. 90(R only)*v.w.*
ν_8	E″	2	R	228	228 *m.* (diffuse)

Table 2. Interpretation of the infra-red sprectum of antimony pentafluoride

Observed frequency (cm^{-1})	Calculated frequency (cm^{-1})	Assignment
1419 *m.**	1426	$2\nu_5$
1140 *w.*†	1139	$2\nu_4 + \nu_5$
760 *s.*	762	$\nu_2 + \nu_6$
727 *s.*	726	$\nu_6 + \nu_8$
710 *s.*	713	ν_5
684 *s.*	684	$3\nu_8$
517 *s.*	522	$\nu_3 + \nu_8$
491 *m.*	498	ν_6
478 *w.*	476	$\nu_2 + \nu_4$
439 *w.*	440	$\nu_4 + \nu_8$
335 *s.*	335	$\nu_7 + \nu_8$
326 *s.*	321	$3\nu_7$
ca 300 *s.*	294	ν_3

* Observed only in the spectrum of the liquid.
† Observed in both the liquid and vapour spectra.

is, for example, in the phosphorus fluorides where the P—F distance is 1·52 Å in the trifluoride and 1·57 Å in the pentafluoride and so 2·00 Å has been taken as the Sb—F distance in antimony pentafluoride. The sum of the covalent radii is 2·05 Å. An error of 0·01 Å in the bond length leads to a error of about 0·03 cal/deg.mole in the values of S^0 and of $-(G - E_0)/T$. On the basis of this bond length and using the fundamental frequencies given in Table 1, the thermodynamic properties have been calculated on the simple harmonic oscillator approximation and are given in Table 3.

Table 3. Calculated thermodynamic properties of antimony pentafluoride gas

T(°K)	S^0 (cal/deg. mole)	C_p (cal/deg. mole)	$-(G-E_0)/T$ (cal/deg. mole)
100	63·03	15·36	52·25
150	69·01	19·14	56·04
200	74·92	21·98	60·04
250	80·07	24·15	63·54
273·1	82·24	24·96	65·03
298·1	84·46	25·71	66·57
350	88·69	26·97	69·54
400	92·25	27·88	72·17
500	98·74	29·10	76·89

Acknowledgements—The authors wish to thank Dr. P. L. ROBINSON for the preparation of the sample of antimony pentafluoride and Mr. A. M. DEANE for his assistance throughout this work.

References

[1] GAUNT J. and AINSCOUGH J. B. *Spectrochim. Acta* 1957 **50** 52—56.
[2] SCHAIR R. C. and SCHURIG W. F. *Industr. Engng. Chem.* 1951 **43** 1624.
[3] GAUNT J. *Trans. Faraday Soc.* 1954 **50** 209.
[4] WILSON E. B. *J. Chem. Phys.* 1934 **2** 432.

VOL.
10
1957/5

Spectrochimica Acta, 1957, Vol. 10, pp. 61 to 69. Pergamon Press Ltd., London

Organische Moleküle in der Glimmentladung—III

Spektroskopische Untersuchungen über das Verhalten von Benzol, Toluol, Chlorbenzol, Diphenyl und Benzylchlorid [1]

H. Schüler und E. Lutz
Forschungsstelle für Spektroskopie
in der Max-Planck-Gesellschaft, Hechingen, Germany

(*Received June 10 1957*)

Abstract—A review is made of the spectra which have been found in the glow discharge with the following substances: (a) benzene, (b) toluene, (c) diphenyl, (d) benzyl chloride, (e) chlorobenzene. When the discharge tube is heated to 200–300°C a spectrum is noticed, designated as "*W*-spectrum," for which the carrier may be C_6H_4 (dehydro benzene). Taking into account other observations on dibenzyl and diphenyl methane, a process is suggested which is designated as "molecular splitting." As an extension to the assumption previously made that an atom or a radical is split off from the main molecule, the possibility is suggested that atoms, or an atom and radical lying close together, may be split off together, and indeed in such a way that the energy of union of this pair to form a molecule is taken into account in the whole energy process.

In einer früheren Arbeit haben die Verfasser [2] gezeigt, wie weit die Versuchsanordnung zur Untersuchung organischer Moleküle in der Glimmentladung bisher ausgebaut wurde. Mit diesen Hilfsmitteln sind weitere Beobachtungen an Benzol, Toluol, Chlorbenzol und Benzylchlorid gemacht worden. In Abb. 1 sind die meisten Spektren, die bisher in der Emission einer Glimmentladung bei den untersuchten Substanzen gefunden wurden, in einer Übersicht zusammengestellt.

1. Benzol (C_6H_6)

Beim Benzol sind bisher folgende Spektren beobachtet worden:

1.1. Im "Endstadium" [2] der Entladung wurde der bekannte Übergang $^1B_{2u} \rightarrow {}^1A_{1g}$ im Bereich etwa 2540–3300 Å (Abb. des Spektrums, siehe [3] Abb. 10 und 12) gefunden.

1.2. Das "*U*-Spektrum" [4]. Abb. des Spektrums, siehe [4] Abb. 3. Es handelt sich um zwei diffuse Gruppen im Bereich 4750–4900 Å und 5000–5400 Å. Das Spektrum tritt in dem Zwischenstadium [2] auf, wo noch schwach die Atomlinien des Trägergases (He) zu sehen sind. Das gleiche Spektrum erscheint auch beim Diphenyl. Der Träger dieses Spektrums ist noch unbekannt.

1.3. Das "*T*-Spektrum." Abb. des Spektrums, siehe [1a] Abb. 1. In einem Stadium noch höherer Anregung [2] als beim "*U*-Spektrum," erkennbar an dem starken Auftreten der Trägergaslinien (He), erscheint das "*T*-Spektrum" [4] im Bereich 4673–6500 Å, dessen Träger zunächst als Diacetylen [5] und in einer neueren Arbeit [6] als Diacetylen $^+$ identifiziert wurde.

1.4. Das "*V*-Spektrum" [7]. Add des Spektrums, siehe [8] Abb. 7. Es erscheint im Bereich 4456–etwa 5900 Å. Das Spektrum tritt im gleichen Entladungsstadium wie das "*U*-Spektrum" auf und hat beim Benzol nur eine sehr geringe Intensität,

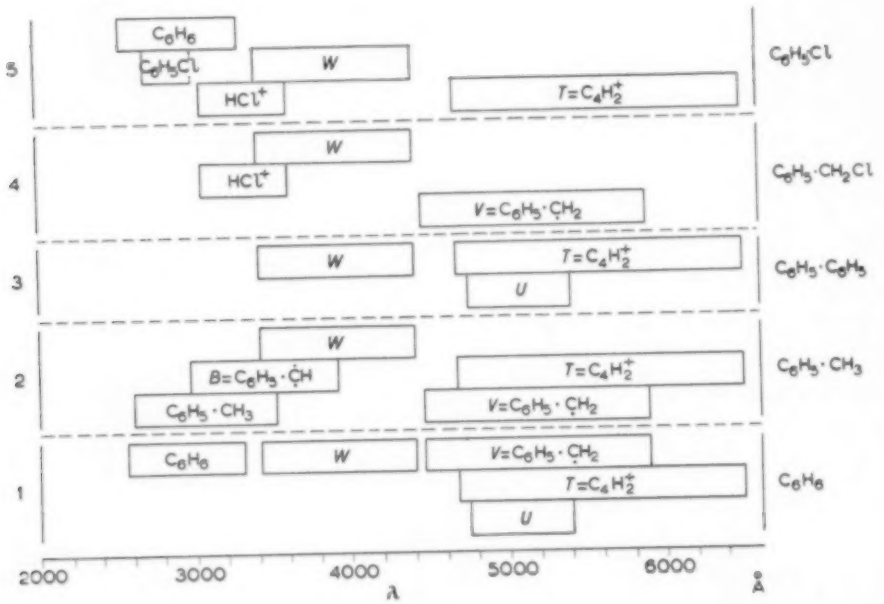

Abb.1. Übersicht der Spektren, die für die Diskussion benötigt werden. Die Spektren, der einzelnen Substanzen treten nicht alle gleichzeitig auf.

weil es sich um eine sekundäre Bildung handelt. Da der Träger als Benzylradikal ($C_6H_5CH_2$) [9] bestimmt wurde, deutet sein Auftreten zumindest auf eine Aufspaltung des Benzolringes hin.

1.5. Im "Zerstörungsstadium" [2], d.h. in einer He-Entladung mit Spuren von Benzol, beobachtet man die Spektren der kleinsten Bruchstücke wie C_2, CH, H_2 [4].

1.6. Das "*W*-Spektrum" (siehe Abb. 4a, 2a, und 2b). Bei grossen Stromstärken (60mA) wurde ein Kontinuum [4] beobachtet, das sich von etwa 3400–4400 Å erstreckt. Das Verhalten dieses Spektrums ist mit den beschriebenen Hilfsmitteln [2] näher untersucht worden.

Da größere Stromstärken sowohl eine höhere Stromdichte als auch höhere Temperaturen in der Entladung zur Folge haben, wurde, um diese gekoppelte Erscheinung zu trennen, zunächst bei kleineren Stromstärken (~5–10 mA) untersucht. Dabei war das "*W*-Spektrum" nicht zu beobachten. Erst wenn man die Entladungsröhre von außen durch einen Ofen heizt, erscheint bei einer Ofentemperatur von etwa 200–300°C das "*W*-Spektrum."

In Abb. 2a ist dieses Spektrum mit Hg als Vergleichsspektrum abgebildet. Bei einer Stromstärke von 20 mA und einer zusätzlichen Temperatur des Entla-

VOL. 10 1957/5

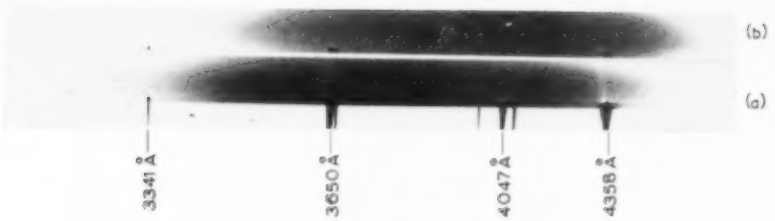

Abb. 2. Das "W-Spektrum" beim Benzol.
He-Druck: 0·9 mm Hg, Röhrenheizung: 200°C, Substanzbad: ~ −7°C, Hg als Vergleichsspektrum, aufgenommen mit dem mittleren Hilger-Quarz-Spektrographen auf Agfa Raman ortho Platten.
(a) Stromstärke: 20 mA, Gesamtdruck: steigt von 2·5 auf 3·2 mm Hg an, Belichtungszeit: 20 sec.
(b) Die Entladung wurde zunächst mit 20 mA eingebrannt. Dabei stieg der H_2-Druck dauernd an; beim Gesamtdruck zwischen 4 und 5 mm Hg sank der Strom auf 1–1·5 mA ab. Dieses Stadium wurde aufgenommen und der Versuch mehrmals wiederholt, bis die Belichtungszeit insgesamt 8 min betrug.

Abb. 3. [9] Entladung im Dibenzyldampf.
Röhrenheizung: 60°C, Stromstärke: 7·5 mA, Belichtungszeit: 15 min.

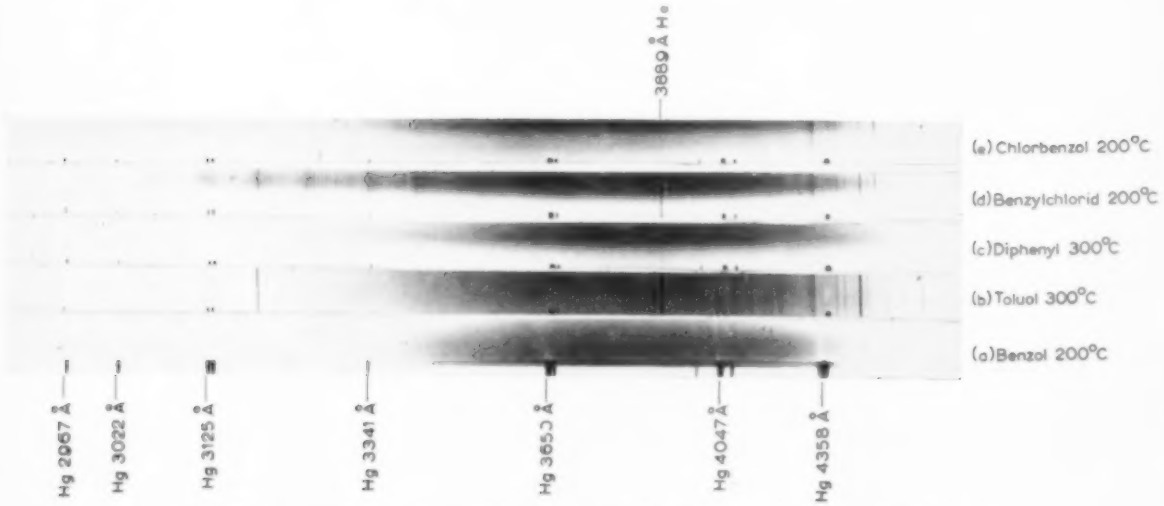

Abb. 4. Aufgenommen mit dem mittleren Hilger-Quarzspektrographen auf Agfa Raman ortho Platten.

	Stromstärke	He-Druck	Substanzbad	Röhrenheizung	Belichtungszeit
(a) Benzol	20 mA	0·9 mm Hg	~ −7°C	200°C	1/3 min
(b) Toluol	5 mA	0·45 mm Hg	−35°C	300°C	2 min
(c) Diphenyl	5 mA	0·8 mm Hg	+75°C	300°C	1 min
(d) Benzylchlorid	2 mA	0·6 mm Hg	+20°C	200°C	5 min
(e) Chlorbenzol	2 mA	0·8 mm Hg	−5°C	200°C	30 min

VOL.
10
1957/5

dungsrohres (Röhrenheizung) von 200°C erscheint das "*W*-Spektrum" isoliert, d.h. bei der Belichtungszeit von 20 sec ist von dem Benzolübergang $^1B_{2u} \rightarrow {}^1A_{1g}$ nichts zu beobachten. Bemerkenswert ist, daß bei dieser Entladung eine starke Bildung von H_2 festgestellt wird. Dies beweisen Druckzunahme [2] und das Auftreten des Viellinienspektrums des H_2 im Handspektroskop [2], beides hinter der Kühlfalle beobachtet. Läßt man diese Entladung einige Minuten brennen, ohne die angelegte Spannung zu ändern, so sinkt in Folge des steigenden H_2-Druckes die Stromstärke langsam ab. Bei etwa 5 mm Hg Gesamtdruck beträgt sie noch etwa 1–1.5 mA. Beim Durchlaufen dieses Stadiums erhielt man die Aufnahme 2b. Der Versuch musste mehrmals wiederholt werden, bis die aus Intensitätsgründen erforderliche Belichtungszeit von 8 min erreicht war.

Der Vergleich mit dem Spektrum von 2a zeigt, dass der Anfang und das Ende von 2b sich mehr nach Rot verlagern. Da es sich vermutlich bei 2a und 2b um den gleichen Träger handelt, ist diese Differenzierung als Folge der Änderung des Druckes und der Stromstärke anzusehen.

2. Toluol ($C_6H_5CH_3$)

In der Glimmentladung mit Toluol findet man folgende Spektren:

2.1. Den bekannten Übergang 2600–etwa 3500 Å, der dem tiefsten Singulett-Singulett Übergang des Toluols entspricht.

2.2. Das "*V*-Spektrum" [7], Benzylradikal [2], vgl. (1.4.). Es tritt stark auf, wenn die Entladungsröhre nicht zusätzlich geheizt wird und ist in und vor dem "Endstadium" [2] zu beobachten. Aus der Abhängigkeit seiner Intensität von der Stromstärke [10] folgt, daß das angeregte Benzylradikal in einem Primärprozeß [10] entsteht.

$$\text{Toluol} + e \rightarrow \text{Benzylradikal}^* + \text{H} + e$$

2.3. Das "*T*-Spektrum" (Diacetylen $^+$), vgl. (1.3.). Es erscheint in einem "Zwischenstadium" [2] (höhere Anregung).

2.4. Das "*B*-Spektrum" (Benzalradikal [9, 11], $C_6H_5\dot{C}H$). Es beginnt bei 2960 Å und erstreckt sich bis 3900 Å, siehe Abb. 3. Zuerst wurde es bei Diphenylmethan und Dibenzyl beobachtet. (Seine Beobachtung beim Stilben hat sich bei extrem reinen Präparaten nicht bestätigt.) Beim Toluol tritt es erst auf, wenn das Entladungsrohr auf 200°C geheizt wird. Hinter den Kühlfallen ist H_2 spektroskopisch zu beobachten.

2.5. Das "Zerstörungsstadium," vgl. (1.5.).

2.6. Das "W_b-Spektrum," vgl. (1.6.), siehe Abb. 4b. Es erscheint erst bei Aufheizung der Röhre auf 300°C. Das Auftreten der stärksten Linien des Trägergases He deutet darauf hin, daß die Aufnahme in dem "Vorendstadium" gemacht wurde. Wie beim "*W*-Spektrum" des Benzols konnte auch hier die Entstehung von H_2 spektroskopisch hinter der Kühlfalle nachgewiesen werden. Eine Druckzunahme wie beim Benzol war nicht zu beobachten. Die größere Ausdehnung des Spektrums nach Violett in Abb. 4b deutet auf das gleichzeitige Auftreten des Benzalradikals hin, denn bei längerer Belichtung setzt sich die Schwärzung bis zur Grenze des Benzalspektrums bei 2960 Å fort.

3. Diphenyl (C_6H_5·C_6H_5)

Beim Diphenyl konnten folgende Spektren beobachtet werden:

3.1. Das "*U*-Spektrum," vgl. (1.2.).

3.2. Das "*T*-Spektrum" (Diacetylen +), vgl. (1.3.).

3.3. Ein Spektrum mit mindestens drei diffusen Banden. Die Maxima der Banden liegen bei etwa 3025, 3130 und 3255 Å. Über die Deutung dieses Spektrums wird an anderer Stelle berichtet.

3.4. Ein Spektrum, das mit dem mittleren Hilger-Quarz-Spektrographen aufgenommen, kontinuierlich erscheint und bei längerer Belichtungsdauer sich von etwa 3100–3800 Å erstreckt. Im allgemeinen tritt es gekoppelt mit dem Spektrum (3.3.) auf. Bei geeignetem Substanzdruck kann es bis 300°C Röhrenheizung beobachtet werden.

3.5. Das "W_c-Spektrum," siehe Abb. 4c, vgl. (1.6.). Es erscheint erst bei einer Röhrenheizung von 270°C und etwas höherer Stromstärke (5 mA und grösser).

4. Benzylchlorid ($C_6H_5CH_2Cl$)

4.1. Ein Spektrum, das der ersten Anregung des Benzylchloridmoleküls entspricht, konnte bisher nicht beobachtet werden.

4.2. Das "*V*-Spektrum" (Benzylradikal), vgl. (2.4.), tritt nur sehr schwach auf. In den Kühlfallen konnte infrarotspektrometrisch die Bildung von Dibenzyl nachgewiesen werden.

4.3. Das Spektrum des HCl^+, auf der Aufnahme 4 d, im Bereich 3600–3050 Å zu sehen, tritt stark auf. In den Kühlfallen ist HCl in grösseren Mengen nachweisbar. Das Spektrum tritt auch noch im "Endstadium" [2] auf.

4.4. Die Anwesenheit von atomarem Cl lässt sich durch die Bogenlinien 4601, 4526, 4390 und 4323 Å nachweisen.

4.5. Das Benzalradikal, vgl. (2.4.), konnte durch sein Spektrum bisher nicht nachgewiesen werden, dagegen konnte die Bildung von Stilben $C_6H_5.CH{:}CH.C_6H_5$ infrarotspektrometrisch nachgewiesen werden.

4.6. Das "W_d-Spektrum," vgl. (1.6.), siehe Abb. 4d, erscheint bei einer Röhrenheizung von 200°C und einer Stromstärke von 2 mA.

5. Chlorbenzol (C_6H_5Cl)

Beim Chlorbenzol wurden folgende Spektren festgestellt:

5.1. Die Anregung des Muttermoleküls wurde durch ein Bandenspektrum [2] nachgewiesen, das bei 2698 Å beginnt und sich als Kontinuum noch über 3000 Å hinaus erstreckt. (Siehe zitierte Arbeit 2, Abb. 4)

5.2. Atomares Cl ist ebenfalls im Endstadium der Entladung nachzuweisen, vgl. (4.4.).

5.3. Das HCl^+-Spektrum (vgl. (4.3.), siehe Abb. 4e). Bemerkenswert ist, daß bei einer Entladung im Endstadium bedeutende Mengen HCl in der Kühlfalle gefunden werden konnten. Z. B. wurden 7% HCl der verdampften Substanz in den Kühlfallen nachgewiesen bei einer Entladung, die unter folgenden Bedingungen brannte, Stromstärke: 3 mA, He-Druck: 0·4 mm Hg, keine zusätzliche Röhrenheizung, Substanzbad: — 5°C, das entspricht einem Dampfdruck von etwa 4·7 mm Hg am Ort der Verdampfung.

VOL. 10 1957/5

5.4. Das "T-Spektrum" (Diacetylen +), vgl. (1.3.), wird auch beim Chlorbenzol im Stadium höherer Anregung ("Zwischenstadium") beobachtet, ist aber im Vergleich zur Benzolentladung nur sehr schwach vorhanden.

5.5. Das unter (1.1.) aufgeführte Benzolspektrum tritt ebenfalls auf, aber hier ist seine Intensität im Vergleich zu einer Benzolentladung um den Faktor 200–300 schwächer [2].

5.6. Im "Zerstörungsstadium" ist H, H_2, C_2 und CH beobachtet worden [12].

5.7. Das "W_c-Spektrum," siehe Abb. 4e. Dieses Spektrum erscheint bereits bei Zimmertemperatur, tritt aber hier gemeinsam mit der ersten Anregung des Chlorbenzols, vgl. (5.1.), auf. Erst bei einer Röhrenheizung von 200°C erscheint es nahezu isoliert.

6. Diskussion

Bei der Bestimmung der Träger, der in den beschriebenen Versuchen beobachteten Spektren, ist folgendes zu berücksichtigen:

Die Aufenthaltsdauer eines Muttermoleküls im Entladungsraum bei der beschriebenen Strömungsanordnung [2] liegt zwischen 1/10 und 1 sec. Für die in der Entladung entstehenden Bruchstücke ist die Aufenthaltsdauer im Mittel noch kleiner, da sie an verschiedenen Stellen der positiven Säule der Glimmentladung erst gebildet werden. Weiter ist noch zu berücksichtigen, daß die Lebensdauer der Bruchstücke im allgemeinen viel kleiner ist als ihre Aufenthaltsdauer.

Wird bei zwei verschiedenen Substanzen das Spektrum des gleichen Radikals mit sehr verschiedener Intensität beobachtet und wird chemisch das Dimerisationsprodukt des Radikals etwa in der gleichen Menge nachgewiesen, so ist daraus zu schliessen, daß bei dem intensiven Radikalspektrum das Radikal bereits im angeregten Zustand entstehen muss, während im andern Fall es nicht angeregt entsteht, vgl. (2.2.) und (4.2).

Das zusätzliche Heizen des Beobachtungsraumes der Entladungsröhre bis 300°C im "End"—und "Vorendstadium" ändert das spektrale Bild. Das Leuchten der Muttermoleküle wird zurückgedrängt, aber nicht so, daß die Entladung in ein "Zwischenstadium" (Zustand höherer Anregung) übergeht, vielmehr treten neue Spektren auf, die in keinem anderen Entladungsstadium zu beobachten sind. Die zusätzliche Röhrenheizung hat bei den untersuchten Substanzen noch keine merkliche thermische Zersetzung zur Folge. Es tritt ein neuer Prozeß in Erscheinung, der den bisherigen Anregungsmechanismus des "End"- oder "Vorendstadiums" voraussetzt und meistens noch eine zusätzliche Erwärmung des Entladungsraumes benötigt.

Für diesen Prozeß möchten wir nun folgenden Vorgang zur Diskussion stellen, der am Beispiel des Benzols erläutert werden soll. Neben der einfachen Abtrennung eines einzelnen H vom Benzol, soll noch ein zweiter Vorgang existieren und zwar derart, daß in *einem* Prozeß sich H_2 abspaltet, wobei die Vereinigung von H und H der Gesamtenergie des Prozesses zuzuschlagen ist. Das würde darauf hinauslaufen, da die Abtrennungsarbeit eines H-Atoms vom Ring etwa gleich der Wiedervereinigungsenergie von zwei H-Atomen zu H_2 ist, daß für den Prozeß:

$$C_6H_6 + e \rightarrow C_6H_4 + H_2 + e \qquad (1)$$

nicht wesentlich mehr Energie aufzuwenden ist, als für den Prozeß

$$C_6H_6 + e \rightarrow C_6H_5 + H + e \qquad (2)$$

Der Prozeß (1) sei als "Molekülabspaltung" bezeichnet, im Gegensatz zu der Abtrennung eines Atoms oder eines Radikals (2).

W-Spektren. Die unter 1–5 beschriebenen "*W*-Spektren" sind in Abb. 4 zusammengestellt. Berücksichtigt man, daß die Spektren, aufgenommen mit dem mittleren Hilger-Quarz-Spektrographen, kontinuierlich erscheinen und der Nachweis der Identität von kontinuierlichen Spektren immer schwierig ist, so liegt die Annahme nahe, daß es sich bei den verschiedenen Substanzen um das gleiche Spektrum handelt. In unserem Fall kommt noch hinzu, daß bei einigen Substanzen Spektren vorhanden sind, die sich mit den "*W*-Spektren" teilweise überlagern. Außerdem hat sich beim Benzol gezeigt, daß das "*W*-Spektrum" unter verschiedenen Versuchsbedingungen, siehe Abb. 2, ein wenig variiert.

Die Originalaufnahmen lassen aber alle in der Gegend 3800–3850 Å ein flaches Maximum erkennen. Allen Spektren ist auch gemeinsam, daß sie erst auftreten, wenn eine zusätzliche Röhrenheizung von 200–300°C vorhanden ist. Nur beim Chlorbenzol findet man die ersten Anzeichen des Spektrums bereits bei Zimmertemperatur, vgl. (5.7.). Weiter ist noch zu bemerken, daß sie alle im "End"- oder "Vorendstadium" auftreten. Die starke He-Linie 3889 Å ist in Abb. 4b bis 4e noch zu sehen. Außer der Röhrenheizung ist für das Auftreten aller bisher beobachteten "*W*-Spektren" ein ziemlich hoher Substanzdruck der Untersuchungssubstanz notwendig. Ferner ist es unwahrscheinlich, daß fünf verschiedene Substanzen, die sich sonst in Bezug auf ihre Spektren sehr verschieden verhalten, alle unter ähnlichen Bedingungen an der gleichen Stelle ein Spektrum anzeigen, das jedesmal einem andern Träger zuzuordnen wäre.

Das "*W*-Spektrum" tritt zwar, wenn es mit dem mittleren Hilger-Quarz-Spektrographen aufgenommen wird, als Kontinuum auf, es ist aber nicht anzunehmen, daß es sich um ein echtes Kontinuum handelt, sondern um eine Überlagerung vieler diffuser Banden, besonders deshalb, weil das Spektrum bei höheren Temperaturen gefunden wird. Die Möglichkeit, echte Kontinua bei organischen Substanzen in der Emission einer Glimmentladung zu beobachten, ist sehr unwahrscheinlich, weil bisher nur Übergänge vom ersten angeregten zum Grundzustand gefunden wurden und der Grundzustand immer stabil sein muß.

Auf Grund der Annahme einer "Molekülabspaltung" möchten wir als Träger des "*W*-Spektrums" das C_6H_4 (Dehydrobenzol) zur Diskussion stellen und einige Beobachtungen anführen, die für diese Auffassung sprechen.

Beim *Benzol* macht sich bei Auf heizung der Röhre auf 200–300°C die "Molekülabspaltung" und damit die Bildung von C_6H_4 durch eine verstärke H_2-Bildung bemerkbar. Die Differenzierung des "*W*-Spektrums", siehe Abb. 2, könnte sich vielleicht daraus ergeben, daß die Stellen am Ring, die nicht durch ein H besetzt sind, sich nicht nur in *o*-Stellung, sondern auch in *p*- und vielleicht auch in *m*-Stellung befinden. Die in Abb. 2 wiedergegebenen "*W*-Spektren" sind ja auch unter sehr verschiedenen Bedingungen aufgenommen worden. Beim Benzol würde man eigentlich zunächst das Auftreten des Phenylradikals erwarten, und bei der ersten Beobachtung des "*W*-Spektrums" wurde auch seine Deutung als

VOL. 10 1957/5

Phenylradikal zunächst diskutiert, jedoch wäre sein Erscheinen erst bei einer Röhrenheizung von 200°C und dann mit einer solch grossen Intensität schwer verständlich. Vielmehr muß man das Erscheinen des Phenylradikals bei Zimmertemperatur im "Vorendstadium" erwarten. Dort erscheint aber nun, vgl. (1.2.), das "*U*-Spektrum." Es ist nicht ausgeschlossen, daß dieses Spektrum, das auch beim Diphenyl beobachtet wird, dem bisher spektroskopisch nicht nachgewiesenen Phenylradikal entspricht.

Das Auftreten des "*W*-Spektrums" beim *Toluol* bei einer Röhrenheizung von 300°C ist nicht mit einer verstärkten H_2-Entwicklung wie beim Benzol verbunden, was verständlich ist, weil die "Molekülabspaltung" hier CH_4 bildet.

Beim *Diphenyl* könnte die "Molekülabspaltung" zur Benzolbildung führen. Dieses wird aber bei 300°C Röhrenheizung in der Entladung wieder weiter zerlegt, wie bereits beschrieben wurde.

Das durch "Molekülabspaltung" erwartete CH_3Cl beim *Benzylchlorid* hat seine erste Anregung bei 1600 Å und sein Eigenleuchten kann deshalb mit einem Quarzspektrographen nicht nachgewiesen werden.

Mit steigender Röhrenheizung (bis 200°C) tritt das "*W*-Spektrum" beim *Chlorbenzol* immer dominierender hervor, vgl. (5.7.). Die HCl^+-Banden werden mit zunehmender Intensität des "*W*-Spektrums" ebenfalls stärker, dies würde auch nach der "Molekülabspaltung" zu erwarten sein.

Der Versuch einer Deutung des "*W*-Spektrums" als C_6H_4, z.B. beim Chlorbenzol setzt die "Molekülabspaltung" des HCl voraus. Die "Molekülabspaltung" gibt noch in anderen Fällen eine Erklärungsmöglichkeit. In Abb. 3 sind die Spektren wiedergegeben, die man bei einer Entladung mit Dibenzyldampf ($C_6H_5CH_2 \cdot CH_2C_6H_5$) bei einer Röhrenheizung von nur 60°C erhält. Man sieht, daß das Spektrum des Benzalradikals viel intensiver auftritt als das Benzylradikal. Dies läßt darauf schließen, daß das Benzalradikal nicht sekundär aus dem Benzylradikal entstanden sein kann. Die "Molekülabspaltung" macht das intensive Auftreten des Benzalradikals verständlich. Das von der "Molekülabspaltung" geforderte Auftreten von Toluol ist durch sein Spektrum in der Abb. 3 nachgewiesen.

Analoge Beobachtungen liegen beim Diphenylmethan ($C_6H_5CH_2C_6H_5$) vor. Das hier durch die "Molekülabspaltung" geforderte Auftreten des Benzalradikals und des Benzols wird durch die Beobachtung dieser beiden Spektren bestätigt.

Beim Toluol ist außer der "Molekülabspaltung" am Ring die "Molekülabspaltung" am CH_3 Substituenten zu erwarten. Tatsächlich wird nun das Benzalradikal bei 200°C Röhrenheizung beobachtet und die Bildung von H_2 hinter den Kühlfallen im Handspektroskop nachgewiesen.

Beim Benzylchlorid wurde bereits auf eine "Molekülabspaltung" am Ring hingewiesen; in Analogie zum Toluol, wäre auch eine am Substituenten CH_2Cl zu erwarten, es müsste danach HCl und das Benzalradikal entstehen. Wie Abb. 4d zeigt, tritt bei 200°C das HCl^+-Spektrum auf. Das Benzalradikal konnte zwar nicht durch sein Spektrum nachgewiesen werden, jedoch zeigte eine infrarotspektrometrische Untersuchung der an den nicht geheizten Stellen der Röhre abgelagerten Kristalle die Bildung von Stilben ($C_6H_5CH{:}CHC_6H_5$). Nach dem

früher Gesagten muß es sich um eine Bildung des Benzalradikals im nichtangeregten Zustand handeln.

Die "Molekülabspaltung" macht das Auftreten des Benzalradikalspektrums bei Dibenzyl, Diphenylmethan und Toluol verständlich. Damit ist die Möglichkeit gegeben, einige Ergebnisse der Pyrolyse mit denen der Glimmentladung zu vergleichen. Horrex und Miles haben [13] bei einer Untersuchung der Dibenzyl-Pyrolyse die Bildung von Toluol, Stilben, Benzol und Styrol nachgewiesen, dabei werden zur Erklärung der Entstehung dieser Substanzen außer H-Atomen drei Radikale gefordert:

(1) das Benzylradikal ($C_6H_5\dot{C}H_2$)

(2) das Diphenyläthylradikal ($C_6H_5\dot{C}HCH_2C_6H_5$)

(3) das Phenyläthylradikal ($C_6H_5CH_2CH_2\cdot$)

Das Benzylradikal wurde in der Glimmentladung durch sein Spektrum nachgewiesen. Wenn in der Glimmentladung der gleiche Reaktionsmechanismus wie bei der Pyrolyse vor sich gehen sollte, dann müsste das von uns als Benzalradikal bezeichnete Spektrum einem der beiden Radikale von 2 oder 3 entsprechen. Da diese Radikale in der Glimmentladung bei Diphenylmethan und Toluol nicht zu erwarten sind, trotzdem aber bei diesen beiden Substanzen das gleiche Spektrum wie bei Dibenzyl auftritt, kann es sich zumindest im Fall der Glimmentladung mit Dibenzyl nicht um einen Prozeß handeln, der über die beiden Radikale 2 und 3 führt. Die "Molekülabspaltung" würde aber die Bildung der genannten Endprodukte auch erklären. Der Einwand, daß das Emissionsspektrum von einem Radikal herrührt, das sekundär aus bereits gebildetem Dibenzyl entstanden sein könnte, ist auszuschliessen, weil das Benzalradikalspektrum bei allen drei untersuchten Substanzen etwa in der gleichen Intensität auftritt.

In wie weit die Ergebnisse der Pyrolyse mit denen der Glimmentladung wirklich verglichen werden dürfen, muß erst durch weitere Versuche geklärt werden.

Aus den vorliegenden Untersuchungen geht also hervor, daß spektroskopische Beobachtungen bei der Glimmentladung auch Hinweise für einen Ablauf des Reaktionsmechanismus liefern.

7. Zusammenfassung

Es werden alle Spektren zusammengestellt, die bisher bei folgenden Substanzen in der Glimmentladung gefunden wurden: 1. Benzol, 2. Toluol, 3. Diphenyl, 4. Benzylchlorid, 5. Chlorbenzol. Bei einer zusätzlichen Heizung des Entladungsrohres (200–300°C) wurde bei den genannten Substanzen ein Spektrum gefunden, das als "*W*-Spektrum" bezeichnet und dessen Träger als C_6H_4 (Dehydrobenzol) diskutiert wird.

Unter Hinzunahme von weiteren Beobachtungen an Dibenzyl und Diphenylmethan wird ein Prozeß zur Diskussion gestellt, der als "Molekülabspaltung" bezeichnet wird. In Ergänzung zu der bisherigen Annahme, daß immer nur ein Atom oder ein Radikal von der Muttersubstanz abgespalten wird, wird auf die Möglichkeit hingewiesen, daß nebeneinanderstehende Atome, bzw. Atom und Radikal, gemeinsam abgetrennt werden und zwar so, daß die Vereinigungsenergie dieser beiden zum Molekül dem Gesamtenergieprozeß zuzuschlagen ist.

VOL. 10 1957/5

Literatur

[1a] Schüler H. *Spectrochim. Acta* 1950 **4** 85. [b] Schüler H. und Reinebeck L. *Spectrochim. Acta* 1954 **6** 288.

[2] Schüler H. und Lutz E. *Z. Naturf.* 1957 **12a** 334.

[3] Schüler H. und Woeldike A. *Phys. Z.* 1941 **42** 390.
vgl. auch Austin J. B. und Black J. A. *Phys. Rev.* 1930 **35** (1), 452.

[4] Schüler H. und Reinebeck L. *Z. Naturf.* 1951 **6a** 160.

[5] Schüler H. und Reinebeck L. *Z. Naturf.* 1954 **9a** 350.

[6] Callomon J. H. und Ramsay D. A. *Canad. J. Phys.* 1957 **35** 129.

[7] Schüler H. Reinebeck, L. und Köberle R. *Z. Naturf.* 1952 **7a** 421.

[8] Schüler, H. Woeldike, A. und Reinebeck, L. *Z. Naturf.* 1949 **4a** 124.

[9] Schüler H. und Michel A. *Z. Naturf.* 1955 **10a** 459.

[10] Schüler H. und Stockburger M. *Z. Naturf.* 1957 **12a** 507.

[11] Schüler H. und Reinebeck L. *Gazz. Chim. Ital.* 1952 **82** 484.

[12] Schüler H. und Reinebeck L. *Naturwissenschaften* 1952 **39** 445.

[13] Horrex C. und Miles S. E. *Disc. Faraday Soc.* 1951 **10** 187.

OL.
10
7/58

Spectrochimica Acta, 1957, Vol. 10, pp. 70 to 84. Pergamon Press Ltd., London

Infra-red spectroscopic studies of hydrogen bonding in methanol, ethanol, and *t*-butanol

URNER LIDDEL and EDWIN D. BECKER
National Institute of Health
Bethesda, Maryland, U.S.A.

(*Received* 10 *June* 1957)

Abstract—The infra-red spectra of methanol, ethanol and *t*-butanol have been investigated in the 3 μ region (fundamental frequency of the OH stretching vibration). The alcohols were studied in CCl_4 solution over a concentration range 0·005–1·0 M and a temperature range $-15°$ to $+60°$C. Quantitative measurements of the intensity of the sharp OH band near 3630 cm^{-1} yielded values for the equilibrium constants and the following values for the enthalpies of dimer formation: methanol, 9·2 ± 2·5; ethanol, 7·2 ± 1·6; *t*-butanol, 4·8 ± 1·1 kcal/mole of dimer. Integrated intensities are given for the dimer band near 3500 cm^{-1} and the polymer band near 3350 cm^{-1}. The high values of ΔH, together with the frequency shift and intensity data, suggest that the alcohol dimer is cyclic with two non-linear hydrogen bonds.

VOL.
10
1957/5

THE study of hydrogen bonding (H-bonding) in alcohols has been the subject of numerous investigations, many of them utilizing infra-red spectroscopy. The general spectral characteristics of H-bonded alcohols in the fundamental OH stretching region were established over 20 years ago by ERRERA *et al.* [1]. Fig. 1 shows spectra of *t*-butanol at several temperatures and concentrations. The plots are typical of all the lower alcohols. The sharp band in the region of 3630 cm^{-1} decreases in peak height with increasing concentration and is clearly assigned to the OH stretching mode of alcohol monomers. The broad bands at lower frequencies (3300–3500 cm^{-1}) increase in intensity with increasing concentration and are assigned to OH stretching vibrations in H-bonded alcohol molecules.

Following ERRERA's work FOX and MARTIN [3] made extensive studies of the spectra of benzyl alcohol, while MECKE and his collaborators [4, 5] have investigated the OH stretching modes of alcohols in both the fundamental and overtone regions. Both groups interpreted their results in terms of chemical equilibria between various H-bonded species. SMITH and CREITZ [6] studied the spectra of several sterically hindered alcohols, and COGGESHALL and SAIER [7] determined equilibrium constants for H-bond formation in some of the lower alcohols. KUHN [8] examined the spectra of a large number of alcohols and diols. Recently ENS and MURRAY [9] studied the first overtone spectra of several alcohols, and FISHMAN and DRICKAMER [10] reported the effect of pressure on the spectrum of *n*-butanol. Measurements of the intensity and frequency of infra-red bands attributed to H-bonded alcohol molecules have been given by TSUBOMURA [11] and by FINCH and LIPPINCOTT [12].

Other physico-chemical measurements have also provided information on H-bonding in alcohols. WELTNER and PITZER [13] deduced values for the energy of H-bonds from measurements of the gas phase heat capacity of methanol;

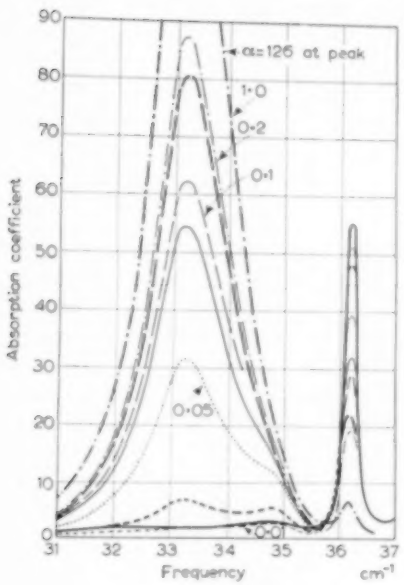

Fig. 1(a)

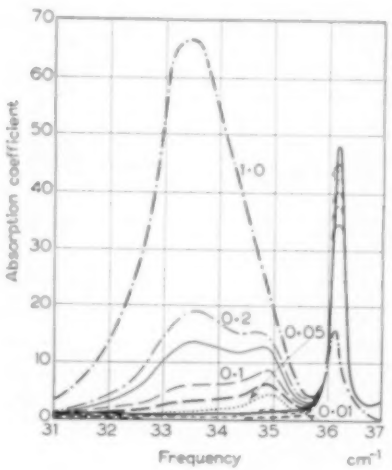

Fig. 1(b)

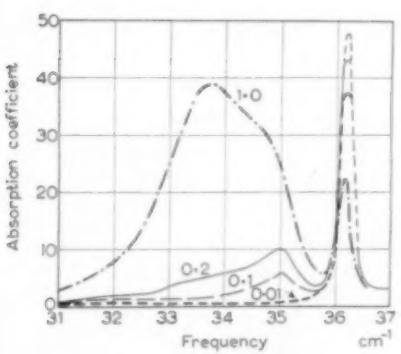

Fig. 1(c)

Fig. 1. Absorption spectrum of *t*-butanol. (a) −12°C; (b) 25°C; (c) 50°C. Absorption coefficient (α or ε) is defined as $(1/Cd)(\log_{10} I_0/I)$, C in moles/l., d in cm. (This figure has appeared in the Transactions of the New York Academy of Sciences [2].

STAVELY and TAYLOR [14] reported on the viscosities of dilute solutions of alcohols in "inert" solvents; CALDWELL and BABB [15] studied diffusion in the methanol–benzene system; BOUD *et al.* [16] investigated the molecular polarization of alcohol solutions in non-polar solvents; SCATCHARD *et al.* [17] measured the vapor pressure of methanol dissolved in CCl_4; BROWN, FOCK and SMITH [18] determined the heats of mixing of ethanol and *iso*propanol with several non-polar solvents; SAROLÉA-MATHOT [19], KRETSCHMER and WIEBE [20], and BARKER and SMITH [21] applied statistical theories of association to alcohols in CCl_4; and BONDI and SIMKIN [22] estimated H-bond energies from the heats of vaporization of aliphatic alcohols.*

Virtually all investigators agree that a solution of an alcohol in a non-polar solvent such as CCl_4 consists of a variety of H-bonded species, as well as unassociated monomers. However, there is controversy over the sizes, shapes and relative numbers of H-bonded molecules. Viscosity data [14] indicate an absence of dimers, with only trimers and higher polymers as H-bonded species. Likewise, the infra-red data of KREUZER and MECKE [4a] show that there are practically no dimers, and MECKE [4b] proposes that cyclic trimers are the smallest stable H-bonded alcohol molecules. On the other hand, a number of investigations have provided strong evidence for the existence of dimers. FOX and MARTIN [3] were able to show that the peak height of the band at 3500 cm^{-1} in benzyl alcohol varied as the square of the total alcohol concentration and assigned it to a dimer. SMITH and CREITZ [6] confirmed the assignment for the corresponding band in 2,4-dimethyl-3-ethyl-3-pentanol. They used the concentration variation of the height of this band as well as that of the monomer band (3625 cm^{-1}) to calculate the equilibrium constant for formation of dimers. COGGESHALL and SAIER [7] studied the concentration dependence of the peak heights of the monomer bands in several simple alcohols and determined equilibrium constants for formation of dimers and higher polymers.

The structure and shape of the hydrogen bonded species of alcohols have also been a matter of some controversy, with advocates of both cyclic and open (chain) structures. Of particular interest is the structure of the dimer (assuming that it exists) since a cyclic structure would require non-linear H-bonds. FOX and MARTIN [3] presented evidence against an open dimer, but SMITH and CREITZ [6] strongly favor an open dimer because of the presence of a band at 3619 cm^{-1} in 2,4-dimethyl-3-ethyl-3-pentanol, which they attribute to the non-bonded hydrogen of the dimer. (In this alcohol the monomer OH absorption is at 3627 cm^{-1}.) VAN THIEL, BECKER and PIMENTEL [23] have recently used the novel matrix isolation technique [24] to study the hydrogen bonding in methanol at 20°K in a solid nitrogen matrix. By varying the ratio of nitrogen to methanol they were able to assign the observed frequencies in the 3 μ region to various H-bonded species, and from the pattern of frequency shifts between species they concluded that the dimer is very probably cyclic and that the trimer is also likely to be cyclic.

* References 1–22 are not intended to provide a comprehensive account of work in this field. The cited articles should be consulted for references to earlier work. Several reviews of H-bonding (L. KELLNER *Rep. Progr. Phys.* 1952 **15** 1; M. DAVIES *Chem. Soc. Ann. Rep.* 1946 **43** 1; and L. HUNTER *Ibid.* 1946 **43** 141) also provide valuable literature references.

VOL. 10 1957/5

In the present work we have used conventional infra-red techniques to study H-bonding of methanol, ethanol and *t*-butanol solutions in CCl_4 over the temperature range $-15°$ to $+60°C$. This investigation differs from previous studies primarily in the coverage of a considerably broader temperature range and in the emphasis that we have placed on the spectral and thermodynamic properties of a single species, the dimer. Many earlier workers have presented treatments which led to the calculation of average properties for a variety of H-bonded species.

Experimental

All spectral measurements were made with a Perkin-Elmer Model 13 spectrophotometer (double beam) that had been modified to scan and record linearly in frequency [25]. A calibrated LiF prism was used with an estimated frequency accuracy of $\pm 4\ cm^{-1}$. The spectral slit width was about $9\ cm^{-1}$ at $3600\ cm^{-1}$ and $6\ cm^{-1}$ at $3000\ cm^{-1}$. A scanning rate of $125\ cm^{-1}$/min was used. Transmission accuracy is estimated at $\pm 0{\cdot}5$ per cent in the region 30–50 per cent T, where most measurements were made, giving an optical density accurate to about 1·5 per cent. The zero and 100 per cent transmission values were measured for each spectrum. A correction was applied for the false energy, which was found to be one per cent in the $3500\ cm^{-1}$ region. The spectrometer was desiccated with P_2O_5 or $Mg(ClO_4)_2$ to reduce water vapor absorption.

The cell employed for most of the measurements* had CaF_2 windows, was water jacketed, and could be varied in thickness from 0·1 mm to 10 mm by use of appropriate lead spacers or copper spacers and teflon gaskets. The 0·1 mm spacer was measured by interference fringes; the others (0·5 mm or greater) were measured with a micrometer. The temperature of the cell could be varied by passing through the jacket water or gylcol solution from baths maintained about $-15°$ and $+60°C$. Spectra at intermediate temperatures were obtained as the cell warmed or cooled. In these cases the temperature change was small and was always measured, while scanning the spectral region of interest, with a copper-constant and thermocouple placed in the solution or soldered in the copper spacer that formed the body of the cell. Estimated temperature accuracy is $\pm 2°C$.

The alcohols were distilled from sodium prior to use. Considerable difficulty was encountered with the absorption of atmospheric water by the CCl_4, and a special procedure was devised to dry it. The CCl_4 (Eastman spectro grade) was placed in an open beaker in an evacuated desiccator over P_2O_5 and was allowed to stand at least 24 hr prior to use. In order to minimize exposure to atmospheric water all transfers of CCl_4 and of solutions were made with hypodermic syringes or with pipettes. Solutions were prepared by successive dilutions from a concentrated solution (usually 1 M) made from a weighed amount of alcohol. Concentrations should be accurate to one per cent. Solutions were prepared just before use in order to minimize evaporation of the alcohol [26].

Each of the eight concentrations between 0·005 M and 0·2 M (and in some cases 1·0 M) was studied as a function of temperature in a cell of appropriate thickness. For each cell thickness a CCl_4 blank was run, and optical densities were determined by a point-by-point calculation. The optical densities were corrected for the variation in the number of molecules in the light path due to density change of the solvent with temperature, and an apparent molar absorption coefficient, ε, was calculated from the relation $\varepsilon \equiv (1/Cd) \log_{10} (I_0/I)$, where C is the total concentration of alcohol in moles/l. and d is the cell length in cm. The values of ε at the peaks of the bands of interest (CH and OH stretching modes) were plotted vs. temperature for each concentration and values read from the resultant smooth curves at temperature intervals of about 10° from $-10°$ to $+45°C$. These interpolated values of ε served as the working data for the calculation of equilibrium constants.

* Spectra of ethanol at concentrations higher than 0·2 M were obtained in standard Perkin-Elmer microcells fitted with BaF_2 windows. Thicknesses were measured by interference fringes. The temperature was not measured but is estimated be to $27° \pm 3°C$.

Results

Calculation of K and ΔH. The feature of primary interest is the sharp band near 3630 cm^{-1} (Fig. 1) and the variation of ε for this band (designated ε_m) with temperature and with concentration. The frequency of the band varies from one alcohol to another and is slightly dependent on temperature, as indicated in the first two columns of Table 1. This band is unquestionable due primarily

Table 1. Frequencies of OH stretching modes

Alcohol	Monomer		Dimer		Polymer	
	Frequency at 25°C	$\Delta\nu/\Delta T$ (cm^{-1}/deg)	Frequency at 25°C	$\Delta\nu/\Delta T$ (cm^{-1}/deg)	Frequency at 25°C	$\Delta\nu/\Delta T$ (cm^{-1}/deg)
Methanol	3643	0·08	3528	0·2	3332	0·85
Ethanol	3634	0·06	3509	0·3	3336	0·8
t-Butanol	3616	0·06	3492	0·25	3352	0·85

to absorption by monomers, although it is possible that non-bonded hydrogen atoms of open dimers or polymers absorb at this frequency also [8, 23]. In 0·005 M solutions, which are sufficiently dilute to preclude formation of an appreciable number of alcohol-alcohol H-bonded species, ε_m displays a marked temperature coefficient, as shown in Fig. 2 for a typical case. We reported this variation of

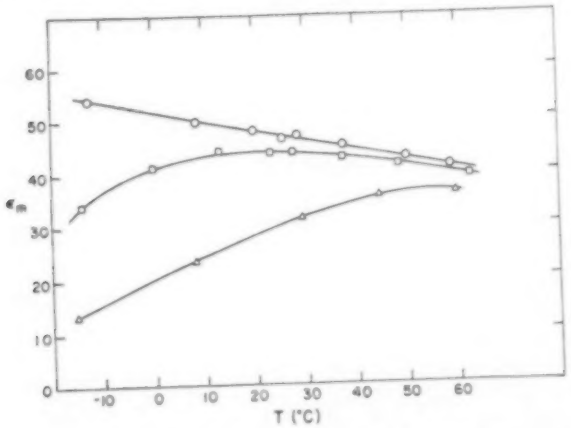

Fig. 2. Apparent absorption coefficient, ε, for the 3635 cm^{-1} (monomer) band of ethanol as a function of temperature at various concentrations.
○ 0·005 M; □ 0·05 M; △ 0·20 M.

intensity with temperature previously and attributed it to a temperature-dependent solvent perturbation resembling very weak H-bonding to the solvent [27]. HUGHES, MARTIN and COGGESHALL [28] reported a similar effect in long-chain alcohols. In more concentrated solutions ε_m is decreased, especially at lower

VOL. 10 1957/5

temperatures, as a result of the depletion of monomers and formation of H-bonded species which absorb at other frequencies. The net result, as indicated in Fig. 2, is the superposition of these two effects, giving, in general, a maximum value of ε_m at an intermediate temperature.

Values of ε_m at various temperatures were plotted vs. concentration and smooth curves drawn through the points. Typical examples are shown in Fig. 3. The

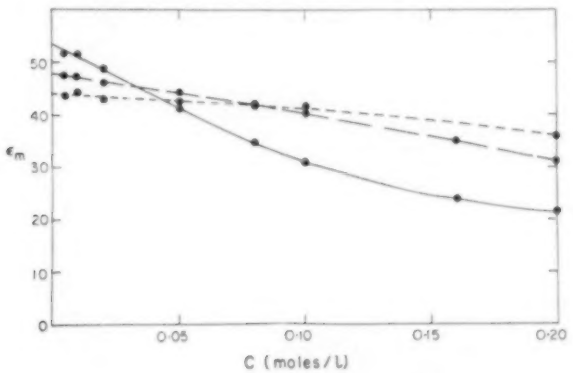

Fig. 3. Apparent absorption coefficient, ε, for the 3635 cm^{-1} (monomer) band of ethanol as a function of concentration at various temperatures.
——— 0°C; — — — 25°C; - - - - 45°C.

extrapolation to zero concentration gives the value of ε_m when all alcohol molecules are in the form of monomers, and is designated ε_m°. This quantity is, as we have noted, temperature-dependent, but is assumed to be independent of concentration (i.e. to obey Beer's Law) over the concentration range of interest.*

Analysis of the chemical equilibrium expression for formation of dimer and polymer (appendix, 1 and 4) shows that the limiting slope of the ε_m vs. C curve is related to the equilibrium constant for dimer formation. If only monomer contributes to ε_m, the relation is

$$(d\varepsilon_m/dC)_{C=0} = -2K_C\varepsilon_m^\circ = -K_X\varepsilon_m^\circ/5,$$

where $K_C = C_d/C_m^2$, $K_X = X_d/X_m^2$, C_d, C_m, X_d, X_m are concentrations and mole fractions of dimer and monomer, and $K_X = 10K_C$ for CCl_4. Such a condition would be applicable in the low concentration region, where higher polymers are unimportant, if the dimer is cyclic. For an open dimer the non-bonded hydrogen might absorb at almost the same frequency as monomer [8, 23] and thus would presumably contribute to the monomer band. If the non-bonded hydrogen of the open dimer has the same absorption coefficient as the monomer, ε_m°, then it is easily shown (appendix, 2) that the value of K calculated above should be multiplied by 2. (If its absorption coefficient is $r\varepsilon_m^\circ$, then K should be multiplied

* The effects of finite resolution discussed by RAMSEY [29] result in a correction factor that is independent of optical density in the range studied.

by $2/(2 - r)$.) The dimer equilibrium constant can alternatively be found from the limiting slope of a plot of $C(\varepsilon_m/\varepsilon_m^\circ)^2$ vs. $(1 - \varepsilon_m/\varepsilon_m^\circ)$ [4], or from the extrapolation of the function $[C(\varepsilon_m/\varepsilon_m^\circ)^2]/[1 - \varepsilon_m/\varepsilon_m^\circ]$ to zero concentration [7]. We actually used all three methods to obtain K's for some temperatures and found

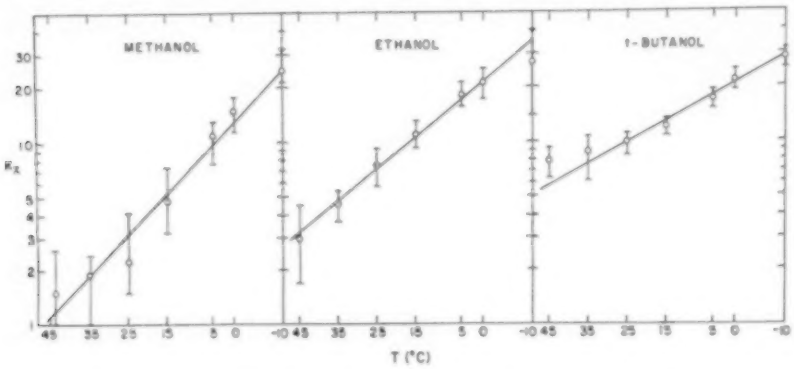

Fig. 4. Variation of the equilibrium constant for dimer formation, K_x, with temperature.

agreement within the accuracy of the data. Since $(1 - \varepsilon_m/\varepsilon_m^\circ)$ is a small quantity at low alcohol concentrations, there is considerable scatter in the plots using that function.

Equilibrium constants for formation of cyclic dimers were calculated and $\log_{10} K$ plotted vs. $1/T$ to obtain the heat of formation, as shown in Fig. 4. It should be noted that a similar plot for open dimer K's would yield the same slope and same ΔH since all K's would be a constant ($\sim$2) times the K's given for a

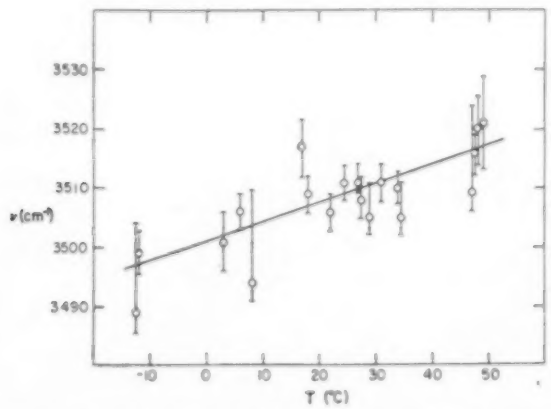

Fig. 5. Frequency of the band near 3510 cm^{-1} in ethanol as a function of temperature.

cyclic dimer. We shall attempt to identify ΔH with the energy of the dimer H-bond (or bonds). This requires the assumption that the difference in solvation energy between the dimer and two monomers is negligible. The calculated ΔH's are listed in Table 2, along with H-bond energies reported by other workers.

VOL. 10 1957/5

We have not calculated equilibrium constants for formation of higher polymers.

Dimer and polymer bands. The calculations of K and ΔH have used data only for the height of the "monomer" band near 3630 cm^{-1}. Additional information is contained in the bands due to associated species at approximately 3500 cm^{-1} and 3350 cm^{-1}. The former feature has been attributed to dimers [3, 6] and hence is of considerable interest in connection with the foregoing calculations. This band is difficult to study in detail, since it is weak in comparison with the features

Table 2. H-bond of energy of alcohols

Alcohol	Solvent	Species	Energy*	Investigators	Method
Methanol	CCl_4	Dimer	9·2 ± 2·5	This work	i.r.
	Vapor	Dimer	3·2	WELTNER and PITZER [13]	Gas heat capacity
	Vapor	Tetramer	6·	WELTNER and PITZER [13]	Gas heat capacity
	Liquid	Polymer	5·5	BONDI and SIMKIN [22]	Heat of vaporization
	CCl_4	Polymer	4·72	MECKE [4b]	i.r.
	C_6H_6	Polymer	3·67	MECKE [4b]	i.r.
	CCl_4	Polymer	5·15	MECKE [4b]	Heat of solution
	CCl_4	(Dimer) (Polymer)	3·6 ± 0·4	SAROLÉA-MATHOT [19]	Statistical; i.r. data of ref. 5
Ethanol	CCl_4	Dimer	7·2 ± 1·6	This work	i.r.
	Liquid	Polymer	5·5	BONDI and SIMKIN [22]	Heat of vaporization
	Cyclo-hexane	Polymer	5·4 ± 1·0	KRETSCHMER and WIEBE [20]	Statistical; thermo-dynamic data
	$CHCl_3$	Polymer	6·74	BARKER and SMITH [21]	Statistical; thermo-dynamic data
t-Butanol	CCl_4	Dimer	4·8 ± 1·1	This work	i.r.
	CCl_4	Polymer	5·3 ± 0·5	HOFFMANN [5]	i.r.

* The values given under this heading for the present work are the enthalpy changes (ΔH) per mole of dimer. For other studies, where polymers are involved, the figure given is generally ΔH divided by the average number of monomeric units in the polymer. The original articles should be consulted for more details.

at 3630 and 3350 cm^{-1}. There is only a small region of temperature and concentration in which this band is of sufficient intensity to be accurately measurable and yet is not submerged in the very broad band at 3350 cm^{-1}. The frequency of the 3500 cm^{-1} band was carefully measured for the most favorable conditions of concentration and temperature for the three alcohols. A plot of ν vs. T for ethanol is shown in Fig. 5. Although there is considerable scatter due to the

inherent breadth of the band and small interference by water vapor, there is no doubt that the frequency is a function of temperature. Such a relation is predicted by the theory of hydrogen bonding of LIPPINCOTT and SCHROEDER [30] and correlates with the studies of alcohol polymers by FINCH and LIPPINCOTT [12]. The frequencies and temperature coefficients for the three alcohols are given in Table 1.

In less favorable cases where the 3350 cm^{-1} band is appreciable, an attempt was made to resolve graphically the 3500 and 3350 cm^{-1} bands and to determine their areas separately. The intensities of the band at 3500 cm^{-1} are known with much less accuracy than the peak heights of the monomer band. These values may, however, be used to check the assignment of this band to the dimer, as well as to make a rough check on the consistency of the dimer equilibrium constants at different temperatures. The integrated intensities of this band were plotted vs. temperature for each concentration and values read from the best smooth curves through the points at temperatures corresponding to those used in the calculation of the dimer K's. At a given temperature the variation of the dimer concentration with total alcohol concentration can be found from the relation

$$C_d = KC_m^2 = KC^2(\varepsilon_m/\varepsilon_m^\circ)^2$$

(assuming only monomer contributes to the 3630 cm^{-1} band.) From the integrated intensity, B_d, of the 3500 cm^{-1} band and the calculated dimer concentration the true integrated molar absorption coefficient, B_d°, can be determined at each concentration and checked for constancy. In both ethanol and t-butanol an approximately constant value was found, but in methanol the calculated dimer absorption coefficient increased with concentration at each temperature. Such behavior indicates either that the 3500 cm^{-1} band is increasing with concentration more rapidly than expected for a dimer absorption or that the concentration of monomer has been underestimated at the higher concentrations of alcohol. The latter is highly improbable, since absorption by other species (non-bonded hydrogens of open dimers or polymers) at the monomer frequency would cause the calculated monomer concentration to be too high, rather than too low. The 3500 cm^{-1} band does not increase rapidly enough with concentration to be due only to trimer, but it is possible that two species, dimer plus, presumably, trimer, absorb at this frequency. No separate band was found for any of the alcohols studied in this work which could be correlated with the band found in the matrix isolation studies at 3445 cm^{-1} and attributed to trimer [23]. It is conceivable that dimer and trimer bands overlap so as to be unresolvable in the temperature range used in the present work.

A rough check on the rate of change of equilibrium constants with temperature (hence a check on the calculated ΔH) is obtained by comparing the values of B_d° found for each temperature. For ethanol B_d° approximately independent of temperature could be obtained with equilibrium constants appropriate to a ΔH of about 5–7 kcal/mole; for t-butanol best agreement is obtained for ΔH in the range 4·5–6 kcal/mole. The failure of B_d° to remain constant with concentration at a given temperature prevented us from using this method to check ΔH for methanol. Values of B_d° for ethanol and t-butanol are listed in Table 3. The

VOL.
10
1957/5

best values of B_d° obtained for an open dimer with an assumed absorption coefficient of ε_m° for the non-bonded hydrogen were approximately half that for the cyclic dimer, giving approximately the same intensity per bonded OH. The calculated concentration variation of the open dimer did not vary sufficiently from that of the cyclic dimer to permit a definite assignment of the 3500 cm^{-1} band to either species.

Measurements of the intensity of the broad polymer band near 3350 cm^{-1} are influenced by the presence of dimers, and accurate measurements of the area of the polymer band are possible only in our most concentrated solutions ($\geq$0·2M).

Table 3. Frequency shifts, band widths and absorption coefficients

Species	Alcohol	$\nu_m - \nu$ (cm^{-1})	$\nu_{1/2}$ (cm^{-1})*	$B^\circ \times 10^{-3}$ (l./mole cm^2)†
Monomer	Methanol	0	22	4·7
	Ethanol	0	24	4·6
	t-Butanol	0	15	3·3
Dimer	Methanol	115 ± 3	80 ± 30	———
	Ethanol	125 ± 5	90 ± 20	15 ± 5
	t-Butanol	124 ± 4	75 ± 15	11 ± 2
Polymer	Methanol	311 ± 6	205 ± 15	54
	Ethanol	298 ± 6	195 ± 15	55
	t-Butanol	264 ± 6	160 ± 15	53

* $\nu_{1/2}$ the band width at half maximum, has been corrected for finite resolution according to the methods given by RAMSEY [29].

† B° is the integrated molar absorption coefficient *per* OH *bond*;
$B_i^\circ \equiv (2{\cdot}3/NC_i d) \int \log_{10} (I_o/I)\, d\nu$, where C_i is the concentration of the species in question in moles/l., d is the cell thickness in cm, and N is the number of OH oscillators per molecule contributing to the band. For monomer a Lorentzian shape was assumed, giving

$$B_m^\circ = 2{\cdot}3/C_m d \,.\, (\log I_c/I)_{\max}\, \nu_{1/2}\, K,$$

where $K(\sim\pi/2)$ is given by RAMSEY [29]. For the H-bonded species B° was determined by graphical integration.

The calculation of the number of alcohol molecules existing as polymers is also subject to uncertainty since the band at 3630 cm^{-1} might contain an appreciable contribution from non-bonded hydrogens of dimers or polymers. Calculations for the two limiting cases—an open trimer, in which 1/3 of all the OH's in the polymer are assumed to contribute to the 3630 cm^{-1} band with intensity ε_m°, and an infinite (or cyclic) polymer, in which none of the hydrogens of the polymer contribute to the 3630 cm^{-1} band—show that the intensity per *bonded* OH is approximately independent of the effect of end group OH's (exactly independent if the amount of dimer is negligible). The polymer intensity data are summarized in Table 3. Most of the data were obtained from solutions less concentrated than 1 M, but for ethanol results at room temperature were obtained up to a concentration of 9 M.

The frequency of the polymer band varies with temperature for all three alcohols, as indicated in Table 1. Our values for the temperature coefficients, $\Delta\nu/\Delta T$, are 2–3 times those found by FINCH and LIPPINCOTT [12] for these

alcohols. We cannot account entirely for this discrepancy, but it presumably reflects a difference in behavior between the relatively small polymers that are probably present in our system and the very large polymers that would be present in the undiluted alcohols studied by FINCH and LIPPINCOTT.

Other spectral effects of H-*bonding.* In addition to the pronounced spectral changes with extent of H-bonding that we have discussed thus far, two other spectral features were found to vary with temperature and concentration. In both methanol and ethanol some of the bands attributable to CH stretching modes intensified slightly with decreasing temperature in dilute solutions [27] and exhibited a pronounced intensification with increasing concentration, especially at low temperature. This effect, which is certainly an indirect result of hydrogen bonding, is being studied in more detail. The results will be published soon.

Another feature which seems to be associated with formation of H-bonds in the alcohols, and which has apparently not been previously discussed, is the appearance of two weak bands near 2600 cm^{-1} in concentrated solutions ($\geq$0·1 M) at low temperature ($\leq 0°$). Although these bands are too weak to permit accurate measurement, their intensities correlate qualitatively with the amount of polymer as indicated by the intensity of the 3350 cm^{-1} polymer band. The weakness of the features and their location at $\sim$2600 cm^{-1} suggest the possible assignment as a combination mode of the polymer. The bands could arise as a difference between the strong 3350 cm^{-1} band and a fundamental (unobserved in the present work) about 750 cm^{-1}. The closest frequency to 750 cm^{-1} that has been reported is a band at 670 cm^{-1} found in a large series of alcohols by STUART and SUTHERLAND [31]. They showed it to be due to a vibration of associated molecules and assigned it to the out-of-plane OH deformation. Coupling between this out-of-plane mode and the OH stretching vibration is expected to be quite weak. Another serious drawback to the assignment of the 2600 cm^{-1} bands as a difference is that the corresponding sum was not observed. No reasonable alternative assignments have occurred to us.

Discussion

It is shown in the appendix that the limiting slope of the ε_m vs. C curve is proportional to the equilibrium constant for dimer formation and that a non-zero value of $(d\varepsilon_m/dC)_{c=0}$ implies that dimers are stable. This treatment is subject only to the requirement that Beer's Law hold over the range in which the slope is calculated. In applying the equations it is, of course, necessary to find the true limiting slope. By expanding the expression for $d\varepsilon_m/dC$ in a power series in C it can be shown that for only monomers and dimers $d\varepsilon_m/dC$ will first deviate appreciably from its limiting value at a concentration $>$0·01 M (for K's in the observed range) and that the initial deviation will tend to decrease the absolute value of the observed slope. The presence of higher polymers in this region would, on the other hand, tend to increase the slope (in absolute value). Even at the lowest temperatures studied there appears to be virtually no polymer (as indicated by the 3350 cm^{-1} band) in the concentration region below 0·02 M. We believe, therefore, that our measurements extend to a sufficiently low concentration to permit direct observation of the limiting slope, and that the non-zero slope found

VOL.
10
1957/5

for all three alcohols at all temperatures shows conclusively that alcohol dimers are stable in CCl_4 solution.

As noted in the introduction, other workers have reached the conclusion that alcohol dimers are not stable. This disagreement is not too surprising in view of the complexity of the system and the practical impossibility of building up an appreciable concentration of a given H-bonded species without considerable interference from other species. For instance, STAVELEY and TAYLOR [14] tested for the presence of dimers by noting the linearity of a function of viscosity plotted vs. concentration. They do not give examples of the plots but indicate indirectly that their data extended to 0·1 or 0·2 M (at 20°C). In this range of concentration and temperature our results predict that any effect of dimers would probably be masked by the larger concentration of higher polymers. HOFFMANN [5] has also concluded from infra-red data that dimers are absent ($K = 0$). However, we have replotted HOFFMANN's data on an ε vs. C curve and from the limiting slope obtain equilibrium constants in reasonable agreement with ours (e.g. ethanol at 21–25°C; HOFFMANN's data, $K_x = 5{\cdot}3$–$11{\cdot}6$; our data, $K_x = 5{\cdot}8$–$9{\cdot}2$). Such a large variation dependent upon the method of plotting the data is quite disturbing and demonstrates the sensitivity of the equilibrium calculations to small errors in the data. A significant increase in the accuracy of determination of K by this method will probably have to await an order of magnitude improvement in the accuracy of photometry. We feel that our conclusions on the presence of dimers are materially strengthened by the inclusion of experiments over a wide range of temperature, particularly below room temperature, where the limiting slope is certainly not zero.

The exact values obtained for the dimer equilibrium constants are dependent on the structure of the dimer and the extent of contribution, if any, of the non-bonded hydrogen of the open dimer to the monomer band. The various alternatives are discussed in the appendix. Because of this ambiguity the K's themselves can contribute little information to our knowledge of the structure of the dimer. The mean values of ΔH obtained from the temperature dependence of K's, as listed in Table 2, are quite high for a single OH—O hydrogen bond, especially one which causes a frequency shift of only 125 cm^{-1} [32]. These values, therefore, suggest that the dimer is formed from two H-bonds (necessarily non-linear) and exists in the cyclic form. An energy of 2·5–4·5 kcal per bond is probably reasonable for such a non-linear bond. The precision of determination of ΔH is not great enough to rule out the single bonded open dimer, but only to make it appear less plausible than the cyclic form. It is conceivable that both open and cyclic dimers co-exist. If so, the K found in this work actually represents the sum of the constant for a cyclic dimer, K_{cd} and half the constant for an open dimer, K_{od} (appendix, 3). In that event, the calculated ΔH would represent an average heat of formation of the two types of dimer and would probably be temperature-dependent. It is unlikely that both cyclic and open dimers would absorb at exactly the same frequency. At high concentrations the absorption of the open dimer (for example) might be hidden under the polymer band, but at lower concentrations there seems to be insufficient absorption in that region to permit the presence of an appreciable amount of dimer.

Table 2 shows that ΔH for dimer formation decreases in absolute value with increasing size of the alcohol. These figures indicate an unusually large variation in the strength of the hydrogen bond(s) of the dimer for molecules that are very similar chemically. Furthermore, the frequency differences between the monomer and dimer bands are nearly the same for the three alcohols, and a large difference in H-bond energy among the three is unexpected in view of the generally accepted correlations between frequency shift and H-bond energy [32]. Some of the discrepancy may be the result of the presence of both cyclic and open dimers, which would give an apparent ΔH that is temperature-dependent. On the other hand, the margin of error in these determinations is almost large enough to permit a more nearly constant ΔH of about 6–7 kcal/mole to be consistent with our data for the three alcohols.

HUGGINS and PIMENTEL [33] have recently published data on frequency shifts, band widths and integrated intensities for a large number of H-bonding systems and have shown that these quantities can be correlated for many such compounds. The frequency and band-width data for all three alcohols given in Table 2 agree rather well with the straight line of HUGGINS and PIMENTEL. There are discrepancies, however, in the intensity-frequency shift correlations. Our intensity values for the 3500 cm^{-1} (dimer) band in ethanol and *t*-butanol are far below that predicted by the *H–P* curve. Part of the discrepancy might be due to error in measurement of the band intensity and in the calculation of dimer concentration. However, if the 3500 cm^{-1} is due to the cyclic dimers, the deviation from the predicted behavior may represent the effect of non-linear H-bonds [33]. Further studies of spectral systematics among systems that are known to form bent H-bonds are needed.

Our values for the intensity of the polymer bands also lie below the *H–P* curve, but are probably well within the combined limits of error of our measurements and of the curve itself. It should be noted, however, that the intensity datum given by *H–P* for methanol is far from their curve and from our value. Their intensity is evidently in error, probably as a result of interference by dimers.

VOL.
10
1957/5

Appendix

Assume that the alcohol molecules exist in the form of monomer, dimer, trimer and higher polymers. The concentrations of the first three species (C_m, C_d, C_t) are related by the equilibrium expressions

$$K_d = C_d/C_m^2; \qquad K_t = C_t/C_m^3.$$

(1) Suppose that ε_m represents the apparent absorption coefficient of the band due *only* to monomer. Then

$$\varepsilon_m = \varepsilon_m^0(C_m/C)$$

$$= \varepsilon_m^0[(C - 2C_d - 3C_t - nC_p)/C],$$

where C is the total concentration of alcohol and C_p is the concentration of the higher (n-fold) polymers. Then

$$\varepsilon_m = \varepsilon_m^0[(C - 2K_dC_m^2 - 3K_tC_m^3 - \text{terms in higher powers of } C_m)/C].$$

Neglecting the terms in powers of C_m greater than 3, and making the approximation that $C_m \approx C$*, we have

$$\begin{aligned} \varepsilon_m &= \varepsilon_m^o[(C - 2K_dC^2 - 3K_tC^3)/C] \\ &= \varepsilon_m^o[1 - 2K_dC - 3K_tC^2] \\ d\varepsilon_m/dC &= \varepsilon_m^o[-2K_d - 6K_tC] \\ \lim_{C\to 0}(d\varepsilon_m/dC) &= -2K_d\varepsilon_m^o. \end{aligned}$$

(2) Suppose that ε_m represents not only monomer absorption ε_m^o but also absorption by the non-bonded OH of an open dimer, $r\varepsilon_m^o$. Then

$$\begin{aligned} \varepsilon_m &= \varepsilon_m^o(C_m/C + rC_d/C) \\ &= \varepsilon_m^o[(C - 2K_dC_m^2 + rK_dC_m^2)/C] \\ &\approx \varepsilon_m^o[1 - (2 - r)K_dC] \\ \lim_{C\to 0}(d\varepsilon_m/dC) &= -(2 - r)K_d\varepsilon_m^o. \end{aligned}$$

Thus K_d is seen to be $2/2 - r$ times as large as in the case 1, and for $r \approx 1$, K_d is about twice that for case 1.

(3) Suppose both cyclic dimers (*cd*) and open dimers (*od*) exist, with the non-bonded OH of the latter contributing to ε_m with an absorption coefficient ε_m^o. Then

$$\begin{aligned} K_{cd} &= C_{cd}/C_m^2; \qquad K_{od} = C_{od}/C_m^2 \\ \varepsilon_m &= \varepsilon_m^o(C_m/C + C_{od}/C) \\ &= \varepsilon_m^o[(C - 2K_{cd}C_m^2 - 2K_{od}C_m^2 + K_{od}C_m^2)/C] \\ &\approx \varepsilon_m^o[1 - 2K_{cd}C - K_{od}C] \\ \lim_{C\to 0}(d\varepsilon_m/dC) &= -2(K_{cd} + K_{od}/2)\varepsilon_m^o. \end{aligned}$$

(4) The monomer-dimer equilibrium can be expressed either in concentration or mole fraction,

$$K_C = C_d/C_m^2; \qquad K_X = X_d/X_m^2.$$

It is easily shown that the equilibrium constants are related by the expression

$$K_X = K_C/V_s \approx 10K_C$$

where V_s, the molar volume of the solvent, is about 0·1 l. for CCl_4.

References

[1] Errera J. and Mollet P. *Nature, Lond.* 1936 **138** 882; Errera J., Gaspart R. and Sack H. *J. Chem. Phys.* 1940 **8** 63.
[2] Liddel U. *Trans. N.Y. Acad. Sci.* In press.
[3] Fox J. J. and Martin A. E. *Proc. Roy. Soc.* A 1937 **162** 419.
[4a] Kreuzer J. and Mecke R. *Z. Phys. Chem.* B 1941 **49** 309.
[4b] Mecke R. *Disc. Faraday Soc.* 1950 **9** 161.
[5] Hoffmann E. G. *Z. Phys. Chem.* B 1943 **53** 179.
[6] Smith F. A. and Creitz E. C. *J. Res. Nat. Bur. Stand.* 1951 **46** 145.
[7] Coggeshall N. D. and Saier E. L. *J. Amer. Chem. Soc.* 1951 **73** 5414.
[8] Kuhn L. P. *J. Amer. Chem. Soc.* 1952 **74** 2492.
[9] Ens A. and Murray F. E. *Canad. J. Chem.* 1957 **35** 170.

* The justification of this assumption at low C can be shown by a detailed exact treatment or by development in a power series in C, as has been done for the monomer-dimer case by Bono [34].

[10] FISHMAN E. and DRICKAMER H. G. *J. Chem. Phys.* 1956 **24** 548.
[11] TSUBOMURA H. *J. Chem. Phys.* 1956 **24** 927.
[12] FINCH J. N. and LIPPINCOTT E. R. *J. Chem. Phys.* 1956 **24** 908; *J. Phys. Chem.* In press.
[13] WELTNER W., JR. and PITZER K. S. *J. Amer. Chem. Soc.* 1951 **73** 2606.
[14] STAVELEY L. A. K. and TAYLOR P. F. *J. Chem. Soc.* 1956 200.
[15] CALDWELL C. S. and BABB A. L. *J. Phys. Chem.* 1955 **59** 1113.
[16] BOUD A. H., CLEVERDON D., COLLINS G. B., and SMITH J. W. *J. Chem. Soc.* 1955 3793.
[17] SCATCHARD G., WOOD S. E., and MOCHEL J. M. *J. Amer. Chem. Soc.* 1946 **68** 1960.
[18] BROWN I., FOCK W., and SMITH F. *Aust. J. Chem.* 1956 **9** 364.
[19] SAROLÉA-MATHOT L. *Trans. Faraday Soc.* 1953 **49** 8.
[20] KRETSCHMER C. B. and WIEBE R. *J. Chem. Phys.* 1954 **22** 1697.
[21] BARKER J. A. and SMITH F. *J. Chem. Phys.* 1954 **22** 375.
[22] BONDI A. and SIMKIN D. J. *J. Chem. Phys.* 1956 **25** 1073.
[23] VAN THIEL M., BECKER E. D., and PIMENTEL G. C. *J. Chem. Phys.* 1957 **27** 95.
[24] BECKER E. D. and PIMENTEL G. C. *J. Chem. Phys.* 1956 **25** 224.
[25] BRACKETT F. S. *J. Opt. Soc. Amer.* In press.
[26] SAIER E. L. and COGGESHALL N. D. *Analyt. Chem.* 1948 **20** 812.
[27] LIDDEL U. and BECKER E. D. *J. Chem. Phys.* 1956 **25** 173. It was erroneously stated in this article that the half-width of the 3645 cm^{-1} band in methanol is 35 cm^{-1}, independent of temperature. In fact, the half-width (corrected according to the tables of reference [29]) varies from 19 cm^{-1} at $-10°C$ to 25 cm^{-1} at $+50°C$.
[28] HUGHES R. H., MARTIN R. J., and COGGESHALL N. D. *J. Chem. Phys.* 1956 **24** 489.
[29] RAMSEY D. A. *J. Amer. Chem. Soc.* 1952 **74** 72.
[30] LIPPINCOTT E. R. and SCHROEDER R. *J. Chem. Phys.* 1955 **23** 1099.
[31] STUART A. V. and SUTHERLAND G. B. B. M. *J. Chem. Phys.* 1956 **24** 559.
[32] BADGER R. M. and BAUER S. H. *J. Chem. Phys.* 1937 **5** 839; BADGER R. M. *Ibid.* 1940 **8** 288.
[33] HUGGINS C. M. and PIMENTEL G. C. *J. Phys. Chem.* 1956 **60** 1615.
[34] BONO D. *C.R. Acad. Sci., Paris* 1956 **242** 637.

VOL.
10
1957/5

Spectrochimica Acta, 1957, Vol. 10, pp. 85 to 98. Pergamon Press Ltd., London

La mésure de la "largeur effective" des raies dans l'analyse des substances en poudre

A. Fiorenza et M. Lachin
Laboratori Gomma, Pirelli S.p.A. Milano

(*Received 5 May* 1957)

Abstract—After discussing the difficulty of applying spectrochemical analysis to powders, the method of measurement used and special photometer required are described. For each element it has been found advisable to measure a group of lines, instead of a single one; and the improvement gained is described. The results indicate some properties of the parameter of "effective line-width" and its importance in the analysis of ashes, especially those of some ingredients used in the rubber industry.

1. Avant-propos

On sait que l'examen analytique qualitatif et quantitatif des matériaux non métalliques au moyen de la spectrométrie a présenté et présente encore de grandes difficultés: les résultats positifs, quoique très nombreux, se bornent à des cas particuliers et les méthodes employées sont très laborieuses. Les causes de ces limitations sont très complexes et ne sont pas entièrement connues, on peut considérer comme dominantes, sans doute, celles qui sont dûes aux effets de perturbation réciproque des éléments entre eux, à la présence des anions avec leurs hauts potentiels d'excitation et à la nécessité de doser des pourcentages élevés.

Il s'en suit que l'application des méthodes adoptées pour l'analyse des échantillons métalliques ne peut guère s'étendre facilement à ces matériaux, vu qu'il est moins aisé d'obtenir des conditions de répétition assez rigoureuses.

2. Méthodes densitométriques et leurs limitations

Suivant les méthodes densitométriques, les mesures sur les raies doivent être limités, comme on le sait [1, 2, 3], à la partie rectiligne de la courbe de noircissement photographique de Hurter-Driffield (Fig. 1), dont l'étendue est non seulement limitée, mais dépend également de la qualité de l'émulsion et des modalités de traitement, et est en outre variable selon la longueur d'onde.

La densité (D), qui est exprimée par le rapport:

$$D = \log \frac{J_0}{J},$$

où

J_0 = flux lumineux incident

J = flux lumineux transmis

a des limites linéaires comprises, comme maximum, entre 0·5 et 1·5 environ, équivalant à des rapports de concentration de 1 à 10 dans les cas les plus favorables. Les noircissements les plus intenses sortent de la partie rectiligne de la courbe et il se produit en même temps un élargissement ou une expansion de la raie

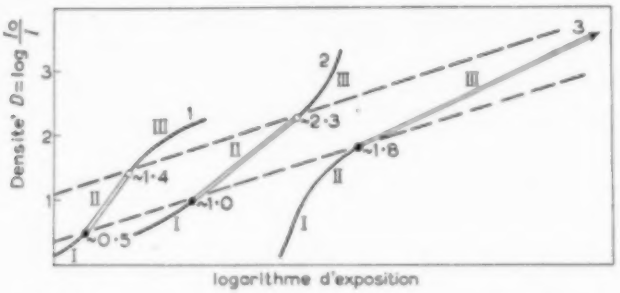

Fig. 1. Caractéristiques de la largeur effective par rapport à la densité du negatif.
1. Courbe densitométrique de Hurter-Driffield
2. Courbe des largeurs effectives à l'échelle linéaire
3. Courbe des largeurs effectives à l'échelle logarathmique
● Limite de validité inférieure
○ Limite de validité supérieure

elle-même, dû à des phénomènes très complexes, parmi lesquels domine la diffusion de la lumière dans la couche sensible.

Dans leur travaux, Junkes et Salpeter [4, 5, 6, 8] n'ont pas seulement signalé, comme résumé des recherches partielles d'autres Auteurs, l'importance de ce phénomène d'expansion des raies spectrales, mais ils ont réussi encore à élaborer une méthode et à imaginer un photomètre qui permet de mesurer rationnellement le phénomène.

3. La largeur effective et sa mesure

Tandis que dans le densitomètre normal on effectue une mesure de la variation du flux à travers une fente fixe, dans le densitomètre Junkes la fente est variable, de facon à ramener le flux à une valeur constante. Le procédé consiste donc à mesurer le flux lumineux qui passe à travers une certaine fente, lorsqu'on projette sur celle-ci une partie de la plaque non impressionnée; la valeur de ce flux, indiqué par la déviation du galvanomètre, dépend de cette dimension initiale, que l'on nomme *largeur fondamentale*. Lorsque la raie qui doit être mesurée est projetée sur la fente, cette dernière s'élargit autant qu'il est nécessaire pour que le galvanomètre indique un passage de flux égal au précédent, c'est-à-dire jusqu'à ce que l'on obtienne *le même effet;* de là l'origine du nom de *largeur effective* donné à ce paramètre, que l'on exprime par un nombre qui représente la largeur géométrique de la fente.

La méthode serait parfaite si toutes les raies étaient monochromatiques et avaient un profil égal et si, en faisant abstraction des imprécisions optiques qui existent même dans les meilleurs spectrographes, l'espace entre deux raies était toujours suffisant. Si l'on ajoute les variations de sensibilité des plaques d'une part et d'efficacité des spectrographes aux différentes longueurs d'onde d'autre part, il est évident que même pour cette méthode il existe des limitations. Malgré

VOL. 10 1957/5

cela, son utilité et son importance ressortent des études de INTONTI [7, 9], qui en a élaboré les premières applications pratiques.

Suivant cet Auteur, les rapports entre la largeur effective et les intensités lumineuses sont représentés par le diagramme-type reproduit à la Fig. 1. On y trouve le tracé des courbes d'expositions croîssantes que l'on obtient en appliquant la méthode densitométrique habituelle en comparaison avec les courbes obtenues avec les valeurs des largeurs effectives ou leurs logarithmes. Comme on le voit, toutes les courbes sont composées de trois zones, dont une rectiligne, qui sera généralement employée. Les valeurs numériques ne représentent qu'un exemple. Leur valeur réelle peut varier considérablement, non seulement pour des raisons de caractère photographique, mais aussi pour des raisons de profil et de loi d'émission de chaque raie à l'intérieur d'un même spectre. Pour chaque raie, la limite inférieure de validité est plus basse pour la courbe densitométrique; puis vient ensuite la représentation linéaire en fonction des largeurs effectives, puis celle donnée par la représentation logarithmique. La limite supérieure suit le même ordre, avec la différence que dans la méthode densitométrique elle est vite atteinte, dans la représentation linéaire de la largeur effective elle est plus éloignée, et, en ce qui concerne la représentation logarithmique, selon INTONTI on ne l'atteindrait même pas après une exposition 1000 fois supérieure à celle qui suffit normalement à l'exécution d'un spectre.

Par conséquent, dans l'emploi de ce paramètre, l'effet peut se trouver à un point différent de la courbe, que l'on ne peut connaître à l'avance, et qui dépend des caractéristiques du matériel sensible, des conditions de l'expérience et de la concentration des matériaux à doser.

4. Essai d'emploi du paramètre pour l'examen des poudres

Quoique le nouveau paramètre proposé ne puisse pas être appliqué, pour les raisons susdites, avec des principes simplistes et généraux, et que ses modalités d'utilisation ne puissent pas être encore complètement définies, on a estimé utile d'en essayer l'emploi pour s'assurer à première vue et approximativement dans quelle proportion l'extension des limites de mesure pourrait contribuer à la recherche des méthodes quantitatives dans le domaine des matériaux non métalliques.

4.1. *Le Photomètre*

Dans la réalisation de l'instrument, tout en tenant compte des expériences précédentes des Auteurs nommés ci-dessus, il a été estimé nécessaire de s'écarter quelque peu des principes de grande précision suivis par eux, en se bornant à une réalisation simple, par des moyens presque rudimentaires, qui soit suffisante aux besoins modestes d'un travail d'exploration. C'est pourquoi on a utilisé (Fig. 2) comme projecteur un microscope muni d'un objectif 10 × et d'un condensateur de Abbe à deux lentilles, sans oculaire. Le spectrogramme est projeté sur le plan de la fente agrandi 50 fois à travers un prisme et un miroir de renvoi. Sous la fente se trouve une cellule photovoltaïque opposée à une deuxième qui recueille un flux constant provenant de la même source lumineuse (constituée par une lampe normale pour microscopie alimentée directement sur courant alternatif) qui peut être diaphragmée de façon à fournir un courant d'opposition correspondant à celui de la largeur fondamentale choisie. Comme indicateur de zéro, il a été employé un galvanomètre d'une grande sensibilité. La fente variable a été réalisée au moyen de deux lamelles, dont l'une est mobile et réglable par une vis à pas fin. Son ouverture est indiquée par un micromètre centésimal de 10 mm de course. L'ensemble fente-cellule peut se déplacer par rapport à l'image, de facon à permettre un centrage précis de la raie. Tout l'ensemble, enfin, peut tourner par rapport à l'image même, de manière à

garantir le parallélisme entre la raie et la fente. Il faut avoir soin que le champ de projection qui touche les déplacements de la fente soit éclairé par un flux uniforme. Comme il ressort du schéma, en remplaçant le diaphragme mobile M par une deuxième fente variable, le photomètre pourrait servir également pour des mesures densitométriques.

Pour rapporter la fondamentale à une valeur constante (le fond des plaques peut être différent

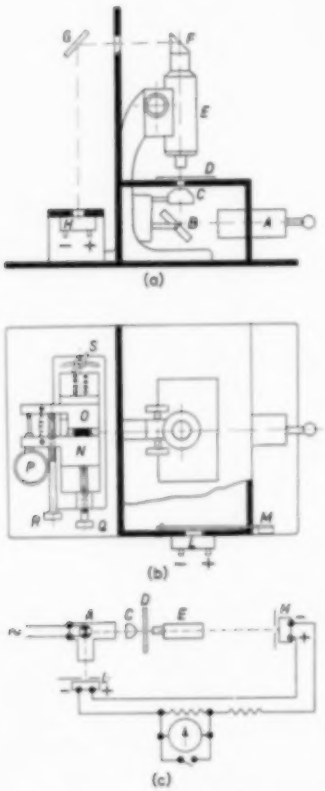

Fig. 2. Photomètre et schéma électrique.

A–Lampe	*M*–Diaphragme de la contre-cellule
B–Miroir	*N*–Lamelle fixe
C–Condenseur	*O*–Lamelle mobile
D–Plaque	*P*–Micromètre
E–Microscope	*Q*–Commande de translation
F–Prisme	*R*–Commande largeur de la fente
G–Miroir	*S*–Commande de rotation
H–Cellule photo-électrique	
L–Contre-cellule	

et non uniforme) il a été adopté le principe d'en fixer la valeur *à vide*, c'est-à-dire sans l'interposition de la plaque, en ayant soin, naturellement, que le microscope se trouve déjà dans la position de mise au point. En pratique, on met l'image au point, on enlève ensuite la plaque, on élargit la fente jusqu'à la valeur de la fondamentale et on règle le contre-courant jusqu'à ce que le galvanomètre marque zéro.

VOL. 10 1957/5

Il est indispensable de contrôler de temps en temps le zéro, parce que, surtout dans la phase de mise en train, le courant de la contre-cellule peut changer sous l'effet des variations de température déterminées par la lampe; les variations de la largeur effective dues à ce phénomène ne sont pas, toutefois, supérieures à $\pm$ 0·02 mm. Ces mesures sont effectuées dans un local dont la lumière est atténuée afin que la cellule n'en ressente pas l'influence lorsque la fente est ouverte au maximum. En mesurant, dans ces conditions, une raie dans ses différentes parties, les valeurs se reproduisent avec des écarts de $\pm$0·03 mm qui ne sont pas à attribuer seulement au photomètre, mais aussi aux irrégularités du négatif ou à des imperfections de la fente du spectrographe.

4.2. *Conditions expérimentales d'exécution des spectrogrammes*

Il a été employé des électrodes de graphite de 5 mm de diamètre avec cratère de 2 mm de diamètre et de 5 mm de profondeur, ainsi que des contre-électrodes plates du même type et de mêmes dimensions; le remplissage du cratère a été fait en plongeant à plusieurs reprises l'électrode dans le mélange des poudres contenu dans un pèse-filtre et en pressant sur le fond à chaque remplissage.

L'appareillage employé consistait en un spectrographe Q 18 Zeiss avec mise au point pour 3013 Å, un diaphragme intermédiaire rectangulaire de 3·2 mm et une fente de la largeur de 0·02 mm. Comme source d'énergie on a employé un générateur Feussner avec une capacité de 1330 pF, une tension de 1200 V, une inductance de 0·08 mH, un interrupteur tournant sur le secondaire; la distance des électrodes était de 2 mm, et la durée de la pose de 120 secondes. Le matériel photographique employé était constitué par des plaques Ferrania photomécaniques ultra contraste ortho, développées pendant 5 minutes à 18°C dans un bain de métol-hydroquinone, fixées dans un bain d'hyposulfite-bisulfite de sodium, lavées dans de l'eau courante et séchées à l'air.

4.3. *Mélanges examinés*

On a examiné des mélanges de quantités pesées de différentes substances, homogénéisées dans un mortier. On a employé des produits purs ou techniques, d'une composition correspondant à celle de certains des ingrédients couramment employés dans l'industrie du caoutchouc. Comme standard interne, ou élément de référence, on a adopté l'oxyde cuivreux et comme diluant complémentaire l'oxyde de zinc. Comme unique exception, pour le dosage de quantités croissantes d'oxyde de zinc, on a adopté, comme diluant, l'oxyde de magnésium. Le schéma des concentrations choisies pour une exploration rapide à vaste rayon a été le suivant:

Substance %	Diluant %	Standard %
1	49	50
2·5	47·5	50
5	45	50
10	40	50
25	25	50
50	—	50

Le but de ce travail étant seulement de contrôler l'efficacité de la méthode, on a recherché a étendre la méthode dans le domaine des fortes concentrations plutôt que d'en rechercher la fidélité à concentrations constantes. On a adopté l'excitation par étincelle afin que les spectres soient moins envahis par les bandes, tout en sachant que de cette manière les résultats auraient été moins reproductibles. En effet, l'étincelle, par son action mécanique, projette à l'extérieur une partie de la poudre. Une portion seulement de la poudre restante est excitée et émet des radiations. Une partie seulement de ces radiations (c'est-à-dire celles qui sont émises dans le champ optique du spectrographe) réussit finalement à atteindre et à impressionner la plaque photographique. La quantité de poudre que l'étincelle réussit à projeter à l'extérieur dépend beaucoup des conditions de la plus ou moins grande compression avec lesquelles elle a été introduite dans le cratère. Le spectre est donc plus intense lorsque la poudre n'est pas compacte, c'est-à-dire lorsqu'à la fin de la pose on en trouve une quantité considérable dans la zone qui

entoure les électrodes. Par conséquent, pendant tout le temps de l'exposition, les radiations frappent la plaque d'une manière intermittente en suivant les lois du hasard et l'effet photographique devient la somme des émissions élémentaires se différençiant entre elles par la fréquence et l'intensité de telle sorte que des valeurs globales, même égales, peuvent produire des effets différents à cause des variations de l'exposant p (exposant de Schwarzchild de la formule bien connue:

$$D = f(J.\, t^p)$$

Ces conditions expérimentales, très discutables du fait que pour le même temps d'exposition on a obtenu des intensitiés de spectre variant de 1 à 3, ont été reconnues comme étant les plus indiquées pour vérifier, avec le plus de facilité et d'évidence, l'effet des méthodes d'évaluation basées sur les propriétés du nouveau paramètre.

4.4. *Methodes d'evaluation des resultats*

On a appliqué le procédé quantitatif de la confrontation interne. Pour exprimer les résultats, on a employé, selon les modalités indiquées dans les travaux d'Intonti, les deux méthodes différentes suivantes:

Methode lineaire. On porte en ordonnée, les différences de largeurs effectives

$$L_1 - L_2$$

où L_1 est égal à la largeur effective de l'élément à doser, et L_2 correspond à la largeur effective de l'élément de référence (standard interne).

Methode logarithmique. On porte en ordonnées, les différences des logarithmes des largeurs effectives, c'est-à-dire le logarithme des rapports:

$$\log L_1 - \log L_2 = \log \frac{L_1}{L_2}$$

Dans les deux méthodes on porte toujours en abscisses le logarithme de la concentration.

Pour examiner l'effet dans la vaste gamme de concentrations explorées, comprises entre 2 et 100%, il a été nécessaire d'exclure les éléments à spectre complexe, à cause de la faible dispersion du spectrographe. Les exemples indiqués se rapportent par conséquent seulement aux éléments pauvres en raies. C'est pour la même raison qu'il a fallu adopter une fondamentale de 0·60 mm à la place de celle de 2 ou 3 mm qui, sur la base de la formule proposée par Intonti, aurait été la plus indiquée. En outre, on a fait coïncider le zéro du micromètre et la valeur pour le flux à vide, c'est-à-dire sans interposition de plaque sur le trajet lumineux, c'est pourquoi, contrairement au principe suivi par Intonti, la valeur de la fondamentale n'est pas comprise dans les nombres indiqués. Pour plus de simplicité, toutes les valeurs relatives aux largeurs effectives ont été indiquées en centièmes de millimètre dans les tables.

4.5. *Résultats des mesures*

Lorsqu'en répétant les expériences de Intonti l'on a tenté d'employer un couple analytique, formé par une seule raie de l'élément et une seule raie du standard, les résultats se distribuaient en des diagrammes dispersés sur une large bande qui, en dehors d'une plus grande extension des concentrations, ne différait guère de celle que l'on aurait obtenue avec la méthode densitométrique classique. Les avantages de la méthode se sont révélés lorsqu'au cours de la recherche des raies les plus

VOL.
10
1957/5

appropriées, on a examiné les spectres d'un point de vue plus général, en mesurant toutes les raies suffisamment intenses d'un élément sur un certain nombre de spectres répétés dans les mêmes conditions. Par suite de la reproductibilité réduite déjà mentionée, les valeurs respectives, au lieu de coïncider, oscillaient entre des limites d'une certaine ampleur. Ces valeurs ont été placées en diagramme (Fig. 3) sans se préoccuper de donner un ordre quelconque aux intensitiés ou aux

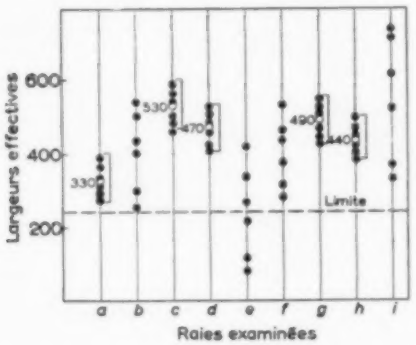

Fig. 3. Dispersion des valeurs des largeurs effectives pour un groupe de raies.

longueurs d'onde; on a immédiatement remarqué que les raies se partageaient en deux groupes, dans l'un la dispersion était à peu près du même ordre, tandis que dans l'autre elle était plus grande et d'une ampleur différente. En traçant sur le diagramme le niveau correspondant à la densité 1·0 du négatif, comme limite inférieure de validité probable, on a observé que le groupe à dispersion constante était celui des raies qui se trouvaient toujours au-dessus de ce niveau, tandis que les autres se trouvaient indifféremment au-dessus ou au-dessous; les raies utiles semblaient donc se trouver dans le groupe des raies les plus intenses. Une fois le groupe à dispersion plus grande éliminé, on a calculé pour les autres la moyenne arithmétique des valeurs, qui, dans l'exemple indiqué, correspond aux nombres cités à côté. Ces valeurs de largeurs effectives moyennes, disposées en ordre croissant et traduites en valeurs proportionnelles par rapport à la valeur plus haute (pour permettre la comparaison avec d'autres éléments), ont permis, en les disposant en abscisses, de vérifier si le rapport entre les largeurs effectives des raies choisies se maintenait proportionnel dans chacun des spectres.

Comme il ressort de la Fig. 4, on observe que, tandis que l'alignement des valeurs reste toujours constant, la pente des droites subit des variations. On peut en déduire que les rapports entre les largeurs effectives de certaines raies d'un même spectre maintiennent leur valeur même en cas de variation des conditions d'exposition. Dans l'exemple mis en diagramme, on a indiqué les valeurs relatives à 4 spectres seulement, pour éviter des superpositions inutiles nuisibles à la clarté. Il y a lieu de penser que les causes de variation de la pente des droites peuvent être multiples et ne sont pas à attribuer seulement à la variabilité de la

caractéristique de l'émulsion photographique. On a observé, en effet, (Fig. 5) que les pentes de deux éléments différents (celui de l'élément dosé et celui de référence) peuvent avoir des valeurs différentes, tandis qu'elles devraient être du même ordre, si elles étaient causées par une variation des caractéristiques du

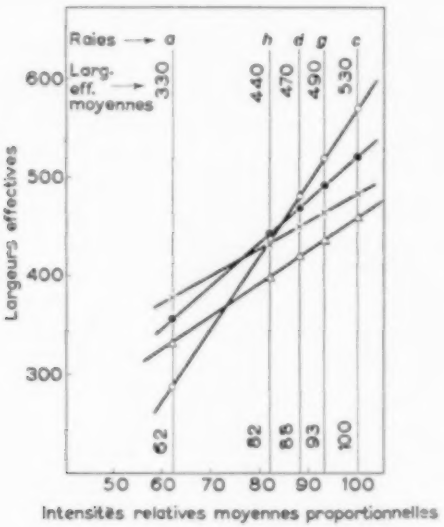

Fig. 4. Caracteres de proportionlité entre les largeurs effectives.

négatif seulement. A la suite de recherches ultérieures il semble qu'elles soient dûes en partie à la fluctuation systématique des intensités relatives aux raies des spectres I et II, causées par des variations de tension au générateur, et en partie à la fondamentale trop restreinte, pour laquelle on ne mesure qu'une portion du profil de la raie élargie. Ce profil semble être indépendant de celui propre à la raie spectrale, cependant il varie avec la marche du phénomène d'expansion de la raie. La nécessité de s'écarter des normes établies par Intonti détermina donc un défaut dans la mesure. On a négligé pour le moment la variation de la pente et l'on a fixé, par contre, l'attention sur l'alignement constant des points, qui pouvait être l'indice d'un caractère d'homogénéité relative. Cette faculté de répétition des alignements est subordonnée naturellement à un choix judicieux des raies. Le cuivre (standard) parmi les éléments qui ont été examinés, se trouve dans des conditions avantageuses, du fait qu'il est plus riche en raies, pourtant, pour les autres éléments aussi il s'est produit la même situation, quoique le nombre plus petit de raies disponibles ait imposé de faire un choix moins rigoureux.

On donne à présent un exemple expérimental obtenu en choisisant, parmi une cinquantaine de cas examinés, les moins reproductibles et les plus significatifs. Dans les diagrammes de la Fig. 5 déjà mentionnée, sont indiquées les valeurs

relevées sur le standard et sur le zinc aux concentrations de 20 et de 50%,* répétées sur des différentes plaques avec des différentes fentes du spectrographe, de façon à augmenter encore les conditions de dispersion. On voit toujours les alignements désormais bien connus, les variations des valeurs absolues et celles des paramètres angulaires.

Calcul numérique et représentation graphique
dans un exemple d'application des moyennes

Plaque *A* = fente spectrographe 0·015mm
Plaque *B* = fente spectrographe 0·025mm

		Cu_2O						ZnO						Différences entre les moyennes Zn—Cu
		Raies					Moyennes	Raies					Moyennes	
λ		2276	2242	2246	2373	2347		2502	2557	3282	3302	3345		
Intensités relat. moyennes proport.		37	48	54	84	100		44	60	73	85	100		
ZnO 50%	Plaque *A*	232	303	344	514	625	403	206	299	304	493	469	354	−49
	Plaque *B*	254	321	361	525	645	421	210	286	307	495	555	371	−50
ZnO 20%	Plaque *A*	169	234	262	428	505	319	26	56	117	173	238	122	−197
	Plaque *B*	293	380	418	700	891	536	172	250	383	428	459	352	−184

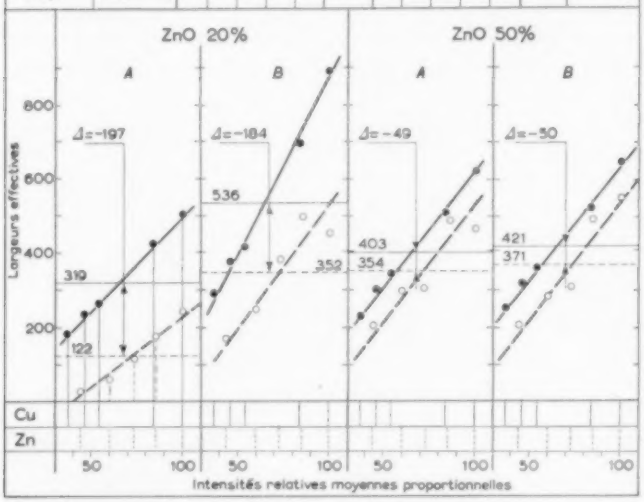

Fig. 5.

Dans ce cas aussi, de même que dans l'exemple déjà illustré dans la Fig. 4, on a porté en abscisses les intensités relatives moyennes proportionelles, déduites de la moyenne des largeurs effectives de 20 spectres.

On a remarqué à ce point que si la représentation graphique n'offrait pas une grande possibilité de se procurer des éléments de jugement, par contre le calcul des moyennes arithmétiques menait à des résultats très concordants. Ce fait,

* Dans les figures 5 et 6 la substance est référée au mélange avec le diluant, hormis le standard.

Table 1. Schéma des opérations de calcul.

Standard						Élément								Différences			
Largeurs effectives					Moyen	Largeurs effectives				Moyennes							
										1	2	3	4				
Raies					$\frac{\sum_1^5 X}{5}$	Raies				Y_1	$\frac{\sum_1^2 Y}{2}$	$\frac{\sum_1^3 Y}{3}$	$\frac{\sum_1^4 Y}{4}$	Δ_1	Δ_2	Δ_3	Δ_4
a	b	c	d	e		a_1	b_1	c_1	d_1								
X_1	X_2	X_3	X_4	X_5	X_m	Y_1	Y_2	Y_3	Y_4	Y_{m_1}	Y_{m_2}	Y_{m_3}	Y_{m_4}	$Y_{m_1} - X_m$	$Y_{m_2} - X_m$	$Y_{m_3} - X_m$	$Y_{m_4} - X_m$

VOL. 10
1957/5

qui s'est constamment répété dans les nombreux cas examinés en appliquant les deux systèmes, a conduit à adopter la méthode de calcul des moyennes, en éliminant la représentation graphique, dont l'utilité se borne seulement au choix des raies.

Dans le but d'obtenir une confirmation supplémentaire de la validité de la méthode, on a tracé une série de diagrammes, lesquels ont mis en évidence l'effet

Table 2. Longueurs d'onde des raies et formules employées pour le calcul des valeurs mis en diagramme dans la Fig. 6.

Standard Cu_2O		Substance					Formules	
Raies	λ in Å		Raies, et λ in Å				Standard	$\frac{a+b+c+d+e}{5}$
			a_1	b_1	c_1	d_1		
a	2276	ZnO	3302	3345	2502	2557	Substance	Colonne
b	2242	MgO	2852	2779	2928	2936		1 a_1
c	2246	$CaCO_3$	3933	3968	4226	3158		2 $\frac{a_1+b_1}{2}$
d	3273	Al (Caolin)	3082	3092	3944	3961		3 $\frac{a_1+b_1+c_1}{3}$
e	3247	Si (Caolin)	2514	2516	2524	2881		4 $\frac{a_1+b_1+c_1+d_1}{4}$

de correction que l'on obtient en augmentant le nombre des raies mesurées. Dans ce cas aussi le nombre des combinaisons a été limité par simplicité, en employant toujours la moyenne de 5 raies pour le standard. On améliore déjà de ce fait les conditions du premier diagramme. Dans la Table 1 est indiqué le schéma de calcul adopté. La Table 2 donne les longueurs d'onde et les formules de calcul employées pour obtenir les courbes d'étalonnage de la Fig. 6. On voit clairement qu'en augmentant le nombre des raies introduites dans le calcul, les résultats tendent à contenir les points expérimentaux dans une bande toujours plus étroite. Si l'on tient compte des conditions d'essai adoptées, un certain optimisme est permis quant aux résultats qui pourraient être atteints si, avec des dispositions appropriées, on créait des conditions plus rationnelles. En dehors de cette caractéristique générale d'homogénéité des raies, les diagrammes présentent d'autres détails de grand intérêt.

En se référant aux courbes caractéristiques de la Fig. 2 et aux diagrammes de la Fig. 6, on remarque pour le zinc et le magnésium que la marche a été linéaire dans toute l'étendue des concentrations; ce qui fait penser que le phénomène enregistré se soit produit entièrement dans la deuxième partie de la courbe, qui semble présenter pour ces deux éléments une extension remarquable.

Pour le calcium, bien que l'on ait agi dans des conditions d'excitation analogue, il est évident que le phénomène se produit décidément dans la troisième partie, en effet, le passage aux logarithmes en rectifie la fonction.

Pour l'aluminium, par contre, étant donné que les raies sont moins intenses, on se trouverait dans la zone de transition entre la première et la deuxième partie de la courbe. La tendance vers la ligne droite dans la partie inférieure, en échelle logarithmique, à laquelle correspond une certaine tendance à la dispersion, en échelle linéaire, est, en effet, trés caractéristique.

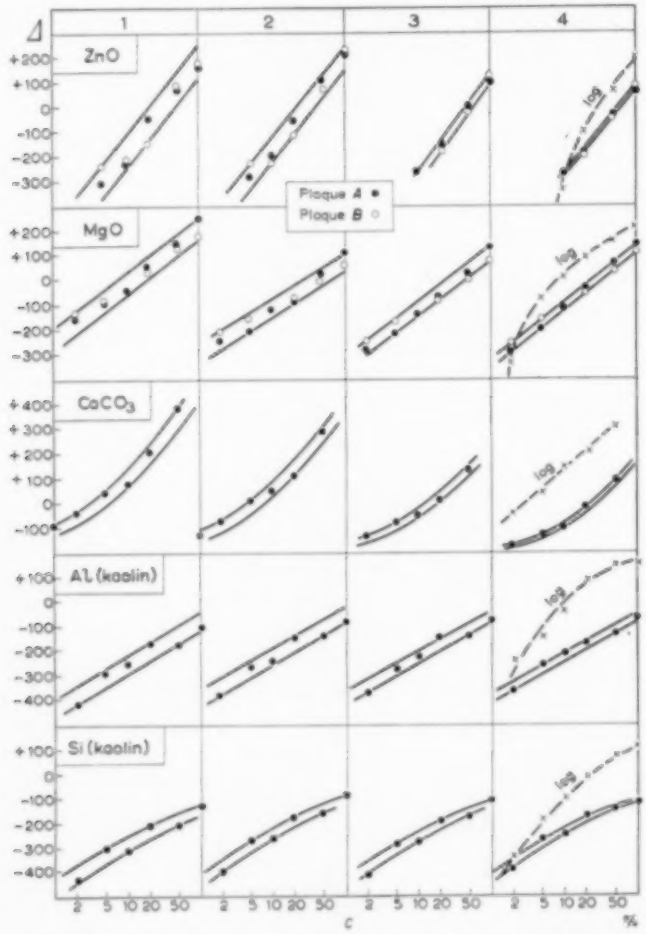

Fig. 6. Effet correctif de moyennes pour les courbes d'étalonnage des différents éléments.

Le silicium, enfin, donne lieu à d'étranges résultats; plus dispersé en échelle linéaire, et mieux aligné en échelle logarithmique, avec laquelle cependant il engendre une courbe à ample rayon que l'on ne saurait attribuer à une zone précise. On dirait que sa courbe caractéristique a une forme différente de celle des autres éléments avec de plus amples raccords et des zones moins définies.

Ces différentes manières de se comporter, indiqueraient que les résultats ne

sont pas dûs à des circonstances fortuites, mais qu'ils sont bien en liaison avec des caractéristiques particulières du paramètre qui, comme on l'a déja dit, ne garde pas la même loi dans toute son étendue et confirmerait, en outre, l'utilité d'effectuer les évaluations au moyen de groupes de raies.

5. Conclusions

Dans le rapide tour d'horizon, qui a fait l'objet de ce mémoire et dont le but était la seule vérification de caractères d'utilité éventuels du nouveau paramètre dans le domaine des matériaux non métalliques, on a vu que malgré les conditions rudimentaires des essais et malgré l'élaboration simpliste, l'emploi du paramètre de la largeur effective, non seulement a fourni une possibilité de reproduction des valeurs qui ne peut être obtenue avec les mesures densitométriques, mais a permis également d'entrevoir de nouvelles possibilités dérivées de l'étude complète et générale du spectre des éléments.

Ces adaptations générales et leur étude systématique auront certainement une très grande importance dans la recherche de méthodes rationnelles et seront utiles à l'étude des perturbations réciproques, c'est-à-dire des phénomènes d'exaltation et d'atténuation [10, 11.]

Il est donc permis d'espérer que bien des préventions au sujet de l'intérêt que l'analyse spectrographique peut présenter dans son application à des matériaux non métalliques pourront bientôt tomber, grâce à l'aide du paramètre étudié par J. Junkes, dont l'adoption pourra certainement donner à la spectrographie en général un développement imprévu.

Nous exprimons nos sincères remerciements à MM. les Pères J. Junkes S. J. et E. W. Salpeter S. J. ainsi qu'à M. le professeur R. Intonti pour l'intérêt bienveillant qu'ils ont montré pour cet ouvrage.

OL.
10
7/58

Sommaire

Après avoir exposé les difficultés d'effectuer des analyses quantitatives sur des matériaux en poudre, on décrit la méthode suivie dans les mesures et le photomètre utilisé. Dans les expériences, il a été adopté le principe de doser les éléments en mesurant un groupe de raies, au lieu d'une seule. Les résultats mettent en évidence quelques caractéristiques du nouveau paramètre et son importance dans l'analyse des cendres, spécialement en ce qui concerne certains ingrédients employés dans l'industrie du caoutchouc.

Bibliographie

[1] Gazzi V. *Spettroscopia applicata all'analisi chimica.* Zuffi Bologna, 1944.
[2] Nachtrieb N. H. *Principles and Practice of Spectrochemical Analysis.* McGraw-Hill, New York, 1950.
[3] Harrison G. R., Lord R. C., et Loofbourow I. R. *Practical Spectroscopy.* Prentice-Hall, New York, 1954.
[4] Junkes J. et Salpeter E. W. *Spectrochim. Acta* 1955 **7** 60–63.
[5] Junkes J. et Salpeter E. W. *Metallurgia (Ital.)* 1 suppl. 23–29 1956 (IV Seminario Spettrochimico A.I.M. 1955).
[6] Junkes J. et Salpeter E. W. VI *Colloquium Spectroscopicum Internationale.* Amsterdam, 1956.

[7] Intonti R. *Metallurgia* (*Ital.*) 1 suppl. 31–34 1956 (IV Seminario Spettrochimico A.I.M. 1955).
[8] Junkes J. *V Seminario Spettrochimico A.I.M.* 1956.
[9] Intonti R., Pfundt H., et Lais A. *V Seminario Spettrochimico A.I.M.* 1956.
[10] Pierucci M. VI *Colloquium Spectroscopicum Internationale.* Amsterdam, 1956; *V Seminario Spettrochimico A.I.M.* 1956.
[11] Gazzi V. VI *Colloquium Spectroscopicum Internationale.* Amsterdam, 1956; *V Seminario Spettrochimico A.I.M.* 1956.

VOL.
10
1957/5

Spectrochimica Acta, 1957, Vol. 10, pp. 99 to 104. Pergamon Press Ltd., London

Zur Ausleuchtung von Spektrographen durch Zwischenabbildung der Lichtquelle

K. D. Mielenz
Feinmechanisch-optische Werkstätten R. Fuess, Berlin-Steglitz

(*Received 5 April* 1957)

Abstract—Various equipments for the intermediate projection of the light source, and especially their ability to homogenize the spectrum, are discussed. Good homogeneity over a large wavelength range with a fully illuminated spectrograph is achieved, if lens I is achromatic. An achromatic intermediate projection is described which can be easily adapted to various electrode distances.

1. Eigenschaften der Zwischenabbildungen

Den üblichen Strahlengang zeigt Abb. 1(a). Außer einem an frei zugänglicher Stelle bequem abblendbaren Zwischenbild Y' der Lichtquelle Y soll hierbei in der Spektrographenapertur ein zweites Lichtquellenbild Y'' so entstehen, daß jeder Punkt jeder Spektrallinie von jedem Punkt der Lichtquelle beleuchtet wird, die Linien also auch durch eine inhomogene Lichtquelle über ihre ganze Länge gleichmäßig geschwärzt werden.

Eine vollständige Ausnutzung der Lichtstärke und der Auflösung des Spektrographen wird bei voller Ausleuchtung der Aperturblende erreicht. Die Voraussetzung hierzu, eine ruhig brennende Entladung, ist in der spektrochemischen Praxis vielfach gegeben, z.B. bei Stahlanalysen. Bei tanzender Lichtquelle dagegen, etwa bei Leichtmetallanalysen, soll die Apertur jede Bewegung der Lichtquelle auffangen. Anderenfalls sind Verfälschungen der Intensitätsverhältnisse im Spektrum und hierduch Analysenfehler möglich [1]. Hier muß auf die volle Ausleuchtung, und damit auf die volle optische Leistung des Spektrographen verzichtet werden. Eine Abhilfe dieses Übelstandes ist nach Preuss durch Verwendung von Rasterlinsen [1, 2] möglich, doch sind derartige Linsen aus Quarz bislang nicht erhältlich.

Die Abstände und Durchmesser der Zwischenabbildungslinsen ergeben sich elementar aus Abb. 1(a). Insbesondere findet man bei voller Ausleuchtung für den Aperturwinkel der Linse I

$$\frac{h}{a} = \frac{Y''}{Y}\frac{L}{f} \tag{1}$$

(Bezeichnungen s. Abb. 1(a). Je vollständiger die Ausleuchtung ist, je mehr also Y'' sich dem Wert H nähert, desto "kurzbrennweitiger" wird die Zwischenabbildung,* desto größer wird nach (1) aber auch das erforderliche Öffnungsverhältnis der Linse I. Es ist durch den Ausleuchtungsgrad, durch die Größe der Lichtquelle und

* d.h.: desto geringer wird der Abstand Funkenstativ-Spalt.

den Spektrographen unveränderlich vorgegeben und kann auch durch Abstands-oder Brennweitenänderungen nicht mehr beeinflußt werden. Ähnliches gilt für die anderen Linsen, sodaß also mit Festlegung der Brennweiten und Abstände keinerlei Freiheiten hinsichtlich einer Variation des Ausleuchtungsgrades oder des Elektrodenabstandes mehr bestehen.

Die von Nordmeyer beschriebene feldlinsenfreie Zwischenabbildung nach

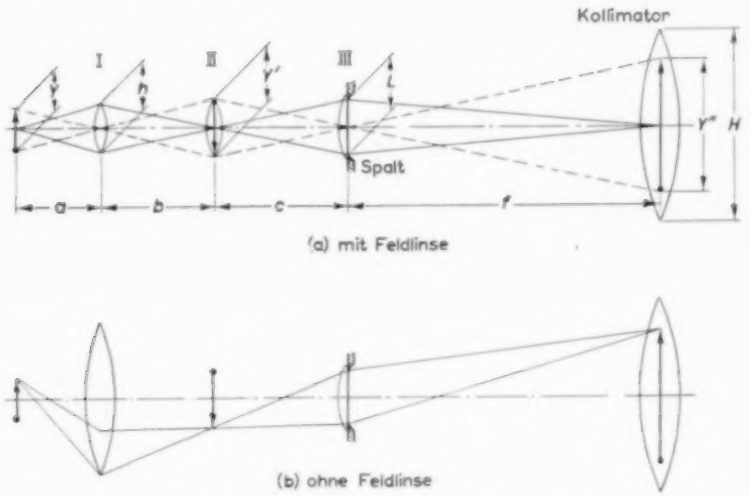

Abb. 1. Zwischenabbildungen mit und ohne Feldlinse.

Twyman [3] vermeidet diesen Nachteil. Gemäß Abb. 1 (b). entfällt bei ihr die Kopplung der Strahlengänge vor und hinter dem Zwischenbild, sodaß es einfach durch Verschiebung des Funkenstativs und der Linse I möglich wird, mit jeder beliebigen Lichtquelle* jeden beliebigen Ausleuchtungsgrad zu erzielen. Nachteilig ist das erforderliche hohe Öffnungsverhältnis der Linse I†, das sich praktisch nur wie bei Nordmeyer mit einem Hohlspiegel realisieren läßt. Der durch den Spiegel geknickte Strahlengang ist aber schwierig zu justieren, erfordert diffizile Verstellmechanismen und kompliziert das Funkenstativ wie den Gesamtaufbau. Wie sich noch zeigen wird, ist die Achromasie der Spiegelanordnung ihr besonderer Vorzug.

2. Die Homogenisierung des Spektrums durch verschiedene Zwischenabbildungen

Hierin erweisen sich einfache, d.h. aus unkorrigierten Linsen bestehende Anordnungen als unzulänglich:

In Abb. 2 sind die Längsprofile von Spektrallinien wiedergegeben, die bei voller Spektrographen-Spalthöhe mit einer einfachen kurzbrennweitigen Zwischenabbildung (volle Ausleuchtung bei 2,5 mm Elektrodenabstand) bei Einstellung der

* Oberhalb einer Mindesthöhe Y_{min}.

† Für Quarzspektrograph Fuess 110 M für $Y_{min} = 2{,}5$ mm etwa 1 : 0,9 (85 mm ϕ bei 80 mm Brennweite).

Linsenabstände auf verschiedene Wellenlängen aufgenommen wurden.* Die Homogenität des Spektrums befriedigt nur für die gerade eingestellten Wellenlängen; in anderen Spektralbereichen genügt schon die normale Inhomogenität des Funkens, um krasse Linieninhomogenitäten zu erzeugen.

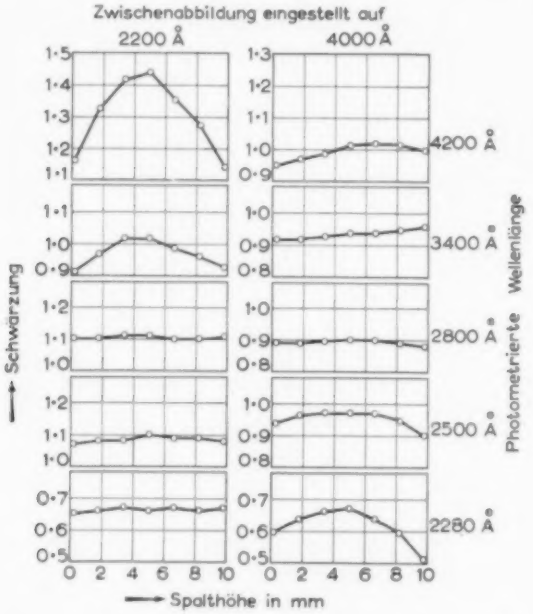

Abb. 2. Linienlängsprofile bei einfacher, nichtachromatischer Zwischenabbildung, volle Kollimator-ausleuchtung.

Zum Vergleich wurde der Versuch mit einer langbrennweitigen Zwischenabbildung (1/3-Ausleuchtung bei 2,5 mm Elektrodenabstand) wiederholt. Das Ergebnis läßt wohl eine bessere Homogenisierung erkennen, doch waren im Vergleich zum ersten Versuch zur Erzielung gleicher Schwärzungen unter sonst gleichen Bedingungen erheblich längere Belichtungszeiten erforderlich.

Offensichtlich erkauft die langbrennweitige Anordnung die gleichmäßigeren Linienprofile, indem sie mit geringeren Öffnungsverhältnissen der Zwischenabbildungslinsen die optische Leistung des Spektrographen nur zum Teil ausnutzt. Dieser Kompromiß ist in Anbetracht des bei Spektrographen ohnehin schlechten Wirkungsgrades der Lichtausnutzung [1] recht unbefriedigend. Es wurde daher versucht, die kurzbrennweitige Zwischenabbildung so abzuändern, daß sie trotz voller Ausleuchtung und demzufolge großer Aperturen das Spektrum gut homogenisiert. Die eigentliche Ursache der Inhomogenitäten in Abb. 2 wurde durch Versuche ermittelt—immer bei voller Ausleuchtung:

(a) *Ohne Zwischenabbildung*, also bei direkter Abbildung der Lichtquelle in der

* Versuchsbedingungen: Fe-Funken; Quarzspektrograph Fuess 110 M, Spalt 30 μ × 10 mm; Spektrenauswertegerät Fuess 118 S, photometrierte Fläche 15 μ × 0,5 mm an 7 verschiedenen Stellen der Linie.

Apertur durch Linse III ergab sich ein gut homogenes Spektrum. Also liegt kein Einfluß der Linse III vor-offenbar wegen einer Lochkammerwirkung des Spaltes.*

(b) Bei *Fortlassung der Feldlinse* II wie auch bei sphärischer Korrektur der Linse I zeigte sich kein Unterschied zu Abb. 2. Damit scheidet auch die Möglichkeit aus, daß der Fehler auf sphärische Aberrationen der Linse I zurückgeht.†

(c) *Ersatz der Linse* I *durch einen Hohlspiegel:* Die feldlinsenlose Anordnung gemäß Abb. 1(b) ergab bei Verwendung eines zweiteiligen Quarzkondensors I, wie nach (b) nicht anders zu erwarten war, ebenso schlechte Linienlängsprofile wie in Abb. 2. Ersetzt man aber den Kondensor I durch einen Hohlspiegel,so erhält man sofort im ganzen Spektrum völlig homogene Linien trotz der schlechten Abbildungseigenschaften des schief beaufschlagten Spiegels vom Öffnungsverhältnis 1 : 0,9.

Damit ist eindeutig der *Farbfehler der Linse* I (der ja gleichfalls mit dem Öffnungsverhältnis wächst) als Fehlerursache erkannt. Infolge der *chromatischen Fokusdifferenzen* entstehen die Lichtquellenbilder Y'' im Spektrographen für verschiedene Wellenlängen an verschiedenen Stellen, und es wird nur derjenige Wellenlängenbereich homogenisiert, für den Y'' am optimalen Ort liegt.

3. Beschreibung einer neuen achromatischen Zwischenabbildung

Die vorstehenden Überlegungen und Ergebnisse legen es nahe, die kurzbrennweitige Anordnung mit Feldlinse beizubehalten, Linse I aber zu achromatisieren. Wenn weiterhin Linse I mit verschiedenen Brennweiten $f_1, f_2, \ldots$ (für volle Ausleuchtung bei Elektrodenabständen $Y_1, Y_2, \ldots$) vorgesehen wird, so werden auch hierbei Freiheiten hinsichtlich des Elektrodenabstandes und des Ausleuchtungsgrades gewonnen. Hält man die Gleichungen

$$\frac{a_1}{Y_1} = \frac{a_2}{Y_2} = \ldots = \frac{fh}{LY''} \tag{2}$$

ein, so können die Linsen II und III wie auch die Abstände aller drei Linsen ungeändert bleiben, sodaß bei einer Änderung der Elektrodenabstände nur die Achromate auszuwechseln und die Abstände $a_1, a_2, \ldots$ durch Verschiebung des Funkenstativs zu ändern sind. Aus Gl. (2) lassen sich unter Zuhilfenahme der Abb. 1(a) alle Daten der gesuchten Zwischenabbildung herleiten.

Achromatische Zwischenabbildungen der vorbeschriebenen Art wurden für die Quarzspektrographen Fuess 100 M und 110 H für volle Ausleuchtung durch die Elektrodenabstände $Y_1 = 2{,}5$ und $Y_2 = 5$ mm berechnet und hergestellt. Zu ihrer Prüfung wurden die unter (2) beschriebenen Versuche wiederholt, jedoch in erheblich verschärfter Form, indem jetzt gemäß Abb. 3 eine Entladung mit einer künstlich erzeugten krassen Inhomogenität benutzt wurde. Diese Entladung ergibt bei unvollkommenen Zwischenabbildungen ein gemischtes Al-Cu-Spektrum mit

* In Übereinstimmung hiermit ist die Beobachtung, daß man bei der Einstellung der Zwischenabbildung auf verschiedene Wellenlängen eine gleich gute Homogenisierung erzielt, wenn man—statt alle Glieder zu verschieben—nur die Lage der Lichtquelle verändert und es bei den übrigen Abständen, insbesondere bei (c), bei einer mittleren Einstellung bewenden läßt.

† Linse I könnte infolge des sphärischen Fehlers ein Strahler mit unterschiedlicher Leuchtdichte in den verschiedenen Linsenzonen sein. Diese zonalen Helligkeitsunterschiede würden dann durch die Feldlinse getreu auf dem Spalt und damit im Spektrum wiedergegeben werden.

VOL. 10 1957/5

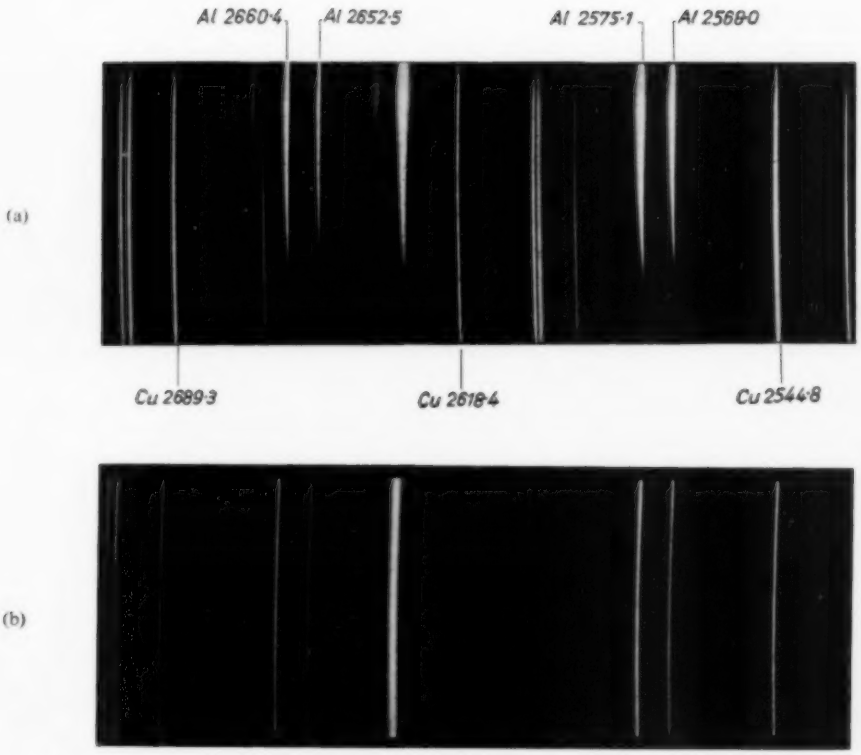

ABB. 4. Ausschnitt des Spektrums der Funkenstrecke nach Abb. 3, (a) nichtachromatische, (b) achromatische Zwischenabbildung. (Quarzspektrograph mittlerer Dispersion FUESS 110 M.)

VOL.
10
1957/5

total deformierten "Linien" (Abb. 4). Die mit den achromatischen Zwischenabbildungen erzeugten Linien sind dagegen nach den Meßbeispielen in Abb. 5 selbst bei exakter Photometrierung im ganzen Spektrum völlig gleichmäßig geschwärzt.

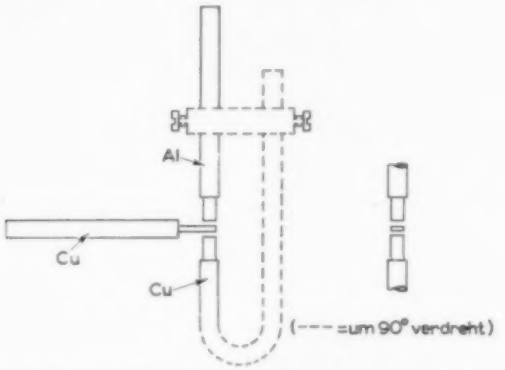

Abb. 3. Funkenstrecke mit künstlicher Inhomogenität.

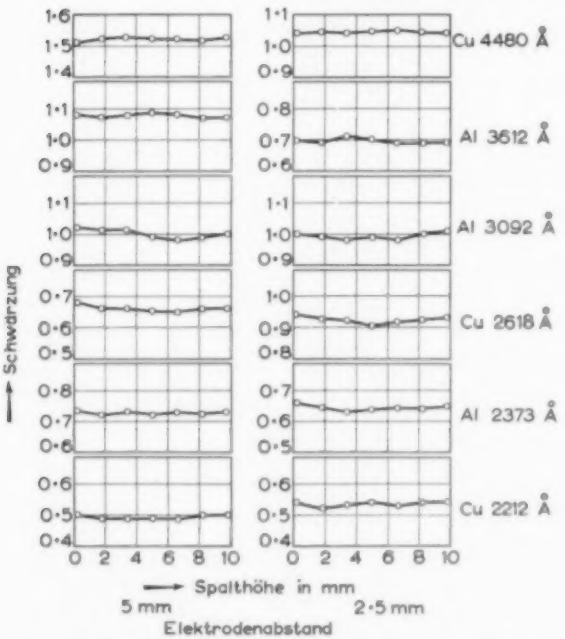

Abb. 5. Linienlängsprofile im Spektrum der Funkenstrecke nach Abb. 3 bei achromatischer Zwischenabbildung, für Quarzspektrograph mittlerer Dispersion Fuess 110 M bei voller Kollimatorausleuchtung mit 2,5 und 5 mm Elektrodenabstand.

4. Zusammenfassung

Verschiedene Anordnungen zur Zwischenabbildung der Lichtquelle werden diskutiert und insbesondere auf ihre Fähigkeit, das Spektrum zu homogensieren,

untersucht. Voraussetzung für gute Homogenität über einen größeren Wellenlängenbereich bei voller Auslechtung des Spektrographen ist Achromasie der Linse 1. Eine achromatische Zwischenabbildung, die auf einfache Weise an verschiedene Elektrodeabstände angepaßt werden kann, wird beschrieben.

Literatur

[1] Mielenz K. D. *Optik*. Im Druck.
[2] Preuss E. *Heidelberg. Beitr. Min.* 1954 **4** 163.
[3] Nordmeyer M. *Spectrochim. Acta* 1955 **7** 128.

VOL.
10
1957/5

Spectrochimica Acta, 1957, Vol. 10, pp. 105 to 109. Pergamon Press Ltd., London

Characteristic infra-red absorption frequencies of substituted naphthalenes

J. G. Hawkins,* E. R. Ward, and D. H. Whiffen
The Chemistry Department, The College of Technology, Leicester;
The Chemistry Department, The University, Birmingham 15

(*Received* 24 *May* 1957)

Abstract—Some characteristic infra-red absorption frequencies of substituted naphthalenes are tabulated in relation to the substitution pattern of the separate rings. The tables have been compiled from the spectra of 170 compounds comprising 80 from the authors' files together with almost the entire range of such spectra so far published. They include predominantly in-plane and out-of-plane carbon-hydrogen deformation frequencies.

The infra-red spectra of a number of nitronaphthalenes and nitronaphthylamines were measured as a means of identification, of investigating the composition of mixtures of known isomers, and of differentiating mixtures of known isomers from new compounds. The spectra were also examined to see to what extent the infra-red spectra could characterize positions of substitution and so be useful in helping to elucidate the orientation of compounds of uncertain structure. The spectra themselves, obtained with the Nujol mull technique on a Grubb Parsons single-beam spectrometer with a rock-salt prism, have been offered to the Documentation of Molecular Spectroscopy punched card collection through which they will be available. The second object, the characterization of unknown orientations, requires the selection of characteristic absorption patterns for each substitution type and this problem is considered here.

The predominant characteristic infra-red absorption bands for substituted benzenes [1–5] are those of the in-plane and especially the out-of-plane C-H deformations. Interaction between the hydrogens substituted in different rings in naphthalene is likely to be small and characteristic frequencies may be sought for each ring separately. This conclusion is borne out by the work of Cencelj and Hadzi [6], Werner, Kennard, and Rayson [7] and of Luther and Günzler [8] which appeared while the present work was in progress.

The findings are summarized in Tables 1–8. These are compiled from the spectra of the following: 26 alkyl naphthalenes measured at the Laboratories of Trinidad Leaseholds and by Anderson, Smith, and Broomfield [9]; 9 polymethyl naphthalenes recorded by Mosby [10]; 12 nitronaphthols and derivatives reported by Luther and Günzler [8]; 33 polychloronaphthalenes recorded by Cencelj and Hadzi [6]; the set of monohalogeno-naphthalenes given by Ferguson and Werner [14]; 24 nitronaphthalenes, the 2 naphthylamines, 39 nitronaphthylamines and 12 miscellaneous nitro- and halogeno-naphthalenes all measured in the present work. The above list makes up a total of 170 spectra considered here which represent the vast majority of the published spectra of naphthalene compounds.

* Present address: Whiffen and Sons Ltd., Derby Road, Loughborough, Leics.

Table 1. Hydrogen pattern 1:2:3:4 (71 compounds)

Mean value cm^{-1}	751	784	957	1028	1137	1239	1269
Range cm^{-1}	726–770	761–800	944–976	1012–1053	1110–1156	1213–1252	1252–1291
Standard deviation cm^{-1}	±11	±10	±8	±10	±10	±9	±8
Number present	71	65	66	63	62	62	59
Number missing	0	6	5	8	8	7	11
Number overlaid	0	0	0	0	1	2	1
General intensity	*s–vs*	*s*	*m*	*var.*	*w–m*	*var.*	*m–s*

Table 2. Hydrogen pattern 1:2:3 (66 compounds)

Mean value cm^{-1}	748	795	1077	1170	1214
Range cm^{-1}	730–774	776–820	1063–1097	1152–1183	1193–1233
Standard deviation cm^{-1}	±9	±9	±8	±8	±10
Number present	55	57	58	58	62
Number missing	0	1	8	6	2
Number overlaid	11	8	0	2	2
General intensity	*s*	*s*	*w–m*	*var.*	*var.*

Table 3. Hydrogen pattern 1:2:4 (59 compounds)

Mean value cm^{-1}	824	864	901	972	1092	1180
Range cm^{-1}	805–847	846–894	884–922	957–990	1067–1118	1163–1200
Standard deviation cm^{-1}	±12	±10	±10	±9	±12	±10
Number present	59	51	55	51	42	50
Number missing	0	7	4	5	12	5
Number overlaid	0	1	0	3	5	4
General intensity	*vs*	*m-s*	*m–s*	*m*	*m–s*	*var.*

Table 4. Hydrogen pattern 1:2 (19 compounds)

Mean value cm^{-1}	734	810	940	1151	1211
Range cm^{-1}	722–753	799–835	920–961	1144–1158	1200–1220
Standard deviation cm^{-1}	±8	±10	±14	±5	±5
Number present	16	17	17	15	14
Number missing	1	0	1	2	1
Number overlaid	2	2	1	2	4
General intensity	*var.*	*s*	*w*	*m*	*var.*

VOL. 10 1957/5

Table 5. Hydrogen pattern 2:3 (22 compounds)

Mean value cm^{-1}	824	1160	1193	1263
Range cm^{-1}	812–834	1147–1174	1178–1202	1247–1287
Standard deviation cm^{-1}	±6	±7	±6	±11
Number present	22	21	15	16
Number missing	0	1	6	2
Number overlaid	0	0	1	4
General intensity	*s–vs*	*var.*	*m–s*	*var.*

Table 6. Hydrogen pattern 1:3 (30 compounds)

Mean value cm^{-1}	861	888	1102	1204
Range cm^{-1}	843–875	867–905	1085–1118	1190–1217
Standard deviation cm^{-1}	±8	±10	±9	±6
Number present	28	26	22	25
Number missing	1	2	3	2
Number overlaid	1	2	5	3
General intensity	*s*	*m–s*	*var.*	*var.*

Table 7. Hydrogen pattern 1:4 (15 compounds)

Mean value cm^{-1}	878	1144
Range cm^{-1}	870–889	1126–1157
Standard deviation cm^{-1}	±5	±9
Number present	13	12
Number missing	1	1
Number overlaid	1	2
General intensity	*s*	*var.*

Table 8. Hydrogen pattern 1 or 2 (25 compounds together)

Mean value cm^{-1}	881	1059	1206
Range cm^{-1}	858–896	1040–1075	1188–1223
Standard deviation cm^{-1}	±9	±9	±9
Number present	22	16	19
Number missing	1	6	2
Number overlaid	2	3	4
General intensity	*m*	*w*	*m*

Abbreviations; *vs* = very strong, *s* = strong, *m* = medium, *w* = weak, *var.* = variable.

The hydrogen patterns as given in the heading of each table indicate the positions that the hydrogen atoms would occupy if given the lowest numbering, e.g. 1:3:7-trichloronaphthalene is considered under hydrogen patterns 1:3 and 1:2:4, which numbers correspond to the hydrogens at 4:2 and 5:6:8 respectively.

The most useful patterns are those of the strong out-of-plane deformation frequencies [1–8] which are near 750 cm^{-1} for four adjacent hydrogen atoms, near 780 cm^{-1} for three, 820 cm^{-1} for two and 870 cm^{-1} for a lone hydrogen atom.

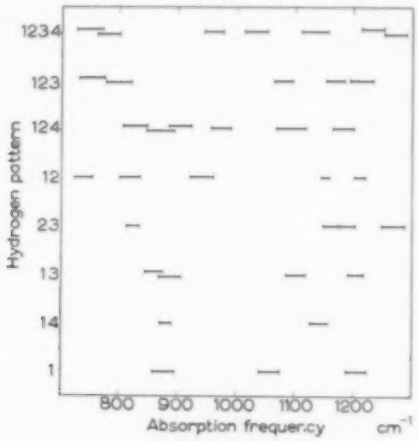

Fig. 1. Chart showing correlation between absorption frequency and position of ring hydrogen atoms in substituted naphthalenes.

The other characteristic frequencies below 1000 cm^{-1} are probably other, weaker out-of-plane hydrogen deformations [4,11] though there is an out-of-plane skeletal vibration likely [12] to be above 700 cm^{-1} somewhat analagous to the benzene frequency at 705 cm^{-1}; with substitution this mode can acquire some C–H deformation character and appear strongly in the infra-red spectra and so account for the extra frequency below 800 cm^{-1} in Tables 1, 2, and 4. The corresponding bands [4] near 697 cm^{-1} for mono-, near 690 cm^{-1} for meta- and near 692 cm^{-1} for 1:3:5-substituted benzenes are all stong in infra-red absorption. The region 1000 to 1200 cm^{-1} contains the majority of the in-plane C–H deformations and again there is a close resemblance to the benzene case, e.g. hydrogen pattern 1:2:3:4 absorb near 1028 and 1137 cm^{-1} and ortho benzenes near 1031 and 1126 cm^{-1} [4]. And again hydrogen pattern 1:2:3 absorbing near 1077 and 1170 cm^{-1} is to be compared with 1:2:3-substituted benzenes near 1073 and 1160 cm^{-1} [4]. The interpretation of the characteristic frequencies above 1200 cm^{-1} is less clear as these may be high in-plane C–H deformations or low C–C stretchings. Above 1300 cm^{-1} there are probably further absorptions which should be considered characteristic but these are not so distinctive of substitution type and are partly obscured in a considerable number of cases by the nitro-group absorptions [13].

It has not been found possible to differentiate between the vibration frequency of single isolated hydrogen atoms situated in the 1- and in the 2-positions. These two patterns unresolved therefore comprise Table 8.

VOL.
10
1957/5

The frequencies considered are displayed in chart form in Fig. 1 which shows that considerable overlapping of ranges occurs and it is unwise to base conclusions about the structure of compounds of unknown orientation on the presence of just one band. The absence of a band may be rather stronger evidence but even this can be unreliable. It is also possible that since approximately half of the compounds from which the tables were compiled contain nitro-groups, this circumstance may have led to average frequencies slightly different from those with other classes of derivative. Nevertheless the tables can be a useful guide as to what spectrum to expect for the corresponding structures.

Acknowledgements—J. G. H. wishes to thank the City of Leicester Education Committee and Genatosan Ltd. for maintenance grants and Professor H. W. MELVILLE for permitting him to make the spectroscopic measurements in the University of Birmingham Chemistry Department. We also wish to thank the Royal Society for a grant for the spectrometer. Finally we would like to thank our colleague Dr. T. M. COULSON and the following who also kindly provided specimens: Drs. R. DEAN (Coal Tar Research Association) and L. SIHLBOM (University of Stockholm), and Dr. M. A. T. ROGERS (I.C.I. Dyestuffs Division) who kindly provided specimens from the collection of the late Professor WYNNE.

OL.
10
7/58

References

[1] THOMPSON H. W. and TORKINGTON P. *Trans. Faraday Soc.* 1945 **41** 246; WHIFFEN D. H. and THOMPSON H. W. *J. Chem. Soc.* 1945 268; THOMPSON H. W. *J. Chem. Soc.* 1948 328.
[2] BELLAMY L. J. *The Infra-red Spectra of Complex Molecules.* Methuen, London, 1954.
[3] COLTHUP N. B. *J. Opt. Soc. Amer.* 1950 **40** 397.
[4] RANDLE R. R. and WHIFFEN D. H. *Molecular Spectroscopy* p. 111. Report on the conference held in London in October 1954 by the Institute of Petroleum.
[5] JONES R. N. and SANDORFY C. *Techniques of Organic Chemistry* Vol. IX, p. 247. 1956.
[6] CENCELJ L. and HADZI D. *Spectrochim. Acta* 1955 **7** 274.
[7] WERNER R. L., KENNARD W., and RAYSON D. *Aust. Naturf. J. Chem.* 1955 **8** 346.
[8] LUTHER H. and GÜNZLER H. *Z. Naturf.* 1955 **10b** 445.
[9] ANDERSON D. G., SMITH J. C., and BROOMFIELD M. *J. Inst. Petrol.* 1952 **38** 424; American Petroleum Institute *Research Project* 44 Catalogue of infra-red and Raman spectra.
[10] MOSBY W. L. *J. Amer. Chem. Soc.* 1952 **74** 2564.
[11] WHIFFEN D. H. *Spectrochim. Acta* 1955 **7** 253.
[12] SCULLY D. B. and WHIFFEN D. H. To be published.
[13] RANDLE R. R. and WHIFFEN D. H. *J. Chem. Soc.* 1952 4153.
[14] FERGUSON J. and WERNER R. L. *J. Chem. Soc.* 1954 3645.

Spectrochimica Acta, 1957, Vol. 10, pp. 110 to 118. Pergamon Press Ltd., London

Analyse isotopique du lithium par spectroscopie optique—I

Utilisation de la raie $\lambda = 4603$ Å

J. Artaud, J. Blaise, et S. Gerstenkorn
Centre d'Études Nucléaires de Saclay, Département de Metallurgie et de Chimie Appliquée et Laboratoire Aime Cotton-Centre National de la Recherche Scientifique (Bellevue)

(*Received* 15 *May* 1957)

Abstract—An interferometric isotopic assay for lithium with the line $\lambda = 4603$ (2P–4D) is described. The light source is a liquid nitrogen-cooled hollow cathode working under low current. Excited in this way, the line $\lambda = 4603$ does not show any self absorption, unlike the red line $\lambda = 6707{\cdot}8$ Å. It is shown that the Doppler width is different for both isotopes of lithium. The value of the natural abundance ratio of lithium isotopes is found to be $12{\cdot}3 \pm 0{\cdot}3$.

1. Introduction

Divers auteurs [1–5] ont déterminé l'abondance isotopique du lithium naturel en utilisant l'effet isotopique dans le spectre optique du lithium. La raie d'analyse utilisée par ces auteurs est la raie rouge $\lambda = 6707{\cdot}8$ Å du lithium correspondant à la transition 2S–2P (Fig. 1).

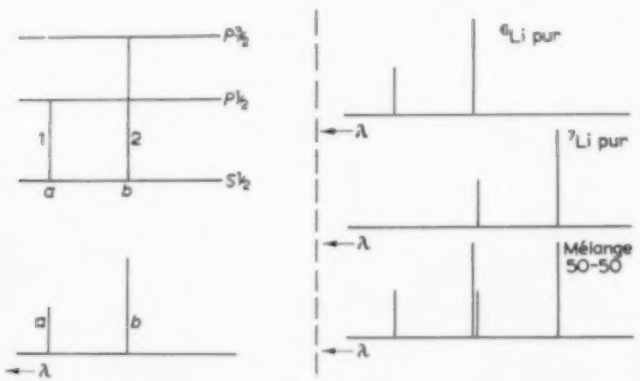

Fig. 1. Structure fine et effet isotopique de la raie Li 6707·8 Å.

C'est la raie de résonance, sujette à l'auto-absorption, présentant un déplacement isotopique de 337 mK [6, 7].* La distance entre les composantes du doublet de structure fine est de 350 mK. Il en résulte une superposition de la grande composante due à l'isotope ^{6}Li avec la petite composante de l'isotope ^{7}Li.

* Suivant les recommandations de la "Joint Commission for Spectroscopy," nous utiliserons comme unité de nombre d'onde: le kayser 1 mK = 10^{-3} cm^{-1}.

Dans notre travail nous avons choisi comme raie d'analyse la raie $\lambda = 4603$ Å correspondant à la transition 2P–4D (Fig. 2). Dans les conditions expérimentales où nous opérons, la raie bleue ne présente pas d'auto-absorption et les tubes photomultiplicateurs d'électrons sont plus sensibles dans le bleu que dans le rouge. De

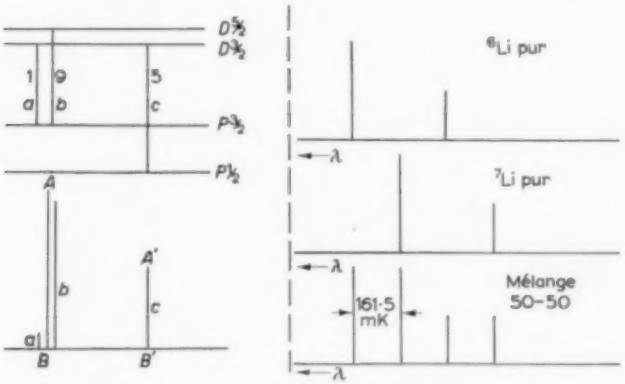

Fig. 2. Structure fine et effet isotopique de la raie Li 6403 Å

plus le déplacement isotopique de 161·5 mK $\pm$ 2 mK permet la séparation et la mesure de la grande composante correspondant à l'isotope ^{6}Li (Fig. 2).

2. Appareillage

L'appareillage utilisé est un spectromètre photoélectrique Fabry-Pérot [8, 9, 10].

Il se compose de:

Source { (a) une cathode-creuse, ordinairement employée à l'étude des structures fines et hyperfines, refroidie à l'azote liquide,

Appareils Analysateurs des Radiations { (b) un premier monochromateur qui est un prisme à déviation constante Pellin-Broca.
(c) un deuxième monochromateur comportant un réseau plan 600 traits/mm,
(d) un interféromètre Pérot-Fabry, à 7 couches diélectriques avec un pouvoir réflecteur d'environ 0·97 pour environ 4700 Å et conservant un pouvoir réflecteur acceptable dans une bande de $\pm$400 Å autour de cette longueur d'onde,

Recepteur { (e) une cellule photoélectrique type RCA 1P 21 refroidie à l'azote liquide,
(f) un amplificateur et un enregistreur direct type MECI.

Principe de l'enregistrement. L'anneau du centre, de rayon nul, est projeté sur la cellule, les longueurs d'onde défilent au centre grâce à la variation de l'indice μ de l'air. Cette variation s'obtient en laissant entrer progressivement l'air dans la cloche renfermant l'interféromètre où le vide a été établi au préalable.

Ainsi, sur l'enregistrement on obtient autant de fois que l'on veut le profil des composantes de la raie étudiée et ceci permet de se rendre compte de la stabilité de la lampe et de la constance de tous les autres facteurs.

De plus, l'enregistrement est linéaire en longueur d'ondes et direct, ce qui n'est pas le cas pour les autres méthodes.

3. Travail experimental

Les Figs. 3(a) et 3(b) montrent des enregistrements types.

L'enregistrement representé par la Fig. 3(a) est celui d'un mélange isotopique enrichi à 50 pour cent en ^{6}Li.* On remarquera les points suivants:

3.1. *La constance du fond enregistré entre les ordres successifs.* Le courant d'obscurité de la celulle est indiqué en bas à gauche (Fig. 3a et 3b—zéro de

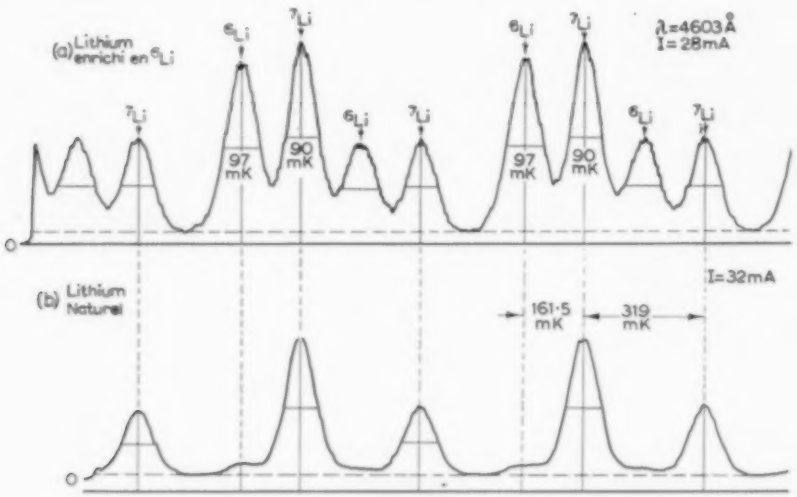

Fig. 3(a). Enregistrement de la raie LiI 4603 Å dans le cas du mélange 50/50.
Fig. 3(b). Enregistrement de la raie LiI 4603 dans le cas du lithium naturel.

l'enregistrement). Le fond enregistré entre deux ordres peut être pris pour fond réel de l'enregistrement, sans erreur appréciable. En effet le pouvoir réflecteur de l'étalon pour $\lambda = 4603$ Å est de l'ordre de 0·97; d'autre part nous avons choisi un intervalle spectral libre de 755·3 mK alors que la distance entre les composantes extrêmes de la structure étudiée est de l'ordre de 480 mK (Fig. 2). La différence entre le fond enregistré et le zéro de l'enregistrement (courant d'obscurité de la cellule) peut être attribuée à la lumière diffusée qu'on peut supposer uniforme sous toute la structure.

3.2. *La stabilité de la décharge.* La durée des enregistrements des Figs. 3(a) et 3(b) est d'une heure environ.

3.3 *Largeurs Doppler différentes pour* ^{6}Li *et* ^{7}Li. Soit y_6 et y_7 les largeurs enregistrées à mi-hauteur des composantes correspondantes à ^{6}Li et ^{7}Li. Sur l'enregistrement 3(a) on a: $y_7 = 89{\cdot}8$ mK, $y_6 = 97{\cdot}2$ mK.

Le rapport $y_6/y_7 = 97{\cdot}2/89{\cdot}8 = 1{\cdot}082$; il est sensiblement égal au rapport $\sqrt{(7/6)} = 1{\cdot}081$ d'où

$$\frac{y_6}{y_7} = \sqrt{\frac{7}{6}}$$

* Le ^{6}Li (pur à 99,8 pour cent) utilisé pour la préparation de ce mélange isotopique provient des laboratoires d'Oak-Ridge de l'U.S.A.E.C.

VOL. 10 1957/5

"Le rapport des largeurs mesurées à mi-hauteur des composantes des isotopes est égal à la racine carrée du rapport des masses des isotopes."

D'autre part l'équation des courbes enregistrées est de la forme

$$I = I_0 \exp(-kx^2) \text{ (voir tableau 1)}$$

où I_0 représente l'intensité de la raie spectrale pour $x = 0$. I est l'intensité correspondant à une abscisse x et K est une constante,

$$K = \frac{-4 \log 2}{(\Delta\sigma)^2}$$

avec $\Delta\sigma$ largeur de la raie à mi-hauteur.

Le Tableau 1 est obtenu de la façon suivante:

On considère la largeur à mi-hauteur de la raie mesurée en mm par exemple. Soit 20·0 mm pour $I = I_0/2$. Si la fonction enregistrée est du type de Gauss il est facile à partir de cette valeur de 20 mm de calculer les largeurs correspondant à diverses intensités (Tableau 1). Ces valeurs figurent dans la 1ère colonne "largeurs calculées." Dans la 2ème colonne figurent les largeurs mesurées aux mêmes ordonnées. On constate que la fonction enregistrée est bien gaussienne, excepté dans la partie inférieure ($I < I_0/4$) où les pieds sont plus larges que ceux d'une fonction de Gauss. Ces pieds sont dus à la fonction d'appareil qui dans notre cas se rapproche d'une fonction d'Airy.

Tableau 1

I/I_0	Largeurs calculées	Largeurs mesurées	Écarts
7/8	9·0	8·8	−0·2
3/4	13·0	12·7	−0·3
5/8	16·5	16·5	0
1/2	20·0	20·0	0
3/8	23·8	24·0	+0·2
1/4	28·2	29·5	+1·3
1/8	34·6	37	+2·4

Si l'on représente par Y la fonction enregistrée, elle est égale au produit de composition de trois fonctions: la fonction source B (du type de Gauss), la fonction d'étalon E (du type d'Airy) et la fonction exploratrice F (du type rectangulaire). Les notations sont celles de CHABBAL [10].

On a:

$$Y = \frac{2\pi S}{\sigma} B \,.\, E \,.\, F$$

où S est la surface utilisée de l'étalon et σ le nombre d'onde de la raie enregistrée.

Soient Z_6 et Z_7 les aires des composantes des isotopes du lithium. On a ([10], paragraphe 3–9–2, page 147):

$$Z_6 = C_6 \cdot y_6 \cdot h_6$$

et

$$Z_7 = C_7 \cdot y_7 \cdot h_7$$

h_6 et h_7 étant les hauteurs mesurées des pics correspondant aux isotopes du lithium. C_6 et C_7 sont des coefficients, appelés coefficients de forme, fonctions des rapports a/y_6 et a/y_7: a étant la largeur à mi-hauteur de la fonction d'appareil.

Enfin, g_6 et g_7 étant les largeurs à mi-hauteur des fonctions sources correspondant aux deux isotopes; on a entre g, a et y les relations suivantes:

$$y_6 = g_6 \oplus a$$
$$y_7 = g_7 \oplus a$$

Le symbole $\oplus$ signifie que la largeur enregistrée y est une fonction des largeurs g et a.

D'autre part si la fonction source est due uniquement à l'effet Doppler on a:

$$g_6 = g_7\sqrt{\frac{7}{6}}$$

puisque

$$g = 0{\cdot}716\sigma \,.\, 10^{-6}\sqrt{\frac{T}{M}}$$

y et σ étant exprimés en kaysers
T: température absolue de la source
M: masse atomique.

Finalement les surfaces Z_6 et Z_7 peuvent s'écrire:

$$Z_6 = C_6 \cdot y_6 \cdot h_6 = C_6 \cdot [g_6 \oplus a] \cdot h_6$$

et

$$Z_7 = C_7 \cdot y_7 \cdot h_7 = C_7 \cdot [g_7 \oplus a] \cdot h_7$$

avec
$$\begin{cases} C_6 = \varphi\left(\dfrac{a}{y_6}\right);\ C_7 = \varphi\left(\dfrac{a}{y_7}\right) \\ \\ g_6 = g_7\sqrt{\dfrac{7}{6}} \end{cases}$$

Ces remarques nous servirons au paragraphe 4 pour le calcul du rapport d'abondance.

3.4. *L'absence d'auto-absorption.* La raie $\lambda = 4603$ Å représente la transition $(4^2D \rightarrow 2^2P)$ et comprend trois composantes (structure fine). Les intensités de ces trois composantes a, b, c, sont proportionnelles aux nombres 1, 9, 5 (Fig. 2).

Les composantes a et b sont très proches l'une de l'autre [11] (18 mK au plus), elles ne sont pas résolues et, en fait, on observe un doublet. La connaissance de la distance entre les composantes a et b et de leur intensité relative [1, 9], nous a permis de calculer le rapport théorique des intensités du doublet que l'on observe (Fig. 2).

Il s'agit de calculer la hauteur AB de la résultante des deux composantes a, b et de faire le rapport $AB/A'B'$.

Supposant d'une part la largeur à mi-hauteur comprise entre 80 et 90 mK (valeurs mesurées) et d'autre part que l'équation de la courbe des raies enregistrées

VOL.
10
1957/5

est de la forme $I = I_0\,(\exp) - Kx^2$ on obtient les valeurs ci-dessous pour le rapport théorique du doublet (vour Tableau 2).

Tableau 2

Distance entre les composantes (comprise entre 15 et 18 mK)	Largeur de la raie à mi-hauteur	Intensité ^{7}Li forte $(a + b)$	Intensité ^{7}Li faible c	Rapport du doublet $\frac{^7\text{Li}(a+b)}{^7\text{Li}\,(c)}$
15 mK	80 mK	9·915	5	1·983
	90 mK	9·932	5	1·986
18 mK	80 mK	9·879	5	1·976
	90 mK	9·904	5	1·981

Le rapport théorique du doublet observé peut donc être pris égal à : 1·98.

Dans le cas de la Fig. 3b par exemple on mesurera ce rapport sur le doublet correspondant au ^{7}Li. Le Tableau 3 montre différentes valeurs obtenues pour ce rapport.

Tableau 3

Intensité du courant	Hauteur des composantes en mm		Rapport du doublet	Ecarts	Résultats
	^{7}Li forte	^{7}Li faible			
25 mA					
	309·0	157·5	1·961	0·027	
	337·0	167·5	2·011	0·022	$\frac{^7\text{Li fort}}{^7\text{Li faible}} = 1{\cdot}99 \pm 0{\cdot}03$
	323·0	165	1·957	0·032	
	337·0	166	2·030	0·041	
moyenne			1·989	0·031	
35 mA					
	416	213	1·953	0·043	
	416	208·5	1·995	0·001	
	417	208·5	2·000	0·004	$\frac{^7\text{Li fort}}{^7\text{Li faible}} = 1{\cdot}99 \pm 0{\cdot}03$
	417	204·0	2·044	0·048	
	413	204·0	2·024	0·028	
	421·5	215·0	1·960	0·036	
moyenne			1·996	0·027	

Le rapport mesuré (1·99) comparé à la valeur théorique 1·98 nous amène à conclure qu'il n'y a pas de correction à effectuer par suite de l'auto-absorption dans les conditions expérimentales dans lesquelles nous opérons.

4. Rapport d'abondance du lithium naturel

4.1. Le rapport d'abondance ρ est égal, en toute rigueur, au rapport des surfaces Z_7 et Z_6 définies au paragraphe précédent.

$$\rho = \frac{Z_7}{Z_6}$$

Mais il est plus commode et plus rapide de représenter l'intensité d'une raie spectrale par la hauteur h des pics enregistrés au lieu de considérer les surfaces Z. On aura donc:

$$\rho = \frac{Z_7}{Z_6} = \frac{C_7}{C_6} \cdot \frac{y_7}{y_6} \cdot \frac{h_7}{h_6}$$

Or, dans notre cas, $\dfrac{C_7}{C_6}$ est peu différent de 1. On a en effet

$$C_7 = 1{\cdot}119 \text{ et } C_6 = 1{\cdot}114 \text{ d'où } \frac{C_7}{C_6} = 1{\cdot}004 \# 1.$$

d'où

$$\rho = \frac{y_7}{y_6} \cdot \frac{h_7}{h_6} \text{ mais } y_6 = \sqrt{\frac{7}{6}}\, y_7 \text{ d'où finalement}$$

$$\rho = \sqrt{\frac{6}{7}} \cdot \frac{h_7}{h_6}$$

Pour avoir le rapport d'abondance il suffira donc de multiplier le rapport des hauteurs mesurées h_7/h_6 par le rapport des largeurs à mi-hauteur des raies enregistrées correspondant aux deux isotopes y_7/y_6.

4.2. *Fonction d'appareil.* Remarquons que le facteur $\sqrt{6/7} = g_7/g_6$, c'est-à-dire que l'on a:

$$\frac{y_7}{y_6} = \frac{g_7 \oplus a}{g_6 \oplus a} \simeq \frac{g_7}{g_6}$$

Cela est dû au fait que dans notre cas la fonction d'appareil (a) est petite devant la largeur g de la fonction source.

Si la fonction d'appareil (a) était plus importante (étalon moins réfléchissant, avec R de l'ordre de 0·8 par exemple) le rapport $y_7/y_6 = g_6 \oplus a/g_7 \oplus a$ tendrait vers 1; dans ce cas les largeurs des composantes des deux isotopes seraient égales et le rapport d'abondance serait simplement pris égal au rapport des hauteurs

$$\rho = \frac{h_7}{h_6}$$

En résumé "le rapport d'abondance est $\rho = K.\ h_7/h_6$, K étant un coefficient variant de $\sqrt{(6/7)}$ à 1, selon l'importance de la fonction d'appareil." Dans notre cas

$$K = \frac{y_7}{y_6} = \frac{89{\cdot}8}{97{\cdot}2} \# \sqrt{\frac{6}{7}} \quad \text{(Fig. 3a).}$$

VOL. 10 1957/5

Le Tableau 4 donne les résultats obtenus pour l'abondance naturelle du lithium; la Fig. 4 représente un enregistrement type.

Tableau 4. Rapport d'abondance du lithium naturel

Intensité du courant dans la cathode	Hauteur des composantes (mm)			Rapport doublet ^{7}Li	Rapport $\frac{^7\text{Li forte}}{^6\text{Li forte}}$	Rapport 1·98 ^{7}Li faible /^{6}Li forte	Rapport d'abondance	Ecart
	Composante ^{7}Li forte	Composante ^{7}Li faible	Composante ^{6}Li forte					
35 mA	309	157·5	23·5	1·96	13·1	13·3	12·1	−0·2
Lithium	309	165·0		1·87		13·8	12·8	+0·7
métal	323	165·0	25·0	1·96	12·9		11·9	−0·4
	323	167·5		1·99		13·3	12·3	0
	337	167·5	24·5	2·01	13·7		12·7	+0·4
	337	166		2·03		13·4	12·4	+0·1
35 mA	416	213	31·5	1·95	13·2		12·2	−0·1
Lithium	416	208·5		1·99		13·1	12·1	+0·2
sous	417	208·5	31·0	2·00	13·4		12·4	+0·1
forme de	417	204		2·04		13·1	12·1	−0·2
Sulfate	413	204	31·5	2·02	13·1		12·1	−0·2
(B)	421·5	215	31·5	1·96	13·4		12·4	+0·1
		215				13·4	12·4	+0·1
Moyenne				1·98 ± 0·03			12·3	±0·25

La valeur trouvée pour l'abondance du lithium naturel est de 12·3 ± 0·3 [1–5].

Conclusion

La raie 4603 Å offre une nouvelle possibilité de doser les mélanges isotopiques du lithium pour des mélanges s'échelonnant entre 7 et 97 pour cent en ^{6}Li.

Cette méthode ne comporte aucune correction, ne nécessite pas de cathode calibrée, ni d'échantillons absolument identiques (même état physique) et évite l'emploi d'étalons déterminés par d'autres méthodes. C'est une méthode de détermination absolue.

Résumé

On décrit une méthode d'analyse isotopique du lithium à l'aide d'un spectromètre photoélectrique Fabry-Pérot. La source est une cathode creuse refroidie à l'azote liquide et fonctionnant sous faible intensité. Dans ces conditions, la raie $\lambda = 4603$ Å ne présente pas d'auto-absorption, contrairement à la raie rouge $\lambda = 6707{\cdot}8$ Å. On met en évidence les langeurs Doppler, différentes pour les deux isotopes. La valeur trouvée pour le rapport d'abondance du lithium naturel est 12·3 ± 0·3.

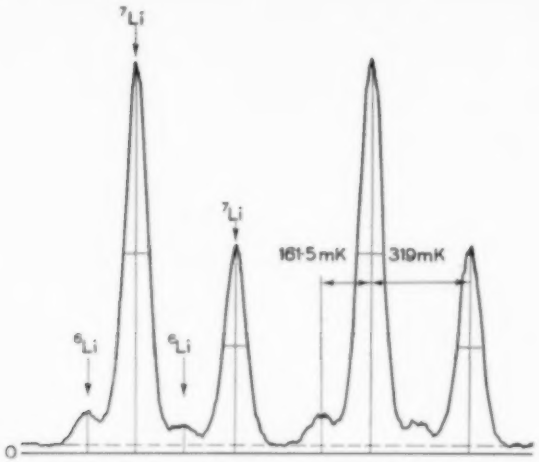

Fig. 4. Enregistrement type du lithium naturel (vitesse d'enregistrement 15 minutes par ordre).
$\lambda = 4603$ Å $\quad I = 10{\cdot}5$ mA

Remerciements—Nous remercions Mr. le Professeur Jacquinot pour l'aide et les conseils qu'il nous a apportés au cours de ce travail, et la Direction Scientifique du Commissariat à l'Énergie Atomique pour l'autorisation de publier ce travail.

VOL.
10
1957/5

Bibliographie

[1] Brody J. K., Fred M., and Tomkins F. S. *Spectrochim. Acta* 1954 **6** 383–412.
[2] Werner G. K., Smith D. D., Overshine S. T., Rudolph O. B., and Macnally J. R. Jr. *J. Opt. Soc. Amer.* 1955 **45** 3, 202–205.
[3] Thorne R. P. *A.E.R.E. C/R* 1732.
[4] Stuckenbrocker G. L., Smith D. D., Werner G. K., and Macnally J. R. Jr. *J. Opt. Soc. Amer.* 1952 **42** 6, 383–386.
[5] Striganov A. R. *Usp. Fizit. Nauk SSSR* 1956 **58** 365–414.
[6] Jackson D. A. and Kuhn *Proc. Roy. Soc.* A1939 **173,** 953.
[7] Hugues H. *Phys. Rev.* 1955 **99** No. 6.
[8] Jacquinot P. and Dufour Ch. *J. Recherches C.N.R.S.* 1948 No. 6.
[9] Brochard J., Chabral R., Chantrel H., and Jacquinot P. *J. Phys. Radium* 1952 **13** 433.
[10] Chabbal R. *J. Recherches C.N.R.S.* 1953, No. 42.
[11] Meissner K. W., Mundie E. G., and Stelson P. H. *Phys. Rev.* 1948 **74** 932.

Spectrochimica Acta, 1957, Vol. 10, pp. 119 to 127. Pergamon Press Ltd., London

RESEARCH NOTES

A slide rule for calculating blackening curve separations

H. J. PHILCOX
Plant Analysis Section, East Malling Research Station, Kent

(*Received* 7 *December* 1956)

Abstract—A slide rule has been devised for simplifying the operations in calculating blackening curve separations, obtained from galvanometer readings, without plotting density curves or using tables.

In its present form the slide rule is suitable only for spectrograms where the background correction is negligible; under such conditions a considerable saving of time and effort is claimed.

Introduction

BLACK [1] described a calculating board in which he made use of Seidel transformations for the determination of blackening curve separations. The essential operations of BLACK's method have been adapted to permit the use of a slide rule technique in place of the tedious plotting and erasing of pencil lines. A brief description of BLACK's calculating board will help the reader to follow the design and operation of the slide rule. (The calculating board holds a piece of paper on which are drawn seven vertical lines spaced 3·0 cm apart (Fig. 1), each line marking

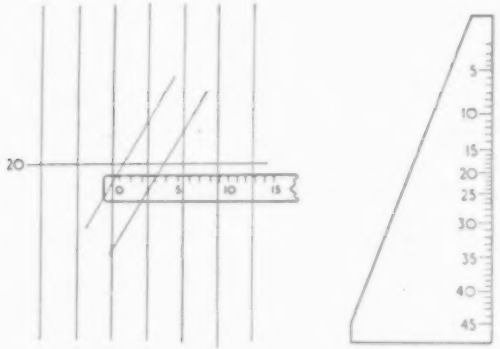

Fig 1. Diagram of the calculating board showing the vertical step lines and the two density lines whose separation is being measured by the linear scale. The set square carries the Seidel Density scale.

off a step or exposure increment obtained by using a six-stepped 2:1 ratio rotating sector. The length of the vertical lines being 27 cm is suitable for working with a microphotometer giving a full scale deflection of 50 for a clear plate.) The

standard density line is drawn horizontally at a convenient height. To draw a density curve slide the set square along to the appropriate step sector line and from the vertical Seidel density scale on the set square plot a point on the paper corresponding to the galvanometer reading. Slide the set square along to the next step sector line and make another plot. The line joining the two plots is the density curve and it must intersect the standard density line. Draw one density line for the element and another for the internal standard. These lines should be parallel and the distance between them, which is measured by means of a millimetre scale, is known as the separation. These operations are illustrated in Fig. 1.

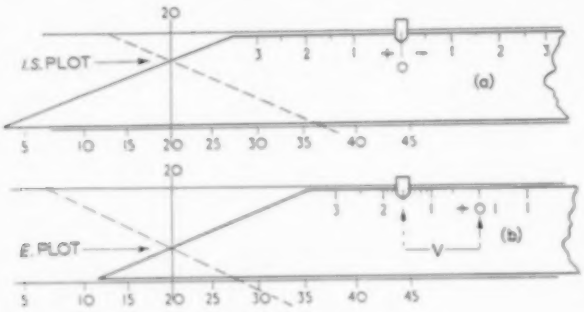

Fig. 2. Diagram of the slide rule showing settings of the slider and the marker for an internal standard (*I.S.*) plot and for an element (*E*) plot. The element line is denser than the internal standard line so a positive separation value of *V* is recorded.

In the slide rule the step sector lines are horizontal and the standard density line vertical, and instead of seven step sector lines there are only two which correspond to the upper and lower edges of the slider.

The Seidel Density scale corresponding to galvanometer readings is marked off horizontally on the fixed part of the slide rule (Fig. 2) and the standard density line is conveniently set at a galvanometer reading of 20 on the calculating board and on the slide rule. The function of the oblique edge of the slider is to transfer a vertical distance up the standard density line to a horizontal scale marked off along the top edge of the slider.

Construction of the slide rule

The slide rule, which is made entirely from Perspex, is illustrated in Fig. 3. The overall length is 30 cm and width 6 cm, the distance between the parallel side of the slider being 3·0 cm, which is equal to the spacing between the vertical lines of the calculating board.

The stationary part of the rule carries the Seidel Density scale (*A*) marked to correspond with galvanometer deflections. The scale, prepared as described by Black [1], is drawn directly on to a piece of Perspex which covers the whole width of the slide rule. The slider (*E*), which moves under this piece of Perspex, has the left hand end (*EE*) cut obliquely, the length of the oblique edge being 9·0 cm. The right hand upper edge of the slider carries a linear scale (*G*) having a centre zero and marked up to 0·3 to the left (+) and 0·3 to the right (−) the distance between 0

VOL. 10 1957/5

and 0·3 in either direction being 9·0 cm. *F* is a sliding marker which is used to set the zero on scale *G*. *C* is the cursor which moves over part of the Seidel Density scale and carries a pivoted arm with a straight edge *D*. The pivot point of arm *D* must move accurately along the upper edge of *E* from the standard density line (*B*) to the left. A zero line (*CC*) is drawn from the pivot point of arm *D* perpendicular to the parallel sides of *E*.

Method of using the slide rule

(1) Obtain galvanometer readings, for successive steps of the step sector, first for the internal standard line on the plate and then for the analysis line.

(2) Set zero line (*CC*) by sliding the cursor (*C*) so that the cursor points to the galvanometer reading of less than 20 for the internal standard line. This operation corresponds to the first-plot reading of the density curve on the calculating board.

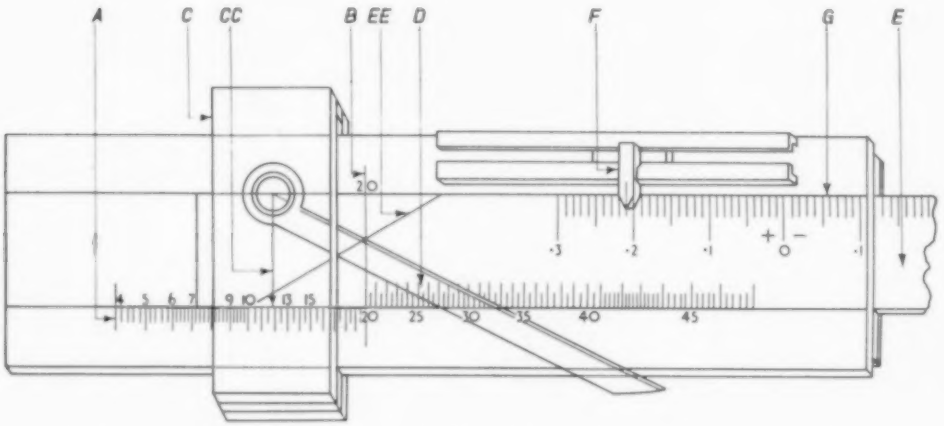

Fig. 3. The complete slide rule showing Seidel Density scale (*A*), standard density line (*B*), the cursor (*C*) carrying the movable arm (*D*), the slider (*E*), the marker (*F*) and the scale of separation values (*G*).

(3) To obtain the second plot of the internal standard density curve, rotate arm (*D*) so that the straight edge cuts scale (*A*) below the standard density line, recording a galvanometer reading greater than 20. This operation enables the straight edge representing the density curve to intersect the standard density line (*B*) at the point *D.B* (Fig. 2a).

(4) The intersection point of the standard density line by the arm (*D*) is now recorded in the following manner. Move the slider (*E*) so that the edge (*EE*) intersects line (*B*) precisely at the point of intersection of (*D.B*). The point of internal standard density curve intersection with standard density line is now recorded by moving the pointer (*F*) to the zero graduation on the linear scale (*G*), pointer (*F*) remains zero during the manipulations for the analysis line density-curve.

(5) Operations (1), (2), and (3) are repeated, this time for the analysis line and the separation value will be shown on scale (*G*) Fig. 2(b).

(6) Note the reading on scale G of the marker F which has not been moved since operation (4). This is the separation value when the galvanometer readings have been taken in the same steps for the two spectrographic lines. If the reading is (+) the second line is stronger and if (−) the second line is weaker than the first.

For every step up add 0·3 to the separation value and for every step down subtract 0·3 from the separation value.

Some examples of calculations are given in Table 1 and these should serve to make the method clear

Table 1

Slide rule examples for minus readings with variable step values

	Line	Galvanometer readings in step nos.				Slide rule readings	Add for step differences	Total separation values
		3	4	5	6			
Galvanometer readings in the same steps	*I.S.* *E*		13·0 19·5	24·2 34·2		−0·170	0	−0·170
Readings for *E* in one step down	*I.S.* *E*	19·5	13·0 34·2	2·42		−0·170	−0·300	−0·470
Readings for *E* in one step up	*I.S.* *E*		13·0	24·2 19·0	34·2	−0·170 −0·170	+0·300	+0·130

Slide rule examples for plus readings with variable step values

Galvanometer readings in the same steps	*I.S.* *E*		12·3 11·2	23·5 23·4		+0·010	0	+0·010
Readings for *E* in one step down	*I.S.* *E*	11·2	12·3 23·4	23·5		+0·010	−0·300	−0·290
Readings for *E* in one step up	*I.S.* *E*		12·3	23·5 11·2	23·4	+0·010	+0·300	+0·310

I.S. = Internal standard *E* = Element for analysis

Acknowledgements—The author wishes to acknowledge the help given by Mr. A. C. Mason in the preparation of this paper, also that of Misses M. J. Jenner and E. Brett for checking the accuracy of this instrument in routine work.

Reference

[1] Black I. A. *Spectrochim. Acta* 1952 **4** 519–524.

VOL. 10 1957/5

Infra-red spectra of solutions of iodine in alkyl benzenes

E. E. Ferguson
Chemical Division U.S. Naval Research Laboratory

(*Received* 11 *April* 1957)

Aromatic compounds form complexes of the electron donor-acceptor type with the halogens [1]. Haller, Jura, and Pimentel [2] have examined the infra-red spectra of iodine solutions of benzene, toluene, mesitylene, and hexamethylbenzene. They found one aromatic absorption band enhanced in solution in each case except mesitylene where they observed two. Recently the infra-red spectrum of benzene has been found to show two enhanced bands in iodine and bromine solutions [3]. Hexadeuterobenzeneiodine solution shows precisely the same two modes enhanced as in benzene [4].

Table 1. Infra-red bands of polymethylbenzenes enhanced in iodine solution

No.	C_6H_6*	Mesitylene†	*p*-xylene	*m*-xylene	*o*-xylene	Toluene
1	992‡ a_{1g}	998 *vw* a_1	835 *w* a_{1g}	1000 *vw* a_1	masked	1002 *m* a_1
2	3062					
3	1340 a_{2g}			1268 *m* b_1		
4	703 b_{2g}					
5	995		962 *vw*? b_{2g}	890 *w* b_2	860 *w* a_2	
6	606 e_{2g}			535 *w* a_1		
7	3047		1204 *vs* a_{1g}		1225 *w*? a_1	1210 *vw* a_1
8	1596					
9	1178					
10	850‡ e_{1g}					842 *w* a_2
11	673 a_{2u}					
12	1010 b_{1u}	575 *w* a_1		723 *vw*? a_1		
13	3060	1300 *vs* a_1				
14	1310 b_{2u}					
15	1152					
16	405 e_{2u}					
17	975					
18	1037 e_{1u}					
19	1485					
20	3080			1252 *m* a_1		
not assigned		880 *m*	943 *w*		930 *vw*?	

(*vw* very weak, *w* weak, *m* medium intensity enhancement, *vs* very strong)
* Benzene assignment from Miller *J. Chem. Phys.* 1956 **24** 996.
† Other assignments from Pitzer and Scott *J. Amer. Chem. Soc.* 1943 **65** 803.
‡ Benzene bands enhanced by iodine (ref. 3).

Reported here are investigations of the spectra of solutions of iodine with toluene, the xylenes, mesitylene, and seven additional monosubstituted alkyl benzenes. The spectra were obtained with a Perkin-Elmer Model 21 spectrophotometer with a NaCl prism and a PE Model 112 instrument using quartz and KBr prisms. Cell thicknesses varied from 0·02 to 1·5 mm. The spectra of the compounds used are nearly identical to the API spectrograms obtained with NBS standard samples of 99·8 to 99·9 mole per cent purity.

The observed changes in the solution spectra are listed in Tables 1 and 2 together with the assignment of the bands as given by PITZER and SCOTT [5]. The spectral changes are attributed to the charge-transfer complexes formed rather than to solvent perturbations.

Table 2. Monoalkylbenzene infra-red bands enhanced by iodine in solution

Compound	Band frequencies (cm^{-1})		
C_6H_6	992	850	
Toluene	1002 *m*	842 *w*	1210 *vw*
Ethylbenzene	1003 *vw*	842 *w*	
n-Propylbenzene	1003 *w*	841 *vw?*	
*Iso*propylbenzene	1001 *vw*	masked	
n-Butylbenzene	1003 *vw*	842 *vw*	
tert.-Butylbenzene	1002 *w*	masked	
sec.-Butylbenzene	masked	840 *w*	
n-Hexylbenzene	1003 *w*	838 *vw*	

(*m* medium, *vw* very weak, *w* weak enhancement)

In benzene, the solubility of iodine is less than 5 mole per cent, of which about 60 per cent is in the form of 1:1 complex [6], and it seems reasonable to assign the increased band intensities to the 3 per cent of new molecular species rather than the 2 per cent solvent influence. In the methylated aromatic cases, the argument is even more compelling, in mesitylene for example BENESI and HILDEBRAND [6] claim that about 85 per cent of the iodine is complexed. Considering the small concentration of iodine, the intensity changes are quite considerable, in some cases giving enhanced "complex" bands with extinction coefficients approaching those of active benzene fundamentals.

Several consistencies appear in Tables 1 and 2. First, for all the monoalkylbenzenes (except where strong absorption interferes) the same two vibrational modes are enhanced as in benzene itself, namely γ_1 near 1000 cm^{-1} and γ_{10a} near 840 cm^{-1}. This indicates that these vibrational modes are altered only very slightly by monoalkylsubstitution. The most conspicuous consistency in the data is that the symmetric ring stretching mode γ_1 is observed enhanced in every case except *o*-xylene where it is masked by strong absorption. The totally symmetric carbon–carbon single-bond stretching frequency (the stretching between the carbon atoms of the aromatic ring and the attached methyl carbons) is enhanced in every case, and generally with more intensity than any other band. The symmetric C—C single bond stretching modes are γ_{13} at 1300 cm^{-1} in mesitylene; γ_7 at 1204 cm^{-1} in *p*-xylene, 1225 cm^{-1} in *o*-xylene, and 1210 cm^{-1} in toluene; γ_{20a} at 1252 cm^{-1} in *m*-xylene.

The remaining bands which are enhanced do not fall into any clear pattern so that no general deductions are warranted. The fact that several bands, not assigned as fundamentals, are observed to be enhanced is not explained. It is quite possible that these bands do correspond to inactive fundamental vibrations and that the original assignments are in error.

References

[1] ANDREWS L. J. and KEEFER R. M. *J. Amer. Chem. Soc.* 1952 **74** 4500; 1955 **77** 2164.
[2] HALLER W., JURA G. and PIMENTEL G.C. *J. Chem. Phys.* 1954 **22** 720
[3] FERGUSON E. E. *J. Chem. Phys.* 1956 **25** 577.
[4] FERGUSON E. E. *J. Chem. Phys.* 1957 **26** 1357.
[5] PITZER K. S. and SCOTT D. W. *J. Amer. Chem. Soc.* 1943 **65** 803.
[6] BENESI H. A. and HILDEBRAND J. H. *J. Amer. Chem. Soc.* 1949 **71** 2703.

VOL. 10 1957/5

Some aspects of the determination of barium in silicate rocks*

D. M. Shaw
Department of Geology, Hamilton College, McMaster University,
Hamilton, Ontario, Canada

Introduction

During the course of recent research into the geochemistry of pelitic sediments, an opportunity arose to compare the analyses of rocks for barium, as obtained by spectrographic and by gravimetric methods, in different laboratories. Accordingly the writer, assisted by Mr. G. R. Pearson, measured the barium content of fifteen rocks, using a d.c. arc spectrographic method. Gravimetric analyses on the same samples were carried out in the Rock Analysis Laboratory at the University of Minnesota, under the direction of Dr. S. S. Goldich. This note is chiefly concerned with an unexpected matrix effect which was detected during standardization of the spectrographic method.

Method

A Jarrell-Ash 21-foot grating spectrograph was used, having a dispersion of 5·2 Å/mm in the first-order spectrum. A 10 mg sample was packed in the crater of a $\frac{1}{4}$ in. platform electrode and burnt at 8 amperes in a d.c.-arc for seventy to ninety seconds (complete burn). The emitted light was focused on the 20 μ slit by a 100 cm cylindrical quartz lens, passing through a rotating 5-step sector with a log-ratio of 0·2. Spectra were photographed on Eastman-Kodak type III-F plates, which were developed for three minutes in D-19 developer at 20°C. An iron-arc spectrum was exposed on each plate for calibration.

The spectral lines used were Ba 4934, La 4921, and Fe 4920. Lanthanum served as internal standard, Line blackness was measured on an ARL Densitometer, and the results converted to arbitrary log intensity units (log I) by the conventional methods of Honerjäger-Sohm and Kaiser [1], using a calculating-board. Background corrections were applied.

Standards

All spectrographers are familiar with the difficulties of making standards which resemble the unknowns in both chemical and physical properties. In this case the unknowns were argillaceous rocks consisting principally of silica and alumina, with minor amounts of potash, iron oxides, other metallic oxides, and water. Accordingly, the first material chosen for a standard matrix was a mixture of SiO_2, Al_2O_3, and KCl in weight proportions of 5 : 3 : 1, free of Ba. Mixtures with $BaCO_3$ were made at various concentrations below 1 per cent Ba, by the usual dilution methods, mixing in an agate mortar. In preparation for arcing, both standards and unknowns were mixed with an equal quantity of graphite powder. La_2O_3 was incorporated in the graphite, for use as internal standard, so that the final mixtures contained 0·25 per cent. At this stage the most obvious difference between standards and unknowns (apart from metallic elements absent in the standards) was the excess of chlorine and carbon dioxide in the standards, and the different state of combination of the elements. The electrodes containing both standards and unknown samples were therefore sintered in a muffle-furnace at red-heat for 15 min, to obviate these differences. After this the electrodes were allowed to cool, then arced.

To study the results, the log intensity of each line was calculated from the density readings, relative to an arbitrary base-level (corresponding to a density of 0·4 on the fourth step). In this way the behaviour of the analysis and internal standard lines

* A paper presented at the first Canadian Symposium on Applied Spectroscopy, held in Ottawa, September, 1954.

can be studied independently, then the final ratio is obtained by difference (i.e., $\log I_{Ba}/I_{La} = \log I_{Ba} - \log I_{La}$). In Fig. 1a are shown these log-I values for seven replicates of a standard mixture and seven of a shale. It is seen first of all that lanthanum is satisfactory as an internal standard, since the Ba and La points rise and fall together, so that the ratio I_{Ba}/I_{La} remains reasonably constant throughout each set of replicates. Secondly, the values of $\log I_{Ba}$ are not very different in standard and unknown, so the Ba concentration is about the same in each. Thirdly, the values of $\log I_{La}$ are in quite different ranges for standard and unknown, yet each contained the same amount (0·25 per cent La_2O_3). This is clearly a matrix effect, and would obviously lead to incorrect analyses if the ratio I_{Ba}/I_{La} were used.

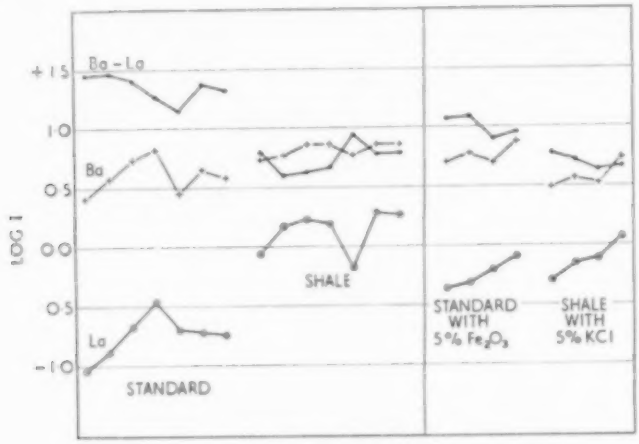

Fig. 1 (a and b)

For the next exposures the standard matrix was changed to include 5 per cent Fe_2O_3, reducing other constituents (including Ba and La) by the same amount. Also 5 per cent KCl was added to the previous shale mixture, reducing its Ba and La content by the same proportion. The results of fourfold replication are shown in Fig. 1b.

It is seen that La and Ba still behave sympathetically, and that the Ba values are still in the same range.* However the La values are now very similar in both sets of samples, *and similar to the previous La values* in the shales. The addition of 5 per cent Fe_2O_3 to the standard has noticeably enhanced the La line. The ratio I_{Ba}/I_{La} should now give a reasonable measure of the Ba content of an unknown, after preparation of a working-curve of $\log I_{Ba}/I_{La}$ vs. log concentration.

This matrix effect is unusual, in that it is controlled by iron rather than by alkalies. Although only a few values are shown in the figure, the behaviour was confirmed throughout the later work of preparing the working-curve and analyzing samples. At the beginning the whole effect was thought to have arisen by a mistake in weighing the La_2O_3, but this supposition was shown to be wrong after a second identical batch was prepared.

Results

A satisfactory method was developed, giving a precision of about ± 20 per cent of the absolute Ba content, for a 95 per cent probability range, using the statistical methods described elsewhere [2]. Unknowns were run in quadruplicate.

* It is possible (though not certain) that the additional alkali has decreased I_{Ba} in the shale. In any case, the alkali content of standard and unknown is now nearly the same.

VOL. 10 1957/5

Table 1

Sample number	Per cent Ba	
	Spectrographic	Chemical
L1	0·049	0·05
L3	0·062	0·05
L8	0·069	0·04
L9	0·063	0·06
L10	0·046	0·03
L11	0·066	0·04
L12	0·103	0·08
L29	0·059	0·07
L41	0·055	0·05
L49	0·044	0·07
L54	0·033	0·04
L55	0·087	0·10
L69	0·035	0·04
L81	0·056	0·06
L82	0·045	0·06

OL.
10
7/58

Fifteen rocks were analyzed, and the results are presented in Table 1, with the gravimetric results included for comparison. Agreement is satisfactory in many cases, especially with the last eight samples. In only three cases out of fifteen (L8, 11, 12) is the disagreement profound enough to introduce the question, "Which method is the more accurate?"

References

[1] Honerjäger-Sohm M. and Kaiser H. *Spectrochim. Acta* 1944 **2** 396–416.
[2] Shaw D. M. and Bankier J. D. *Geochim. et Cosmochim. Acta* 1954 **5** 111–123.

Book reviews

F. Wever, W. Koch und S. Eckhard: **Erfahrungen mit der spektrochemischen Analyse von Gefügebestandteilen des Stahles** (Inclusions in Steel) Forschungsberichte des Wirtschafts-und Verkehrsministeriums Nordrhein-Westfalen. Nr. 244 1956. Westdeutscher Verlag-Köln und Opladen. DM 11.20.

This supplements and amplifies the 48th report of the same series on the spectrochemical analysis of inclusions in steel; dealing with improvements in technique consequent on the adoption of this method for routine analysis at the Max Planck Institute for Steel Research. A source unit giving a choice of Feussner spark, interrupted arc, and alternating-current arc with high-frequency ignition is described, with automatic exposure-timing devices.

Micromanipulators are used to introduce the sample into a fused borax bead, which is then treated with cobalt citrate as an internal standard element and dissolved in water. The iron and other main constituents are determined chemically; while the qualitative analysis of a part of the solution is followed by a quantitative estimation of the remaining elements in the spectrum. Mn, Cr, Ti, Ni, Si, Al, Cu, Ca, and Mg may be estimated spectrochemically; but for recommended wavelengths the previous report must be consulted. Typical analyses, tests of reproducibility and comparisons of spectrochemical with other micro-analytical techniques are given.

E. van Someren

Paul W. Merrill: **Lines of the Elements in Astronomical Spectra** Carnegie Institution of Washington Publication 610, Washington, D.C., 1956. Quarto, vii + 167 pp. $1.60 paper bound; $2.00 cloth bound.

This monograph is designed to be useful to physicists, chemists, and spectroscopists, as well as astronomers. The author's aim is to provide a résumé and partial bibliography of observations of lines in astronomical spectra. The compilation is arranged by elements rather than by wavelengths or stellar types. The discussion for each element includes a brief historical statement followed by a detailed survey of present knowledge on the occurrence and behaviour of lines of that element in the spectra of various astronomical bodies. Numerous reference citations are arranged by journal in the bibliography. A list of 108 references to tables of wavelengths of astronomical spectra is also included. A new collection of partial Grotrian energy level diagrams is found in the appendix. Although there is a strong astronomical bias in these diagrams, the analytical emission spectroscopist faced with the selection of internal-standard line pairs will find these diagrams very useful.

The reviewer feels that this is a valuable reference compilation for spectroscopists of every kind, and that every spectroscopic library should have a copy on its shelves.

Velmer A. Fassel

VOL. 10 1957/5

Chemical Applications of Spectroscopy Edited by W. West. Vol. IX (of **Technique of Organic Chemistry,** Edited by A. Weissberger. Interscience Publishers Inc., New York, 1956. xxiv + 787 pp., 15 × 23 cm. $15.00).

This book deals with the entire spectral range from the vacuum ultra-violet to the radiofrequency region. Emphasis is on the understanding and interpretation of spectra, and experimental details are scarcely mentioned. Although the book is one of a series on organic chemistry, it will be of greater interest to spectroscopists, and this review is addressed primarily to them. Let it be understood at the beginning that the reviewer regards the book as a valuable one. Although he will point out some aspects in which it seems to him that it could have been improved, they are minor faults beside the overall accomplishment.

Before the book as a whole is evaluated, it is desirable to comment briefly on the individual chapters. Chapter I, Introductory Survey of Molecular Spectra, by W. West (70 pp.), includes the usual—and highly desirable—survey of the entire gamut of molecular spectra. It also contains an odd mixture of other topics, such as the induced infra-red absorption of H_2, O_2, and N_2, and a brief section on the variation method. The Franck-Condon principle and predissociation spectra appear here rather than in the chapter on electronic spectra. One gets the impression that certain subjects were inserted in this chapter when it was found that they were not treated by the other authors.

Chapter II, Microwave and Radiofrequency Spectroscopy, by Walter Gordy (115 pp.), covers pure rotational spectra, electronic magnetic resonance, and nuclear magnetic resonance. The reviewer is not competent to judge this critically, but he enjoyed reading it. The material is well organized and clearly written. The author does a skilful job of explaining the physical processes involved, and in indicating those aspects of the subject which are of special interest to chemists. The chapter concludes with a 13-page discussion of spectrochemical analysis at microwave and radio frequencies which summarizes the potentialities well. This is one of the best chapters in the book.

Chapter III, Theory of Infrared and Raman Spectra, by A. B. F. Duncan (59 pp.), was rather disappointing. This is due in no small part to the magnitude of the task. The author has attempted to treat in 59 pages, material to which Herzberg, in his excellent book *Infrared and Raman Spectra*, has devoted many times that number. It is understandable that the present chapter suffers by comparison. But it is also true that the author's treatment lacks that lucidity, that sparkle and crispness that distinguishes an excellent writing job from a pedestrian one. It is likely that a neophyte will have thorny going in reading this chapter, and it is doubtful whether he will obtain much understanding of the subject therefrom. Nowhere in the book, for example, is there an illustrative case of a vibrational analysis using actual data. On the other hand, the chapter may be a convenient reference for one who has some familiarity with the material. For instance, the depolarization ratios of Raman lines are worked out explicitly, and the reviewer knows of only one other place where this can be found in English. Whether it is important enough to warrant inclusion is another matter. It was noted that Kohlrausch's *Ramanspektren* (1943) was omitted from a list of books on this subject.

Chapter IV, The Application of Infrared and Raman Spectrometry to the Elucidation of Molecular Structure, by R. Norman Jones and Camille Sandorfy (334 pp.), is the outstanding chapter of the book. It deals with the use of empirical group frequencies in determining the structure of complex molecules. Although the chief emphasis is on infra-red spectra, Raman spectra are given a considerable amount of attention. The chapter is authoritative, well written, and a pleasure to read. It contains a welcome discussion of what the authors call Experimental Techniques which includes the representation of infra-red spectra, errors in spectrophotometry, intensities of infra-red bands, slit-width effects, the effect of physical state, the choice of solvents, polarization, and several other pertinent topics. The last two hundred pages are devoted to characteristic group frequencies. There is a 16-page table giving the frequency of the carbonyl stretching band in a large number of compounds, and a 25-page table summarizing the various group frequencies. Almost one thousand references are cited. The senior author has contributed much to the literature on the subject, and the entire chapter bears the stamp of authority and comprehensiveness. The only lapse noted by the reviewer was a minor one in the discussion

of the out-of-plane hydrogen vibrations of substituted aromatics, where the useful correlation with the number of adjacent hydrogen atoms was not used.

A comparison with BELLAMY's fine book, *The Infrared Spectra of Complex Molecules*, will be of interest. BELLAMY devotes two hundred and twenty pages to group frequencies, compared to two hundred in this chapter. The extent of the coverage is therefore about the same, and the quality is comparable. BELLAMY's book is somewhat easier to use, because of its division into chapters with their introductory discussions and tables. The present chapter has more spectra, figures, and structural formulas in the body of the discussion to clarify and illustrate the material. Both use wavenumbers exclusively. Because of JONES and SANDORFY's additional inclusion of Experimental Techniques, their chapter is the best treatment of chemical applications of infra-red spectra available in English, and probably in any language. It alone will be worth the cost of the book to the practising infra-red spectroscopist, and the volume will surely stand with BELLAMY's as the current bibles of the art. Many will wish that this portion could be obtained separately for daily use in the laboratory.

Chapter V, Electronic Spectra in the Visible and Ultraviolet Regions, is divided into two parts. Part 1, Theory of Electronic Spectra, is by A. B. F. DUNCAN (48 pp.). It is devoted to classification of electronic transitions, wave functions for molecules (molecular orbital and valence bond methods), and the computation of intensities. Again, it is a poor place to study the subject for the first time.

Part 2, Applications of the Theory of Electronic Spectra, by F. A. MATSEN (78 pp.), opens with a section on theory which does not unduly duplicate that in Part 1. The bulk of the chapter is an effort to use the molecular orbital approach to understand and correlate some of the salient observations in electronic spectra. The goal is a worthy one. On the one hand, there is an enormous welter of data in this field, widely scattered and scarcely understood. On the other hand, the past ten years has seen vigorous activity in developing the theory, but the results, unfortunately, are still widely scattered in the literature. An attempt to summarize the most useful theoretical conclusions and apply them in an orderly way to the experimental observations is therefore timely. Prof. MATSEN has succeeded rather well in this. The chapter is not primarily concerned with empirical correlations between electronic spectra and structure, although many are introduced in the course of the discussion. For a detailed survey of them one would have to go elsewhere, such as to GILLAM and STERN's book, or to the comprehensive article by PESTEMER and BRÜCK in HOUBEN-WEYL's Methoden der Organische Chemie, Vol. 3, Part 2.

Chapter VI, Fluorescence and Phosphorescence, by W. WEST (52 pp.), was found to be well written and interesting, and is a very good discussion of the subject.

Some general comments can now be made about the book as a whole. An 8-page index of symbols, giving the name and the page where they are first introduced, is a convenient feature. There are of course some errors, but not an unreasonable number. The index seems satisfactory, and the general quality of the printing and binding is good.

It is common to find in a joint venture of this sort that the quality is not uniform, and this book is no exception. There is evidence that it would have benefited by better planning between the authors. It appears that the area to be covered by each writer was not always clearly defined and fitted into the plan of the book. This is especially true with the theory of electronic spectra. Molecular orbitals, for instance, are discussed in three separate places by three separate authors: in Chapter I by WEST, in Chapter V by DUNCAN, and again in Chapter V by MATSEN.

The book will be of little use for teaching purposes; it is not a textbook, nor was it intended as one. For the practising molecular spectroscopist, and for the chemist with strong interests in that direction, the book will be excellent. Its greatest value probably consists in gathering in one place a great amount of information. It may not contain the most thorough treatment of one's own specialty, but it will provide a valuable source of information about those other aspects of spectroscopy with which one is less well acquainted. A notable exception to this is the chapter by JONES and SANDORFY; this is for expert and dabbler alike.

The reviewer regards this book as a valuable contribution to the field of molecular spectroscopy, and is certain that his copy will receive extensive use. Its status on his bookshelf will be

VOL. 10 1957/5

just below the definitive volumes by HERZBERG. Anyone who pretends a serious interest in molecular spectroscopy will want a copy, and many with only casual interest will find it useful in one way or another.

FOIL A. MILLER

HERBERT M. HERSHENSON: **Ultra-violet and Visible Absorption Spectra: Index for 1930–1954** Academic Press, Inc., New York, 1956. 205 pp., $12.00.

THIS book represents a monumental effort that should be greatly appreciated by everyone working in ultra-violet and visible spectra. The difficult problems of nomenclature and indexing perhaps have not been solved by the author. It is indeed troublesome to search under many different headings to find spectra of compounds of a given parent substance. Also, it is rather inconsistent to have one list of references under dinaphthyls and a different list of references under binaphthyls, with both lists referring to the same compounds. But within the practical limitations of labour, size, and consequent price the system used by the author is a suitable compromise. Complete cross-indexing would be prohibitive. At first the book may be difficult to use, but one quickly becomes accustomed to looking under various headings for a particular compound.

The very extensive compilation of inorganic complex compounds should prove invaluable to the analytical chemist. The listing of various dyes under their common names is probably the best arrangement for those working in dye chemistry, but it is not convenient for others. The author has included references to spectra under such interesting headings as corn syrup, gasoline, gas oil, lignin, lubricating oil, and liver. In this reviewer's opinion such references are commendable and might well have been expanded.

There are two glaring omissions from the references to spectra of organic compounds. One is the collection of American Petroleum Institute spectra; the other is the spectra contained in "Aromatische Kohlenwasserstoffe," by E. CLAR, Springer-Verlag, 1953, second edition. It is unfortunate that all of the spectra of polynuclear hydrocarbons in CLAR's book were not listed. Most of CLAR's spectra are to be found in the literature, but there are several spectra of polynuclear aromatics which are to be found only in CLAR's book.

The work involved in this compilation should be greatly appreciated and the author should be encouraged "to see to it that subsequent literature will be covered in a supplementary index."

R. A. FRIEDEL

Vistas in Astronomy. Edited by A. BEER, Pergamon Press, London, New York, Paris. Vol. I. xiv + 776 pp. £9. 9s. 1955. Vol. II. 1000 pp. £15. 15s. 1956.

SECTIONS 13 and 14 of this famous work are devoted specifically to spectroscopy and spectral peculiarities of celestial objects. In addition, articles in other sections deal *inter alia* with visible and infra-red Fraunhofer lines, the calculation of atomic transition probabilities, intensity of emission lines, and resonance fluorescence. Two major articles review developments and possibilities in the design of spectrographs; direct-intensity microphotometers, and spectra obtained with shock-wave tubes are also discussed.

As to manner, each article is written at research level and at the same time designed to be accessible to those, whether in other branches of astronomy or in neighbouring disciplines, who are not specialists in the author's own field.

As to matter, although the approach is primarily astro-physical, much that is contained in these articles will interest spectroscopists more generally. The theory and instrumentation presented are, of course, of quite general applicability; and in many other cases the astronomical work is clearly linked with laboratory spectroscopy, to which it forms a natural extension. The Sun, because it presents such a bright extended surface, enables the lines of the elements occurring in its spectrum to be studied in great detail. The occurrence of P, S, Si, Mg, and Fe is especially discussed, for example. The high temperatures, low densities, great atmospheric depths and dilute radiation sometimes found in celestial objects, tend to emphasize lines of high excitation potentials and forbidden transitions; many lines are thus prominent which can be observed otherwise only with difficulty, if at all, in the laboratory; the nebular lines of O III and N II, and the coronal lines of Fe XIV, etc., are famous examples. Among the new identifications of this type discussed is that of transitions of C IV in the Wolf-Rayet stars on the basis of predictions from laboratory spectra of C at lower temperatures. Some stars show isotopic ratios for certain elements different from those found on the Earth. We are always kept aware that our knowledge of the general chemical composition of matter in the Universe as a whole is largely derived from the spectro-chemical analysis of starlight.

Altogether, the spectroscopist will find in abundance material that interests and concerns him in the pages of this book, one of the most comprehensive surveys of our days.

P. B. Fellgett

VOL.
10
1957/5

ERRATUM

Charles E. White, Donald E. Hoffman, and John S. Magee Jr.: Fluorescence emission spectra, fluorescence excitation spectra, and absorption spectra of some metal chelates.

Spectrochim. Acta 1957 **9** 105

Introduction, line 11, p. 105, for azonaphthalene-3-sulphonic acid . . . read azonaphthalene-4-sulphonic acid.

Spectrochimica Acta, 1957, Vol. 10, pp. 133 to 148. Pergamon Press Ltd., London

Materialabbau in Funkenentladungen. Experimentelle Untersuchungen an Zinkkathoden

K. Bunge*
Mitteilung aus dem Institut für Spektrochemie und angewandte Spektroskopie in Dortmund

(*Received* 5 *April* 1957)

Zusammenfassung—Es wird eine Methode beschrieben, die es gestattet, das von einer Metallelektrode beim Abfunken abgebaute Material quantitativ zu bestimmen. Die Methode wird speziell auf den Abbau an Zinkkathoden angewendet. Es ergibt sich, dass die abgebaute Mange, bezogen auf die durch die Funkenstrecke geflossene Ladung, weitgehend unabhängig von den gewählten Entladungsbedingungen ist. Sie beträgt etwa $5 \cdot 10^{-5}$ gr pro Coul. Die Abbrandflecke und die Spektren der verwendeten Funken werden untersucht. Sie werden in Zusammenhang mit den Abbauerscheinungen gebracht. Einige Anwendungen der gewonnenen Ergebnisse auf Untersuchungen über Abfunk und ähnliche Effekte werden skizziert.

1. Einleitung

Nach einer grundlegenden Arbeit von Kaiser und Wallraff [1] wenden sich eine Reihe von Autoren den Problemen der Physik spektrochemischer Lichtquellen zu. Eingehende Untersuchungen finden sich über die Vorgänge in den Metalldampfwolken, die bei der Entladung von den Elektroden fortgeschleudert werden (neuere Veröffentlichungen [2, 3]). Weniger bekannt ist der Prozess, durch den das Metall von der Elektrodenoberfläche entfernt wird. Erst in letzter Zeit sind hierzu, vor allem von Cundall und Craggs [4], eingehendere Untersuchungen angestellt worden. Hier, sowie u.a. bei Hurwitz [5], Laqua [6] und Stetter [7] finden sich auch Angaben über die im folgenden hauptsächlich behandelte Frage nach der Menge des von der Elektrode abgebauten Materials.

Bei den Untersuchungen über den Abbau werden meist Versuchsbedingungen gewählt, wie sie auch sonst in der spektrochemischen Praxis üblich sind. Dabei treten eine Reihe von Erscheinungen auf, wie Erwärmung der Elektrode, Abfunkeffekte, Oxydation usw., die die Verhältnisse komplizieren. Im folgenden werden solche Nebeneffekte vermieden: Alle für einen Abbauversuch verwendeten Entladungen sind gleichwertig. Das Ziel der Arbeit ist:

(1) Ausarbeiten einer allgemeinen Methode zur Bestimmung der beim Übergehen elektrischer Entladungen von Metalloberflächen abgebauten Materialmengen.

(2) Sammeln experimenteller Unterlagen über den Abbau von Zinkkathoden.

2. Allgemeine Methodik zur Bestimmung des Abbaus von Elektroden. Anwendung auf Zinkkathoden

2.1. *Charakterisierung der Methode*

Zunächst werde das benutzte Verfahren in grossen Zügen gekennzeichnet. Das zu untersuchende Material liegt als zylindrischer Metallstab vor. Dieser

* Die Arbeit ist im wesentlichen ein Auszug eines Teils einer Dissertation, Bonn, Febr. 1955.

wird in schraubender Bewegung unter einer Gegenelektrode hinweg durch ein Entladungsgefäss geführt, wobei seine Oberfläche abgefunkt wird. Die sich im Gefäss ansammelnden abgebauten Metallmengen werden nach dem Versuch aus dem Gefäss entfernt und bestimmt. Die Anzahl der pro sec übergehenden Funken ist so gewählt, dass jeder Funke im wesentlichen auf eine Stelle des Metalls schlägt,

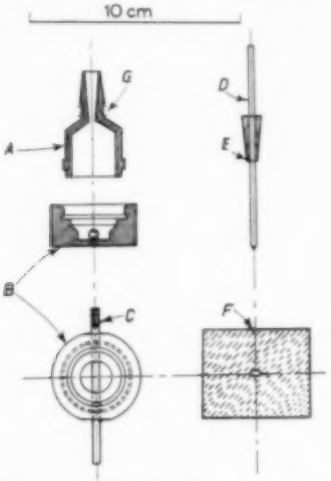

Abb. 1. Entladungsgefäss mit Elektroden und Papierhülle.
A, *B* Entladungsgefäss — *C* abzufunkende Elektrode
D Gegenelektrode — *E* Konus
F Papierhülle — *G* Metallmanschette

die von vorhergehenden Funken nicht angegriffen wurde. Auch die sonstigen von dem übergehenden Funken angetroffenen Bedingungen (z.B. Elektrodentemperatur, Zusammensetzung der Luft im Entladungsgefäss usw.) ändern sich nur in vernachlässigbarer Weise: die Funken sind untereinander gleichwertig.

2.2. *Versuchsanordnung*

(a) *Entladungsgefäss.* Abb. 1 zeigt das Entladungsgefäss (*A*, *B*), die abzufunkende Elektrode (*C*), die Gegenelektrode (*D*), über die der Konus (*E*) geschoben ist, und die mit einem Loch versehene Papierhülle (*F*). Die um den Hals des Gefässes gelegte, geerdete Metallmanschette (*G*) erleichtert das Übergehen der Zündfunken. Gefäss und Konus bestehen aus Plexiglas, die Hülle aus dünnem Transparentpapier. Beim Vorbereiten des Gefässes für den Versuch werden seine beiden Teile ineinander verschraubt, die Gegenelektrode eingesetzt, die Hülle in der gezeichneten Weise um die Elektrode gelegt, nach unten stramm gezogen und auf dem Boden des Gefässes mit einem Streifen Tesafilm fixiert. Beim Abfunken schlägt die Entladung durch das Loch in der Hülle auf die Elektrode über. Ist der Versuch beendet, so werden die Elektrode und das Papier aus der Durchbohrung im Unterteil (*B*) des Gefässes entfernt. Die Löcher und der Schlitz in (*B*) werden mit einem Streifen Tesafilm von aussen überklebt. Aus dem nunmehr abgeschlossenen Innenraum des Gefässes kann ohne Verlust das abgebaute Material herausgelöst werden.

VOL.
10
1957/5

Bei den Versuchen tritt folgende Schwierigkeit auf: Ein Teil des ursprünglich abgebauten Materials setzt sich stets auf der Elektrode selbst wieder ab. Da es nicht gelang, diesen Teil mit zur Bestimmung heranzuziehen, wurde versucht, ihn wenigstens möglichst klein zu halten. Die Anordnung mit der Papierhülle verfolgt diesen Zweck. Eine Bewegungseinrichtung (Synchronmotor, Getriebe usw.) schraubt die Elektrode (C) durch das Entladungsgefäss (Vorschub: $\frac{1}{2}$ mm, Umdrehungszahl: 1 Umdrehung in 10 sec).

(b) *Elektrische Anordnung.* Die elektrischen Entladungen liefert im allgemeinen ein Niederspannungsfunkenerzeuger; für ergänzende Versuche wird ein Hochspannungsfunkenerzeuger verwendet.

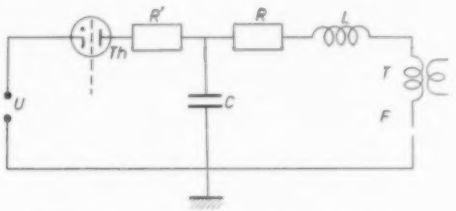

Abb. 2. Niederspannungsfunkenerzeuger.

Ladekreis		Funkenkreis	
U	Ladespannung 2 kV	C	Speisekondensator 0,1–10 μF
Th	Thyratron ASG 5017	R	Dämpfungswiderstand 1–1000 Ω
R'	Ladewiderstand 1 kΩ	L	Induktivität 0–10 mHy
C	Ladekondensator 0,1–10 μF	T	Teslatransformator
		F	Analysenfunkenstrecke

(α) *Niederspannungsfunkenerzeuger:* Abb. 2 zeigt den für das folgende allein wichtigen Lade- und Entladekreis des Funkenerzeugers. Gegenüber den üblichen Niederspannungsfunkenerzeugern ist u.a. folgende Veränderung angebracht: Die Anzahl der Funken pro sec ist nicht fest vorgegeben, sondern kann von etwa 1 bis 100 variiert werden. Der im Mittel fliessende Strom ist daher nicht von vornherein durch die Schaltelemente im Funkenkreis festgelegt. (Näheres über den benutzten Funkenerzeuger vergleiche [8]). Die Sekundärinduktivität des Teslatransformators T ist möglichst klein gehalten, da von ihr die maximale im Entladekreis erreichbare Stromstärke abhängt ($I_{\max} = U\sqrt{C/L}$). Sie beträgt etwa 5 μHy; bei diesem Wert ist es schon nicht ganz einfach, eine zur Zündung der Analysenfunkenstrecke hinreichende Spannung im Entladekreis zu induzieren.

Die Verhältnisse in der Funkenstrecke werden stark von in der Nähe befindlichen Isolatoren beeinflusst. So kann z.B. ein in freier Luft völlig regelmässig übergehender Funke im Entladungsgefäss cet. par. zu "stottern" beginnen und schliesslich ganz aussetzen. Die geerdete Metallmanschette (Abb. 1) beseitigt in einfacher Weise diese recht lästige Störung. Ihre Wirkung beruht wahrscheinlich darauf, dass Wandladungen unter Mithilfe des bei der Zündung auftretender starken Feldes zwischen Manschette und Gegenelektrode beseitigt werden. Ein solches Feld könnte auch erklären, warum sich nach Anbringen der Manschette in deren Nähe mehr Material absetzt als zuvor.)

Messung der elektrischen Grössen. Die beim Übergehen eines aperiodisch gedämpften Funkens abgebaute Materialmenge wird im folgenden stets auf die durch die Funkenstrecke geflossene Ladung bezogen. Sie ist $Q = C\Delta U$ mit

$\Delta U = U_L - U_R$, wenn C die Kapazität des sich entladenden Kondensators, U_L seine Spannung vor der Entladung ("Ladespannung") und U_R seine Spannung danach ("Restspannung") ist. U_L wird mit einem Scheitelspannungsmesser bestimmt. U_R wird in leicht verständlicher Weise in der Schaltung gemäss Abb. 3 gemessen. Dazu wird an der Batterie B solange gestöpselt bis der Indikator In (Mikroamperemeter, Oszillograph) Strom anzeigt. Der Einsatzpunkt

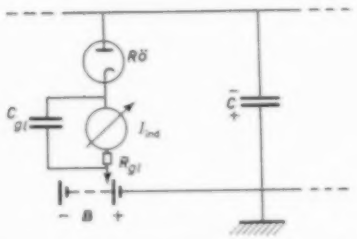

Abb. 3. Messung der Restspannung des Speicherkondensators.
$Rö$ Hochspannungsgleichrichter AG 1006
R_{gl} Glättungswiderstand 200 kΩ
C_{gl} Glättungskondensator 32 μF
C Speicherkondensator
In Stromindikator
B Anodenbatterie

ist ziemlich scharf. (Gelegentlich wurde auch U_R direkt mit einem statischen Voltmeter gemessen.) Kapazitäten, Induktivitäten und Widerstände werden nach den üblichen Verfahren gemessen, kleine Induktivitäten nach den im Kohlrausch [9] angegebenen Formeln berechnet. (Es handelt sich um die Induktivität von einlagigen Zylinderspulen.) Die Bestimmung der Ladung Q ist mit einem Fehler von etwa 1%, in ungünstigen Fällen bis etwa 2% behaftet. Die Anzahl von Funken pro sec wird bis zu einem Wert von an 10 die Netzfrequenz angeschlossen. Bei kleineren Funkenfolgen gibt ein Telephonzähler die Anzahl direkt wieder.

(β) *Hochspannungsfunkenerzeuger:* Zu ergänzenden Versuchen dient der in Abb. 4 skizzierte "tandem-gap"-Funkenerzeuger. Er arbeitet mit Gleichrichtung und liefert 50 Funken pro sek. Um regelmässiges Abfunken zu erreichen, muss $R'C$ etwa 10^{-2} sec sein. An der Tandemfunkenstrecke TF wird der Wert der Spannung eingestellt, bei dem sich der Kondensator entladen soll. Die Ladespannung des Kondensators wird ähnlich wie oben mit einem Scheitelspannungsmesser bestimmt, die Restspannung meist nur abgeschätzt (Messfehler s.o.)

(c) *Kolorimetrische Bestimmung.* Das als abzubauendes Material verwendete Zink wird im wesentlichen nach einem bei Sandell [10] angegebenen Verfahren kolorimetrisch bestimmt. (Photometer: Zeiss, Elko II, Lichtquelle: Glühlampe, Filter: S 53 (grün). Relative Standardabweichung bei der Bestimmung etwa 2%).

2.3. *Versuchsbedingungen*

Die in der vorliegenden Arbeit gewählten Versuchsbedingungen lehnen sich zwar nach Möglichkeit an die in der Spektrochemie auch sonst üblichen an; im einzelnen werden jedoch erhebliche Änderungen in Kauf genommen, wenn man erhoffen kann, dadurch leichter ausdeutbare Ergebnisse zu erhalten. Die wichtigsten Massnahmen in dieser Richtung sind: Es wird ein chemisch

VOL. 10 1957/5

reines Material verwendet; jeder Funke schlägt im allgemeinen auf ein bis dahin unbearbeitetes Gebiet der Elektrode; der Strom fliesst in der Entladung nur in einer Richtung.

(a) *Material.* Es wird der Abbau an Zink untersucht (Zink pa., Merck). Zink empfielt sich für die ersten Versuche vor allem durch folgende Vorzüge: Wegen seines niedrigen Siedepunktes kann man erwarten, dass es kräftig abgebaut

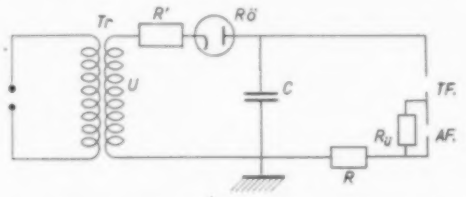

Abb. 4. Hochspannungsfunkenerzeuger.
Tr Hochspannungstransformator 220/10 kV
U Sekudärspannung des Transformators etwa 10 kV
R' Ladewiderstand
Rö Hochspannungsgleichrichter AG 1006
C Lade = und Speicherkondensator 700–2400 pF
R 10 Ω–10 kΩ
TF Tandemfunkenstrecke
AF Analysenfunkenstrecke
Rü Uberbrückungswiderstand

wird; es kann in geringen Mengen bestimmt werden; es lässt sich leicht zu Elektroden giessen und mechanisch bearbeiten. Dazu kommt folgendes: Es liegen eingehende Untersuchungen über den Mechanismus der Bogenkathode bei Quecksilber vor. Will man aus ihren Ergebnissen auf die Verhältnisse bei anderen Elementen schliessen, so kommen als solche Elemente vor allem das dem Quecksilber nahe stehende Zink und das Cadmium in Frage.

(b) *Oberfläche.* Die Beschaffenheit der Oberfläche (Oxyd- und Fettschichten, Kratzer usw.) ist für die Abbauerscheinungen von Bedeutung [10]. Die Zinkelektrode wird unmittelbar vor den Versuchen mit feinem Schmirgelpapier abgerieben und mit sauberem Filtrierpapier kräftig abgewischt. Anschliessend wird sie peinlichst vor jeder Verunreinigung bewahrt.

(c) *Gegenelektrode.* Die Gegenelektrode besteht aus Wolfram (bei vergleichenden Versuchen auch aus Silber). Wolfram wird wenig abgebaut; es ist zu erwarten, dass es die Abbauerscheinungen an der Zinkelektrode nicht wesentlich beeinflusst.

(d) *Geometrie der Anordnung.* Die Form und Anordnung der Elektroden ist aus Abb. 1 zu ersehen. Ihr Abstand beträgt gewöhnlich 2 mm (bei vergleichenden Versuchen auch 1 und 3 mm).

(e) *Umgebendes Medium.* Es wird in sorgfältig getrockneter Luft unter Normaldruck gearbeitet. (Feuchtigkeit im Gefäss gibt anscheinend zu Fehlern Anlass.) Zu den Bestandteilen der Luft gesellen sich im Laufe des Abfunkens noch Stickoxyde (an bräunlicher Färbung erkennbar) und Dämpfe von Zinkoxyd (milchige Schwaden). Im allgemeinen werden bei einem Versuch insgesamt etwa 200 γ Zink abgebaut. Bei vollständiger Oxydation dieser Menge Zink zu ZnO würden einige Prozent des im Gefäss befindlichen Sauerstoffs während des Versuches verbraucht werden.

(f) *Verwendete Entladungen.* In der Hauptsache werden die Abbauerscheinungen beim Übergehen aperiodisch gedämpfter Kondensatorentladungen auf Zinkkathoden untersucht. Der Entladungsstrom hat also angenähert die Gestalt $I = I_0 \exp(-t/T)$ (I_0, T Parameter). Ein aperiodisch gedämpfter Funke lässt sich kennzeichnen durch Angabe der gesamten von der Anode zur Kathode geflossenen Elektrizitätsmenge Q and einer gewissen Stromstärke I ($Q = C\Delta U$, $I = U/R$; I ist angenähert die Spitzenstromstärke während der Entladung. Bezeichnungen wie in 2.2 b). Die verschiedenen Entladungen, die zu gleichem I und Q führen, sollen als äquivalent bezeichnet werden. Es ist zweckmässig,

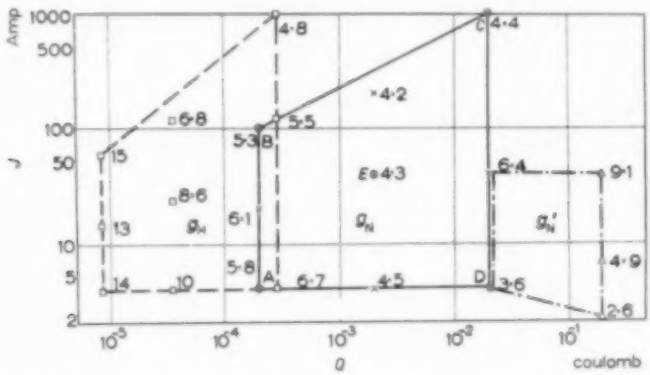

Abb. 5. Übersicht über die Entladungen, deren Abbau gemessen wurde.

g_N Gebiet in dem die Hauptversuche unternommen wurden

$g_{N'}$ Gebiet in dem die ergänzenden Versuche mit dem Niederspannungsfunkenerzeuger unternommen wurden

g_H Gebiet in dem die ergänzenden Versuche mit dem Hochspannungsfunkenerzeuger ausgeführt wurden

Der spezifische Abdampfverlust wurde für die durch die eingetragenen Punkte gekennzeichneten Entladungen bestimmt. Der jeweilige Mittelwert ist neben den Punkten eingetragen.

alle Entladungen, denen das gleiche I and Q zugeordnet ist, als Entladungen der *Art* (Q/I) zusammenzufassen. Ferner werden alle Entladungen, denen das gleich Q zugeordnet ist, als solche der *Gattung* (Q) bezeichnet. In Abb. 5 sind Q und I in doppelt logarithmischen Massstab aufgetragen. Jedem Punkt der Q,I-Ebene entspricht genau eine *Klasse* äquivalenter Entladungen der Art (Q/I). Die Versuche umfassen das Gebiet $G = g_N + g_{N'} + g_H$. (Randpunkte zählen zum Gebiet.) Die Funken in g_N und $g_{N'}$ werden mit dem Nieder spannungs-, die in g_H mit dem Hochspannungsfunkenerzeuger hergestellt.

Das Gebiet g_N, das die Funken der "Hauptversuche" (s.u.) enthält, ist nicht willkürlich abgegrenzt; vielmehr treten, wenn man die Grenzen wesentlich überschreitet, gewisse Schwierigkeiten auf. Seite AB ($Q = 2 \cdot 10^{-4}$ Coul): die Funken werden sehr schwach; der Zündfunke beeinflusst die Entladung nennenswert. (Anstelle der fremdgezündeten Entladungen des Niederspannungs- werden daher äquivalente selbstgezündete Entladungen des Hochspannungsfunkenerzeugers in dem Gebiet mit $Q < 2 \cdot 10^{-4}$ Coul verwendet.) Seite AD ($I = 4$ Amp): der Strom wird so klein, dass sich voraussichtlich der normale Bogenmechanismus nicht ausbilden kann. Seite DC ($Q = 2 \cdot 10^{-2}$ Coul): für kleine I erhält man sehr lang dauernde

Entladungen (Zeitkonstante einige 10^{-2} sec). Es handelt sich in diesen Fällen bereits um eine Art Dauerbogen, dessen Abbau zu untersuchen hier nicht die Aufgabe ist. Für mittlere I hinterlassen die Funken tiefe Krater auf der Elektrode (vgl. z.B. den Funkeneinschlag bei 70 Amp Abb. 7); bei dem explosionsartigen Ausbruch des verdampfenden Materials kommt es vor, dass auch etwas flüssiges Metall verspritzt; es wird mit bestimmt und fälscht die Ergebnisse. Auch bei grossem I scheint Verspritzen möglich zu sein. Seite BC ($I^2 = U^2C/4L$): die Seite charakterisiert die Entladungen mit kritischer Dämpfung. Wird BC in Richtung nach grösseren I zu überschritten, so werden die Entladungen oszillierend.

(g) *Thermische Belastung der Elektrode.* Bei den sich auf g_N beziehenden Versuchen wird die Funkenfolge so gewählt, dass im Mittel $2 \cdot 10^{-2}$ Amp fliessen. (Bei Entladungen mit $Q = 2 \cdot 10^{-2}$ Coul sind das also etwa 10 Funken pro sec usw.) Die Elektroden werden 4 min lang abgefunkt. Dabei erwärmen sie sich nur geringfügig (um etwa 10°C).

2.4. *Versuche*

(a) *Allgemeiner Ablauf eines Versuches* (siehe auch 2.2, b). Die saubere Zinkelektrode wird gemeinsam mit der Papierhülle in das mit trockener Luft gefüllte Entladungsgefäss eingeführt. Die Hülle wird am Gefäss fixiert. Die Elektrode wird mit der Bewegungseinrichtung in Verbindung gebracht. Bewegungseinrichtung und Funkenerzeuger werden in Betrieb genommen. Nach etwa 4 min. ist der Versuch beendet. Elektrode und Hülle werden aus dem Gefäss entfernt und der Teil B des Gefässes mit einem Streifen Tesafilm verschlossen. Der Niederschlag im Gefäss, auf der Gegenelektrode und auf der Papierhülle wird in Salzsäure gelöst und der kolorimetrisch bestimmt.

Die Versuche zerfallen in Vor-, Haupt- und ergänzende Versuche. Die bisher beschriebenen Bedingungen beziehen sich vorwiegend auf die Hauptversuche; die Bedingungen für die Vor- und ergänzenden Versuche sollen nicht im einzelnen wiedergegeben werden.

(b) *Vorversuche.* Zunächst wurde das Gebiet g_N mit etwa 60 Versuchen sondiert. Führt man als Abdampfverlust M der Kathode bei einer Entladung die abgebaute Zinkmenge (in gr.) pro Funken ein; nennt man weiter das Verhältnis von M zur durchgeflossenen Ladung (in Coul.), Q, den spezifischen Abdampfverlust μ: so lässt sich das Ergebnis der Vorversuche in überraschend einfacher Weise so formulieren: Entladungen der gleichen Art haben gleiches Aussehen der Abbrandflecke, gleiches M und gleiches μ; Entladungen der gleichen Gattung haben gleiches M und μ; alle Entladungen in g_N haben gleiches μ.

Um festzustellen, wie μ auf Abänderungen der Versuchsbedingungen reagiert, wurden folgende Versuche unternommen: (1) die Funkenfolge wurde auf etwa 1/5 herabgesetzt; (2) sie wurde gegenüber (1) auf den 10-fachen Wert gesteigert; (3) die Wolframelektrode wurde durch eine Silberelektrode ersetzt; (4) der Elektrodenabstand wurde auf 1 mm herabgesetzt; (5) er wurde auf 3 mm erhöht. (1) bis (5) zeigten keinen Einfluss auf die für μ gemessenen Werte.

(c) *Hauptversuche.* Bevor auf ihre Ergebnisse eingegangen wird, muss diskutiert werden, welche Bedeutung dem in der Versuchsanordnung bestimmten Abdampfverlust M der Elektrode zukommt. Wenn es überhaupt einen Sinn haben soll, M zu messen, so muss M eine selbstständige physikalische Bedeutung haben. M ist jedenfalls nicht mit dem primär aus dem Kathodenbrennfleck

austretenden Material identisch. Dieses ist überhaupt nicht ohne weiteres bestimmbar. Ein nennenswerter Teil davon kehrt nämlich in Form positiver Ionen zur Kathode zurück (vgl. entsprechende Bermerkungen für den Dauerbogen [11]). Bestimmt werden kann jedoch der Materialverlust der Kathode durch die mit grosser Geschwindigkeit ausbrechenden Dampfwolken. Da diese den Hauptteil des emittierten Lichtes liefern, ist ihre Masse eine physikalisch besonders bedeutsame Grösse. Sie dürfte in guter Näherung mit dem in der Versuchsanordnung bestimmten Abdampfverlust der Kathode übereinstimmen. (Das Wort "Abdampfverlust" deutet darauf hin, dass es sich um einen Verlust von Kathodenmaterial durch die ausbrechenden Dampfwolken handelt. Die Elektrode kann nämlich auch auf andere Weise, z.B. durch Abspritzen festen oder flüssigen Metalls Material verlieren.)

Da es sich bei den Vorversuchen nur um grob ausgeführte Übersichtsversuche handelt, wurden ihre Ergebnisse durch die sorgfältig ausgeführten Hauptversuche verifiziert. Nach den Vorversuchen ändert sich jedenfalls μ nur wenig in g_N; daher ist es hinreichend, die Hauptversuche auf einige Punkte des Gebietes, die Randpunkte A, B, C, D und den inneren Punkt E zu beschränken. Tabelle 1 gibt die Ergebnisse der Hauptversuche wieder. Unter der Art der Entladung sind die für μ gemessenen Werte eingetragen. In der gleichen Spalte eingetragene Werte gehören zu der gleichen Versuchsreihe, in verschiedenen Spalten aufgeführte Eintragungen liegen z.T. einige Monate auseinander. Die Mittelwerte der Messungen sind ausserdem in Abb. 5 verzeichnet.

VOL.
10
1957/5

Neben den zufälligen Fehlern, deren Grösse man aus den Angaben in Tabelle 1 abschätzen kann, können auch noch systematische Fehler auftreten. Sie können z.B. dadurch zustande kommen, dass flüssiges Metall verspritzt und einen zu grossen Abdampfverlust vortäuscht. Der Effekt könnte eine Rolle spielen bei Entladungen mit grossem Q und mittlerem, eventuell auch grossem I. Als weitere Fehlerquelle ist die schon oben erwähnte Selbstbestäubung der Kathode zu erwähnen.

2.5. *Ergänzende Versuche*

(α) *Zündfunken:* Schliesst man den Kondensator im Funkenkreis kurz und lässt nur den Zündfunken überschlagen, so bestimmt man eine Zinkmenge, die etwa 10^{-9} g pro Zündfunke entspricht. Dies ist etwa 10% der ermittelten Menge für einen Funken der schwächsten Entladungsgattung in g_N ($Q = 2 \cdot 10^{-4}$ Coul). Da also immerhin der Einfluss des Zündfunkens die Messergebnisse verfälschen könnte, werden die Entladungen der eben erwähnten Gattung durch äquivalente selbstgezündete Funken nachgebildet und deren Abbau untersucht (s.u.).

(β) *Abbau für Zink als Anode:* Wird Zink als Anode geschaltet, so bestimmt man bei Funken mit $Q = 2 \cdot 10^{-2}$ Coul etwa 5% der Niederschlagsmenge in der anderen Polung, bei $Q = 2 \cdot 10^{-3}$ Coul kommt die Menge schon in die Nähe der unter für den Zündfunken bestimmten, um bei $Q = 2 \cdot 10^{-4}$ Coul überraschenderweise kleiner als diese zu werden. Die Erklärung könnte folgende sein: Das niedergeschlagene Zink rührt praktisch nur von dem Zündfunken her. Nun liegt aber bei den hier in Rede stehenden Versuchen vor dem Durchschlag eine Spannung von etwa 2 kV an, die die Funkenstrecke entionisiert. Daher erfolgt der Durchbruch erst, wenn die Entladung im Primärkreis des Teslatransformators schon zum Teil abgeklungen ist. Da aus ihr die Energie des Zündfunkens gespeist wird, ist dieser schwächer als der unter (α) beschriebene.

(γ) *Oszillierende Funken:* Es werde ein oszillierender Funke betrachtet, bei dem in der i-ten Teilentladung (Zink als Kathode) die Ladung Q_i durch die Funkenstrecke fliesst und die Spitzenstromstärke I_i herrscht. Der Punkt (Q_1, I_1) liege in g_N. (Die Teilentladung kann also

durch die Entladung der Art (Q_1/I_1) approximiert werden.) Man wird vermuten, dass $\mu = M/Q_{osz}$ ebenfalls angenähert $5 \cdot 10^{-5}$ g/Coul sei, wenn $Q_{osz} = \Sigma Q_i$ gesetzt wird (Σ ist die Summe über alle i mit 4 Amp $\leq I_i$). Die Vermutung bestätigt sich. Tabelle 2 enthält die elektrischen Bedingungen und Ergebnisse der Versuche. Auffallend sind die grossen Werte für $C = 10\ \mu$F. Hierfür ist wahrscheinlich das schon erwähnte Verspritzen von Metall verantwortlich.

Tabelle 1. Ergebnisse der Hauptversuche

$(2 \cdot 10^{-4}/100)$			$(2 \cdot 10^{-3}/200)$			$(2 \cdot 10^{-2}/1000)$		
4,8	7,0	5,4			3,9	3,5	5,3	5,2
5,3		5,4			4,5	4,0		6,3
4,3						3,8		
5,0						3,6		
5,3						3,8		
	5,3			*4,2*			*4,4*	
$(2 \cdot 10^{-4}/20)$			$(2 \cdot 10^{-3}/40)$			$(2 \cdot 10^{-2}/40)$		
		6,1	4,7	5,1	4,3			6,9
		6,1	4,2	5,1	3,6			5,8
			4,2					
			4,3					
			3,5					
	6,1			*4,3*			*6,4*	
$(2 \cdot 10^{-4}/4)$			$(2 \cdot 10^{-3}/4)$			$(2 \cdot 10^{-2}/4)$		
4,9	6,0	6,3			4,9	3,5	3,6	3,6
5,1		6,2			4,2	3,7		3,5
5,9′						3,7		
5,1						3,7		
5,3						3,6		
	5,8			*4,5*			*3,6*	

Spezifischer Abdampfverlust μ der Kathode für die Entladungen der Art (Q Coul/I Amp) in Einheiten 10^{-5} g/Coul. (Mittelwert von μ kursischrift.)

(δ) *Langdauernde Funken:* Um den Anschluss an den Dauerbogen herzustellen, werden auch Entladungen mit $Q = 2 \cdot 10^{-1}$ Coul verwendet (Ergebnisse siehe Abb. 5). Der niedrige Wert von μ für $(2 \cdot 10^{-1}/2{,}2)$ dürfte auf die geringe Stromstärke zurückzuführen sein (vgl. Bemerkung unter 2.3(f); auch bei den Entladungen mit $2 \cdot 10^{-4} \leq Q \leq 2 \cdot 10^{-2}$ Coul und $I \leq 4$ Amp fällt μ ab).

(ε) *Selbstgezündete Funken:* Um den Einfluss des Zündfunkens auszuschalten, werden die in g_N liegenden Entladungen, die pro Funken nur einen geringen Abbau zeigen, als selbstgezündete Funken hergestellt. Bei diesen Versuchen, die mit dem Hochspannungsfunkenerzeuger ausgeführt werden, liegt die Funkenfolge mit 50 pro sec fest. Es wird solange gefunkt, bis der Niederschlag etwa 300 γ Zink enthält. Der spezifische Abdampfverlust steigt nach kleinem Q erheblich an (Ergebnisse siehe Tabelle 2).

2.6. *Zusammenfassung*

(1) Der spezifische Abdampfverlust einer Zinkkathode ist in g_N und g'_N im wesentlichen unabhängig von der Art der Entladung und beträgt $\mu = 5 \cdot 10^{-5}$ gr. Zink pro Coul. In g_H steigt μ mit abnehmenden Q stark an.*

(2) Wird Zink als Anode geschaltet, so werden Zinkmengen in der Anordnung bestimmt, die um einen Faktor von mehr als zehn kleiner sind als die bei der umgekehrten Polung.

Tabelle 2. Ergebnisse der Versuche mit oszillierenden Funken

(0,1/0,005)	(1/0,012)	(10/0,012)
4,2	6,1	6,0
6,5	4,1	5,4
(0,1/0,12)	(1/0,5)	(10/2)
7,9	6,3	10
7,2	6,7	7,9
(0,1/4)	(1/15)	(10/40)
6,7	7,8	10,4
7,0	7,2	9,2

Spezifischer Abdampfverlust μ in Einheiten 10^{-5} g/Coul. Die Entladungen sind charakterisiert durch Angabe der Kapazität in μF und der Induktivität in mHy (C μF/L mHy).

(3) Für oszillierende Funken, deren Halbwellen durch Entladungen in g_N approximiert werden können, gilt ebenfalls $\mu(=M/Q_{\text{osz}}) = 5 \cdot 10^{-5}$ gr/Coul mit $Q_{\text{osz}} = \Sigma Q_i$ (siehe γ).

(a) *Allgemeinere Betrachtungen.* Da bei den untersuchten, sehr verschiedenartigen Enladungsbedingungen der spezifische Abdampfverlust $\mu = M/Q$ in g_N konstant ist, liegt es nahe, anzunehmen, dass dies sogar für den momentanen spezifischen Abdampfverlust $\mu_{\text{m}} = dM/dQ$ bei beliebigen unipolaren Entladungen (Zink als Kathode geschaltet) der Fall ist. (Man muss natürlich fordern, dass Q in g_N liegt und $4 \leq I \leq 1000$ Amp für alle während der Entladung auftretenden Stromstärken gilt. Sollte sich diese Annahme als stichhaltig erweisen, so könnte das Problem des Materialabbaus für den hier behandelten Fall als gelöst angesehen werden.

Wie die Versuche zeigen, liegen bei Entladungen mit kleinem Q (Q etwa $2 \cdot 10^{-4}$ Coul) die Verhältnisse nicht so einfach. Wahrscheinlich ist bei diesen Funken der für Entladungen

* Es ist interessant, den in der vorliegenden Arbeit bestimmten spezifischen Abdampfverlust μ mit dem nach den Angaben in der Veröffentlichung von Cundall und Craggs [4] berechneten zu vergleichen. Die Autoren benutzen eine Entladung der Stromstärke 600 Amp und der Zeitdauer 3 μsec in Wasserstoffatmosphäre. Sie erhalten die abgebaute Menge durch Wägung der Elektrode vor Beginn des Abfunkens und nach dem Übergehen von 1000 Funken. Dabei ergibt sich μ zu $6{,}1 \cdot 10^{-5}$ g/Coul Die verwendete Entladung entspricht in der Notierung der vorliegenden Arbeit etwa einer solchen von der Art $(1{,}8 \cdot 10^{-3}/600)$. Für ähnliche Entladungen ergeben sich nach Tabelle 1 für μ Werte von etwa $4{,}5 \cdot 10^{-5}$ g/Coul.

VOL. 10 1957/5

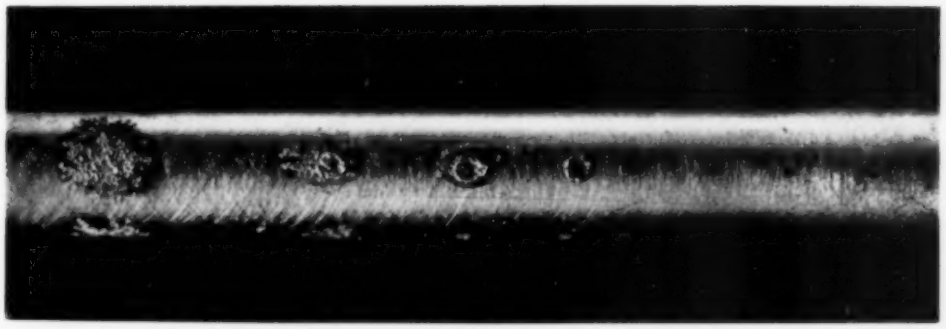

Abb. 7. Abbrandflecke von Funken der Gattung mit $Q = 6 \cdot 10^{-2}$ Coul.
Die Stromstärken der einzelnen Funken, I, sind 1000, 400, 200, 68, 20, 6,8, 4, 2,2 Amp.
(1000 Amp. entspricht dem ersten Funken von links, 400 dem zweiten usw.). Alle Funken
dieser Serie bauen gleich viel Material ab!

OL.
10
7/58

VOL.
10
1957/5

mit grösserem Q charakteristische Mechanismus noch nicht voll ausgebildet. Auch bei grossem Q ($Q >$ etwa $2 \cdot 10^{-2}$ Coul) treten Abweichungen ein. Das Ansteigen von μ in diesen Fällen dürfte auf eine Zunahme von μ gegen Ende der Entladung zurückzuführen sein. Eine solche Zunahme ist nicht verwunderlich, wenn man bedenkt, dass gegen Ende der Entladung grössere Gebiete der Kathode auf hohe Temperaturen aufgeheizt werden. (Auch im Dauerbogen hängt der Abbauverlust erheblich von der Temperatur ab [11]).

3. Abbrandflecke und Spektren

3.1. *Abbrandflecke*

Als Abbrandfleck werde die bleibende Veränderung der Elektrodenoberfläche nach dem Einschlagen eines Funkens bezeichnet. (Neuere Arbeiten über Abbrandflecke siehe [12] und [13].

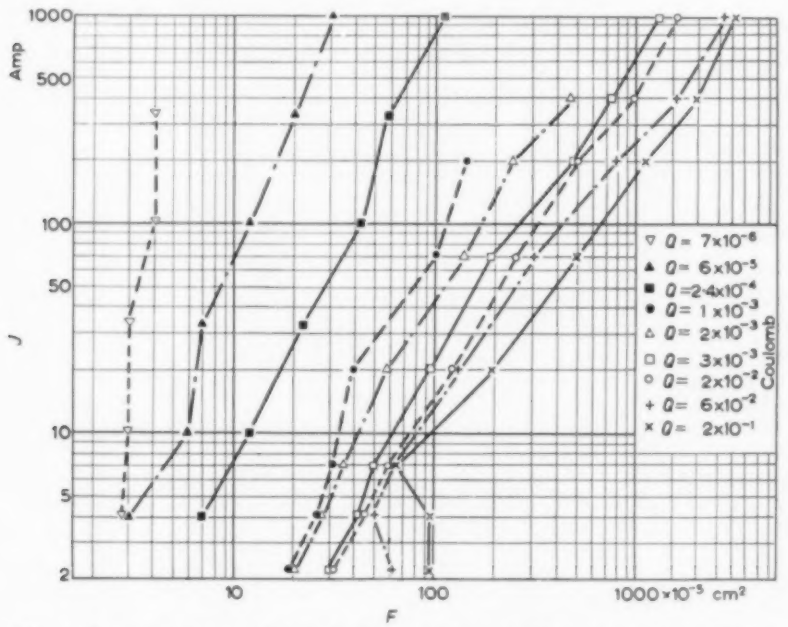

Abb. 6. Zusammenhang zwischen der Stromstärke I der Entladung und der Fläche F des Abbrandfleckes für Entladungen der gleichen Gattung.

Für eine Reihe von Entladungsarten, insbesondere für die in g_V, wurden die Abbrandflecke im Mikroskop vermessen. Jeder der in Abb. 6 gezeichneten Geradenzüge gibt den Zusammenhang von I und der Fläche des Abbrandfleckes für die Entladungen einer bestimmten Gattung wieder. Abb. 7 zeigt Funken der Gattung $Q = 6 \cdot 10^{-2}$ Coul. Alle diese Entladungen, deren Abbrandflecke so unterschiedlich aussehen, zeigen als Entladungen gleicher Gattung gleichen Abdampfverlust. Für die spektrochemische Analyse ist es wichtig, dass man aus der Fläche des Abbrandfleckes und dem Abdampfverlust für den entsprechenden Funken seine mittlere Eindringtiefe in die Elektrode abschätzen kann. Dies ist von Bedeutung für alle Probleme, bei denen die Oberflächenbeschaffenheit eine Rolle spielt.

Bei den anodischen Abbrandflecken hat man den Eindruck, als sei die bearbeitete Fläche zwar flüssig gewesen, jedoch nur wenig Material verdampft. Nur bei Funken mit grossem Q (Q etwa $5 \cdot 10^{-2}$) sieht man, vor allem bei mittleren Stromstärken, Gebilde, die aufgeplatzten Blasen ähneln und auf Materialabbau hindeuten. In der Tat ist auch bei diesen Funken der Materialverlust ziemlich gross. Für $Q = 10^{-3}$ Coul kann man die anodischen Flecke von der Umgebung kaum unterscheiden.

Die Abbrandflecke oszillierender Funken zeigen im allgemeinen soviel Teilflecke wie der Funke Entladungen aufweist. Es besteht kein Zweifel daran, dass jeder Teilfleck einer Halbwelle zuzuordnen ist, in der die Elektrode Kathode war. Unter Berücksichtigung dieser Tatsache erscheinen die Ergebnisse über den Abdampfverlust oszillierender Funken fast selbstverständlich.

3.2. *Spektren*

Die Spektren der Entladungen in $G = g_N + g'_N + g_H$ wurden aufgenommen, um die Verbindung zwischen den Erscheinungen des Materialabbaus und den für die Spektrochemie besonders wichtigen Prozessen in den leuchtenden Metalldampfwolken herzustellen. Leider mussten die Spektren photographiert werden. Dabei treten eine Reihe von Schwierigkeiten auf (s.u.). Die Ergebnisse tragen daher vor allem qualitativen Charakter. Es wäre interessant die Versuche mit lichtelektrischen Empfängern zu wiederholen.

(a) *Versuchsanordnung, Aufnahmebedingungen, usw.* Anordnung und Bewegung der Elektroden, Abfunkbedingungen usw. entsprechen den für die Abbauversuche verwendeten; nur werden die Elektroden nicht in dem abgeschlossenen Gefäss, sondern in freier Luft abgefunkt. Die Spektren werden in der üblichen Weise mit einem Spektrographen (Zeiss, Q12) geringer Dispersion aufgenommen. Für die Untersuchung werden die Funkenlinien Zn II bei 2502 Å (F_2), 2558 Å (F_1) und die Bogenlinien Zn I bei 2756 Å (B_3), 2771 Å (B_2), 2801 Å (B_1) verwendet.

Die Ebene, die Elektrode und Gegenelektrode enthält, ist um etwa 45° gegen die optische Achse des Kollimators geneigt, so zwar, dass die Einschlagsstelle des Funkens dem Spalt zugewendet ist. Es tritt daher das von dem Brennfleck ausgehende Licht ungehindert in den Spektrographen ein. (Bei der üblichen Anordnung kann ein Teil der Funkenbahn vom Spalt her gesehen verdeckt sein; da sich die Intensität der Funken- und Bogenlinien ungleichmässig über die Funkenbahn verteilt, wird dabei das gemittelte Intensitätsverhältnis gefälscht.)

(b) *Intensitätsverhältnis und spezifische Intensitäte einer Linie.* Es werde jetzt eine bestimmte Entladung E ins Auge gefasst. Die Intensität der Linien F sei J_F, die der Linien B sei J_B, der Abdampfverlust der Kathode sei M. Entsprechendes gelte für die mit Null indizierten Grössen einer Bezugsentladung E^0. Man gelangt dann in üblicher Weise zu einer für E charakteristischen Grösse, indem man das Verhältnis $\alpha = J_F/J_B$ bildet. Will man die Entladung E nicht selbst kennzeichnen, sondern nur mit anderen Entladungen vergleichen, so bildet man α/α° oder auch $Y = \log \alpha/\alpha^\circ$: Damit ist Y für alle Entladungen E eindeutig festgelegt.

Auch die Intensität einer Linie, z.B. die von B, J_B, ist charakteristisch für E. J_B hängt direkt und in trivialer Weise von der Masse der strahlenden Dampfwolke ab. Es liegt nahe, J_B in J_B/M und M zu zerspalten, wobie J_B/M diese triviale Abhängigkeit nicht mehr zeigt. J_B/M ist ebenfalls für E charakteristisch; es hat als Gesamtintensität der Linie B, die bei der Entladung E von der Masseneinheit ausgestrahlt wird, eine unmittelbare physikalische Bedeutung. Betrachtet man neben E die Bezugsentladung E^0, so gelangt man wie oben von $\beta = J_B/M$ zu $X = \log \beta/\beta^0$ mit $X^0 = 0$.

VOL. 10 1957/5

Entsprechend J_B könnte man auch noch andere Grössen auf die Masseneinheit reduzieren, z.B. die Gesamtstrahlung der Wolke. Falls man den Abdampfverlust nicht kennt, könnte man auch aushilfsweise auf die durch die Funkenstrecke in einer Richtung geflossene Ladung Q reduzieren.

(c) *Ergebnisse.* Es werde jetzt F mit F_2, B mit B_2 und E° mit der Entladung der Art $(2 \cdot 10^{-2}/20)$ identifiziert. Weiter werde zunächst die Gültigkeit des Reziprozitätsgesetzes für den photochemischen Umsatz vorausgesetzt.

Tabelle 3. Logarithmus des Intensitätsverhältnisses der Funkenlinie F_2 und der Bogenlinie B_2 in den ausgewerteten Spektren $Y = \log \alpha/\alpha_0$ mit $Y^\circ = 0$ für die Entladung der Art $(2 \cdot 10^{-2}/20)$ als Normierung

Amp \ Coul	$7 \cdot 10^{-6}$	$3 \cdot 10^{-5}$	$2{,}4 \cdot 10^{-4}$	$2 \cdot 10^{-4}$	$2 \cdot 10^{-3}$	$2 \cdot 10^{-2}$	$2 \cdot 10^{-1}$
1000			2,19 2,12			2,00 2,17	
200	1,33	1,88	2,31 2,25 2,23 2,23		2,17 2,04	1,48 1,68	
100				2,22 2,18	1,74 1,67	1,18 1,13	
40	1,27	1,69 1,86	1,71 1,63 1,71 1,63	1,62 1,64	0,97 0,84	0,55 0,52	0,50 0,48
20				0,89 0,88	0,34 0,35	Null (Normierung)	
10	0,89	0,90	0,49 0,49	0,59 0,59	−0,03 −0,02	−0,32 −0,27 −0,34 −0,25	−0,58 −0,59
4				0,19 0,23	−0,18 −0,17	−0,29 −0,28	−0,46 −0,51

Tabelle 3 gibt die Y-Werte für die untersuchten Entladungen E an. Von zwei in der Tabelle untereinander stehenden Zahlen bezieht sich die obere auf einen Versuch mit einer Wolfram-, die untere mit einer Silbergegenelektrode. Das Hauptergebnis ist: Die Y-Werte nehmen von der linken unteren zur rechten oberen Ecke stark zu. (Entsprechendes gilt auch für die aus den anderen Kombinationen der F und B gewonnenen Y-Werte.) Diese Resultate decken sich mit den von anderen Autoren z.T. an Zinklegierungen z.T. an anderen Elementen gewonnenen [14, 15].

Es wurden auch die X-werte für die benutzten Entladungen berechnet. Sie sollen jedoch nicht wiedergegeben werden, weil in ihnen grosse und in ein und derselben Richtung wirkende systematische Fehler enthalten sind (s.u.). Im allgegeinen sind die X-Werte für Entladungen derselben Gattung nicht stark von I abhängig. Dagegen steigen sie sehr stark von Entladungen mit kleinem Q nach solchen mit grossem Q hin an. So ist z.B. $X^2 - X^1$ etwa $+3$ für $E^2 = (2 \cdot 10^{-1}/40)$, $E^1 = (7 \cdot 10^{-6}/40)$.

Die Ergebnisse für die Y-Werte spiegeln die bekannte Tatsache wieder, dass, je kürzer und intensiver eine Entladung ist, desto funkenähnlicher ihr Charakter [6].: Das Verhalten der X-Werte könnte man versuchsweise folgendermassen deuten

Die leuchtenden Metalldampfwolken haben unabhängig von den speziellen Versuchsbedingungen eine "Anregungstemperatur" von etwa 5000–7000°C [7]. Da bei Entladungen gleicher Gattung überdies die Wolken gleiche Masse besitzen, strahlen sie den gleichen Teil ihrer Energie als Licht aus und liefern folglich auch gleiche X-Werte. Von zwei Entladungen verschiedener Gattung dagegen hat die mit grösserem Q die grössere Masse der Metalldampfwoke. Bei grösserer Masse der Wolke ist aber das Verhältnis des Volumens der Wolke zur Oberfläche grösser: es wird daher ein grösserer Bruchteil der Energie in Form von Strahlung und ein kleinerer in Form von Wärmeleitung abgegeben. Daher nehmen bei Vergrösserung von Q die X-Werte zu.

(d) *Fehlerquellen.* Wie schon erwähnt, werden die Intensitätsverhältnisse der Linien nach einem photographischen Verfahren bestimmt. Man würde nur dann zu quantitativ richtigen Ergebnissen gelangen, wenn die Linien sich nicht in der Zeitdauer ihres Leuchtens, sondern nur in ihrer Intensität unterschieden. Dies ist jedoch, wie man besonders aus neueren Untersuchungen mit lichtelektrischen Empfängern weiss, nicht einmal für Linien, die aus der gleichen Entladung entstammen, der Fall. Die Belichtungsdauer der Platten ist bei den verwendeten Funken nicht nur sehr unterschiedlich, sondern absolut gesehen sehr kurz. In solchen Fällen zeigen Photoemulsionen starke Abweichungen vom Reziprozitätsgesetz ("Kurzzeit-", "Ultrakurzzeiteffekt" [16]). Da sich jedoch die Intensitätsverhältnisse um Zehnerpotenzen ändern, können zwar die eben genannten Effekte das quantitative Bild modifizieren, nicht jedoch das qualitative Bild ändern.

4. Anwendungen

4.1. *Abfunk-und ähnliche Effekte*

(a) *Allgemeines.* Die spektrochemische Analyse erlaubt es, aus Intensitätsverhältnissen von Linien auf Konzentrationen von Elementen in der untersuchten Ausgangssubstanz zu schliessen. Viel bedeutungsvoller für das Spektrum sind aber die Konzentrationen in den Dampfwolken, die das Licht emittieren. Sie zu kennen ist geradezu eine Voraussetzung für die Lösung einer ganzen Reihe vorwiegend praktischer Probleme. Wie die entwickelte Methode auf diese Probleme angewendet werden könnte, soll im folgenden skizziert werden. (Das behandelte Gebiet ist sehr umfangreich. Es wurden nur ganz wenige Übersichtsversuche unternommen, die im einzelnen nicht angeführt werden sollen. Neue Arbeit über Abfunkeffekt usw. [17], dort auch weitere Literaturangaben.)

(b) *Abfunkeffekt.* Hierunter versteht man die Erscheinung, dass in der Spektorchemie interessierende Grössen, insbesondere Intensitätsverhältnisse von Linien, sich während des Abfunkens ändern (vor allem zu Beginn der Analyse). Für diese Anderungen von Intensitätsverhältnissen sind sicher zu einem wesentlichen Teil Änderungen von Konzentrationen in der Dampfwolke verantwortlich; doch können, wenigstens in speziellen Fällen auch andere Einflüsse wirksam werden [18]. Die Konzentrationen in den Wolken könnte man ohne Schwierigkeit bestimmen indem man das abgebaute Material der Analyse unterwirft. (Es kann auch hinreichen einen Teil des Materials zu bestimmen [19].) Besonders interessant wäre es, die Elektrode zu wiederholten Malen durch das Gefäss zu drehen und die Konzentrationen in den jeweils erhaltenen Niederschlägen zu vergleichen mit den Intensitätsverhältnissen in der Ausgangssubstanz.

(c) *Destillationseffekt.* Unter Destillationseffekt versteht man die Erscheinung,

VOL. 10 1957/5

dass der Funke aus Mehrkomponenten-Systemen vorzugsweise und für längere Zeit (Grössenordnung eine Minute) gewisse Komponenten (z.B. die mit niedrigem Siedepunkt) in den Gasraum befördert. Die Ausführungen des vorigen Abschnittes lassen sich m.m. auch auf diesen Effekt anwenden. Übrigens ist es nützlich, auch die Beobachtungen über Abbrandflecke mit zu berücksichtigen. So wird z.B. gewöhnlich angenommen, dass Fraktionierung der Komponenten besonders bei lang dauernden stromschwachen Entladungen eintreten könne. Betrachtet man jedoch die tiefausgehöhlten Gruben, die diese Entladungen in der Oberfläche hinterlasser so gerät man in Zweifel, ob eine solche Fraktionierung schon im einzelnen Funken möglich ist. Diese Frage lässt sich natürlich nur durch das Experiment entscheiden.

(d) *Störung durch dritte Partner.* Im allgemeinen hängen bei einem vorgegebenen Analysenverfahren die Intensitätsverhältnisse der Linien zweier zu bestimmender Elemente nur von deren Konzentrationen in der Ausgangssubstanz ab. Dies trifft jedoch in manchen Fällen nicht mehr zu, wenn man gewisse Stoffe in eventuell nur geringen Mengen zusetzt. Eine Analyse des abgebauten Materials würde es ermöglichen festzustellen, ob solche Irregularitäten darauf zurückzuführen sind, dass die Konzentration in den leuchtenden Dampfwolken nicht gleich denen im massiven Ausgangsmaterial sind, oder, ob der dritte Partner die Anregungsbedingungen in der Wolke verändert. (Neuere Arbeit über dritte Partner siehe Calker und Wienecke [20].)

4.2. *Sonstige Anwendungen*

Die Beobachtung über Abbrandflecke kann man zu Rate ziehen, wenn bei der Analyse die Oberflächenbeschaffenheit der Elektrode eine wesentliche Rolle spielt. Dieser Fall tritt z.B. ein bei der Untersuchung galvanischer Niederschläge, von Plattierungen, Korrosionsprodukten auf Oberflächen, Oxydbeschlägen, wärmebehandelten Oberflächen usw. So wäre z.B., um einen konkreten Fall zu nennen, zu überlegen, ob man zur empfindlichen Analyse eines dünnen galvanischen Bezuges die sonst für empfindliche Untersuchungen bevorzugten weichen Funken benutzen soll. Diese graben sich männlich tief in die Elektrode ein und befördern zum grossen Teil das gar nicht interessierende Grundmaterial in die Funkenstrecke. Der sonst nicht besonders empfindliche harte Funke könnte hier viel angemessener sein; denn er greift hauptsächlich den oberflächlichen Überzug an. Umgekehrt wird man etwa zur Lokalanalyse besser weiche Entladungen benutzen, da diese eng begrenzte Abbrandflecke liefern.

5. Schlussbemerkungen

In der Arbeit werden eine Reihe von Fragestellungen berührt, die weiter zu behandeln lohnend erscheint. Einige besonders wichtige dürften die folgenden sein: Wie verhalten sich die Abbauerscheinungen bei Zink in Abhängigkeit von der Oberflächenbeschaffenheit der Elektrode, dem umgebenden Gas und dem Druck? Welche Erscheinungen treten bei ähnlichen Metallen (etwa Cadmium), welche bei wesentlich verschiedenen (z.B. Kupfer, Silber, Gold) auf? Welche Besonderheiten zeigen sich bei Legierungen? Bestehen etwa Zusammenhänge zwischen den Abbauerscheinungen und dem Zustandsdiagramm der Legierung?

Für theoretische Untersuchungen dürfte es von grosser Bedeutung sein, den Abdampfverlust in Abhängigkeit von der Elektrodentemperatur zu bestimmen. Bei gleichzeitiger Beobachtung der Spektren, ev. auch der Brennspannungen, könnten daraus wichtige Rückschlüsse zu der bislang anscheinend noch nicht geklärten Frage gezogen werden, welcher Teil der zur Kathode gelieferten Energie zur Verdampfung von Material, welcher zur Erwärmung der Elektrode verwendet wird.

Meinem verehrten Lehrer, Herrn Professor Doktor H. Kaiser, möchte ich an dieser Stelle für die Anregung zu der Arbeit herzlich danken. Zu ihrer Durchführung stellte er grosszügig die mittel des Institutes für Spektrochemie und angewandte Spektroskopie (Dortmund) zur Verfügung.

Literatur

[1] Kaiser H. und Wallraff A. *Ann. Phys. Lpz.* 1939 **34** 297–340.
[2] Steinhaus D. W., Crosswhite H. M. und Dieke *Spectrochim. Acta* 1953 **5** 436–451.
[3] Tsui-Fang, Cundall C. M. und Craggs J. D. *Spectrochim. Acta* 1953 **5** 452–459.
[4] Cundall C. M. und Craggs J. D. *Spectrochim. Acta* 1955 **7** 149–164.
[5] Hurwitz J. K. *Spectrochim. Acta* 1955 **7** 1–13.
[6] Laqua K. *Spectrochim. Acta* 1952 **4** 446–466.
[7] Stetter A. *Spectrochim. Acta* 1953 **5** 350–363.
[8] Bunge K. *Spectrochim. Acta* 1955 **6** 134–140.
[9] Kohlrausch F. *Praktische Physik* Bd. 2. Leipzig 1944.
[10] Sandell E. B. *Colorimetric Determination of Traces of Metals.* New York 1950.
[11] Seelinger R. und Wulfhekel H. *Ann. Phys. Lpz* 1930 **6** 87–104.
[12] Somerville J. M., Blevin W. R. und Fletcher N. H. *Proc. Phys. Soc.* B 1952 **65** 963–970.
[13] Cobine J. D. und Gallagher C. J. *Phys. Rev.* 1948 **74** 1524–1530.
[14] Sinclair D. A. *J. Opt. Soc. Amer.* 1949 **39** 958–966.
[15] Corless Ch. H. *Spectrochim. Acta* 1952 **5** 378–388.
[16] Angerer E. v. *Wissenschaftliche Photographie.* Leipzig 1952.
[17] Keil A. *Spectrochim. Acta* 1956 **7** 367–372.
[18] Kaiser H. *Transactions, Instruments and Measure Conference.* Stockholm 1949.
[19] Sventitskii N. S. und Taganov K. T. *Izv. Akad. Nauk SSSR* 1948 **12** 396–401.
[20] Calker J. v. und Wienecke *Z. Angew. Phys.* 1952 **4** 210.

VOL.
10
1957/5

Spectrochimica Acta, 1957, Vol. 10, pp. 149 to 153. Pergamon Press Ltd., London

The solvent effect in infra-red intensities

THEODORE L. BROWN
Noyes Chemical Laboratory, University of Illinois, Urbana, Illinois

(*Received* 28 *May* 1957)

Abstract—The problem of the effect of the solvent upon the intensity of infra-red absorption is discussed. Equations relating the intensities measured in solutions to one another and to the vapor intensity are derived and compared with experimental results. An equation based on a model which takes into account the shape of the solute molecule as well as the dielectric constant of the surrounding medium is capable of accounting, at least qualitatively, for the variety of observed solvent effects.

DURING the past few years there has arisen a considerable interest in the measurement of infra-red absorption intensities. Because the number of molecules which can be studied as vapors is limited, measurements are frequently made on compounds in solution. It is desirable, therefore, that the possibilities of correcting data obtained for compounds in solution to vapor phase values be investigated. A less formidable but perhaps equally important objective is the correlation of intensity data obtained for compounds in different solvents. Although some experimental results regarding the effect of solvent on infra-red intensities are available in the literature, an adequate theory has not been advanced as yet. In this paper some of the factors which must be involved in affecting the intensities in solution are considered, and equations based on various models are evaluated.

Theory

The intensity of infra-red absorption, A, may be expressed as

$$A = \frac{1}{n}\,\frac{N\pi}{3\bar{c}}\left(\frac{\partial\mu}{\partial Q}\right)^2 \tag{1}$$

where N is Avogadro's number, $\bar{c}$ is the velocity of light, n is the refractive index of the medium surrounding the absorbing molecule, μ is the dipole moment, and Q is the vibration co-ordinate. Although the value of n measured at the wavelength of the absorption being observed should be used in this and the following equations, the optical values are good approximations for the solvents which are considered. In order to compare the intensities for a compound in two different media the term $(\partial\mu/\partial Q)$ must be evaluated for the two cases.

Let it be assumed that for solutions in *non-polar solvents* the electric moment of a solute molecule, μ_s, is a function of these variables; (a) the vapor state moment, μ_v; (b) the dielectric constant of the solvent, ϵ_m, and of the solute, ϵ_s; (c) a factor $\bar{g}$ which is dependent on the shape of the solute molecule and the location of the dipole within it.

Since the vibrational amplitudes are small in comparison with molecular dimensions, the factor g will not in general be a function of Q, nor will ϵ. Then,

$$\frac{\partial \mu_s}{\partial Q} = \frac{\partial \mu_s}{\partial \mu_v} \cdot \frac{\partial \mu_v}{\partial Q} \tag{2}$$

The ratio of intensities for two different media of refractive indices n_{m2} and n_{m1} is then,

$$\frac{A_2}{A_1} = \frac{n_{m1}}{n_{m2}} \cdot \frac{(\partial \mu_{s2}/\partial \mu_v)^2}{(\partial \mu_{s1}/\partial \mu_v)^2} \tag{3}$$

Several equations which have been developed to relate μ_s to μ_v, and which are based upon a model which takes into account some or all of the factors listed above can be adapted to the present problem. For example, ONSAGER has obtained the following equation [1]:

$$\mu_s = \frac{n^2{}_m(n^2{}_s + 2)}{2n^2{}_m + n^2{}_s}\ \mu_v \tag{4}$$

Application to equation (3) leads to

$$\frac{A_2}{A_1} = \frac{n_{m1}}{n_{m2}} \left[\frac{n^2{}_{m2}(2n^2{}_{m1} + n^2{}_s)}{n^2{}_{m1}(2n^2{}_{m2} + n^2{}_s)}\right]^2 \tag{5}$$

The simple Debye model does not permit an evaluation of a solvent effect for dilute solutions in non-polar solvents, and thus the Debye and Onsager models do not lead to equivalent results except for the limiting case of pure liquids discussed by POLO and WILSON [2].*

Equation (5) predicts a positive solvent effect which is dependent only on the dielectric constants of solvent and solute. It will be indicated in more detail later that this prediction is not always in accord with experiment; the magnitude of the solvent effect varies widely, and may even be zero or of the opposite sign from that predicted. Several semi-empirical expressions relating μ_s and μ_v have been developed which take into account the shape of the solute molecule [4]. One of the more successful of these, due to FRANK [5], is of the form

$$\mu_s = [1 + C - C/n^2{}_m]\mu_v \tag{6}$$

The sign and magnitude of the constant C is determined by the geometry of the solute molecule; zero or negative solvent effects are admissible. The corresponding expression for A_2/A_1 is

$$\frac{A_2}{A_1} = \frac{n_{m1}}{n_{m2}} \left[\frac{1 + C - C/n^2{}_{m2}}{1 + C - C/n^2{}_{m1}}\right]^2 \tag{7}$$

In the application of equation (6) to electric moment changes, the value of the constant is not easily determined *a priori*, but some generalizations can be drawn from the theory regarding the magnitude of the solvent effect. However, in applying these considerations to intensity changes a complicating factor arises. The vibration co-ordinate (taken as an internal co-ordinate), even when it can be assumed to be essentially localized in one bond of the molecule, may not coincide

* HIROTA [3] has obtained an expression for A_s/A_v from the ONSAGER model which differs from that given by POLO and WILSON. Equation (5) involves the same assumptions as those made by the latter authors.

VOL. 10 1957/5

with the direction of the primary dipole. For example, in the O—H stretching of alcohols the vibration co-ordinate makes an angle of about 55° with the primary dipole; the vibrational transition will involve then not only a change in the magnitude of the vector electric moment, but also a change in direction. It is to be expected that in general the magnitude of the solvent effect will be different for the intensities from that for the electric moments, although the same general form of equation should still be applicable.

Experimental

Materials. Reagent grade carbon tetrachloride, chloroform, and carbon disulfide were used without further treatment other than drying with anhydrous magnesium sulphate. Commercial grade hexane and tetrachloroethylene were purified by fractionation with an efficient packed column. The benzonitriles were Eastman Kodak White Label materials, purified by recrystallization. Propargyl alcohol, a gift from Antara Chemicals, division of General Aniline and Film Corp., was purified by fractional distillation.

Procedure. The experimental procedures employed have been described elsewhere [10]. Spectral slit widths of 1·8, 4·2, and 4·5 cm^{-1} were employed for the C≡N, ≡C—H and O—H bands, respectively. An integration interval of 50 cm^{-1} was chosen for the C≡N band, while for the ≡C—H and O—H bands the interval was 150 cm^{-1}.

Comparison with experiment

Although studies of the solvent dependence of the intensity for infra-red absorption are not numerous, there is considerable evidence that equation (5) is not adequate for many compounds. The magnitude of the solvent effect varies considerably for different classes of compounds, whereas it is predicted by the equation to be constant. In addition, even negative solvent effects have been observed for the C—C stretching band of acetonitrile [6], and the 1200 cm^{-1} C—O—R band of methyl formate measured in non-polar solvents [7]. In both of these last cases the vibration co-ordinate is nearly centrally located and lies along the long axis of the molecule, an arrangement for which FRANK's theory predicts a negative solvent effect for the static moments. Equation (7) is capable of accounting in a reasonable way for the variations in the magnitude of the solvent effect, and even for the few cases of negative solvent effect.

The variation in intensity with change in solvent for molecules in which the vibrational co-ordinate lies near the end of the molecule has not been examined as yet. In Table 1 are shown the results of intensity measurements on some compounds of this type. It is seen that the magnitude of the solvent effect varies considerably for the absorptions studied. For the ≡C—H bond in particular, the solvent effect is nearly zero.

If equation (7) is applied to the results for the ≡C—H band of propargyl alcohol, C being obtained by averaging the values calculated for all possible pairs of solvents, a value for A_e of 0·60 ± 0·01 intensity units is obtained. Treating the results obtained for the C—O—R band of methyl formate in non-polar solvents [7] in the same manner, a value for A_e of 1·38 ± 0·03 results. This is much larger than the reported value of 1·00 which may, however, be low; the effect of pressure

broadening was not studied, and the one atmosphere of air which was employed may have been inadequate. A completely satisfactory test is not possible until values of A_v are available for comparison with those calculated from solution data, but the above results show at least that a consistent value for A_v can be obtained from use of equation (7) in cases where equation (5) is altogether unsatisfactory.

Table 1. The integrated intensity of some infra-red absorption bands in non-polar solvents

Compound	A*	ν_m	$\Delta\nu_{\frac{1}{2}}$	Solvent
p-Methylbenzonitrile C≡N stretch	0·21	2226	6·5	C_6H_{14}
	0·28	2226	6·5	CCl_4
	0·26	2226	6·5	C_2Cl_4
	0·48	2227	10·5	$CHCl_3$
p-Fluorobenzonitrile C≡N stretch	0·15	2224	6·5	C_6H_{24}
	0·20	2224	6·0	CCl_4
	0·18	2223	6·0	C_2Cl_4
	0·37	2223	11·0	$CHCl_3$
Propargyl alcohol O—H stretch	0·39	3629	27	C_6H_{14}
	0·60	3619	22	CCl_4
	0·59	3617	22	C_2Cl_4
	0·68	3608	22	CS_2
Propargyl alcohol ≡C—H stretch	0·66	3321	13	C_6H_{14}
	0·68	3318	14	CCl_4
	0·66	3316	12	C_2Cl_4
	0·64	3312	12	CS_2

* In units of 1×10^4 mole^{-1} litre cm^{-2}

Discussion

A quantitative test of any theory of the solvent effect in infra-red intensities is very difficult to make because of the extreme sensitivity of the intensity to specific interactions, particularly those involving the functional group under study. For example, the C≡N intensity of benzonitriles increases by about 80 per cent in chloroform as compared with carbon tetrachloride (Table 1), presumably because of hydrogen bonding [8]; the C—D stretching band of chloroform —*d* varies by a factor of 36 in a variety of solvents [9]. The large increase in the O—H intensity of propargyl alcohol in the other three solvents as compared with hexane (Table 1) is probably due to weak hydrogen bonding effects. Nevertheless it does appear that, apart from specific interactions, the geometrical character of the solute molecules is important in determining solvent effects in non-polar solvents.

It is interesting to note that the solvent effect for the intensities does not always parallel that for the frequencies (Table 1). For non-polar solvents the frequency shifts appear to depend only on the dielectric constant of the solvent, as predicted by the Kirkwood–Bauer–Magat equation [6].

VOL. 10 1957/5

References

[1] Onsager L. *J. Amer. Chem. Soc.* 1936 **58** 1486.
[2] Polo S. and Wilson M. K. *J. Chem. Phys.* 1955 **23** 2376.
[3] Hirota E. *Bull. Chem. Soc. Japan* 1954 **27** 295.
[4] Smith J. W. *Electric Dipole Moments* Chap. 6. Butterworths, London 1956.
[5] Frank F. C. *Proc. Roy. Soc.* 1935 A **152** 171.
[6] Bayliss N. S., Cole A. R. H. and Little L. H. *Aust. J. Chem.* 1955 **8** 26.
[7] Russell R. A. and Thompson H. W. *J. Chem. Soc.* 1955 479.
[8] Steel G. and Thompson H. W. *Trans. Faraday Soc.* 1956 **52** 1451.
[9] Huggins C. M. and Pimentel G. C. *J. Chem. Phys.* 1955 **23** 896.
[10] Brown T. L., Sandri J. M. and Hart H. *J. Phys. Chem.* 1957 **61** 698.

OL.
10
7/58

Spectrochimica Acta, 1957, Vol. 10, pp. 154 to 160. Pergamon Press Ltd., London

Proton resonance spectra of some crystals containing nitrogen and fluorine

J. B. Leane and R. E. Richards
The Physical Chemistry Laboratory, Oxford

(*Received* 26 *July* 1957)

Abstract—The preparation and analysis of a pure sample of ammonia–boron trifluoride is described. The proton and fluorine magnetic resonance spectra of this compound and also of ammonium fluorotitanate and ammonium fluorogermanate have been measured. The spectra from the fluorine nuclei at 90°K are consistent with a rigid arrangement of the fluorine nuclei in the lattice. The proton resonance spectra are, however, narrower than is possible in a rigid lattice structure and require reorientation of the NH_3 group and of the ammonium ions even at 20°K. This indicates a surprising weakness in the hydrogen bonds between the nitrogen and fluorine atoms. Other evidence which supports this conclusion is assembled in the discussion.

1. Introduction

The nuclear resonance spectra of molecular crystals are profoundly modified when molecular motion occurs. For example, a study of the proton resonance of the ammonium halides by Sachs, Turner and Purcell [1] and by Bersohn and Gutowsky [2] has provided detailed information about the type and the frequency of the molecular motion and the potential barriers which hinder it. The motion of the ammonium ion depends on the interactions between the ions in the crystal and occurs more easily and at lower temperatures when these interactions are weak.

Hydrogen bonding would provide a strong interaction between the ions and therefore increase the barrier hindering their motion. This is in fact observed in ammonium fluoride and hydrazine difluoride. The crystal structures of these compounds indicate that strong hydrogen bonds are formed, and the nuclear resonance spectra imply that they have a rigid lattice [3, 4].

There is, however, evidence that hydrogen bonding between nitrogen and fluorine is sometimes remarkably weak. Confirmation of the frequent weakness of these bonds has been found from the proton magnetic resonance spectra of ammonia–boron trifluoride and the ammonium salts of some complex fluoro-acids.

2. Experimental

Ammonia–boron trifluoride adduct

Preparation. The gas-phase reaction between ammonia and boron trifluoride has a high heat of reaction (about 41 kcal/mole [5]), and thermal decomposition of the product into ammonium fluoroborate and boron nitride occurs easily. A somewhat modified version of an earlier procedure for preparing this material [6] was therefore adopted.

A glass apparatus was so constructed that boron trifluoride gas, dry nitrogen, and then dry ammonia could be successively passed over about 150 ml of anhydrous ether contained in a 1 l. flask. The ammonia was dried by condensing it over

VOL.
10
1957/5

sodium at −80°C and the nitrogen was dried first with calcium chloride and then with phosphorus pentoxide.

The ether was first saturated with boron trifluoride, yielding the addition compound $Et_2O{\cdot}BF_3$. Excess gas was then expelled by passing dry nitrogen through the apparatus, so preventing deposition of ammonia–boron trifluoride in the connecting tubes and taps when ammonia is admitted. An approximately equal volume of dry ether was next added to the etherate; this was found to improve the quality of the final product and greatly reduced the proportion of ammonium fluoroborate produced.

Ammonia was then allowed to evaporate slowly from a cooled solution of sodium in liquid ammonia and to pass into the reaction vessel. This vessel was cooled in an ice-salt freezing mixture and gently agitated during the addition of ammonia. After about 45 min the reaction was complete and the flask was disconnected; the ether layer was poured off and the product which had deposited was dried for 24 hr *in vacuo*. It was then recrystallized from water, the temperature never exceeding 35°C in order to avoid hydrolysis. The crystals were filtered, washed, and dried.

Analysis. The most probable impurity in this product was ammonium fluoroborate, and so qualitative tests were made for the NH_4^+ and BF_4^- ions. By mixing a strong aqueous solution of the sample with sodium tetraphenyl boron solution there was shown to be less than 0·01 per cent NH_4^+ present; similarly, the BF_4^- concentration was shown to be less than 0·05 per cent by the absence of a precipitate with a 10 per cent solution of "Nitron" in 5 per cent acetic acid.

Quantitative analysis of the nitrogen by the Kjeldahl method gave a mean value of 16·48 per cent. The theoretical value is 16·50 per cent.

The boron was estimated by the following procedure. A weighed quantity of the compound was hydrolysed by boiling with a slight excess of sodium hydroxide; excess calcium chloride was then added to precipitate the fluoride ions, which interfere with the indicators. The solution was cooled and neutralized with hydrochloric acid, using methyl red as indicator, and the boron was then estimated by the mannitol method. A mean value of 12·91 per cent boron was found, the theoretical value being 12·76 per cent.

Ammonium fluorotitanate and ammonium fluorogermanate were kindly provided by Dr. A. Sharpe of Cambridge.

Measurements. The nuclear magnetic resonance spectra were recorded with the apparatus described by Richards and Smith [7] and Pratt and Richards [8]. A twin-T radio frequency bridge system was used, care being taken to avoid saturation of the spin system by use of too much r.f. power. The derivative curves of the absorption signal were plotted automatically on a recording milliammeter. The second moments were calculated from these curves and were corrected for modulation broadening [9] and for the effect of field inhomogeneity.

3. Results

The second moments were measured from the proton absorption signals and are given in Table 1. The errors stated are standard deviations.

The averaged derivative curves are shown in Figs. 1, 2, and 3.

Table 1. Second moments of the proton resonance signals

Compound	Temperature (°K)	Second moment (gauss^2)	Number of measurements
$H_3N{\cdot}BF_3$	293	12·74 ± 1·18	9
$H_3N{\cdot}BF_3$	20	15·34 ± 0·74	11
$(NH_4)_2TiF_6$	90	6·14 ± 0·23	7
$(NH_4)_2TiF_6$	20	11·06 ± 0·12	5
$(NH_4)_2GeF_6$	90	6·60 ± 0·20	5
$(NH_4)_2GeF_6$	20	10·18 ± 0·54	4
NH_4BF_4 [10]	20	14·35 ± 1·25	9

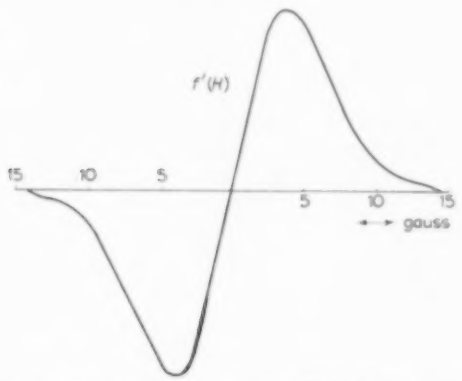

Fig. 1. Proton resonance signal of $H_3N{\cdot}BF_3$ at 20°K.

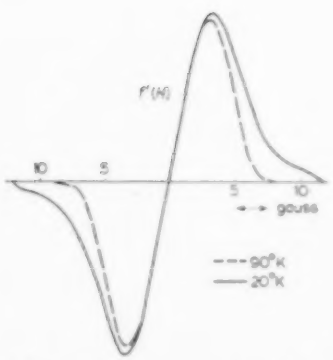

Fig. 2. Proton resonance signal of $(NH_4)_2TiF_6$ at 90°K and 20°K.

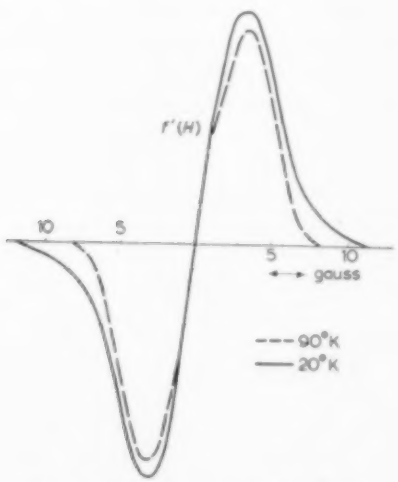

Fig. 3. Proton signal of $(NH_4)_2GeF_6$ at 90°K and 20°K

The second moments of the fluorine signals were also measured at 90°K and are given in Table 2.

Table 2. Second moments of the flourine resonance signals

Compound	Temperature (°K)	Second moment (gauss²)	Number of measurements
$H_3N{\cdot}BF_3$	90	25·08 ± 1·18	8
$(NH_4)_2TiF_6$	90	9·71 ± 0·38	7
$(NH_4)_2GeF_6$	90	11·18 ± 0·56	8
NH_4BF_4	90	22·26 ± 1·60	10

4. Discussion

Ammonia–boron trifluoride. If an N—H bond distance of 1·02 Å and a B—N—H bond angle of 107° is assumed in ammonia–boron trifluoride (as suggested by Hoard, Geller and Cashin [11]), it is found that intramoleculer broadening alone should contribute 35·6 gauss² to the second moment. The observed second moment is much lower than this and some reorientation of the NH_3 group must be assumed.

The most probable motion in this compound is rotation of the NH_3 group about the B—N bond. Gutowsky and Pake [12] have shown that rotation of a triangular group of nuclei at resonance about their threefold axis reduces the intramolecular broadening to one-quarter of the rigid lattice value. Here this amounts to 8·9 gauss², leaving from 3·8 gauss² (at 293°K) to 6·4 gauss² (at 20°K) to be accounted for by intermolecular broadening. This is approximately the figure to be expected, and it is therefore concluded that this motion about the C_3 molecular axis accounts for the narrowness of the absorption line.

The ammonium salts. The intra-ionic broadening of a stationary ammonium ion is about 43 gauss² [13] and the additional intermolecular broadening usually raises the total second moment to about 50 gauss². Since, in the salts studied here, the second moments lie in the range 6·1 to 14·3 gauss², it is clear that the absorption line is being narrowed by some form of reorientation. The absorption line-width is reduced when the molecular reorientation frequency exceeds a critical value near 10^5 c/s. When a narrow line is observed, therefore, it is concluded that the molecular motion occurs at a frequency greater than this.

It is not, however, easy to specify the reorientation process here; Pendred and Richards [10] suggest that rotation of the ammonium ion about a C_2 axis accounts for the second moment of 14·35 gauss² for the fluoroborate at 20°K.

The results of about 6 gauss² for the fluorotitanate and fluorogermanate at 90°K are so low as to require complete and random reorientation of the ammonium ions; interionic interactions are then entirely responsible for the broadening. At 20°K, however, the second moments show that the motion can no longer be random. The reorientation mechanism may be rotation about a C_2 axis or some rocking motion with very large amplitude. The latter seems the more probable.

General. It has been shown [13] that the potential barrier hindering the motion of the ammonium ion in the ammonium halides is approximately proportional to the temperature of the line-width transition in their proton resonance spectra. If this relationship is assumed to apply to the fluorogermanate and fluorotitanate, it would imply that here the ammonium ion is hindered by a barrier of less than 740 cal/mole. This is much smaller than the barrier in ammonium chloride (4740 cal/mole [13]); if any hydrogen bonds do occur between the ammonium ions and the fluorine atoms, they must be extremely weak.

The results are remarkable, for these bonds are known to be quite strong in many cases; for example, the N—H bending vibration is found at 1494 cm^{-1} in ammonium fluoride [14] compared with 1397 cm^{-1} in the chloride and iodide. Similarly, the low N—F separation of 2·62 Å in hydrazine difluoride [15] provides evidence of hydrogen bonding. They do, however, confirm other measurements of an entirely different kind which indicate that strong hydrogen bonds are not always formed to fluorine atoms.

Cote and Thompson have found [16] that certain infra-red bands associated with the fluoroborate ion occur at the same frequency in the ammonium salt as in the sodium and potassium salts; hydrogen bonding, if it occurred, would displace some of these bands in the ammonium salt.

Cox and Sharpe have determined the unit cell constants of a large number of complex fluorides from X-ray data [17–20]. They showed that the cell dimensions of the ammonium salts are in general slightly greater than those of the corresponding rubidium derivatives [17]. Furthermore, they compared the molecular volumes of the salts of several complex fluoro-, chloro-, and bromo-acids [18]. In the case of the complex chloro- and bromo-acids, the volume of the ammonium salt lies between those of the potassium and rubidium derivatives, yet in all the complex fluorides (except the hexafluorosilicates) the molecular volume of the ammonium salt is approximately equal to or greater than that of the rubidium compound. If hydrogen bonds occur, a contraction of the N · · · F distance would be expected, probably leading to a smaller molecular volume.

The infra-red band associated with the N—H bending mode, which occurs at about 1400 cm^{-1}, has been observed for many of the above salts [18] and is shown in Table 3. Hydrogen bonding raises the frequency of this vibration, but it is clear that, of those listed, only in ammonium fluoride is there an appreciable increase in frequency.

Lastly, the absence of any difference in the O—H stretching frequency of benzyl alcohol when dissolved in toluene and benzyl fluoride [21] demonstrates how weak the hydrogen bond from a hydroxyl group to a fluorine atom can be. This contrasts with the significant shift which is observed, for example, when benzyl alcohol is mixed with anisole.

The number and distance of the nearest fluorine neighbours about the nitrogen atoms in the compounds studied also shows no indication of the formation of hydrogen bonds. The results of X-ray measurements are given in Table 4. Detailed data are not available for the fluorotitanate, but its structure is known to be very similar to the fluorogermanate [18].

These N—H · · · F distances may be compared with the much smaller separations

VOL.
10
1957/5

of 2·66 Å in ammonium fluoride [24] and 2·62 Å in hydrazine difluoride [15]; this again indicates the absence of hydrogen bonding.

It also seems likely that even if weak hydrogen bonds are formed, the protons may adopt a large number of nearly equivalent positions which will be separated by

Table 3. Frequency of the N—H bending mode of some ammonium salts

Compound	Frequency (cm^{-1})	Compound	Frequency (cm^{-1})
NH_4F	1494	$(NH_4)_2TiF_6$	1408
NH_4Cl	1397	$(NH_4)_2GeF_6$	1408
NH_4Br	1407	$(NH_4)_2BeF_4$	1426
NH_4I	1397	NH_4BF_4	1430
$(NH_4)_2SiF_6$	1405		

Table 4. Number and distance of the nearest fluorine neighbours about the nitrogen atoms

Compound	Number of neighbours	Distance (Å)
$H_3N{\cdot}BF_3$ [11]	6	2·98–3·15
$(NH_4)_2GeF_6$ [22]	9	2·97–3·00
NH_4BF_4 [23]	8	2·83–3·08

Table 5. X—F and N—H separations in the ions, $XF_6^{=}$ and XF_4^{-}

Ion	Separation (Å)	Ion	Separation (Å)
$TiF_6^{=}$ [25]	1·917	BF_4^{-} [23]	1·43
$GeF_6^{=}$ [22]	1·77	NH_4^{+} [2]	1·03

only a small potential barrier; it is therefore possible that rotational movement would not be much restricted.

The anions of these salts are much larger than the ammonium ions, as shown in Table 5. Relatively large spaces may therefore be left for the ammonium ions and their motion may not then be much restricted. It is interesting to note that the highest observed second moment for the ammonium salt of a complex fluoro-acid, corresponding to the least free reorientation, is found for the fluoroborate, in which the anion is smallest.

Finally, the second moments of the fluorine signals range from 9·7 to 25·1 gauss^2 and are all compatible with a rigid arrangement of the fluorine atoms in the lattices.

Acknowledgements—We thank the Hydrocarbon Research Group of the Institute of Petroleum for financial help, and the Ministry of Education for a maintenance grant to one of us (J. B. L.).

References

[1] Sachs A. M., Turner E. H. and Purcell E. M. *Phys. Rev.* A 1949 **76** 466.
[2] Bersohn R. and Gutowsky H. S. *J. Chem. Phys.* 1954 **22** 651.
[3] Drain L. E. *Disc. Faraday Soc.* 1955 **19** 200.
[4] Deeley C. M. and Richards R. E. *Trans. Faraday Soc.* 1954 **50** 560.
[5] Laubengayer A. W. and Condike G. F. *J. Amer. Chem. Soc.* 1948 **70** 2274.
[6] Kraus C. A. and Brown E. H. *J. Amer. Chem. Soc.* 1929 **51** 2690.
[7] Richards R. E. and Smith J. A. S. *Trans. Faraday Soc.* 1951 **47** 1261.
[8] Pratt L. and Richards R. E. *Trans. Faraday Soc.* 1953 **49** 744.
[9] Andrew E. R. *Phys. Rev.* 1953 **91** 425.
[10] Pendred D. and Richards R. E. *Trans. Faraday Soc.* 1955 **51** 468.
[11] Hoard J. L., Geller, S. and Cashin W. M. *Acta Cryst.* 1951 **4** 396.
[12] Gutowsky H. S. and Pake G. E. *J. Chem. Phys.* 1950 **18** 162.
[13] Gutowsky H. S., Pake G. E. and Bersohn R. *J. Chem. Phys.* 1954 **22** 643.
[14] Plumb R. C. and Hornig D. F. *J. Chem. Phys.* 1955 **23** 947.
[15] Kronberg M. L. and Harker D. *J. Chem. Phys.* 1942 **10** 309.
[16] Coté G. L. and Thompson H. W. *Proc. Roy. Soc.* A 1951 **210** 217.
[17] Cox B. and Sharpe A. G. *J. Chem. Soc.* 1953 1783.
[18] Cox B. and Sharpe A. G. *J. Chem. Soc.* 1954 1798.
[19] Cox B. *J. Chem. Soc.* 1954 3251.
[20] Cox B. *J. Chem. Soc.* 1956 876.
[21] McDonald R. S., Gibbs J. H. and Ladd J. R. *J. Chem. Phys.* 1955 **23** 1170.
[22] Hoard J. L. and Vincent W. B. *J. Amer. Chem. Soc.* 1939 **61** 2849.
[22] Hoard J. L. and Blair V. *J. Amer. Chem. Soc.* 1935 **57** 1985.
[24] Zachariasen W. *Z. Phys. Chem.* 1927 **127** 218.
[25] Ibers J. A. and Holm C. H. *Acta Cryst.* 1957 **10** 139.

VOL.
10
1957/5

Spectrochimica Acta, 1957, Vol. 10, pp. 161 to 169. Pergamon Press Ltd., London

Infra-red spectrum of tetramethylhydrazine

D. C. McKean
Chemistry Department, University of Aberdeen, Scotland

(*Received* 17 *July* 1957)

Abstract—The infra-red spectrum of gaseous tetramethylhydrazine has been measured from 4500 to 400 cm^{-1}, using a conventional prism spectrometer. The region below 1500 cm^{-1} has also been investigated in the liquid and solid states, in solution and in the gas phase at 120°C.

The spectra in the gaseous and condensed phases are similar, with the exception of a few bands, possible reasons for whose appearance are suggested. No alteration in the spectrum occurs with change in temperature which can be attributed to the occurrence of more than one structural isomer.

Moments of inertia were calculated for a series of likely models and used to interpret and assign some bands with characteristic contours observed in the 10 μ region.

A plausible assignment of the skeletal stretching and methyl rocking vibrations can be made on the basis of the Penney–Sutherland model for the hydrazine skeleton.

Introduction

The structure of hydrazine has been the subject of considerable theoretical interest [1] and various physical methods have been employed in its determination [1–5]. A successful attack by means of infra-red spectroscopy awaits the interpretation of spectra obtained by the use of very high resolving power [6]. The infra-red spectra of several methyl-substituted hydrazines have recently been published [7a,b,c], but little structural information has so far been forthcoming, due in part to a lack of symmetry in these molecules.

In tetramethylhydrazine, however, the symmetry of the parent molecule is virtually restored, and it should be easier to make definite assignments of its vibration frequencies. In addition, the molecule is still sufficiently light for one to expect to find characteristic band contours in the gas phase.

The structure of tetramethylhydrazine is of particular interest, since the recent synthesis and examination of the chemical properties of tetrasilylhydrazine [8a]. The difference in chemical behaviour between the methyl and silyl compounds should be reflected in a difference in structure.

Experimental

Samples of tetramethylhydrazine were prepared by Aylett in this laboratory [8b]. One sample, which had been purified by mixing with acetic anhydride, contained a very small proportion of this substance. Other samples may have contained minute traces of *sym*-dimethylhydrazine, since a very small change in intensity occurred from one sample to another in the contour of the strong band at 720 cm^{-1}. A weak band at 1045 cm^{-1} is attributed below to another unknown impurity.

The spectrometer used was a Hilger H800 instrument equipped with NaCl and KBr prisms. A conventional 15 cm cell was used to study the gas at room temperature and in an oven at approximately 120°C. Liquid cells were filled in

a dry box flushed with nitrogen and no trace of decomposition could be detected by the spectrometer. For the solid state measurements, a solid film was deposited on a KBr window cooled to liquid-air temperatures in the usual type of low temperature absorption cell [9].

The spectrometer calibration was checked using the data of Downie, Magoon, Purcell and Crawford [10] and Plyler and Peters [11], the frequencies quoted below being reliable to ± 1 cm^{-1} below 1500 cm^{-1} and 5–10 cm^{-1} above 2000 cm^{-1}.

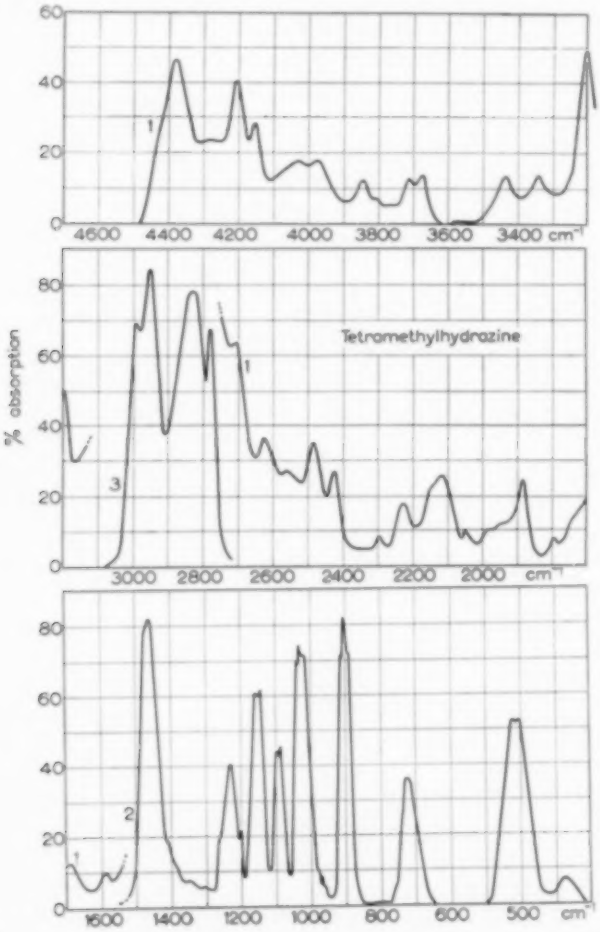

Fig. 1. Spectrum of tetramethylhydrazine vapour between 4500 and 400 cm^{-1}. Optical path lengths pL: (1)—260, (2)—50, (3)—15, in cm Hg cm.

Results

Discussion of spectra

The spectrum of the gas between 4500 and 1300 cm^{-1} is shown in Fig. 1: spectra in the gas, liquid, solution in carbon tetrachloride and solid between 1300

and 700 cm^{-1} are illustrated in Fig. 2. The spectrum in the gas phase at 120°C, not given, showed only a slight symmetrical broadening of each band consistent

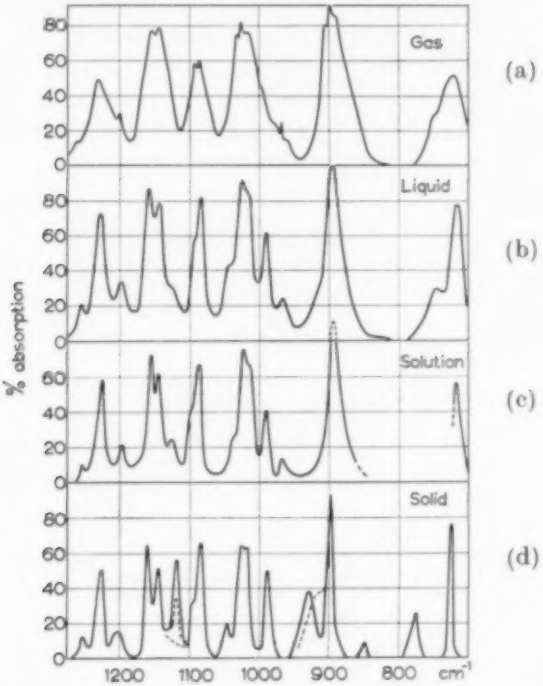

Fig. 2. Spectra of tetramethylhydrazine in (a) vapour, $pL = 50$; (b) liquid, $L = 0{\cdot}03$ mm; (c) 10 per cent by weight solution in carbon tetrachloride, $L = 0{\cdot}1$ mm; (d) solid film at ~80°K.

Table 1. Infra-red absorption frequencies in cm^{-1} of tetramethylhydrazine vapour above 1300 cm^{-1}

4380	3205	2220
4205	3090	2115
4160	2960	2045
4015	2835	1980
3965	2780	1947
3850	2705	1886
3795	2618	1792
3710	2562	1694
3675	2493	1588
3440	2425	1460
3340	2293	

with a normal alteration in the population of the ground state J levels. The gaseous frequencies are listed in Table 1. Table 2 is devoted to a comparison of

VOL. 10 57/58

the frequencies occurring below 1300 cm^{-1} in the various phases for tetramethylhydrazine together with the gas phase frequencies of dimethylamine.

In the region above 1300 cm^{-1} there appear the usual bands due to CH_3 stretching and deformation vibrations, together with considerable absorption due to overtone or combination frequencies.

Table 2. Infra-red frequencies and assignments in dimethylamine and tetramethylhydrazine in the region below 1300 cm^{-1}

$(CH_3)_2NH$[a]			$(CH_3)_4N_2$				
ν_{gas}	Contour	assignment[c]	ν_{gas}	Contour	ν_{liquid}	ν_{solid} (−190°C)	Assignment[c]
1276 vw		δCH_3 *sym.*[b]			1255 w	1253 w	
			1231 s		1228 s	1225 s	δCH_3 *sym.* (a) and (a)
			1201 w		1198 w	1203 m	
1155 vs	*PQR* *A* type	δCH_3 *anti.*	1151 vs	*PR* ~11 cm^{-1}	1157 vs 1144 vs	1160 vs 1146 vs	δCH_3 *anti.* (b) and (b)
					1126 w	1119	overtone or combination
					1094 sh	1089 sh	overtone or combination
			1089 s	*PR* ~8 cm^{-1}	1084 vs	1084 vs	ν_{CN} *anti.* (a)
					1041 w	1046 w	impurity
1018 s	*PQR* *A* type	ν_{CN} *anti.*	1026 vs	*PQR* ~15 cm^{-1}	1023 vs	1021 vs	ν_{CN} *anti.* (b)
					1017 sh	1017 vs	ν_{CN} *sym.* $-\nu_{NN}$(a)
			969 w	*PQR* ~22 cm^{-1}	989 s	987 s	δCH_3 *perp.* (b)
					966 w	–	" " (a)
						927	898 + libr.
925 m	*PR* *B* type	ν_{CN} *sym.*	899 vs	*PQR* ~15 cm^{-1}	895 vs	898 vs	ν_{CN} *sym.* (b)
						848 w	overtone or combination
			748 sh		746 sh	766 w	overtone or combination
			722 s		718 s	721 s	ν_{CN} *sym.* + ν_{NN} (a)
			509 vs	*PR* ~7 cm^{-1}	510 vs	517 vs 510 vs	skeletal bend (b)
			435 m		440 m	440 m	skeletal bend ?
					405 w	405 w	?

[a] *Ibid.* See also J. R. Barcelo and J. Bellanato *Spectrochim. Acta* 1956 **8** 27.
[b] The corresponding mode is identified more certainly in dimethyl ether at 1244 cm^{-1}.
[c] *sym.*, *anti.*, and *perp.* refer to the C_3-axis and plane respectively of the $(CH_3)_2N$ group.

In the region below 1300 cm^{-1}, the spectra in the gaseous and condensed phases resemble each other closely, the principal bands at 1231, 1151, 1089, 1026, 899 and 722 cm^{-1} in the gas occurring in practically identical positions in the liquid and solid. The bands at 1151 and 1026 cm^{-1}, however, become doublets in the liquid and solid states respectively. Two bands, those at 969 and 746 cm^{-1}, appear to be shifted about 20 cm^{-1} by a change in phase, the most likely correlation being shown in Table 2.

There are also four bands appearing in the liquid or solid which appear to be unrepresented in the gas. These lie at 1120, 1045, 927 and 848 cm^{-1}, and they all exhibit some form of irregular behaviour. The band at 1045 cm^{-1}, for instance, during the evaporation of the melted film diminished in intensity much less rapidly than the rest of the spectrum: its assignment to an impurity less volatile than tetramethylhydrazine seems unavoidable.

VOL. 10 1957/5

The band at 927 cm^{-1} in the solid film was unaltered in intensity when the film warmed up, but moved to about 915 cm^{-1} on the side of the intense band at 894 cm^{-1}. This behaviour, together with its unusual width, suggests that the band may be due to an overtone or combination involving a low-lying fundamental whose frequency is noticeably affected by a change of phase from solid to liquid. A combination involving the fundamental at 894 cm^{-1} and a librational frequency is a possible choice [12].

The intensity of the band at 1120 cm^{-1} varied greatly, as shown in Fig. 2, according to the particular solid film deposited; moreover, the same sample of liquid which was used to deposit the film showed no trace of the band in a check made on the gas. When the low-temperature cell was allowed to warm up, an initial thickening of the film occurred due to material evaporating off the surrounding metal block on to the window, the temperature of which lagged behind that of the block. With one specimen the band at 1120 cm^{-1} increased in intensity relative to the other bands in the spectrum: in another it decreased during this thickening. Since tetramethylhydrazine readily supercools, the above behaviour is explained if the intensity of this band depends to a large extent on the crystallinity of the film and if the degree of crystallinity varied widely from one specimen to another, according to the exact circumstances of deposition.*

This behaviour of the band at 1120 cm^{-1} was paralleled by that of the weaker band at 848 cm^{-1}.

An important question to be answered before discussing the problem of assignment is whether or not the molecule exists in more than one configuration.

Examination of the modes of vibration likely to occur between 1300 and 600 cm^{-1} shows that the bands arising are very little altered in frequency by a rotation of the end groups with respect to each other, although their intensities are greatly affected. The bands of isomers such as those shown in Fig. 3 will therefore overlap, and it might be hard to detect a small change in the relative abundance of two forms by observing the effect of a change in temperature on the spectrum. Over a range of 100°C, no changes could in fact be detected in the spectrum of the gas, and it will be assumed that the molecule exists in only one form.

Moments of inertia and band contours

As an aid to assignment, moments of inertia were calculated for a series of restricted internal rotor models having the following dimensions:

$$r_{CH} = 1{\cdot}09\ \text{Å}, \qquad r_{CN} = 1{\cdot}47\ \text{Å}, \qquad r_{NN} = 1{\cdot}45 \text{ or } 1{\cdot}50\ \text{Å},$$

$$\angle HCH = \angle CNC = \angle CNN = 109°28'$$

The angle θ between the planes bisecting the $(CH_3)_2N$ groups was varied from 0°, corresponding to the *cis* configuration (Fig. 3), to 180°, for the *trans* model. Fig. 4 shows the values of I_A, I_B, and I_C which result. While the directions of two of the principal axes vary, that of the third remains fixed along the C_2-symmetry

* The fact that any particular configuration of the molecule other than the *cis* or *trans* forms can exist as two optically active isomers may be connected with this phenomenon.

axis of the molecule. This is the principal axis for the largest and intermediate moments of inertia respectively for $\theta < 83$ and $> 83°$. The vibrations of the molecule fall into two classes A and B, which are symmetric and antisymmetric respectively with respect to the C_2-axis. In the A class, therefore, the dipole

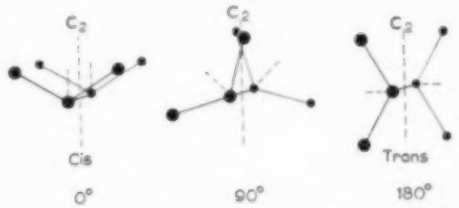

Fig. 3. Configurations of the hydrazine skeleton, assuming tetrahedral interbond angles.

moment change lies along the C_2-axis and we expect to observe either pure C or pure B type bands according to whether $\theta < 83$ or $> 83°$. At the same time the bands in the B class will be either hybrid A—B or hybrid A—C type bands. For $\theta \approx 83°$ the molecule is an accidental symmetric top, but for practically all other

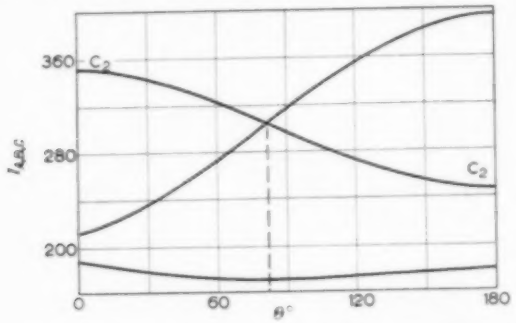

Fig. 4. Values of moments of inertia I_A, I_B, and I_C, for tetramethylhydrazine models, as functions of the relative orientation of the end groups.
$r_{NN} = 1{\cdot}45$ Å. Units: 10^{-40} c.g.s.

configurations the calculations of Badger and Zumwalt [13] for asymmetric top molecules show that A, B and C type bands will appear having P—R separations respectively of about 15 cm^{-1}, 7 cm^{-1}, and 22 cm^{-1}.

The bands at 1026 and 899 cm^{-1} in the gas are therefore identified as predominantly A type, those at 507 and 1089 as B type, and that at 969 cm^{-1} as C type. The band at 1152 cm^{-1} in the gas would be B type except for its PR separation of 11 cm^{-1}, which is too high. The appearance of two strong bands at the same frequency in the liquid suggests that it is not, in fact, hybrid, but composite.

Assignments

The forty-eight normal vibrations of tetramethylhydrazine may be divided into five groups:

(1) Twelve CH_3 stretching modes, in the 3 μ region.

(2) Twelve CH_3 deformations, lying between 1300 and 1470 cm^{-1}.

VOL.
10
1957/5

(3) Eight CH_3 rocking modes, (δ), which vary more widely in frequency but will certainly not be found outside the range 1300–800 cm^{-1}.

(4) Twelve skeletal modes, including five C—N or N—N stretching (ν) and seven bending motions, the former lying between 1100 and 700 cm^{-1}, the latter at rather low frequencies.

(5) Four restricted rotations of the methyl groups.

Between 1300 cm^{-1} and 700 cm^{-1} there will therefore be thirteen modes which may all be infra-red active, provided the molecule does not have a centre of symmetry, as in the *trans* configuration. The form of these modes will closely resemble the corresponding vibrations of dimethylamine. The latter may be classified, using the approximate C_{2v}-symmetry of dimethylamine, as follows:

A_1—δCH_3 *sym.*, ν_{CN} *sym.* B_2—δCH_3 *perp.*

B_1—δCH_3 *anti.*, ν_{CN} *anti.* A_2—δCH_3 *perp.**

Of these, δCH_3 *perp.* (A_2) is infra-red inactive and δCH_3 *perp.* (B_2) is missing from the spectrum.†

In tetramethylhydrazine we accordingly expect in each symmetry class: δCH_3. *sym.*, δCH_3. *anti.*, δCH_3. *perp.* (2), ν_{CN} *anti.* and ν_{CN} *sym.*, with the addition of ν_{NN} to the *A* class only. However one of the δCH_3 *perp.* modes in each class will almost certainly be missing from the infra-red spectrum and the other possibly also. ν_{NN} in the *A* class will not have an intrinsic dipole moment change but will mix mechanically with ν_{CN} *sym.* to produce two active modes.

If the molecule possesses also a centre of symmetry the above modes will be contained in four classes as follows:

A_g δCH_3 *sym.*, δCH_3 *perp.* (2), ν_{CN} *sym.*, ν_{NN}.
A_u δCH_3 *anti.*, ν_{CN} *anti.*
B_g δCH_3 *anti.*, ν_{CN} *anti.*
B_u δCH_3 *sym.*, δCH_3 *perp.* (2), ν_{CN} *sym.*

Formally six infra-red active modes result, but one at least of these should be missing, namely δCH_3 *perp.* Since six strong bands are to be found in the spectrum of the gas, the *trans* structure can be eliminated.

If a direct comparison is made between the frequencies observed in dimethylamine, tetramethylhydrazine, and, in one case, dimethylether, several assignments can be made immediately.

These are: δCH_3 *sym.*, in both classes, at 1230 cm^{-1}.
δCH_3 *anti.*, in the two classes, at 1157 and 1144 cm^{-1}.

The overlapping of the bands in each class presumably prevents the appearance of characteristic band contours in the spectrum of the gas.

ν_{CN} *sym.* and ν_{CN} *anti.* in the *B* class of tetramethylhydrazine should lie very near to the corresponding modes in dimethylamine and almost certainly produce the *A* type bands at 899 and 1026 cm^{-1}. The likely positions of the two modes compounded of ν_{CN} *sym.* and ν_{NN} in the *A* class were calculated by borrowing CN

* "*sym.*", "*anti.*" and "*perp.*" denote symmetry with respect to the C_2-axis and plane respectively of the $(CH_3)_2N$ group.

† No *C* type band is visible in the spectrum of dimethylamine between 1500 and 650 cm^{-1}.

and NN stretching force constants from dimethylamine and hydrazine respectively, the bending motions being ignored. The predicted frequencies* are 715 and 1029 cm^{-1} respectively, the agreement with the bands observed at about 720 cm^{-1} in all phases and at 1017 cm^{-1} in the liquid and solid being very satisfactory. It is assumed that the higher mode is invisible under the *B* class band at 1026 cm^{-1} in the gas.

The strong band at 1089 and the weak one at 969 cm^{-1} in the gas remain unassigned: the only fundamentals left are ν_{CN} *anti.* in the *A* class and the four δCH_3 *perp.* modes, at least two of which should not be active. 1089 cm^{-1} is a little high for a CN stretching mode which does not to a first approximation mix mechanically with either ν_{CN} *sym.* or ν_{NN} in the same class. The frequency and relative intensity of this band are remarkably constant during phase changes, however, a characteristic of the skeletal stretching modes already assigned. By contrast, the band at 969 cm^{-1} is markedly affected by the phase change from gas to liquid and it seems more reasonable to assign it to a δCH_3 *perp.* mode, which should in any case be weak, by analogy with dimethylamine.

The band at 1089 cm^{-1} is accordingly assigned as ν_{CN} *anti.* (a).

The remaining bands in the spectrum, at about 1255, 1198, 1126, 1094, 966, 848 and 746 cm^{-1}, are probably overtones or combinations. If the band at 1084 cm^{-1} is correctly assigned to the *A* symmetry class, then its type *B* contour implies that $\theta > 83°$.

A strong suggestion that the angle is in fact close to 90°, within 10°, arises from a consideration of the relative intensities of the *A* and *B* class bands. If unit intensity is ascribed to each mode of the $(CH_3)_2N$ group such as δCH_3 *anti.* or ν_{CN} *anti.*, and if it is assumed that the dipole moment changes at the two ends of the hydrazine molecule are strictly additive, then the relative intensities of *A* and *B* class modes of each type (CN stretch or CH_3 rock) may readily be calculated as a function of θ.

For $\theta = 90°$, ν_{CN} *anti.* and δCH_3 *anti.* are predicted to have identical intensities in the two symmetry classes. (A 10° change in θ leads to a 30 per cent change in relative intensity.) In the assignment adopted here, the observed intensities respectively of the *A* and *B* class bands, due to ν_{CN} *anti.* or δCH_3 *anti.*, are very nearly the same.

While the assignment proposed above seems to be open to few objections, confirmatory evidence would be welcome. It is unfortunate that the band at 722 cm^{-1}, which can only be an *A* class mode, could not be resolved.‡

The structure indicated for the molecule is, however, one to be expected from the work of Penney and Sutherland on hydrazine itself. Experiment with a Stuart atomic model using an N—N distance of about 1·45 Å suggests that even in the eclipsed, or 120°, configuration there is no steric repulsion between the methyl groups at the two ends of the molecule: the same theoretical considerations should therefore apply to tetramethylhydrazine as to hydrazine itself.

* The two modes are approximately the in-phase and out-of-phase combinations respectively of the symmetric CN and NN stretching motions.

‡ While a *B* type contour could readily be obscured by a small amount of absorption due to an impurity or an overtone or combination band, the same is much less likely to be true of a type *C* band with its prominent *Q* branch. There is therefore slight negative evidence to suggest a *B* type contour for this band.

VOL. 10 1957/5

Acknowledgement—I am greatly indebted to Dr. B. J. Aylett for making available a number of samples of tetramethylhydrazine.

References

[1] Penney W. G. and Sutherland G. B. B. M. *Trans. Faraday Soc.* 1934 **30** 898.
[2] Giguere P. A. and Schomaker V. *J. Amer. Chem. Soc.* 1943 **65** 2025.
[3] Beamer W. *J. Amer. Chem. Soc.* 1948 **70** 2979.
[4] Collin R. L. and Lipscomb W. N. *Acta Cryst. Camb.* 1951 **4** 10.
[5] Giguere P. A. and Liu I. D. *J. Chem. Phys.* 1952 **20** 136.
[6] Mould H. M., Price W. C., Wilkinson G. R. and Wood R. *International Meeting of the European Molecular Spectroscopy Group, Freiburg.* July 1957.
[7] (a) Axford D. W. E., Janz G. J. and Russell K. E. *J. Chem. Phys.* 1951 **19** 704.
(b) Shull E. R., Wood J. L., Aston J. G. and Rank D. H. *J. Chem. Phys.* 1954 **22** 1191.
(c) Olsen A. L. and Kruse H. W. *J. Chem. Phys.* 1956 **24** 1106.
[8] Aylett B. J. (a) *J. Inorg. Nucl. Chem.* 1956 **2** 325.
(b) *J. Chem. Soc.* 1957 4152.
[9] Wagner E. L. and Hornig D. F. *J. Chem. Phys.* 1950 **18** 296.
[10] Downie A. R., Magoon M. C., Purcell T. and Crawford B. L. *J. Opt. Soc. Amer.* 1953 **43** 941.
[11] Plyler E. K. and Peters C. W. *J. Res. Nat. Bur. Stand.* 1956 **45** 462.
[12] cf. Hexter R. M. and Dows D. A. *J. Chem. Phys.* 1956 **25** 504.
[13] Badger R. M. and Zumwalt L. R. *J. Chem. Phys.* 1938 **6** 711.

OL.
10
7/58

Spectrochimica Acta, 1957, Vol. 10, pp. 170 to 178. Pergamon Press Ltd., London

Normal vibrations of urea and urea-d_4

A. YAMAGUCHI, T. MIYAZAWA, T. SHIMANOUCHI and S. MIZUSHIMA
Chemical Laboratory, Faculty of Science, Tokyo University
Hongo, Tokyo, Japan

(*Received* 24 *June* 1957)

Abstract—Infra-red absorption spectra of urea and urea-d_4 have been measured. Infra-red dichroic measurement and Raman measurement have been made for urea in the crystalline state. The normal vibrations of the planar C_{2v} model have been calculated as an eight-body problem and the assignment of the observed frequencies has been made.

Introduction

THE Raman and infra-red spectra of urea have been observed by several investigators [1].* The normal vibration calculation has been published by KELLNER, assuming non-planar structure. However, since the planarity of urea molecule has been established by WALDRON and BADGER [3] and by ANDREW and HYNDMAN [4], we have recently calculated the normal modes of vibration for the C_{2v} model, using a potential function of the Urey–Bradley type. Furthermore, we have made remeasurement of the Raman and infra-red spectra. In the present paper we should like to report the result of these theoretical and experimental researches, particularly the part which differs from those of the previous investigators.

Experimental results and discussion

Infra-red absorption spectra of urea and urea-d_4 have been measured as Nujol mull. Infra-red dichroic measurement has been made for oriented crystal prepared from ethanol solution. Raman measurement has also been made in the crystalline state to study low frequency vibrations.

Based on the result of these measurements and that of the normal vibration calculation to be described below, the assignment of observed frequencies has been made. This is not much different from that made by WALDRON and STEWART except the following points.

The band at 1150 cm^{-1} has been assigned by WALDRON and STEWART to a band of A_1 type. However, we conclude this band to be a stronger A_1 type band overlapped by a weaker B_2 type band. One might consider the latter to be a A_1 type band appearing due to the imperfect orientation of the crystal or to the use of not perfectly polarized light. However, even when the 1464 cm^{-1} band disappears completely for the polarized light with electric vector vibrating along the C_2 axis, the 1150 cm^{-1} band appears as weak absorption for the polarized light with vectors vibrating in the direction perpendicular to C_2 axis.

STEWART [1] assigned the 1153 cm^{-1} band to the NH_2 rocking vibration of A_1 type and a broad band centred at 1064 cm^{-1} to the same vibration of B_2 type. However, we assigned the rocking vibrations of both A_1 and B_2 types to the band

* The references to previous investigations are given in this paper.

VOL.
10
1957/5

at 1150 cm^{-1}. A broad band at 1050 cm^{-1} was also observed for guanidinium ion for which only observable NH_2 rocking vibration is of E type which was assigned to the band at 1180 cm^{-1} [5].

As to the skeletal deformation frequencies, the values 570 and 556 cm^{-1} observed as absorption in the crystalline state are considerably different from the Raman values 601 and 534 cm^{-1} observed in aqueous solution. The difference seems to be due to the difference in state, since in our Raman measurement in the crystalline state, we observed two sharp lines at 555 and 575 cm^{-1} in this frequency region.

The Raman line at 534 cm^{-1} of aqueous solution was reported to be depolarized. Consequently, STEWART assigned this line to NH_2 twisting vibration which corresponds to the infra-red band at 520 cm^{-1} and not to the band at 557 cm^{-1}. According to this view, we have to consider that the Raman line arising from NH_2 twisting vibration is strong and that arising from skeletal deformation vibration escapes detection in aqueous solution, whereas reverse is the case in the crystal. Since we have shown that there is considerable shift of the vibrational frequencies between the crystal and aqueous solution, the assignment made by us as above can be considered to be more reasonable.

The part of the Raman spectra of the crystal in the region 490–650 cm^{-1} reported by REITZ and WAGNER [6] is quite different from that observed by us. This necessarily results in the difference of the assignment of the observed frequencies in this region.

OL.
10
7/58

Calculation of normal vibrations

The normal vibrations of the urea molecule were calculated by KELLNER on the assumption of the non-planar model [2]. However, the dichroic measurement of the infra-red band arising from the NH stretching vibration by WALDRON and BADGER [3] and proton magnetic resonance absorption measurement by ANDREW and HYNDMAN [4] concluded the planar structure of the urea molecule.

We have, therefore, calculated the normal vibrations of the C_{2v} model of this molecule as an eight-body problem. The significance of the internal co-ordinates will be clear from Fig. 1. The symmetry co-ordinates used in this calculation are listed in Table 1.

A potential function of the Urey–Bradley type has been used [7, 8]. The secular equation $|GF - E\lambda| = 0$ is set up according to WILSON's method [9], where the expressions for the matrices G and F are shown as in Table 3. The force constants K, H, and F have been calculated from the eighteen observed frequencies by the least-squares method. Here K, H, and F are the force constants for the bond stretching, bond angle deformation, and interaction between non-bonded atoms, respectively. The best set of force constants so obtained is shown in Table 2, and the normal frequencies calculated therefrom are compared with those observed in Table 4. We see that the values of force constants obtained here are reasonable, if we compare them with the corresponding constants obtained for the molecule with similar structure [5, 8, 10].

The symmetry co-ordinates, S, are related linearly to the normal co-ordinates, Q, through the matrix expression

$$S = LQ.$$

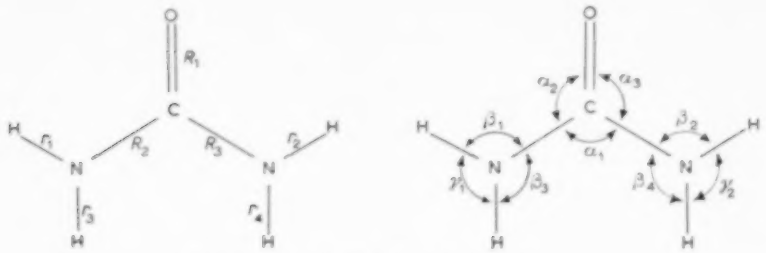

Fig. 1. Internal co-ordinates of urea.

Table 1. Symmetry co-ordinates

Symmetry type	Vibrational mode	Symmetry co-ordinate
A_1	S_1 (CO stretch.)	ΔR_1
	S_2 (NH_2 bend.)	$(2\Delta\gamma_1 + 2\Delta\gamma_2 - \Delta\beta_1 - \Delta\beta_2 - \Delta\beta_3 - \Delta\beta_4)/2\sqrt{3}$
	S_3 (NH_2 rock.)	$(\Delta\beta_1 + \Delta\beta_2 - \Delta\beta_3 - \Delta\beta_4)/2$
	S_4 (CN stretch.)	$(\Delta R_2 + \Delta R_3)/\sqrt{2}$
	S_5 (skel. def.)	$(2\Delta\alpha_1 - \Delta\alpha_2 - \Delta\alpha_3)/\sqrt{6}$
	S_6 (NH_2 sym. stretch.)	$(\Delta r_1 + \Delta r_2 + \Delta r_3 + \Delta r_4)/2$
	S_7 (NH_2 antisym. stretch.)	$(\Delta r_1 + \Delta r_2 - \Delta r_3 - \Delta r_4)/2$
B_2	S_8 (NH_2 bend.)	$(2\Delta\gamma_1 - 2\Delta\gamma_2 - \Delta\beta_1 + \Delta\beta_2 - \Delta\beta_3 + \Delta\beta_4)/2\sqrt{3}$
	S_9 (CN stretch.)	$(\Delta R_2 - \Delta R_3)/\sqrt{2}$
	S_{10} (NH_2 rock.)	$(\Delta\beta_1 - \Delta\beta_2 - \Delta\beta_3 + \Delta\beta_4)/2$
	S_{11} (skel. def.)	$(\Delta\alpha_2 - \Delta\alpha_3)/\sqrt{2}$
	S_{12} (NH_2 sym. stretch.)	$(\Delta r_1 - \Delta r_2 + \Delta r_3 - \Delta r_4)/2$
	S_{13} (NH_2 antisym. stretch.)	$(\Delta r_1 - \Delta r_2 - \Delta r_3 + \Delta r_4)/2$

Table 2. Force constants in 10^5 dynes/cm

K_{CN}	5·24	H_{NCN}	0·72
K_{CO}	6·49	F_{ON}	1·57
H_{OCN}	0·12	F_{NN}	0·61
H_{CNH}	0·36	F_{CH}	0·46
H_{HNH}	0·38	F_{HH}	0·00 (assumed)

VOL. 10 1957/5

Table 3a. Elements of G matrix*

	A_1 type
$g_{1,1}$	$\mu_C + \mu_O$
$g_{1,3}$	$2\tau_2 \sin \alpha_2 \cdot \mu_C$
$g_{1,4}$	$\sqrt{2} \cos \alpha_2 \cdot \mu_C$
$g_{1,5}$	$\sqrt{6}\tau_2 \sin \alpha_2 \cdot \mu_C$
$g_{2,2}$	$3\tau_3^2[\mu_H + (1 - \cos \gamma)\mu_N]$
$g_{2,4}$	$\sqrt{6} \cdot \tau_3 \sin \beta \cdot \mu_N$
$g_{2,6}$	$-\sqrt{3} \cdot \tau_3 \sin \gamma \cdot \mu_N$
$g_{3,3}$	$2\tau_2[\mu_N + (1 - \cos \alpha_1)\mu_C] - 4\tau_2\tau_3 \cos \beta \cdot \mu_N + \tau_3^2[\mu_H + (1 + \cos \gamma)\mu_N]$
$g_{3,4}$	$-\sqrt{2} \cdot \tau_2 \sin\alpha_1 \cdot \mu_C$
$g_{3,5}$	$\sqrt{6} \cdot \tau_2^2[\mu_N + (1 - \cos \alpha_1)\mu_C] - \sqrt{6} \cdot \tau_2\tau_3 \cos \beta \cdot \mu_N$
$g_{3,7}$	$-2\tau_2 \sin \beta \cdot \mu_N - \tau_3 \sin \gamma \cdot \mu_N$
$g_{4,4}$	$\mu_N + (1 + \cos \alpha_1)\mu_C$
$g_{4,5}$	$-\sqrt{3} \cdot \tau_2 \sin \alpha_1 \cdot \mu_C$
$g_{4,6}$	$\sqrt{2} \cos \beta \cdot \mu_N$
$g_{5,5}$	$3\tau_2^2[\mu_N + (1 - \cos \alpha_1)\mu_C]$
$g_{5,7}$	$-\sqrt{6} \cdot \tau_2 \sin \beta \cdot \mu_N$
$g_{6,6}$	$\mu_H + (1 + \cos \gamma)\mu_N$
$g_{7,7}$	$\mu_H + (1 - \cos \gamma)\mu_N$
	B_2 type
$g_{8,8}$	$3\tau_3^2[\mu_H + (1 - \cos \gamma)\mu_N]$
$g_{8,9}$	$\sqrt{6}\tau_3 \sin \beta \cdot \mu_N$
$g_{8,12}$	$-\sqrt{3}\tau_3 \sin \gamma \cdot \mu_N$
$g_{9,9}$	$\mu_N + (1 - \cos \alpha_1)\mu_C$
$g_{9,10}$	$\sqrt{2}\tau_2 \sin \alpha_1 \cdot \mu_C$
$g_{9,11}$	$-2\tau_1 \sin \alpha_2 \cdot \mu_C - \tau_2 \sin \alpha_1 \cdot \mu_C$
$g_{9,12}$	$\sqrt{2} \cos \beta \cdot \mu_N$
$g_{10,10}$	$2\tau_2^2[\mu_N + (1 + \cos \alpha_1)\mu_C] - 4\tau_2\tau_3 \cos \beta \cdot \mu_N + \tau_3^2[\mu_H + (1 + \cos \gamma)\mu_N]$
$g_{10,11}$	$-\sqrt{2}\tau_2^2[\mu_N + (1 + \cos \alpha_1)\mu_C] + 2\sqrt{2}\tau_1\tau_2 \cos \alpha_2 \cdot \mu_C + \sqrt{2}\tau_2\tau_3 \cos \beta \cdot \mu_N$
$g_{10,13}$	$-2\tau_2 \sin \beta \cdot \mu_N - \tau_3 \sin \gamma \cdot \mu_N$
$g_{11,11}$	$2\tau_1^2(\mu_C + \mu_O) - 4\tau_1\tau_2 \cos \alpha_2 \cdot \mu_C + \tau_2^2[\mu_N + (1 + \cos \alpha_1)\mu_C]$
$g_{11,13}$	$\sqrt{2}\tau_2 \sin \beta \cdot \mu_N$
$g_{12,12}$	$\mu_H + (1 + \cos \gamma)\mu_N$
$g_{13,13}$	$\mu_H + (1 - \cos \gamma)\mu_N$

$\tau_1 = 1/R_1$ $\qquad$ $\tau_2 = 1/R_2 = 1/R_3$

$\alpha_1 = \alpha_1$ $\qquad$ $\alpha_2 = \alpha_2 = \alpha_3$

$\beta = \beta_i$ $\qquad$ $\gamma = \gamma_i$

* Elements other than those shown in the table vanish.

Table 3b. Elements of F matrix

	A_1 type
$f_{1,1}$	$K_{CO} + 2(t_1^2F_{OX} + s_1^2F'_{OX})$
$f_{1,4}$	$\sqrt{2}(t_1t_2F_{OX} - s_1s_2F'_{OX})$
$f_{1,5}$	$-\sqrt{2}R_2[t_1s_2F_{OX} + s_1t_2F'_{OX}]/\sqrt{3}$
$f_{2,2}$	$R_2r[H_{CXH} + s_3s_4F_{CH} - t_3t_4F'_{CH}]/3 + 2r^2[H_{HXH} + s_5^2F_{HH} - t_5^2F'_{HH}]/3$
$f_{2,4}$	$-\sqrt{2}r[t_3s_4F_{CH} + s_3t_4F'_{CH}]/\sqrt{3}$
$f_{2,6}$	$-R_2[t_3s_4F_{CH} + s_3t_4F'_{CH}]/\sqrt{3} + 2rs_5t_5(F_{HH} + F'_{HH})/\sqrt{3}$
$f_{3,3}$	$R_2r[H_{CXH} + s_3s_4F_{CH} - t_3t_4F'_{CH}]$
$f_{3,7}$	$R_2[t_3s_4F_{CH} + s_3t_4F'_{CH}]$
$f_{4,4}$	$K_{CX} + 2t_0^2F_{XX} + t_2^2F_{OX} + s_2^2F'_{OX} + 2(t_3^2F_{CH} + s_3^2F'_{CH})$
$f_{4,5}$	$2R_2s_0t_0(F_{XX} + F'_{XX})/\sqrt{3} - R_1[s_1t_2F_{OX} + t_1s_2F'_{OX}]/\sqrt{3}$
$f_{4,6}$	$\sqrt{2}(t_3t_4F_{CH} - s_3s_4F'_{CH})$
$f_{5,5}$	$2R_2^2[H_{XCX} + s_0^2F_{XX} - t_0^2F'_{XX}]/3 + R_1R_2[H_{OCX} + s_1s_2F_{OX} - t_1t_2F'_{OX}]/3$
$f_{6,6}$	$K_{XH} + t_4^2F_{CH} + s_4^2F'_{CH} + 2t_5^2F_{HH}$
$f_{7,7}$	$K_{XH} + t_4^2F_{CH} + s_4^2F'_{CH} + 2s_5^2F'_{HH}$
	B_2 type
$f_{8,8}$	$R_2r[H_{CXH} + s_3s_4F_{CH} - t_3t_4F'_{CH}]/3 + 2r^2[H_{HXH} + s_5^2F_{HH} - t_5^2F'_{HH}]/3$
$f_{8,9}$	$-\sqrt{2}r[t_3s_4F_{CH} + s_3t_4F'_{CH}]/\sqrt{3}$
$f_{8,12}$	$-R_2[t_3s_4F_{CH} + s_3t_4F'_{CH}]/\sqrt{3} + 2rs_5t_5(F_{HH} + F'_{HH})/\sqrt{3}$
$f_{9,9}$	$K_{CX} + 2s_0^2F'_{XX} + t_2^2F'_{OX} + s_2^2F'_{OX} + 2(t_3^2F_{CH} + s_3^2F'_{CH})$
$f_{9,11}$	$R_1(s_1t_2F_{OX} + t_1s_2F'_{OX})$
$f_{9,12}$	$\sqrt{2}(t_3t_4F_{CH} - s_3s_4F'_{CH})$
$f_{10,10}$	$R_2r(H_{CXH} + s_3s_4F_{CH} - t_3t_4F'_{CH})$
$f_{10,13}$	$R_2(t_3s_4F_{CH} + s_3t_4F'_{CH})$
$f_{11,11}$	$R_1R_2(H_{OCX} + s_1s_2F_{OX} - t_1t_2F'_{OX}$
$f_{12,12}$	$K_{XH} + t_4^2F_{CH} + s_4^2F'_{CH} + 2t_5^2F_{HH}$
$f_{13,13}$	$K_{XH} + t_4^2F_{CH} + s_4^2F'_{CH} + 2s_5^2F'_{HH}$

$s_0 = R_2 \sin \alpha_1/q_{XX}$	$t_0 = R_2(1 - \cos \alpha_1)/q_{XX}$
$s_1 = R_2 \sin \alpha_2/q_{XO}$	$t_1 = (R_1 - R_2 \cos \alpha_2)/q_{XO}$
$s_2 = R_1 \sin \alpha_2/q_{XO}$	$t_2 = (R_2 - R_1 \cos \alpha_2)/q_{XO}$
$s_3 = r \sin \beta/q_{CH}$	$t_3 = (R_2 - r \cos \beta)/q_{CH}$
$s_4 = R_2 \sin \beta/q_{CH}$	$t_4 = (r - R_2 \cos \beta)/q_{CH}$
$s_5 = r \sin \gamma/q_{HH}$	$t_5 = r(1 - \cos \gamma)/q_{HH}$

q_{ij} is the distance between non-bonded atoms i and j.

VOL. 10 1957/5

It can be shown that the potential energy for a given normal mode of vibration (Q_a) is expressed as

$$V_a = \tfrac{1}{2} Q_a^2 \Sigma F_{kl} L_{ka} L_{ea}.$$

Table 4. Calculated and observed frequencies in cm^{-1}

	$OC(NH_2)_2$			$OC(ND_2)_2$		
Symmetry type	Calc.		Obs.	Calc.		Obs.
A_1	ν_1	1648	1686	ν_1'	1597	1610
	ν_2	1615	1603	ν_2'	1265	1245
	ν_3	1143	1150	ν_3'	986	1001
	ν_4	1012	1000	ν_4'	874	887
	ν_5	555	556	ν_5'	476	475
B_2	ν_6	1639	1629	ν_6'	1477	1490
	ν_7	1461	1464	ν_7'	1174	1154
	ν_8	1152	1150	ν_8'	893	887
	ν_9	558	570	ν_9'	523	512

Therefore, the distribution of the potential energy among symmetry co-ordinates can approximately be expressed as $\frac{1}{2} F_{ii} L_{ia}^2$. This has been calculated as shown in Table 5. From this table we can tell the nature of vibration of each normal mode accurately.

Based on the result of these calculations, we can make the assignment of observed frequencies as follows:

To the vibrations of the frequencies 1686 and 1603 cm^{-1} there are considerable contributions of both CO stretching and NH_2 bending motions, whereas STEWART assigned the 1688 cm^{-1} band to CO stretching vibration and the 1603 cm^{-1} band to NH_2 bending motion. Our calculations shows that for the band at 1686 cm^{-1} the contribution of the NH_2 bending motion is greater than that of CO stretching motion.

The band at 1629 cm^{-1} corresponds to almost pure NH_2 bending vibration. As the diagonal terms of the G and F matrices of the NH_2 bending motion of A_1 type is equal to that of B_2 type, the A_1 type band should have a frequency of about 1630 cm^{-1}, if there is no coupling between NH_2 bending and CO stretching motions. On the other hand, the observed frequency of 1610 cm^{-1} of urea-d_4 is assigned to almost pure skeletal vibration. Therefore we can conclude that the interaction between the 1630 and 1610 cm^{-1} vibrations gives rise to the two observed bands at 1686 and 1603 cm^{-1}.

The infra-red bands of urea-d_4 at 1245 and 1154 cm^{-1} are assigned, respectively, to A_1 type and B_2 type ND_2 bending vibrations. This assignment is consistent with the observed depolarization degrees of the Raman lines. The large frequency

Table 5. Percentage potential energy distribution among symmetry co-ordinates ($F_{ii}L_{i\alpha}^2/\lambda_\alpha$)

$OC(NH_2)_2$

A_1 type

	ν_1	ν_2	ν_3	ν_4	ν_5
S_1 (CO stretch.)	0·20	**0·40**	0·35	0·12	0·01
S_2 (NH_2 bend.)	**0·61**	**0·38**	0·00	0·02	0·00
S_3 (NH_2 rock.)	0·08	0·15	**0·64**	0·06	0·07
S_4 (CN stretch.)	0·24	0·07	0·02	**0·65**	0·07
S_5 (skel. def.)	0·07	0·12	0·00	0·00	**0·83**

B_2 type

	ν_6	ν_7	ν_8	ν_9
S_8 (NH_2 bend.)	**0·94**	0·07	0·00	0·00
S_9 (CN stretch.)	0·15	**0·80**	0·15	0·00
S_{10} (NH_2 rock.)	0·00	0·14	**0·84**	0·02
S_{11} (skel. def.)	0·01	0·14	0·00	**0·95**

$OC(ND_2)_2$

A_1 type

	ν_1'	ν_2'	ν_3'	ν_4'	ν_5'
S_1 (CO stretch.)	**0·68**	0·08	**0·32**	0·00	0·00
S_2 (ND_2 bend.)	0·01	**0·76**	0·12	0·12	0·00
S_3 (ND_2 rock.)	0·12	0·00	**0·29**	**0·39**	0·02
S_4 (CN stretch.)	0·32	0·18	0·07	**0·44**	0·05
S_5 (skel. def.)	0·19	0·00	0·07	0·02	**0·75**

VOL. 10 1957/5

B_2 type

	ν_6'	ν_7'	ν_8'	ν_9'
S_8 (ND_2 bend.)	0·11	**0·86**	0·03	0·01
S_9 (CN stretch.)	**1·00**	0·04	0·07	0·00
S_{10} (ND_2 rock.)	0·04	0·04	**0·84**	0·08
S_{11} (skel. def.)	0·12	0·06	0·03	**0·89**

difference between the A_1 and B_2 vibrations is due to the fact that in the A_1 vibration the cross term related to the CN stretching vibration is large.

The 1464 cm^{-1} frequency of urea is assigned to the CN stretching vibration of B_2 type. The corresponding frequency of urea-d_4 is observed at 1490 cm^{-1}.

It has been stated above that the 1150 cm^{-1} band is assigned to NH_2 rocking vibrations of both A_1 and B_2 types. The normal vibration calculation yields almost the same value for these frequencies.

The Raman line at 1000 cm^{-1} of urea is strong, whereas the corresponding absorption band is weak. The assignment of this frequency to CN stretching vibration of A_1 type is confirmed by the calculation of potential energy distribution. In the case of urea-d_4 we observed two frequencies at 1001 and 887 cm^{-1}, both of which are fairly strong in both the scattering and absorption. The calculation shows that the coupling of CN stretching vibration with ND_2 rocking motion is considerable.

To the 1000 cm^{-1} CN vibration there is also a contribution of CO stretching motion, where both CN and CO motions are in phase. The corresponding out-of-phase vibration of urea-d_4 is observed as a band at 1610 cm^{-1}. The coupling of these two stretching motions naturally takes place, since the mass of O is equal to NH_2 and, due to the resonance, the difference between the force constants K(C=O) and K(C—N) becomes less. In other words, the skeletal stretching vibrations of urea become similar to those of planar XY_3 molecule, and the said in-phase and out-of-phase motions of urea may be considered to correspond, respectively, to the totally symmetric and degenerate vibrations of XY_3 molecule.

The band at 570 cm^{-1} of urea is assigned to a skeletal vibration of B_2 type and that at 556 cm^{-1} to a vibration of A_1 type. In urea-d_4 the observed frequencies 512 and 475 cm^{-1} are assigned to fairly pure skeletal vibrations of B_2 and A_1 types, respectively.

As shown in Table 6, the product rule holds for in-plane vibrations. This confirms the assignment made above.

Broad bands observed at 1050, 785, 719, and 500 cm^{-1} are assigned to vibrations of B_1 type. From the crystal structure of urea it is seen that we cannot distinguish vibrations of B_1 type from those of B_2 type by dichroic measurement. However, the application of product rule shows all the four bands mentioned above are not to be included among B_2 vibrations. The bands at 785 and 717 cm^{-1} are considered

to arise from a mixed motion of NH_2 wagging and CO out-of-plane bending vibrations.

In urea-d_4 are observed broad bands centred at 776, 750, and 620 cm^{-1}. The

Table 6. The product rule for in-plane vibrations

	Observed $\frac{\Pi\nu_a}{\Pi\nu'_a}$	Calculated $\left(\frac{G(H)}{G(D)}\right)^{\frac{1}{2}}$
A_1 type	2·05	2·06
B_2 type	1·99	1·90

bands in the region below 400 cm^{-1} could not be observed by the spectrophotometer used in the present measurement, although we would expect to observe a band at about 350 cm^{-1} from the isotopic shift.

References

[1] Stewart J. E. *J. Chem Phys.* 1957 **26** 248.
[2] Kellner L. *Proc. Roy. Soc.*, A1941 **177** 456.
[3] Waldron R. D. and Badger R. M. *J. Chem. Phys.* 1950 **18** 566.
[4] Andrew E. R. and Hyndman D. *Proc. Phys. Soc.* A1953 **66** 1187.
[5] Angell C. L., Sheppard N., Yamaguchi A., Shimanouchi T., Miyazawa T. and Mizushima S. *Trans. Faraday Soc.* 1957 **53** 589.
[6] Reitz A. W. and Wagner J. *Z. Phys. Chem.* B1939 **43** 339.
[7] Shimanouchi T. *J. Chem. Phys.* 1949 **17** 245, 734.
[8] Mizushima S. *Structure of Molecules and Internal Rotation* p. 188. Academic Press, New York 1954.
[9] Wilson E. B. *J. Chem. Phys.* 1939 **7** 1047; *Ibid.* 1941 **9** 76.
[10] Mizushima S., Shimanouchi T., Nakagawa I. and Miyake A. *J. Chem. Phys.* 1953 **21** 215.

VOL.
10
1957/5

Spectrochimica Acta, 1957, Vol. 10, pp. 179 to 194. Pergamon Press Ltd., London

Interference filters for the infra-red

O. S. Heavens,* J. Ring† and S. D. Smith‡

(*Received* 1 *August* 1957)

Abstract—The possibilities are examined of using multilayer filters in the infra-red region of the spectrum. The properties of certain potentially useful systems are examined from theoretical considerations. Techniques suitable for the preparation of multilayer systems including details of the controlled deposition of layers are discussed. The results obtained with multilayer filters employing germanium and cryolite are given and the present factors limiting the range and performance of filters of this type are discussed. A narrow band interference filter with a variable air-gap as spacer is considered and is shown to have some advantages over all-solid filters.

1. Introduction

Progress in optical multilayers has reached a stage such that interference filters of various types may be constructed for infra-red wavelengths from the longest visible wavelengths up to 20 μ. The component films of the multilayer systems are usually deposited by vacuum evaporation and accurate methods of thickness control have been developed (Giacomo and Jacquinot [1], Ring [2]). The infra-red region is particularly suitable for the application of multilayer interference techniques since transparent materials are available with a wide range of refractive indices. The design possibilities are considerable and narrow band, wide band and low (frequency) pass filters have been evolved. However, the greater thickness of film required for infra-red filters compared with those for the visible region of the spectrum brings difficulties from the deterioration of the optical qualities of evaporated films with increasing thickness. This limits at present the performance of some filters.

Used as monochromators, narrow band interference filters possess considerable advantages over prism and grating instruments in luminosity as a function of resolving power. Jacquinot [3] has shown that the gain in luminosity may be of the order 100. Thus in any region where resolution is energy-limited, considerable improvement may be expected with the introduction of interference monochromators.

All interference filters possess unwanted side-bands at multiples or fractions of their fundamental wavelength. It is therefore necessary to employ auxiliary filtering. This is achieved by a combination of interference methods and the use of suitable absorbing materials.

2. Simple theory of the Fabry–Perot interference filter

The filters consists of two reflecting surfaces of reflectance R and transmittance T separated by a spacer of thickness t and refractive index n. The transmittance

* Royal Holloway College, University of London.
† University of Manchester.
‡ Royal Aircraft Establishment, Ambarrow Court.

as a function of wave number is given by the Airy sum:

$$T(\nu) = \frac{1}{1 + F \sin^2 \theta} \tag{1}$$

where $F = \dfrac{4R}{(1 - R)^2}$ and $\theta = 2\pi nt/\lambda = 2\pi nt\nu$. The system has pass bands centred at the points at which $T = 1$, i.e. where $\sin^2 \theta = 0$ or $2\pi nt\nu_p = N\pi$, where N is the order of the filter, whence $\nu_p = N/2nt$.

The effects of absorption in the reflecting surfaces and of phase changes on reflection at these surfaces have been neglected in the above treatment. If the absorption of each reflecting surface is A, so that $R + T + A = 1$, the transmittance of the filter may be written

$$T(\nu) = \frac{1}{(1 + A/T)^2} \cdot \frac{1}{1 + F \sin^2 \theta} . \tag{2}$$

Thus the shape of the transmission band is unaffected by the presence of absorption. The effect of a phase change $\phi(\nu)$ on reflection at each surface can be included in θ; maxima occur when $\theta = 2\pi nt\nu + 2\phi(\nu) = N\pi$, where N is an integer.

The width of the pass band, measured between points at which $T = T_{\max}/2$ is given approximately by

$$W = \frac{\nu_0(1 - R)}{N\pi R^{\frac{1}{2}}} = \frac{4\nu_0}{N\pi F^{\frac{1}{2}}} . \tag{3}$$

Thus for an efficient narrow band filter we require a high value of R combined with a low value of A/T. For visible wavelengths the required conditions are approached by silver films and are much improved by the use of multilayer high-reflecting stacks (Polster [4]). In the infra-red, the performance of silver films is significantly worse than for the visible, and multilayer stacks are necessary. Quarter-wave stacks of germanium with cryolite or fluorite show high reflectance with quite small numbers of layers as shown by the calculated reflectances in Table 1. The refractive indices are quoted for a wavelength of about 2 μ.

Table 1

System	Calculated reflectance at λ_0
DH	0·69
$DHLH$	0·96
$DHLHLH$	$0{\cdot}99_8$

D = massive quartz substrate $\quad n_D = 1{\cdot}45$

H = $\lambda/4$ germanium | optical thicknesses $\quad n_H = 4{\cdot}0$

L = $\lambda/4$ cryolite | thicknesses $\quad n_L = 1{\cdot}35$

The limit to the number of films which can be used in a narrow band filter is set by the optical quality of the component films which limits the maximum obtainable reflectance (Section 8).

VOL. 10 1957/5

The simple narrow band filter may take two forms according to whether the spacer layer is of high or low index, thus:

High-index spacer	$HL \ldots\ldots HL(NHH)LH \ldots LH$	where N is order of the filter.
Low-index spacer	$HLH \ldots\ldots (NLL) \ldots HLH$	

The transmittance around the fundamental pass band of the filter is given approximately by equation (2) as the reflectance of the stacks is nearly constant near λ_0. Away from λ_0, the reflectance of the stacks changes rapidly with wave number, falling sharply and giving rise to a broad transmission band in the filter. The calculated transmittance of the filter $DHLHHLH$ is compared with the appropriate Airy sum in Fig. 1. The transmittance curve of the multilayer follows

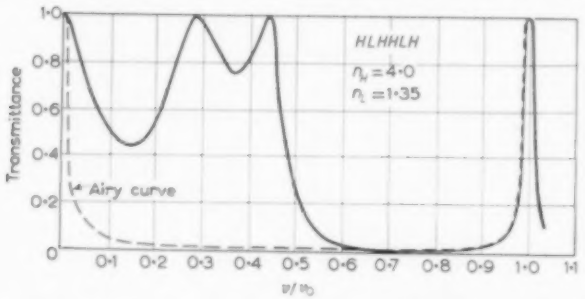

Fig. 1. Computed transmittance of the system $HLHHLH$ compared with the Airy summation.

closely the Airy curve over the transmission band of the filter. The divergence of the curves for $\lambda_0/\lambda > 1{\cdot}4$ shows the characteristic difference between the multilayer single half-wave filter, as we may call this type, and the metallic film type, which follows the Airy curve throughout.

Since these "side-bands" of transmission are caused by the fall in reflectance of the multilayer stacks on either side of the spacing layer, attempts have been made to extend the range of high reflectivity in such stacks. BAUMEISTER and STONE [5] have shown that by "staggering" the thickness of individual layers in the stack the width of the reflecting region may be doubled. Such broad-band reflectors exhibit anomalous dispersion of phase change on reflection which can give rise to several narrow pass-bands at wavelengths other than λ_0 when they are incorporated in interference filters; however, the problem of auxiliary filtering (discussed in Section 4) is much mitigated by their use. The dispersion of phase change on reflection has been neglected in calculating the Airy curve of Fig. 1. There is some variation of phase change on reflection with wavelength in the case of metal films and a much larger change for high-reflecting multilayer stacks. The effect of the phase change is to narrow the pass band slightly compared with that for a constant phase-shift filter. In the case illustrated in Fig. 1 the effect is small. The effect can be augmented by a suitable design of reflecting stack and can be used to narrow filter pass-bands by making θ (equation 2a) change more rapidly as a function of ν. BAUMEISTER and JENKINS [6] have attempted to narrow the pass-bands of interference filters for visible wavelengths

in this way but with limited success, due to the difficulties of thickness control implicit in these deliberately mismatched reflecting stacks. The narrow band reflecting stack (described in Section 4) is an alternative system with a high dispersion of phase change on reflection but is not easy to construct for infra-red wavelengths.

Effect of non-normal incidence

If an interference filter is placed in a converging beam of radiation the pass band is broadened, the maximum transmission is reduced and the position of the peak is shifted to shorter wavelengths. The effects are often small, especially with a spacer layer of high refractive index. If the angle of refraction in the spacer layer is r, the condition for a maximum is : $2nt \cos r + \phi(r) = N\lambda$, where ϕ represents the effect of phase shifts on reflection from the stacks. For the range of angles of incidence found in spectroscopic equipment the variation of $\phi(r)$ with angle of incidence may be neglected. With this approximation the wavelength shift of the pass band on changing from normal incidence to an angle i is $\Delta\lambda/\lambda = 1 - \cos r$, where $\sin i = n \sin r$. The advantage of a high-index spacer is apparent. For a germanium spacer and an angle of incidence of 25°, $\Delta\lambda/\lambda = 0{\cdot}0056$. This shift of pass band is sufficiently small for the filter to be usable in a converging beam, except where the limiting performance is required.

3. Double and treble half-wave systems as band pass filters

The shape of the pass band of the single half-wave filter as described above is not ideal since one half of the energy transmitted by the filter lies outside the band defined by the half width in Section 2. If two similar filters are used in series, the band width is reduced by 36 per cent and the proportion of energy within the half width is 65 per cent. This does not represent a very useful gain. The properties of multilayer systems containing two half-wave films, each surrounded by high-reflecting quarter-wave stacks have been investigated by Smith. The characteristics of this type of filter include a pass band which may have twin peaks on either side of the fundamental wavelength λ_0.

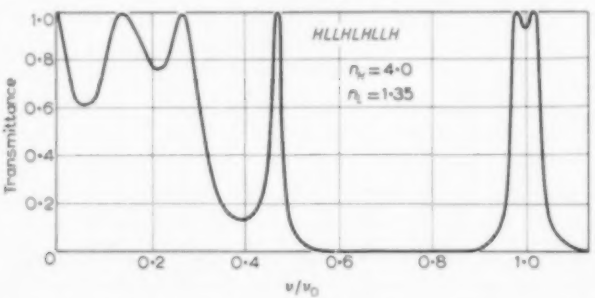

Fig. 2. Computed transmittance of the system *HLLHLHLLH*.

Double half-wave systems may be designed as band-pass filters of either moderate or very narrow bandwidths with pass bands showing either a twin peak or a single peak. The twin peak form is suitable for a band-pass filter, the band

showing steeper sides and a more rapid transition from stop band to pass band than a single half-wave filter of comparable bandwidth. The computed transmittance of the double half-wave filter *HLLHLHLLH* is shown in Fig. 2. The half-width (defined as before) is 0·08 λ_0 and the proportion of energy transmitted within the half-width is over 80 per cent. A much narrower double half-wave filter is the system *HLHHLHLHLHHLH*; the computed transmittance of this (Fig. 3) shows a half-width of 0·02 λ_0 and otherwise similar characteristics. Double half-wave systems show excellent rejection in stop-band regions.

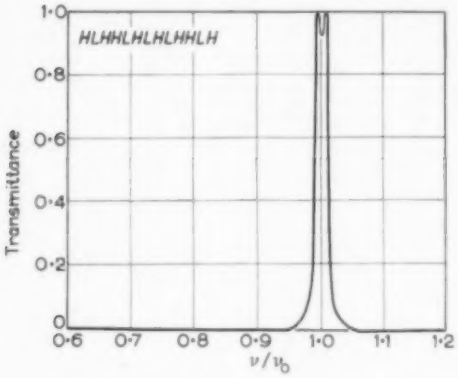

Fig. 3. The narrow-band double half-wave system *HLHHLHLHLHHLH*.

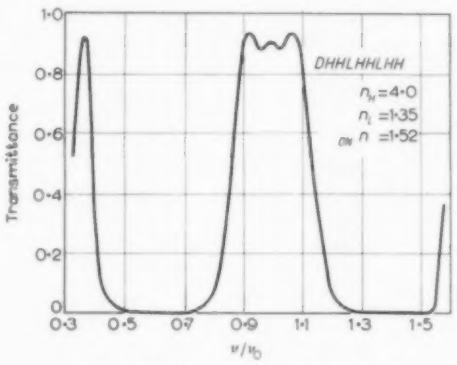

Fig. 4. Wide-band triple half-wave system *DHHLHHLHH*.

A further interesting and useful feature is that in the centres of the pass band the "effective number of beams" contributing to the interference is at a minimum, whereas in the rejection bands this number is large. This has the consequence that the effect of imperfections in the films is smallest at the centre of the transmission band and greatest in the rejection band, where losses are less important. Thus double half-wave filters show higher transmission at the centre of their pass bands than single half-wave filters with the same number of films, for which the effective number of beams is constant. Turner *et al.* [7] have investigated the properties of treble half-wave systems which show multipeak pass bands. These systems are useful for wider-band filters than can be made with double half-waves and can also be designed as narrow-band filters. An example of a wide-band filter *DHHLHHLHH* is shown in Fig. 4.

Auxiliary filtering

All the multilayer systems described above show unwanted pass bands at wavelengths shorter than λ_0. For example, the "free filter range" of the filter *DHLHHLH*, defined as the range within which the transmission in the stop band is <2 per cent, is from $1{\cdot}4 > \lambda_0/\lambda > 0{\cdot}6$. If germanium or tellurium is used as the high index material, the absorption in these semi-conductors is sufficiently high to suppress completely the bands below 1·0 and 2·0 μ respectively. In general, however, auxiliary filters must be used to isolate the fundamental band of the primary filter.

4. Narrow-band reflecting filters

Since most infra-red optical systems employ mirrors, multilayer reflecting coatings may be used as auxiliary filters with the additional advantage of reducing the losses caused by metallic reflections. Several multilayer reflecting stacks in series will deliver to a detector a sharply defined spectral band centred on λ_0 (the wavelength of maximum reflectivity of each stack) whose width may be controlled by adjusting the number and material of the layers constituting the multilayer. In particular, a large number (say 40) of alternate quarter-wave layers of two substances of nearly equal refractive index (e.g. CaF_2/MgF_2 or ZnS/Se) will reflect a band with a half-width of $\sim 0{\cdot}1\lambda_0$ with no further reflectance on the long-wavelength side and with the next reflecting band on the short-wave side at $\lambda_0/3$. This may simplify the problem of auxiliary filters by removing the necessity for a long-wave cut filter and extending the suppression band of other filters to shorter wavelengths. Such filters may prove useful as coatings for mirrors in grating monochromators since they would suppress all even multiples of the fundamental reflected wave number.

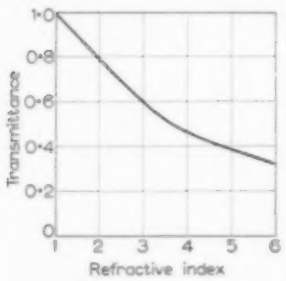

Fig. 5. The transmittance of a plane parallel-sided slab as a function of refractive index.

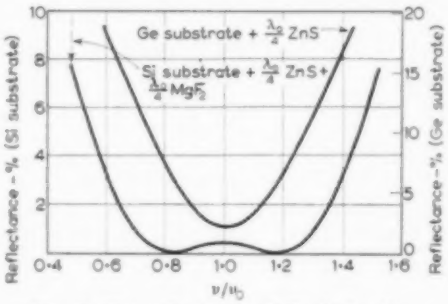

Fig. 6. The reflectance of Ge (refractive index = 4·0) and Si (refractive index = 3·0) when bloomed with simple antireflecting coatings. The uncoated reflectances are Ge—36 per cent and Si—25 per cent.

5. Semi-conductor low pass filters

A number of semi-conducting materials provide convenient low-(wave number) pass filters, since they are transparent at wavelengths longer than a characteristic steep absorption edge which corresponds to the energy required to raise electrons from the valence to conduction band. For smaller quanta, i.e. at longer wavelengths, absorption is essentially due to free carriers (either electrons in the conduction band or holes in the valence band), and is very much smaller. The absorption in this region depends upon the number of free carriers, which in turn depends at room temperature on the purity of the material and the size of the energy gap between valence and conduction bands. In some cases the long-wave absorption is sufficiently high to necessitate the use of thin samples. However, the thicker the specimen the sharper is the cut-off at the absorption edge. There is thus an optimum thickness of material for the most effective filtering. A list of materials giving positions of absorption edges and suitable thicknesses is given in Table 2.

VOL.
10
1957/5

Table 2.

Material	Transparent beyond absorption edge (μ)	Thickness (mm)	Refractive index	Comments
Se	0·7	1	2·5	Can be cast from liquid
Si	1·1	>0·1	3·5	Thin single crystal
Ge	1·7	>0·2	4·0	Thin single crystal
PbS	3·0	0·006	4·2	Evaporated film on heated substrate (BRAITHWAITE) [8]
Te	3·4	>0·1	5·0	Crystal
PbTe	3·8	0·005	5·5	Evaporated film on heated substrate (BRAITHWAITE) [8]
InAs	3·8	0·1–0·2		
PbSe	4·2	0·007	4·7	Evaporated film on heated substrate (BRAITHWAITE) [8]
InSb	3·5–7 depending on purity	0·02–0·1	3·96	This crystal requires to be thinnest for the short-wave edge of the impure material

Thin crystals may be readily prepared by grinding with fine grade carborundum and aluminium oxide followed by polishing with aluminium oxide on photographic paper. For very thin specimens it is convenient to glue the crystals on to a substrate whilst a mm or so thick and to remove them on completion of grinding and polishing. Hot shellac (which dissolves readily in boiling alcohol) is useful for the purpose.

Table 2 shows that all the materials have high refractive indices. This entails a large reflection loss, as shown in Fig. 5, and it is therefore necessary to coat the surface with antireflecting layers. A single quarter-wave layer of refractive index equal to the square root of the substrate index reduces the reflectance of the surface to zero at one wavelength. This is sufficient if the wavelength region to be transmitted is restricted to, say, $\lambda_0 \pm 5$ per cent. Two- and three-layer antireflecting systems can be designed to extend the range, giving zero reflectance at two and three points respectively. Typical antireflecting coatings suitable for silicon and germanium have the characteristics shown in Fig. 6.

6. Multilayer low-pass filters

For a region in which there is no convenient absorbing filter multilayer methods may be conveniently used. The design of a multilayer low-pass filter depends upon the property that the transmission of a quarter-wave film increases steadily as the wavelength increases from the quarter-wave position and never falls again. Similarly a multilayer system composed of films of thickness not greater than a quarter-wave at λ_0 shows secondary minima of transmission beyond this wavelength but the minima never reach the low values obtained at λ_0 and shorter wavelengths. Double half-wave systems may be used as low-pass systems. Fig. 7 shows the

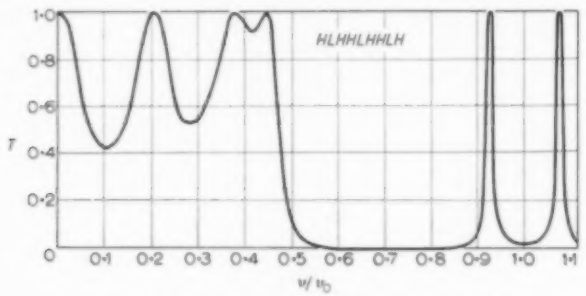

Fig. 7. The double half-wave as a low-pass filter.

computed curve for the system $HLHHLHHLH$. This filter shows a steep rise in transmission around $2\lambda_0$ and thereafter only feeble minima. These secondary minima may be further suppressed by suitable choice of the refractive index of the substrate, when the transmission beyond $2\lambda_0$ never falls below 70 per cent. Several such filters may be used in series.

Long-wave cut filters

Suppression of long-wavelength radiation can usually be achieved by choice of suitable absorbing substrates such as glass (2·5 μ), quartz (4·0 μ), magnesium oxide crystal or fluorite (9·0 μ), rocksalt (16 μ), $PbCl_2$ (20 μ), KBr (27 μ). Choice of thickness gives a measure of control over the wavelength of the final cut-off.

7. Experimental techniques

Multilayer films are made by vacuum deposition (at pressures $\sim 10^{-5}$ mm Hg) and the methods used for infra-red coatings are very similar to those which have been developed over the past decade to construct multilayers for the visible region of the spectrum [9]. Commercial evaporation plants can be suitably modified with ease. There are three features of special interest; evaporation sources, thickness control systems and the uniformity of thickness of layers over the substrate.

(a) *Evaporation sources*

The conditions to be satisfied by a source are that it should be capable of being heated to a temperature of 1000–1500°C without reacting chemically with the substance being evaporated and that the angular distribution of evaporating material should remain constant for successive layers.

VOL. 10 1957/5

The source should contain enough of the evaporating material to suffice for a complete filter, thus confining the number of sources required to the number of different substances in the multilayer—normally two. For large diameter filters (which are made with a source and filter distance of about 30 cm) 10 g of each substance will suffice.

The only source which is of universal application is a "boat" made from thin sheet molybdenum or tantalum (Fig. 8). Such boats can be heated by passing an electric current through them, a power of a few hundred watts being required. They tend, however, to become brittle in time and some substances (e.g. germanium) will ruin a boat after only a few evaporations.

Fig. 8. Evaporation source of molybdenum or tantalum sheet.

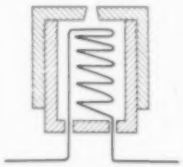

Fig. 9. Central heating in a pyrophillite crucible.

The angular distribution from a given boat is reasonably constant but differs between boats of the same type. For most evaporation materials a crucible of a refractory substance such as alumina or pyrophillite (a form of steatite), with a a tungsten or molybdenum wire heater wound internally or externally, proves to be more satisfactory. If the material being evaporated does not react with the heater, the form of crucible shown in Fig. 9 is very useful, since the filament acts as a "super-heater" for the evaporating molecules and there is very little loss of energy by radiation from the crucible. The refractive index of evaporated germanium films has been found to depend markedly on the type of source used and molybdenum boats, or carbon crucibles heated externally, have been found most suitable.

(b) *Thickness control systems*

Techniques have been developed which allow the optical thickness of each layer in a filter to be controlled during deposition with an error of less than 1/3 per cent. The simplest monitoring system is obtained by passing a beam of substantially monochromatic radiation through (or reflecting it from) the substrate being coated and receiving it on a detector coupled to a meter or preferably a recorder. When a layer reaches an optical thickness equal to a multiple of $\lambda_c/4$ (λ_0 being the mean wavelength of the control beam) the transmittance or reflectance reaches a maximum or minimum value, at which point deposition is stopped. Such methods are accurate to 1–2 per cent and are simple in application though some skill is needed in judging the stationary points. As many as ten layers can be successively controlled thus; for more complicated stacks clean control plates are introduced as required.

If the wavelength of the monitoring beam is rapidly alternated between two wavelengths on either side of λ_0, then the quarter-wave condition is indicated by a disappearance of the difference signal between the two intensities (provided they were equalized before the deposition commenced). Such systems have been

used to construct complicated interference filters using only one control surface. They demand little skill on the part of the operator. The position of the pass-band can be placed to within $\pm 0{\cdot}005\lambda_0$.

(c) *Uniformity of films*

The finite size of evaporation plants results in a non-uniform deposition of material on a substrate and equation (1) shows that the position of the band transmitted by various points over the area of a filter will change in the same way as the deposited thickness. This problem has been largely removed by the use of rotating substrates [10] and filters can be made sufficiently uniform over a diameter approximately equal to the radius of the evaporation plant.

8. Experimental infra-red interference filters

We have seen in sections 2, 3 and 4 that filming materials are required with a variety of refractive indices. In Table 3 several materials are listed in order of increasing refractive index together with the wavelength region for which they are transparent.

The major experimental problem lies in the deposition of films of good optical quality of suitable thickness for infra-red wavelengths. Two distinct types of deterioration are observed in evaporated films of increasing thickness; "cracking" and "clouding". In "cracking" mechanical stresses are set up in the film as its thickness increases which eventually results in mechanical failure of the film; deep cracks are formed or complete disruption occurs. In the "clouding" form of deterioration the crystallite size within the deposited film increases progressively with thickness and is first detected when the crystallites become large enough to scatter visible light. The films then show a whitish "bloom". Smith has shown experimentally that this scatter decreases approximately as $1/\lambda^4$ as predicted by the Rayleigh expression. Thus a layer of germanium of optical thickness 4 μ shows significant loss at 2 μ but negligible loss at 4 μ. Imperfect optical quality of films is a limiting factor at present on multilayer filters for infra-red wavelengths.

Experimental filters have been made by the authors for the region 1–5 μ and by Greenler [11] for longer wavelengths. Quarter-wave stacks are an essential part of all the multilayer systems discussed in this paper. In Fig. 10 is shown the transmittance of a three-layer germanium/cryolite stack *DHLH* (*D* denotes a glass substrate) centred at 1·8 μ. The wavelength variation of the reflectance of the stack is shown by the plot of $1-T$ in Fig. 10. The reflectance is subject to a small correction due to losses within the stack. The rapid fall in the transmittance below 1·3 μ is due to absorption in the germanium layers. The figure indicates how a simple high-reflecting stack may be used in conjunction with an absorption edge to form a band-pass filter. The absorption edge of a slab of semi-conductor may also be steepened by the use of a quarter-wave stack with its peak reflectance at a wavelength somewhat shorter than that of the absorption edge.

9. Single half-wave (ADI) filters

Fig. 11 shows the transmittance of a five-layer single half-wave filter *DHLHHLH* constructed for 2·37 μ from germanium and cryolite. From the

VOL. 10 1957/5

Table 3.

Material	Index	Transparent region	Comments
CaF_2	1·25–1·35	to 9 μ	Forms porous films, of variable index. Bulk index 1·43. Shows visible scatter at 1 μ optical thickness
Na_3AlF_6 (Cryolite)	1·34	visible to 10 μ	Forms good films until mechanical failure sets in with optical thickness $\sim$2 μ. Tensional stress
MgF_2	1·39	visible to 10 μ	Hard films formed and shows mechanical failure at 1 μ optical thickness. Tensional stress
NaCl	1·54	visible to 15 μ	Shows visible scatter when thick
KBr	1·56	0·6–30 μ	
MoO_3	2·0		
ZnS	2·35	0·5–14 μ	Compressive stress
Sb_2S_3	2·5	0·5–10 μ	
Se	2·5	0·7–20 μ	
Ge	4·0 (at 2·0 μ)	1·7–20 μ	
Te	4·9 (at 6·0 μ)	3·4–20 μ	

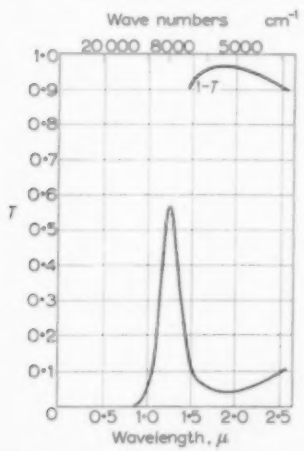

Fig. 10. Experimental three-layer filter *DHLH*. High-index layer of Ge: low-index layer of cryolite.

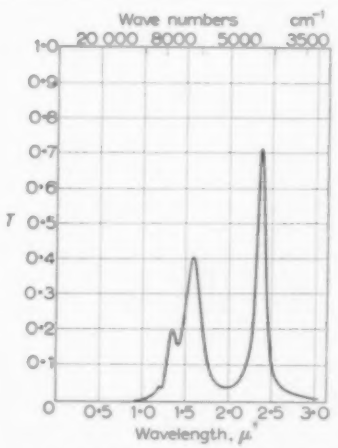

Fig. 11. Experimental five-layer Ge and cryolite filter *DHLHHLH*.

measured half-width (0·05 μ) we may deduce the effective value of F from equation (3) and hence a value for the effective reflectance (R_e) of the quarter-wave stacks. Furthermore, from equation (2),

$$T_{\max} = \frac{1}{(1 + A/T)^2} \tag{4}$$

so that the experimental $T_{\max}$ (0·71) gives a value for A/T. From the relation $R_e + T + A = 1$ we may deduce A, the loss by absorption and scattering, in the stacks. A comparison of the experimental performance with theory is shown in Table 4.

Table 4.

	λ_0 (μ)	Half-width (μ)	$\frac{\Delta\lambda}{\lambda_0}$	Ratio of half-width to spacing	Effective reflectance	$T_{\max}$	A
Theoretical	2·37	0·11	0·046	1:11	0·87	0·96	0
Experimental	2·37	0·12	0·05	1:10	0·85	0·72	0·015

Although the losses in the stacks are small in the above case, they limit the performance of stacks constructed with greater numbers of layers. Single half-wave filters of seven and nine layers (i.e. *DHLHLLHLH* and *DHLHLHHLHLH*) were found to be scarcely better than the five-layer filter described above. Attempts to produce small band widths by the use of high-order (e.g up to five) spacer layers resulted in but slight improvement over first-order filters. The deterioration in the layers of these materials with increasing thickness thus sets a limit to the complexity of filter which can be constructed. This state of affairs is likely to be improved as techniques of making layers improve.

One technique at present being tried consists of using a cleaved lamina of mica as the spacing layer and coating both sides of it with conventional reflecting stacks. A sheet of mica 25 μ thick would give a tenth-order spacer at a wavelength of 5 μ and it seems probable that a half-width of $<0{\cdot}01$ μ can be obtained in this way. A low-order filter can be used in series to eliminate adjacent orders of the mica filter.

10. Filters for longer wavelengths

Single half-wave filters for wavelengths from 5 to 20 μ have been investigated by Greenler [11]. The materials used are tellurium for high-index and NaCl or KBr for low-index layers. Greenler finds that optical thicknesses of 18 μ for tellurium and 10 μ for NaCl films are obtainable without cracking or peeling. The performances of a three-layer Te/NaCl filter *DHLLH* and a five-layer Te/NaCl filter *DHLHHLH* constructed for $\lambda_0 = 10$ μ are shown in Table 5.

The losses in the five-layer filter at 10 μ are much greater than those for the 2 μ filter described in the above paragraph, showing that there is some deterioration in films of thickness suitable for the filter.

Useful filtering can be achieved with three-layer filters, particularly if two are used in series whilst the use of filters with air-gap spacers in this region should lead to very significant improvement in performance.

Table 5.

Filter	λ_0 (μ)	Half-width (μ)	$\frac{\Delta\lambda}{\lambda_0}$	Ratio of half-width to spacing	T_{max}
DHLLH	10	1	0·1	1:5	0·8
DHLHHLH	10	0·5	0·05	1:10	0·35

11. Experimental double half-wave filters

The single half-wave filters described above are relatively more sensitive to film imperfections than double half-wave systems. Fig. 12 shows the measured transmittance of a seven-layer band-pass double half-wave filter *DHLLHLHLLH* constructed from germanium and fluorite for $\lambda_0 = 2\,\mu$. The dotted curve in the same figure shows the transmittance of a five-layer single half-wave filter centred

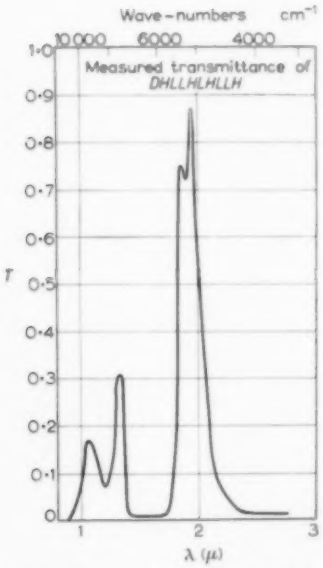

Fig. 12. Experimental double half-wave filter *DHLLHLHLLH*.

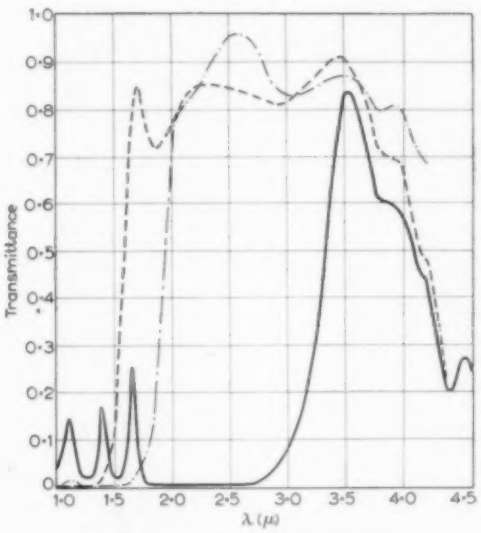

Fig. 13. Experimental low-pass systems.

at the same wavelength. By comparison the peak transmittance of the double half-wave filter is significantly higher, the transition from pass band to stop band more rapid and the rejection in the stop band greater than for the single half-wave filter, although the latter's bandwidth is smaller.

Fig. 13 shows the measured transmittance of three low-pass double half-wave systems. All the systems are *DHLHHLHHLH* with λ_0 at 0·75, 0·95, 1·5 μ respectively, leading to "edges" (defined by wavelength for 50 per cent transmission) at 1·6, 2·0, 3·3 μ. Agreement with theory (Fig. 7) is satisfactory, the fall in transmittance beyond 3·8 μ being due to absorption in the quartz substrates.

12. A tunable interference filter with air gap as spacer layer

There are three immediate advantages in using an air gap as the spacer layer:

(i) The position of the pass band can be tuned to any desired wavelength within the reflectance region of the stacks.

(ii) The filter may be used at various orders and hence bandwidths.

(iii) The number of films in any one assembly is reduced compared with that of a "solid" filter with the same reflecting stacks. This latter feature is important

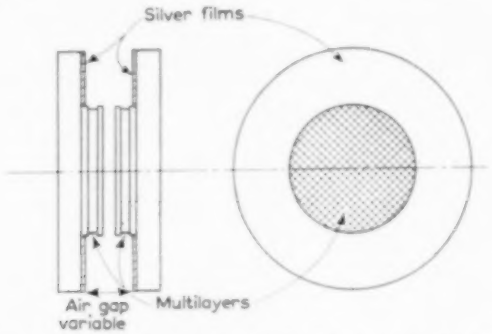

Fig. 14. Arrangement of films on the plates of the tunable interference filter.

as the losses in the stacks increase with increasing numbers of films and total thickness of stack. Such a filter (Smith and Heavens [12]) has been constructed for $\lambda_0 = 2\ \mu$ with three-layer germanium/cryolite stacks. The filter takes the form shown in Fig. 14. Semi-transparent silver annuli enable the plates to be set

Table 6.

	λ_0 (μ)	Half-width (μ)	$\frac{\Delta\lambda}{\lambda_0}$	Ratio of half-width to spacing	Effective reflectance	Spacing of peaks at 2 μ (μ)
Theoretical	2·0	0·004	0·002	1:65	0·95	0·25
Experimental	2·0	0·01	0·005	1:26	0·89	0·25

parallel through observation of Fabry–Perot rings in visible light. The mechanical problems in adjusting the air gap while keeping the plates parallel are not severe over the small range of movement required. The performance of the filter with its seventh-order peak at 2 μ is described in Table 6.

We observe that the characteristic ratio of half-width to spacing has risen from 1 : 10 to 1 : 26 compared with "solid" filter described above. Fig. 15 shows the pass band of the filter (with its third order at 2 μ) in series with a low-pass auxiliary filter. No unwanted bands then occur between 1 and 3 μ. The pass band may be easily adjusted to any wavelength within ± 12 per cent of λ_0. Alternatively the

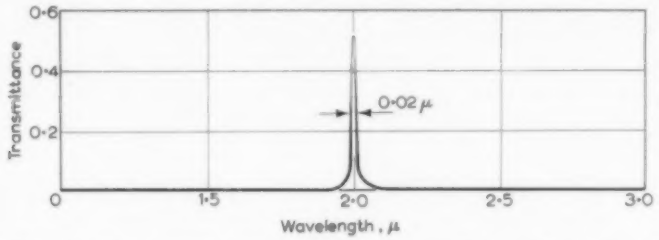

Fig. 15 Experimental transmittance of variable air-gap filter combined with double half-wave low-pass filter from 1·0 to 3·0 μ.

band may be continuously scanned over the same wavelength range by continuous variation of the air gap; this has been done conveniently by the use of a pressurized capsule.

For work at high resolution, a Fabry–Perot interferometer with a variable gap is a most attractive alternative to the conventional scanning monochromator. It has been shown by JACQUINOT [3] to be about one hundred times more luminous for a given resolving power than the best blazed grating of the same size. The interferometer transmits a number of pass-bands whose spectral separation decreases as the interferometer gap increases. Each pass-band can have a half-width which is about one-thirtieth of the separation of adjacent bands. It is therefore possible to use a conventional monochromator to isolate one such pass-band and the interferometer will increase the resolving power of the system without the necessity of decreasing the slit-width. This is made possible by the large angular dispersion of the interferometer which is such as to give a relation between slit-width and resolution as shown in Table 6:

Table 6.

f/5 Collimator Slit size	Resolving power	*f*/20 Collimator Slit size
4·5 cm	1,000	18 cm
1·5 cm	10,000	6 cm
0·45 cm	100,000	1·8 cm

(Slit-width vs. resolving power for a 10 cm diameter interferometer for two different collimator focal ratios).

The only requirement in scanning such a monochromator through an extended spectral range is that the width of the interferometer gap should be varied in a

saw-tooth fashion over a range of half a wavelength. This causes the transmission bands to drift by an amount equal to their separation. By selecting each of these bands successively by scanning the conventional monochromator a wide spectral range can be explored.

This variation has been introduced in two ways. The mechanical method described above has been found satisfactory if the interferometer is properly constructed. An alternative method is to keep the gap physically constant and to vary its optical thickness by changing the gas pressure in the interferometer. Jacquinot [13], Jaffe, Rank, and Wiggins [14] have described systems in which the pressure of air is varied from 0–1 atm. However, this gives a range of 0·001 μ at 3 μ (1 cm^{-1} at 3000 cm^{-1}) which is useful only for high resolution monochromators. Other gases, used under pressure, allow this range to be increased by a factor of twenty without much difficulty.

13. Conclusions

The experimental filters show that the most significant limitation to the performance of infra-red interference filters is in the optical quality of thick evaporated films. Very considerable advances could be made if the growth of the large crystallites, which cause the losses, could be inhibited. Useful filters can be constructed, however, with the present qualities obtainable although the useful numbers of layers in any one assembly is limited. The use of air gaps as spacer layers leads to considerably improved performance and the practicability of tuning the pass band to a given wavelength and of continuous scanning has been demonstrated. The design possibilities of multiple half-wave filters are considerable and these filters show less dependence on film imperfections than do filters of the Fabry–Perot type. It should therefore be possible to provide an interference system as a wide or narrow band filter or monochromator for any chosen (but restricted) wavelength region between 1 and 20 μ. The experimental results show that the advantages of interference monochromators over grating and prism instruments predicted by Jacquinot can be realized to a considerable extent in the near infra-red region of the spectrum.

References

[1] Giacomo P. and Jacquinot P. *J. Phys. Radium* A1952 **13** 59.
[2] Ring J. Ph. D. Thesis, University of Manchester, 1957.
[3] Jacquinot P. *J. Opt. Soc. Amer.* 1954 **44** 761.
[4] Polster H. D. *J. Opt. Soc. Amer.* 1952 **42** 21.
[5] Baumeister P. W. and Stone J. M. *J. Opt. Soc. Amer.* 1956 **46** 228.
[6] Baumeister P. W. and Jenkins F. A. *J. Opt. Soc. Amer.* 1957 **47** 57.
[7] Turner A. F. *Infra-red Transmission Filters.* Bausch and Lomb Technical Reports, Nos. 1–6.
[8] Braithwaite J. G. N. *J. Sci. Instrum.* 1955 **32** 10.
[9] Holland L. *Vacuum Deposition of Thin Films.* Chapman and Hall 1956.
[10] Lissberger P. H. and Ring J. *Optica Acta Paris* 1955 **2** 43.
[11] Greenler R. G. *J. Opt. Soc. Amer.* 1957 **47** 130.
[12] Smith S. D. and Heavens O. S. *J. Sci. Instrum.* In press.
[13] Jacquinot P. *J. Rech.* 1948 **6** 91.
[14] Jaffe J. H., Rank D. H. and Wiggins T. A. *J. Opt. Soc. Amer.* 1955 **45** 636.

VOL.
10
1957/5

Spectrochimica Acta, 1957, Vol. 10, pp. 195 to 200. Pergamon Press Ltd., London

The spectrochemistry of actinium

WILLIAM F. MEGGERS
National Bureau of Standards, Washington, D.C.

(*Received* 23 *May* 1957)

Abstract—For spectrochemical detection or determination of actinium ($_{89}$Ac) the wavelengths and estimated relative intensities (100 or greater) of 109 strong lines are presented. The wavelengths range from 2558·08 to 7866·10 Å. Thirty-two lines are characteristic of Ac I, 63 belong to Ac II, 7 are assigned to Ac III, 2 possibly to Ac IV, and 5 to Ac0. The energy levels involved in the production of lines in the first three spectra of actinium are given. Within the range of these observations the strongest Ac I line is the transition $6d7s^2\,{}^2D_{1\frac{1}{2}}$–$6d7s(a^3D)7p\,{}^2F^\circ_{2\frac{1}{2}}$ with wavelength 4179·98 Å and intensity 1000 in the arc or hollow cathode. The strongest line of Ac II appears to be $6d7s\,{}^3D_3$–$7s(^2S)7p\,{}^3P^\circ_2$ with wavelength 4088·44 Å, and intensity 3000 in the spark. The strongest observed line has a wavelength 2626·44 Å, and intensity 5000 in the spark; it represents the transition $7s\,{}^2S_{0\frac{1}{2}}$–$7p\,{}^2P^\circ_{1\frac{1}{2}}$ in Ac III, and must be regarded as the *raie ultime* in high-voltage condensed electrical discharges.

OL.
10
7/58

In 1899, soon after the discovery of radium and polonium, a third new element, actinium, was found in pitchblende [1]. It was separated from other elements by chemical means, and was revealed by its radioactivity. Later research established the fact that actinium occurs in nature only as the daughter of protactinium, which in turn results from the spontaneous decay of the relatively rare isotope of uranium with atomic number 92 and mass 235—the isotope that produced the first atomic bomb. The atomic number of actinium is 89, and its mass is 227. Its half-life is about 22 years. Through a series of α- and β- emissions actinium forms a succession of unstable atoms of diminishing mass until it is transformed into a stable isotope of lead with atomic number 82 and mass 207. The terrestrial abundance of actinium is reported to be 3×10^{-10} g per metric ton, that is about 3 parts in 10^{16}.

Because of its low abundance, radioactive instability, and lack of commercial uses, actinium had never been concentrated in pure form from mineral sources. For a long time, therefore, little was known about its chemical or physical properties. However, after the discovery of nuclear fission and the construction of uranium piles, neutrons became available in sufficient quantities to produce, by transmutation, ponderable amounts of any desired element. Thus, several milligrams of actinium were made at the Argonne National Laboratory by bombarding radium with neutrons, thereby transmuting radium of atomic number 88 and mass 226 to actinium of atomic number 89 and mass 227.

Although actinium was artificially prepared primarily for chemical research, portions of the samples were loaned to physicists for investigation of the optical emission spectra. Because the Argonne laboratory was fully equipped with devices for the safe handling of "hot" materials, the actinium spectra were photographed there; the spectrograms were then shipped to the National Bureau of Standards,

where they were measured and interpreted. The results of this co-operative investigation have been published as a research paper entitled "Emission Spectra of Actinium" [2], which may be consulted for full details.

Because of large-scale production of thorium and uranium in recent years it seems likely that the refinement of these metals would yield as by-products considerable quantities of rarer elements, possibly including actinium. During these years also the emission spectra of the elements have increasingly found application to the detection and quantitative determination of the elements in ores, metals, solutions, and concentrates. For this purpose it is necessary to know the wavelengths, relative intensities, and excitation potentials of spectral lines of each element so that coincidences with lines of other elements can be avoided, the strongest line can be used to find traces, and so that lines of equal or comparable excitation may be chosen for quantitative analysis by the internal standard method [3]. Such information was previously given for technetium and promethium [4], two artificial elements now available commercially as fission products of uranium. Similar information is now given for actinium.

Unlike technetium and promethium, which have never been detected in terrestrial sources, actinium, as stated above, was first found in pitchblende. Furthermore, despite its low concentration in the earth's crust, actinium, at least once, has been sufficiently enriched to detect spectroscopically. Thus, in 1937, LUB [5] examined the spark spectra of lanthanum solutions containing 0·05 mg of actinium and published the wavelengths of nine new lines (presumably actinium) that appeared among 900 lanthanum lines. The following wavelengths in ångströms (and intensities) of actinium lines were reported by LUB: 4061·58 (4), 4088·37 (5), 4168·40 (5), 4179·93 (4), 4359·09 (3), 4386·37 (5), 4413·17 (5), 4507·20 (5), and 4812·25 (4). These are indeed identifiable with intense lines in our description of emission spectra of actinium, but it is now known that only one of these belongs to neutral actinium atoms, seven originate in singly ionized atoms, and one belongs to doubly charged ions. This assignment of several hundred actinium lines to successive spectra (Ac I, Ac II, Ac III, and possibly Ac IV) was based upon intensities in different light sources, the hollow cathode, the electric arc, and the high-voltage spark [2]. The quantum interpretation of these spectra was successful in accounting for most of the observed lines as transitions between atomic or ionic energy levels that could be grouped into spectral terms and correlated with electron configurations. The ground state of Ac I was found to be $(6d7s^2)^2D_{1\frac{1}{2}}$, that of Ac II is $(7s^2)^1S_0$, and that of Ac III is $(7s)^2S_{\cdot 0\frac{1}{2}}$.

Since spectrographers are interested primarily in wavelengths, relative intensities, and atomic energies associated with spectral lines, such information for 109 actinium lines has been selected from our research paper [2] and presented here in Table 1. Many of the actinium lines are widened by hyperfine structure which complicates the measurement of wavelengths and the estimation of relative intensities. However, the probable error in any actinium wavelength is usually less than 0·01 Å, as shown by good agreement of different measurements and by the close coincidence of calculated and observed wave numbers.

The estimated intensities of actinium lines appearing in arc, spark, and hollow-cathode sources range from 1 to 5000, but only lines of intensity 100, or more,

VOL.
10
1957/5

Table 1. Emission spectra of actinium

Wavelength (ångströms)	Intensity			Spectrum	Energy levels (kaysers)
	Arc	Spark	Hollow cathode		
2558·08		200*h*		IV?	
2626·44	20*de*	5000*h*		III	0–38063
2657·81	40*c*	100*c*	2*c*	II	7427–45040
2682·90	3*e*	400*h*		III	801–38063
2793·90		200*Hw*		IV?	
2847·16	50	300*hl*		II	9088–44200
2896·82	50*c*	100*c*		II	7427–41937
2923·02	80	100		II	7427–41628
2952·55	30*c*	4000*h*		III	4204–38063
2994·17	200	400	60	II	0–33389
3019·87	200*c*	300*c*	4*c*	II	5267–38372
3043·30	200	1000	10*c*	II	9088–41937
3069·36	80	400	5	II	13236–45807
3078·07	40	300		II	14949–47428
3086·04	70	300	7	II	16757–49152
3087·37	150	200	20*c*	II	7427–39807
3112·83	300	400	6	II	4740–36856
3120·16	200	300	6	II	4740–36780
3143·71	100	10	80	I	0–31800
3153·09	500*c*	1000*c*	80*cs*	II	5267–36973
3154·41	600	1000*c*	60*cs*	II	7427–39119
3164·81	300	500*cs*	10*cs*	II	5267–36856
3171·17	150	15	60	I	2231–33756
3219·08	20	100*h*	2	II	22199–53255
3230·59	300*cs*	400*cs*	10*cs*	II	7427–38372
3237·70	200*cs*	300*cs*	10*cs*	II	5267–36144
3239·86	20	100	2	II	19203–50060
3260·91	500	1000	80	II	4740–35397
3318·01	200	300	6*cs*	II	5267–35397
3383·53	200*c*	400	20*cs*	II	7427–36973
3392·78	20*de*	3000*dh*	10*d*	III	0–29466
3413·84	300	400	60	II	9088–38372
3417·77	500	600	200	II	0–29250
3481·16	500	1000	200*cs*	II	7427–36144
3487·59	40	4000	15	III	801–29466
3489·53	300	400	100	II	4740–33389
3527·31	50	200	20	II	13236–41579
3529·24	50	200	15	II	14949–43276
3534·63	50	250	15	II	16757–45040
3554·99	300	400	10*cs*	II	5267–33389
3565·59	1000	2000	150*cs*	II	5267–33305
3694·88	50	150	20	II	9088–36144
3701·30	80	10	100	I	0–27010
3756·67	400*c*	500*c*	80*cs*	II	5627–31879
3799·82	100	200	30	II	9088–35397
3835·32	100	8	150	I	0–26066
3843·04	300	20	600*c*	I	

Table 1. Emission spectra of actinium—*continued*

Wavelength (ångströms)	Intensity			Spectrum		Energy levels (kaysers)
	Arc	Spark	Hollow cathode			
3863·12	1000*cs*	2000*c*	200*cs*	II		7427–33305
3885·56	400	40	400*c*	I		0–25729
3914·47	100	200	100*c*	II		7427–32966
3977·36	40	100	8	II		13236–38372
4034·63	200	30	80*c*	I		2231–27010
4061·60	400*c*	500*c*	400*cs*	II		5267–29881
4063·10	200	20	200*cs*	I		2231–26836
4078·70	150	200	50*c*	II		4740–29250
4088·44	2000*cs*	3000*cs*	300*cs*	II		7427–31879
4168·40	1500*cs*	2000*cs*	200*cs*	II		5267–29250
4179·98	1000	50	1000	I		0–23917
4183·12	500	20	800	I		0–23899
4194·40	400	20	400	I		2231–26066
4209·69	80	300	200*cs*	II		7427–31175
4225·99	80	3	100	I		
4359·13	300	400	100	II		5267–28201
4384·53	300*c*	30*c*	150*cl*	I		0–22801
4386·41	500	1500	100*cl*	II		9088–31879
4396·71	400	30	200	I		2231–24969
4402·11	100	10	10*c*	I		12078–34788
4413·09	40*c*	3000*h*			III	801–23454
4452·19	600	700	50*cs*	II		7427–29881
4462·73	400	50	300*c*	I		0–22402
4507·20	2000*cl*	2000*cl*	150*cl*	II		0–22181
4552·18	100*c*	5*c*	15*c*	I		10906–32867
4569·87	50*c*	4000*h*			III	4204–26080
4605·45	1000	1000	100*c*	II		4740–26447
4610·10	100	5	10	I		2231–23917
4613·93	300	20	100*c*	I		2231–23899
4682·16	100*c*	6*c*		I		12078–33430
4705·78	200*c*	10*c*	30*cs*	I		2231–23476
4716·58	500	20	200*cs*	I		0–21196
4720·16	1000	1000	100*cs*	II		5267–26447
4740·51	50	200	5	II		20848–41937
4807·83	60	100	10*c*	II		9088–29881
4812·22	500	600	150*c*	II		7427–28201
4860·16	150*c*	10	60*c*	I		2231–22801
4945·18	150	200	8*c*	II		16757–36973
4958·23	200	200	6*c*	II		9088–29250
4960·87	100	150	4	II		13236–33389
5258·24	300*c*	20*c*	200*c*	I		0–19012
5271·56	150	8	100	I		2231–21196
5344·74	100	4	30	I		9864–28568
5446·38	300	400	9	II		14949–33305
5569·26	200*c*	10*c*	200*c*	I		0–17951
5636·60	100*c*	4*c*	80*c*	I		0–17736
5718·44	100*Bl*	1			AcO	

VOL.
10
1957/5

Table 1. Emission spectra of actinium—*continued*

Wavelength (ångströms)	Intensity			Spectrum		Energy levels (kaysers)
	Arc	Spark	Hollow cathode			
5718·66	200*Bl*	2	8*Hl*		AcO	
5729·15	180*Bl*		6*Hl*		AcO	
5732·05	200*cl*	200*cl*	60*cl*	II		4740–22181
5740·00	150*Bl*		5*Hl*		AcO	
5751·41	120*Bl*		5*Hl*		AcO	
5758·97	300*c*	400*c*	40*c*	II		9088–26447
5910·85	1000*c*	1000*c*	400*c*	II		5267–22181
6164·75	500*c*	600*c*	200*cl*	II		4740–20956
6167·83	50*cl*	100*cl*	20*cl*	II		16757–32966
6242·83	300*c*	300*c*	10*c*	II		13236–29250
6359·86	300*c*	20*c*	500*c*	I		2231–17951
6691·27	200*cl*	20*cl*	300*c*	I		0–14941
6695·23	150	200	20	II		14949–29881
7290·40	10*c*		300*c*	I		0–13713
7866·10	2*cl*		200*cl*	I		2231–14941

OL.
10
7/58

are included in Table 1. The relative intensities in different sources lead unambiguously to the assignment of each line to its proper spectrum, as shown in column 5. Literal symbols accompanying the intensity numbers have the following meanings: *B*, molecular band; *c*, complex; *d*, double; *e*, enhanced at electrode; *h*, hazy; *H*, very hazy; *l*, shaded to longer waves; *s*, shaded to shorter waves; and *w*, wide.

Finally, the energy levels that produce particular lines in a specified spectrum are given in the last column of Table 1. Instead of representing these by spectroscopic symbols, they are expressed in wave number units (1K = 1 cm^{-1}), rounded to the nearest whole unit. Conventionally the normal (unexcited) state in any spectrum is called 0 (zero), so that these numbers are exactly proportional to excitation energies. These energies may be converted to electron-volts by dividing the wave number values by 8067·5(1 eV = 8067·5K) but it is preferable to retain the former because they facilitate finding the corresponding spectral terms, quantum numbers, and electron configurations in other actinium tables [2], and their difference is the vacuum wave number of the spectral line.

The atomic energy levels that produce Ac I lines require no correction, but those responsible for Ac II and Ac III need to be increased respectively by the first and second ionizaion potentials, if the total energy is desired. The first ionization potential of actinium has been predicted [6] to be 6·89 $\pm$ 0·6 eV(6·89 eV = 55585K), and a second ionization potential of 12·0 eV(12·0 eV = 96810K) has been derived [2] from a spectral series in Ac II. Thus, to measure the total energies involved in exciting Ac II lines all energy level values for these lines in Table 1 should be increased by 55585K. Likewise to obtain the total energies required for the exeitation of Ac III lines the energy level values shown in Table 1 must be increased by 55585 + 96810 = 152395K. Each of the actinium spectra, Ac I,

Ac II, and Ac III, exhibits lines of outstanding intensity which may be looked for when seeking small concentrations of this element.

Within the range of these observations the strongest Ac I line is the transition $6d7s^2\,{}^2D_{1\frac{1}{2}} - 6d7s(a^3D)7p\,{}^2F^\circ_{2\frac{1}{2}}$ with wavelength 4179·98 Å, and intensity 1000 in the arc or hollow cathode. The strongest line of Ac II appears to be $6d7s\,{}^3D_3 - 7s(^2S)7p\,{}^3P^\circ_2$ with wavelength 4088·44 Å, and intensity 3000 in the spark. If the light source favours the production of doubly-charged ions (Ac^{++}), and excitation of Ac III, the strongest line will undoubtedly be $7s\,{}^2S_0 - 7p\,{}^2P^\circ_{2\frac{1}{2}}$ with wavelength 2626·44 Å (5000), because this represents the transition of a single electron between p and s states, the latter defining the ground state of Ac III [7].

References

[1] DEBIRNE A. *C. R. Acad. Sci. Paris.* 1899 **129** 593; *Ibid.* 1900 **130** 906.
[2] MEGGERS W. F., FRED M. and TOMKINS F. S. *J. Res. Nat. Bur. Stand.* 1957 **58** 297, Research Paper 2763.
[3] MEGGERS W. F. *Spectrochim. Acta* 1947 **3** 5.
[4] MEGGERS W. F. *Spectrochim. Acta* 1951 **4** 317.
[5] LUB W. A. *Koninkl. Akad. Wetenschap. Amsterdam* 1937 **40** 584.
[6] FINKELNBURG W. and HUMBACH W. *Naturwissenschaften* 1955 **42** 35.
[7] MEGGERS W. F. *J. Opt. Soc. Amer.* 1941 **31** 39, 605.

VOL.
10
1957/5

Spectrochimica Acta, 1957, Vol. 10, pp. 201 to 212. Pergamon Press Ltd., London

Untersuchung der statistischen Streuung der Restgehaltsbestimmung nach dem spektrochemischen Zugabeverfahren

F. Rosendahl
Institut für Spektrochemie und angewandte Spektroskopie, in Zusammenarbeit mit der Westfälischen Wilhelms-Universität zu Münster, Dortmund-Aplerbeck

(*Received* 18 *June* 1957)

Zusammenfassung—Es wird ein geschlossener mathematischer Ausdruck für die statistische Streuung der Restgehaltsbestimmung nach dem Zugabeverfahren abgeleitet, aus dem sich die optimalen Bedingungen für diese Methode ablesen lassen.

Einleitung

In den letzten Jahren sind spektrochemische Analysenmethoden in immer stärkerem Maße zur *quantitativen* Spurenanalyse angewendet worden. Einmal der Schnelligkeit wegen, mit der diese Methoden einen vollständigen Überblick über die Zusammensetzung der untersuchten Substanz geben, zum anderen wegen der durchweg hohen Nachweisempfindlichkeit.

Die einzige brauchbare Möglichkeit, bei der spektrochemischen Bestimmung kleiner Spurengehalte zu einer unabhängigen Eichung zu kommen, ist das bereits von Duffendack und Wolfe [2] mitgeteilte Zugabe-oder Additionsverfahren, das heute vielfach benutzt wird. Zur vollkommenen Beherrschung dieser Eichmethode ist es jedoch unerläßlich, die Grenzen ihrer Anwendbarkeit und Genauigkeit zu kennen. Eichhoff und Mainka [3] geben einen Anhalt über die erzielbaren Genauigkeiten, indem sie in praktischen Beispielen mit angenommenen fehlerhaften Intensitätswerten rechnen und die dabei auftretenden Abweichungen der Konzentrations angaben bestimmen. Im folgenden soll in mathematisch geschlossener Form eine *allgemeingültige* Untersuchung über die statistische Analysengenauigkeit, die mit dem Zugabeverfahren erreichbar ist, angestellt werden.

Überblick über das Zugabeverfahren

Die Grundlage des spektrochemischen Zugabeverfahrens ist der nahezu lineare Zusammenhang zwischen dem Logarithmus der Konzentration eines Elementes und dem Logarithmus der Intensität seiner Nachweislinie. Unter dieser wesentlichen Voraussetzung ist der Leitgedanke dann folgender: Zu der gegebenen gering verunreinigten Substanz gibt man eine geeignete bekannte Menge des zu untersuchenden Elementes hinzu ("Nennkonzentration"). Auf diese Weise bereitet man einige Eichproben, die in der Grundzusammensetzung genau der zu prüfenden Substanz entsprechen und von denen man die Konzentration des gefragten Elementes bis auf einen kleinen Restgehalt kennt. Dieser Restgehalt ist in allen so hergestellten Eichproben gleich.

Trägt man in doppeltlogarithmischem Maßstab die Intensität der Nachweislinie gegen die Nennkonzentration auf, so erhält man eine Kurve, die zu kleineren

* Diese Arbeit enthält im wesentlichen den ersten Teil der 1955 bei der mathematisch-naturwissenschaftlichen Fakultät der Universität Bonn eingereichten Dissertation von F. Rosendahl.

Gehalten hin immer steiler verläuft. Addiert man zu der Nennkonzentration einer jeden Eichprobe einen geeigneten konstanten Betrag, so läßt sich diese Kurve in eine Gerade überführen. Der konstante Betrag, der überall addiert werden muß, ist die unbekannte Restkonzentration, die auf diese Weise bestimmt werden kann. Die Gerade, die nach der Korrektur vorliegt, ist die Eichkurve für den betreffenden Konzentrationsbereich.

Während der Grundgedanke des Zugabeverfahrens bei den verschiedensten Autoren immer wiederkehrt, schlägt jedoch jeder einen anderen Weg vor, die Korrektur durchzuführen. Neben Duffendack und Wolfe griffen noch Gatterer [4], Pierce und Nachtrieb [10] sowie Kaiser [8] die Frage auf. In dieser Arbeit soll dem Vorschlag von Kaiser entsprechend vorgegangen werden. Danach kann die Restkonzentration errechnet werden, wenn die Steilheit η der doppeltlogarithmisch aufgetragenen Eichgeraden gleich eins ist. Die Anwendungsmöglichkeit läßt sich jedoch in einfacher Weise auf den Bereich der übrigen Vorschläge erweitern, so daß die einschränkende Bedingung, zwischen der Intensität und der Konzentration müsse ein linearer Zusammenhang bestehen, hinfällig wird.

Rechnerischer Gang der Restgehaltskorrektur

Wird die Linearität einer spektrochemischen Eichkurve vorausgesetzt, so läßt sie sich in der üblichen Bezeichnungsweise [6] in folgender Form niederschreiben:

$$\lg k^* = \eta \Delta Y + \lg k_0 \tag{1}$$

Ist in einer Probe neben der bekannten Konzentration k ein unbekannter Restgehalt k_r, so gilt:

$$k^* = k + k_r \tag{2}$$

und damit

$$\lg (k + k_r) = \eta \Delta Y + \lg k_0 \tag{3}$$

Wenn ΔY_r der Logarithmus des Intensitätsverhältnisses für die Probe ohne Zusatz ist, dann ist:

$$\lg k_r = \eta \Delta Y_r + \lg k_0 \tag{4}$$

ein Sonderfall von Gleichung (3). Subtrahiert man Gleichung (4) von Gleichung (3), so gelangt man zu:

$$\lg \left(1 + \frac{k}{k_r}\right) = \eta(\Delta Y - \Delta Y_r) \tag{5}$$

Ist die Steilheit η bekannt, so läßt sich nach Kaiser k_r in einfacher Weise durch die Anwendung der Seideltransformation [5] und anschließende Auflösung der Gleichung aus den Meßwerten der Probe ohne Zusatz und einer Probe mit bekanntem Zusatz bestimmen. Ist η unbekannt, so benötigt man auf jeden Fall noch eine zweite Probe mit einer bekannten Zumischung zu k_r, so daß man ein System von zwei transcendenten Gleichungen für die beiden Unbekannten η und k_r zur Hand hat. Die Lösung dieses Systems findet man zweckmäßig mittels graphischer Methoden. Ist die Restkonzentration k_r bestimmt worden, so braucht man nur

VOL. 10 1957/5

die Meßwerte ΔY gegen die entsprechenden $k^* = k + k_r$ auf halblogarithmischem Papier aufzutragen, um eine Eichgerade zu erhalten. Mit dieser Eichgeraden kann man dann ohne weitere Zwischenrechnung Proben mit in dem erfaßten Bereich liegenden Gehalten analysieren. Soweit die eigentliche Rechenoperation, die notwendig ist, um eine Eichgerade zu gewinnen.

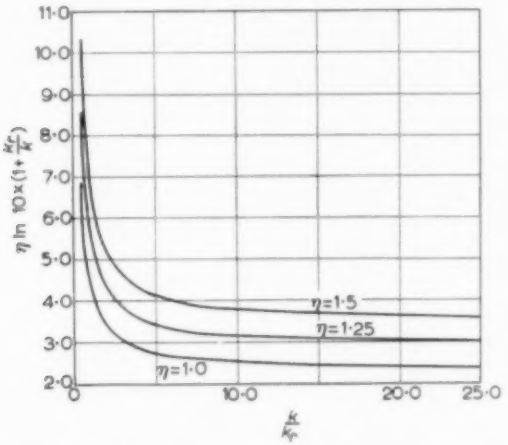

Abb. 1. Fehlerübertragungsfaktor für die Restgehaltsbestimmung bei bekannter Steilheit der Eichgeraden. Aufgetragen als Funktion von k/k_r.

Statistische Genauigkeit der Restgehaltsbestimmung

(a) *Lineare Eichkurven.* Die ungenaue Kenntnis der zugemischten Konzentrationen und die Unsicherheit der Meßwerte ΔY sind die hauptsächlichen Fehlerquellen des Zugabeverfahrens.

Wie die Erfahrung zeigt, können wir die erste Fehlerquelle außer Betracht lassen. Die Zumischungen können bei sorgfältiger und zweckmäßiger Arbeitsweise so präzise durchgeführt werden, daß man die beigemischten Konzentrationen k praktisch als fehlerfrei ansehen kann. Damit hinterbleibt nur noch die Unsicherheit der Meßwerte ΔY.

Das Ziel dieser Untersuchung ist es, die Streuung von k_r als Funktion der Meßwertfehler auszudrücken. Damit ergibt sich dann gleichzeitig eine Abschätzung für die statistisch mögliche Fehlerhaftigkeit der nach dieser Methode aufgestellten Eichgeraden, die später als systematischer Fehler allen Konzentrationsbestimmungen anhaftet, die nach dieser Eichung vorgenommen werden.

Zunächst wollen wir die Fehlerbetrachtung für den einfacheren Fall einer bekannten Steilheit η durchführen. Da ΔY und ΔY_r unabhängige Variable sind, kann man bei bekanntem η die Streuung $[\sigma_{k_r}]_\eta$, die durch die Meßwertstreuung verursacht wird, nach dem Fehlerfortpflanzungsgesetz [9] berechnen. Es gilt:

$$[\sigma_{k_r}]_\eta^2 = \left(\frac{\partial k_r}{\partial \Delta Y}\right)^2 \sigma_{\Delta Y}^2 + \left(\frac{\partial k_r}{\partial \Delta Y_r}\right)^2 \sigma_{\Delta Y_r}^2 \qquad (6)$$

Hiernach errechnet sich aus Gleichung (5):

$$\frac{[\sigma_{k_r}]_\eta}{k_r} = \eta \ln 10\left(1 + \frac{k_r}{k}\right)\sqrt{(\sigma^2_{\Delta Y} + \sigma^2_{\Delta Y_r})} \tag{7}$$

In Abb. 1 ist der Übertragungsfaktor $\eta \ln 10[1 + (k_r/k)]$ der Meßwertstreuungen auf die "relative Streuung" $[\sigma_{kr}]_\eta/k_r$ bei bekanntem η als Funktion von k/k_r für verschiedene η aufgezeichnet. Man erkennt, daß der Faktor für kleine Werte k/k_r stark ansteigt, während er für große Werte nahezu konstant ist. Damit die Streuung $[\sigma_{k_r}]_\eta$ nicht zu groß wird, sollte man also dafür sorgen, daß k/k_r nicht kleiner als 1 wird. Das bedeutet, daß die kleinste Nennkonzentration nicht kleiner als die Restkonzentration sein sollte.

Für den einfacheren Fall, daß η bekannt ist, wird die Streuung der Restkonzentrationsbestimmung um so kleiner, je größer das Verhältnis der Nennkonzentration zur Restkonzentration ist. Notwendige Voraussetzung ist natürlich dazu, daß die Eichgerade über einen genügend großen Bereich geradlinig ist und extrapoliert werden kann.

Wir wenden uns nun dem allgemeineren Fall zu, bei dem η unbekannt ist. Hier liegt ein System von 2 transcendenten Gleichungen für k_r und η vor, das nicht explizit nach k_r aufgelöst werden kann.

$$\lg\left(\frac{k_1}{k_r} + 1\right) = \eta(\Delta Y_1 - \Delta Y_r);\ \lg\left(\frac{k_2}{k_r} + 1\right) = \eta(\Delta Y_2 - \Delta Y_r) \tag{8}$$

Hier und auch im weiteren Verlauf der Arbeit sind die zur kleinsten Nennkonzentration gehörenden Werte mit 1 und die zur höchsten gehörenden mit 2 indiziert.

Auch in diesem allgemeineren Fall kann die Streuung von k_r nach dem Fehlerfortpflanzungsgesetz errechnet werden, da die drei statistischen Variablen ΔY_1; ΔY_2; ΔY_r unabhängig sind. Es gilt demnach:

$$\sigma_{k_r}{}^2 = \left(\frac{\partial k_r}{\partial \Delta Y_1}\right)^2 \sigma^2_{\Delta Y_1} + \left(\frac{\partial k_r}{\partial \Delta Y_2}\right)^2 \sigma^2_{\Delta Y_2} + \left(\frac{\partial k_r}{\partial \Delta Y_r}\right)^2 \sigma^2_{\Delta Y_r} \tag{9}$$

Durch Division der beiden Gleichungen (8) und nach einer Umstellung erhalten wir für k_r folgende implizite Funktion

$$\frac{\lg[(k_2/k_r) + 1]}{\lg[(k_1/k_r) + 1]} - \frac{\Delta Y_2 - \Delta Y_r}{\Delta Y_1 - \Delta Y_r} = F(k_r;\ \Delta Y_1;\ \Delta Y_2;\ \Delta Y_r;\ k_1;\ k_2) = 0 \tag{10}$$

Unter der Voraussetzung:

$$\frac{\partial F}{\partial_{k_r}} = F_{k_r} \neq 0 \tag{11}$$

erhalten wir dann

$$\frac{\partial k_r}{\partial \Delta Y_1} = -\frac{F_{\Delta Y_1}}{F_{k_r}};\ \frac{\partial k_r}{\partial \Delta Y_2} = -\frac{F_{\Delta Y_2}}{F_{k_r}};\ \frac{\partial k_r}{\partial \Delta Y_r} = -\frac{F_{\Delta Y_r}}{F_{k_r}} \tag{12}$$

VOL. 10 1957/5

Führen wir die Differentiationen durch und setzen die Ergebnisse in Gleichung (9) ein, so gelangen wir nach einigen Umformungen zu folgendem Ausdruck für die Streuung σ_{k_r} der k_r-Bestimmung:

$$\frac{\sigma_{k_r}}{k_r} = \eta\varphi\left(\frac{k_1}{k_r};\frac{k_2}{k_r}\right)\sqrt{\left[\sigma^2_{\Delta Y_1} + \left(\frac{\Delta Y_1 - \Delta Y_r}{\Delta Y_2 - \Delta Y_r}\right)^2 \sigma^2_{\Delta Y_2} + \left(1 - \frac{\Delta Y_1 - \Delta Y_r}{\Delta Y_2 - \Delta Y_r}\right)^2 \sigma^2_{\Delta Y_r}\right]} \quad (13)$$

Die Funktion φ in Gleichung (13) hat dabei folgende Form:

$$\varphi\left(\frac{k_1}{k_r};\frac{k_2}{k_r}\right) = \ln 10 \cdot \frac{1 + k_r/k_1}{1 - [(1 + k_r/k_1)\lg(1 + k_1/k_r)/(1 + k_r/k_2)\lg(1 + k_2/k_r)]} \quad (14)$$

Zunächst kann man aus Gleichung (13) herauslesen, daß die Streuungen $\sigma_{\Delta Y_r}$ der Meßwerte ΔY_1; ΔY_2 und ΔY_r mit verschiedenen Gewichten in das Ergebnis eingehen. Die Meßwertstreuungen der niedrigsten Nennkonzentration sind dabei mit dem größten Gewichtsfaktor versehen.

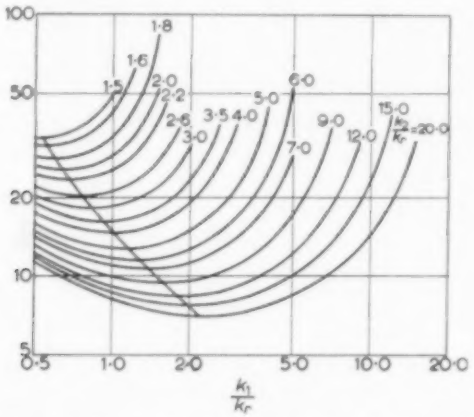

Abb. 2. Fehlerübertragungsfaktor $\varphi[(k_1/k_r);(k_2/k_r)]$ für die Restgehaltsbestimmung bei unbekannter Steilheit der Eichgeraden. Aufgetragen als Funktion von k_1/k_r (kleinere Nennkonzentration) mit k_2/k_r (grössere Nennkonzentration) als Parameter. Die Minima sind durch einen Kurvenzug miteinander verbunden.

Die Funktion $\varphi(k_1/k_r\,;k_2/k_r)$, die in Gleichung (12) erscheint, übt einen erheblichen Einfluß auf die Größe der Streuung aus. In Abb. 2 ist φ als Funktion von k_1/k_r für verschiedene Parameter k_2/k_r in dem praktisch interessierenden Bereich aufgetragen. Alle Kurven durchlaufen ein Minimum, das um so höher im Wert und um so schärfer definiert ist, je kleiner das als Parameter gewählte Verhältnis k_2/k_r ist. Die Minima sind in Abb. 2 durch einen Kurvenzug miteinander verbunden. Ihre Lagen ergeben sich aus folgender Gleichung:

$$\left(\frac{k_1}{k_r}\right)_{\min} = \ln 10\left(1 + \frac{k_r}{k_2}\right)\lg\left(1 + \frac{k_2}{k_r}\right) - 1 \quad (15)$$

Es gibt also zu jedem Verhältnis k_2/k_r der höheren Nennkonzentration eine für die Restgehaltsbestimmung optimale zweite kleinere Nennkonzentration. Ferner ist die Streuung der k_r-Bestimmung erheblich kleiner und die Auswahl der kleineren

Nennkonzentration wesentlich unkritischer, wenn der Konzentrationsbereich, über den sich die Nennkonzentrationen erstrecken, groß ist. Als Faustregel mag hier gelten: Die kleinere Nennkonzentration soll ungefähr der gleiche und die höhere wenigstens der zehnfache Betrag der Restkonzentration sein. Um einen Begriff von der Größenordnung der Streuung von k_r zu bekommen, wollen wir für $\eta = 1$ und die Konzentrationsverhältnisse $k_1/k_r = 1$ und $k_2/k_r = 20$ aus Abb. 2 und nach Gleichung (13) σ_{k_r}/k_r berechnen. Den hier angenommenen Werten entsprechen bei $\eta = 1$ nach Gleichung (8) die Meßwertdifferenzen $\Delta Y_1 - \Delta Y_r = 0{,}3$ und $\Delta Y_2 - \Delta Y_r = 1{,}32$, so daß wir erhalten:

$$\frac{\sigma_{k_r}}{k_r} = 8{,}2\sqrt{[\sigma^2_{\Delta Y_1} + 0{,}23^2\,\sigma^2_{\Delta Y_2} + (1 - 0{,}23)^2\sigma^2_{\Delta Y_r}]} \tag{14a}$$

Nehmen wir an, daß die Meßwertstreuungen $\sigma_{\Delta Y_1} = \sigma_{\Delta Y_2} = \sigma_{\Delta Y_r} = 0{,}010$ sind, so erhalten wir eine Streuung für die k_r-Bestimmung von ungefähr 11% des Restgehaltes. Eine solche Streuung ist aber für ein derartig kompliziertes Eichverfahren nicht verwunderlich und bei Spurenanalysen durchaus vertretbar.

Diese kurze Rechnung läßt erkennen, daß an die Genauigkeit der Meßwerte ΔY_r hohe Anforderungen gestellt werden. Andererseits wendet man jedoch die Zugabemethode hauptsächlich bei der Spurenanalyse im Bogen an. Bei einer Bogenanalyse muß man durchschnittlich mit einer Streuung der Einzelmessung von ungefähr 10% rechnen, d.h. $\sigma_{\Delta Y_r} \approx 0{,}040$. Um also nach Gleichung (13) ein σ_{k_r}/k_r innerhalb vernünftiger Grenzen zu bekommen, ist die Anwendung der Zugabemethode dann nur sinnvoll, wenn die Meßwerte, die zur Rechnung benutzt werden, Mittelwerte aus einer hinreichend großen Zahl von Einzelmessungen sind. Dann kann nämlich für $\sigma_{\Delta Y_r}$ die Streuung des Mittelwertes eingesetzt werden, die sich durch eine grössere Anzahl von Meßwerten herunterdrücken läßt. Das ist besonders für $\sigma_{\Delta Y_r}$ wichtig, da ΔY_r oft an der Bestimmungsgrenze (6) liegt und dadurch die Streuung, allein durch das Plattenkorn bedingt, schon größer als 10% ist.

Während theoretisch zur Bestimmung von k_r bei unbekanntem η nur zwei Eichproben mit verschiedenen Nennkonzentrationen notwendig wären, benutzt man in der Praxis oft mehr Proben und gewinnt durch Mittelung der einzelnen $k_{r\mu}$ einen Mittelwert $\bar{k}_r$. Da jedoch die einzelnen $k_{r\mu}$ keine unabhängigen Variablen sind, da der Meßwert ΔY_r bei allen Berechnungen derselbe ist, kann ohne nähere Untersuchung nichts über die Streuung von $\bar{k}_r$ ausgesagt werden. Wir wollen deshalb diesen Fall in unsere Fehlerbetrachtung einbeziehen. Jedoch werden wir uns darauf beschränken, daß mit Ausnahme von ΔY_r jeder Meßwert ΔY_ν nur einmal zur Restgehaltsbestimmung herangezogen wird. Die Variablen $k_{r\mu}$ hängen untereinander nur durch den zu ihrer Berechnung gemeinsam benutzten Meßwert ΔY_r zusammen.

Bezeichnen wir mit $k_{r\mu}$ den Restgehalt, der sich aus dem Gleichungssystem (8) für die Nennkonzentrationen $k_{2\mu}$ und $k_{2\mu-1}$ errechnet, so gilt:

$$k_{r\mu} = k_{r\mu}(\Delta Y_r;\ \Delta Y_{2\mu-1};\ \Delta Y_{2\mu}) \tag{16}$$

$$\bar{k}_r = \frac{1}{m}\sum_{\mu=1}^{m} k_{r\mu} \tag{17}$$

VOL. 10 1957/5

Da die Meßwerte ΔY_τ unabhängige Variable sind, erhalten wir für den gebildeten Mittelwert $\bar{k}_\tau$ folgende Streuung:

$$\sigma_{\bar{k}_\tau}^2 = \left(\frac{\partial \bar{k}_\tau}{\partial \Delta Y_\tau}\right)^2 \sigma_{\Delta Y_\tau}^2 + \sum_{\mu=1}^{m}\left[\left(\frac{\partial \bar{k}_\tau}{\partial \Delta Y_{2\mu-1}}\right)^2 \sigma_{\Delta Y_{2\mu-1}}^2 + \left(\frac{\partial \bar{k}_\tau}{\partial \Delta Y_{2\mu}}\right)^2 \sigma_{\Delta Y_{2\mu}}^2\right] \tag{18}$$

Unter Berücksichtigung von Gleichung (16) und (17) können wir Gleichung (18) schreiben:

$$m^2\sigma_{\bar{k}_\tau}^2 = \left(\sum_{\mu=1}^{m}\frac{\partial k_{\tau\mu}}{\partial \Delta Y_\tau}\right)^2 \sigma_{\Delta Y_\tau}^2 + \sum_{\mu=1}^{m}\left[\left(\frac{\partial k_{\tau\mu}}{\partial \Delta Y_{2\mu-1}}\right)^2 \sigma_{\Delta Y_{2\mu-1}}^2 + \left(\frac{\partial k_{\tau\mu}}{\partial \Delta Y_{2\mu}}\right)^2 \sigma_{\Delta Y_{2\mu}}^2\right] \tag{19}$$

Oder nach weiterer Umschreibung:

$$m^2\sigma_{\bar{k}_\tau}^2 = \sum_{\mu=1}^{m}\left[\left(\frac{\partial k_{\tau\mu}}{\partial \Delta Y_{2\mu-1}}\right)^2 \sigma_{\Delta Y_{2\mu-1}}^2 + \left(\frac{\partial k_{\tau\mu}}{\partial \Delta Y_{2\mu}}\right)^2 \sigma_{\Delta Y_{2\mu}}^2 + \left(\frac{\partial k_{\tau\mu}}{\partial \Delta Y_\tau}\right)^2 \sigma_{\Delta Y_\tau}^2\right] + 2\sigma_{\Delta Y_\tau}^2 \sum_{\substack{\rho;\tau=1\\ \rho<\tau}}^{m} \frac{\partial k_{\tau\rho}}{\partial \Delta Y_\tau}\frac{\partial k_{\tau\tau}}{\partial \Delta Y_\tau} \tag{20}$$

Unter Berücksichtigung von Gleichung (9) und Anwendung der Indizierung auf die Streuung erhalten wir:

$$\sigma_{\bar{k}_\tau} = \frac{1}{m}\sqrt{\left(\sum_{\mu=1}^{m}\sigma_{k_{\tau\mu}}^2 + 2\sigma_{\Delta Y_\tau}^2 \sum_{\substack{\rho;\tau=1\\ \rho<\tau}}^{m} \frac{\partial k_{\tau\rho}}{\partial \Delta Y_\tau}\frac{\partial k_{\tau\tau}}{\partial \Delta Y_\tau}\right)} \tag{21}$$

Die partiellen Ableitungen $\partial k_{\tau\mu}/\partial \Delta Y_\tau$ in Gleichung (21) haben folgende Form:

$$\frac{\partial k_{\tau\mu}}{\partial \Delta Y_\tau} = \eta k_{\tau\mu}\varphi\left(\frac{k_{2\mu-1}}{k_{\tau\mu}}; \frac{k_{2\mu}}{k_{\tau\mu}}\right)\left(1 - \frac{\Delta Y_{2\mu-1} - \Delta Y_\tau}{\Delta Y_{2\mu} - \Delta Y_\tau}\right) \tag{22}$$

wobei die Funktion $\varphi\,[(k_{2\mu-1})/k_{\tau\mu};\ k_{2\mu}/k_{\tau\mu}]$ identisch ist mit der in Gleichung (13) auftretenden, die in Abb. 2 wiedergegeben ist. Ziehen wir $1/m$ unter die Wurzel, so geht unter der Voraussetzung, daß für die $\sigma_{k_{\tau\mu}}$ eine obere Schranke existiert, der erste Summand unter der Wurzel für $m \to \infty$ wie $1/m$ gegen Null. Der zweite Summand dagegen strebt für $m \to \infty$ gegen einen endlichen Grenzwert > 0, wenn es für die $\partial k_{\tau\mu}/\partial \Delta Y_\tau$ eine obere Schranke und eine untere Schranke > 0 gibt. Da in allen praktisch möglichen Fällen immer gilt:

$$100 > \frac{k_{2\mu}}{k_{2\mu-1}} > 1 \tag{23}$$

sind diese Voraussetzungen erfüllt. Damit können wir aus Gleichung (21), wie zu erwarten war, folgendes herauslesen: Durch eine Mittelung verschiedener $k_{\tau\mu}$, die alle aus einem gemeinsamen Meßwert ΔY_τ, sonst aber aus verschiedenen Werten ΔY_τ berechnet wurden, kann die Streuung verringert werden. Sie geht für eine grosse Anzahl von Einzelbestimmungen $k_{\tau\mu}$ jedoch nicht auf Null, sondern es bleibt ein Anteil, der von der Streuung des Meßwertes ΔY_τ herrührt. Dieser Anteil kann nur durch ein kleineres $\sigma_{\Delta Y_\tau}$ verkleinert werden.

Bei der praktischen Durchführung einer Restgehaltsbestimmung geht man jedoch aus Zeitgründen selten über vier verschiedene Nennkonzentrationen hinaus

und hat somit nur zwei k_r Werte zur Mittelung. Um auch dann noch einen Vorteil aus der Mittelwertbildung zu ziehen, sollte man besonders streng die Auswahl und Kombination der Nennkonzentrationen unter dem Gesichtspunkt der Abb. 2 bzw. Gleichung (14) vornehmen. In den meisten Fällen wird es angebracht sein, zur Restgehaltsbestimmung die höchste Nennkonzentration mit der zweitniedrigsten und die niedrigste mit der zweithöchsten zu kombinieren.

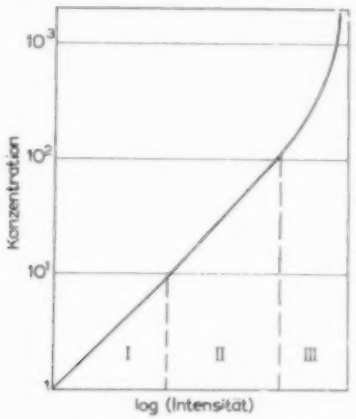

Abb. 3. Schematische Darstellung einer Eichkurve mit Selbstabsorption über einen grossen Konzentrationsbereich. In Bereich I ist das Zugabeverfahren anwendbar. In Bereich II ist das Zugabeverfahren bedingt anwendbar. In Bereich III ist das Zugabeverfahren nicht mehr anwendbar.

(b) *Nichtlineare Eichkurven.* Wie bereits eingangs erwähnt, stützt sich das ganze Zugabeverfahren auf die Linearität der Eichkurven. Diese Voraussetzung läßt sich nicht umgehen, es sei denn, man wüßte, wie die Steilheit von der Konzentration abhängt.

Zum Teil hat man es in der Hand, dafür zu sorgen, daß die Eichkurve geradlinig verläuft. Kaiser [7] beschreibt sowohl den Einfluß des Untergrundes als auch einer ungenauen Plattenkalibrierung auf die Eichkurve. Eine Krümmung der Eichkurve, deren Ursache hierin zu suchen ist, läßt sich aus dem Wege räumen. Anders ist es dagegen, wenn die Nichtlinearität durch Selbstabsorption der Nachweislinie hervorgerufen wird. Um diesen Einfluß auszuschalten oder wenigstens abzuschwächen, wählt man eine Analysenlinie aus, die weniger zur Selbstabsorption neigt, oder man versucht, die momentane Teilchendichte des betreffenden Elementes in der Lichtquelle herabzusetzen. Beide Möglichkeiten bewirken jedoch immer eine Einbuße an Nachweisempfindlichkeit, so daß ihre Anwendbarkeit nicht unbeschränkt ist.

In Abb. 3 ist über einen großen Konzentrationsbereich schematisch eine Eichkurve gezeichnet, bei der die Analysenlinie Selbstabsorption aufweist. Der erfahrungsgemäße Einfluß der Selbstabsorption auf eine Eichkurve wurde u.a. durch theoretische Überlegungen von Cowan und Dieke [1] bestätigt.

Im eingezeichneten Bereich I, bei kleinen Gehalten, ist noch nichts von Selbstabsorption zu merken. Die Intensität wächst linear mit der Konzentration, d.h. die Steilheit η der Eichkurve ist in diesem Bereich gleich eins.

VOL.
10
1957/5

Im Bereich II macht sich der Einfluß bereits bemerkbar. Die Steilheit nimmt allmählich zu. Allerdings läßt sich in diesem Bereich die Eichkurve innerhalb begrenzter Konzentrationsbereiche jeweils noch durch eine Gerade annähern, deren Steilheit größer als eins ist. In diesem Bereich kann man die Zugabemethode noch anwenden. Die gefundene Eichkurve darf jedoch nach keiner Seite hin extrapoliert werden. Daß diese Annäherung durch eine Gerade nur in einem

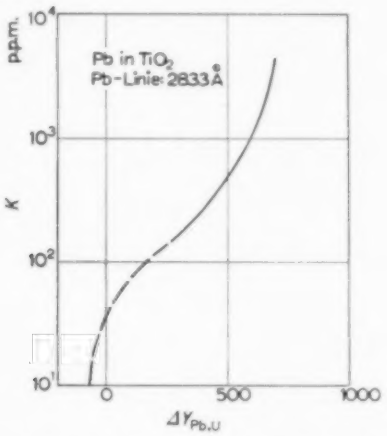

Abb. 4. Unkorrigierte Eichkurve mit starker Selbstabsorption, bei der das Zugabeverfahren nicht angewendet werden kann. Gemessen an der Pb-Linie 2833 in TiO_2. Der ausgezogene Kurventeil ist gemessen. Der gestrichelte Kurventeil ist extrapoliert.

begrenzten Konzentrationsbereich möglich ist, beeinträchtigt die Erfüllung der Forderung nach einem möglichst großen Bereich. Nach Gleichung (13) und Abb. 2 wird daher die k_r Bestimmung um so ungenauer, je begrenzter der Bereich ist.

Wendet man im Bereich II die Zugabemethode an, so muß man damit rechnen, daß der ermittelte Restgehalt kleiner ist als der tatsächliche. Maßgebend für die Größe der Abweichung ist das Verhältnis der am Anfang und Ende des erfaßten Konzentrationsbereichs vorliegenden Steilheiten. Solange die gefundene Steilheit ungefähr gleich eins ist, kann es sich jeweils nur um kleine Abweichungen handeln. Es gibt vernünftige Gründe anzunehmen, daß die wahre Steilheit nicht kleiner als eins ist. Berechnet man mit der niedrigsten Nennkonzentration für $\eta = 1$ den k_r Wert, so erhält man, abgesehen von Meßfehlern, die obere Grenze. Durch den gefundenen Mittelwert k_r liegt die untere Grenze von k_r fest. Die Korrektur ist nämlich darauf abgestimmt, eine Gerade als Eichkurve zu bekommen, und damit erschiene eine Eichkurve mit allmählich wachsender Steilheit, wie sie im Falle von Selbstabsorption vorliegt, als überkorrigiert.

In dem Bereich III läßt sich das Zugabeverfahren ohne weiteres nicht mehr anwenden. Man erkennt das meist schon an dem Verlauf der unkorrigierten Eichkurve. Sie weist selbst bei kleinen Nennkonzentrationen noch einen Durchhang nach unten auf. Selbstverständlich kann eine solche Kurve durch die eingangs beschriebene Korrektur nicht in eine Gerade übergeführt werden. Man erkennt somit sofort, daß die Voraussetzung der Linearität der Eichkurve nicht gegeben

ist. In Abb. 4 ist eine derartige unkorrigierte Eichkurve gezeichnet, wie sie beispielsweise für die Pb-Linie 2833 gemessen wurde.

PIERCE und NACHTRIEB schlagen vor, die Konzentration gegen die Intensität nicht logarithmisch, sondern linear aufzutragen. In dieser Darstellung bewirkt eine Restkonzentration lediglich eine Parallelverschiebung der Eichkurve in der Richtung der Konzentration. Die beiden Autoren extrapolieren diese Kurve zu kleineren Gehalten und lesen die Restkonzentration am Schnittpunkt der Kurve mit der Konzentrationsachse ab. Sie vertreten dabei die Ansicht, daß auf diese Weise die Schwierigkeiten, die durch Selbstabsorption der Nachweislinien entstehen, entfallen. Der Einfluß der Selbstabsorption kann jedoch durch eine andere Auftragungsart in keiner Weise ausgeschaltet werden, ihrem Verfahren haftet durch die Extrapolation dieselbe Unsicherheit an wie all den übrigen Korrekturmöglichkeiten.

Anhang

Zahlenbeispiel für die hergeleiteten Formeln

Die vorangegangenen Überlegungen wurden angestellt in Zusammenhang mit der Ausarbeitung spektrochemischer Arbeitsvorschriften zur Spurenbestimmung in TiO_2 und zur Analyse von Titanmetall auf Verunreinigungen.* Am Beispiel der Mg-Bestimmung in Titanmetall soll nun die Streuung der Restgehaltsbestimmung errechnet werden.

Folgende Meßwerte lagen vor:

Nennkonzentration (%)	Mittelwert $\overline{\Delta Y_r}$	Anzahl der Meßwerte N	Standard-abweichung $\sigma_{\Delta Y_r}$	Streuung des Mittelwertes $\sigma_{\Delta Y_r}/\sqrt{N}$
k_r 0	−0,504	28	0,014	0,0027
k_1 $1{,}41 \times 10^{-2}$	−0,148	16	0,018	0,0045
k_2 $2{,}99 \times 10^{-2}$	0,069	15	0,026	0,0066
k_3 $7{,}04 \times 10^{-2}$	0,385	16	0,021	0,0053
k_4 $14{,}08 \times 10^{-2}$	0,682	14	0,023	0,0061

Trägt man nach Gleichung (8) k_r gegen η mit den verschiedenen Nennkonzentrationen k_r als Parameter auf, so findet man den Schnittpunkt der Kurven k_1 und k_3 bei $k_{r_1} = 1{,}23 \times 10^{-2}\,\%$ und den der Kurven k_2 und k_4 bei $k_{r_2} = 1{,}3 \times 10^{-2}\,\%$. Als Mittelwert erhält man also $\bar{k}_r = 1{,}27 \times 10^{-2}\,\%$ (Abb. 5). Für die Steilheit η liest man einen Mittelwert $\bar{\eta} = 0{,}92$ ab. Die Bestimmung der Restkonzentration und die Aufstellung der Eichgeraden ist damit erledigt.

Nach Gleichung (13) und mit Hilfe von Abb. 2 errechnen wir nun die Streuungen für k_{r_1} und k_{r_2}. Für die gewünschte Genauigkeit reicht es dabei aus, wenn wir in Gleichung (13) für k_r und η die Mittelwerte aus den zwei Bestimmungen einsetzen.

* Die Arbeitsvorschriften wurden im Auftrage der Titangesellschaft m.b.H., Leverkusen, ausgearbeitet, der ich, besonders Herrn Dr. TILLMANN, für die tatkräftige Unterstützung herzlich danke.

VOL. 10 1957/5

Wir erhalten dann:

$$\frac{k_1}{k_r} = 1{,}1 \qquad \frac{k_3}{k_r} = 5{,}5 \qquad \frac{k_2}{k_r} = 2{,}4 \qquad \frac{k_4}{k_r} = 11$$

$$\left(\frac{\Delta Y_1 - \Delta Y_r}{\Delta Y_3 - \Delta Y_r}\right)^2 = 0{,}16; \quad \left(1 - \frac{\Delta Y_1 - \Delta Y_r}{\Delta Y_3 - \Delta Y_r}\right)^2 = 0{,}36;$$

$$\left(\frac{\Delta Y_2 - \Delta Y_r}{\Delta Y_4 - \Delta Y_r}\right)^2 = 0{,}23; \quad \left(1 - \frac{\Delta Y_2 - \Delta Y_r}{\Delta Y_4 - \Delta Y_r}\right)^2 = 0{,}27$$

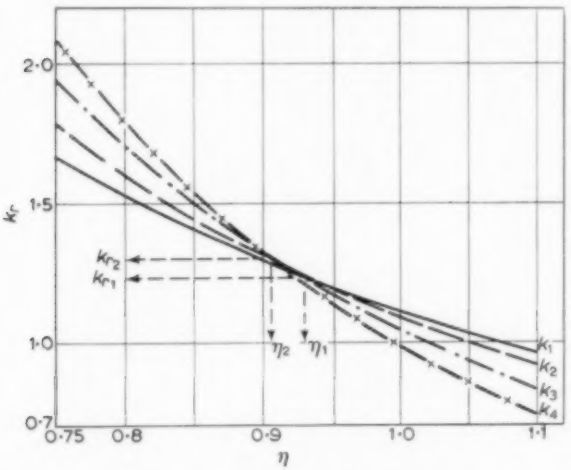

Abb. 5. Graphische Bestimmung des Restgehaltes k_r und der Steilheit η aus dem Gleichungssystem (8) für das Zahlenbeispiel.

Gleichung (13) liefert somit folgende relative Streuungen:

$$\frac{\sigma_{k_{r1}}}{k_r} = \eta\varphi\left(\frac{k_1}{k_r}; \frac{k_3}{k}\right)\sqrt{(\sigma^2_{\Delta Y_1} + 0{,}16\sigma^2_{\Delta Y_3} + 0{,}36\sigma^2_{\Delta Y_r})} = 0{,}059$$

$$\frac{\sigma_{k_{r2}}}{k_r} = \eta\varphi\left(\frac{k_2}{k_r}; \frac{k_4}{k_r}\right)\sqrt{(\sigma^2_{\Delta Y_2} + 0{,}23\sigma^2_{\Delta Y_4} + 0{,}27\sigma^2_{\Delta Y_r})} = 0{,}06$$

wenn man die Werte der Funktion φ entweder nach Gleichung (14) berechnet oder der Abb. 2 entnimmt und unter der Wurzel die entspr. Streuungen der Mittelwerte einsetzt.

Bezeichnen wir $\varphi[(k_1/k_r);\ (k_3/k_r)]$ mit φ_1 und $\varphi[(k_2/k_r);\ (k_4/k_r)]$ mit φ_2 so ergeben Gleichung (21) und (22) für den Mittelwert der Restgehaltsbestimmung eine relative Streuung von:

$$\frac{\sigma_{\bar{k}_r}}{k_r} =$$

$$\frac{1}{2}\sqrt{\left[\left(\frac{\sigma_{k_{r1}}}{k_r}\right)^2 + \left(\frac{\sigma_{k_{r2}}}{k_r}\right)^2 + 2\eta^2\varphi_1\varphi_2\left(1 - \frac{\Delta Y_1 - \Delta Y_r}{\Delta Y_3 - \Delta Y_r}\right)\left(1 - \frac{\Delta Y_2 - \Delta Y_r}{\Delta Y_4 - \Delta Y_r}\right)\sigma^2_{\Delta Y_r}\right]}$$

$$= 0{,}044$$

In diesem Beispiel ist damit die Restgehaltsbestimmung mit einer Streuung von ~4,5% möglich gewesen. Dieser relativ günstige Wert beruht wesentlich auf der kleinen Streuung der Meßwerte.

Ich mochte auch an dieser Stelle meinem verehrten Lehrer, Herrn Prof. Dr. H. Kaiser für viele Diskussionen über dieses Thema danken.

Literatur

[1] Cowan R. D. und Dieke G. H. *Rev. Mod. Phys.* 1948 **20** 418.
[2] Duffendack O. S. und Wolfe R. A. *Industr. Engng. Chem.* (*Anal.*) 1938 **10** 161.
[3] Eichhoff H. J. und Mainka E. *Mikrochim. Acta* 1955 298.
[4] Gatterer A. *Spectrochim. Acta* 1940 **1** 513.
[5] Kaiser H. *Spectrochim. Acta* 1941 **2** 1.
[6] Kaiser H. *Spectrochim. Acta* 1947 **3** 40.
[7] Kaiser H. *Spectrochim. Acta* 1947 **3** 297.
[8] Kaiser H. *Spectrochim. Acta* 1951 **4** 351.
[9] Kohlrausch F. *Praktische Physik* Vol. 1. Teubner, Leipzig, 1944.
[10] Pierce W. C. und Nachtrieb N. H. *Industr. Engng. Chem.* (*Anal.*) 1941 **13** 774.

VOL.
10
1957/5

Spectrochimica Acta, 1957, Vol. 10, pp. 213 to 237. Pergamon Press Ltd., London

REPORTS OF MEETING

The Annual Symposium on Molecular Structures and Spectroscopy

THIS Symposium was held at Ohio State University, Columbus, Ohio, 10–14 June 1957, under the sponsorship of the Department of Physics and Astronomy, The Graduate School of the University and the Office of Naval Research. The following papers were presented at the meeting.

INFRA-RED INSTRUMENTATION AND TECHNIQUES

Commercial infra-red instrumentation. VAN ZANDT WILLIAMS, The Perkin Elmer Corporation, Norwalk, Connecticut.

Instrumentation for high resolution. E. K. PLYLER, National Bureau of Standards, Washington, D.C.

Military instrumentation. LLOYD G. MUNDIE, Willow Run Laboratories, Michigan.

Recent developments in infra-red at Baird-Atomic. D. Z. ROBINSON, R. D. HAY and E. DUBOIS, Baird Atomic, Inc., Cambridge, Mass.

Recent developments in infra-red instrumentation at Baird-Atomic are discussed. These developments include several new accessories. Particular attention is given to the *KM*–1 infra-red spectrophotometer and various components which may be added to increase the performance of this expandable instrument.

Report on Cary model 81 Raman spectrometer. D. G. REA, California Research Corporation, Richmond, Calif.

This paper takes the form of an "up-to-the-minute" progress report describing our experiences with the Cary model 81 Raman spectrometer. Instrument characteristics, including determination of spectral slit widths and slit function, stability, frequency calibration, and recommended scanning conditions are given. Specific attention is given to the factors which determine the inter-laboratory exchange of Raman spectral data—particularly for the American Petroleum Institute spectral files. Typical spectra of a variety of materials are shown. Other associated problems which are discussed briefly include fluorescence, source design and lifetimes, polarization accessories, and the stability of filter solutions.

A photoelectric scale-reader. FRED P. DICKEY and R. C. NELSON, Ohio State University.

Putting grating-circle readings on the chart of a direct-recording spectrometer by observation and pipping is tiresome and usually not precise enough to utilize the full quality of the graduations. A photoelectric reading device will be described which can be used in a vacuum spectrometer. The reticle of the reading microscope is replaced by an evaporated-film cadmium sulfide photoconductive cell having narrow, closely spaced electrodes. The electrodes may be used as a bifilar reticle visually or to indicate scale graduations photoelectrically in conjunction with a 10 c/s amplifier and a lamp with modulated filament.

An improved optical null infra-red spectrophotometer. L. W. HERSCHER, H. D. RUHL and N. WRIGHT, Dow Chemical Company, Michigan.

A new spectrophotometer is described and some demonstrations of its performance are given. The design embodies several new features directed toward improved quantitative accuracy of

chemical analysis, particularly differential analysis. An arrangement for bypassing a small amount of radiation around the sample cell provides a dynamic balance at zero transmission; a means for automatic gain control during differential recording permits the beam-balancing servo to remain active through absorption bands of the reference material as deep as 95 per cent absorbed; a new type of radiation attenuator is used which permits simpler optical design and provides exact linearity between pen movement and percent transmitted. Other features include improved scan-speed control, expansion of pen-travel in ordinate direction, and use of a non-linear ($\lambda^{\frac{1}{2}}$) wavelength scale. Differential performance is demonstrated using the difficult example of an impurity of propylbenzene in ethylbenzene.

The IR-7 infra-red spectrophotometer—an optical null grating instrument. Joseph Ashley and William M. Ward, Beckman Instruments, Inc., Fullerton, Calif.

A modification of the IR–4 infra-red spectrophotometer has been made, such that the second section of the monochromator contains a grating as the dispersing element. Improved resolution compared to a double prism instrument will be demonstrated. Examples of exchanging this advantage in favour of speed, or signal to noise ratio, will be shown. Continuous scans are possible by use of an automatic order changing system which preserves linear abscissa presentation. All other features of the IR–4 have been maintained, such as the single beam–double beam choice.

Optical materials for the infra-red: current status. Stanley S. Ballard, University of California.

The properties of available optical materials are of critical importance in the design of infra-red equipments. The principal uses in laboratory instruments such as spectrometers are for prisms and absorption-cell windows; in field instruments refractive materials are used for large entrance windows and for corrector plates in catadioptric systems. A review is given of the important optical and other physical properties of the materials used in present-day instrumentation, with emphasis on refractive index, transmission region, and mechanical and thermal properties. The current status of availability and usefulness of materials is assessed in terms of the need for prisms transmitting to long wavelengths and windows suitable for field equipments employing photo-conductive or thermal detectors. Generally speaking, the situation is much less satisfactory for field equipments than for laboratory equipments.

Vibrational relaxation in carbon monoxide by the spectrophone method.* G. C. Turrell, W. D. Jones, and J. C. Decius, Oregon State College.

An infra-red spectrophone for study of vibration relaxation was developed and applied to the measurement of relaxation in carbon monoxide. CO was chosen for its theoretically predicted behavior. Application of the Schwartz–Slawsky–Herzfeld [1] theory predicts a very long lifetime for pure CO, with a high dependence on reduced collision mass, low mass giving shorter lifetime. Special interest was directed toward CO–H_2 mixture, because of the predicted effect of H_2 and the fact that H_2 is an impurity in commercial CO. The lifetimes at room temperature for the collision CO + M, extrapolated to one atmosphere pressure of M, varies from 1·6 μsec for $M = H_2$ to 190 μsec for M = CO.

Automatic analysis of infra-red spectra. R. H. Taplin, Federal Telecommunication Laboratories, Nutley, N.J.

Progress is reported on a group of related projects at Federal Telecommunication Laboratories directed towards automatic infra-red analysis.

Digital techniques are employed including the concept of total spectral information in the fingerprint region.

The discussion of the results obtained in a difficult problem in steroid analysis is presented

* Supported by the Office of Naval Research.

[1] Schwartz R. N., Slawsky Z. L. and Herzfeld K. F. *J. Chem. Phys.* 1952 **20** 1591.

VOL.
10
1957/5

particularly in the light of the inherent numerical accuracy obtainable by total spectral matching in the digital system.

INFRA-RED AND RAMAN SPECTRA OF MOLECULES

Infra-red spectroscopy in the field of bacteriology.* Harrmon M. Randall and Donald W. Smith, University of Michigan and University of Wisconsin.

This presentation brings up to date the results of a research project of which previous reports have been made at these meetings. In the beginning, the work is purely exploratory to see to what extent infra-red spectroscopy could be used in biological research where complex mixtures were involved. The specific problem is concerned with the lipid mixtures extracted from the tubercle bacillus. It is demonstrated that with highly standardized procedures, reproducible results could be obtained. Certain strains of the tubercle bacillus were identified by the infra-red spectra of some of these simpler mixtures. Column chromatography was adopted to obtain still simpler mixtures, and in some instances single compounds were identified in the eluates.

The compounds thus isolated from the lipid extracts of the tubercle bacillus and related micro-organisms are recognized as compounds by their infra-red spectra. It begins to appear that each class of mycobacteria may be characterized by the chemical content of its lipid extract. The chemical identification of the atypical strains, micro-organisms which cause a disease resembling tuberculosis, is highly desired because no adequate biological tests have yet been developed. The chemical identification of this group of organisms has been attempted, and the results are presented.

Spectroscopy of molecules in the infra-red. K. Narahari Rao and Edward D. Palik, Ohio State University and University of Michigan.

The structures of some inorganic hydrides. M. Kent Wilson, Tufts University, Mass.

The vibrational spectra of phthalocyanin and related molecules.† F. W. Karasek and J. C. Decius, Oregon State College.

Although a complete assignment of the vibrations for a molecule of the size of phthalocyanin ($C_{32}H_{18}N_8$) is at present not feasible, a comparison of the infra-red spectra of phthalocyanin, several of its metal derivatives, the deuterated molecule, and the hexadecachlorinated copper derivative make possible a reasonably convincing assignment of most of the thirteen active normal modes associated with the two central and sixteen peripheral hydrogen atoms. The assumption is made that the molecule obeys D_{4h} (square planar) selection rules except for the motion of the imino hydrogens which are apparently in or near the plane of the molecule in the transposition.

The infra-red and Raman spectrum and thermodynamic functions of *cyclo*propyl cyanide. Lawrence H. Daly and Stephen E. Wiberley, Rensselaer Polytechnic Institute, N.Y.

*Cyclo*propane is the only molecule containing the *cyclo*propane ring which has been thoroughly investigated from a spectroscopic viewpoint. *Cyclo*propyl cyanide was selected as an interesting derivative to study. The infra-red spectrum of the liquid and vapor has been measured from 2 to 25 μ using lithium fluoride, sodium chloride and cesium bromide prisms. The Raman spectrum of the liquid and qualitative polarization data have been obtained. A normal co-ordinate analysis was done on the skeletal molecule assuming a C-point group. Using the calculated values and data on related molecules a complete vibrational assignment of the experimentally determined frequencies has been made. The moments of inertia have been calculated and the thermodynamic functions tabulated.

* Supported in part by the Faculty Research Fund, University of Michigan, The American Trudeau Society, and the Research Corporation.
† Supported by the Research Corporation.

The infra-red and Raman spectra of PCl_5. J. K. Wilmshurst and H. J. Bernstein, National Research Council, Ottawa.

The infra-red spectrum of PCl_5 in the vapour state and as a solution in CS_2 has been obtained. The Raman spectrum of a solution of PCl_5 in benzene has been obtained photoelectrically together with depolarization ratios. A complete vibrational assignment has been made on the basis of D_{3h} symmetry, and force constants have been calculated. Thermodynamic functions have been computed from the assigned fundamentals and used to interpret the equilibrium of the reaction $PCl_3(g) + Cl_2(g) = PCl_5(g)$ giving $E_0^0 = -20{,}525 \pm 160$ cal mole^{-1}.

The vibrational spectra and structure of *cyclo*-octane. Harold E. Bellis and Emil J. Slowinski, Jr., University of Connecticut.

Infra-red and Raman spectra of *cyclo*-octane have been obtained under several conditions of temperature and state of aggregation.

The infra-red spectra of gaseous, liquid, and solid *cyclo*-octane contain essentially the same bands. No unequal dependence of band intensities on temperature is observed in either the Raman or infra-red spectrum of the liquid. This behavior is taken to imply that only one structural isomer of *cyclo*-octance is present under ordinary conditions.

The number of lines observed in the vibrational spectrum and the presence of several coincidences serve in a general way to eliminate from consideration those structures for *cyclo*-octane which possess either very high or very low symmetry or a center of symmetry. Actual selection of the most probable structure for the molecule is made by dividing the vibrational spectrum into regions characteristic of the group frequencies present in the system, and by comparing in each region the observed spectrum with that predicted for the various possible models. This approach reduces the number of reasonable structures to two, the "tub" form (point group D_{2d}) and the "distorted crown" form (point group D_4). Further consideration of coincidences to be expected from these two structures gives some evidence that the "tub" form is the most probable structure for *cyclo*-octane.

The assignment of frequencies to the fundamental vibrations and overtones of the molecule on the basis of the D_{2d} "tub" model is found to proceed without difficulty.

The infra-red spectrum of polyacrylonitrile. S. Krimm and C. Y. Liang, University of Michigan.

The infra-red spectrum of polyacrylonitrile has been measured from 3200 to 70 cm^{-1}. Polarization measurements were obtained on stretched and rolled specimens in the range of 3200 to 350 cm^{-1}. The bands have been assigned with the aid of previous studies of high polymer spectra, including an analysis of the skeletal vibrations, and an approximate-calculation of the normal frequencies of the nitrile group. A detailed analysis of the spectrum is discussed.

The infra-red spectrum of silyl *iso*cyanide. H. Richard Linton and Eugene R. Nixon, University of Pennsylvania.

The infra-red spectra of both SiH_3NC and SiD_3NC have been examined over the range from 400 to 4000 cm^{-1}. In each case seven of the fundamental vibrations have been observed and the eighth (the SiNC skeletal bending) has been inferred from its first overtone. The spectral assignments, together with the Coriolis coupling coefficients, are discussed.

The infra-red spectra and the structure of some homophthalimides. Aaron L. Bluhm, Quartermaster Research and Development Center, Mass.

The number of tautomeric forms which homophthalimides, $C_6H_4CR'R''CONRCO$, can assume has continually raised the question of the structure of these compounds. Past studies of the chemical behavior and the ultra-violet and infra-red spectra of these compounds, although enlightening, have not been without ambiguity in the assignment of a keto or enol configuration.

In the 3 μ region the R = H homophthalimides in the solid phase exhibit two absorptions at about 3·15 and 3·25 μ, arising from associated NH stretching vibrations. In solutions of decreasing concentration, these two bands disappear and are replaced by one band at 2·96 μ.

VOL.
10
1957/5

In the 6 μ region, the dilute solution spectra show two strong absorptions at about 5·82 and 5·87 μ, arising from unassociated C=O stretching vibrations. One of these vibrations is apparently perturbed in the solid phase, in which the absorptions occur at about 5·87 and 5·96 μ.

The R=CH_3 homophthalimides show no absorptions in the 3 μ region (other than CH stretching modes), and the two strong absorptions at about 5·84 and 5·97 μ are unchanged in both the solid and solution phase spectra.

The spectra, including the concentration dependent band shifts and intensity changes, of this group of homophthalimides are discussed with respect to the type of hydrogen bonding which occurs and to the assignment of a diketo configuration for the homophthalimides.

Importance of the *ortho* effect in hydrogen bonding to very weak bases. A. W. Baker, Dow Chemical Company, Calif.

Hydrogen bonding between hydroxyl groups and very weakly basic groups such as the halogens, electron bonds and sulfur is ordinarily not observable or else the hydroxyl frequency shifts are extremely slight. If these groups occur on an aromatic ring *ortho* to each other, their distances of interaction are stabilized to such an extent that hydrogen bonding is demonstrated by fairly large frequency shifts. Intramolecular hydrogen bonding of this type will be discussed for such compounds as *o*-allyl phenol and *o*-propenyl phenol. Steric effects of groups substituted *meta* to the hydroxyl (3-position) are presented.

Correlations of infra-red group frequencies and electronegativity. Lester W. Daasch, U.S. Naval Research Laboratory, Washington, D.C.

It has previously been demonstrated that the stretching frequency of the P=O and C=O groups increases in a linear fashion with an increase in the sum of the electronegativities of adjacent substituents. Evidence of similar relationships for the stretching frequencies of the SO_2, NO_2 and C=S groups are presented. The slopes of the straight line for the C=O, P=O, SO_2 and C=S group plots of frequency vs. electronegativity sum are found to be very nearly equal, which may have implications in regard to the relative contributions of the inductive and mesomeric effects of the substituents. It has been possible to assign effective electronegativity values to polyatomic groups which can usually be used in all the correlations.

Normal vibration calculation of monosubstituted amides. San-Ichiro Mizushima, Takehiko Shimanouchi and Tatsuo Miyazawa, Tokyo University.

Monosubstituted amide molecules, in which carbonyl oxygen and amide hydrogen are in the *trans* position, give six characteristic absorption bands in the region 1800–400 cm^{-1}. These are 1650, 1550, 1270, 730, 630, and 600 cm^{-1} in the case of R—CONH—R′, and 1650, 1450, 950, 630, 620, and 500 cm^{-1} in the case of R—COND—R′. Of these the first four are due to the in-plane vibrations and are related to the C=O and C—N stretching, and O=C—N and N—H(N—D) bending modes. The other two are due to the out-of-plane vibrations and are related to N—H(N—D) and C=O bending modes. A normal co-ordinate treatment has been made in order to elucidate the nature of the characteristic in-plane vibrations. An intramolecular potential function of the Urey–Bradley type has been used, and the force constants have been transferred from other molecules which are closely related to peptide molecules.

Diformylhydrazine (H—CONH—)$_2$ and its N-deuterated compound have been studied first. This molecule possesses a simple absorption spectrum, giving only six bands in the region 1800–400 cm^{-1}, four of which are due to the in-plane vibrational modes of the peptide group. Frequencies and normal modes as well as potential energy and kinetic energy distributions have been calculated for the infra-red active in-plane vibrations (B_u) of (H—CONH—)$_2$ and (H—COND—)$_2$. Observed and calculated frequencies agree within 2 per cent except for one case. Similar calculations have been carried out for the *trans* and *cis* isomers of *n*-methylacetamide, CH_3—CONH—CH_3 and CH_3—COND—CH_3, with the methyl groups being treated as point masses. In this case, frequency agreement is within 4 per cent except for two cases. Calculated results of normal modes and energy distributions give a clear picture of the nature of the characteristic vibrations.

Infra-red spectra of organo-phosphorus compounds: new correlations. R. A. Nyquist, Dow Chemical Company, Michigan.

This investigation characterizes the stretching (valence) frequencies of the $-\overset{\overset{\displaystyle O}{\|}}{\underset{|}{P}}-O-\phi$ (phenyl) and the $-\overset{\overset{\displaystyle O}{\|}}{\underset{|}{P}}-O-R$ linkages in a large number of organo-phosphorus compounds.

The frequency range of the P—Cl bond in several types of compounds has also been established.

Infra-red spectrum and vibrational energy distribution of carbon dioxide at temperatures up to 1273°K.* Richard H. Tourin and Paul M. Henry, The Warner and Swansey Research Corporation, New York, N.Y.

The energy distribution in the infra-red spectrum of carbon dioxide has been studied as a function of temperature, up to 1273°K. Values of spectral absorption and integrated absorption were calculated from spectra of heated CO_2—N_2 mixtures.† Composition and pressure of the samples were constant; hence the temperature effect could be isolated.

The effect of temperature on the observed spectrum is related to the change with temperature of the vibrational energy distribution. In order to study this effect, the vibrational distribution of the molecular population was calculated for temperatures up to 1273°K. All appreciably populated vibrational levels were included in the calculations. Comparison of the calculated distributions to the spectral data will be described.

Rotation-vibration spectrum of lithium hydride. Wilfred G. Norris and William Klemperer, Harvard University.

The rotation-vibration spectrum of LiH has been measured with a small grating spectrometer in the region 1600 to 900 cm^{-1}. Three bands, 0–1, 1–2, 2–3 are prominent. The intensities of lines in these bands are discussed.

Infra-red spectrum of beryllium chloride vapor. Alfred Buchler and William Klemperer, Harvard University.

The infra-red spectrum of beryllium chloride vapor has been measured from 2000 to 200 cm^{-1}. The vibrations of the linear triatomic molecule $BeCl_2$ are assigned as $\nu_3 = 1113\ cm^{-1}$ and $\nu_2 = 484\ cm^{-1}$. Several vibrations of the polymeric species present in the vapor in equilibrium with the liquid have been measured.

Infra-red spectra of the airglow and aurora between 0·9 and 2·0 μ. A. W. Harrison and A. Vallance Jones, University of Saskatchewan.

Spectra of the airglow and aurora from 0·9 to 2·0 μ have been obtained with a PbS cell infra-red spectrometer which is designed to work at low resulution (25–200Å) with very weak sources. Auroral spectra have been obtained which show that 0–0 N_2^+ Meinel band at 1·11 μ and further bands of the $\Delta = -1$ sequence of this system between 1·5 and 1·6 μ. In the twilight airglow spectrum the 0–1 band of the $^1\Delta_g - {}^3\Sigma_g^-$ atmospheric O_2 system has been detected as an emission feature which decays in a way which suggests that band is emitted as a result of a phosphorescent excitation by solar radiation. The night airglow spectrum in this region consists entirely of the intense $\Delta = 2$ and $\Delta = 3$ sequences of Meinel OH vibration-rotation bands. Absolute intensity measurements have been made of the bands studied.

Infra-red radiation from the sky.‡ E. E. Bell and I. L. Eisner, Ohio State University.

Data will be presented to show the measured spectral radiance of the sky (0°K reference temperature) in the 1–20 μ wavelength region. The relative importance of atmospheric

* Supported in part by United States Air Force.

† Tourin R. H. Ohio Symposium, 1955, paper *M*8.

‡ This work was done under contract between Wright Air Development Center and The Ohio State University Research Foundation.

VOL. 10 1957/5

emission [1–4] and scattered sunlight will be shown. The importance of the temperature, water-vapor content, altitude, sun angle, elevation, and azimuth will be illustrated with typical spectra. A semi-quantitative explanation of the effects of these variables will be given on the basis of a simple model of the atmosphere.

Infra-red emission from flames.* E. Bell, P. Burnside, F. Dickey, C. Dam, S. Kopczynski and R. Rowntree, Ohio State University.

The emission from small flames, mainly hydrocarbons, have been measured and the spectral radiance of a few are shown. The goodness of the temperature determination from this data are illustrated by examples and the method is described [5]. The general features of such flames are explained. The spectral radiance of several non-hydrocarbon flames is also discussed.

Direct observation of the derivative of infra-red spectra with applications. C. W. Peters and R. W. Terhune, University of Michigan.

The derivative of an infra-red spectrum can be approximated by alternately sampling the spectrum at two adjacent wavelengths with the same detector and amplifying the differential signal. This has been done with a grating spectrometer by inserting a small mirror which was vibrated at 90 c/s before the exit slit. A synchronous detector was used to observe both the phase and the amplitude of the signal.

Such a technique has advantages for particular applications such as observations of details in line profiles and detection of small percentage absorptions.

Electric field induced absorption spectra of H_2 and D_2.† R. W. Terhune and C. W. Peters, University of Michigan.

The infra-red absorption of the fundamental vibration rotation band of H_2 induced by an applied electric field was first observed by Crawford and Dagg [6]. By a slightly different method, we have measured the frequencies and intensities of several lines in the Q and S branches of both H_2 and D_2.

The absorption produced by an alternating electric field of strengths up to 100,000 V per cm was analyzed with a grating spectrometer and was synchronously detected. Absorptions as small as 1 part in 50,000 at a resolution of 1 cm^{-1} could be detected.

A spectrometric determination of the abundance of nitrous oxide in ground level air at Columbus, Ohio.‡‡ J. W. Birkeland and J. H. Shaw, Ohio State University.

A multiple traversal absorption cell has been used to obtain spectra of ground level air and various mixtures of N_2, CO_2, and N_2O over paths ranging from 250 to 700 m. Comparison of these spectra in the region near 4·5 μ allows an estimate of the abundance of N_2O in ground level air to be made. The values obtained agree with estimates [7] made from the spectra of ground level air taken by Taylor and Yates [8] over paths of 10·1 miles, 3·4 miles and 1000 ft and with values quoted by Miller [9].

---

* This work was done under contract between Rome Air Development Center and The Ohio State University Research Foundation.

† Supported partially by a tri-service contract administered by the Signal Corps.

‡‡ This work has been sponsored by the Geophysics Research Directorate, Air Force Cambridge Research Center, Air Research and Development Command, under contract with the Ohio State University Research Foundation.

[1] Butler NRL June, 1952, Report 3984.
[2] Oetjen, Bell, Young and Metter *J. Opt. Soc. Amer.* 1955 **45** 403.
[3] Sloan, Shaw and Williams *J. Opt. Soc. Amer.* 1955 **45** 455.
[4] Burch and Shaw *J. Opt. Soc. Amer.* 1957 **47** 227.
[5] Bell E., Burnside P. and Dam C. *J. Opt. Soc. Amer.* 1955 **45** 405.
[6] Crawford M. F. and Dagg I. R. *Phys. Rev.* 1953 **91** 1569.
[7] Birkeland J. W., Burch D. E. and Shaw J. H. *J. Opt. Soc. Amer.* In press.
[8] Taylor J. H. and Yates H. W. *J. Opt. Soc. Amer.* 1957 **47** 223.
[9] Miller L. *Geophysical Research Papers* 1955 No. 39.

Vibrational frequencies and assignments for some metallic borohydrides. A. R. Emery and R. C. Taylor, University of Michigan.

Raman spectra of the borohydride ion have been obtained from solutions of lithium, sodium, and potassium borohydrides dissolved in liquid ammonia at temperatures of about −50°C. The investigation included the various isotopic species, $^{11}BH_4^-$, $^{11}BD_4^-$, $^{10}BH_4^-$, $^{10}BD_4^-$, and both NH_3 and ND_3 were used as solvents. All fundamentals were observed and a satisfactory assignment has been made which agrees with the polarization data and the product rule.

The vibrational assignments of $Al(BH_4)_3$ are discussed briefly in terms of the Raman spectra of the four isotopic species in the liquid state at 0°C.

Molecular association of phenol. D. G. Rea, California Research Corporation.

The molecular complexes formed by hydrogen bonding between phenol molecules have been studied, the emphasis being placed on determination of thermodynamic properties. The association of phenol in carbon tetrachloride at various concentrations was followed by observing the intensity of the first overtone of the O—H stretching vibration of the monomeric phenol molecule. These measurements were carried out at temperatures from 15–60°C. Due to experimental error, no conclusions can yet be drawn about the thermodynamic properties of the dimer. For the formation of trimer from monomer, the measured properties are:

$$\Delta H_{13}^\circ = -6{\cdot}7 \text{ kcal}$$

$$\Delta S_{13}^\circ = -18 \text{ cal deg}^{-1}$$

Overlapping of the association band with the monomer band makes uncertain any measurement at the high concentrations required for determination of the properties of higher polymers. Certain considerations lead to the conclusion that the phenol polymers are cyclic. Hence, the heat of formation of a hydrogen bond in a cyclic phenol trimer is −2·2 kcal.

Skeletal vibrational frequencies of cyclic compounds. Harold Boaz, Eli Lilly and Co., Indiana.

The infra-red spectra of *cyclo*pentane, *cyclo*pentene, *cyclo*hexane, *cyclo*hexene, tetrahydropyran, dihydropyran, *p*-dioxane, trioxane and quinolizidine have been examined in the interval 650–5000 cm^{-1}. Skeletal frequencies from 100 to 250 cm^{-1} are observed in combination and difference with the ring stretching fundamental (850–1000 cm^{-1}), with the C=C stretching fundamental and with their overtones. The number of skeletal frequencies is consistent with the symmetry of the molecule.

SPECTRA OF SOLIDS

Infra-red bands in crystalline α-quartz. Darwin L. Wood and Dorothy M. Dodd, Bell Telephone Laboratories, N.J.

Several optical absorption bands of α-quartz at wavelengths near 3 μ have been studied in both natural and synthetic crystals. These bands can be attributed to electronic transitions. Their appearance, which depends on the origin of the crystal, can be modified by low temperatures, X-irradiation, electrodiffusion of ions within the lattice, and annealing. The origin of the bands is discussed in terms of the energy levels associated with defects and impurity centers in the lattice, and tentative interpretation of the spectra is given.

The optical anisotropy of a color center specific to germanium-doped synthetic quartz. Alvin J. Cohen and Herbert L. Smith, University of Pittsburgh.

The optical anisotropy of the color center system related to substitutional aluminum impurity in quartz has been investigated recently [1,2]. The color center intensity at 275 μ produced by X-irradiation in two specimens of Bell synthetic quartz varies as the germanium content. It is absent in all other synthetic and natural quartz examined. The color center band

[1] Mitchell E. W. J. and Paige E. G. S. *Phil. Mag.* 1955 **46** 1353.
[2] Cohen J. *J. Chem. Phys.* 1956 **25** 908.

VOL.
10
1957/5

is anisotropic with maximum absorption in the σ-direction (electric vector perpendicular to the c-axis). In the π-direction (electric vector parallel to the c-axis) the absorption is poorly resolved into two bands. The color center absorption is caused by an electric dipole transition and bleaches more rapidly than the other color center bands present in the specimens. A possible model for the center will be discussed.

The rule of mutual exclusion and the Born–Raman controversy in crystals. T. VENKATARAYUDU and T. S. G. KRISHNAMURTY, Andhra University, Waltair, India.

The following 24 point space groups contain centre of inversion as a symmetry operation:

C_i C_{2h}^1 C_{2h}^3 D_{2h}^1 D_{2h}^{10} D_{2h}^{23} D_{2h}^{25} C_{4h}^1 C_{4h}^5
D_{4h}^1 D_{4h}^{17} C_{3i}^1 C_{3i}^2 D_{3d}^1 D_{3d}^3 D_{3d}^5 C_{6h}^1 D_{6h}^1
T_h^1 T_h^3 T_h^5 O_h^1 O_h^5 O_h^9.

Crystals belonging to any one of these groups may be studied experimentally whether or not there are any coincidences of spectral lines Raman effect and infra-red absorption. In all these cases, the spectra are mutually exclusive according to Raman's theory and are not so according to Born's theory.

Fluorescence of single anthracene crystals at low temperatures. J. FERGUSON, National Research Council, Ottawa.

A low-temperature cell of the type described by DUERIG and MADOR [1] was used to study the polarized fluorescence from anthracene sublimation flakes at 77 and 4°K. A recording spectrometer was used to measure accurately the relative intensity of the two crystal polarizations (parallel to the b and a axis respectively) and also to determine differences in the fluorescence spectrum between 77 and 4°K. The polarization ratio (b/a) was found to decrease through the spectrum in an unusual manner and measurements taken at 77 and 4°K indicate that there is more than one emitting level and that these have different polarization properties. The fluorescence, as is well known, arises from regions of weak absorption in the crystal and the interpretation of these levels is discussed.

The polarized fluorescence excited from anthracene crystals containing traces of tetracene is reported. It was found that the transfer efficiency can either increase or decrease in going from 77 to 4°K depending on a random selection of crystal samples, and here again the results can be interpreted in terms of more than one emitting level for the anthracene fluorescence. The depolarization of the tetracene fluorescence at low temperatures reported by SIDMAN [2] was not found.

In addition, the polarized absorption spectrum of each crystal was determined, but these will not be reported except where relevant to the fluorescence spectra.

Application of crystal field theory to the electronic spectra and structure of 4- and 6-co-ordinated Ni(II) chelates. GILDA MAKI, University of California.

A calculation of the electronic energy levels in 4- and 6-co-ordinated Ni(II) complexes was made using crystal field theory. In order to test the theory most rigorously, only the assumptions inherent in its original form were used. Thus, unadjusted experimental free-ion intermultiplet separations were used, and no explicit account was taken of the effect of "exchange energy" on the various states. Only those states of the free ion arising from the ground state configuration were considered, and were characterized by the quantum numbers L and S and a term energy. All such states of the same multiplicity and symmetry were allowed to interact, including those from different terms of the free ion. Calculations were made for four pertinent symmetries: octahedral, tetragonal, *cis*-and *trans*-planar.

The results were employed (1) to assign the symmetry forbidden optical absorption spectra obtained for several types of Ni chelates (2) to explain the multiplicity of the ground states and

[1] DUERIG W. H. and MADOR I. L. *Rev. Sci. Instrum.* 1952 **23** 421.
[2] SIDMAN W. *J. Chem. Phys.* 1956 **25** 122.

(3) to explain some observed changes in magnetic moment in going from the solid form to various solvents.

In cases where the symmetry was unknown, several plausible assignments of the spectra were made, comparison of which, permitted a prediction of structure. For some chelates with inequivalent ligands, assignment was made for the correct local symmetry and also for the higher symmetry obtained by considering all the ligands to be equivalent. In every case, a more applicable assignment could be made in the lower symmetry. In general, it was possible to explain observed spectra and magnetic properties with very consistent values of parameters. These results indicate that crystal field theory is quite effective in explaining properties of the complex which are closely associated with the central ion.

Infra-red study of the hydrogenation and dehydrogenation of chemisorbed olefins and acetylene. W. A. Pliskin and R. P. Eischens, Texace Research Center, Boston, N.Y.

Various unsaturated hydrocarbons were chemisorbed on Cabosil-supported nickel and then exposed to hydrogen to form absorbed alkyl groups. Infra-red spectra show that these chemisorbed alkyl goups can be dehydrogenated by evacuation to form a surface carbide type chemisorbed species. By re-exposure to hydrogen at room temperature, the surface carbide is easily rehydrogenated to form adsorbed alkyl groups. The spectra show that some polymerization can occur during this procedure. This is especially interesting in the case of acetylene which on chemisorption forms both adsorbed ethyl groups and an appreciable quantity of surface carbide. Subsequent hydrogen exposure results in an infra-red spectrum indicating mainly adsorbed butyl groups, consistent with the fact that hydrogenation of acetylene produces a product containing a high percentage of butane.

Infra-red absorption spectra of solid solutions. H. W. Morgan, Oak Ridge National Laboratory, Tennessee.

Studies have been made of the spectra of simple inorganic molecules and of complex ions in solution in ionic solids. Solutions are prepared by quenching a melt of the solvent to which has been added a small amount (<1 per cent) of solute. The alkali halides have been used most frequently as solvents, since the resultant solution may be pressed into a window for convenient examination. By the technique of solution, near neighbor interactions are minimized, and sharpened, more intense spectra are observed. These represent equilibria frozen at the melting point of the solvent. In this manner the spectra of monomeric SeO_2 and TeO_2, which exist as chain polymers in their solid phases, have been studied and assigned. The solution spectra of certain complex ions is discussed, including frequency shifts and other solid state interactions which are observed.

Infra-red spectrum of cyanate ion in alkali halide lattices. A. G. Maki, Jr and J. C. Decius, Oregon State College.

The fundamental frequencies as well as numerous combinations and overtones of NCO^- have been observed in single crystals of KI, KBr, KCl, and NaCl in which the cyanate ion is present to the extent of a few tenths of a percent. Cooling such crystals with liquid air permits the identification of upper stage bands based on one or two quanta of the bending frequency as well as the isotopic components of the "anti-symmetric" stretching mode due to $(^{14}N^{12}C^{16}O)^-$, $(^{14}N^{13}C^{16}O)^-$, $(^{15}N^{12}C^{16}O)^-$, and $(^{14}N^{12}C^{18}O)^-$, in their natural abundances, as well as $(^{15}N^{13}C^{16}O)^-$, etc. in ^{13}C enriched samples.

The constants for the anharmonic energy levels, including a Fermi resonance, are being calculated along with the force constants; a qualitative discussion of the small but systematic shifts of the frequencies with host lattice is given.

The Raman spectrum of single crystal hydrogen peroxide. Robert C. Taylor, University of Michigan.

From the known crystal structure of hydrogen peroxide, one predicts under the unit cell approximation that each frequency of the free H_2O_2 molecule with C_2-symmetry will contribute

VOL.
10
1957/5

three components to the crystal spectrum. All components arising from the A-frequencies will be Raman active but only two of the B-components will be allowed. In view of the relatively strong intermolecular forces created by the network of hydrogen bonds in the crystal, one may also expect not only that these components will be split appreciably but that quite probably the accidental degeneracy of the stretching and bending hydrogen fundamentals of the free molecule may be removed.

In support of these predictions, the Raman spectrum of large single crystals of H_2O_2 at $-10°C$ is observed to be remarkably rich in bands as compared to the liquid spectrum. An assignment of the observed frequencies has been made which is consistent with the X-ray symmetry and shows splittings of 10–30 cm^{-1} between the crystalline components arising from any particular hydrogen frequency. Bands arising from the accidentally degenerate A and B hydrogen stretching motions of the free molecule appear separated by somewhat more than 100 cm^{-1} in the crystal.

HIGH RESOLUTION INFRA-RED AND RAMAN SPECTROSCOPY

The pure rotational absorption spectrum of formaldehyde. Cecil F. Dam and Ely E. Bell, Ohio State University.

The CH_2O absorption spectrum between about 20 and 80 cm^{-1} was recorded with the far infra-red spectrograph at the Ohio State University. Asymmetric rigid rotator energy term values $F(J_\tau)$ were calculated using the rotational constants reported by Lawrance and Strandberg [1]. The comparison of the observed and the calculated spectra shows excellent agreement, both in wavelength positions, and in intensities.

The transmission of water vapor in the far infra-red. Phillips B. Burnside, Ely E. Bell and Edward D. Palik, Ohio State University.

The transmission of water vapor in paths of various lengths has been measured over the spectral range 50–500 cm^{-1}. The experimental results have been applied to the Goody[2] statistical theory of water vapor transmission. Goody's expression relating the average transmission and absorber concentration can be written in terms of two parameters, which are simple functions of the absorption line half width, the mean line spacing, and the mean line strength. The variation of these two parameters in the far infra-red is shown.

The infra-red spectrum of methyl chloride in the 1·6 μ region.* R. G. Brown and T. H. Edwards, Michigan State University, Maryland.

The parallel component of $2\nu_4$ has been resolved and analyzed. Q branches of the sub-bands up to $K = 10$ have been measured, part of the structure of the P and R lines has been resolved, and the $K = 3$ sub-band analyzed. Preliminary results give $\nu_0 = 6015{\cdot}56$ cm^{-1}, $(A'-B') - (A''-B'') = -0{\cdot}0481$ cm^{-1}, $B' = 0{\cdot}4433$ cm^{-1}, $B'' = 0{\cdot}4432$ cm^{-1} and $B' - B'' = 0{\cdot}00043$ cm^{-1}.

Rotation-vibration constants of ammonia. W. S. Benedict† and Earle K. Plyler, Johns Hopkins University, Maryland, and National Bureau of Standards, Washington, D.C.

We have observed under high resolution the spectra of NH_3 and ND_3 between 1800–7100 cm^{-1}, and have analyzed 14 bands of the former and 9 bands of the latter species in that interval. The strongest combinations and overtones of the E-vibrations are in general the perpendicular bands. Effective values of the rotation-vibration interaction constants and of ζ_3 and ζ_4 can be

* This work was aided by a grant from the Research Corporation.
† Work supported by the U.S. Air Force, Office of Scientific Research, under Contract No. AF 18(600)–1557.

[1] Lawrance R. B. and Strandberg M. W. P. *Phys. Rev.* 1951 **83** 363.
[2] Goody R. M. *J. R. Met. Soc.* 1952 **336** 165.

obtained from each analyzed band; these however show small variations in different combinations, so that it is difficult to obtain their limiting value at infinitesimal amplitude with a precision comparable to that of the measurements. One of the interactions responsible for this situation is the Fermi resonance between $2\nu_4^0$ and ν_1, which is particularly marked in ND_3; another is the presence of the low potential barrier to inversion. Table 1 gives the best available values for the rotational constants in the ground state, their variation with vibration, and the resulting equilibrium dimensions.

Table 1. Rotational constants and molecular dimensions of ammonia

Constant	$-B$, α	NH_3 A, γ	ζ	B, α	ND_3 A, γ	ζ
0	9·9443	6·196		5·1426	3·117	
1	−0·135	−0·078		−0·032	−0·052	
2	−0·015	−0·098		−0·054	−0·0288	
3	−0·176	0·009	0·0422	−0·0650	0·0002	0·1331
4	0·232	0·066	−0·255	0·080	−0·025	(−0·321)
e	9·963	6·341		5·1708	3·182	
	Molecule, state	NH_3, eq.	NH_3, eq.	NH_3, $\kappa = 0$	ND_3, $\kappa = 0$	
	I, 10^{-40} g cm^{-2}	2·8094	5·4131	2·8147	5·4428	
	h, 10^{-8} cm	0·3819	0·3805	0·3670	0·3687	
	r, 10^{-8} cm	1·0126	1·0108	1·0173	1·0155	

VOL. 10 1957/5

The infra-red spectra of the deuterium and tritium substituted ammonia molecules. P. A. Staats, H. W. Morgan and J. H. Goldstein, Oak Ridge National Laboratory, Tennessee.

The absorption spectra of the nine isotopic ammonia molecules, including NHDT, were studied with prism resolution over the region 5000–500 cm^{-1}. The majority of the normal modes were assigned to observed bands. Through the use of four cells and the double beam technique, the spectrum of each of the molecules NH_2D, NHD_2, and ND_3 was obtained free from the absorptions of other isotopic species. A normal co-ordinate analysis has been performed, and corrections for the anharmonicity introduced by the use of modified "spectroscopic masses" in computing elements of the G-matrices. Satisfactory agreement has been obtained between the predicted and observed frequencies for the assigned modes. Evidence is presented for reassignment of the band center of ν_3 in ND_3. The discussion includes the observed inversion splittings and the variations in band shapes and intensities resulting from the isotopic substitutions.

Remarks on the infra-red spectra of HCOF, DCOF and $2\nu_2 - \nu_2$ of NO_2.* R. F. Stratton, J. W. Keller and A. H. Nielsen, University of Tennessee.

(a) HCOF and DCOF [1] are accidentally nearly symmetric tops having components of the dipole moments along both the least and intermediate axes of inertia. The absorption regions often appear as widely spaced Q branches superposed on bands with PQR structure. At this time all of the fundamentals have been examined with a grating spectrograph and all except the C—H stretch in DCOF were resolved. A number of overtones and combination bands have also been

* Supported by the Office of Ordnance Research, U.S. Army.

[1] Morgan H. W., Staats P. A., and Goldstein J. H. *J. Chem. Phys.* 1956 **25** 337; Stratton R. F. and Nielsen A. H. *APS Bull. II* 1956 **1** 259.

examined. The analysis of the FCO bend and C—F stretch are complete and the analysis of the planar C—H bending is well begun in both molecules. A slide showing the constants calculated to date was shown.

(b) The fundamental bending vibration, ν_2, of NO [1] was reinvestigated, and the difference band $2\nu_2 - \nu_2$ was recorded for the first time. The band centers and rotational constants were determined for each band from a rotational analysis performed using combination relations. From the band centers, the anharmonic constant, X_{22}, was calculated.

The line frequencies, rotational constants, and band center found for the ν_2 band were seen to agree very well with previous results, while the value obtained for the anharmonic constant, X_{22}, differed substantially from the only previously quoted value [2].

In 1953, MOORE [3] observed nine overtone and combination bands of NO_2. Using these frequencies, as well as an earlier determination of ν_2, he obtained a complete set of vibrational constants, including $X_{22} = -8{\cdot}1 \pm 3{\cdot}3\ \text{cm}^{-1}$. The value of X_{22} found in this investigation is $-0{\cdot}6\ \text{cm}^{-1}$.

A new set of vibrational constants was determined using MOORE's data together with present measurements. Calculated frequencies of bands using this new set were found to agree quite as favorably as those computed from MOORE's constants.

The internuclear distance and *l*-type doubling in $C^{32}S_2$.* A. H. GUENTHER, T. A. WIGGINS and D. H. RANK, Pennsylvania State University.

The $3\nu_3$ and $\nu_2 + 3\nu_3 - \nu_2$ bands at 4566·810 and 4547·464 cm^{-1} respectively, were analyzed and B_{000}, α_3 and α_2 evaluated. By using α_1 as determined from $B' - B''$ of the $2\nu_1 + \nu_3$ band as measured by ALLEN, PLYLER and BLAINE [3], B_e was calculated. The values $r_o = 1{\cdot}554_5$ Å and $r_e = 1{\cdot}553$ Å are in excellent agreement with the C—S distance in OCS as measured by microwave methods.

The R branch of the $3\nu_3$ band, which covers less than $5{\cdot}5\ \text{cm}^{-1}$, exhibits a Fortrat parabola such that $R(100)$ is adjacent to $R(0)$. It was possible to resolve all but seven lines of this branch.

The value of q'' ($6{\cdot}7 \times 10^{-5}\ \text{cm}^{-1}$) the splitting constant of the ν_2 state, is within experimental error of the value $q'' = 7{\cdot}7 \times 10^{-5}$ as calculated by NIELSEN's theory [4].

From the band origins measured in this investigation and origins of other bands previously determined by other investigations, a complete set of ω's and anharmonicity constants are evaluated for $C^{32}S_2$.

The molecular constants determined are in cm^{-1}:

$$B_{003} = 0{\cdot}10697 \pm 0{\cdot}00002 \qquad \alpha_3 = 0{\cdot}00071_0$$
$$B_{000} = 0{\cdot}10910 \qquad \alpha_2 = -0{\cdot}00025_6$$
$$B_{013}^{-} = 0{\cdot}10726 \qquad \alpha_1 = 0{\cdot}00015_3{}^1$$
$$B_{013}^{+} = 0{\cdot}10932 \qquad D'' = D' = (1{\cdot}1 \pm 0{\cdot}3) \times 10^{-8}\ \text{cm}^{-1}$$
$$B_{010}^{+} = 0{\cdot}10719$$

Rotation-vibrational Raman spectroscopy at high resolution.† H. L. WELSH, G. G. SHEPHERD, E. H. RICHARDSON, M. A. THOMAS and A. WEBER, University of Toronto.

A new apparatus for Raman spectroscopy of gases will be described. The Raman tube is 24 ft in length, and is in two 10 ft glass sections, 6 in. in diameter. Illumination is from four water-cooled mercury lamps 10 ft long, of a design previously described.‡

The spectrograph is a plane grating instrument in a Littrow arrangement, using an $f/10$

* This Research was assisted by support from Contract Non r-656(12) NR 019–401 of the U.S. Office of Naval Research.

† This research was supported by Grant No. 1001–01, Project D46–10–01–01, of the Defence Research Board of Canada.

‡ Presented at the Symposium in 1955.

[1] KELLER F. L. and NIELSEN A. H. *J. Chem. Phys.* 1956 **24** 636.
[2] MOORE G. E. *J. Opt. Soc. Amer.* 1953 **43** 1045.
[3] ALLEN H. C. JR., PLYLER E. K. and BLAINE L. R. *J. Amer. Chem. Soc.* 1956 **78** 48 43.
[4] NIELSEN H. H. *Phys. Rev.* 1950 **77** 130.

off-axis paraboloidal mirror. The 5 × 8 in. grating has 1200 lines per mm, and in the third order a dispersion of about 6 cm^{-1} per mm at 4358 Å. A ninefold gain in intensity without any loss of resolution is obtained by means of a cylindrical lens in front of the plateholder.

The Q branches of the oxygen and nitrogen fundamentals have been resolved; these and other preliminary results are discussed.

Raman spectrum of CS_2 vapor. B. P. Stoicheff, National Research Council, Ottawa.

The pure rotational spectrum and the vibrational spectrum of CS_2 vapor have been photographed with a 21 ft grating. Rotational lines up to $J = 94$ have been measured and values of the constants B_0 and D_0 have been determined. As is well known, the vibrational Raman spectrum of CS_2, similar to that of CO_2, consists of the Fermi diad ν_1, $2\nu_2$ with some additional "hot" bands. In CS_2, the resonance is not as strong as in CO_2 and the ν_1 Q branch is by far the most intense line observed. In the present research, a total of fourteen sharp Q branches were photographed in the region of the diad (630–820 cm^{-1}). Also the rotational structure of the ν_1 vibrational band was observed and analyzed. These results, together with published data on the infra-red spectrum, are used to determine B_e and the vibrational constants ω_i and π_{ik}.

INTENSITIES IN INFRA-RED AND RAMAN SPECTRA

Some problems in the measurement and interpretation of infra-red intensities. John Overend, University of Minnesota.

Infra-red intensities: perturbations and interactions. David F. Eggers, Jr., University of Washington.

Modulation techniques for observing infra-red absorption spectra.* James C. Gilfert and Dudley Williams, Ohio State University.

Several modulation methods for observing infra-red absorption spectra were discussed by Magnuson and Smith at this Symposium in 1955. One of these methods, in which pressure modulation is employed, has been used in this laboratory [1]. The present paper describes recent results and will discuss the possibility of using the method for determining curves of growth of single spectral lines in terms of absorber concentration w, partial pressure p of the absorbing gas, and the total pressure P of the gas sample.

Strengths and widths of pressure-broadened HCl infra-red lines.† Harold J. Babrov, George A. Ameer and William M. Benesch, University of Pittsburgh.

As part of an investigation of the various aspects of the pressure broadening of infra-red adsorption lines, we have undertaken the measurement of the line strengths and widths of several of the P-branch lines of the fundamental vibration-rotation band of HCl. The value here obtained for the band adsorption coefficient, $S^\circ_{1,0}$, is 143 cm^{-2} atm^{-1}. This is based on a line strength for the $P-1$ line, S°_{P-1}, of 6·60 cm^{-2} atm^{-1} at 300°K. The line width of the $P-1$ line when broadened by nitrogen is $\alpha^\circ_{P-1} = 0{\cdot}12$ cm^{-1} atm^{-1} at 300°K.

One of the favorable aspects of the present method is the use of a single large absorption cell into which are introduced easily reproducible mixtures of gases under moderate pressures. The resulting lines are large and easily planimetered. The resulting equivalent widths are treated in a manner indicated by the following equation:

$$\frac{W^{35}\alpha^{37}}{W^{37}\alpha^{35}} = \frac{f(\beta x^{37})}{f(x^{37})}$$

where $x = \dfrac{SL}{2\pi\alpha}$, $\beta = \dfrac{x^{35}}{x^{37}}$, and the function $f(x)$ is well known and tabulated [2]. S is the line

* Supported in part by a contract between the Air Force Combridge Research Center and the Ohio State University Research Foundation.

† This research was supported by the United States Air Force through the Air Force Office of Scientific Research of the Air Research and Development Command under contract no. *AF*18(600)–986.

[1] Gilfert J. C. and Williams D. *Bull. Ams. Phys. Soc.* 1957 **2** No. 4, 212.

[2] Kaplan and Eggers *J. Chem. Phys.* 1956 **25** 876.

VOL. 10 1957/5

absorption coefficient, L is the optical path length, and α is the line half-width produced by relatively large nitrogen pressures. The superscripts refer to the two isotopic lines of HCl. To obtain a large value of β, the less abundant isotope at very low HCl pressure and high ($\sim$ one atmosphere) N_2 pressure is used in one half of the experiment, while the more abundant isotope at higher HCl pressure and low ($\sim \frac{1}{6}$ atmosphere) N_2 pressure is used in the second half. It may be noted that this method is not inherently dependent on the presence of isotopes.

Vibrational intensities in distorted *n*-paraffins. O. Theimer, University of Oklahoma.

The infra-red and Raman spectrum of distorted n-paraffins is investigated theoretically. The deviations from the straight chain are assumed to be of the simple type which can be fully described by the number of gauche connexions between neighboring CH_2 groups. For the case of chains which contain only one such connexion, intensity formulas are obtained by perturbation methods. One finds that the number of active fundamentals per chain is not affected by the distortion. The bearing of this result on the spectroscopic investigation of rotational isomers is discussed.

Intensity in the Raman effect—V. Photoelectrically recorded Raman spectra of some simple molecules in the gas phase. T. Yoshino and H. J. Bernstein, National Research Council, Ottawa.

The Raman spectra of gaseous H_2, D_2, O_2, N_2, CO, CO_2, CH_4, C_2H_2, H_2O, NH_3, SiH_4, PH_3 have been recorded photoelectrically using a multireflection gas cell (1–2 atm) and a White Raman spectrometer. Pure rotational spectra and some vibration-rotation bands of relatively high signal–noise ratio have been obtained with slit widths of 1·5–5 cm^{-1}. Intensities and depolarization ratios of the Raman bands have been obtained and a simple model useful for estimating the Raman intensity of the totally symmetrical fundamental in hydrides is discussed.

Infra-red intensities in condensed phases solid benzene films. Charles A. Swenson and Willis B. Person, University of Iowa.

The relative intensities of infra-red absorption bands of solid benzene films have been measured in an attempt to determine the possibility of reliable intensity measurements for solids. Influence of temperature and slit width on the measured intensities has been studied. The absolute intensities have also been estimated. These have been compared with the gas-phase intensities.

Intensities of "inactive" infra-red bands in liquid solutions. Eldon Ferguson, U.S. Naval Research Laboratory, Washington, D.C.

Molecular vibrations which are infra-red inactive according to selection rules appropriate to the isolated molecule are commonly observed to absorb radiation in the liquid state as a consequence of molecular collisions. The intensities of such bands have been measured for several molecules in a variety of solvents.

A system of "solvent ordering" according to the ability of a solvent to enhance (or diminish) the intensity of an inactive fundamental of a particular compound is found to exhibit considerable internal consistency, i.e. this ordering is maintained for other compounds.

This spectroscopic solvent ordering can be related to such liquid properties as surface tension, solubility parameter, compressibility, etc. The best correlation found is with values of mean polarizability divided by molar volume, which is equivalent to a correlation between collision-induced absorption intensity and London dispersion forces.

Studies with the spectrophone. S. H. Bauer and Masako Kinoshita, Cornell University.

Studies are being continued in this laboratory on the utility of the spectrophone for the measurement of specific radiation intensities and the determination of relaxation times for the transfer of energy from vibrational to translational degrees of freedom. Herein we report on measurements of the amplitudes of the oscillatory signals rather than their phase lags. We have attempted to answer several questions:

(1) What information regarding integrated absorption coefficients can be obtained from measurement of the amplitude of the signal? Let κ be an unknown constant for the particular geometry, transducer-amplifier sensitivity, and gas; $J_\nu\phi_\nu$ the known product of the source emission frequency function with the transmission function for the filter used; α_ν the spectral absorption coefficient.

$$\langle\alpha\rangle_i^n = \kappa \int_{\nu_i} J_\nu\phi_\nu \alpha_\nu^n \, d\nu; \quad n = 1, 2, 3, 4$$

Magnitudes of the moments can be obtained. Typical values for CO_2 for three bands will be cited and compared (for $n = 1$) with results available form pressure broadening experiments.

(2) How do design parameters (cell dimensions, chopping frequency, type of transducer, etc.) affect the amplitude and phase of the spectrophone signal? Summaries of several experiments are presented, and a method outlined which should permit an absolute calibration to be made of both the amplitude and phase for a variety of damping factors. As yet, the limiting feature is the theory for the steady state temperature distribution in the cell.

Intensity relations in C_{3v} molecules. Harvey Hanson and Harold H. Nielsen, Ohio State University.

The electric moment, E_A, of a C_{3v} type of molecule has been transformed by a contact transformation $TE_AT^{-1} = E_A$ [1]. T is so chosen that $TH_0T^{-1} = H_0' = H_0$, $TH_1T^{-1} = H_1' = 0$, H being the Hamiltonian for the molecule. The latter is tantamount to stipulating that the wave functions of $H_0 + H_1'$ are, to first order of approximation, those for the unperturbed Hamiltonian H_0. The matrix elements of E_A' have been evaluated for fundamental "parallel" vibrations, for fundamental "perpendicular" vibrations and for the pure rotation spectrum.

The selection rules for the parallel type transition remain $\Delta J = \pm 1{\cdot}0$; $\Delta K = 0$. The significant selection rules for the perpendicular type transition remain $\Delta J = \pm 1{\cdot}0$; $\Delta K = \Delta l = \pm 1$. Certain other transitions are allowed in this case, but they are almost certainly negligible.

In all instances, the relations for the matrix elements of the electric moment consist of the usual unperturbed term plus correction terms depending in a more or less complicated manner upon the rotational quantum numbers J and K. On inspection one sees that the relations are hybrid functions showing the effect discussed by Nielsen [2] and the effect discussed by Herman and Wallis [3].

Internal barrier of acetyl cyanide from the microwave spectrum.* Lawrence C. Krisher, Harvard University.

The microwave spectra of acetyl cyanide, CH_3COCN, and the completely deuterated species, CD_3COCN, have been studied in the region of 10,000–34,000 Mc. Transitions up to $J = 12$ have been assigned and the moments of inertia of the two isotopic species have been determined, allowing a partial determination of the structure to be made. Splittings due to hindered internal rotation of the methyl group have been observed for lines of the ground torsional state. These splittings are found to be in good agreement with the theory of Wilson and co-workers for a barrier to internal rotation, $V(\alpha) = V_3(1 - \cos 3\alpha)/2$, of $V_3 = 1250$ cal/mole (437 cm^{-1}).

The microwave spectrum and barrier to internal rotation of acetic acid.† William J. Tabor, Harvard University.

The microwave spectra of CH_3COOH and CD_3COOH have been measured leading to a three-

* This research was made possible in part by support extended Harvard University by the Office of Naval Research under ONR Contract Nonr 1866 (14), and by a grant from the California Research Corporation.

† This research was made possible in part by support extended Harvard University by the Office of Naval Research under ONR Contract Nonr 1866 (14), and by a grant from the California Research Corporation.

[1] Hanson R. H., Nielsen H. H., Waggoner J. and Shaffer W. H. *J. Chem. Phys.* In press.
[2] Nielsen H. H. *Bull. Soc. Sci. Liège* 1951 Nos. 6–7. 440.
[3] Herman R. C. and Wallis R. F. *J. Chem. Phys.* 1955 **23** 637.

VOL. 10 1957/5

fold barrier of 483 ± 25 cal/mole. To treat this relatively low barrier case in the usual high barrier representation, it was necessary to include perturbation terms up to fourth order. A structure of acetic acid was determined assuming the carboxyl group is the same as that in formic acid.

Microwave spectra of normal and isotopic nitrogen dioxide. JOHN RASTRUP-ANDERSEN, JAMES C. BAIRD and GEORGE R. BIRD, The Rice Institute, Houston, Texas.

New observations [1] on $^{14}N^{16}O_2$ have yielded precise frequencies for the six strong and four weak lines with $\Delta F = \Delta N$ of the rotational transition $9_{19} \rightarrow 10_{0,10}$ near 41 kMc. The six strong lines of the transition $22_{1,21} \rightarrow 21_{2,20}$ have also been measured. As expected, combination rules govern some of the frequencies of the $9_{19} \rightarrow 10_{0,10}$ transition.

The microwave spectrum of $^{15}N^{16}O_2$ is calculated to be blank from 5 to 50 kMc, except for lines with $N > 35$. The transition $9_{19} \rightarrow 10_{0,10}$ was predicted near 52 kMc, and four lines have now been measured in this region. These are presumably the four strong lines with $\Delta F = \Delta N$ of $9_{19} \rightarrow 10_{0,10}$ of $^{15}N^{16}O_2$. An improbable assignment not yet rigorously excluded would attribute these to a magnetic pole transition of $^{14}N^{16}O_2$.

Sufficient data are now available to test the theory developed by LIN [2] for an accidentally-symmetric top free radical and to calculate the six magnetic constants of $^{14}N^{16}O_2$. Even if the magnetic quantum numbers of the individual lines were known, secular equations with several sets of real roots would have to be solved, and these roots tested against additional data. Since the quantum numbers are not now known, the calculation is very difficult indeed. The magnetic constants calculated by LIN from the earlier data on $8_{08} \rightarrow 7_{17}$ of $^{14}N^{16}O_2$ are incompatible with the present data on $9_{19} \rightarrow 10_{0\,10}$. A satisfactory solution has not been obtained, but preliminary calculations indicate that the theory will have to be extended to include corrections for the finite asymmetry of NO_2. One of us (J. C. B.) is currently working with LIN to accomplish this.

This work has been supported by grants from the Research Corporation and the Robert A. Welch Foundation. We wish to acknowledge many helpful conversations with Dr. CHUN C. LIN.

Microwave spectra of acetone. J. D. SWALEN, National Research Council, Ottawa.

The microwave spectra of acetone and acetone-d_6 have been observed. From a number of low J transitions, the average rotational constants were determined. A preliminary structure consistent with these constants and using some parameters from the structure of acetaldehyde [3] is as follows:

$$\begin{aligned} d_{cc} &= 1{\cdot}511 \pm 0{\cdot}005 \text{ Å} \\ d_{co} &= 1{\cdot}216 \text{ Å (assumed)} \\ d_{ch} &= d_{cd} = 1{\cdot}087 \text{ Å (assumed)} \\ \angle\text{CCC} &= 116^\circ\,37' \pm 1^\circ \\ \angle\text{HCH} &= \angle\text{DCD} = 108^\circ\,16' \text{ (assumed)} \end{aligned}$$

Stark effect measurements gave a dipole moment of 2·90 ± 0·03 Debye.

Each transition consisted of a multiplet structure caused by the internal rotation of the methyl groups. This multiplet pattern is being analyzed to determine the potential energy hindering internal rotation. The theory of internal rotation for the case of two symmetric tops attached to an asymmetric frame will also be discussed.

Electronic structure of oxygen bonds in molecules.* M. J. STEVENSON,† Columbia University, New York.

The quadrupole hyperfine structure due to the ^{17}O nucleus observed in microwave rotation spectra gives information on the bonds of various molecules containing oxygen. The value of the

* Work supported jointly by the Signal Corps, the Office of Naval Research, and the Air Force Office of Scientific Research.

† John Tyndall Fellow.

[1] These extend the earlier results by BIRD G. R. *J. Chem. Phys.* 1956 **25** 1040.
[2] LIN C. C. *Selected Topics in Microwave Spectroscopy* Doctoral Thesis, Harvard University, 1955.
[3] KILB R. W., LIN C. C. and WILSON E. B., JR. *J. Chem. Phys.* In press.

^{17}O quadrupole moment obtained from a measurement of the quadrupole coupling constant in $HD^{17}O$ is $-0{\cdot}03 \pm 0{\cdot}01 \times 10^{-24}$ cm^2, about six times greater than the value accepted thus far. Therefore, the quadrupole spectrum of ^{17}O should be resolvable in most molecules.

The measurement of the hyperfine structure in the $HD^{17}O$ rotational spectrum yields $e\left(\frac{\delta^2 V}{\delta a^2}\right)_{ave} Q = -10{\cdot}3$ Mc. A larger amount of hybridization than previously expected is indicated by the small value of the asymmetry parameter $\eta = 0{\cdot}472$. The molecular orbital calculations of Ellison and Shull [1] will be compared with the experimental data. Nethercot and Rosenblum [2] have obtained $eqQ = +4{\cdot}43$ Mc for $C^{17}O$. This result is in disagreement with the MO calculations for CO [3,4], with the generally accepted valence bond picture of CO, and also with the measured eqQ of OCS [5]. Large amount of hybridization of the $2p\sigma$ oxygen orbital or inclusion of π-bonded C^+–O^- structure is necessary to obtain the experimental value of eqQ in CO. A comparison of the experimental and theoretical data on several molecules containing oxygen will be made.

ULTRA-VIOLET AND ELECTRONIC BAND SPECTRA

The 3960 Å absorption system of H_2CO.* S. E. Hodges, J. R. Henderson and J. B. Coon, A and M College of Texas.

The absorption spectrum of H_2CO vapor shows a weak system of bands between 3600 and 4260 Å. Absorption paths varying from 5–120 m atm reveal nine bands in this region which have envelopes distinctly different from those of the well-known 3530 Å system. Each band appears double, having two absorption maxima of about equal peak intensity. Four of these bands have been previously reported [6, 7, 8].

A band at 25243 cm^{-1} is probably the (0, 0) band of this system. Four much weaker bands lying to the red side of the origin are regarded as temperature sensitive. Two of these bands involve the frequency $\nu_2'' = 1746$ cm^{-1} of the ground state. An excited state interval of 1183 cm^{-1} is interpreted as ν_2'. The principle problem of the analysis is the interpretation of an interval of 535 cm^{-1} between the (0, 0) band and its nearest neighbor toward the violet. This interval can be explained in terms of an inversion in the nonplanar bending mode of the excited state. The results are: $(1^+–0^+)$ 535 cm^{-1}, $(0^–0^+)$ 29 cm^{-1}, $(1^–1^+)$ 240 cm^{-1}. The latter two intervals are based on the assumption that two of the temperature sensitive bands involve the nonplanar bending mode of the ground state.

The long path, low-temperature absorption spectrum of formaldehyde. Velta Erdmanis and G. Wilse Robinson, Johns Hopkins University, Maryland.

The spectrum in the near ultra-violet region obtained at high resolution with a multiple pass cell cooled to dry ice temperature exhibited a number of interesting new features. Collision broadening of the rotational lines was reduced to a near minimum so that the limitations in resolving power were essentially those imposed by the instrument itself, in this case about 240,000. The absence of high temperature structure permitted important new bands to be found.

A progression of six very weak, double-headed, temperature insensitive bands was found to the long wavelength side of the n–π^* system. While some of these have been reported previously, this is the first indication that they belong to a new electronic transition.

In addition to these bands, the absence of high rotational lines in the vibronic transition at 28,313 cm^{-1} (A-band) permitted identification of a relatively weak parallel type band at 28,190

* Supported by the Air Force Office of Scientific Research of the ARDC.

[1] Ellison F. O. and Shull H. *J. Chem. Phys.* 1955 **23** 2348.
[2] Nethercot A. H. and Rosenblum B. To be published.
[3] Sahni R. C. *Trans. Faraday Soc.* 1953 **49** 1.
[4] Mulliken R. S. *J. Chem. Phys.* 1955 **23** 1833.
[5] Geschwind, Gunther-Mohr and Silvey *Phys. Rev.* 1952 **85** 474.
[6] Ebers E. S. PhD Thesis, Harvard University 1935.
[7] Cohen D. and Reid C. *J. Chem. Phys.* 1956 **24** 85.
[8] Robinson G. W. *Canad. J. Phys.* 1956 **34** 699.

VOL. 10 1957/5

cm^{-1}. This is the (0–0) band of the n–π^* transition which is forbidden under the strict total vibronic C_{2v} selection rules. Parallel bands of similar appearance are observed throughout the longer wavelength regions of the system and are due to transitions from the ground vibronic state to symmetric members of higher inversion doublets, alone or in combination with v_2. The relative intensity of this system as compared with that of the "allowed" part of the electronic transition gives an indication of the deviation from C_{2v} symmetry of the electronic wave functions in the nonplanar excited state.

This work supported in part by OOR, Project No. TB2–0001 of Contract No. DA–36–034–ORD–2169.

The electronic absorption spectrum of ND_2. K. Dressler and D. A. Ramsay, National Research Council, Ottawa.

The absorption spectrum of ND_2 which lies in the region 5000–7600 Å has been analyzed following the recently accomplished analysis of the corresponding NH_2 bands. Rotational constants for the ground state are found to be

$$A''_{000} = 13{\cdot}31\ cm^{-1}, \qquad B''_{000} = 6{\cdot}48\ cm^{-1}, \qquad C''_{000} = 4{\cdot}30\ cm^{-1}.$$

The bond length and bond angle, as deduced from these constants, are identical with the corresponding values for NH_2, viz.

$$r''_{000}(ND) = 1{\cdot}025\ Å, \qquad <(D - N - D) = 103^\circ\ 20'.$$

The spectrum consists mainly of a long progression of bands involving successive quanta of the bending vibration in the linear upper state. A few bands involving excitation of an N—D stretching vibration in the upper state have also been identified. The vibronic structure of the upper state has been studied and compared with the structure calculated by Renner for an electronic Π state.

Ultra-violet absorption spectra of LiH and LiD. R. Velasco, National Research Council, Ottawa.

The absorption spectra of LiH and LiD have been photographed in the 2300–3200 Å region, using the third order of a 21 ft grating spectrograph. Multiple reflection mirrors have been used in the absorption tube to obtain path lengths up to 16 m. For each molecule a new ($^1\Pi$–$X^1\Sigma^+$) band system, showing a clear breaking off of the fine structure due to rotational predissociation, has been found. The rotational and vibrational analyses of both systems have been made and, from the observed predissociation limits, the dissociation energies (D_0) of LiH and LiD in the ground state have been found to be, 2·429 ± 0·001 eV and 2·451 ± 0·001 eV, respectively.

The electronic spectrum of HNO. F. W. Dalby, National Research Council, Ottawa.

A new absorption system, in the region 6500–7700 Å has been photographed during the flash photolysis of : nitromethane, nitroethane, *iso*amyl nitrite, and mixtures of nitric oxide and ammonia. The fine structure analysis of the bands of the system and the method of production both strongly suggest that the absorbing molecule is HNO.

The analysis of the 0–0 band of the system yields the following ground state rotational constants:

$$A_v = 17{\cdot}14\ cm^{-1}, \qquad B_v = 1{\cdot}41\ cm^{-1}, \qquad \text{and} \qquad C_v = 1{\cdot}31\ cm^{-1}$$

By assuming the N—H distance to be 1·02 Å, the NO distance is determined to be 1·22 Å and the HNO angle 102°.

Bands corresponding to the NO stretching frequency and the HNO bending frequency in the upper state have also been analyzed. The rotational constants and the geometry of the molecule in the excited electronic state and a preliminary analysis of the DNO spectrum is also presented.

Substituent effects on the ultra-violet spectra of catacondensed hydrocarbons. John A. Petruska, University of Chicago.

By considering the catacondensed hydrocarbons, $C_{4r+2}H_{2r+4}$ (e.g. naphthalene, anthracene, phenanthrene, benzanthracene, etc.), as distorted cyclic polyenes with "cross-link" perturbations,

it becomes a relatively simple matter to calculate by group theory and perturbation theory how substituent-induced changes in the π-electronic spectra of catacondensed hydrocarbons should depend on the number and relative positions of the substituent groups. Within the approximation of first and second order perturbation theory, the formulae for the frequency shifts and intensity changes derived on this basis are particularly simple, being analogous to the well-known Sklar–Forster rules for substituted benzenes. In this paper, the method of deriving the appropriate formulae for any transition between two π-electronic states is discussed briefly. The remaining time was spent in discussing the application of theoretical results to the correlation and interpretation of various sets of spectroscopic data on substituted catacondensed hydrocarbons available in the literature to date.

Effects of high pressure on the near ultra-violet vapor absorption spectrum of benzene in various diluent gases.* W. W. Robertson and S. E. Babb, Jr., University of Texas.

The near ultra-violet vapor absorption spectrum of benzene has been recorded in various diluent gases covering a density range that extends from the vapor density of benzene through the density region of liquid hydrocarbons. The wavelength of absorption shifts to the red smoothly with an increasing slope with increasing density of diluent gas, but is linear with dielectric constant. The frequency of absorption then decreases with increasing dielectric constant and has an increasing slope. The smoothness of the curves suggests that there is no essential difference in mechanism between that described by the collision theory generally used to interpret wavelength shifts resulting from intermolecular interactions at low densities and the mechanism described by the statistical theory that would be applied in the region of liquid densities. Data are presented on carbon dioxide as a diluent, both above and below the critical temperature. Behavior in liquid and gaseous phases at equal densities is presented.

VOL.
10
1957/5

Energy level calculations for small diatomic molecules. Frank E. Harris, University of California.

An *IBM* type 701 data processing machine has been programmed to compute matrix elements of the Hamiltonian of an arbitrary many-electron diatomic molecule, in terms of a basis consisting of products of one-electron spheroidal wave functions. The program uses the auxiliary functions denoted by Kotani $A_n(\alpha)$, $B_n(\alpha)$, $G^p{}_\tau(m, \alpha)$, and $W^p{}_\tau(m, n; \alpha, \beta)$, and tables of these functions for wide ranges of all the variables were obtained as a by-product of the present investigation. We are beginning to test various methods of introducing configuration interaction among these product wave functions to improve energy level calculation in small molecules such as H_2, LiH, and Li_2. A report on our progress in this direction is given.

A theory for the spectral variations among the metal porphyrins. Martin Gouterman, University of Chicago.

The visible and near ultra-violet porphyrin bands are assumed to be due to transitions between a filled pair of *MO*'s which have angular momentum 4 (in a $D_{\infty h}$ group) to an empty pair with angular momentum 5. Some plausibility arguments can be given to justify the application of this interpretation to porphyrin, where the actual symmetry is D_{4h}. One then considers the effects on these states of metal substitutions, which are good substitutions to consider as they preserve the symmetry of the molecule. With some simplifying assumptions as to how the metal affects the Hamiltonian, it is possible to explain for a number of metals the observed relations of: (a) the oscillator strength to the energy for the visible band of the tetraphenyl porphins; (b) the same for the octa-alkyl porphins; (c) the visible band energy of the octa-alkyl to that of the tetraphenyl porphins; (d) the ultra-violet band energy to the visible band energy for the tetraphenyl porphins.

Recent theoretical studies of bond properties. C. A. Coulson, Oxford University, England.

---

* This work was supported by the Air Force Office of Scientific Research, Air Research and Development Command, Contract *A.F.* 49(638)-35, project no. 19750.

Electron-spin resonance studies of unstable free radicals. David J. E. Ingram, University of Southampton, England.

Interaction of two excited hydrogen atoms in either 2*s* or 2*p* states. Bruno Linder and J. Hirschfelder, University of Wisconsin.

Higher ionization potentials of linear triatomic molecules. Y. Tanaka, A. S. Jursa and F. J. LeBlanc, Air Force Cambridge Research Center, Mass.

Using the rare gas continuum as a background, we observed several Rydberg absorption series for each of the following molecules: CO_2, N_2O, CS_2, and COS. The ionization potentials obtained by the analysis of the series are shown below.

Molecule	I.P.	Series	Molecule	I.P.	Series
CO_2	18·01 ± 0·01 eV	I	CS_2	14·47 ± 0·01 eV	I
	18·08 ± 0·01 eV	I′		14·47 ± 0·01 eV	I′
	18·23 ± 0·01 eV	II		16·19 ± 0·01 eV	II
				16·19 ± 0·01 eV	II′
	19·38 ± 0·01 eV	III			
	19·39 ± 0·01 eV	III′		19·51 ± 0·05 eV	III
N_2O	16·39 ± 0·01 eV	I	COS	16·15 ± 0·01 eV	I
	16·39 ± 0·01 eV	I′		16·15 ± 0·01 eV	I′
	16·55 ± 0·01 eV	II			
	20·10 ± 0·01 eV	III			
	20·10 ± 0·01 eV	III′			

Experimental observation of the polarizations of electronic transitions. Richard Williams, Harvard University.

Monochromatic polarized light was used to excite fluorescence in aromatic hydrocarbons dissolved in a rigid glass of propylene glycol. The polarization of the resulting fluorescence was observed. When the transitions responsible for absorption and emission are not identical, the relative polarizations of the two transitions are obtained. In this way, the polarizations of the higher electronic transitions are directly observed for several representative aromatic hydrocarbon systems. Results are compared with theoretical predictions.

Triplet-singlet emission spectra in crystalline toluene at 4 and 77°K and in EPA solution at 77°K.* Yoshiya Kanda and H. Sponer, Duke University, North Carolina.

A study of the triplet-singlet emission spectra of toluene crystals at 4 and 77°K showed that the spectra are different at the two temperatures. At 4°K a spectrum of sharp bands appears with a 0,0 transition at 28,785 cm^{-1}. This spectrum has been analyzed. There is also a diffuse spectrum underlying the sharp bands. The diffuse spectrum looks like the toluene spectrum obtained in rigid EPA solution, except for a small shift of the latter to shorter wave

* Supported by the National Science Foundation.

lengths. Our explanation is that the sharp spectrum belongs to the crystal and the diffuse spectrum to the amorphous state or to a conglomerate of extremely small crystals.

The crystals spectrum at 77°K looks entirely different. It consists of seven rather broad diffuse bands going from 25,290 cm^{-1} toward longer wavelengths. By slowly raising the temperature above 4°K while keeping exposure times and sector rotation constant, we obtained between 20·6 and 22·7°K the diffuse "short λ" spectrum and only a few of the sharp bands. From 24·5°K on the spectrum has changed. It begins with a line-like band on the short wavelength side of the first diffuse band which is also the first band of the 77°K crystal spectrum, while the "'short λ" spectrum is entirely gone. The life times of the two sets of spectra at 4°K and above 25°K are also different: the short λ spectrum has a life time of 8–10 sec, and the long λ spectrum has a life time of 0·2–1 sec. The sharp bands of the second set disappear when the temperature is raised still further, and the diffuse bands become identical with those of the crystal spectrum at 77°K.

Since the 77°K crystal spectrum has no analog in EPA solution, it is not characteristic of the toluene crystal. The question arises then whether it is due to an impurity of whether its carrier could have been produced photochemically. Since great care was taken in purifying the samples, the possibility of photochemical reactions under the influence of light illumination was examined. If produced photochemically, the carrier of the "long λ" spectrum must be formed at the cost of the carrier of the "short λ" spectrum. Experiments were carried out in which toluene crystals were subjected to a long illumination at 77°K during which a few exposures were taken. Immediately after the illumination the crystal was transferred to the liquid helium container. The result was that the "short λ" spectrum—sharp and diffuse bands—appeared again, but the "long λ" spectrum was absent. As is discussed, these results indicate that a higher temperature is needed for the sensitized excitation of an impurity which is photochemically formed.

Theory of forbidden transitions in diatomic molecules. William Lichten, Columbia University, New York.

Selection rules and a scheme for estimating intensities of forbidden electronic transitions of diatomic molecules are presented. The intensity derived from perturbations depends on the magnitude of the matrix elements of spin orbit interactions. In many cases, these matrix elements can be estimated semi-empirically by means of measured values of multiplet splittings and other perturbations.

The vibrational intensities and sum rules (Franck–Condon principle) are shown to have special forms for forbidden transitions.

Estimates of intensities of forbidden transitions in O_2, CO and N_2 agree with observed absorption spectra and lifetime measurements. The expected intensity and position of unobserved absorption spectra is discussed for several molecules.

Similarities and differences with the case of polyatomic molecules are drawn.

Information about electronic transitions in aromatic crystals from photoconductivity. Dr. L. E. Lyons, University of Sydney, Australia.

Two types of information about electronic transitions may be obtained from photoconductivity measurements:

(1) The close resemblances between the absorption spectrum and the spectral dependence of the photocurrent, including the dependence upon the polarization of the incident light, enable conclusions to be drawn about the polarization of the transitions in the crystal. This will be illustrated for several substances including some for which polarization ratios have not yet been reported from absorption spectroscopy.

(2) Electronic levels in the crystal due to the removal of an electron from one molecule to another or to freedom within or without the crystal must occur to explain intrinsic photo effects such as are observed. The energies and probabilities of transitions to such "ionized" levels in e.g. anthracene and naphthalene have been calculated. The relation of the results to photoconductivity are discussed.

VOL.
10
1957/5

Structure of nitrogen dioxide in its low lying excited state. G. Wilse Robinson, Johns Hopkins University, Maryland.

The absorption spectrum of NO_2 in the visible and photographic infra-red has been studied at moderately high resolution. The principal feature of the spectrum from about 4500 Å to the origin near 9000 Å is a progression of bands with an average ΔG of 700 cm^{-1}. The complexity of these bands increases rapidly towards shorter wavelengths where the widths of the bands become of the same magnitude as the distance between them.

The gross structure can be explained on the basis of a linear or near linear equilibrium structure in the excited electronic state. Transitions occur from rotational sub-levels in the ground state to v_2 vibrational levels in the excited state. Because of the strong Franck–Condon effect, the bands near the origin are extremely weak, long path length techniques being required to avoid excessive pressure broadening of the rotational structure.

Absorption spectra of neodymium complexes with aliphatic carboxylic acids. R. C. Vickery, Horizons Inc., Ohio.

The formation of complexes between neodymium and aliphatic carboxylic acids has been studied by spectrophotometric techniques and the results obtained correlated with other physico-chemical data on complex stabilities. Absolute success has not been obtained in this correlation, and an anomaly has been found in that, whilst with monocarboxylic acids the Nd 576 mμ band shifts toward higher wavelengths with increasing stability, a similar shift is found in polycarboxylic acids, with decreasing stability of the complex. In general, the band shift may be correlated with the molecular weight of the complexing agent, but not entirely with the stability of the complex formed.

Spectra of afterglows from nitrogen-oxygen mixtures. A. M. Bass, U. Kurzweg and H. P.–Broids, National Bureau of Standards, Washington.

A systematic survey has been made of the spectra of the afterglows resulting from electric discharges in mixtures of nitrogen and oxygen. The spectra have been photographed for mixtures ranging from 100 per cent nitrogen to 100 per cent oxygen, pressures from 1–5 mm, flow rates from 2 to 20 cm^3/sec, and as a function of time after the discharge. The spectrum range covered is from 3000 to 11,000 Å, making use of both a prism spectrograph (f/4) and a grating spectrograph (f/0·8). Curves have been prepared to show the relative variations of the individual spectral features as function of the various parameters.

MOLECULAR DYNAMICS

The interaction of rotational and vibrational motion in polyatomic molecules. C. F. Curtiss, University of Wisconsin.

A review of work in internal rotation. D. G. Burkhard, University of Colorado.

Theory of the overtone and combination bands of the methane molecule. Karl T. Hecht, University of Michigan.

MICROWAVE SPECTROSCOPY

The contribution to the rotational constant of H_2 and HD due to the electrons in the molecule.* Stewart K. Kurtz, Ohio State University.

When the electrons are included in the complete Hamiltonian for a diatomic molecule [1], a term

$$\mu_{xx}\,\pi_x\,P_x + \mu_{yy}\,\pi_y\,P_y \qquad (1)$$

* Supported in part by the Office of Ordnance Research, U.S. Army, through contracts with the Ohio State University Research Foundation.

[1] Nielsen H. H. *Hand. Physik.* In press.

occurs which is of some interest. The π_x and π_y are operators representing the components of internal angular momentum of the electrons, and P_x and P_y represent components of the total angular momentum. It follows that the term (1) represents a Coriolis type interaction between the rotational motion of the molecule and the internal motions of the electrons. A second order perturbation calculation has been carried out for H_2 and HD using the term in (1). The results are expressible in the form of a correction to the rotational constant.

In the case of H_2 the calculations have been carried out using several of the existing approximations to the ground state wave function. Results indicate a close dependence of the magnitude of the correction on the form of the wave function. The numerical values of the correction factor are in fair agreement with those calculated from figures based on an irrotational flow model [1].

Some aspects of the theory of *l*-type doubling and *l*-type resonance. GILBERT AMAT, Laboratoire d'Infrarouge, Paris, France.

Discussion on the sign of the q constant of l-type doubling and on the possible occurrence of a vibrational l-type doubling (or resonance), connected with terms in the Hamiltonian which do not depend upon rotational operators is presented.

Angular momentum quantum numbers in symmetric molecules.* TIEN CHI CHEN, Duke University, North Carolina and IBM Research Laboratory, New York.

The generalized united-atom theory of molecules suggests that electronic states of symmetric molecules may be characterized by means of "atomic" quantum numbers.

When the one-electron potential of a molecule is expanded in terms of co-ordinates of the center of symmetry, the angular terms may be considered to be perturbations on a basically spherical potential. For H_2^+, the latter is a Coulomb potential with cut-off. Using WANNIER's theory [2], the ground state of H_2^+ is shown to be 95 per cent pure s in character. The quantum number l becomes increasingly pure with increase in energy.

For cyclic polyenes, an analogous treatment in cylindrical co-ordinates indicates that the Hückel ring quantum number is the magnetic quantum number m_l. The one-electron wavefunctions for the low-lying levels have essentially the same (ρ, z) dependent part, and are distinguished by their ϕ dependence. Molecular symmetry splits the $m_l = \pm N$ levels for a cyclic polyene of $2N$ carbon atoms. The results are compared with *LCAO* and electron-gas theories. Additional perturbations due to substitution or cross-link formation are discussed in terms of the ϕ dependence.

Hindered internal rotation in the propylene oxide molecule. DUDLEY R. HERSCHBACH and JEROME D. SWALEN, Harvard University and National Research Council, Ottawa.

The microwave spectrum of propylene oxide has been observed in order to study the hindered internal rotation of the methyl group. Because "tunnelling" through the hindering barrier splits each torsional state v into two sublevels (species A and E of symmetry group C_3) the rotational lines appear as doublets with strongly barrier dependent separation. The barrier is high enough that these doublets were not resolvable for most ground torsional state transitions of low J, but small splittings ($\sim$0·2 mc) were observed for one Q branch series. However, the splittings are magnified by factors of 50 and 1200 in the first and second excited torsional states, respectively, and a large number of satellite lines from molecules in these states were assigned. Both the splittings and transition frequencies of the low J lines from the $v = 0, 1, 2$ torsional states are in good agreement with the theory of hindered internal rotation developed by WILSON and co-workers, for a barrier $V(\alpha) = V_3(1 - \cos 3\alpha)/2$ of $V_3 = 2560$ cal/mole (895 cm^{-1}).

For the ground torsional state one rP branch and three pR branches extending from $J = 1$–45 and $K_{-1} = 1$–23 were also studied. For high K, the contributions from asymmetry ($\kappa = -0{\cdot}88$), centrifugal distortion, and internal rotation can to good approximation be treated separately. When grouped according to the average value of $\tau = K_{-1} - K_{+1}$, the transitions within each

* Supported in part by the National Science Foundation.

[1] ESPE I. *Phys. Rev.* 1956 **103** 1254.
[2] WANNIER G. H. *Phys. Rev.* 1943 **64** 358.

VOL. 10 1957/5

branch are nearly equally spaced. The centrifugal distortion shifts follow the symmetric rotor formula, and increase with the average value of τ. Internal rotation here produces a triplet fine structure (1·0 mc in extent) consisting of two E lines and a single A line of twice the intensity: since the rigid rotor asymmetry splitting is negligible for high K, the A line is nearly K-degenerate, but this degeneracy is split by the internal angular momentum present for the E-level. The relative position of the three lines is periodic in K, following the pattern predicted by KOEHLER and DENNISON for a symmetric hindered rotor (selection rules prevent its observation for a true symmetric rotor), and the splittings agree well with the barrier determined from the low J spectra.

A quantum mechanical interpretation of the force constant–internuclear distance relationships for diatomic molecules. J. N. MURRELL,* University of Chicago.

The change in energy arising from the displacement of the nuclei of a diatomic molecule from their equilibrium positions can be obtained by perturbation theory. By considering the second-order change in energy involved in both a symmetrical and an anti-symmetrical displacement of the nuclei along the molecular axis, an expression for the force constant of the molecule can be obtained as follows:

$$K/2Z_AZ_B = e^2/r_0^3 - e^2\sum_n (D_{on}^{(1)}|\cos\theta_{ai}/r_{ai}^2)\,(D_{on}^{(1)}|\cos\theta_{bi}/r_{bi}^2)/(E_n - E_o)$$

In this expression the contribution from the nuclear repulsion, e^2/r_0^3 appears as the largest term, r_0 being the equilibrium separation. The sum over all the excited states of the molecule can be regarded as the electronic contribution: it appears as a result of allowing the electrons to follow the nuclei during the vibration. Individual terms in this sum are determined by the interaction of the one-electron transition density function $D_{on}^{(i)}$ between the ground state and the nth excited state, and the dipolar fields $\cos\theta_{ai}/r_{ai}^2$ and $\cos\theta_{bi}/r_{bi}^2$ centred on the two nuclei. This sum contains both positive and negative terms (unlike the usual second-order perturbation equation) and should converge quite rapidly.

Plotting a graph of $K/2\ Z_AZ_B$ against e^2/r_0^3 for a number of diatomic molecules, shows that certain regularities exist in the magnitude of the electronic contribution. It is very nearly constant for molecules belonging to the same isoelectronic series, and varies regularly in a given period or group of the periodic table. An explanation of these regularities can to some extent be found by analysing the individual integrals involving atomic orbitals, which go to make up the electronic contribution.

The harmonic force field of nitric acid. ANN PALM, University of California Radiation Laboratory.

A normal co-ordinate treatment was carried out for the HNO_3 and DNO_3 molecules employing the Wilson FG matrix method and a general quadratic potential function. By means of a preliminary C_{2v} approximation, it was possible to evaluate sets of reasonable force constants as a function of the N=O, N—O bond–bond interaction constant. The derived quantities have been correlated with corresponding ones of structurally related molecules.

---

* Commonwealth Fund Fellow, 1956–57.

Spectrochimica Acta, 1957 ,Vol. 10, pp. 238 to 239. Pergamon Press Ltd., London

Symposium on Spectrochemical Analysis for Trace Elements

THIS Symposium was held at the Sixtieth Annual Meeting of American Society for Testing Materials, 17–21 June 1957, Atlantic City, New Jersey.

Emission spectrometric determination of oxygen in metals. V. A. FASSEL, W. A. GORDON and R. W. TABELING.

The problems encountered in extending emission spectrometric methods to the determination of the oxygen content of metals will be surveyed and several techniques for surmounting some of these problems will be discussed. Methods for the determination of oxygen in steel, titanium, the rare earths, and other metals will be discussed in detail. These procedures are based on the liberation of the oxygen content of the metal into an argon atmosphere by the high temperatures attained in direct-current arc discharges. The intensity ratio of the line pair $\frac{\text{O } 7771{\cdot}9}{\text{A } 7891{\cdot}1}$ is related to the oxygen content of the metal sample. The results of preliminary studies on the emission spectrometric determination of hydrogen and nitrogen in metals will be summarized.

The determination of trace elements in metals. J. A. NORRIS.

The determination of trace (less than 100 p.p.m.) quantities of various elements in metals such as iron and steel, copper, aluminum, and others will be surveyed. The methods will be divided in general into four categories: (1) direct determination, (2) chemical pretreatment, (3) carrier techniques, and (4) total separation with or without new matrix.

VOL.
10
1957/5

Trace analysis by means of the graphite spark. JAMES M. MORRIS and FRANCIS X. PINK.

A method is described for the determination of trace impurities below the 1 p.p.m. level. Although the method was developed for the analysis of semiconductor materials, it may be applied to a wide variety of samples. A concentrational step and chemical separation are employed prior to spectrographic analysis. An a.c. spark is used between graphite electrodes, resulting in increased precision and accuracy. The samples, in solution form are pipetted on to the surface of high purity graphite electrodes. The solutions are evaporated to dryness and sparked. Excitation conditions, standard preparation, and analytical data are given. Millimicrograms of impurities are determined with an average standard deviation σ of 2·7 at 5 times the sensitivity limit.

Medical and biological materials. BERT VALLEE and PETER BENT.

Plants and soils. W. G. SCHRENK.

Spectrographic methods may be developed in this field of study by following the general principles of sample preparation, buffers, internal standards, electrode preparation, and excitation conditions, developed by spectrographers in all fields. The general techniques used in applying spectroscopy to plant and soil samples will be reviewed.

Problems concerning spectrographic analysis of plants and soils will differ depending on the type of information desired. In certain cases special spectroscopic techniques may need to be developed.

To illustrate methods used and results that may be expected, data obtained in several problems studied at the Kansas Agricultural Experiment Station were presented.

Geological materials. K. J. MURATA.

Because 99 per cent of the earth's crust consists of only ten elements, all with atomic numbers smaller than 27, most of the elements are trace constituents of the crust. Semiquantitative and quantitative spectrochemical methods are being used extensively in basic geochemical studies on the distribution of the elements in crustal rocks, in systematic exploration for hidden ore deposits, and in determination of by-product elements in ores. Trace analysis of natural crystals are of interest with respect to structure-sensitive properties such as fluorescence. Trace elements in river and ocean waters constitute a challenging subject for research.

OL.
10
7/58

Spectrochimica Acta, 1957, Vol.10, pp. 240 to 241. Pergamon Press Ltd., London

RESEARCH NOTE

Vibrational band intensity of the NH group in substituted acetanilides

R. Moccia and H. W. Thompson
The Physical Chemistry Laboratory, Oxford, England

(*Received* 20 *June* 1957)

Abstract—The frequency, intensity and half-band width of the NH group vibration in a number of substituted acetanilides has been measured. All three quantities appear to be unaffected by the nature or position of *meta* and *para* substituents in the aromatic nucleus. This result is in contrast with those found for related structures such as the substituted N-methyl anilines.

In several recent papers from this laboratory, the effect of other substituents in an aromatic nucleus upon the frequency and intensity of a vibrational chromophore attached to it have been measured. It seems likely that by measurements of this kind, the inductive and mesometric factors contributing to the whole molecular structure may be better understood. This paper summarizes results on the stretching vibration of the NH group in substituted acetanilides.

The experimental method was similar to that described in earlier papers. The spectra were measured on a Perkin Elmer 12C spectrometer, with lithium fluoride prism, the effective slit widths being about 10 cm^{-1}. Absorption cells 0·67 cm and 2·0 cm in length were used, with concentration below 0·005 molar. Owing to the very low solubility of the solutes in carbon tetrachloride, chloroform was used as solvent. The acetanilides were recrystallized before use, and their purity was checked by melting points. The integrated band areas were measured graphically, and

$$B = \frac{1}{cl}\int \ln\left(\frac{T_0}{T}\right)_\nu . d\nu$$

was plotted against $\ln (T_0/T)_{max}$ in order to obtain the required true intensity A by extrapolation to zero absorbance.

As already reported elsewhere, the N-monosubstituted amides show a pair of bands between 3350 cm^{-1} and 3460 cm^{-1} which are best interpreted as being associated respectively with the *cis* and *trans* modifications of the amide link [1]. In the case of acetanilides the higher frequency component greatly predominates, almost to the exclusion of the low frequency band. With the first six compounds listed below in Table 1 the integrated intensity of the main band was about 90 per cent of the intensity of the combined pair, and with the remaining substances it was even greater. For our present purpose it was therefore sufficient to determine the whole intensity of the pair of bands and to assume equivalent absorption characteristics for each. This assumption cannot affect seriously the main conclusions reached.

The results are given in Table 1. When comparisons are possible [2], the vibration frequency of the NH group is always slightly lower in chloroform than in carbon tetrachloride, and its intensity is somewhat greater. These trends apply in other cases also,

VOL.
10
1957/5

but it is at present uncertain whether they result from hydrogen bonding with the solvent or from other causes. The main feature of the present data is that both the frequency and intensity of the NH group vibration are unaffected by substituents on the aromatic ring, over a wide range of Hammett σ factors. With N-methyl anilines, increasing σ leads to an increase in both frequency and intensity of the NH group vibration [3]. It is evident that mesomeric effects in the amide group outweigh any polar influence of a substituent. With compounds of the type Ar—CO—R, in which R = H, OC_2H_5, C_6H_5, or CH_3, substituents on the aromatic nucleus have little effect upon the intensity of the carbonyl group vibration but they cause a change in its frequency [4].

Table 1. Acetanilides, NH group stretching vibration. ν in cm^{-1}, A in cm^2 molecule^{-1} sec^{-1} ($\log_e$)

Substituent	σ	ν (*trans*)	ν (*cis*)	$\Delta\nu^{\circ}_{1/2}$	$A' \times 10^7$
pN$(CH_3)_2$	−0·6	3439	3390	17·8	3·85
$p$$CH_3O$	−0·268	3438	3390	17·8	3·56
$p$$C_2H_5O$	−0·25	3437	3388	17·5	3·80
$p$$CH_3$	−0·17	3437	3389	17·0	3·68
$m$$CH_3$	−0·069	3438	3388	18·0	4·02
H	0	3436	3388	17·5	3·6
pCl	0·227	3436	3389	18·0	3·8
pBr	0·232	3436	3388	18·0	3·75
pI	0·276	3438	3387	18·7	3·8
$m$$NO_2$	0·727	3434	3388	19	3·83

The apparent half band widths of the NH group appears also to be unaffected by the substituents on the aromatic ring. With N-methyl anilines, by contrast, it shows a large variation with σ. The value of about 18 cm^{-1} with acetanilide is to be compared with 32 cm^{-1} for N-methyl aniline.

Acknowledgements—This work was supported by a grant from the Hydrocarbon Research Group of the Institute of Petroleum for which we express thanks. One of us (R. M.) also acknowledges gratefully the award of a scholarship by the Consiglio Nazionale delle Ricerche of Italy.

References

[1] Russell R. A. and Thompson H. W. *Spectrochim. Acta* 1956 **8** 138.
[2] Russell R. A. and Thompson H. W. *Proc. Roy. Soc.* A1956 **234** 318.
[3] Krueger P. J. and Thompson H. W. *Proc. Roy. Soc.* 1957 In press.
[4] Thompson H. W., Needham R. W. and Jameson D. *Spectrochim. Acta* 1957 **9** 208.

MEETINGS AND NEWS ITEMS

Fifth Annual Conference of the Western Spectroscopy Association

The fifth annual conference of the Western Spectroscopy Association will be held at Asilomar, California on Thursday and Friday, 6 and 7 February 1958.

Those interested in attending this meeting may obtain information concerning accommodation by writing to:—

Dr. Kenneth J. Palmer,
United States Department of Agriculture,
800, Buchanan Street, Albany 10, California.

VOL.
10
1957/5

Ninth Pittsburg Conference on Analytical Chemistry and Applied Spectroscopy: 3–7 March 1958

Ninth Annual Symposium of the American Association of Spectrographers: 9–11 June 1958, Chicago, Ill.

Organizers of gatherings of spectroscopists, of national or international scope, are invited to send to this journal not only the dates of the meetings, but also the names and addresses of the organizing secretaries.

Fifth Ottawa Symposium on Applied Spectroscopy

The fifth Ottawa Symposium of the Canadian Association for Applied Spectroscopy is to be held in Ottawa, on 15, 16, and 17 September 1958.

Papers are invited for presentation on the subjects of applied spectroscopy including emission, ultra-violet, infra-red and X-ray work in the field of instrumental analysis.

Titles and brief extracts of papers should be submitted before 2 June 1958 to Mr. N. Tomingas, c/o Canadian Copper Refiners Ltd., P.O. Box 338, Place d'Armes, Montreal, Quebec.

Papers to be published in future issues

J. R. Barcelo: The infra-red spectrum of some metallic chelates

E. Lieber, T. S. Chao and C. N. R. Ramachandra Rao: The ultraviolet absorption spectra of substituted phenyl amino-1,2,3-triazoles

G. Michel and G. Duyckaerts: Contribution à la spectrometric Raman—II. Intensite de la raie du-carbonyle aliphatique

P. Krumholz: Spectroscopic studies on rare-earth compounds.—I. Instrumentation

P. Krumholz: Spectroscopic studies on rare earth compounds.—II. A comparative study of the absorption spectra of the neodymium ion in aqueous solution and in crystalline salts

R. M. Hexter: High-resolution, temperature-dependent spectra of calcite

R. M. Hexter: Infra-red spectroscopic investigation of anion rotational disorder in sodium nitrate

H. R. Linton and E. R. Nixon: Infra-red spectra of silyl and silyl-d_3 cyanides

E. R. Lippincott and R. D. Nelson: The vibrational spectra and structure of ferrocene and ruthenocene

A. K. Rusanov and V. G. Khitrov: Spectrographic analysis of ores by introducing the powder into the arc in a stream of air

L. H. Jones: Systematics in the vibrational spectra of uranyl complexes

R. A. Spurr and T. A. Chubb: Absorption coefficients of four organic fluorine compounds in the vacuum ultra-violet

L. F. H. Bovey: A tuneable microwave cavity for excitation at 2540 Mc/s of an optical spectroscopic source

G. A. Crosby and M. Kasha: Intramolecular energy transfer in ytterbium organic chelates

C. G. Cannon: The nature of hydrogen bonding

R. C. Taylor and A. R. Emery: The Raman spectra of four isotopic varieties of diborane in the gas phase

L. Bovey: Emission and absorption spectra of plutonium excited in a King furnace

F. González-Sánchez: Infra-red spectra of the benzene carboxylic acids

H. R. Linton and E. R. Nixon: Infra-red spectrum and force constants of silyl-d_3 iodide

A. N. Zaĭdel: Spectral-isotopic method for the determination of hydrogen in metals

Papers to be published in future issues

C. Rimington, S. F. Mason and O. Kennard: Porphin

L. B. Archibald and A. D. E. Pullin: Solvent effects in infrared spectra of compounds containing the carbonyl group

A. Stojiljkovic and D. H. Whiffen: The vibration frequencies of unsymmetrical para dihalogenobenzenes

A. Stojiljkovic and D. H. Whiffen: The vibration frequencies of the symmetrical para dihalogenobenzenes

N. S. Ham and A. Walsh: Microwave-powered Raman sources

R. A. Ford and F. Parry: Electronic and vibrational states of carbonyl compounds—I. Electronic states of camphorquinone

E. Bright Wilson, Jr.: Determination of the order of atoms in a linear molecule

VOL.
10
1957/5

Spectrochimica Acta, 1958, Vol. 10, pp. 245 to 249. Pergamon Press Ltd., London

The infra-red spectrum of some metallic chelate compounds—I Rubeanates*

José R. Barceló
Institute of Optics, Madrid

(*Received* 14 *April* 1957)

Abstract—Some investigators have attempted to study the structural changes that appear in the chelation through the infra-red spectrum. Acetylacetone and its compounds, and the oximes and dioximes have been studied by these methods.

In the present paper one of the reagents which forms chelate compounds is examined the molecule of which contains no hydroxyl groups, namely rubeanic acid, the diamine of thioxalic acid. Copper, nickel, cobalt, silver and mercury derivatives of this acid have also been studied and formulae have been proposed for the reagent and its metal compounds in the solid state.

As is well known, the metallic chelate compounds are of extraordinary interest in qualitative and quantitative analysis. It is, therefore, not surprising that besides an abundant bibliography dealing with their analytical applications there should also exist publications in which attempts are made to study both the nature of the reagent itself and of the metallic compounds which it forms.

For this purpose infra-red spectrometry has been used. Lecomte [1] has studied the infra-red spectrum of metallic acetylacetonates. Voter *et al.* [2] have examined the nature of the hydrogen bond in nickel dioximes, and Duyckaerts [3] has also measured the infra-red spectra of oximes.

It may be noted that in these measurements with acetylacetone and the oximes, interest has centred mainly around the OH group. In this paper we propose to study another reagent in this group, namely the rubeanic acid or thiamide of oxalic acid. This compound differs from those so far studied by the absence of the OH group from its molecule, although it is one of the simplest molecules among those which produce metallic chelate compounds.

Experimental work

The substances studied were rubeanic acid and its metallic derivatives of copper, nickel, cobalt, silver, and mercury. The rubeanic acid used was a commercial sample. The rubeanates were obtained from metallic salts in highly dilute solution (so that the process of obtaining them might resemble the formation of the substance in analytical practice) and in a neutral medium, except that of mercury, which was prepared in an acidic medium. To these solutions of dilute metallic salts we added a 0·5 per cent alcoholic solution of rubeanic acid. When the precipitate was filtered, washed, and dried at 110°C, the corresponding metallic compound was obtained.

The powders prepared were: copper rubeanate, of a greenish-black colour; nickel rubeanate, violet-bluish black; cobalt rubeanate, orange-brown; silver

* Presented at the XV Congress of the I.U.P.A.C., Lisbon, 1956.

rubeanate, dark greenish-brown; and mercuric rubeanate, white and of low density, turning sienna when heated.

The infra-red spectrum was run with a D209 Hilger spectrometer, between 4000 and 400 cm^{-1}, using LiF, NaCl and KBr prisms.

Since the metallic derivatives are insoluble and the solubility of rubeanic acid is low in suitable infra-red solvents, the spectra of all the substances were obtained by means of the potassium-bromide pellet technique.

In the case of rubeanic acid, concentrations in the 0·3–0·5–0·75 and 1 per cent range were used. As regards the metallic compounds, the concentration used is not known, but it was varied in each case so as to obtain a satisfactory spectrum.

Discussion

The rubeanic acid or thiamide of oxalic acid can be represented by three different formulae

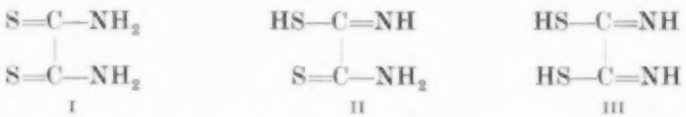

I II III

diamine I, hemiacid II, and imide or acid III, and in each one of these the *cis*, *trans*, or other intermediate positions can exist. The X-rays study of rubeanic acid [4] suggest a planar molecule with a centre of symmetry. The study of the infra-red spectrum, in the region of higher frequencies, would seem to indicate that the most acceptable structure is I, at least for the substance in the solid state.

In spite of our having sought very carefully for the frequency corresponding to group S—H, which should appear in the region of 2500–2600 cm^{-1}, this frequency was not found in the spectra of rubeanic acid at the concentrations studied.

Special interest attaches to the part of the spectrum corresponding to the valency vibrations of the N—H. As is well known, the free N—H link shows an absorption band at about 3500–3400 cm^{-1}, whereas the associated N—H link has this frequency at much lower values between 3300–3200 cm^{-1}. In this range and near it, rubeanic acid shows three intense bands at 3304 cm^{-1}, 3205 cm^{-1}, and 3135 cm^{-1}; and three other less intense bands at 2930 cm^{-1}, 2850 cm^{-1}, and 2756 cm^{-1}. All these bands imply the existence of an associated N—H group.

To make a more detailed study of this matter, this spectrum should be compared with that of *N*-methylacetamide, which has been described by San-Ichiro Mizushima [5]. The latter molecule has been studied because it is the simplest one containing a peptide bond and can be regarded as a fragment of a polypeptide chain. If this molecule

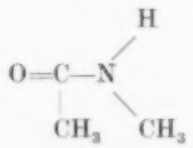

is compared with that of rubeanic acid, similarities may be noted. The chief difference lies in the fact that instead of the S=C group it contains the O=C

VOL. 10 1957/5

group and that N is joined only to an H, since the other valency is saturated with a methyl group.

In *N*-methylacetamide, in the vapour state, a band appears at 3500 cm^{-1}, which indicates the existence of a free N—H group, whereas in the solid or liquid form the N—H frequency moves to 3250 cm^{-1} and 3300 cm^{-1} respectively, which points to an associated N—H link. MIZUSHIMA remarks that a band in the infra-red spectrum of the solid which appears at 3105 cm^{-1} is difficult to interpret

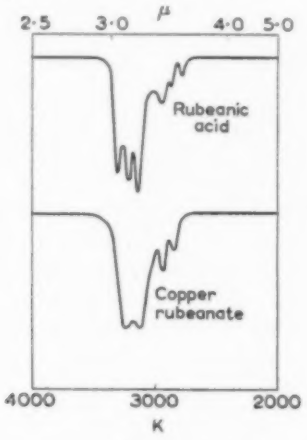

Fig. 1.

since there is only one hydrogen atom, and there cannot be two valency vibration frequencies. In the spectrum of this substance in the solid state there also exist the weak bands at 2985 cm^{-1}, 2910 cm^{-1}, and 2720 cm^{-1}, which are not explained.

In the spectrum of rubeanic acid (Fig. 1), in this region there appear six bands, namely three strong ones at 3304 cm^{-1}, 3205 cm^{-1}, and 3135 cm^{-1}, and three weak ones at 2930 cm^{-1}, 2850 cm^{-1}, and 2756 cm^{-1}. As will be seen, this part of the spectrum is very similar to that of *N*-methylacetamide. The fundamental difference consists in the fact that, here, there are two N—H frequencies, which accords with the existence of the NH_2 group, whereas in *N*-methylacetamide the group present is =NH. In rubeanic acid, also, the intense band appears at 3135 cm^{-1}, which might apparently be considered as an N—H frequency; but this cannot be so since in the spectrum of the metallic derivatives it remains unchanged, whereas the other two are replaced by a single band which lies at an intermediate position.

The study of the association in chloroacetic acids [6] shows that in the case of an association a series of weak bands appear in the region of 2900 cm^{-1}, and these also occur in other associated carboxylic acids. Many authors have studied this series of bands and have given interpretations which, for the time being, are not considered final. However, it must be acknowledged that these bands are closely bound up with the existence of hydrogen bridges. In rubeanic acid these bands are intense at 3135 cm^{-1}, and weak at 2930 cm^{-1}, 2850 cm^{-1}, and 2756 cm^{-1}.

It would seem to follow from the above that the formulae for rubeanic acid in the solid state must be of the following type if we consider the *trans* form in accord with the X-ray study.

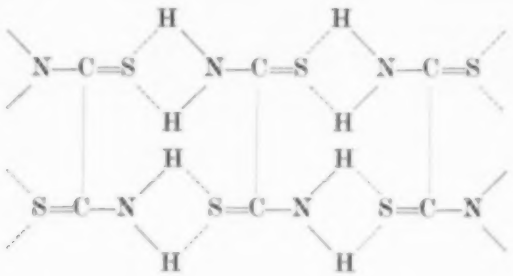

The spectrum of the metallic derivatives in this region of higher frequencies is rather similar for copper, nickel, and cobalt. With the silver compound, it has not been possible to define the absorption clearly; and with mercury the absorption appears as a very wide band around 3400 cm^{-1}, the existence of which is rather uncertain.

As regards the first three of these compounds, it is clearly seen that the NH_2 bands of rubeanic acid have become reduced to one, which appears around 3230 cm^{-1}, i.e. between those of the acid itself. The band at 3135 cm^{-1} remains unchanged, which shows that it is not closely related to the N—H valency frequency. The three weakest bands at a lower frequency have become reduced to two and their positions differ only slightly from those occupied by the corresponding bands of the acid. The last of these bands at 2756 cm^{-1} has disappeared from the spectra of the metallic derivatives, except that of mercury, in which, moreover, another band appears at 2325 cm^{-1}.

This leads us to think that the constitution of the metallic derivatives, at least as regards copper, nickel, and cobalt, may possibly be of the following type:

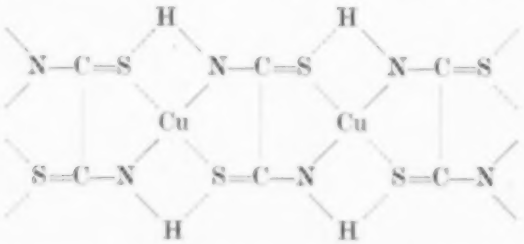

The part of the spectrum between 2000 and 400 cm^{-1} is more difficult to interpret, but some general considerations may be noted.

Rubeanic acid must possess 24 fundamental frequencies, some of which may be inactive in the infra-red spectrum. In the spectrum some characteristic frequencies can be assigned, such as the deformation and rocking of N—H, C—N and the S=C—N group. It is worthy of mention that the deformation frequency of the NH_2 group, which in the case of free hydrogen appears around 1600 cm^{-1},

VOL. 10 1957/5

in the present case occurs at 1555 cm^{-1}, and this would also appear to be related to the existence of associated hydrogen atoms.

As other authors have observed, when passing from the acid to the metallic derivatives the spectrum in the region 2000–400 cm^{-1} undergoes a great change. This would seem to be attributable to two main causes. On the one hand, the presence of a heavy atom bound to the molecule groups by valency and co-ordination forces causes the frequencies of these groups to undergo a considerable displacement. On the other hand, as inferred from the formulae we have suggested, the introduction of the metallic atom changes the symmetry of the molecule. In the rubeanic acid molecule, with its hydrogen bonds, a ring of eight atoms appears:

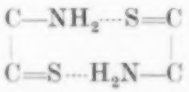

whereas in that of the metallic compounds there exists one pentacyclic ring.

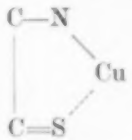

This change in the symmetry may explain the variation of the spectrum when passing from the acid to its metallic derivatives. In the case of the compounds of copper, nickel, and cobalt the difference, though not very great, is noticeable, and this, in the case of nickel and cobalt, cannot be attributed to differences in the mass, since this is practically the same and is also not very different from that of copper.

These differences are much more marked when comparing mercury and silver derivatives with the others, and therefore, the formula given for the metallic derivatives may possibly not apply to those of silver and mercury, in which some chemical transformation may perhaps occur when the preparative reaction takes place. However, the monovalent nature of silver and the acid medium in which the compound of mercury was precipitated may be the causes of these differences in structure.

References

[1] Lecomte J. *Disc. Faraday Soc.* 1950 **9** 125.
[2] Voter R. C., Banks Ch. V., Fassel V. A. and Kores P. W. *Analyt. Chem.* 1951 **23** 1730.
[3] Duyckaerts G. *Bull. Soc. Roy. Sci. Liége* 1952 **4–5** 196.
[4] Long B., Markey P. and Wheatley P. J. *Acta Cryst.* 1954 **7** 140.
[5] San-Ichiro Mizushima *Structure of Molecules and Internal Rotation*. Academic Press, New York, 1954.
[6] Jorge M. P. and Barceló J. *An. Soc. Esp. Fis. Quim.* B 1957 **53** 339.

Spectrochimica Acta, 1958, Vol. 10, pp. 250 to 258. Pergamon Press Ltd., London

The ultra-violet absorption spectra of substituted phenyl amino-1,2,3-triazoles

E. Lieber,* C. N. R. Rao† and T. S. Chao‡
Departments of Chemistry, DePaul University, Chicago 14, Ill. and
Purdue University, Lafayette, Ind., U.S.A.

(*Received* 22 *October* 1956)

Abstract—The ultra-violet absorption spectra of isomeric substituted phenyl amino-1,2,3-triazoles have been studied. The influence of the substituents in the 1-, 4-, and 5-positions is discussed. The spectra of these triazoles have been of significant use for analytical and structural studies in this heterocyclic system.

Introduction

The earlier studies of Ramant-Lucas and Hoch [1] showed that the phenyl aminotriazoles,§ unlike other phenyl triazoles exhibited strong absorption bands

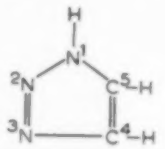

which pictures the parent compound (Ring Index Number 76).

in the ultra-violet region. As part of an investigation on the synthesis and isomerization of substituted phenyl amino-1,2,3-triazoles (2), a detailed study of the near ultra-violet absorption spectra of the compounds synthesized was concurrently carried out. The substituted phenyl amino-1,2,3-triazoles are an interesting class of compounds that undergo a rather facile thermal isomerization which involves an equilibrium, I ⇌ II (2):

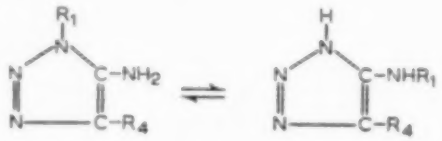

I II

This communication deals with the influence of R_1 and R_4 on the near ultra-violet absorption characteristics of compounds of type I and II and its application to analytical and structural problems in this field.

Experimental

Preparation of the compounds used in this study. The 1-substituted phenyl-4-phenyl-5-amino-1,2,3-triazoles, III ($\phi = C_6H_5$) were prepared by the condensation

* Department of Chemistry, De Paul University, to whom all correspondence and requests for reprints should be sent.

† Purdue University.

‡ Archer Daniels Midland Company, Minneapolis, Minn., U.S.A.

§ The vicinal or v-triazoles, also known as 1,2,3-triazoles, are five-membered, doubly unsaturated heterocycles, the ring consisting of three sequentially linked nitrogen atoms and two carbon atoms. The numbering system used in this communication is in accordance with A. M. Patterson and L. T. Capell *The Ring Index*. Reinhold, New York 1940.

VOL. 10 1957/5

of an organic azide with phenylacetonitrile in the presence of sodium methoxide. 4-Phenyl-5-substituted-phenyl amino-1,2,3-triazoles, IV, were obtained by the

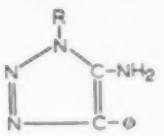

III

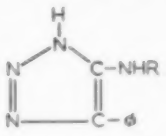

IV

irreversible isomerization of type III compounds in boiling dry pyridine. In general, type II ("amino-N-phenyl") isomers could be prepared by refluxing type I ("ring-N-phenyl") isomers in a basic solvent. The details of the synthesis and isomerization of substituted phenyl amino-1,2,3-triazoles have been discussed elsewhere [2]. 1-Phenyl-5-amino-1,2,3-triazole (I, $R_1 = \phi$; $R_4 = H$) and 1-methyl-5-anilino-1,2,3-triazole, V, were prepared by the method of DIMROTH [3]. The

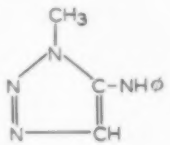

V

aniline and substituted anilines used in this investigation were commercially available and were used after suitable purification.

Experimental procedure. A Cary recording spectrophotometer was used for all the measurements. Molar absorptivities (ϵ) are in units of liters per (mole cm). The instrument was calibrated using the didymium glass as a standard. All the spectra were determined in 95 per cent ethanol. The wavelengths are recorded in mμ.

Results and discussion

In general, the near ultra-violet absorption characteristics of the substituted triazoles can be interpreted in terms of the resonance conjugation brought about by the substituents in the 1-, 4-, and 5-positions of the parent compound and their interaction with the triazole nucleus. Therefore, absorption in the near ultra-violet will occur when substituents capable of appreciable resonance conjugation with the triazole nucleus are present. RAMART-LUCAS and HOCH [1] have studied

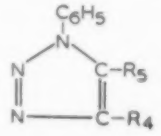

VI

the near ultra-violet spectra of phenyl triazoles, VI, and have observed that the spectroscopic behavior of the compounds VI varied considerably according to the nature of the substituents in the 4- (R_4) and 5- (R_5) positions. They found that the

compounds are in non-absorbant forms in the near ultra-violet region when R_5 is a hydrogen, methyl, phenyl or carboxylic group and R_4 is a hydrogen or a carboxyl group. They explain this observation by the negligible interaction between the aromatic and heterocyclic nuclei. However, 1,4-diphenyl-5-amino-1,2,3-triazole (VI; $R_5 = NH_2$; $R_4 = \phi$) and ethyl 1-phenyl-5-amino-1,2,3-triazole-4-carboxylate (VI; $R_5 = NH_2$; $R_4 = CO_2Et$) are in absorbant form, which they

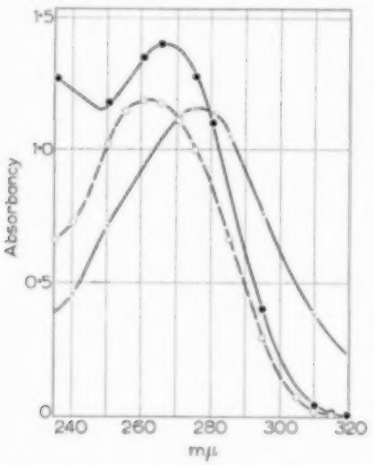

Fig. 1. Ultra-violet absorption spectra of 1-substituted-4-phenyl-5-amino-1,2,3-triazoles in 95 per cent ethanol:
●——● III, R = ϕ;
○ · · · ○ III, R = $C_6H_5CH_2$
×——× III, R = 4-$NO_2C_6H_4$.

explain as due to an energetic interaction between the aromatic nucleus in the 1-position and the rest of the molecule.

The results reported in this communication deal with the near ultra-violet spectra of the isomeric 1-substituted phenyl-5-amino- (I; the "ring-N-phenyl") and the 5-substituted phenyl amino- (II; the "amino-N-phenyl") triazole derivatives and the influence of the different substituents on the spectra. Fig. 1 shows the spectra of some typical 1-substituted phenyl-4-phenyl-5-amino-1,2,3-triazoles (III) and Table 1 lists the wavelengths corresponding to the absorption maxima (λ_{max}) and the molar absorptivities. The results in Table 1 indicate that the 1-phenyl-, 1-(*p*-tolyl)- and the 1-benzyl-derivatives exhibit a strong absorption band at 260–265 mμ. This corresponds to the absorption band observed by Ramant-Lucas and Hoch [1] at 267–268 mμ in the case of 1,4-diphenyl-5-amino-1,2,3-triazole, this latter value being obtained by extrapolation from their absorption curves. It is interesting to note that the introduction of a nitro group on the benzene ring situated at the 1-position varies the wavelength of the absorption maximum. Doub and Vandenbelt [4] have shown that while the primary band of benzene is not shifted to any considerable extent by substituents like the methyl, chloro or bromo group on the ring, it is shifted to a great extent by strongly

VOL. 10 1957/5

interacting groups like the nitro group. 1-Substituted phenyl-4-phenyl-5-amino-1,2,3-triazole can be regarded as disubstituted benzenes of the form VII:

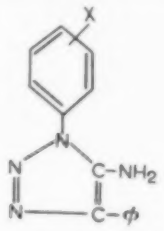

VII

The influence of the substituent X on the λ_{max} of these triazoles is of the same relative magnitude as that on the λ_{max} of the primary band of benzene. Accordingly, the spectra can be considered to be due to electronic transitions arising from the benzene rings modified by various substituents, including the 1,2,3-triazole ring, and is the "main" benzene transition, identified by DOUB and VANDENBELT [4] as

Table 1. Ultra-violet absorption spectra of 1-substituted 4-phenyl-5-amino-1,2,3-triazoles

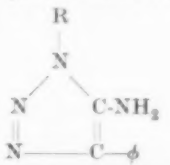

R	λ_{max}	$\epsilon \times 10^{-4}$
C_6H_5	265	1·58
4-$NO_2C_6H_4$	275	2·26
3-$NO_2C_6H_4$	242·5	2·38
4-$CH_3OC_6H_4$	260	1·78
4-$CH_3C_6H_4$	265	1·95
$C_6H_5CH_2$	262	1·01

"first primary bands". The *p*-nitro group shifts the λ_{max} of 1,4-diphenyl-5-amino-1,2,3-triazole to a greater extent than the *p*-methyl or *p*-methoxy group. The *p*-nitrophenyl compound, VIII:

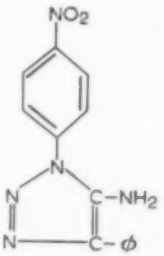

VIII

has a λ_{max} of about 275 mμ which is very close to the λ_{max} of nitrobenzene (269 mμ).

In Table 2 are tabulated the λ_{max} values and the corresponding molar absorptivities of a number of 4-phenyl-5-(substituted phenyl) amino-1,2,3-triazoles, IX:

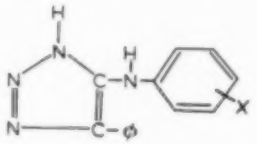

IX

Some typical absorption spectra of type IV compounds (the "amino-N-phenyl" type) are shown in Fig. 2. Most of the 4-phenyl-5-(substituted phenyl) amino-1,2,3-triazoles, exhibit an absorption band at 240–245 mμ. An unresolved shoulder

Table 2. Ultra-violet absorption spectra of 4-phenyl-5-substituted amino-1,2.3-triazoles

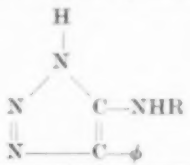

R	λ_{max}	$\epsilon \times 10^{-4}$
C_6H_5	240	1·72
4-ClC_6H_4	245	1·93
3-ClC_6H_4	245	1·56
4-$CH_3C_6H_4$	240	1·75
4-$CH_3OC_6H_4$	240	1·62
4-$NO_2C_6H_4$	235	1·36
	367·5	1·43
3-$NO_2C_6H_4$	259	2·37
	370	0·17
$C_6H_5CH_2$	285	0·70

is also present in these cases at about 265 mμ. 4-Phenyl-5-benzylamino-1,2,3-triazole, X, has a λ_{max} of 285 mμ. The 4-phenyl-5-(substituted phenyl) amino-1,2,3-triazoles, VIII, can be regarded as substituted anilines, in which the entire

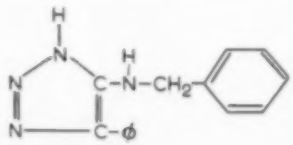

X

heterocyclic nucleus is a substituent on the NH_2 group attached via the 5-position of the heterocyclic ring. Comparison of the λ_{max} of these triazoles with those of

VOL. 10 1957/5

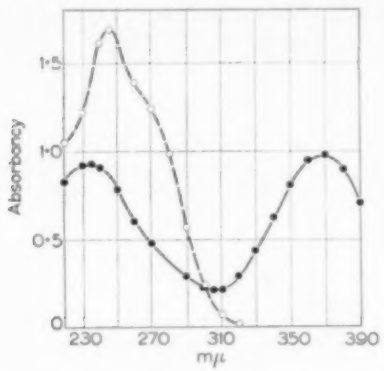

Fig. 2. Ultra-violet absorption spectra of 4-phenyl-5-(substituted phenyl) amino-1,2,3-triazoles in 95 per cent ethanol:
○ · · · ○ IV, R = 4-BrC_6H_4
●——● IV, R = 4-$NO_2C_6H_4$

Table 3. Comparison of the λ_{max} values of 4-phenyl-5-(substituted phenyl) amino-1,2,3-triazoles and substituted anilines

R	Values of λ_{max}	
	Vicinal triazole*	Substituted aniline†
H	240	234·5
4-Cl	245	243
4-Br	245	244
4-CH_3	240	235
4-CH_3O	240	235
4-NO_2	235	229
	367·5	374
3-NO_2	259	280
	370	370

* Structure is

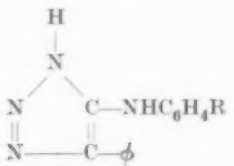

† Structure is $RC_6H_4NH_2$

the corresponding substituted anilines in Table 3 shows an extraordinary similarity between the two. The similarity is rather striking in the case of the nitro derivatives.

The results on the influence of the 4-position on the ultra-violet spectra of the substituted phenyl amino-1,2,3-triazoles, XI:

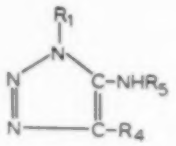

XI

are summarized in Table 4. Replacement of the phenyl group in the 4-position of 1,4-diphenyl-5-amino-1,2,3-triazoles by a hydrogen or a carbethoxy group decreases the λ_{max} considerably, while a similar replacement in 4-phenyl-1,2,3-triazole increases the λ_{max}. Replacement of the hydrogen in the 1-position of

Table 4. Influence of the substituent in 4-position on the ultra-violet spectra of substituted amino-1,2,3-triazoles

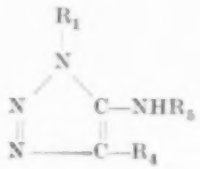

R_1	R_4	R_5	λ_{max}	$\epsilon \times 10^{-4}$
C_6H_5	C_6H_5	H	265	1·58
H	C_6H_5	C_6H_5	240	1·72
C_6H_5	H	H	221	0·90
H	H	C_6H_5	251	1·58
C_6H_5	CO_2Et	H	223	1·68
H	CO_2Et	C_6H_5	260	2·26

5-anilino-1,2,3-triazole by a methyl group (XI; $R_1 = CH_3$; $R_4 = H$; $R_5 = \phi$) increases the λ_{max} from 251 to 266 mμ. In 1-phenyl-5-amino-1,2,3-triazole (XI; $R_1 = \phi$; $R_4 = H$; $R_5 = H$) and ethyl 1-phenyl-5-amino-1,2,3-triazole-4-carboxylate (XI; $R_1 = \phi$; $R_4 = CO_2C_2H_5$; $R_5 = H$) there appears to be another band at about 260 mμ. A similar shoulder is observed in the absorption spectra of the corresponding 5-anilino isomers at wavelengths of about 265 and 300 m respectively.

Ramant-Lucas and Hoch [1] have observed that a methyl group causes a prominent hypsochromic effect while a phenyl group produces a small bathochromic effect in the ultra-violet spectra of phenyl triazoles and that the influence of the substituents is more in position 5 than in position 4. Comparison of the results in

Tables 1 and 2 shows that the shifting of a phenyl group from the 1-position to the 5-position produces considerable hypsochromic effect while a similar shifting of the benzyl group produces a bathochromic effect. From Table 4 it can be seen that when the substituent in the 4-position is a nonresonating group like hydrogen or a carbethoxy group, the shifting of the phenyl group from position 1 to 5 produces a large bathochromic effect. This bathochromic effect is larger in magnitude with the carbethoxy group in the 4-position when compared to hydrogen in the same position. It thus appears that a highly resonating group like the phenyl group provokes a bathochromic effect in type I ("ring-N-phenyl" type) compounds when in the 1-position and a hypsochromic effect in type II ("amino-N-phenyl" type) compounds when in the 5-position, only if the substituent in the 4-position is another resonating group, as in compounds of type I ($R_4 = \phi$) and II ($R_4 = \phi$). In general, when one of the substituents in the 1- and 4-positions is a resonating group and the other is a nonresonating group, there is a hypsochromic effect in type I ("ring-N-phenyl") compounds, and, similarly, a bathochromic effect is observed in type II ("amino-N-phenyl") compounds if one of the substituents in the 4- and 5-positions is a resonating group and the other a nonresonating group. The magnitude of the bathochromic effect in type II ("amino-N-phenyl") compounds is enhanced when hydrogen in position 1 is replaced by a more electropositive and nonresonating group like the methyl group. It is interesting to note that the intensity of the absorption bands both in type III ("ring-N-phenyl") and type IV ("amino-N-phenyl") compounds is very great with a highly interacting group like the *p*-nitrophenyl group, while it is the least with an aliphatic-like group such as the benzyl group. Further, results in Table 4 indicate that a marked increase in the intensity of the band (hyperchromic effect) is caused by shifting a resonating group in the 1-position to the 5-position, when the substituent in the 4-position is a nonresonating group.

From the results in Tables 1, 2, and 4, it can be seen that the near ultra-violet absorption spectra of the two isomers I and II are distinctly different and provide a means for the qualitative and quantitative determination of either isomer. The isomers of type II ("amino-N-phenyl") are weak acids and can be estimated accurately in nonaqueous media [5]. In order to investigate the position of the acidic hydrogen in type II compounds, the acidity of 1-methyl-5-anilino-1,2,3-triazole (XI; $R_1 = CH_3$; $R_4 = H$; $R_5 = \phi$) was determined in 18 per cent ethanol utilizing the ultra-violet absorption spectra of the free and protonated forms in solution of measured pH. The results [6] clearly indicated that the acidic hydrogen was in the 1-position. The aqueous alkaline solutions of the type II ("amino-N-phenyl") isomers slowly develop a pink color which is probably due to an indicator behavior of these compounds. Such a colored solution of 4-phenyl-5-anilino-1,2,3-triazole exhibited an absorption band at 248 mμ in the near ultra-violet region and an absorption band at 475 mμ in the visible region. Preliminary determinations of the pK_a values of various 4-phenyl-5-(substituted phenyl)-amino-1,2,3-triazoles using their ultra-violet spectra have shown that the pK_a depends on the electron withdrawing or electron donating power of the substituent on the anilino group in the 5-position. In general, the near ultra-violet absorption spectra of the isomeric substituted amino-1,2,3-triazoles, I and II, provide a

powerful analytical and structural diagnostic tool for investigations in this heterocyclic system.

Acknowledgements—The authors are indebted to the Office of Naval Research for a grant-in-aid which made this study possible and to Mr. Edward Choplinski for his assistance in taking the spectra.

References

[1] Ramant-Lucas and Hoch J. *Bull. Soc. Chim. Fr.* 1949, 451.
[2] Lieber E., Rao C. N. R. and Chao T. S., *J. Org. Chem.* 1957 **22** 654.
[3] Dimroth O. *Liebigs Ann.* 1909 **364** 183.
[4] Doub L. and Vandenbelt J. M. *J. Amer. Chem. Soc.* 1947 **69** 2714.
[5] Lieber E., Rao C. N. R. and Chao T. S. *Analyt. Chem.* 1957 **29** 932.
[6] Lieber E., Rao C. N. R. and Chao T. S. *Curr. Sci.* 1957 **26** 14.

VOL.
10
1957/5

Spectrochimica Acta, 1958, Vol. 10, pp. 259 to 268. Pergamon Press Ltd., London

Contribution à la spectrométrie Raman—II

Intensité de la raie du carbonyle aliphatique

GILBERT MICHEL et GEORGES DUYCKAERTS
Service de Chimie Analytique, Université de Liège, Belgique

(*Received* 15 *July* 1957)

Abstract—The authors have investigated the Raman carbonyl stretching vibration of different aliphatic ketones, esters and aldehydes.

The results concerning the frequency of the carbonyl are in agreement with those of previous workers; the mean values for an homologous series of saturated aliphatic ketones and esters are 1715 $\pm$ 3 cm^{-1} and 1738 $\pm$ 5 cm^{-1}.

The scattering coefficient of the carbonyl line has been measured with an accuracy of 4 per cent and the following observations have been made:

(1) The scattering coefficient of a non-conjugated carbonyl is relatively constant and proportional to the number of independent carbonyl groups in the molecule.

(2) Conjugation of the carbonyl group with an ethylenic double bond increases strongly the scattering coefficient by a factor depending on the nature of the carbonyl (aldehyde, ketone or ester) the nature of the substituents on the molecule and the degree of conjugation allowed by steric factors.

EXCEPTION faite pour les dosages qui sont évidemment basés sur la mesure des intensités des raies, les autres applications de la spectroscopie de diffusion reposent presqu'exclusivement sur les fréquences des raies.

BOURGUEL [1] et plus tard WOLKENSTEIN [2] ont déja attiré l'attention sur l'intérêt des intensités des raies pour la résolution de problèmes de structure moléculaire.

L'introduction de la mesure photoélectrique du spectre Raman par RANK et ses coll. [3] a ouvert la voie à l'étude systématique des corrélations structure-intensité. Des auteurs russes [4] ont déjà publié une série d'articles de ce genre sur les hydrocarbures non saturés notamment. Notons aussi un travail fait par enregistrement photographique [5] étudiant l'influence de la conjugaison sur les raies Raman.

La présente note se rapporte principalement à la vibration de valence de la fonction carbonyle de composés aliphatiques.*

Partie expérimentale

Tous les spectres ont été enregistrés avec l'installation photoélectrique décrite dans une publication antérieure [6]. Les mesures de fréquences ont été effectuées soit sur un enregistrement photoélectrique; dans ce dernier cas, on superpose au spectre Raman un spectre d'émission de gaz rares (Ne, A, He).

Tous les coefficients de diffusion ont été obtenus au moyen de l'installation photoélectrique.

La radiation excitatrice 4358 Å d'une lampe à vapeur de mercure type Toronto (A.R.L.) est filtrée par une solution de nitrite potassique à 60%.

* Les premiers résultats de cette étude avaient déjà fait l'objet d'une communication (G.M.) au Colloque de spectroscopie Moléculaire d'Oxford en 1955.

Les enregistrements photoélectriques quantitatifs sont obtenus dans les conditions suivantes:

largeur spectrale de la fente: 8 cm^{-1}
vitesse de balayage: 10 cm^{-1}/min.
constante de temps: 4 secondes.

Coefficients de diffusion

L'intensité d'une raie Raman étant, suivant la théorie, proportionnelle au nombre des molécules, on peut proposer la relation suivante pour un mélange de substances non associées [7]:

$$I_A^{\nu 1}/I_B^{\nu 2} = K_A^{\nu 1}/K_B^{\nu 2} \cdot N_A/N_B \qquad (1)$$

$K_A^{\nu 1}$, $K_B^{\nu 2}$ étant les coefficients de diffusion des raies choisies des substances A et B.

N_A, N_B étant les nombres de moles.

Devant la difficulté de déterminer les valeurs des coefficients, on a convenu de rapporter les valeurs à une raie de référence, soit généralement, à la 459 cm^{-1} [8] du tétrachlorure de carbone soit aussi à la 315 cm^{-1} de la même substance ou à la 802 cm^{-1} du cyclohexane (4); c'est le coefficient de diffusion relatif:

$$k_A^{\nu 1} \equiv K_A^{\nu 1}/K_{CCl_4}^{459}.$$

Il existe deux méthodes de détermination du coefficient de diffusion relatif k_A^{ν} qui fournissent des valeurs assez voisines:

1. Prendre le spectre d'une solution dans le tétrachlorure de carbone de la substance à concentration connue et calculer le coefficient à partir de la relation (1).

2. Prendre séparément dans des tubes identiques et dans les mêmes conditions les spectres de la substance et du tétrachlorure; dans ces conditions

$$k_A^{\nu 1} = I_A^{\nu 1}/I_{CCl_4}^{459} \cdot (M/d)_A \cdot (d/M)_{CCl_4} \cdot (n_A/n_{CCl_4})^2 \qquad (2)$$

où M et d sont le poid moléculaire et la densité de la substance et du tétrachlorure

n_A et n_{CCl_4} sont les indices de réfraction de la substance et du tétrachlorure.

Ce coefficient de diffusion tient compte du volume effectif de liquide vu par le spectromètre et du nombre de molécules différent pour les deux enregistrements. Nous n'avons pas retenu les autres facteurs de la formule développée par BERNSTEIN et ALLEN [9].

Précision des mesures

Les coefficients de diffusion rassemblés dans les tableaux 1 et 3 sont des valeurs moyennes de 3 à 8 mesures; de la sorte l'erreur moyenne relative ne dépasse jamais 4 pourcent, alors que l'erreur sur une seule mesure, pour les faibles coefficients de diffusion, monte quelquefois à 10 pourcent.

Fréquence de vibration de la fonction carbonyle

Du point de vue de sa fréquence, la vibration de valence de la fonction carbonyle a fait l'objet de nombreux travaux de spectroscopie infra-rouge et Raman: des interprétations faites sur la base des théories de la résonance ont été proposées

VOL. 10 1957/5

Chaque substance a été purifiée et distillée immédiatement avant la prise du spectre: le fractionnement à été fait soit avec une colonne de Crismer de 50 cm, soit avec une colonne de Todt; le point d'ébullition et l'indice de réfraction ont été pris comme critères de pureté:

Substance	Origine		t_E	$n_D^{22°}$
Acétone	U.C.B. p.a.	(a)	56,1°	1,358
Méthyl éthyl cétone	B.D.H. pure	(b)	79,5°	1,380
Méthyl n-propyl cétone	B.D.H. pure	(a)	101,7°	1,390
Méthyl iso-propyl cétone	B.D.H. pure	(a)	95,4°	1,389
Diéthyl cétone	B.D.H. pure	(a)	102,5°	1,392
Méthyl isobutyl cétone	B.D.H. pure	(a)	116,2°	1,395
Di-n-propyl cétone	B.D.H. pure	(a)	144°	1,406
Di-iso-propyl cétone	B.D.H. pure	(c)	123,6°	1,399
Di-iso-butyl cétone	B.D.H. pure	(a)	56–56,5° (11 mm)	1,413
Acétonylacétone	Erba p.a.	(a)	137,4° (150 mm)	1,429
Allylacétone	Schuckardt p.a.	(a)	129,3°	1,410
Benzyl méthyl cétone	B.D.H. pure	(b)	104–5° (13 mm)	1,516
Méthyl 6-heptène-5-one 2	Fluka pure	(a)	51° (4 mm)	1,440
Diacétone-alcool	U.C.B. pure	(a)	55° (10 mm)	1,428
Monochloracétone	B.D.H. pure	(a)	35° (29 mm)	1,430
Cyclopentanone	B.D.H. pure	(a)	130,6°	1,439
Cyclohexanone	B.D.H. pure	(a)	46,5° (11 mm)	1,453
Fenchone	B.D.H. pure	(a)	82,5° (20 mm)	1,463
Acétate de méthyle	U.C.B. p.a.	(a)	57°	1,359
Acétate d'éthyle	U.C.B. p.a.	(a)	77,1°	1,372
Acétate de n-propyle	East. Kodak p.a.	(a)	101,5°	1,384
Acétate de n-butyle	East. Kodak p.a.	(a)	126,4°	1,395
Acétate d'isobutyle	East. Kodak p.a.	(a)	116,4°	1,391
Acétate de butyle sec.	East. Kodak p.a.	(a)	112,4°	1,389
Acétate d'allyle	East. Kodak p.a.	(a)	103-4°	1,404
Acétate de cyclohexyle	East. Kodak p.a.	(a)	172°	1,442
Acétate de bornyle	East. Kodak p.a.	(a)	114° (22 mm)	1,463
Acétate de benzyle	East. Kodak p.a.	(a)	110° (26 mm)	1,523
Propionate d'éthyle	B.D.H. pure	(a)	99°	1,384
Butyrate d'éthyle	B.D.H. pure	(a)	121,2°	1,391
Monochloracétate d'éthyle	B.D.H. pure	(a)	142–143°	1,429
Glycolate d'éthyle	B.D.H. pure	(a)	159°	1,416
Malonate d'éthyle	Chimie organ. (†)	(a)	96° (15 mm)	1,413
Succinate d'éthyle	Chimie organ.	(a)	104–5° (15 mm)	1,420
Tributyrate de glycéryle	B.D.H. pure		186–7° (10 mm)	1,435
Vinyl méthyl cétone*	Michel	(d)	34° (120 mm)	1,408
Ethylidéne acétone*	Michel	(d)	123–124°	1,435
Isopropényl méthyl cétone*	Michel	(d)	97,5–98°	1,420
Oxyde de mésityle	U.C.B. pure	(a)	57° (55 mm)	1,445
Isophorone	B.D.H. pure	(a)	103° (24 mm)	1,505
Acroléine*	Chimie organ. (†)	(d)	52,5°	1,400
Crotonaldéhyde	B.D.H. pure	(a)	102–102,5°	1,436
Acrylate d'éthyle*	Chimie phys. (*)	(d)	50,5 (30 mm)	1,405
Crotonate d'éthyle	B.D.H. pure	(a)	80° (80 mm)	1,424
Méthacrylate de méthyle*	Chimie phys. (*)	(d)	50° (30 mm)	1,413
$\beta.\beta'$-diméthylacrylate d'éthyle	Chimie organ. (†)	(a)	72–73° (48 mm)	1,440
Maléate d'éthyle	U.C.B. pure	(a)	136–7° (90 mm)	1,439
Fumarate d'éthyle	U.C.B. pure	(a)	133–4° (90 mm)	1,439

(a) Purification par distillation.
(b) Purification en passant par la combinaison bisulfitique et distillation.
(c) Traitement au sulfate ferreux et distillation.
(d) Purification par distillation sur cuivre.
(*) Ces substances, photosensibles, ont été traitées avec grand soin:
(1) La distillation s'est effectuée à l'abri de la lumière.
(2) Plusieurs tubes identiques (3 ou 4) ont été remplis de la même substance,
(3) Un seul enregistrement des raies C=O et C=C était fait sur chaque tube, afin d'éviter les erreurs dues à la polymérisation, nous avons en effet contrôlé pour la vinylméthylcétone et l'acroléine surtout une polymérisation tellement rapide qu'un troisiéme enregistrement des raies précitées présentait déjà une diminution notable de leurs coefficients de diffusion.
(4) L'enregistrement de ces substances s'effectuait dans des conditions spéciales ce que nous permettait la forte intensité des raies C=O et C=C:
constante de temps: 1,5 secondes vitesse de balayage: 25 cm^{-1}/minute
de la sorte, l'enregistrement de la zone spectrale intéressante ($\sim$100 cm^{-1}) prenait 4 min à peine.
(*) Nous remercions de tout coeur le prof. Desreux et ses collaborateurs Delava et Devalériola qui nous ont donné ces produits.
(†) Ces substances nous ont été fournies par le prof. Baudrenghien, nous l'en remercions vivement ainsi que ses deux chefs de travaux Jadot et Huls.

par HARTWELL, RICHARDS et THOMPSON [10] et plus récemment amplifiées par CHIORBOLI [11]. Des mises au point récentes sur la question ont été publiées par LECOMTE [12] et par JONES et SANDORFY [13].

Nous avons jugé utile de renseigner les fréquences dans les tableaux 1 et 3 pour montrer qu'il existe une bonne concordance entre la fréquence Raman moyenne que nous avons mesurée pour les cétones et les esters non substitués soit respectivement 1715 $cm^{-1} \pm 3$ cm^{-1} et 1738 $cm^{-1} \pm 5$ cm^{-1} et les valeurs trouvées en infrarouge; ceci confirme les résultats récemment publiés par LASCOMBE et JOSIEN [14].

Citons encore, à l'examen de ces tableaux, les différents facteurs responsables des déplacements de fréquences et mis en évidence par les auteurs mentionnés ci-dessus:

(1) L'effet de masse des groupements situés sur le carbone du carbonyle est négligeable.
(2) L'effet inductif d'un chlore en position α se marque par une augmentation de fréquence (comparer acétone et chloroacétone, ainsi que acétate et monochloracétate d'éthyle).
(3) L'effet de conjugaison entre le carbonyle et une double liaison éthylénique se traduit par un abaissement de fréquence plus important pour les cétones que pour les esters.
(4) L'effet de tension d'un cycle qui augmente la fréquence s'observe pour la fenchone.

Coefficient de diffusion de la raie C=O

En examinant les substances aliphatiques que nous avons étudiées du point de vue du coefficient de diffusion de la raie de vibration du carbonyle, nous avons été tout naturellement amenés à les répartir en deux catégories, suivant que leur carbonyle est conjugué ou non à une liaison éthylénique. L'exaltation de l'intensité de la raie C=O par suite de conjugaison, a été remarquée depuis longtemps déjà, mais jusqu'à présent aucune étude systématique sur l'intensité de la raie Raman du carbonyle n'a encore été entreprise.

A. *Substances à fonction carbonyle non conjuguée.* Nous avons mesuré le coefficient de diffusion molaire de la raie C=O d'un certain nombre de cétones, d'aldéhydes et d'esters aliphatiques à chaînes droites ou ramifiées, contenant éventuellement une liaison éthylénique non conjuguée ou un groupement benzyle ainsi que quelques cétones cyclaniques.

Les résultats rassemblés dans le tableau 1 nous ont permis de tirer les conclusions suivantes:

(1) Le coefficient de diffusion est relativement constant pour une série homologue de cétones ou d'esters; la valeur moyenne est de $0{,}123 \pm 0{,}005$ pour les cétones et de $0{,}105 \pm 0{,}009$ pour les esters. On peut cependant se demander si la nature du radical alcoolique n'a pas une influence sur le coefficient de diffusion; entre autre, il semble que la longueur de la chaîne du radical alcoolique augmente systématiquement l'intensité de la raie C=O.

Notons que la présence dans la molécule d'une double liaison éthylénique ou

VOL. 10 1957/5

Tableau 1

Cétones aliphatiques	νcm^{-1}	$k_{C=O}$	Esters aliphatiques	νcm^{-1}	$k_{C=O}$
Acétone	1710	0,107	Acétate de méthyle	1742	0,092
Méthyl éthyl cétone	1712	0,120	Acétate d'éthyle	1737	0,104
Méthyl-n-propyl cétone	1716	0,123	Acétate de n-propyle	1740	0,090
Méthyl-isopropyl cétone	1715	0,123	Acétate de n-butyle	1739	0,103
Diéthyl cétone	1716	0,118	Acétate de butyle sec.	1734	0,103
Méthyl-isobutyl cétone	1715	0,131	Acétate d'isobutyle	1731 / 1744	0,109
Di-n-propyl cétone	1716	0,125			
Di-isopropyl cétone	1715	0,129	Acétate d'allyle	1745	0,112
Di-isobutyl cétone	1714	0,133	Acétate de cyclohexyle	1739	0,124
Acétonylacétone	1712	0,248	Acétate de bornyle	1737	0,142
Allylacétone	1716	0,113	Acétate de benzyle	1738	0,115
Benzyl méthyl cétone	1710 / 1721	0,125	Propionate d'éthyle	1735	0,090
			Butyrate d'éthyle	1736	0,105
Méthyl-6-heptène-5-one-2	1719	0,117	Chloracétate d'éthyle	1740 / 1754	0,102
Diacétone alcool	1700 / 1719	0,126	Glycolate d'éthyle	1747	0,123
Monochloracétone	1720 / 1736	0,129	[Oxalate d'éthyle]	1740 / 1762	[0,308]
Moyenne	1715 ±3	0,123 ±0,005	Malonate d'éthyle	1729 / 1745	0,201
			Succinate d'éthyle	1736 / 1766	0,190
			Tributyrate de glycéryle	1740 / 1752	0,310
			Moyenne	1738 ±5	0,105 ±0,009
Cétones cyclaniques.					
Cyclopentanone	1728 / 1743	0,180	*Aldéhyde aliphatique*		
Cyclohexanone	1709	0,200	Butyraldéhyde	1718	0,111
Fenchone	1735	0,218			

d'un cycle aromatique n'amène aucune modification marquante pour autant qu'il n'y ait pas de conjugaison avec le carbonyle.

(2) Le coefficient de diffusion des cétones cyclaniques est nettement plus élevé que celui des cétones à chaînes droites ou ramifiées. Le peu de substances examinées ne permet pas de donner une valeur moyenne.

(3) Le coefficient de diffusion molaire observé est proportionnel au nombre de C=O, pour autant qu'il n'y ait aucune interaction entre eux. Le fait ressort clairement du tableau 2; il faut cependant remarquer l'exaltation de la raie C=O lorsque les carbonyles se trouvent sur des carbones voisins, comme c'est le cas pour l'oxalate d'éthyle (voir tableau 2).

(4) Lorsque la raie du carbonyle est dédoublée, le coefficient global des deux composantes est égal à celui du carbonyle simple. Ce fait semble déjà indiquer que ce dédoublement n'est pas dû à une résonance de Fermi; on ne trouve d'ailleurs pas non plus de raie intense aux environs de la moitié de la fréquence moyenne du doublet.

Tableau 2

Substances	Nombre de C=O	$\Sigma k_{C=O}$	$k_{C=O}$
Monocétone	1	0,123	0,123
Acétonylacétone	2	0,248	0,124
Monoester	1	0,105	0,105
Malonate d'éthyle	2	0,201	0,101
Succinate d'éthyle	2	0,190	0,095
Tributyrate de glycéryle	3	0,310	0,103
Oxalate d'éthyle	2	0,308	0,154

Il semble plûtôt que ce dédoublement soit dû à une isomérie rotationnelle, comme l'ont montré MIZUSHIMA et ses collaborateurs [15] pour la monochloracétone.

B. *Substances à fonction carbonyle conjuguée.* Nous avons groupé dans le tableau 3 les résultats des mesures relatives non seulement à la C=O, mais également à la C=C.

Nous avons tiré les conclusions qui résultent de l'examen de ce tableau en considérant comme l'a proposé HARRANT [5], ces composés comme des dérivés de substitution de l'acroléine:

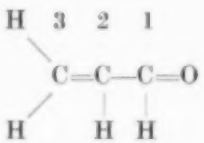

Substances	Substituant en 1	$k_{C=O}$	$k_{C=C}$
Acroléine	—H	0,79	0,38
Vinylméthylcétone	—CH_3	0,64	0,53
Acrylate d'éthyle	—OC_2H_5	0,30	0,68
	Substituant en 2		
Vinylméthylcétone	—H	0,64	0,53
Isopropénylméthylcétone	—CH_3	0,67	0,50
Acrylate d'éthyle	—H	0,30	0,68
Méthacrylate d'éthyle	—CH_3	0,35	0,48

VOL. 10 1957/5

(1) La substitution de l'hydrogène en 1 par un radical alkyle ou alcoyle conduit à une diminution du coefficient de diffusion de la raie C=O et une augmentation de la raie C=C et la substitution subséquente de l'hydrogène 2 par un radical $—CH_3$ produit une variation inverse, mais moins importante.

(2) La substitution du premier H en 3 par un $—CH_3$ se traduit, pour l'aldéhyde, la cétone ou l'ester, par une augmentation importante du coefficient de diffusion de la C=O, comme de la C=C; la substitution du second H en 3 par un autre $—CH_3$ se traduit encore par une augmentation supplémentaire du coefficient de la C=C, mais une diminution de celui de la C=O.

Substances	Nombre de CH_3 en 3	$k_{C=O}$	$k_{C=C}$
Acroléine	0	0,79	0,38
Crotonaldéhyde	1	1,78	1,21
Vinylméthylcétone	0	0,64	0,53
Ethylidène acétone	1	1,13	1,08
Oxyde de mésityle	2	$0,28_2$	2,30
Acrylate d'éthyle	0	0,30	0,68
Crotonate d'éthyle	1	0,53	0,93
β, β'-diméthyl acrylate d'éthyle	2	0,47	1,75

Il est à remarquer que la même augmentation du coefficient de diffusion de la C=C s'observe également dans la substitution progressive des H terminaux par des $—CH_3$ en partant du butadiène [16];

Substances	Formules	$k_{C=C}$
Diméthyl-1-3-butadiène	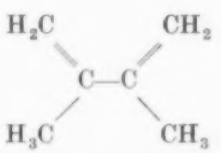	1,83
1-3-hexadiène	$CH_3—CH_2—CH_2=CH—CH=CH_2$	2,53
2-4-hexadiène	$CH_3—CH=CH—CH=CH—CH_3$	3,65
2-5-diméthyl-2-4-hexadiène	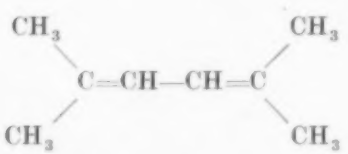	4,78

(3) La substitution d'un H en 3 par un $—COOC_2H_5$ pour l'ester éthylique se traduit par une exaltation de la C=O et de la C=C, dans le cas de l'isomère

trans; pour le dérivé cis, on observe une additivité pour la C=O et une diminution pour la C=C:

	$k_{C=O}$	$k_{C=C}$
Acrylate d'éthyle	0,30	0,68
Maléate d'éthyle (cis)	0,62	0,44
Fumarate d'éthyle (trans)	1,35	1,91

On sait que l'atmosphère des électrons π d'une double liaison possède un plan de symétrie et que le degré de conjugaison entre deux doubles liaisons dépend de la coplanarité de leurs plans de symétrie, dès lors un empêchement stérique peut réduire fortement la conjugaison; on voit ainsi que l'exaltation du coefficient de diffusion des liaisons doubles conjuguées varie parallèlement avec le degré de conjugaison, en effet dans le fumarate d'éthyle, la coplanarité est possible, tandis qu'il y a empêchement stérique dans le maléate.

(4) L'exaltation du coefficient de diffusion de la C=O par introduction dans la molécule d'une liaison ethylénique en position de conjugaison se fait suivant un facteur qui augmente de l'ester, à la cétone et à l'aldéhyde; notons que ce facteur d'exaltation est plus faible si la double liaison conjuguée est en bout de chaîne.

Substances	$k_{C=O}$	Facteur d'exaltation
Ester (moyenne)	0,105	—
Acrylate d'éthyle	0,30	3
Crotonate d'éthyle	0,53	5
Cétone (moyenne)	0,123	—
Vinylméthylcétone	0,64	5
Ethylidène acétone	1,13	9
Cyclohexanone	0,200	—
Isophorone	1,70	8,5
Butyraldéhyde	0,111	—
Acroléine	0,79	7
Crotonaldéhyde	1,78	16

Cette note sera suivie d'un exposé des résultats des mesures de coefficient de diffusion de la raie C=O conjuguée avec les cycles aromatiques et d'une discussion générale des résultats.

Remerciements—Que la patrimoine de l'Université de Liège et le F.N.R.S. trouvent ici tous nos remerciements pour leur aide matérielle sans laquelle ce travail n'aurait pu être mené à bien.

Nous remercions aussi Mr. le Prof. L. D'OR qui nous a facilité le travail par ses encouragements et son aide matérielle.

VOL. 10 1957/5

Tableau 3

Substances	Formules	$\nu_{C=C}$	$k_{C=C}$	$\nu_{C=O}$	$k_{C=O}$
Allylacétone	$CH_2=CH-CH_2-CO-CH_3$	1645	0,35	1716	0,113
Vinylméthylcétone	$CH_2=CH-CO-CH_3$	1618	0,53	1677	0,64
Ethylidène-acétone	$CH_3-CH=CH-CO-CH_3$	1630 1642	0,78 0,30	1672	1,13
Isopropénylméthyl cétone	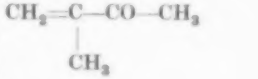	1631	0,50	1678	0,67
Oxyde de mésityle	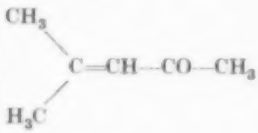	1619 1633	1,90 0,40	1687	0,28
Isophorone	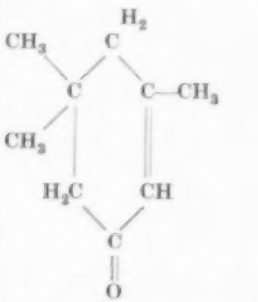	1635	1,74	1667	1,70
Butyraldéhyde	$CH_3-CH_2-CH_2-CO-H$			1718	0,111
Acroléine	$CH_2=CH-CO-H$	1618	0,38	1690	0,79
Crotonaldéhyde	$CH_3-CH=CH-CO-H$	1640	1,21	1684	1,78
Butyrate d'éthyle	$CH_3-CH_2-CH_2-COOEt.$			1736	0,105
Acrylate d'éthyle	$CH_2=CH-COOEt.$	1638	0,68	1721	0,30
Crotonate d'éthyle	$CH_3-CH=CH-COOEt.$	1649 1661	0,93	1718	0,53
Méthacrylate de méthyle		1640	0,48	1722	0,350
β,β'-diméthylacrylate d'Et.	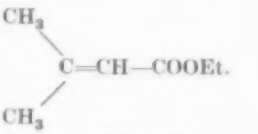	1656	1,75	1706 1715	0,10 0,37
Maléate d'éthyle	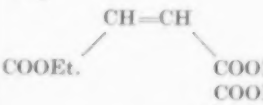	1645 1660	0,44	1727	0,62
Fumarate d'éthyle	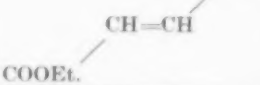	1645 1659	0,59 1,32	1725	1,35

Bibliographie

[1] LESPIAU R. et BOURGUEL M. *Bull. Soc. Chim. Fr.* 1930 **47/48** 1365.
[2] WOLKENSTEIN M. W. *J. Phys. U.S.S.R.* 1941 **5** 185.
[3] RANK D. H. et WIEGAND R. V. *J. Opt. Soc. Amer.* 1946 **36** 325.
[4] SHORIGIN P. P. *Usp. Chim.* 1950 **19** 419;
AKISHIN P. A. et TATEVSKII B. H. *Dokl. Akad. Nauk SSSR* 1951 **76** 527.
SUSCHINSKII M. M. *Izv. Akad. Nauk SSSR* 1947 **11** 341.
[5] HARRANT M. et MARTIN H. *Bull. Soc. Chim. Fr.* 1956 **23** 1383.
[6] MICHEL G. et DUYCKAERTS G. *Spectrochim. Acta* 1957 **8** 356.
[7] MICHEL G. *Spectrochim. Acta* 1952 **5** 218.
[8] FENSKE M. R., BRAUN W. G., WIEGAND R. V., QUIGGLE D., MACCORMICK R. H. et RANK D. H. *Analyt. Chem.* 1947 **19** 700.
[9] BERNSTEIN H. J. et ALLEN G. *J. Opt. Soc. Amer.* 1955 **45** 237.
[10] HARTWELL E. J., RICHARDS R. E. et THOMPSON H. W. *J. Chem. Soc.* 1948 1436.
[11] CHIORBOLI P. *Gazz. Chim. Ital.* 1952 **82** 227; *Ann. Chim. Appl. Roma* 1955 **45** 1193.
[12] LECOMTE J. *Bull. Soc. Chim. Fr.* 1955 **22** 717.
[13] JONES R. N. et SANDORFY C. Chemical applications of spectroscopy. *Technique of Organic Chemistry* Vol. IX. Interscience, New York, 1956.
[14] LASCOMBE J. et JOSIEN M. L. *Bull. Soc. Chim. Fr.* 1955 **22** 1227.
[15] MIZUSHIMA S., SHIMANOUCHI T., MIYAZAWA T., ICHISHIMA I., KURATANI K., NAKAGAWA I. et SHIDO N. *J. Chem. Phys.* 1953 **21** 815.
[16] BRAUN N. G., SPOONER D. F. et FENSKE M. R. *Analyt. Chem.* 1950 **22** 1074.

VOL.
10
1957/5

Spectrochimica Acta, 1958, Vol. 10, pp. 269 to 273. Pergamon Press Ltd., London

Spectroscopic studies on rare-earth compounds—I

Instrumentation

P. KRUMHOLZ
Research Laboratory of Orquima S.A., Sao Paulo, Brazil

(*Received* 1 *August* 1957)

Abstract—A grating spectrophotometer covering the range of 3600–9500 Å with a spectral band width of less than 1 Å and showing excellent reproducibility of the wavelength setting is described. The instrument is provided with a simple device making blank readings nearly independent of the wavelength setting.

Introduction

ABSORPTION spectra of solutions of rare-earth compounds show an almost unique feature among solution spectra of inorganic compounds, by consisting of narrow, partly overlapping bands with half-band widths sometimes as small as a few Å. We were interested for two reasons in exact measurements of such spectra, firstly, in order to compare such solution spectra with the spectra of crystalline rare-earth compounds, and secondly in order to study equilibria in solutions containing rare-earth complexes and ion pairs. For both purposes it was found necessary to use spectral band widths of the order of 1 Å and to be able to reproduce wavelength settings with a precision of a few tenths of an Å. It was further necessary to measure the absorbance with a precision of at least 1 per cent.

Commercially available spectrophotometers, even of the most elaborate design, hardly meet all those requirements, especially that of a very precise reproducibility of the wavelength setting. We decided therefore to build an instrument with the desired characteristics. A grating was chosen as dispersing element owing to the necessity of maintaining the full performance of the instrument up to about 9000 Å. The necessary precision of the wavelength setting was achieved by means of a tangent screw drive operating on a lever arm of sufficient length. As mountings with movable entrance or exit slit permit, for a given wavelength difference, twice the angular displacement of mountings using rotating reflecting elements, the former mounting was chosen.

The instrument described below is of relatively simple design, constructed with commercially available components and meets all the requirements specified above.

Construction of the spectrophotometer. The monochromator of the instrument is built on a similar principle to that described previously [1], but incorporates some important optical and mechanical improvements. Its construction is shown schematically in Fig. 1. The grating (Bausch and Lomb C.P. transmission grating, 32 × 30 mm ruled area, 600 lines per mm, blazed for 5500 Å), the achromatic collimator lens of 275 mm focal length and aperture 1 : 6·5, and the fixed entrance slit and its illuminating system [1] are all mounted on a common lever arm, revolving

around the centre line of the grating. The U-shaped lever arm of stainless steel is welded to a cylindrical block, housing a double row, angular contact, ball-bearing. The bearing shaft is tightly pressed into the bearing and rigidly fixed on the base of the instrument. The lever arm is further supported at a distance of 250 mm

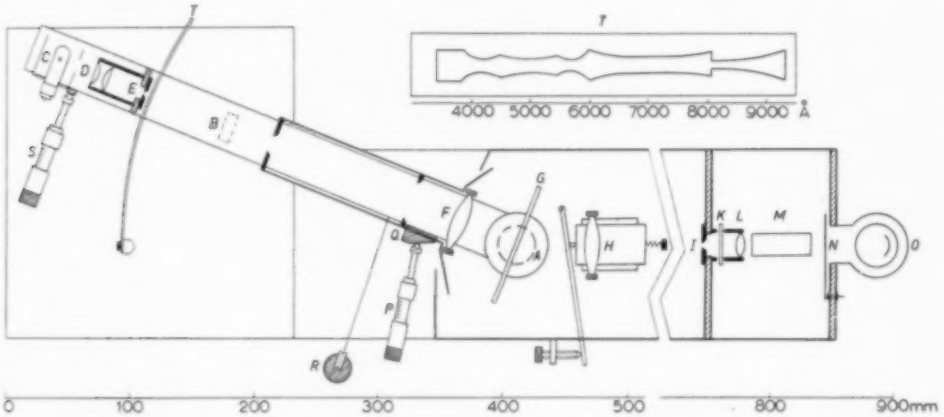

Fig. 1. A—central bearing, B—tangential bearing, C—lamp, D—condenser, E—entrance slit, F—collimator lens, G—grating, H—telescope lens, I—exit slit, K—filter, L—condenser, M—absorption cell, N—shutter, O—photocell, P—micrometer screw, Q—steel piece, R—counter weight, S—auxiliary micrometer screw, T—constant spectral sensitivity diaphragm.

from the centre of rotation by a small ball-bearing, mounted tangentially on the lower side of the lever arm and sliding on a carefully ground and levelled brass plate.

The tangent screw drive consists of a micrometer screw, provided on its top with a carefully centred steel ball of 4 mm diameter, working against the hardened surface of a steel piece, fixed in radial direction on one side of the lever arm. The mounting of the tangent screw is somewhat unconventional, the screw being perpendicular to the steel surface at the extreme long wavelength setting of the instrument. This setting means a greater deviation from the linearity of the wavelength drive than in the conventional centre setting, but permits a full correction of the non-linearity by properly curving the surface of the steel piece. The steel ball contacts the lever arm at such a distance from the centre of rotation (about 85 mm), that one revolution of the micrometer screw, corresponding to a linear displacement of 0·5 mm, corresponds exactly to 100 Å. In order to obtain better reproducibility of the wavelength settings, an auxiliary micrometer screw was set against the lever arm at a distance of about 400 mm from the centre of rotation, so that every revolution corresponds to about 20 Å. As this auxiliary screw covers only a small wavelength range, provision is made for its stepwise displacement.

The telescope lens is identical with the collimator lens and mounted on a dovetail slide, which permits focusing exactly within $\pm 10\ \mu$. The exit slit is of the monolateral type and is reproducible within $\pm 1\ \mu$. The remaining part of the monochromator is similar to that of the instrument previously described [1].

VOL. 10 1957/5

Additional provision was made for thermostatting the absorption cells. The absorption cell carrier is made of massive copper and fixed on a dovetail slide made of a heavy brass plate and provided with channels for circulating water from a thermostat. Temperature may thus be maintained constant within $\pm 0{\cdot}5°$ or better in the range from 3 to 60°.

The photocells used are a R.C.A. 1 P 39, with its base removed, for the visible, and a Cetron C.E. 31 V for the red and near infra-red region. The cells were selected for good reproducibility and low dark current, which amounted to about 10^{-13} A. The photocells are located in brass cylinders, held dry by means of silica gel.

The photocurrent is amplified by means of a 954 acorn tube used in an internally balanced circuit and operated under conditions as specified by NIELSEN [2]. The measuring instrument is a reflecting galvanometer of about 1 μA full-scale sensitivity. The sensitivity of the amplifier is regulated by means of a ten-turn Helipot potentiometer used as an Ayrton shunt of the galvanometer. Over an input range of 100 mV the linearity of the amplifier is better than 0·5 per cent [2] and is further improved to about 0·1 per cent by suitable tilting of the galvanometer scale. Random fluctuations are about $\pm 0{\cdot}1$ per cent of full scale at the highest sensitivity of the amplifier (20 mV full scale with a load resistor of 10^{10} Ω).

Performance of the spectrophotometer

Wavelength calibration. The wavelength scale was calibrated by means of reference spectra emitted by suitable gas discharge tubes. The curvature of the steel piece was adjusted until deviations from the linearity were, in the range from 4000 to 8500 Å, smaller than 2 Å. As the corresponding correction curve showed no discontinuities greater than 0·5 Å, the absolute precision of the wavelength measurements should be within ± 1 Å or better. Wavelength settings can be consistently reproduced within $\pm 0{\cdot}3$ Å, using the principal wavelength drive and within $\pm 0{\cdot}1$ Å, using the auxiliary micrometer screw. The wavelength calibration changed after 1000 hr of operation by less than 2 Å.

Resolution. The effective spectral band width as determined by measurements with suitable line sources [3] is between 0·8 and 1 Å for slit widths of 10 μ. Fig. 2 shows the resolution as well as the reproducibility of the wavelength settings for the group of mercury lines around 3650 Å.

Stray light. Stray light, as determined by means of suitable sharp cut-off light filters [4], is of the order of 0·1 per cent in the region of maximal spectral response. In regions of low-spectral sensitivity of the phototubes it may easily be reduced to this value by means of suitable light filters [1]. If, however, stray light is determined from the apparent deviations from Beers' law [5] of absorption spectra consisting of narrow bands, considerably higher values are found. Deviations from Beers' law as determined with solutions of rare-earth salts indicate a stray light of the order of 0·5 per cent and up to 1 per cent if measurements are performed on very narrow bands, for instance the 4272 Å band of the neodymium ion. This observation indicates that most of the stray light of the monochromator is concentrated near to the wavelength used for the measurement and coincides with similar observations of TUNNICLIFF [6] on such "nearby stray radiation."

In the case of a grating monochromator, it is possible that such a stray radiation originates at least partly from the ghosts of the grating, whose intensity for the special grating now used amounts to about 0·2 per cent of that of the parent line.

Photometric accuracy. The precision of the photometric measurements is essentially limited by the stability of the dark current and of the photocurrent of

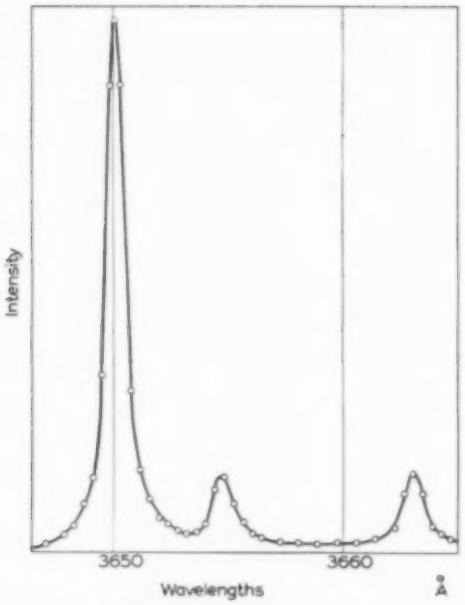

Fig. 2. Emission spectrum of a mercury discharge tube. Lines at 3650·15 Å, 3654·83 Å, and 3663·27 Å.

the phototubes. The dark current, especially that of the red sensitive tubes, increases with increasing illuminations and takes about 30 sec to re-establish its value in the dark. In the region below 6000 Å absorbance values between 0·2 and 1 may be consistently reproduced within $\pm$0·5 per cent. At higher wavelengths the error may be twice as big. The absolute values of the absorbance may be influenced by the geometry of the light path and by stray light. At absorbancies between 0·2 and 0·8 the stray light error should be smaller than 1 per cent, except perhaps for the narrowest bands.

Constant spectral sensitivity device. Measurements of absorption spectra consisting of many narrow bands are extremely tedious if performed as point by point measurements. In order to increase the speed of the measurements we used a simple device, which makes the blank readings nearly independent of the wavelength settings. It consists of fixed diaphragms, placed just behind the entrance slit and cut in such a way as to alter the light flux according to the variable spectral response of the monochromator–photocell combination. In this simple way blank readings can be maintained constant within 1 per cent or better over spectral

VOL.
10
1957/5

ranges of 500–2000 Å. This device should be especially valuable for the rapid location of absorption maxima of low intensity in analytical applications of absorption spectroscopy.

References

[1] Krumholz P. *Rev. Sci. Instrum.* 1951 **22** 362.
[2] Nielsen C. E. *Rev. Sci. Instrum.* 1947 **18** 18.
[3] Hogness T.R., Zscheile F. P., Jr. and Sidwell A.E., Jr. *J. Phys. Chem.* 1937 **41** 379.
[4] Cary H. H. and Beckman A. O. *J. Opt. Soc. Amer.* 1941 **31** 683.
[5] Mellon M. G. *Analytical Absorption Spectroscopy* pp. 247, 275. Wiley, New York 1950.
[6] Tunnicliff D. D. *J. Opt. Soc. Amer.* 1955 **45** 963.

OL.
10
7/58

Spectrochimica Acta, 1958, Vol. 10, pp. 274 to 280. Pergamon Press Ltd., London

Spectroscopic studies on rare-earth compounds—II

A comparative study of the absorption spectra of the neodymium ion in aqueous solution and in crystalline salts

P. KRUMHOLZ
Research Laboratory of Orquima S.A., São Paulo, Brazil

(*Received* 1 *August* 1957)

Abstract—The absorption spectra of aqueous solutions of neodymium perchlorate between 4000 Å and 9000 Å have been measured at 3° using a spectral bandwidth of 1 Å. Several new bands and inflections are reported. A rather pronounced similarity was found between these spectra and the spectrum of crystalline neodymium bromate-enneahydrate.

The absorbancy indexes of the principal absorption maxima of aqueous solutions of neodymium perchlorate were found to depend linearily on the reciprocal of the absolute temperature in the range between 3 and 60°.

IT IS well known [1] that the absorption spectra of solutions of rare-earth salts show a general similarity with the spectra of crystalline rare-earth compounds. More detailed studies have been restricted, however, essentially to the spectra of europium compounds. FREED and co-workers [2] concluded from such studies, that the molecular or ionic environment of the metal ion in solution has an ordered structure similar to that existing in the crystal.

The absorption spectrum of the neodymium ion is particularly sensitive to changes of its ionic or molecular environment. The spectra of solutions of neodymium salts consist, however, contrary to the spectra of europium salts, of rather broad bands and were thus thought to be not suitable for a detailed comparison with crystal spectra. We found, however, that carefully measured spectra of such solutions reveal similarities with the spectra of crystalline neodymium compounds, which are much more pronounced than has generally been admitted.

Whereas the spectrum of the neodymium ion in aqueous solution has been measured by many authors, it has never been obtained with all of its details. PRANDL and SCHEINER [3] determined the wavelengths of the absorption maxima of neodymium chloride up to 7000 Å. The photographic method used can hardly reveal small inflections. The entire spectrum has been measured by HOOGSCHAGEN *et al.* [4], using a photoelectric method. The resolution was insufficient to find all absorption maxima recorded by the previous workers. Moreover, the listed values of the absorbance indices show a systematic error, being about twice the correct values. Fully resolved band structures have been reported only for the band systems around 5200 and 5800 Å by HELLWEGE [5] and by OETJEN [6]. Little attention has been paid, too, in earlier measurements to the influence of the temperature on the absorption spectrum. We found not only a general broadening of the absorption bands [7] but also a considerable decrease of the absorbance values with increasing temperature.

It is the aim of this paper to obtain as full as possible information on the spectrum of the neodymium ion in aqueous solution and to compare it with the spectrum of crystalline neodymium salts. The measurements were performed on solutions of neodymium perchlorate at 3° in order to minimize interactions with the anion and to enhance as far as possible the structure of the absorption bands.

Experimental

Neodymium perchlorate solutions were prepared from neodymium oxide of 99·9 per cent purity. The solutions were 10^{-3} N in free perchloric acid.

The spectroscopic equipment used in this study was described in a previous communication [8]. Measurements were performed with a spectral band width of 1 Å and at an optical depth of 25 mm. The temperature of the solutions was maintained constant within $\pm 0{\cdot}5°$ by circulating thermostated water through the cell holder. The condensation of water-vapour on the cell windows at temperatures below room temperature was prevented by placing silica gel in the cell compartment. Formation of gas bubbles at temperatures above room temperature was prevented by heating the filled absorption cells during 1 hr to a temperature slightly higher than that chosen for the measurements. Concentrations of the solutions were varied between 0·01 and 1 M. Absorbance values were, within the experimental error of 1 per cent, proportional to the concentration, except for the sharpest bands at 4272 and 7316 Å [8]. The spectrum shows a continuous background corresponding to a molar absorbance of 0·01 to 0·02, which might be due to impurities. Wavelength measurements of the sharper absorption maxima should be correct within ± 1 Å [8]. The wavelengths of the inflections, corresponding to hidden bands, were obtained by an appropriate band analysis. The error of the location of the (hidden) maxima is estimated to ± 2 Å for the more pronounced inflections.

Results and discussion

The spectrum of aqueous solutions of neodymium perchlorate, measured between 4000 and 9000 Å at 3° is reproduced in Figs. 1–5. Table 1 lists the wavelengths and the molar absorbance values of the absorption maxima and inflections as compared with the data of PRANDL and SCHEINER [3] and of HOOGSCHAGEN *et al.* [4]. The absorption maxima at 6252 and 7344 Å as well as many inflections have not been recorded previously.

We recorded further in Figs. 1–5 the absorption lines of single crystals of $Nd(BrO_3)_3 \cdot 9H_2O$ as measured by SATTEN [9] at 77°K. The spectrum of the crystal consists of more or less widely separated groups of lines. Similarly, the spectrum of the solution consists of groups of more or less distinct bands.

It is fairly well established [1] that each group of lines in the spectrum of a crystalline rare-earth compound corresponds to a (forbidden) transition between 4*f*-levels of the free ion. It is very probable that this explanation is equally valid for the groups of lines in the spectrum of solutions of rare-earth compounds. "Corresponding" groups of bands (in the spectrum of the solution) and groups of lines (in the spectrum of the crystal) should thus originate from transitions between the same levels of the free ion.

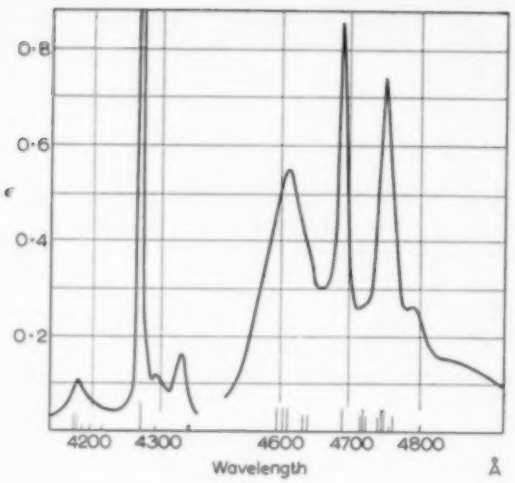

Fig. 1. Absorption spectrum of aqueous solutions of neodymium perchlorate at 3°. Lines on the abscissa represent the lines in the absorption spectrum of single crystals of $Nd(BrO_3)_3 \cdot 9H_2O$ taken from SATTEN's paper [9]. The height of the lines is a relative measure of their intensity.

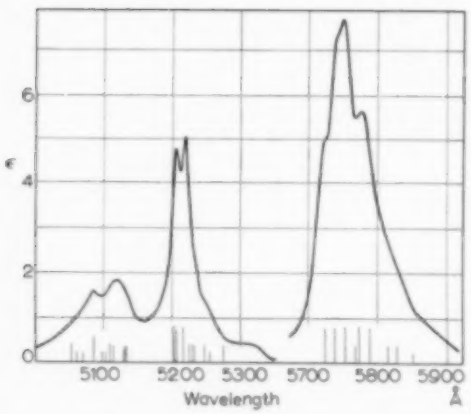

Fig. 2. Absorption spectrum of aqueous solutions of neodymium perchlorate at 3°.

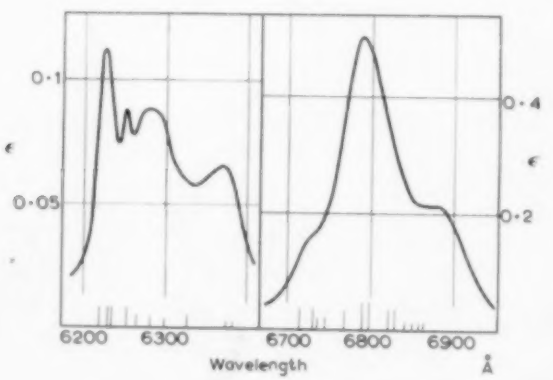

Fig. 3. Absorption spectrum of aqueous solutions of neodymium perchlorate at 3°.

VOL.
10
1957/5

The individual lines in the spectrum of a crystalline rare-earth compound result, according to current explanations [1] essentially from a Stark-effect splitting of the free ion levels in the crystal field. The individual bands in the spectrum of a solution of rare-earth compounds are similarly supposed to result

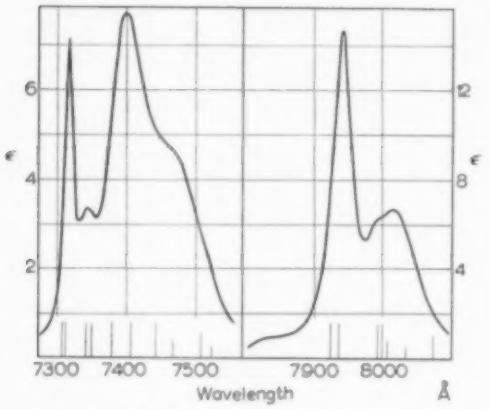

Fig. 4. Absorption spectrum of aqueous solutions of neodymium perchlorate at 3°.

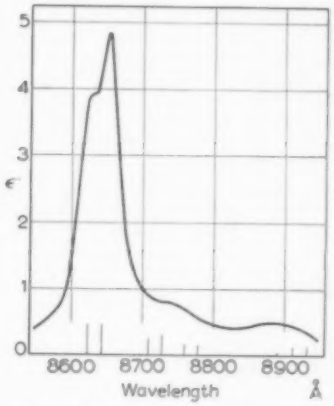

Fig. 5. Absorption spectrum of aqueous solutions of neodymium perchlorate at 3°.

from a splitting of the free ion levels in the field of the neighbouring ions or polar molecules [2].

Figs. 1–5 show that many absorption maxima and inflections in the spectrum of the solution of neodymium perchlorate coincide with individual lines or groups of closely spaced lines in the spectrum of crystalline $Nd(BrO_3)_3 \cdot 9H_2O$. This coincidence appears still clearer in Table 1, where individual lines in the spectrum of the crystal have been tentatively assigned to individual bands in the spectrum of the solution.

Whereas the spectra of other crystalline rare-earth compounds still show a general similarity with the spectrum of the solution, the splitting patterns of the line and band groups are rather different. This follows clearly from Fig. 6, which compares the wavelength of the components of the group around 5800 Å of several crystalline neodymium salts, measured recently by DIEKE and HEROUX [10] at 4°K, with the wavelengths of the components of the corresponding group in the spectrum of the solution. It may thus be concluded that the water molecules around the neodymium ion arrange themselves in the aqueous solution in a definite pattern [2] and that the field produced by this ordered structure is similar to the crystal field in $Nd(BrO_3)_3 \cdot 9H_2O$. The neodymium bromate crystal belongs to the point group C_{6v} [11]. The Zeeman splitting observed on the spectrum of the crystal [10] indicates, however, only trigonal symmetry (C_{3v}) of the crystal field.

A further similarity between the Stark levels in the crystal and in the solution appears in the band group around 4300 Å. This group consists in the spectrum of the solution (see Fig. 1) of a strong and sharp band (half-band width 5 Å) at 4272 Å, accompanied by two weak bands at 4294 and 4331 Å. Furthermore,

Table 1. Wavelengths (λ) and molar absorbance values (ε) of the absorption maxima and inflections (I) of aqueous solutions of neodymium perchlorate at 3°.

λ, Å			ε	λ, Å			ε
(1)	(2)	(3)	(1)	(1)	(2)	(3)	(1)
4182	4182	—	0·11	5740*I*		5740·1	
4200*I*				5752	5752	5754·1	7·7
4272	4272	4273·7	1·3	5779	5784	5776·3	5·6
4282*I*				5820*I*			
4294	4296	4294·7	0·12	6225	6228		0·12
4305*I*				6252		6252·8	0·09
4331	4332		0·16	6275			0·09
4342*I*				6290*I*	6288		
4612	4612	4612·7	0·55	6368	6369		0·065
4640*I*		4639·7		6720*I*			
				6790	6786	6787·7	0·50
4690	4691	4690·7	0·85	6875*I*	6877		
4754	4755	4748·3 } *r*	0·74	7316	7320[a]	7308·9 } *r*	7·15
		4751·3 }				7312·8 }	
4795	4802		0·26	7344		7343 } *r*	3·4
4840*I*						7350·7 }	
5089	5090	5086·5	1·55	7400	7400[a]	7380·7	7·75
5119	5129?		1·85			7408·7	
5206	5207	5202·2 }	4·8	7455*I*			
		5204·6 } *r*		7515*I*			
		5206·9 }		7940	7940[a]	7935·4	14·7
5218	5219	5216·9	5·0	7995*I*	7985[a]		
5240*I*				8012	8010[a]		6·6
5255*I*				8630*I*		8622·6	3·9
5270*I*				8652	8660[a]	8642·5	4·75
5305*I*				8735*I*			
5722*I*	5724	5724·5	5·0	8890	8890[a]		0·5

(1)—this paper. (2)—PRANDTL and SCHEINER [3]. (2a)—HOOGSCHAGEN *et al.* [4]. (3)—tentative assignment of lines in the spectrum of crystalline $Nd(BrO_3)_3 \cdot 9H_2O$ (SATTEN [9]). *r*—barely resolved lines.

Table 2. Temperature coefficients (α), wavelengths (λ), and molar absorbance values at 3° (ε) of the principal absorption maxima of neodymium perchlorate

λ (Å)	$\alpha \times 10^{-2}$	ε	λ (Å)	$\alpha \times 10^{-2}$	ε
4272	4·7	1·3	5752	2·6	7·7
5089	0·9	1·55	7316	4·7	7·15
5119	1·6	1·85	7400	2·0	7·75
5206	3·1	4·8	7940	4·2	14·7
5218	2·7	5·05	8652	4·4	4·75

The values of α are corrected for the thermal expansion of the solutions.

VOL. 10 1957/5

each of these bands shows, as demonstrated in Fig. 7, a weak inflection on the long wavelengths wing, in a distance of about 10 Å from the top of the corresponding band. The relative spacing of those six components corresponds to about 0, 55, 120, 180, 320, and 380 cm^{-1}.

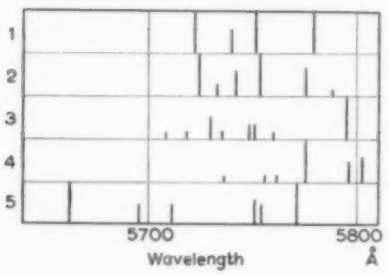

Fig. 6.

Components of the 5800 Å group of the neodymium ion. (1) aqueous solution. (2) $Nd(BrO_3)_3 \cdot 9H_2O$. (3) $Nd(C_2H_5SO_4)_3 \cdot 9H_2O$. (4) $(Nd + La)Cl_3 \cdot 6H_2O$. (5) $2Nd(NO_3)_3 \cdot 3Mg(NO_3)_2 \cdot 24H_2O$. The height of the lines is a relative measure of their intensity.

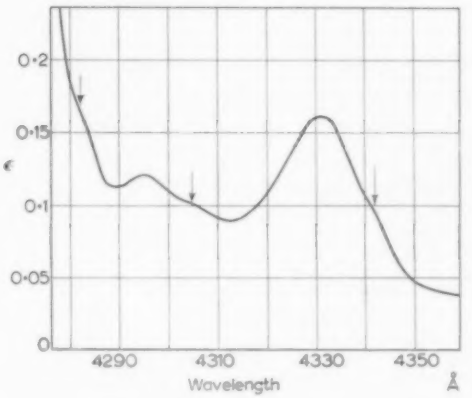

Fig. 7.

Absorption spectrum of aqueous solutions of neodymium perchlorate at 3°. Details of the 4300 Å band system. Arrows indicate inflection points.

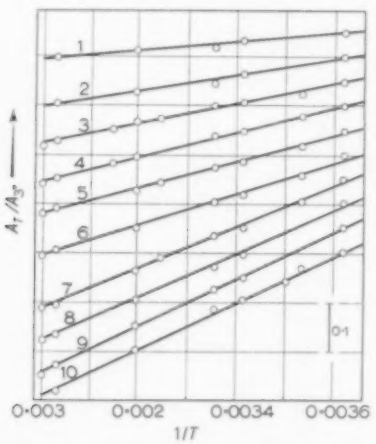

Fig. 8. Temperature dependence of the relative absorbencies, A_T/A_3, at the principal absorption maxima of aqueous solutions of neodymium perchlorate. (1) 5119 Å; (2) 5089 Å; (3) 7400 Å; (4) 5752 Å; (5) 5218 Å; (6) 5205 Å; (7) 7940 Å; (8) 8652 Å; (9) 7316 Å; (10) 4272 Å.

In the spectrum of crystalline $Nd(BrO_3)_3 \cdot 9H_2O$ this group consists [9] of a strong line at 4273·7 Å and three weak lines at 4294·7, 4340·9, and 4344·3 Å. According to SATTEN [9], this group originates from transitions between the ground state ($^4I_{9/2}$) of the neodymium ion, split in the crystal field into five levels at 0,

115, 184, 363 and 382 cm^{-1} and an apparently single upper level. The 184 cm^{-1} level is actually missing in the 4300 Å group, but has been identified by SATTEN [9] in other groups.

The relative spacing of five of the components of the 4300 Å group in solution agrees rather well with the "crystal levels" of the ground state of the neodymium ion. However, the appearance of an additional level at 55 cm^{-1} in the solution spectrum lacks an explanation, and makes it unwise to over-emphasize this agreement.

We determined finally the quantitative dependence of the molar absorbance of the principal absorption maxima of aqueous solutions of neodymium perchlorate upon the temperature. At least within the limited temperature range from 3 to 60° the absorbance may be represented, as shown in Fig. 8, as linear function of the reciprocal of the absolute temperature, according to

$$A_T = A_0\{1 + \alpha(1/T - 1/T_0)\}$$

where A_T represents the absorbance at the temperature T and A_0 its value at a chosen reference temperature, T_0. Table 2 lists the values of the relative temperature coefficient α, for $T_0 = 3°$, for several absorption maxima of aqueous solutions of neodymium perchlorate.

The temperature coefficient is greatest at the corresponding absorption maximum, decreasing rapidly on both wings of the absorption band and finally changing its sign. Thus temperature increase extends the half-band width and broadens the whole absorption band. Accordingly, the total oscillator strengths of an absorption band is less dependent on the temperature than the absorbance index at the absorption maximum.

Acknowledgements—The author is much indebted to Prof. H. STAMMREICH for many valuable suggestions and discussions.

References

[1] YOST D. M., RUSSEL H. and GARNER C. S. JR. *The Rare Earth Elements and Their Compounds*. Wiley, New York 1947.
[2] FREED S. *Rev. Mod. Phys.* 1942 **14** 105.
SAYRE E. V., MILLER D. G. and FREED S. *J. Chem. Phys.* 1957 **26** 109.
[3] PRANDL W. and SCHEINER K. *Z. Anorg. Chem.* 1934 **220** 107.
[4] HOOGSCHAGEN J., SNOEK A. P. and GORTER C. J. *Physica Grav.* 1946 **10** 693.
[5] CHOW Y. K. and HELLWEGE K. H. *Z. Physik*, 1948 **125** 18.
[6] OETJEN G. W. *Z. Naturforsch.* 1949 **4a** 1.
[7] JONES H. C. and STRONG W. W. *Amer. Chem. J.* 1910 **45** 1.
[8] KRUMHOLZ P. *Spectrochim. Acta* 1958 **10** 267.
[9] SATTEN R. A. *J. Chem. Phys.* 1953 **21** 637.
[10] DIEKE G. H. and HEROUX L. *Absorption Spectra and Zeeman Effects of Neodymium Salts at* 4°K. Technical Report NYO 3977. The Johns Hopkins University, Department of Physics, Baltimore 18, Maryland.
[11] DONNAY J. D. H. and NOVACKI W. Crystal data. *Geol. Soc. Amer. Mem.* 1945.

VOL.
10
1957/5

Spectrochimica Acta, 1958, Vol. 10, pp. 281 to 290. Pergamon Press Ltd., London

High-resolution, temperature-dependent spectra of calcite*†

R. M. HEXTER‡
Baker Laboratories, Cornell University, Ithaca, New York

(*Received* 13 *August* 1957)

Abstract—High-resolution absorption spectra of the 2·0–3·5 μ region of a basal section of calcite are reported and analyzed. The resolution was accomplished with a 7500 ruling per inch "Merton-N.P.L." replica grating mounted in place of the Littrow mirror of a Perkin-Elmer Model 13 Spectrometer, with a KBr prism left in place.

A new explanation of some of the observed "splittings" in the 2·0–3·5 μ region is presented and tested. This analysis is similar to that suggested previously as an explanation of observed fine structure in the spectra of crystalline iodoform and brucite. Spectra of calcite were obtained from 78 to 873°K; the observed modifications in the spectra confirm the hypothesis of "librational interaction".

Introduction and discussion of previous work

IN THE early history of infrared spectroscopy, the mineral calcite played an important part in the development of both technique and theory [1–15]. The availability of excellent samples of the mineral and the ease of sampling begged its examination by early spectroscopists. The ease of manipulation of the classical equations of motion of its fundamental unit, the carbonate ion, made for reasonably close agreement between its calculated and observed vibrational spectrum. Moreover, its geometry, made precise with advances in structure determination by X-ray diffraction techniques, together with the early but thorough experimental spectroscopic history [1–15] of the mineral, have made it a touchstone in the application of various modern theories of spectra of the solid state.

The most recent investigation of the spectrum of calcite was that reported by LOUISFERT [16], who obtained new data in the long wavelength region (~30 μ) and also suggested a new assignment for some parts of the very dense 7 μ region of the spectrum of this substance. Very complete analyses of the spectrum were reported in the 1940's by BHAGAVANTAM [17], CABANNES [18], HALFORD [19] and HORNIG [20], while pioneering interpretations [21, 22, 9, 11] preceded these by approximately 20 years.

The major features in the spectrum of calcite were understood by 1926 [8], in that by that date, correct assignment of the more intense bands to the fundamental modes of the carbonate ion had been accomplished. However, as of 1926, the assignment of certain weak bands [11] was at least doubtful, and the curious "doubling" throughout much of the spectrum [20] was not at all well understood. Indeed, the suggestion that the oxygen nuclei of the anion might define an isosceles,

* This research was in part supported by the Office of Ordnance Research, U.S. Army.
† Presented at the Symposium on Molecular Structure and Spectroscopy, The Ohio State University, Columbus, Ohio, June, 1956.
‡ Present address, Mellon Institute, Pittsburgh 13, Pennsylvania.

rather than equilateral triangle, was seriously considered [9] as a possible explanation for this phenomenon. A satisfactory explanation was not in fact forthcoming until various theoretical treatments [17–20] accounted for the effect in terms of the interaction of the motion of the carbonate ion with the motion of the entire lattice of ions of which the crystal is constructed. Some of the features of these interactions can be summarized within a correlation diagram, shown in Fig. 1. In terms of this diagram, the aforementioned "doubling" may be understood in terms of the excitation of binary combinations of the form $\nu(E) \pm R(E), T(E)$,

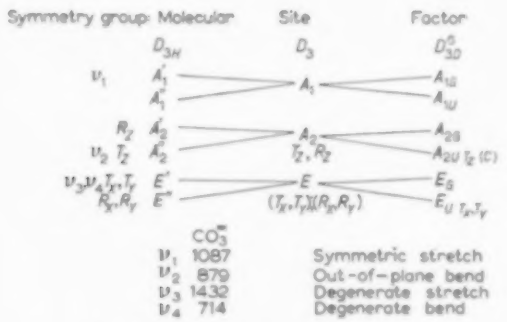

Fig. 1. Correlation diagram for calcite.

in addition to the excitation of the degenerate fundamental $\nu(E)$ itself.* Such combinations have been discussed by HALFORD [19] and by WINSTON and HALFORD [23]. It is possible that the upper state of the additive binary combination, of symmetry $A'_1 + A'_2 + E'$ under the molecular group D_{3h} of the isolated carbonate ion, will be split by the anharmonic coupling of the individual fundamental motions. The transition to the A'_1 level will continue to be inactive; however, in the "site group" approximation [19], transitions to the A'_2 and E' levels, due to the decreased symmetry of the ion's environment in the crystal, can be active. Due to the coupling between the motion of the two unit cell occupants, each of these modes of the site occupant will develop into two unit cell modes, only one of each, however (the ungerade components) being active in the "factor group" approximation [23]. These may then have a separation in frequency due to the original anharmonic coupling of the internal and lattice fundamentals. The upper state of the degenerate internal fundamental, $\nu(E)$, cannot itself be split, nor can the upper or lower state of the subtractive binary combination, $\nu(E) - R(E), T(E)$. However, due to the coupling between the motion of the two unit cell occupants,

* $R(E)$ and $T(E)$ represent doubly degenerate lattice motions of rotational and translational origin, respectively.

* Where V_a = the lattice potential-function, with no interactions with the internal vibrations of the molecules, V_i' = the potential function for the internal motion of individual molecules with no interaction between such motion of various molecules or between such motion and lattice motions, V_{mm}' = the potential energy due to the coupling of the internal motions of different molecules, and V_{ml} = the potential energy due to interaction of lattice and internal motions, and where the zeroth order calculation (upon which V_{ml} is considered a perturbation) is based solely on the first *two* terms of equation (1).

VOL. 10 1957/5

each of the last mentioned levels of the site occupant develops into a gerade and ungerade level of the unit cell. The following transitions are then possible: $\nu_L(E_u) \rightarrow \nu(E_g)$; $\nu_L(E_u) \rightarrow \nu(E_u)$; $\nu_L(E_g) \rightarrow \nu(E_u)$; and $\nu_L(E_g) \rightarrow \nu(E_g)$. Because only $g \leftrightarrow u$ transitions are allowed under the factor group, only the first and third of these may be excited by dipole radiation. Thus, the complex, ν_3, $\nu_3 \pm L(E)$ (where $L(E) = R(E)$ or $T(E)$), may even be observed as a quintet. A thin calcite plate cut parallel to the c axis, inclined at a 30° angle to the propagation vector of the light (under such conditions all allowed transitions, including those polarized along different cystallographic directions, may be observed for this crystal), demonstrates [10], in the vicinity of ν_3, the degenerate stretching mode, four definite sub-maxima and the hint of a fifth.

Another view due to HORNIG [20], predicts that if the term V_{ms} in the potential energy of a crystal,

$$V = V_s + \sum_{[j]}\sum V_j^r + V_{mm'} + V_{ms} \tag{1}$$

is considered as the basis of a perturbation calculation of the crystal energy, that motions of the type $T(E)$ and/or $R(E)$ of the site group D_3 may split the degenerate fundamentals and any overtones or combinations whose species contains a degenerate irreducible representation.

The principal endeavor in the present research has been a high resolution and temperature variation study of the high-frequency bands of calcite in the 2·0–3·5 μ region. This study has given rise to certain revisions in the assignments of these bands, assignments which were originally made during the 1920–1930 period of spectroscopic investigation [7–10] of this substance. The earlier experimental study of this region was of course done with considerably less resolution than is possible today. Nevertheless the rather asymmetric contours of the bands in this region were at least hinted in these spectra, giving rise to the conjecture that the "doubling" characteristic of the lower frequency region (discussed above) remained as a feature of the 2·0–3·5 μ region. Due to the lack of a suitable theory, all shoulders of bands were consequently assigned in a rather arbitrary way.

In the following sections, the results of the present research are reported and interpreted in terms of a model which has been of considerable value in the understanding of complex spectra of crystallographically similar substances [25, 26]. The experimental results demonstrate that the bands under consideration (in the 2·0–3·5 μ region) do *not* have the doublet structure discussed above, but do have a characteristic, temperature dependent, and understandable asymmetry. The earlier assignment of the bands in the 2·0–3·5 μ region is given in Table 1. It will be observed that there are sufficient disagreements between predicted and observed spectra (as to the spectrum of which ray in which the bands may be found) to make the assignments suspect.* Similar disagreements in other spectral regions have been discussed by MATOSSI [11]. Moreover, the band shapes of these lines, and their relative positions with respect to the overtone $2\nu_3$ (whose assignment is unquestioned), were highly reminiscent of similar shapes and relative

* It should be noted that selection rules for combination bands (either between several internal modes or between internal and external modes) are valid insofar as the "factor group" approximation is valid. See Ref. 23, p. 616.

positions with respect to well-identified bands found in previous studies in these laboratories of the infra-red spectra of single crystals of iodoform [25] and

Table 1

Band no.	cm^{-1} (this work)	$\lambda(\mu)$ (this work)	$\lambda(\mu)$ (SCHAEFFER-MATOSSI [24]	Assignment (S and M)†	Species	Predicted ray‡	Observed ray‡
I	4219	2·37	2·30 2·33	$3\nu_3$	$A_1' + A_2' + E'$	Both	o
II	3922	2·55	(2·500) 2·533	$2\nu_3 + \nu_1$	$A_1' + E'$	o	o
II	3546	2·82	(2·74) 2·786	$2\nu_3 + \nu_2$	$A_2'' + E''$	Both	o
IV	3130	3·20	3·04 3·10 3·25*	$\nu_3 + \nu_4 + \nu_1$ $2\nu_1 + \nu_2$	$A_1' + A_2' + E'$ A_2''	Both e	o e
V	2860	3·50	3·33 3·47 3·71*	$2\nu_3$ $3\nu_2$	$A_1' + E'$ A_2''	o e	Both e
VI	2500	4·00	3·87 3·93	$\nu_3 + \nu_1$	E'	o	o

* In extraordinary ray spectrum
† HERZBERG's nomenclature
‡ o = ordinary, e = extraordinary.
( ) Hint

$Mg(OH)_2$ [26]. The crystal structures of these substances belong to the trigonal system, as does that of calcite. Indeed, on a microscopic scale, there are many similarities in the crystal structures of the three substances. This band structure has been heretofore explained [25, 26] as being a branch system in the libration-vibration spectrum of the restricted rotating (librating) molecule—here the carbonate ion.

In the previous studies in this series [25, 26] there have been various experimental difficulties encountered in the performance of temperature variation studies of this branch spectrum. Such studies are important in testing this theory [26], as it predicts the manner of change of band shape and origin. These difficulties have in part been due to unavailability of good samples [$Mg(OH)_2$] and thermal instability [CHI_3]. Calcite withstands both objections: excellent samples may be readily obtained and its thermal and mechanical stability are excellent, even at temperatures as high as 600°C.*†

* We are indebted to the Polaroid Corporation, and especially to Mr. L. W. CHUBB, Jr., of that company, for their very gracious gift of excellent basal sections of calcite.
† At this temperature, the dissociation pressure of calcite is less than 1 mm.

VOL. 10 1957/5

Experimental and spectra

The dispersing element used was a 7500 l.p.i. "Merton-N.P.L." replica grating* installed in place of the Littrow mirror in a Perkin-Elmer Model 13 spectrometer, equipped with a thermocouple detector and a KBr prism, in order

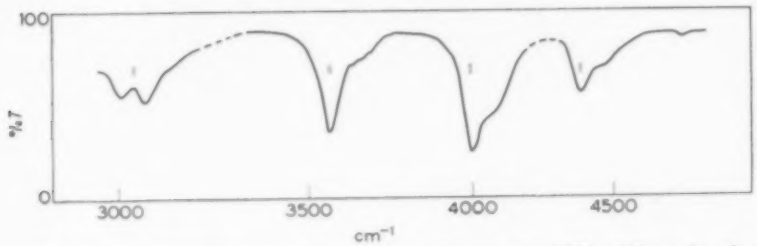

Fig. 2. Absorption spectrum of monocrystalline calcite, 3000–4500 cm^{-1} region. (Room temperature).

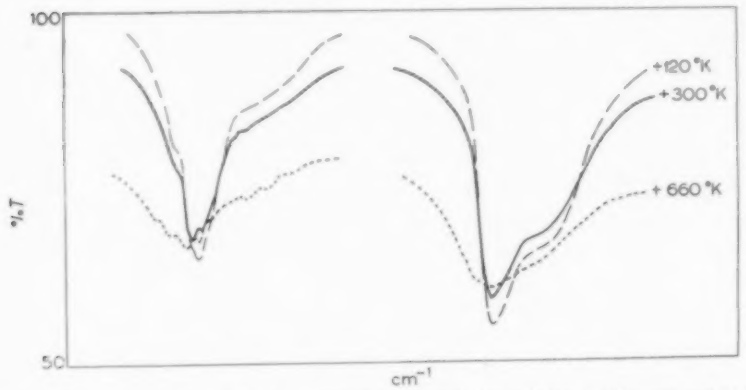

Fig. 3. Temperature-dependent spectra, monocrystalline calcite; 3546 cm^{-1} and 3922 cm^{-1} bands.

that the usual slits and paraboloid could be used. Atmospheric absorption in the 3700 cm^{-1} region was avoided by flushing all housings and sampling spaces of the instrument with Seaford grade nitrogen at a rate of approximately 40 l/min.†

Spectra of the four bands under investigation, with the sample at room temperature, are shown in Fig. 2. High- and low-temperature spectra of two of the four bands are shown in Fig. 3. Spectral slit widths are indicated in Fig. 2. The low-temperature spectra were obtained with a conventional cold cell [27] with the calcite sample sandwiched between two NaCl windows mounted in vacuo on a liquid-nitrogen-cooled brass block, and the high-temperature spectra were obtained with a cell similar in design to that in use some years ago as a hot

* We are indebted to the Light Division, National Physical Laboratories, Teddington, England, for their very gracious gift of this grating.

† To be compared with the rate of 20 l/min used in single beam work by R. C. Lord and T. K. McCubbin *J. Opt. Soc. Amer.* **45** 441 1955.

stage for a melting point microscope [28]. In the cold cell, temperatures recorded were those of the window holding the calcite. In the hot cell, the thermocouple was actually in contact with the crystal. A description of the temperature gradients in such a cell has been given by VOLD and DOSCHER [29]. In all spectra, the sample was a 1·06 mm thick basal section of calcite and the light, while not polarized, was normally incident upon the section.

Results and discussion

Examination of Fig. 2 demonstrates that the band *shapes* of at least three, and possibly all four, of the bands studies are in qualitative accord with the shapes predicted in our earlier article [26] on the theory of these spectra, wherein the envelope was predicted to be given by a Boltzmann distribution among the excited states of a degenerate librator. The *changes* in shape and band origin with temperature, illustrated in Fig. 3, are also in qualitative accord with this theory, which predicts that due to various mechanisms [26] these bands will shade to either high or low frequencies, and upon changing the temperature the band origins will accordingly shift. From the separations of the band origins at room temperature from the band center of $2\nu_3$ at 2860 cm^{-1}, the fundamental libration frequency and its overtones may be calculated [26]. These are shown in Table 2. Examination

Table 2

μ	(cm^{-1})	Separations from $2\nu_3$ center (cm^{-1})	Assignments	Separations between adjacent bands (cm^{-1})
2·37	4219	1359	$2\nu_3 + 270 + 3 \times 416$	297
2·55	3922	1062	$2\nu_3 + 270 + 2 \times 416$	376
2·82	3546	686	$2\nu_3 + 270 + 416$	416
3·20	3130	270	$2\nu_3 + 270$	270
3·50	2860	0	$2\nu_3$	

of the table indicates that there are at least two libration frequencies combining with $2\nu_3$; namely 270 and 416 cm^{-1}. The remaining separations (376 and 297 cm^{-1}) are assigned as the excited levels in the energy level scheme of the 416 cm^{-1} librational fundamental; their decreasing magnitude is a measure of the anharmonicity in this motion.

Other bands whose assignment may be of the same type, but not studied in this research are those reported in the ordinary ray spectrum of calcite [8] at 1755 and 1175 cm^{-1}, and in addition the strong band in the extraordinary ray spectrum [10] at 1587 cm^{-1}. The band at 1755 cm^{-1} has given considerable

VOL.
10
1957/5

difficulty in assignment heretofore [11]. The reasons for this difficulty are the same as those given earlier in this article as objections to the early assignments of the four high-frequency bands experimentally studied here (disagreements between the predicted and observed ray spectrum). The band at 1175 cm^{-1} has had little discussion. If these two bands are assigned as lattice mode combinations with the 1432 cm^{-1} fundamental, the lattice frequencies which result are 323 and 257 cm^{-1}. The third band, whose early assignment [10] MATOSSI [11] has already criticized in this manner, if assigned similarly results in the well-known lattice frequency of 155 cm^{-1} (Table 3).

It remains now to compare these assignments with those made from infra-red investigations of the lattice fundamentals themselves (either from residual ray,

Table 3. Lattice frequencies of calcite

Residual ray [6]	Absorption [12]*	Raman effect [30, 31, 32, 33]	This study
	385 cm^{-1} ?		
	366 ?		
357 cm^{-1} (A_{2u})	338 (A_{2u})	[397] (A_{2u})	416† (A_{2u})
320 (E_u)	310 (E_u)	[344] (E_u)	323‡ (E_u)
		[295] (A_{1u})	
		⟨282⟩ (E_g)	
		[269] (A_{2g})	270† (A_{2g})
			257‡ (A_{2g})
		[260] (E_u)	
{182} (E_u)			
		⟨155⟩ (E_g)	155‡ (E_g)
106 (A_{2u})		⟨106⟩ (A_{2u})	
106 (E_u)		⟨106⟩ (E_u)	
		[99] (A_{2g})	

* Study limited to >280 cm^{-1}.
† In combination with $2\nu_3$.
‡ In combination with ν_3.
{ } Hint
[ ] Calculated
⟨ ⟩ Assumed in calculation
Italicized numbers: observed in Raman effect.

i.e. reflection, studies, or from direct-absorption measurements in the far infrared) or from studies of the Raman effect of calcite. Residual ray studies were made by LIEBISCH and RUBENS [6], and direct-absorption experiments on both single crystals and finely powdered samples were recently accomplished by LOUISFERT [16]. Raman studies were made by GIULOTTO *et al.* [30–33], who in addition solved [33] the classical vibration problem for a single-unit cell of calcite, and thereby predicted the frequencies of lattice motions inactive in the Raman effect. The results of these three investigations are shown in Table 3. In this table, the species assignments for the bands observed in the present study have been made by simply transferring those obtained in the earlier studies where there is near

coincidence of frequencies. This assignment is to be checked below by agreement or lack thereof with "ray prediction".

It should be borne in mind that in general, frequencies found in reflection will be greater than those found in absorption. Furthermore, Haas [34] has shown that in absorption measurements, in general, only powdered samples yield true mechanical frequencies. In addition, it will be observed that one of the lattice

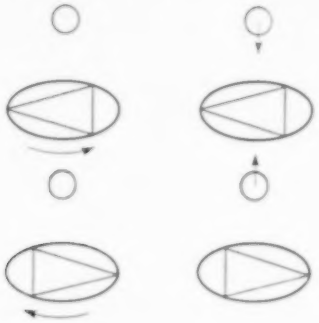

A_{2u} A_{1u}

Fig. 4. The A_{1u} and one of the A_{2u} symmetry co-ordinates of the unit cell of calcite (after Giulotto and Loinger [33]).

VOL. 10 1957/5

frequencies resulting from the present study (416 cm^{-1}) is greater than any of those previously observed or calculated. There is, in addition, some caution necessary in making a direct comparison with Giulotto's calculation [33]. First, the calculation is based upon the motion of the molecules in a single-unit cell, overlooking all coupling effects. Secondly, frequencies reported in reflection (see above) are used in the calculation. Finally, there is some reason to be uncertain whether the mechanics of the problem, as stated, have been set-up correctly, in that the A_{1u} symmetry co-ordinate of Giulotto and Loinger [33] is drawn as is shown in Fig. 4, while one of the A_{2u} co-ordinates (also shown in Fig. 4) certainly should be that for the species A_{1u}, rather than for the species A_{2u}.

The validity of the new assignments presented here for the bands at 4219, 3922, 3546, 3130, 1755, 1587 and 1175 cm^{-1}, as lattice combinations is, as was mentioned above, amenable to still another method of checking; namely, that based on the orientation-dependent selection rules. Predictions of this sort are amenable to confirmation by comparison of the ordinary and extraordinary ray spectra as Matossi [11] first suggested. It should be borne in mind that the ability to make such predictions is subject to the validity of the factor group approximation, which is somewhat questionable in the instance of combination bands [23]. In addition, in order to make a "ray prediction," the species to which the lattice mode belongs must be known, and by virtue of the difficulties mentioned earlier with the only symmetry co-ordinate analysis of this system, species assignment is, at best, tenuous. Nevertheless, if the species of the several lattice fundamentals discussed above are assigned as shown in Table 3, it is interesting to note that the ray prediction for the 2·0–3·5 μ bands (Bands I–IV, Table 1) agree perfectly with

observation. In addition, the results for the 1755, 1587, and 1175 cm^{-1} bands, shown in Table 4, are again in excellent agreement with experiment. Thus, while the lattice frequencies obtained by the present study show some differences with those obtained by previous studies, these new assignments provide impressive

Table 4

Band no.	(cm^{-1}) this work	Species	Predicted ray	Observed ray
VII	1755	$A_{1u} + A_{2u} + E_u$	Both	Both
VIII	1587	$A_{1u} + A_{2u} + E_u$	Both	Both
IX	1175	E_u	*o*	*o*

agreement between the observed and predicted spectra obtained with the crystal in several orientations.

The behavior of the shapes and origins of bands studied, as well as the orientation dependence of their intensities, conform to theoretical prediction. Nevertheless, their assignment as lattice combination bands is not what can be called certain. In another paper in this series [35] similar studies on solid and molten $NaNO_3$ are reported. The crystalline phase of this substance, isomorphous with calcite at room temperature, undergoes a transition at 275°C to a state in which the NO_3^- ions have been reported [36] to be in a state of free rotation. Other studies [37, 38] have indicated that the transition is simply of the order $\rightleftharpoons$ disorder variety which has been discussed by various authors [39, 40, 41], in connection with the motion of polyatomic cations (such as NH_4^+) in solids. These phase transitions (of both first and second order) offer both a means of distinguishing between the two types of disorder, and a conclusive method of verification of the present assignments of the types of bands discussed above.

Acknowledgement—The author wishes to acknowledge many valuable discussions with Dr. David A. Dows during the course of this investigation.

References

[1] Merritt E. *Ann. Phys., Lpz.* 1895 **55** 49.
[2] Konigsberger J. *Ann. Phys., Lpz.* 1897 **61** 687.
[3] Pfund A. H. *Astrophys. J.* 1906 **24** 19.
[4] Coblentz W. W. *Investigations of Infra-red Spectra.* Parts III and IV., p. 65. Carnegie Institution of Washington Publication 1906.
[5] Nyswander R. E. *Phys. Rev.* 1909 **28** 291.
[6] Liebisch T. and Rubens H. *Ber. Dtsch. Chem. Ges.* 1919 **12** 198.
[7] Schaefer C. and Schubert M. *Ann. Phys., Lpz.* 1916 **50** 283.
[8] Schaefer C., Bormuth C. and Matossi F. *Z. Phys.* 1926 **39** 648.
[9] Schaefer C., Matossi F. and Dane F. *Z. Phys.* 1927 **45** 493.
[10] Matossi F. *Z. Phys.* 1928 **48** 616.
[11] Matossi F. *Phys. Z.* 1933 **34** 230.

[12] Randall H. M. and Nielsen H. H. *Phys. Rev.* 1928 **31** 1131.
[13] Plyler E. K. *Phys. Rev.* 1929 **33** 948.
[14] Ellis J. W. *Proc. Nat. Acad. Sci. Wash.* 1930 **16** 315.
[15] Silverman S. *Phys. Rev.* 1932 **39** 72.
[16] Louisfert J. *C. R. Acad. Sci., Paris* 1955 **241** 940.
[17] Bhagavantam S. and Venkatarayudu T. *Proc. Indian Acad. Sci.* A 1939 **9** 224; A **13** 543 1941.
[18] Cabannes J. *Rev. Sci., Paris* 1942 **80** 407.
[19] Halford R. S. *J. Chem. Phys.* 1946 **14** 8.
[20] Hornig D. F. *J. Chem. Phys.* 1948 **16** 1063.
[21] Brester C. J. *Z. Phys.* 1924 **24** 324.
[22] Kornfeld H. *Z. Phys.* 1924 **26** 205.
[23] Winston H. and Halford R. S. *J. Chem. Phys.* 1949 **17** 607.
[24] Schaefer C. and Matossi F. *Das Ultrarote Spektrum* p. 341. Springer, Berlin, 1930.
[25] Hexter R. M. and Cheung H. *J. Chem. Phys.* 1956 **24** 1186.
[26] Hexter R. M. and Dows D. A. *J. Chem. Phys.* 1956 **25** 504.
[27] Wagner E. L. and Hornig D. F. *J. Chem. Phys.* 1950 **18** 296.
[28] Wallace E. H. and Willard M. L. *J. Chem. Educ.* 1931 **8** 706.
[29] Vold M. J. and Doscher T. M. *Industr. Engng. Chem. (Anal.)* 1946 **18** 154.
[30] Giulotto L. and Olivelli G. *J. Chem. Phys.* 1948 **16** 555.
[31] Giulotto L. and Olivelli G. *Nuovo Cim.* 1948 **5** 52.
[32] Giulotto L. and Olivelli G. *Rend. Lat. Lomb.* 1949 **82** 387.
[33] Giulotto L. and Loinger A. *Nuovo Cim.* 1951 **8** 476.
[34] Haas C. *European Molecular Spectroscopy Group. Paper No.* 12. Meeting at Oxford University, July, 1955.
[35] Hexter R. M. *Spectrochim. Acta.* 1958 **10** 289.
[36] Bijvoet J. M. and Ketelaar J. A. A. *J. Amer. Chem. Soc.* 1932 **54** 625.
[37] Ketelaar J. A. A. and Strijk B. *Rec. Trav. Chim. Pays-Bas.* 1945 **64** 174.
[38] Siegel L. A. *J. Chem. Phys.* 1949 **17** 1146.
[39] Frenkel J. *Acta Phys.-chim. URSS.* 1935 **3** 23.
[40] Nagamiya T. *Proc. Phys. Math. Soc. Japan* 1952 **24** 137.
[41] Gutowsky H. S., Pake G. E. and Bersohn R. *J. Chem. Phys.* 1954 **22** 643.

VOL.
10
1957/5

Spectrochimica Acta, 1958, Vol. 10, pp. 291 to 298. Pergamon Press Ltd., London

Infrared spectroscopic investigation of anion rotational disorder in sodium nitrate

R. M. HEXTER*
Baker Laboratory of Chemistry, Cornell University, Ithaca, N.Y.

(*Received* 13 *August* 1957)

Abstract—Absorption spectra in the 5000 to 3000 cm^{-1} region of a basal section of $NaNO_3$ at temperatures of 20°C, 270 and 302, and of molten $NaNO_3$ are reported. Assignments of bands in this region are made as librational combinations with vibrational bands. These bands persist in the temperature range between the second order transition and the melting point, and disappear in the spectrum of the melt. This thermal behavior conclusively eliminates the hypothesis of free rotation of NO_3^- ions above the λ-point; the hypothesis may still be valid for the liquid state. The interpretation of the crystal structure above 275°C as disordered is in harmony with the data here presented.

Introduction

ROTATIONAL or near-rotational motion of polyatomic ions in solids has been studied by a variety of methods, by various investigators, for many years. It is interesting that few attempts have been made to observe the consequences of such motion in a direct manner. It is well known that there are basically two fundamental theories of the nature of such motion: namely, that proposed by PAULING [1] and elaborated by FOWLER [2], NIELSEN [3], DEVONSHIRE [4] and CUNDY [5], and that suggested by FRENKEL [6, 7] and LANDAU [8]. Most experimental work to date in the study of these phenomena has been of an indirect nature. On the one hand, there have been X-ray crystallographic investigations [9, 10, 11, 12, 13] of various kinds, which have endeavored to distinguish between the two types of motion which have been proposed; one of these studies [12] appears to have been definitive in answering the question in a certain class of compounds† in a qualitative manner. On the other hand, recent proton magnetic resonance experiments [14, 15, 16] have very definitely shown that "free rotation [1] cannot be going on in one class of compounds of small molecular weight‡ and in a variety of compounds of moderate and large molecular weight [16]. In the case of the small molecules there remain some difficulties§ which do not permit of certain verification of the Frenkel–Landau model. It should also be mentioned that a still more indirect method has served as an excellent guide to the NMR work—namely, the very precise heat capacity studies of STEPHENSON and his co-workers [17, 18, 19].

"Direct" observations of the motion have been made by HORNIG in the case of the ammonium halides [20] using spectroscopic techniques, and the structural conclusions forthcoming from these studies have been corroborated by LEVY and

* Present address: Mellon Institute, Pittsburgh 13, Pa.
† Those containing relatively heavy anions, such as CN^- and NO_3^-.
‡ NH_4^+ and its isostere, BH_4^-.
§ Reference [15], p. 238.

Peterson [21], using neutron-diffraction techniques. In these studies, it was of course the motion of the polyatomic cation which was under investigation. It is the purpose of this article to report on a similar study of the rotation-like motion of a polyatomic anion—NO_3^-. Similar investigations in the same system were carried out by Pattabhiramayya [22] and Nedungadi [23] using the Raman effect in 1938. Nedungadi compared the low-frequency Raman spectrum of the melt of sodium nitrate with that of the crystal at 290°C. Pattabhiramayya compared the same spectrum of the crystal at 280°C with that of the crystal at temperatures below the transition temperature. It may be concluded from their results [22, 23] that "free rotation" of the NO_3^- ion is not achieved in $NaNO_3$ until at least the melting point is reached.

The existence of a λ-type transition in $NaNO_3$ was first recorded (but not interpreted as such) by Goodwin and Kalmus [24]. The elucidation of the nature of the transition was, in fact, the reason for the X-ray crystallographic studies [9, 10, 11, 12, 13] referred to earlier. Similar transitions take place in various isomorphous and isoelectronic carbonates [13]. The early investigators [9, 10, 11] either postulated free rotation for these rather heavy anions in their high-temperature phases, or recognized that the transition could be of the order–disorder type and that the motion in the high-temperature phase could be torsional rather than rotational but could not distinguish experimentally between the two possibilities. Siegel's [12] work did accomplish the distinction, although, in the sense of the present study, in an indirect manner.

In connection with a related study of the high-resolution infrared spectrum of calcite [25], a study of the temperature dependence of the high-frequency region of the high-resolution infrared spectrum of a single crystal of $NaNO_3$ was undertaken. The two studies were complementary. Because of the presumed torsional origin of the bands studied in calcite, and of their analogs in sodium nitrate, a spectrum of either crystal, recorded at some temperature whereat the motion of the ion is so free as to no longer be deemed torsional, should lack these bands. Such a temperature is most certainly any temperature above the melting points of these substances. The early "indirect" studies referred to above, however, suggested that at temperatures below the melting points but above the λ-points rotation of the ions had already become "free." These temperatures, for calcite and sodium nitrate are, respectively, 975 and 275°C. The dissociation of calcite becomes a problem at temperatures greater than 600°C; this fact, together with the greater ease of reaching the high-temperature phase of sodium nitrate determined the substance chosen for the experiment. The experiment to be done was therefore to record the spectrum of $NaNO_3$ in this region of lattice combination bands at temperatures below and above the λ- and melting-points.

Experimental and spectra

The spectrometer and the special techniques which have been developed in these laboratories for obtaining high-resolution spectra in the 3700 cm^{-1} water vapor region have been described elsewhere [25]. The high-temperature spectra of solid $NaNO_3$ were obtained using the same "hot cell" used in the earlier study of calcite [25]. The samples used in obtaining the spectra of the solid phases were

VOL.
10
1957/5

single basal sections of $NaNO_3$, circular in shape, with diameters of approximately 1 in., and thicknesses of approximately 2 mm.*

Spectra of molten $NaNO_3$ were obtained in a quartz cuvette† similar in design to one described by SUNDHEIM and GREENBERG [26]. The windows for this cell were 2 mm thick sections of Commercial grade quartz furnished by the Amersil Co.‡ This quartz has a transmission coefficient (corrected for reflection loss) of 100 per cent from 2 to 2·70 μ, its absorption band at 2·75 μ amounts to a light loss of only 5 per cent; from 2·85 μ to 3·45 μ the transmission coefficient is 98 per cent, becomes 50 per cent at 4·25 μ and is opaque at 4·85 μ. $NaNO_3$ and silica are, of course, a Lewis acid–base pair, so that after several recordings of the spectrum of the liquid had been made, the inner surfaces of the cuvette were very much clouded; the transmitting qualities of the cell were however not affected by this chemical attack. No attempt was made to record the spectrum of the melt at a carefully controlled temperature; heat was supplied to the base of the cuvette by a small micro-burner at a rate which prevented crystallization *and* decomposition (which may be followed by the evolution of oxygen).§

Results and discussion

Fig. 1 illustrates the envelopes of the four bands under investigation in the spectrum of solid $NaNO_3$ at various temperatures. These bands are assigned analogously to those reported in the previous study of calcite [25]. Due to their overlap of the 3700 cm^{-1} water-vapor region, double-beam methods were used, together with our nitrogen flushing technique [25]. In order to flush the sample space with dry nitrogen, this technique requires the installation of numerous windows in the several covers of the instrument, with a subsequent light loss of such an extent that relatively large slits must be used. As a result, spectral slit widths are quite large relative to those usually obtained with the particular diffraction grating used [25]. The spectral slit widths for the 3125, 3472, 3817 and 4115 cm^{-1} bands shown in Fig. 1 are, respectively, 2·9, 3·7, 4·5, and 5·3 cm^{-1}.

Comparison of the envelopes of these bands in the spectra recorded at room temperature and at 270°C illustrates again our thesis that these are lattice combination bands, in that their envelopes are given by a Boltzmann distribution among the excited states of a degenerate librator [27]. From the separations of the origins of these bands (at room temperature) from the band center of ν_3¶ at 2810 cm^{-1}, the fundamental lattice (libration) frequency and its overtones may be calculated. As in calcite [25], two lattice frequencies are found. These are shown in Table 1(a), and will be discussed in the light of previous studies (Raman

* I am indebted to the Polaroid Corporation, and especially to L. W. CHUBB, Jr., of that company, for their very gracious gift of these samples.

† Fabricated by the Pyrocell Manufacturing Company, New York, New York.

‡ Amersil Company, Inc., Hillside, New Jersey.

§ It should be noted that by virtue of the design of the spectrometer used (a Perkin-Elmer Model 13) wherein the signal is chopped before the sample space, neither the hot cuvette used in obtaining the spectrum of the melt nor the hot cell used in recording the spectrum of the heated crystal contribute any emission background to the spectra. In addition, the hot gases from the microburners do not contribute their emission spectra to the recorder spectrum. Their absorption spectra in the region studied are very weak.

¶ ν_3 is the degenerate stretching mode of the nitrate ion.

effect and Restrahlen) below. We shall say no more about the assignment of these bands at this point except that the validity of the assignment on the basis of the evidence presented so far is as certain (or as uncertain) as that made for calcite [25]. Further confirmation will be based upon the results of the spectra of the high-temperature solid phase and of the melt, to be discussed now.

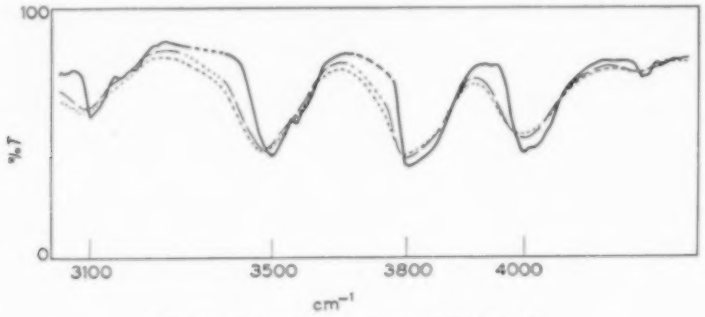

Fig. 1. Absorption spectrum of $NaNO_3$ (*s*).
——— 30°C
– – – – 270°C
..... 302°C

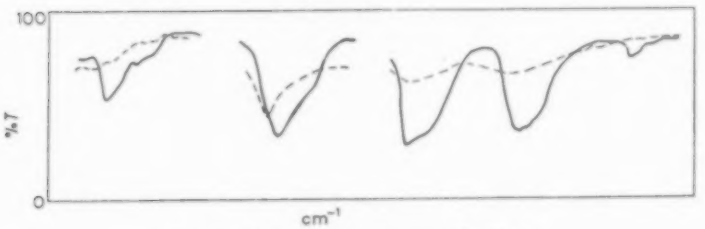

Fig. 2. Absorption spectrum of $NaNO_3$.
——— solid (30°C)
– – – – liquid

Fig. 2 compares the spectrum of the melt with that of the solid at room temperature. It is evident that the bands at 3125, 3817 and 4115 cm^{-1} have disappeared, while that at 3472 cm^{-1} has shifted. This then, supports the assignment of the first three mentioned as lattice combinations, but makes dubious the similar assignment of the last. The dubious nature of the assignment of the 3472 cm^{-1} band requires amendment of Table 1(a). This will also be discussed below in connection with previous studies of the lattice frequencies of sodium nitrate.

Fig. 1 also illustrates the spectrum of the high-temperature phase, as it contains a tracing of the spectrum of the crystal recorded at a temperature just 3° below the melting point. This spectrum differs little from the spectrum of the crystal recorded at 270° (5° below the transition temperature). The small change is in accord with our model of band shape being determined by the Boltzmann distribution among the excited states of a degenerate librator [27]. It is therefore concluded that the high-temperature phase of sodium nitrate unequivocally does not contain freely rotating nitrate ions. The ion, even at room temperature

librates; as the temperature is increased, to be sure, the amplitude of this libration increases. It does not become "free," however, until at least the melting point is reached. This result confirms, then, the conclusions of SIEGEL [12], PATTABHIRAMAYYA [22], and NEDUNGADI [23].*

Lattice frequencies

The procedure outlined above for obtaining the lattice frequencies (by difference from $2\nu_3$) has rendered the two results: 315 cm^{-1} and 347 cm^{-1}. Amendment of Table 1(a), necessitated by the persistence of the 3472 cm^{-1} band in the spectrum of

Table 1(a)

μ	cm^{-1}	Separation from $2\nu_3$ center in cm^{-1}	Separation of neighboring bands in cm^{-1}
2·43	4115	1305	
			298
2·62	3817	1007	
			345
2·88	3472	662	
			347
3·20	3125	315	
			315
$2\nu_3$	2810	0	

the melt, requires that the lattice frequencies be assigned as 315cm^{-1} and 692 cm^{-1} as indicated in Table 1(b). Lattice frequencies for $NaNO_3$ have been previously reported by LIEBISCH and RUBENS [31] and by RAMAN and NEDUNGADI [32]. The first of these was a residual ray investigation while the second was a study of the Raman spectrum. Various authors [33, 34, 35] have classified the several types of "external" modes of the unit cell of calcite or sodium nitrate. Table 2 makes use of their species assignment in summarizing the previous experimental studies.

The assignments for the A_{2u} modes, ν_1' and ν_2' are considered here to be doubtful for two reasons, one theoretical and the other experimental. First, upon inspection of the symmetry co-ordinates developed by GIULOTTO [35], it is difficult to conceive of motions as distinctly different as ν_1' and ν_2'' or as ν_2' and ν_1'' having exactly the same frequency. Second, the observations of ν_1' and ν_2' by LIEBISCH and RUBENS is made in the "extraordinary" residual ray spectrum, which bears a striking resemblance to the ordinary ray spectrum. Now the latter spectrum is unique; it may be obtained in only one way, easily defined. But there

* The persistence of lattice bands in the spectrum of the liquid state is not unknown. SIDOROVA [28] has recorded low-frequency lines in the Raman spectrum of liquid bromoform and acetic acid corresponding to similar lines in the Raman spectrum of the crystalline substances which can only be assigned as lattice frequencies [30]. GROSS and VUKS [29] have also discussed this phenomenon.

Table 1(b)

μ	cm^{-1}	Assignment*	Separation from $2\nu_3$ center (cm^{-1})	Separation of neighboring bands (cm^{-1})
2·43	4115	$2\nu_3 + 2\nu_l + \nu_l'$ or $2\nu_3 + 2\nu_l$	1305	298
2·62	3817	$2\nu_3 + \nu_l + \nu_l'$ or $2\nu_3 + \nu_l + n\nu_l''$	1007	692
3·20	3125	$2\nu_3 + \nu_l$	315	315
$2\nu_3$	2810	$2\nu_3$	0	

* $\nu_l = 315$ cm^{-1} $\quad \nu_l' = 692$ cm^{-1} $\quad \nu_l''$ = unknown

Table 2

Mode*	Species*	I†	R‡
ν_1	$E_g^{(t)}$		189
ν_2	$E_g^{(p)}$		100
ν_1'	$A_{2u}^{(p)}$	71 (?)	
ν_2'	$A_{2u}^{(t)}$	218 (?)	
ν	$A_{1u}^{(t)}$	(inactive)	
ν_1''	$E_{u(1)}^{(t)}$	218	
ν_2''	$E_u^{(p)}$	71	
ν_3''	$E_{u(2)}^{(t)}$	133	
ν_1'''	$A_{2g}^{(t)}$	(inactive)	
ν_2'''	$A_{2g}^{(p)}$	(inactive)	

* Reference [35]
† Reference [31]
‡ Reference [32]

VOL. 10 1957/5

are many types of extraordinary rays. Any spectrum of a uniaxial crystal in which the electric vector is not in a plane perpendicular to the optic axis is an extraordinary ray spectrum. All such spectra will contain *both* A_{2u} *and* E_u components. Only if light is propagated perpendicular to the optic axis *and* has its electric vector in a plane containing the optic axis, i.e. if the spectrum is taken of a section of the crystal perpendicular to a basal section, will the spectrum contain *only* an A_{2u} component. These comments are valid for either absorption or reflection spectra. It is therefore possible that the reported [31] ν_1' and ν_2' are simply ν_2'' and ν_1'' again.

Thus the set of frequencies to be compared with those of Table 1(b), are 71, 100, 133, 189, and 218 cm^{-1}. None of these is as large as the smallest reported here (315 cm^{-1}). Inspection of Table 2 demonstrates that there are at least three and perhaps five previously unreported frequencies (see the preceding paragraph). This was true in the early comparisons of the calcite studies [25] with the early reflection [31] and Raman effect [35] investigations. Long wave length infrared absorption results of calcite have been recently recorded by Mlle. LOUISFERT [36]. She reports two bands (at 366 and 385 cm^{-1}) which are higher in frequency than any of those previously reported in the reflection or Raman studies of calcite. The 315 cm^{-1} lattice frequency for $NaNO_3$ resulting from the present study is therefore not unreasonable. This accounts in a reasonable manner for the lattice combination band at 3125 cm^{-1}. Possible assignments for the bands at 3817 cm^{-1} and 4115 cm^{-1} are given in Table 2b. In this table the lattice frequencies $\nu_l = 315\ cm^{-1}$ and $\nu_l' = 692\ cm^{-1}$ are used, together with an unidentified fundamental, ν_l''.

Conclusions

The incomplete nature of the long wave length infrared studies make provisional the specific assignments presented here. Qualitatively, the assignments of three of the four bands under investigation as lattice combinations are felt to be quite certain, due to their disappearance in the spectrum of the melt. Their persistence in the spectrum of the high-temperature phase of crystalline sodium nitrate confirms the conclusions of SIEGEL [12], PATTABHIRAMAYYA [22], and NEDUNGADI [23] that, in that phase, the NO_3^- ions are *not* freely rotating.

References

[1] PAULING L. *Phys. Rev.* 1930 **36** 430.
[2] FOWLER R. H. *Proc. Roy. Soc.* 1935 **149** 1; 1935 **151** 1.
[3] NIELSEN H. H. *J. Chem. Phys.* 1935 **3** 189.
[4] DEVONSHIRE A. F. *Proc. Roy. Soc.* 1936 **153** 601.
[5] CUNDY H. M. *Ibid.* 1938 **164** 420.
[6] FRENKEL J. *Acta Physicochim. U.R.S.S.* 1935 **3** 23.
[7] FRENKEL J. *Kinetic Theory of Liquids* Chap. II. Oxford University Press, London, 1946.
[8] LANDAU L. *Phys. Z. Sowjet.* 1937 **11** 26, 545.
[9] KRACEK, F. C., POSJNAK E. and HENDRICKS S. B. *J. Amer. Chem. Soc.* 1931 **53** 1183, 2609, 3339.
[10] BIJVOET J. M. and KETELAAR J. A. A. *J. Amer. Chem. Soc.* 1932 **54** 625.
[11] KETELAAR J. A. A. and STRIJK B. *Rec. Trav. Chim. Pays-Bas* 1945 **64** 174.
[12] SIEGEL L. A. *J. Chem. Phys.* 1949 **17** 1146.
[13] LANDER J. J. *J. Chem. Phys.* 1949 **17** 892.

[14] Gutowsky H. S., Pake G. E. and Bersohn R. *J. Chem. Phys.* 1954 **22** 643, 651.
[15] Ford P. T. and Richards R. E. *Disc. Faraday Soc.* 1955 **19** 230.
[16] Andrew E. R. *J. Chem. Phys.* 1950 **18** 607.
[17] Stephenson C. C., Landers L. A., and Cole A. G. *J. Chem. Phys.* 1952 **20** 1044, 1046.
[18] Stockmayer W. H. and Stephenson C. C. *J. Chem. Phys.* 1953 **21** 1311.
[19] Stephenson C. C., Rice D. W. and Stockmayer W. H. *J. Chem. Phys.* 1955 **23** 1960.
[20] Wagner E. L. and Hornig D. F. *J. Chem. Phys.* 1950 **18** 296, 305.
[21] Levy H. and Peterson S. W. *J. Amer. Chem. Soc.* 1953 **75** 1536.
[22] Pattabhiramayya P. *Proc. Indian Acad. Sci.* A 1938 **7** 229.
[23] Nedungadi T. M. K. *Proc. Indian Acad. Sci.* A 1938 **8** 397.
[24] Goodwin H. M. and Kalmus H. T. *Phys Rev.* 1909 **28** 1.
[25] Hexter R. M. *Spectrochim. Acta* 1957 **10** 279.
[26] Sundheim B. R. and Greenberg J. *Rev. Sci. Instrum.* 1956 **27** 703.
[27] Hexter R. M. and Dows D. A. *J. Chem. Phys.* 1956 **25** 504.
[28] Sidorova A. I. *Acta Physicochim. U.R.S.S.* 1937 **7** 193.
[29] Gross and Vuks *Nature, Lond.* 1935 **135** 100, 431, 998.
[30] Hexter R. M. and Cheung H. *J. Chem. Phys.* 1956 **24** 1193.
[31] Liebisch T. and Rubens H. *Ber. Dtsch. Chem. Ges.* 1919 **12** 198.
[32] Raman C. V. and Nedungadi T. M. K. *Nature, Lond.* 1939 **143** 679.
[33] Cabannes J. *Rev. Sci. Paris* 1942 **80** 407.
[34] Mathieu J. P. *Spectres de Vibration et Symetrie des Molecules et des Cristaux* p. 461. Hermann et Cie, Paris 1954.
[35] Giulotto L. and Loinger A. *Nuovo Cim.* 1951 **8** 475.
[36] Louisfert J. *C. R. Acad. Sci., Paris* 1955 **241** 940.

VOL.
10
1957/5

Spectrochimica Acta, 1958, Vol. 10, pp. 299 to 306. Pergamon Press Ltd., London

Infrared spectra of silyl and silyl-d_3 cyanides*

H. Richard Linton and Eugene R. Nixon
Department of Chemistry, University of Pennsylvania, Philadelphia, Pennsylvania

(*Received* 25 *June* 1957)

Abstract—The infrared spectra of silyl and silyl-d_3 cyanides in the gaseous state have been examined over the region from 300 to 3500 cm^{-1}. In each case seven of the eight fundamental vibrations are observed directly; the low frequency skeletal bending fundamental is inferred from its first overtone. Coarse rotational structure of two of the perpendicular fundamentals of SiH_3CN are analyzed in terms of the Coriolis coefficients. Isotopic shifts produced by ^{13}C and ^{15}N in the CN stretching mode of SiD_3CN provide strong evidence for the normal cyanide structure rather than the earlier postulated *iso*cyanide form.

Introduction

It was demonstrated long ago by Gautier [1] that methyl iodide and silver cyanide react at 120°C to form an addition compound which, when treated with aqueous KCN solution, produces a good yield of methyl *iso*cyanide. McBride and Beachell [2] have carried out the reaction between $(CH_3)_3SiI$ and AgCN and found that the product readily adds one atom of sulfur, a fact which they claim is proof for the trimethylsilyl *iso*cyanide structure. More recently MacDiarmid [3] has examined the product obtained by passing SiH_3I vapor through a charge of AgCN. While none of the chemical or physical properties reported by him provides any proof of the structure, MacDiarmid concluded that by analogy with the methyl case it was reasonable to assume the product to be silyl *iso*cyanide.

We have attempted to react sulfur with the compound described by MacDiarmid but have found that no reaction occurs at room temperature and that excessive decomposition takes place at higher temperatures. However, in the infrared study reported in this paper we believe that rather clear-cut evidence for the normal cyanide structure is presented. For this reason we have interpreted our spectra in terms of that model.

Silyl cyanide is a symmetric top with C_{3v} symmetry. To calculate the approximate moments of inertia, we have assumed the following geometry: tetrahedral angles in the SiH_3 group; an SiH distance of 1·48 Å, the value reported for SiH_3D and SiH_3X [4]; a CN distance of 1·16 Å, the microwave value in CH_3CN [5]; and an SiC distance of 1·87 Å, an average value from a number of different compounds [6]. The calculated moments are $I_A = 9{\cdot}78 \times 10^{-40}$ and $I_B = I_C = 172{\cdot}5 \times 10^{-40}$ g cm^2 and the corresponding rotational constants are $A = 2{\cdot}86$ and $B = C = 0{\cdot}162$ cm^{-1}. From the results of Gerhard and Dennison [7], one would expect each of the four parallel A_1 fundamental vibrational bands to exhibit a Q branch with an intensity of not more than about 5 per cent of that of the entire band and a spacing of 17·4 cm^{-1} between the P and R maxima. The spacing of the individual

* Taken from a thesis to be presented by H. Richard Linton in partial fulfillment of the requirements for the Ph.D. degree in the Graduate School of the University of Pennsylvania.

lines within the P and R branches will be approximately $2B$ (0·32 cm^{-1}), too small to be resolved in the present study.

The four degenerate E fundamentals should each display a series of zero lines (Q branches of the sub-bands) with alternating intensities "strong, weak, weak, strong, . . ." and if the dependence of the rotational constants upon vibrational state is neglected, the frequencies of these Q lines will be given by the formula [8],

$$\nu_0(Q_K) = \nu_0 + [A(1 - 2\zeta) - B] \pm 2[A(1 - \zeta) - B]K \quad (1)$$

where ζ is the Coriolis coefficient and ν_0 is the band center. It follows then that

$$A(1 - \zeta) - B = ({}^RQ_K - {}^PQ_K)/4K \quad (2)$$

Cowan [9] has shown that for the four E vibrations,

$$\zeta_5 + \zeta_6 + \zeta_7 + \zeta_8 = B/2A + 1 \quad (3)$$

With SiD_3CN the same angles and internuclear distances give $A = 1{\cdot}43$, $B = C = 0{\cdot}148$ cm^{-1} and a value of 17·2 cm^{-1} for the P–R spacing in the parallel bands.

Experimental

Silyl cyanide was prepared by the method described by MacDiarmid [3] and purified by fractional distillation in a cold trap system. At the highest gas pressure used in the infrared spectra we detected just one extraneous absorption band. This band, at 1107 cm^{-1}, was doubtless due to disiloxane [10], which is formed along with HCN in the hydrolysis of SiH_3CN. Repeated fractionation reduced the intensity of the band to an undetectable level.

The preparation of SiD_3CN followed the same procedure except that D_2O (99·6 per cent pure) and $LiAlD_4$ (unstated purity) were used in making the intermediate SiD_3I. We estimate the isotopic purity of the final product as 97–98 per cent. At 0°C the vapor pressure of our SiD_3CN was 3·75 cm, compared with a value of 4·15 cm for the SiH_3CN. Several weak bands in the spectrum of the deuterated cyanide, discussed below, were reduced in intensity, though not completely eliminated, by fractionation.

The spectra were recorded on a Perkin–Elmer single-beam, double-pass spectrometer with LiF, NaCl, KBr and CsBr prisms. The 10 cm gas cells were of glass fitted with either KBr or polyethylene windows. Our results are plotted in Figs.1 and 2 and summarized in Table 1.

A_1 fundamentals of SiH_3CN

The parallel A_1 fundamentals comprise the symmetric SiH stretch ν_1, the CN stretch ν_2, the symmetric SiH_3 deformation ν_3 and the SiC stretch ν_4.

Both ν_1 and ν_2, in addition to the perpendicular SiH stretch ν_5, lie in the 2200 cm^{-1} region. From the intensity distribution (see Fig. 1) it would appear that either ν_1 and ν_2 are nearly coincident or that one of them is appreciably weaker than the other. Now in SiD_3CN both ν_1 and ν_5 are shifted to about 1600 cm^{-1} leaving ν_2 as the band at 2212 cm^{-1} and as nearly as we can judge ν_1 and ν_2 are of comparable intensities and each is perhaps half as intense as ν_5. Further, the

VOL. 10 1957/5

symmetric SiH stretching modes in silyl flouride, chloride and bromide all fall within the range 2200–2206 cm^{-1} [11]. It is in fact possible to account satisfactorily for the shape of the 2200 cm^{-1} absorption in SiH_3CN by assuming

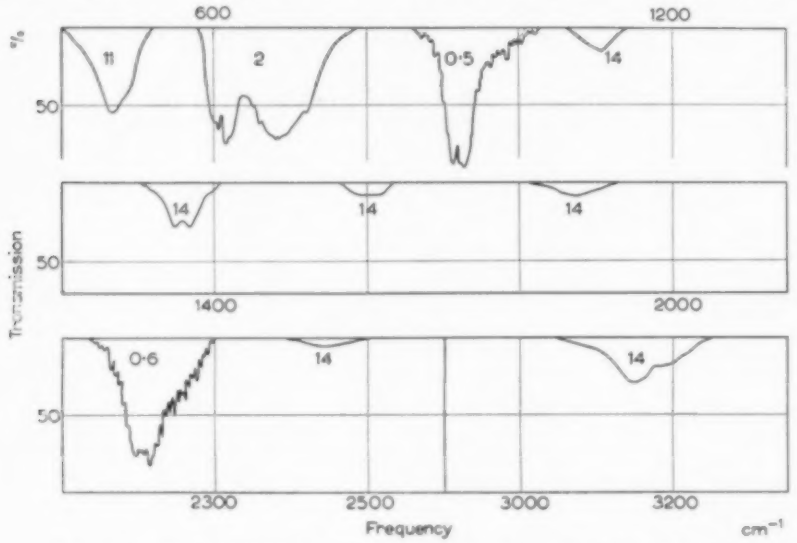

Fig. 1. Infrared spectrum of SiH_3CN in the gas phase at 28°C. Gas pressures (cm) in 10 cm cell shown in figure.

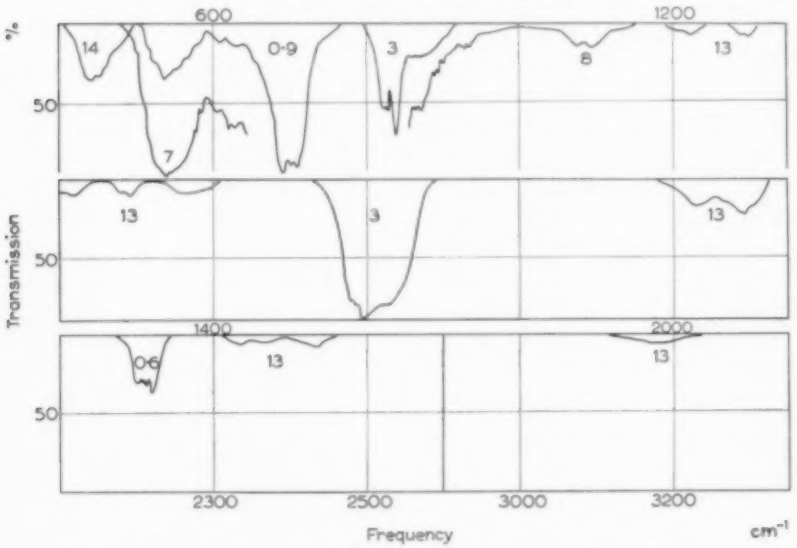

Fig. 2. Infrared spectrum of SiD_3CN in the gas phase at 28°C. Gas pressures (cm) in 10 cm cell shown in figure.

the center of one parallel band near 2205 and the center of another parallel band of about equal intensity at about 2210 cm^{-1}. Since ν_2 in SiH_3CN should lie at

Table 1. Vibrational assignments for SiH_3CN and SiD_3CN

Assignment	SiH_3CN freq. (cm^{-1})	Rel. int.	SiD_3CN freq. (cm^{-1})	Rel. int.
$2\nu_8(A_1 + E)$	469	*m*	442	*m*
	601 *P*		585 *P*	
$\nu_4(a_1)$	608 *Q*	*s*	592 *Q*	*m*
	617 *R*		605 *R*	
$\nu_7(e)$	682	*s*	542	*s*
	913 *P*		691 *P*	
$\nu_3(a_1)$	920 *Q*	*vs*	701 *Q*	*vs*
	928 *R*		709 *R*	
$\nu_8(e)$	941	*s*	(675)	*s*
	1352 *P*		1072 *P*	
$2\nu_7(A_1 + E)$	(1362) *Q*	*w*	1081 *Q*	*w*
	1372 *R*		1089 *R*	
$\nu_3 + \nu_7(E)$ or $\nu_6 + \nu_7(A_1 + E)$	1608	*w*	1215	*w*
$2\nu_6(A_1 + E)$ or $\nu_3 + \nu_6(E)$	1880	*w*	1365	*w*
			1580 *P*	
$\nu_1(a_1)$	(2205)	*s*	1588 *Q*	*s*
			1596 *R*	
			2201 *P*	
$\nu_2(a_1)$	(2212)	*s*	2212 *Q*	*s*
			2219·5 *R*	
$\nu_5(e)$	2227·0	*vs*	(1624)	*s*
$\nu_2 + \nu_8(E)$	2436	*w*	2435	*w*
$\nu_3 + \nu_5(E)$	3135	*w*		
$\nu_{1,2,5} + \nu_6$	3165	*w*		
$\nu_1 + \nu_5$			3175	*w*
unassigned			829	*s*
unassigned			(865)	*m*
unassigned			1290	*w*
unassigned			2035	*w*
unassigned			2095	*w*
unassigned			2332	*w*
unassigned			2370	*w*

VOL. 10 1957/5

least as high as ν_2 in SiD_3CN, we shall somewhat arbitrarily assign ν_2 at 2212 cm^{-1} and ν_1 at 2205 cm^{-1}. Higher resolution is obviously necessary to locate these band centers with more certainty.

The SiH_3 deformation ν_3 is assigned as the parallel band at 920 cm^{-1}. In the silyl halides [11] the comparable vibration lies in the range 930 to 990 cm^{-1}.

The final A_1 vibration, the SiC stretch ν_4, is assigned to the strong parallel band at 608 cm^{-1}. It might be noted that this frequency is somewhat lower than the values (640–764 cm^{-1}) assigned to the symmetric stretches in the methyl chlorosilanes [12].

E fundamentals of SiH_3CN

The antisymmetric SiH stretch ν_5 is clearly the perpendicular band near 2200 cm^{-1} which exhibits the expected alternation of intensities of the Q branches. Judging from the band contour, we place the ${}^RQ_0$ line at 2229·5 cm^{-1} as shown

Table 2. Rotational analysis of the 2227·0 cm^{-1} band of SiH_3CN

K	${}^RQ_K$	${}^PQ_K$	$({}^RQ_K - {}^PQ_K)/4K$
0	2229·5		
1	2234·6	2224·5	2·53
2	2240·0	2219·3	2·59
3	2245·2	2214·1	2·59
4	2250·1	2209·0	2·57
5	2255·0	2202·3	2·64
6	2260·0	2197·3	2·61
7	2264·8	2192·0	2·60
8	2269·3	2186·8	2·58
9	2274·5	2180·3	2·62
10	2278·8	2175·3	2·59
11	2283·4	2169·5	2·59
12	2288·5	2163·3	2·61
13	2293·4	2158·0	2·60
14	2298·0	2152·5	2·60
		Average	2·59

in Table 2. Equation (2) with the calculated rotational constants and the average value of $({}^RQ_K - {}^PQ_K)/4K$ gives +0·04 for the Coriolis coefficient ζ_5. In the analogous SiH stretching mode in SiH_3I [13] the coefficient is +0·02. The calculated band center of ν_5 falls at 2227·0 cm^{-1}.

The SiH_3 deformation ν_6 overlaps the more intense ν_3 and while a number of the Q lines are well resolved, the region of the band center is more obscure. The ${}^RQ_0$ line is either at 961·5 or at about 944·5 cm^{-1}. We favor the second choice chiefly because the resulting assignments (Table 3) lead to a more nearly constant value for $({}^RQ_K - {}^PQ_K)/4K$. The average value of this latter quantity yields $\zeta_6 = -0{\cdot}16$ and the band center at about 941 cm^{-1}. In SiH_3I the corresponding Coriolis coefficient is −0·20.

There is little indication of Q line structure in the SiH_3 rocking vibration ν_7 at 682 cm^{-1}, although the small absorption maxima at 659, 678, 682 and 719 cm^{-1} suggest some unresolved fine structure. It follows from equations (1) and (2) that the sum of the average Q branch spacings in the four E bands is

$$\sum \Delta\nu_i = 6A - 9B = 15{\cdot}7 \text{ cm}^{-1} \tag{4}$$

Since $\Delta\nu_5 = 5{\cdot}18$ and $\Delta\nu_6 = 6{\cdot}30$ cm^{-1}, this leaves only 4·2 cm^{-1} as the sum of $\Delta\nu_7 + \Delta\nu_8$. The Coriolis coefficient ζ_8 must certainly be close to +1. It would

Table 3. Rotational analysis of the 941 cm^{-1} band of SiH_3CN

K	${}^RQ_K$	${}^PQ_K$	$({}^RQ_K - {}^PQ_K)/4K$
3	961·5		
4	968·3		
5	975·0		
6	983·0		
7	989·0		
8	995·8	895·5	3.14
9	1002·0	888·5	3·15
10	1008·3	882·0	3·16
11	1014·5	875·5	3·16
12	1020·5	869·5	3·15
13	1027·5	863·0	3·16
14	1032·5	857·0	3·13
15	1038·8	849·5	3·16
16	1045·0	843·0	3·16
17	1051·1	835·8	3·17
18	1056·0	829·0	3·15
		Average	3·15

be exactly unity for the bending mode of the linear SiCN skeleton and in fact it has values of +0·95 and +0·94 in CH_3CN [14] and CH_3NC [15] respectively. If we assume $\zeta_8 = +0{\cdot}95$ in SiH_3CN, then $\zeta_7 = +0{\cdot}20$, the same value as reported for the corresponding coefficient in SiH_3I. The average spacing $\Delta\nu_7$ should then be about 4·3 cm^{-1}, probably close to the limit of resolution in this region.

Finally the SiCN bending mode ν_8 lies beyond the spectral range covered here. We assign the perpendicular band at 469 cm^{-1} as $2\nu_8$, which would place the fundamental itself at about 235 cm^{-1}.

As may be seen from Table 1, the several weak bands in the spectrum can all be accounted for satisfactorily as overtones or combinations, although in some instances there is more than one possible assignment. A shoulder on the high frequency side of the R peak in the band at 608 cm^{-1} may be due to a weak overlapping band.

Spectrum of SiD_3CN

The SiD stretching modes ν_1 and ν_5 overlap in the 1600 cm^{-1} region (Fig. 2). Since the P and R maxima of ν_1 are discernible, it is possible to place the band

VOL. 10 1957/5

center at close to 1588 cm^{-1}. From the intensity distribution the center of ν_5 must be about 1624 cm^{-1}. The strong parallel band at 2212 cm^{-1} is clearly ν_2. We assign the SiD_3 deformations ν_3 and ν_6 at 701 and 675, the SiC stretch ν_4 at 592, the SiD_3 rocking at 542 and finally $2\nu_8$ at 442 cm^{-1}. The assignments are summarized in Table 1. Application of the Teller–Redlich product rule to the observed fundamentals yields the following results:

A_1 vibrations

$$(1588)(2212)(701)(592)/(2205)(2212)(920)(608) = 0{\cdot}535$$

$$\text{harmonic value} = 0{\cdot}515$$

E vibrations

$$(1624)(675)(542)(221)/(2227)(941)(682)(235) = 0{\cdot}391$$

$$\text{harmonic value} = 0{\cdot}380$$

In the case of the deuterated compound there is no resolvable fine structure in the perpendicular bands.

At the bottom of Table 1 are listed several unassigned bands which appeared in the spectrum of SiD_3CN. Each of these decreased in relative intensity with repeated fractionation of our sample. For this reason it does not seem likely that they are due to simply partially hydrogenated cyanide. The identity of the impurities causing these absorptions is unknown and the band at 829 cm^{-1} is especially puzzling because of its large intensity.

In order to clarify the actual structure of our molecule, we have measured the shifts in the CN stretching frequency produced by the isotopic substitution of ^{13}C and ^{15}N. A sample of SiD_3CN containing about 10 at. per cent of ^{13}C and another sample enriched to about the same extent with ^{15}N were prepared and each was examined both as a gas at room temperature and as a polycrystalline film at liquid air temperature. The results are plotted in Fig. 3.

To calculate the expected shifts, we have treated the molecule as a linear triatomic, taking the SiD_3 group as a single atom. The reason for choosing to examine this effect in SiD_3CN rather than in SiH_3CN is that in the former case the SiC and CN stretching frequencies are fairly well separated from the other two A_1 vibrations. From the two observed frequencies 592 and 2212 cm^{-1}, we have evaluated the two harmonic stretching-force constants in our triatomic model and then calculated the shifts in the 2212 cm^{-1} vibration. For the normal cyanide, the calculated shifts are -51 cm^{-1} for ^{13}C and -31 cm^{-1} for ^{15}N. On the other hand, the *iso*cyanide gives shifts of -43 cm^{-1} for ^{13}C and -38 cm^{-1} for ^{15}N. Admittedly our model is a rather crude one but the calculated shifts, being differences in frequencies, should be more reliable. In fact we have demonstrated that the calculated shifts are not very sensitive to the frequencies assumed for the stretching vibrations.

Fig. 3 shows that the observed shifts produced by ^{13}C are -51 cm^{-1} in both the gas and the solid. With ^{15}N the shift in the solid is -32 cm^{-1} and while overlapping of bands occurs in the gas, the shift is certainly just about -30 cm^{-1}. We consider these results as very strong evidence for the normal cyanide rather than the *iso*cyanide structure.

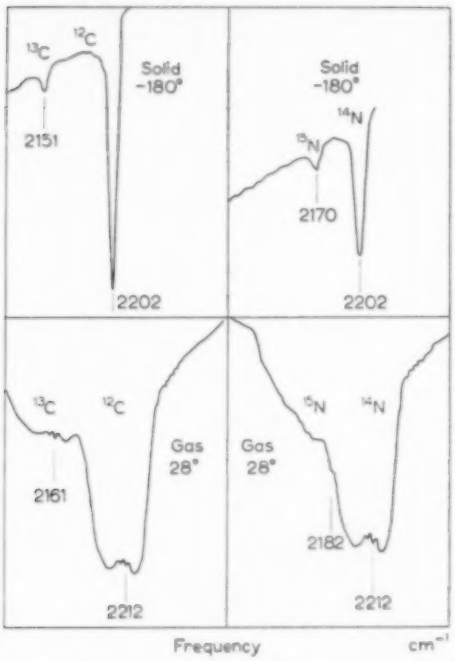

Fig. 3. The CN stretching vibration in isotopically enriched samples of SiD_3CN.

Acknowledgements—We wish to acknowledge the advice and aid of Dr. A. G. MacDiarmid in the preparation and purification of our compounds. One of us (H. R. L.) acknowledges his gratitude to the Armstrong Cork Company for a Fellowship under which this research was performed.

References

[1] Gautier A. *Ann. Chim.* (*Phys.*) 1869 No. 4, 203.
[2] McBride J. J., Jr. and Beachell H. C. *J. Amer. Chem. Soc.* 1952 **74** 5247.
[3] MacDiarmid A. G. *J. Inorg. Nucl. Chem.* 1956 **2** 88.
[4] Polo S. R. and Wilson M. K. *J. Chem. Phys.* 1954 **22** 1559.
[5] Kessler M., Ring H., Trambarulo R. and Gordy W. *Phys. Rev.* 1950 **79** 54.
[6] Keidel F. A. and Bauer S. H. *J. Chem. Phys.* 1956 **25** 1218.
[7] Gerhard S. L. and Dennison D. M. *Phys. Rev.* 1933 **43** 197.
[8] Herzberg G. *Infrared and Raman Spectra of Polyatomic Molecules* p. 429. Van Nostrand, New York 1945.
[9] Cowan R. D. *J. Chem. Phys.* 1950 **18** 1101.
[10] Lord R. C., Robinson D. W. and Schumb W. C. *J. Amer. Chem. Soc.* 1956 **78** 1327.
[11] Newman C., O'Loane J. K., Polo S. R. and Wilson M. K. *J. Chem. Phys.* 1956 **25** 855.
[12] Smith A. L. *J. Chem. Phys.* 1953 **21** 1997.
[13] Dixon R. N. and Sheppard N. *J. Chem. Phys.* 1955 **23** 215.
[14] Venkateswarlu P. *J. Chem. Phys.* 1951 **19** 293.
[15] Williams R. L. *J. Chem. Phys.* 1956 **25** 656.

VOL. 10 1957/5

Spectrochimica Acta, 1958, Vol. 10, pp. 307 to 329. Pergamon Press Ltd., London

The vibrational spectra and structure of ferrocene and ruthenocene

ELLIS R. LIPPINCOTT* and RICHARD D. NELSON†‡

(*Received* 16 *May* 1957)

Abstract—The infrared and Raman spectra of ferrocene, ferrocene-*d*-10 and ruthenocene are reported. The observed spectra were found to be consistent with the D_{5d} model proposed for the bis*cyclo*pentadienyl metal compounds. A detailed assignment of frequencies to the fundamental modes of vibration has been made for these compounds.

A normal co-ordinate analysis has been carried out using the vibrational assignment for a ferrocene *cyclo*pentadienyl ring. The similarity of the valence force symmetry constants between benzene, tropylium ion and the *cyclo*pentadienyl ring has confirmed the aromatic nature of the C_5H_5 ferrocene rings.

Introduction

PREVIOUS publications have given the tentative results of a spectroscopic study of some metal *cyclo*pentadienyl compounds [1, 2]. The completion of the vibrational analysis on $Fe(C_5H_5)_2$, $Ru(C_5H_5)_2$ and $Ni(C_5H_5)_2$ has allowed an assignment of frequencies to be made to the fundamental modes of vibration for these molecules. The frequency assignment was facilitated and checked through the vibrational analysis of $Fe(C_5D_5)_2$. We wish to present here a detailed explanation of these frequency assignments as well as the results of a normal co-ordinate analysis on a *cyclo*pentadienyl ring of ferrocene.

Experimental

Ferrocene was prepared by the Grignard reaction described by KEALY and PAUSON [3]. The product obtained was purified by repeated recrystallization from ethyl alcohol followed by sublimation. Upon purification, orange-red crystals were obtained which melted at 173–174°C.

Ruthenocene was prepared by the same procedure that was used for ferrocene. However, in this case it was necessary to first prepare $RuCl_3$ as none was available. The $RuCl_3$ was prepared by a procedure described in SIDGWICK [4]. In this method chlorine was passed over ruthenium powder heated to approximately 700°C in the presence of carbon monoxide.

Purification of the ruthenocene product from the Grignard reaction by repeated recrystallization from ethyl alcohol followed by sublimation yielded light yellow crystals which melted at 196°C.

The method for the preparation of naphthalene-*d*-8 described by LIPPINCOTT and O'REILLY [5] was slightly modified and used to prepare ferrocene-*d*-10.

Calcium oxide was prepared by the thermal decomposition of reagent grade calcium carbonate. $Ca(OD)_2$ was prepared by adding 99·8 per cent deuterium

* Department of Chemistry, University of Maryland, College Park, Maryland.
† Department of Chemistry, Kansas State College, Manhattan, Kansas.
‡ A thesis presented as partial fulfillment of the requirements for the degree of Doctor of Philosophy in Chemistry at Kansas State College.

oxide to the calcium oxide. The exchange reaction was carried out in the following manner. Five grams of $Ca(OD)_2$ and 0·5 g of ferrocene were placed in a Carius tube which was then evacuated and sealed. The tube was heated for 24 hr at 320°C in a Carius furnace. At the end of a run the ferrocene was removed from the $Ca(OD)_2$ by sublimation, placed with fresh $Ca(OD)_2$ and the exchange reaction rerun. After each run an infrared spectrum was taken to determine the degree of exchange. As the deuterium content increased the intensity of the frequency corresponding to CH stretching decreased. The low intensity of this frequency was taken as an indication that the exchange was practically complete.

Added information on the deuterium content was gained through observation of the infrared frequency corresponding to the anti-symmetric ring breathing mode. This frequency occurs at 1108 cm^{-1} in ferrocene and shifts to 1044 cm^{-1} in ferrocene-*d*-10. In partially exchanged ferrocene both of these frequencies appear as well as several other frequencies which lie between 1108 and 1044 cm^{-1}. As the deuterium content increased the intensity of the frequency at 1044 cm^{-1} increased while the intensity of all the others decreased. The frequencies between 1105 and 1044 cm^{-1} are thought to be due to *cyclo*pentadienyl rings containing one, two, three and four deuterium atoms, respectively.

The sample on which the spectral analysis was made was estimated to have a deuterium content 96 per cent of theoretical.

Infrared spectra were obtained by a Perkin–Elmer model 12-C single beam, single pass, automatic recording spectrophotometer. The region 400–1200 cm^{-1} was studied with samples dissolved in Nujol using KBr optics. Spectra in the region 1000–3500 cm^{-1} were obtained in CS_2 and CCl_4 solutions using NaCl optics.

The same instrument converted to double pass was used for the vapor spectra. Vapor spectra were obtained through the use of a Perkin–Elmer model 021–0081 one meter gas cell fitted with KBr windows. Vapor spectra were obtained on ferrocene in the region 400–3500 cm^{-1}; ferrocene-*d*-10 in the region 400–3500 cm^{-1}; and ruthenocene in the region 700–3500 cm^{-1}.

All infrared spectra obtained are reproduced in Figs. 1–6. Infrared spectra of ferrocene and ruthenocene were obtained in this laboratory as a check to solution spectra in the region 700–3500 cm^{-1} given in the literature [6–8].

Raman spectra were obtained using a Hilger 612 spectrograph. This is a two prism instrument which records photographically, having a camera aperture of *f*/5·4. Raman spectra in CS_2, CCl_4, $CHCl_3$ and benzene solutions were obtained. Spectra on ruthenocene were obtained with both Hg 4358 Å and 5461 Å excitation using the filters and photographic plates listed in Table 1 and Table 2. Ferrocene absorbs throughout much of the visible region. Excitation was accomplished with the Hg 5770–5790 Å doublet as well as the Hg 5461 Å line using the filters and photographic plates listed in Table 1 and Table 2. Spectra on ferrocene and ferrocene-*d*-10 were also obtained with the Na 5890–5895 Å doublet. The Na 5890–5895 Å excitation was accomplished with the use of a sodium vapor lamp unit described elsewhere [9].

It was found that the intensity of the Raman scattering for ferrocene was rather sharply dependent on the concentration. Attempts to obtain Raman spectra on highly concentrated ferrocene solutions gave very poor results. This

VOL. 10 1957/5

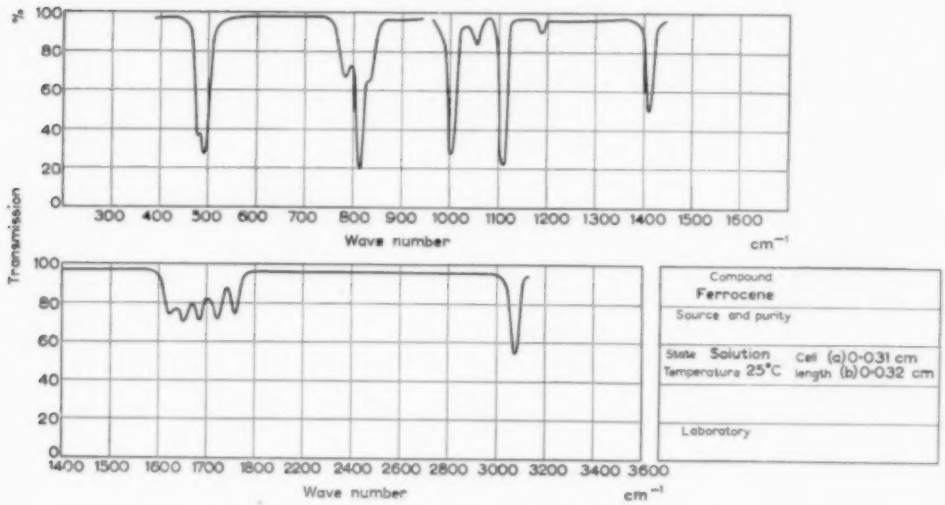

Fig. 1. The infrared spectrum of ferrocene in solution.
(a) 0·45 M in CCl_4 (b) 0·22 M in Nujol solution.

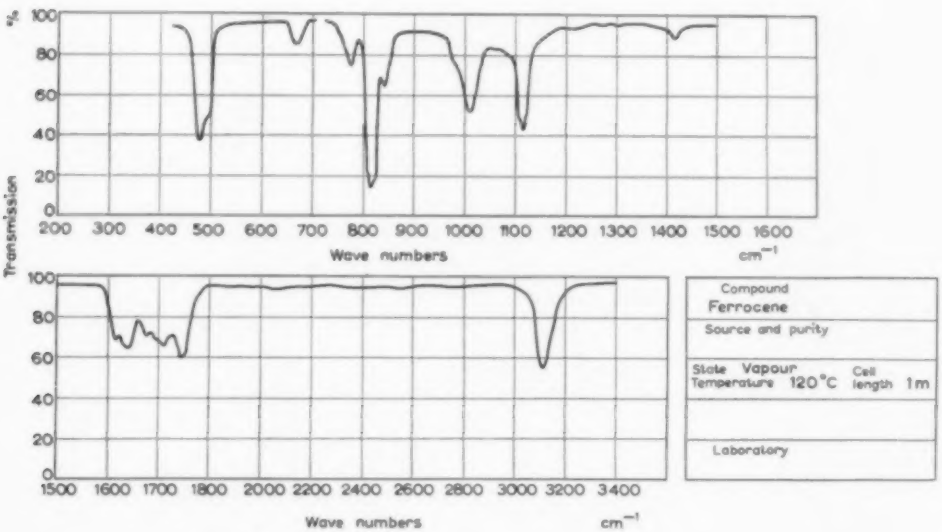

Fig. 2. The infrared spectrum of ferrocene vapor.

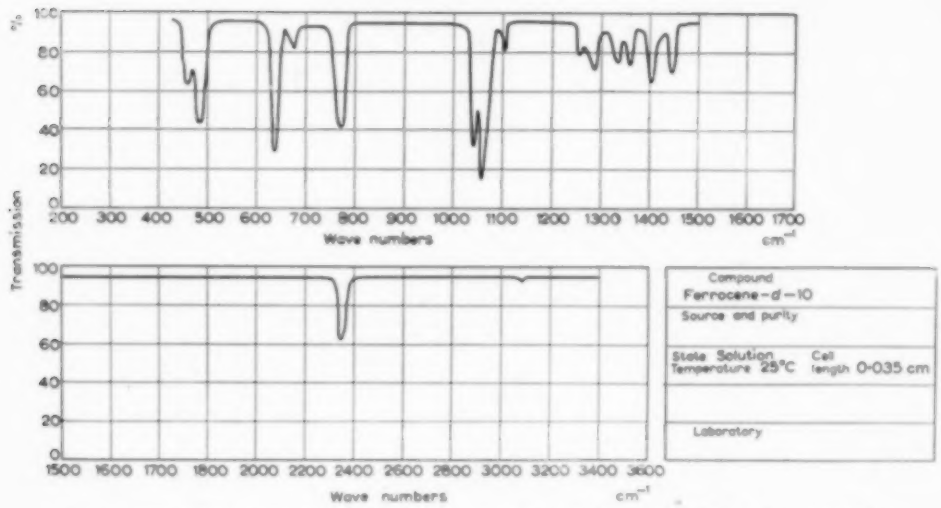

Fig. 3. The infrared spectrum of ferrocene–*d*-10 in solution; 400–600 cm^{-1}, 0·15 M in Nujol solution; 600–800 cm^{-1}, 0·32 M in CS_2; 800–3400 cm^{-1}, 0·45 M in CCl_4.

VOL.
10
1957/5

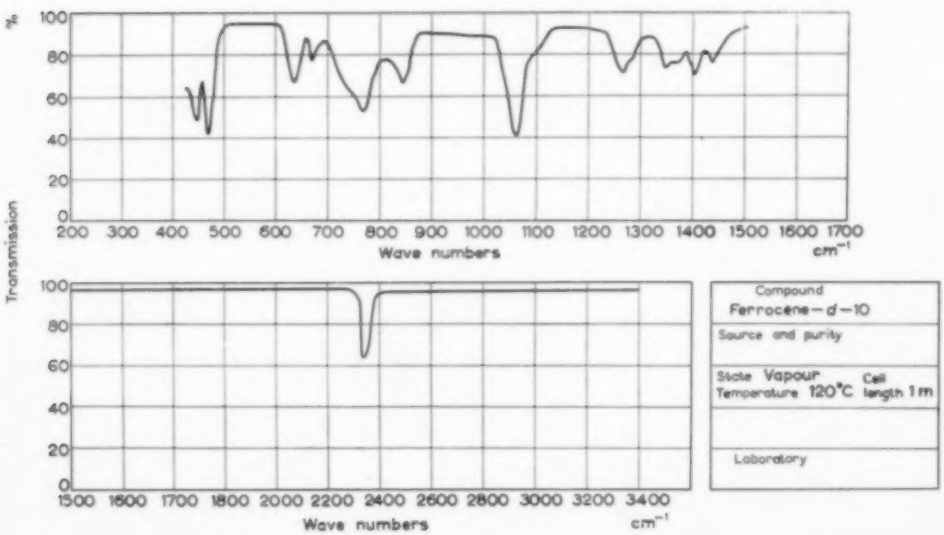

Fig. 4. The infrared spectrum of ferrocene-*d*-10 vapor.

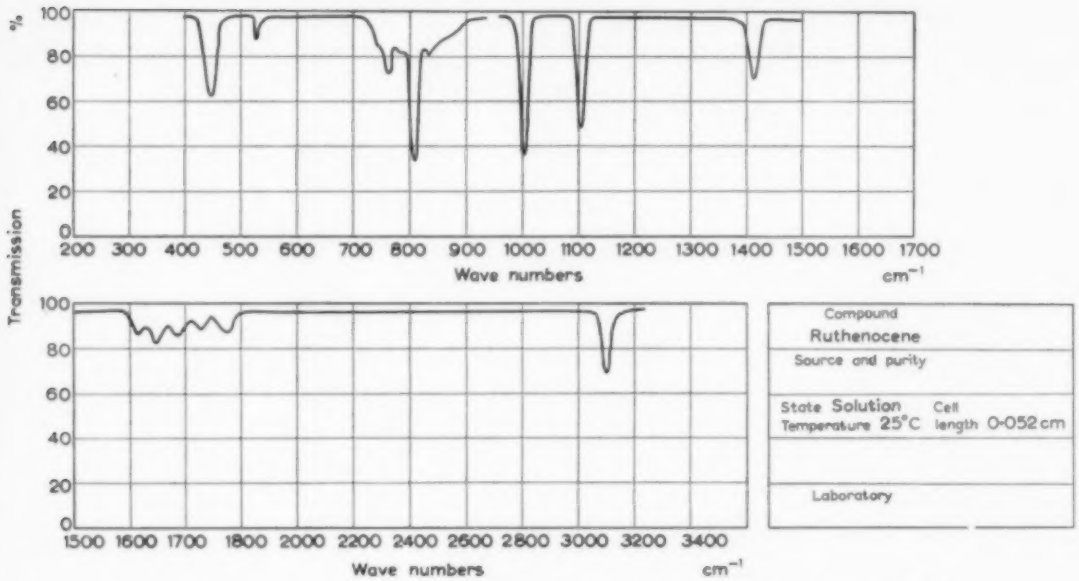

Fig. 5. The infrared spectrum of ruthenocene in solution; 400–600 cm^{-1}, 0·035 M in Nujol solution; 600–950 cm^{-1}, 0·035 M in CS_2, 950–3400 cm^{-1}, 0·05 M in CCl_4.

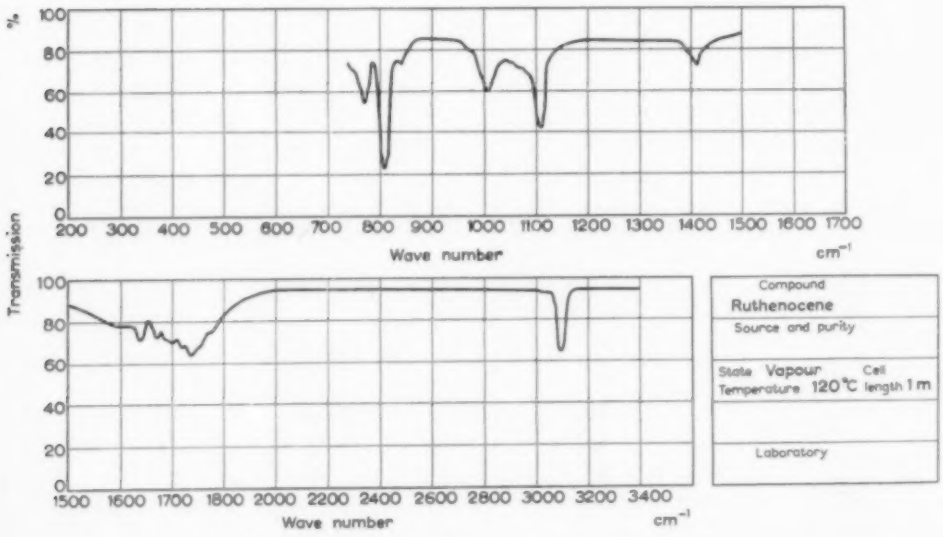

Fig. 6. The infrared spectrum of ruthenocene vapor.

Table 1. Filters for Raman spectra using different excitation wavelengths

Hg excitation	High frequencies	Low frequencies
4358 Å	dilute Rhodamine (5 DGN extra) dilute $PrCl_3$	saturated $NaNO_2$
5461 Å	saturated $NdCl_3$ saturated $NiSO_4$	saturated K_2CrO_4
5770–5790 Å	saturated $NiSO_4$	saturated $K_2Cr_2O_7$

Table 2. Photographic plates for Raman spectra using different excitation wavelengths

Hg excitation	Photographic plates
4358 Å	Eastman Kodak 103 J backed
5461 Å	Eastman Kodak 103 AE backed
5770–5790 Å	Eastman Kodak 103 AE backed

was caused by the partial absorption of the exciting radiation before scattering followed by the partial absorption of the Raman radiation after scattering. It was also found that a maximum intensity for scattering was attained at a concentration considerably less than that of a saturated solution. A detailed description of this optimum concentration effect is given by FISHER [10].

In order to obtain better filtering it was necessary to circulate a filter solution instead of water through the cooling compartment of the filter cell. The Raman tube was sealed to the bottom of the filter cell with rubber tape creating another compartment which held filter solution. A fourth filter was gained by wrapping the Raman tube with a Kodak Wratten filter number 55 when using Hg 5461 Å excitation. Iron spectra were used as a standard for reading the spectral plates.

The vibrational spectra of ferrocene, ferrocene-*d*-10, and ruthenocene are listed in Table 3. Polarization measurements of the Raman spectra were not taken because of the long exposure times required for such colored substances.

Frequency assignment

The distribution of the fundamental modes of vibration among the symmetry species of the D_{5d} character table is shown in Table 4. Raman active fundamentals are in species A_{1g}, E_{1g} and E_{2g} and infrared active fundamentals are in species A_{2u} and E_{1u}. In the following discussion, modes which involve motion perpendicular to the *cyclo*pentadienyl rings will be designated by ($\perp$) and modes which involve motion parallel to the rings will be designated by ($\parallel$).

The assignment of frequencies corresponding to motion within the *cyclo*pentadienyl rings was facilitated by comparison to similar modes in benzene. Frequencies due to ring–metal–ring vibrations were found to be roughly analogous to frequencies observed for linear XY_2 molecules and were assigned accordingly.

VOL. 10 1957/5

Table 3. The vibrational spectra of ferrocene, ruthenocene and ferrocene-*d*-10

Ferrocene			Ruthenocene			Ferrocene-*d*-10		
Raman	Infra-red	I.R. vapor	Raman	Infra-red	I.R. vapor	Raman	Infra-red	I.R. vapor
	170 m					291 m*		
303 cm^{-1} m*			330 s			355 w*		
388 w			402 m				457 s	452 s
	478 s	480 s		446 s			485 s	476 s
	492 s	496 s		528 w		614 w	637 s	638 m
	782 w	776 w		763 w	770 m		679 w	671 w
	811 s	816 s	804 w	806 s	808 s		771 s	775 s
	834 w	840 w		835 w	840 w	849 m		846 m
1010 w	1002 s	1012 s	996 m	1002 s	1008 s	1049 s†	1044 s	1070 s
1050 w*	1051 w		1056 m	1050 w				
1105 s*	1108 s	1112 s	1104 s	1103 s	1105 s		1260 w	1270 m
1178 m	1188 w		1193 w			1290 m*	1290 m	1290 m
1356 w			1360 w				1334 m	1334 m
1408 m	1411 s	1416 w	1412 m	1413 m	1413 w		1358 m	1358 m
1560 vw†								
	1620 m	1620 m		1622 m	1618 m		1403 m	1403 m
	1650 m	1644 m		1651 m	1640 m		1444 m	1444 m
	1684 m	1680 m		1684 m	1690 m	2318 w		
	1720 m	1716 m		1727 m	1732 m	2335 s	2354 m	2354 m
	1758 m	1748 m		1774 m	1775 m			
3085 m			3089 m					
3099 s	3085 s	3106 m	3104 s	3100 m	3108 m			

vw = very weak; w = weak; m = medium; s = strong; * = obtained by Hg and Na radiation; † = obtained by Na radiation.

Table 4. Selection rules for D_{5d} sandwich structure

Species	Number of frequencies	Activity
A_{1g}	4	R
A_{1u}	2	inactive
A_{2g}	1	inactive
A_{2u}	4	IR
E_{1g}	5	R
E_{1u}	6	IR
E_{2g}	6	R
E_{2u}	6	inactive

R, Raman active; IR, infrared active.

The spectra of ferrocene-*d*-10 proved very useful for the frequency assignment particularly in distinguishing between CC and CH modes. The ratio of the observed frequencies in ferrocene to the corresponding frequencies in ferrocene-*d*-10 was calculated. These values were compared to similar values for benzene in Table 6.

The Teller–Redlich product rule was used as a measure of the correctness of the assignment of frequencies. Anharmonicity will cause the observed ratio of frequency products to be slightly greater than the calculated ratio. Because some of the frequencies in species E_{2g} were not observed the product rule was not applied to this species. The results of this calculation are as follows: species A_{1g} ratio observed 0·524, ratio calculated 0·500; species A_{2u} ratio observed 0·537,

Table 5. Description of fundamental modes of vibration

Species	Frequency number	Description
A_{1g}	1	sym. CH stretching
	2	sym. CH bending ($\perp$)
	3	sym. ring breathing
	4	sym. ring metal stretch
A_{1u}	5	CH bend ($\parallel$)
	6	internal rotation
A_{2g}	7	CH bend ($\parallel$)
A_{2u}	8	CH stretching
	9	CH bending ($\perp$)
	10	antisym. ring breathing
	11	antisym. ring metal stretch
E_{1g}	12	CH stretching
	13	CH bending ($\parallel$)
	14	CH bending ($\perp$)
	15	sym. CC stretch
	16	sym. ring tilt
E_{1u}	17	CH stretching
	18	CH bending ($\parallel$)
	19	CH bending ($\perp$)
	20	antisym. CC stretch
	21	antisym. ring tilt
	22	ring metal ring bending
E_{2g}	23	CH stretching
	24	CH bending ($\parallel$)
	25	CH bending ($\perp$)
	26	CC stretch
	27	ring distortion ($\parallel$)
	28	ring distortion ($\perp$)
E_{2u}	29	CH stretching
	30	CH bending ($\parallel$)
	31	CH bending ($\perp$)
	32	CC stretch
	33	ring deformation ($\parallel$)
	34	ring deformation ($\perp$)

VOL. 10 1957/5

ratio calculated 0·513; species E_{1g} ratio observed 0·368, ratio calculated 0·365; species E_{1u} ratio observed 0·401, ratio calculated 0·363.

An examination of Table 3 shows several features which are consistent with a molecule having D_{5d} symmetry. The number of Raman and infrared frequencies observed is rather small for a molecule having 57 vibrational degrees of freedom. The selection rules for a molecule with D_{5d} symmetry predict the appearance of 15 Raman and 10 infrared fundamental vibrational frequencies. D_{5d} selection rules are also followed by the model in which free internal rotation is occurring (cf. BAUMAN R. P. *J. Chem. Phys.* 1956 **24** 13).

D_{5d} symmetry would require planar rings with equivalent bonds. This would predict that only one type of CH bond is present. Consistent with this is the appearance of only one type of CH frequency in either the infrared or Raman spectrum. The appearance of multiple bond frequencies near 1410 cm^{-1} and 1560 cm^{-1} is further evidence for equivalent multiple bonds which result from the delocalization of the π-electrons.

Examination of Table 3 shows some rather unusual features in the vibrational spectra of ferrocene and ruthenocene. For example, many of the infrared and Raman frequencies are coincidences or near coincidences. However, since a D_{5d} model has a center of symmetry, the rule of mutual exclusion should hold [11]. The fact that coincidences do exist was interpreted to mean that the symmetric and antisymmetric modes of vibration involving displacements associated with the *cyclo*pentadienyl rings show little interaction. Consequently these coincidences were assigned to the CH and CC modes of vibrations. Also requiring explanation is the appearance of the band systems around 1700 cm^{-1} in the infrared spectrum of both ferrocene and ruthenocene. It is not believed that these frequencies can

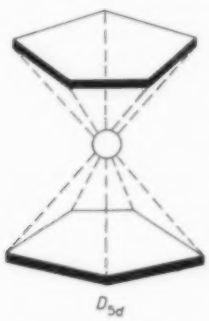

Fig. 7. D_{5d} model.

be interpreted in terms of fundamental modes of vibration, for if they were similar frequencies should appear in the Raman spectra. Also, the D_{5d} model has no structural features that would lead one to predict the appearance of fundamental vibrations in this region. This band system was originally interpreted as being related to the restricted rotation of the *cyclo*pentadienyl rings with respect to one another [1]. However, examination of the position of this band system in ferrocene-*d*-10 reveals that it extends from 1290 cm^{-1} to 1444 cm^{-1}. This represents shifts by factors of 1·21 to 1·25 which would imply that these bands are associated with

Table 6. Frequency shifts produced by substituting D for H in ferrocene

Type vibration	$\frac{C_6H_6}{C_6D_6}$	$\frac{Fe(C_5H_5)_2}{Fe(C_5D_5)_2}$
CH stretching	1·30–1·35	1·31–1·34
H (∥) bending	1·20–1·28	1·3
H (⊥) bending	1·20–1·28	1·22–1·3
CC stretching	1·05	1·09–1·1
Ring breathing	1·05	1·05–1·06
C (∥) bending	1·05	
C (⊥) bending	1·1	
Ring metal stretch		1·04
Ring tilt		1·01–1·09

CH modes (Table 6) and not hindered rotation. Benzene and its substituted derivatives show similar bands which have been interpreted as overtones and combination bands involving CH modes [12]. Because of these facts the band system in ferrocene and ruthenocene is interpreted as combination and overtone bands involving CH modes. No completely satisfactory assignment has been made for these bands.

Comparison of the ferrocene and ruthenocene spectra show that frequencies due to vibrations within the rings are at essentially the same position, whereas frequencies due to ring–metal–ring vibrations occur at different positions. This was interpreted to mean that the strength of the CC and CH bonds are essentially of the same magnitude in the two compounds, whereas the strength of the ring–metal bonds is different. The ring–Ru–ring symmetric stretching frequency occurs at 330 cm^{-1}, whereas the ring–Fe–ring symmetric stretching frequency occurs at 303 cm^{-1}, indicating the rings are bound more tightly to the ruthenium atom than to the iron atom. The ring–Ni–ring symmetric stretching frequency has been calculated to be at 200 cm^{-1} indicating that the rings are bound less tightly to the nickel atom than to either the iron or ruthenium atom.

A frequency assignment is also given for nickelocene, $Ni(C_5H_5)_2$. This assignment is somewhat more empirical than that for ferrocene or ruthenocene in that no Raman spectrum was obtained. More emphasis was placed on the positions of infrared frequencies and comparisons to ferrocene and ruthenocene. The frequency assignment was carried out for nickelocene in order that the thermodynamic functions could be calculated and compared with the corresponding functions for ferrocene and ruthenocene.

A_{1g} Species (Raman)

A_{1g} frequencies are generally strong, sharp, and polarized. Frequencies which received immediate consideration because of their intensity were 3099 cm^{-1} and 1105 cm^{-1} in ferrocene and 3104 cm^{-1}, 1104 cm^{-1} and 330 cm^{-1} in ruthenocene. The totally symmetric CH stretching frequency occurs at 3062 cm^{-1} in benzene and is quite intense. The 3099 cm^{-1} band in ferrocene and 3104 cm^{-1} band in

ruthenocene were assigned to ω_1. The ferrocene 3099 cm^{-1} band shifted to 2335 cm^{-1} in ferrocene-*d*-10.

The symmetric ring breathing mode occurs at 992 cm^{-1} in benzene. It is expected that the frequency due to this mode in ferrocene and ruthenocene would occur somewhat higher due to the fact that the five-membered ring has a smaller C—C—C angle than in benzene, as well as to the influence of the metal–ring bonds. The frequencies 1105 cm^{-1} in ferrocene and 1104 cm^{-1} in ruthenocene were of comparable intensity and sharpness to the 992 cm^{-1} frequency in benzene and were assigned to ω_3. The 1105 cm^{-1} ferrocene frequency shifted to 1049 cm^{-1} in ferrocene-*d*-10. This is only a shift by a factor of 1·05 which is typical of CC modes. This assignment was also suggested by the occurrence in the infrared spectra of frequencies of similar position and intensity which could be assigned to the antisymmetric ring breathing mode.

The 330 cm^{-1} frequency was the lowest band obtained in the Raman spectra of ruthenocene. The corresponding frequency in ferrocene occurred at 303 cm^{-1}. These frequencies are undoubtedly due to similar modes of vibration in the two compounds. The two modes remaining to be assigned in this species are ω_2 CH bend ($\perp$) and ω_4 ring-metal stretch. The 303 cm^{-1} ferrocene frequency shifts to 291 cm^{-1} in ferrocene-*d*-10. This shift is by a factor of 1·04. The ferrocene 303 cm^{-1} frequency and the ruthenocene 330 cm^{-1} frequency were assigned to ω_4. If the two rings are considered as having their mass at the center of mass of the ring then ω_4 is a linear XY_2 type mode.

The ω_2 CH bend ($\perp$) remains to be assigned. This mode is infrared active in benzene and occurs at 671 cm^{-1} with high intensity. The infrared spectra of both ferrocene and ruthenocene contained intense bands at approximately 800 cm^{-1} which were established to be CH modes (see the assignment for species A_{2u}). The appearance of these infrared bands suggested that similar bands should appear in the Raman spectra. Solvent bands in this region made the detection of bands practically impossible. The broadness and increased intensity of a solvent band in the ruthenocene spectra indicated a frequency at 806 cm^{-1}. Ferrocene-*d*-10 has a band at 614 cm^{-1}. No Raman bands were observed in ferrocene from 500 cm^{-1} to 1000 cm^{-1}. If the 614 cm^{-1} ferrocene-*d*-10 frequency had shifted from 1000 cm^{-1} in ferrocene the shift would be by a factor greater than 1·6 which is unreasonable in that the largest possible shift is by a factor of 1·41. The infrared bands at approximately 800 cm^{-1} in ferrocene shifted to 630–680 cm^{-1} in ferrocene-*d*-10 suggesting the 614 ferrocene-*d*-10 Raman band shifted from approximately 800 cm^{-1}. These shifts agree reasonably well with those observed for benzene. On this basis ω_2 was assigned values of 804 cm^{-1} in ferrocene and 805 cm^{-1} in ruthenocene.

The assignment of nickelocene frequencies to the species A_{1g} was based solely on infrared positions and the A_{1g} assignment for ferrocene and ruthenocene. ω_1 was assigned a typical value of 3100 cm^{-1}. A strong infrared band at 770 cm^{-1} which had structural features similar to the 800 cm^{-1} bands in ferrocene and ruthenocene led to the assigning of 770 cm^{-1} to ω_2. ω_2 has an appreciably lower value in nickelocene than in ferrocene or ruthenocene. This may be due to a combination of factors. The ring metal distance in nickelocene is greater than it is in ferrocene or ruthenocene which might cause the rings to be more aromatic in

nickelocene. Weakly bound rings would cause the CH and CC frequencies to become more benzene-like. Also, since the ring–metal bond is weaker in nickelocene than it is in ferrocene or ruthenocene ω_2 may not be perturbed in nickelocene to the extent it is in ferrocene or ruthenocene. The infrared spectra also contained a strong band at 1110 cm^{-1}. ω_3 was assigned a value of 1105 cm^{-1} ω_4 was assigned a value of 220 cm^{-1} for reasons that will be discussed in the A_{2u} assignment.

A_{1u} Species (inactive)

The modes of vibration in this species are ω_5, CH bend ($\|$), and ω_6 an internal rotation.

The fundamental in benzene similar to ω_5 is also inactive but has been calculated to have a value of 1190 cm^{-1}. ω_5 was assigned a value of 1200 cm^{-1} in ferrocene, ruthenocene, and nickelocene. This assignment is thought to be justified on the basis of the position of other CH ($\|$) bending modes. These modes have frequencies which are reasonably close to the frequencies due to corresponding modes in benzene (see assignment for ω_{13}, ω_{18} and ω_{24}). ω_6 was assigned to free internal rotation. Several investigators have suggested that no barrier to internal rotation exists [13–14].

A_{2g} Species (inactive)

Species A_{2g} contains only one fundamental mode of vibration, a ω_7 CH bend ($\|$). This mode is analogous to ω_5. On the basis of the assignment for ω_5 and following the observation that symmetric and anti-symmetric CC and CH modes show coincidence, ω_7 was also assigned a value of 1200 cm^{-1} for ferrocene, ruthenocene and nickelocene.

A_{2u} Species (infrared)

The four fundamental modes of vibration in this species involve the same type of motion as the four modes in species A_{1g}. Because of the similarity between symmetric and antisymmetric CC and CH modes it would be expected that ω_8, ω_9, and ω_{10} would be coincident or nearly coincident with ω_1, ω_2, and ω_3 respectively.

A check of Table 3 reveals that infrared frequencies for both ferrocene and ruthenocene were observed that are coincidences or near coincidences with the frequencies in the Raman spectrum assigned to modes ω_1, ω_2, and ω_3. The 3085 cm^{-1} frequency in ferrocene and the 3100 cm^{-1} frequency in ruthenocene can obviously be assigned to ω_8.

There are a number of infrared frequencies that would fit ω_9. They are 782 cm^{-1}, 811 cm^{-1} and 834 cm^{-1} in ferrocene and 763 cm^{-1}, 806 cm^{-1} and 835 cm^{-1} in ruthenocene. Comparison of the ferrocene spectra to the ferrocene-*d*-10 spectra shows that the ferrocene 782 cm^{-1} frequency can not be readily interpreted as a fundamental CH band. The 811 cm^{-1} ferrocene band and the 637 cm^{-1} ferrocene-*d*-10 band are due to the same mode of vibration. Likewise the 835 cm^{-1} ferrocene band and the 679 cm^{-1} ferrocene-*d*-10 band are due to the same mode of vibration. The shifts in these bands from ferrocene to ferrocene-*d*-10 are by factors of 1·27 and 1·22 which are characteristic of this type of CH mode. If the 782 cm^{-1} band shifted by a similar amount, a third band should appear about 600 cm^{-1} or greater

VOL.
10
1957/5

in ferrocene-*d*-10. Since a third band did not appear, the 782 cm^{-1} band was not interpreted as a CH fundamental. It will be seen later that 782 cm^{-1} band in ferrocene and 763 cm^{-1} band in ruthenocene can be conveniently interpreted as combination bands. We now have the choice of assigning 811 cm^{-1}, 806 cm^{-1} or 835 cm^{-1}, 834 cm^{-1} to ω_9. An examination of the vapor spectra of ferrocene and ruthenocene shows that the ferrocene 811 cm^{-1} band and the ruthenocene 806 cm^{-1} band are very intense and show PQR structure and are probably parallel bands. Nondegenerate modes of vibration in a symmetric top molecule give rise to parallel bands. The only infrared active nondegenerate species is A_{2u}. Therefore 806 cm^{-1} in ruthenocene and 811 cm^{-1} in ferrocene must be assigned in species A_{2u}. Since they are CH bending modes the only assignment that can be made for 811 cm^{-1} in ferrocene and 806 cm^{-1} in ruthenocene is ω_9.

The appearance of an intense frequency at 1108 cm^{-1} in ferrocene and 1103 cm^{-1} in ruthenocene suggested that these may be ring breathing frequencies coincident with the Raman active ω_3 modes. The 1108 cm^{-1} ferrocene band shifted to 1044 cm^{-1} in ferrocene-*d*-10. This was by a factor of 1·06 which compared favorably to the shift observed for ω_3 and also to the shift observed for the similar mode in benzene. The vapor spectra of ferrocene and ruthenocene reveal that the 1108 cm^{-1} ferrocene band and the 1103 cm^{-1} ruthenocene band also show PQR structure and are therefore parallel bands.

ω_{11} is another XY_2 type mode. For molecules of this type the following expression approximately holds.

$$\frac{\omega_{11}}{\omega_4} = \left(1 + \frac{2M_y}{Mx}\right)^{\frac{1}{2}}$$

In the case of bis-*cyclo*pentadienyl metal compounds M_y is the total mass of a ring and M_x is the mass of the metal atom. The observed ratio is generally less than the calculated ratio due to anharmonicity. Since ω_4 is 303 cm^{-1} for ferrocene and 330 cm^{-1} for ruthenocene, 478 cm^{-1} and 492 cm^{-1} for ferrocene and 446 cm^{-1} for ruthenocene approximately fit the above relationship. Therefore, ω_{11} can be assigned to 446 cm^{-1} for ruthenocene. The ferrocene 478 cm^{-1} frequency corresponds to the ruthenocene 446 cm^{-1} frequency and was therefore assigned to ω_{11}. This assignment agrees well with the ferrocene-*d*-10 spectra. The 303 cm^{-1} and 478 cm^{-1} ferrocene frequencies shift to 291 cm^{-1} and 457 cm^{-1} in ferrocene-*d*-10. As might be expected both shifts are by a factor of 1·04.

Once the ferrocene and ruthenocene frequencies had been assigned for species A_{2u} the nickelocene assignment was straightforward for its infrared spectra is very similar to that of ferrocene and ruthenocene. The frequency at 3075 cm^{-1} was assigned to ω_8. The nickelocene 773 cm^{-1} band was similar in appearance to the ferrocene 806 cm^{-1} band and was therefore assigned to ω_9. The later reasoning also led to the assignment of the nickelocene 1110 cm^{-1} band to ω_{10}. These frequencies are due to CC or CH modes and would not be expected to change much from molecule to molecule. Frequencies due to linear XY_2 type modes, however, would be expected to vary from molecule to molecule as the metal atom is changed. Therefore, the linear XY_2 type modes can not be assigned on the basis of coincidences. The frequency observed at 355 cm^{-1} in nickelocene was similar to the

478–492 cm^{-1} pair observed in ferrocene and was assigned to ω_{11}. The basis for assigning 220 cm^{-1} to ω_4 in nickelocene can now be explained. The mass of a nickel atom is only slightly different from the mass of an iron atom. From the relationship for linear XY_2 type molecules the ratio ω_{11}/ω_4 would be expected to be approximately the same for ferrocene and nickelocene. On this basis a value of 220 cm^{-1} was calculated for ω_4.

E_{1g} Species (Raman)

The ferrocene 3085 cm^{-1} band and the ruthenocene 3089 cm^{-1} band were assigned to ω_{12}. The ferrocene 3085 cm^{-1} band shifted to 2318 cm^{-1} in ferrocene-*d*-10.

The mode in benzene which is similar to ω_{13} in ferrocene and ruthenocene is infrared active and gives an intense band at 1037 cm^{-1}. Two ferrocene frequencies 1010 cm^{-1} and 1050 cm^{-1}, and two ruthenocene frequencies, 996 cm^{-1} and 1056 cm^{-1}, are in the vicinity of the benzene band. Raman frequencies due to vibrations in species E_{1g} would be expected to have coincidences in the infrared due to vibrations in species E_{1u} since the CH and CC modes involve the same type of motion in both species. Inspection of the observed frequencies shows that all of the above bands have coincidences in the infrared spectrum. However neither the ferrocene 1057 cm^{-1} infrared band nor the ruthenocene 1050 cm^{-1} infrared band were observed in the vapor spectrum indicating they are not due to active fundamental modes. The ferrocene 1010 cm^{-1} band and the ruthenocene 996 cm^{-1} band were assigned to ω_{13}.

The mode in benzene similar to ω_{14} gives a band at 849 cm^{-1}. A band was observed in the Raman spectra of ruthenocene at 804 cm^{-1}. Ferrocene and ruthenocene both had infrared frequencies which could be interpreted as near coincidences with Raman bands near 800 cm^{-1}. The ruthenocene 806 cm^{-1} frequency was assigned to ω_{14}. ω_{14} in ferrocene was assigned a value of 800 cm^{-1}. A normal co-ordinate analysis of the five-membered ring also led to a prediction of 800 cm^{-1} for ω_{14}.

ω_{15} corresponds to a symmetric CC stretching mode of vibration. The frequency due to a similar vibration in benzene is infrared active and occurs at 1485 cm^{-1}. This benzene frequency shifts by a factor of 1·1 to 1333 cm^{-1} in benzene-*d*-6. Ferrocene and ruthenocene have Raman bands at approximately 1410 cm^{-1} which have coincidences in the infrared as would be expected. The ferrocene 1408 cm^{-1} band shifts to 1290 cm^{-1} or by a factor of 1·09 in ferrocene-*d*-10. Therefore 1408 cm^{-1} in ferrocene and 1412 cm^{-1} in ruthenocene were assigned to ω_{15}.

ω_{16} a symmetric ring tilt mode, was expected to have a low frequency and to be shifted only slightly from ferrocene to ferrocene-*d*-10. The remaining low Raman frequencies are 388 cm^{-1} in ferrocene and 402 cm^{-1} in ruthenocene. These were assigned to ω_{16}. The 388 cm^{-1} ferrocene band shifted to 355 cm^{-1} or by a factor of 1·09 in ferrocene-*d*-10.

The nickelocene frequencies were again assigned by comparison with the assignments for ferrocene and ruthenocene and comparison with nickelocene infrared bands. Infrared bands available are 3075 cm^{-1}, 1000 cm^{-1}, 1430 cm^{-1} and 800 cm^{-1}. ω_{12} was assigned a value of 3085 cm^{-1}. ω_{13} was assigned a value of

VOL. 10 1957/5

1010 cm^{-1}. This is slightly higher than the observed infrared band as is ω_{13} in the two other compounds. ω_{14} for ferrocene and ruthenocene is similar to ω_2 and ω_9. ω_{14} was assigned a value of 770 cm^{-1}. ω_{15} was assigned a value of 1425 cm^{-1} which is slightly less than the observed infrared band as is ω_{15} in the other two compounds. ω_{16} was assigned strictly on the comparison with ferrocene. The ratio ω_{11}/ω_{16} was calculated for ferrocene. Assuming the ratio to be the same for nickelocene ω_{16} would have a value of 275 cm^{-1}.

Species E_{1u} (infrared)

There are six frequencies associated with this degenerate species. ω_{17} was assigned typical values of 3075 cm^{-1} for ferrocene and 3100 cm^{-1} for ruthenocene. Ferrocene and ruthenocene both had infrared bands at 1002 cm^{-1}. The ferrocene 1002 cm^{-1} band shifted to 771 cm^{-1} or by a factor of 1·3 in ferrocene-*d*-10 indicating that it is a CH mode. The 1002 cm^{-1} band was assigned to ω_{18} for ferrocene and ruthenocene.

The ferrocene 834 cm^{-1} band and the ruthenocene 835 cm^{-1} band have been interpreted as near coincidences with Raman bands near 800 cm^{-1}. The ferrocene band shifted by a factor of 1·22 to 679 cm^{-1} in ferrocene-*d*-10 indicating a CH mode. These bands were assigned to ω_{19}.

The 1411 cm^{-1} frequency in ferrocene and 1413 cm^{-1} frequency in ruthenocene were assigned to ω_{20}. The ferrocene 1411 cm^{-1} band shifted by a factor of 1·10 to 1260 cm^{-1} in ferrocene-*d*-10.

The frequency due to ω_{21} is expected low. The shift of ω_{21} from ferrocene to ferrocene-*d*-10 would also be expected to be small as for ω_{16}. The 492 cm^{-1} frequency in ferrocene and 528 cm^{-1} frequency in ruthenocene were assigned to ω_{21}. The ferrocene 492 cm^{-1} band shifted by a factor of 1·01 to 485 cm^{-1} in ferrocene-*d*-10 which was expected.

ω_{22} is the degenerate linear XY_2 bending mode of vibration. This is the lowest fundamental frequency that occurs in linear XY_2 molecules. It was noted that this vibration in CO_2 and CS_2 had a frequency that was roughly half the frequency for the symmetric X–Y stretch. On that basis ω_{22} would be expected to have a value in the neighborhood of 150 cm^{-1} for ferrocene. A band was observed at 170 cm^{-1} in ferrocene by PALIK [15] and was assigned to ω_{22}. ω_{22} for ruthenocene was calculated with the aid of the ratio ω_4/ω_{22} observed in ferrocene. This yielded a value of 185 cm^{-1}.

The frequencies in nickelocene available for assignment to species E_{1u} were mentioned in the E_{1g} nickelocene assignment. These frequencies were assigned as follows: ω_{16} to 3075 cm^{-1}, 1000 cm^{-1} to ω_{18}, 800 cm^{-1} to ω_{19}, 1430 cm^{-1} to ω_{20}. The intensity and structural features of the 355 cm^{-1} band led to the interpretation that it was similar to the 478–492 cm^{-1} pair in ferrocene, and 355 cm^{-1} was also assigned to ω_{21}.

ω_{22} was assigned in the same manner discussed for ruthenocene. The value calculated for ω_{22} was 125 cm^{-1}.

E_{2g} Species (Raman)

This species is degenerate and has six fundamental frequencies.

The typical values of 3085 cm^{-1} for ferrocene and 3089 cm^{-1} for ruthenocene were assigned to ω_{23}. The mode in benzene similar to ω_{24} has a frequency of 1178 cm^{-1}. The ferrocene 1178 cm^{-1} band and the ruthenocene 1193 cm^{-1} band were assigned to ω_{24}.

The Raman spectra of ruthenocene contained a band at 1056 cm^{-1} and the spectra of ferrocene contained a band at 1050 cm^{-1}. The ferrocene 1050 cm^{-1} band shifted by a factor of 1·25 to 849 cm^{-1} in ferrocene-*d*-10 indicating that it is a CH mode. Therefore 1050 cm^{-1} in ferrocene and 1056 cm^{-1} in ruthenocene were assigned to ω_{25}.

The frequency in the Raman spectrum of benzene due to a mode similar to ω_{26} is at 1584 cm^{-1}, indicating that the ferrocene 1560 cm^{-1} band should be assigned to ω_{26}. A similar assignment was made for ruthenocene.

ω_{27} and ω_{28} were originally assigned values 900 cm^{-1} and 500 cm^{-1} respectively strictly on the basis of comparison with benzene [2]. Theoretical calculations however predicted that ω_{27} would have a value of 880 cm^{-1} for ferrocene. Infrared studies of ferrocene crystals by WINTER [16] yielded frequencies of 885 cm^{-1} and 569 cm^{-1} which were assigned to ω_{33} and ω_{34} respectively. It would be expected that ω_{33} and ω_{34} would be coincident with ω_{27} and ω_{28}. Therefore ω_{27} and ω_{28} were assigned values of 885 cm^{-1} and 569 cm^{-1} respectively for ferrocene and ruthenocene.

The nickelocene assignment for this species must be made purely on the basis of frequency positions for corresponding modes in ferrocene and ruthenocene. The values assigned correspond quite closely to the values in ferrocene and ruthenocene. They are $\omega_{23} = 3085$ cm^{-1}, $\omega_{24} = 1180$ cm^{-1}, $\omega_{25} = 1050$ cm^{-1}, $\omega_{26} = 1560$ cm^{-1}, $\omega_{27} = 885$ cm^{-1} and $\omega_{28} = 569$ cm^{-1}.

VOL. 10 1957/5

Species E_{2u} (inactive)

Because this species is inactive, assignment of frequencies was made on the basis of coincidences between symmetric and antisymmetric modes. None of the modes in this species and species E_{2g} involve motions which are associated with the central atom. Since the modes in species E_{2g} involve the same type of motion as the modes in species E_{2u}, the frequencies in these two species would be approximately at the same cm^{-1} values for corresponding modes of vibration. On the basis of this argument the following approximate assignment was made for all three compounds. $\omega_{29} = 3100$ cm^{-1}, $\omega_{30} = 1170$ cm^{-1}, $\omega_{31} = 1050$ cm^{-1}, $\omega_{32} = 1560$ cm^{-1}, $\omega_{33} = 885$ cm^{-1}, and $\omega_{34} = 569$ cm^{-1}.

Assignment of observed non-fundamental frequencies

Frequencies that were not assigned to active fundamental modes of vibration are the Raman 1356 cm^{-1} band and the infrared peaks 782 cm^{-1}, 1051 cm^{-1}, and 1188 cm^{-1} in ferrocene and the Raman 1360 cm^{-1} band and infrared 763 cm^{-1} peak in ruthenocene.

The 1356 cm^{-1} and 1360 cm^{-1} bands can be assigned as the combination $\omega_4 + \omega_{25}$. The symmetry requirements are $A_{1g} \times E_{2g} = E_{2g}$ or that the combination band be Raman active.

The ferrocene 782 cm^{-1} band and the ruthenocene 763 cm^{-1} band can be

assigned as $\omega_4 + \omega_{11}$. Since $A_{1g} \times A_{2u} = A_{2u}$ this combination would be infrared active. If this is applied to ferrocene-*d*-10 a band would be predicted in the neighborhood of 748 cm^{-1}. The 771 cm^{-1} solution band and the 775 cm^{-1} vapor band are broad. This broadness may be due to a band slightly lower than 770 cm^{-1} which could be $\omega_4 + \omega_{11}$ combination.

Attempts to assign the ferrocene 1051 cm^{-1} infrared band to a combination have met with little success. $\omega_{22} + \omega_{27}$ or $\omega_{22} + \omega_{33}$ would explain this band. However nickelocene also has a weak infrared band at 1050 cm^{-1} which can not be explained by this assignment. This ferrocene band does not appear in the vapor spectra. It is believed that the appearance of this band is due to a breakdown of the selection rules. Since a Raman band at 1050 cm^{-1} was assigned in species E_{2g} it is reasonable to assume that it would have a coincidence in species E_{2u}. The ferrocene crystal which has C_i symmetry produced a very intense infrared band at 1050 cm^{-1} [16] and the 1050 cm^{-1} solution band might be due to ω_{31}. This would also explain the appearance of an infrared band at 1050 cm^{-1} in nickelocene since ω_{31} would not be expected to vary much from molecule to molecule.

The ferrocene 1188 cm^{-1} infrared band might also be explained in the same manner since a coincidence with ω_{24} would be expected in the inactive species E_{2u}. A band was observed in the crystal at about this position and was assigned by WINTER to ω_{30} which would be coincident with ω_{24}. 1188 cm^{-1} might also be the combination $\omega_{16} + \omega_9$ since $A_{2u} \times E_{1g} = E_{1u}$ which would make the combination infrared active.

The 846 cm^{-1} band observed in the vapor spectrum of ferrocene-*d*-10 was due to impurity arising from the decomposition of the gaskets of the gas cell.

WINTER made an independent frequency assignment based on the infrared spectra of ferrocene crystals and vapor. As stated previously the crystal has C_i symmetry and because of this the inactive infrared modes for a D_{5d} point group are active. WINTER observed and assigned frequencies to species A_{1u} and E_{2u}. The values postulated for these species in the above assignment agree reasonably well with what those observed for the crystal. For example, ω_5 was postulated to be 1200 cm^{-1} and was observed to be 1257 cm^{-1}; ω_{27} was postulated to be 900 cm^{-1}, calculated to be 880 cm^{-1} and observed to be 885 cm^{-1}; and ω_{28} was postulated to be 500 cm^{-1} and observed to be 569 cm^{-1}.

The complete assignment of frequencies to the fundamental modes of vibration is given in Table 7. The assignment of observed ferrocene-*d*-10 frequencies is also given in this table.

Normal co-ordinate analysis

A successful completion of normal co-ordinate analysis of the tropylium ion, $(C_7H_7)^+$, provided interesting results [17]. Specifically it was found that the valence force symmetry constants compared quite favorably with those of benzene and it was concluded that the tropylium ion must be a planar, aromatic 7-membered ring. Since ferrocene contains planar, aromatic 5 membered rings, a similar analysis on the ferrocene *cyclo*pentadienyl rings may yield interesting comparisons among the 5-, 6- and 7-membered aromatic rings.

It was decided to employ the Wilson *FG* method [18] for the analysis of a

Table 7. Assignment of frequencies for ferrocene, ferrocene-*d*-10, ruthenocene and nickelocene

Species		$Fe(C_5H_5)_2$	$Fe(C_5D_5)_2$	$Ru(C_5H_5)_2$	$Ni(C_5H_5)_2$
A_{1g}	1	3099	2335	3104	(3100)
	2	(804)	614	(805)	(770)
	3	1105	1049	1104	(1105)
	4	303	291	330	(220)
A_{1u}	5	(1200) 1257[b]		(1200)	(1200)
A_{2g}	7	(1200)		(1200)	(1200)
A_{2u}	8	3085	2354	3100	3075
	9	811	637	806	773
	10	1108	1044	1103	1110
	11	478	457	446	355
E_{1g}	12	3085	2318	3089	(3085)
	13	1010	(771)	996	(1010)
	14	(800)[a]	(614)	804	(770)
	15	1408	1290	1412	(1425)
	16	388	355	402	(275)
E_{1u}	17	3075	2354	3100	3075
	18	1002	771	1002	1000
	19	834	679	835	800
	20	1411	1260	1413	1430
	21	492	485	528	355
	22	170	(162)	(185)	(125)
E_{2g}	23	3085	2318	3089	(3085)
	24	1178	(1045)	1193	(1180)
	25	1050	849	1056	(1050)
	26	1560	(1540)	(1560)	(1560)
	27	(900) 880[a]	(640)	(900)	(900)
	28	(500)	(465)	(500)	(500)
E_{2u}	29	(3100)		(3100)	(3100)
	30	(1170)		(1170)	(1170)
	31	(1050)		(1050)	(1050)
	32	(1560)		(1560)	(1560)
	33	(900)		(900)	(900)
	34	(500)		(500)	(500)

( ) means unobserved.
Superscript "*a*" means calculated by a normal co-ordinate analysis.
Superscript "*b*" means observed in crystal.

VOL. 10 1957/5

ferrocene ring, (C_5H_5). The analysis of (C_5H_5) was greatly simplified because many of the methods worked out for ($C_7H_7^+$) could be used for (C_5H_5) [19]. A preliminary report of this work has been given previously.

Table 8. Distribution of observed frequencies in ferrocene rings of D_{5h} symmetry

Species	Frequencies
A_1'	$\omega_1 = \omega_8$ $\omega_3 = \omega_{10}$
A_2''	$\omega_2 = \omega_9$
E_1'	$\omega_{12} = \omega_{17}$ $\omega_{13} = \omega_{18}$ $\omega_{15} = \omega_{20}$
E_1''	$\omega_{14} = \omega_{19}$
E_2'	$\omega_{23} = \omega_{29}$ $\omega_{24} = \omega_{30}$ $\omega_{26} = \omega_{32}$ $\omega_{27} = \omega_{33}$

Table 9. Symmetry co-ordinates for a ferrocene D_{5h} *cyclo*pentadienyl ring

Species	Coefficient j					N	VFC
	1	2	3	4	5		
A_1'	1	1	1	1	1	$\sqrt{(1/5)}$	S
	1	1	1	1	1	$\sqrt{(1/5)}$	t
A_2''	1	1	1	1	1	$\sqrt{(1/5)}$	γ
E_1'	1	C1	C2	C2	C1	$\sqrt{(2/5)}$	S
	0	1 − C2	C1 − C2	C2 − C1	C2 − 1	0·3326	β
	1 + C1	C1 + C2	2C2	C1 + C2	1 + C1	0·3909	t
E_1''	1	C1	C2	C2	C1	$\sqrt{(2/5)}$	γ
E_2'	1	C2	C1	C1	C2	$\sqrt{(2/5)}$	α
	1	C2	C1	C1	C2	$\sqrt{(2/5)}$	S
	0	1 − C1	C2 − C1	C1 − C2	C1 − 1	0·538	β
	1 + C1	C2 + C1	2C1	C2 + C1	1 + C2	1·023	t

N = Normalization factor; C1 = $\cos\phi$; C2 = $\cos 2\phi$; $\phi = 360°/5$

The FG method involves the solution of the secular equation

$$|F - G^{-1}\lambda| = 0$$

where F is the force constant matrix, G the kinetic energy matrix and λ is the

diagonal frequency matrix. The methods of evaluating the elements of G and solving the secular equation are described by WILSON *et al.* [18].

A C_5H_5 ring has D_{5h} symmetry. It is important to know in which species of the D_{5h} character table the observed ferrocene ring vibrations will occur. This information is presented in Table 8.

Table 10. Comparison of valence force symmetry constants for the *cyclo*pentadienyl, tropylium ion and benzene rings

Type	No.[a]	$(C_5H_5)^-$, (cm^{-1})	C_6H_6, (cm^{-1})	$(C_7H_7^+)$, (cm^{-1})	$(C_5H_5)^-$ *VFSC*, (dyn/cm)	C_6H_6[b,c] *VFSC*	$(C_7H_7^+)$[c,d] *VFSC*
CH stretching	1	3099	3062	3060	4·99 $\times 10^5$	5·12 $\times 10^5$	5·16 $\times 10^5$
CC stretching	2	1105	992	868	6·97 $\times 10^5$	7·62 $\times 10^5$	7·66 $\times 10^5$
CH ($\perp$) bending	4	811	671	633	0·42 $\times 10^{-11}$	0·228 $\times 10^{-11}$	0·256 $\times 10^{-11}$
CH stretching	12	3085	3099	3020	5·18 $\times 10^5$	5·15 $\times 10^5$	5·00 $\times 10^5$
CC stretching	13	1411	1485	1477	5·50 $\times 10^5$	6·14 $\times 10^5$	7·40 $\times 10^5$
CH ($\parallel$) bending	14	1002	1037	992	0·96 $\times 10^{-11}$	1·02 $\times 10^{-11}$	0·96 $\times 10^{-11}$
CH stretching	15	3085	3047	3075	5·218 $\times 10^5$	5·04 $\times 10^5$	5·18 $\times 10^5$
CC stretching	16	1560	1596	1594	5·50 $\times 10^5$	5·66 $\times 10^5$	6·09 $\times 10^5$
CH ($\parallel$) bending	17	1178	1178	1210	0·95 $\times 10^{-11}$	0·99 $\times 10^{-11}$	1·16 $\times 10^{-11}$
CC ($\parallel$) bending	18	885	606	433	1·78 $\times 10^{-11}$	1·45 $\times 10^{-11}$	1·02 $\times 10^{-11}$

[a] Frequency number 11, the Raman active CH bending mode, was not observed in the spectra. [b] CRAWFORD B. L. and MILLER F. *J. Chem. Phys.* 1949 **17** 249. [c] Stretching and bending *VFSC* are in units of dyn/cm and dyn cm respectively. [d] For $C_7H_7^+$ the $F_{t\beta}$ interaction constant has values of 2·36 $\times 10^{-3}$ dyn and 0·22 $\times 10^{-3}$ dyn in species E_1' and E_2' respectively. For C_5H_5 the $F_{t\beta}$ interaction in species E_1' has a value of 2·10 $\times 10^{-3}$ dyn.

In the following, the subscripts α refer to ring distortion modes ($\parallel$), β to CH bending modes ($\parallel$), γ to CH bending modes ($\perp$), s to CH stretching modes, and t to CC stretching modes.

The symmetry co-ordinates calculated for use in the analysis are given in Table 9. Expressions for the G elements and their calculated values are given in Tables 11 and 12.

The unobserved frequency ω_{14} was calculated by a slight adjustment of the force constant of benzene.

The results of this analysis are given in Table 10. Also given in Table 10 are the valence force symmetry constants for C_6H_6 and $(C_7H_7)^+$.

A detailed normal co-ordinate analysis for the entire ferrocene molecule rather than just the *cyclo*pentadienyl rings will be given in a separate publication.

Comparison of force constants

A comparison of the force constants and frequencies of the 5-, 6- and 7-membered (CH) rings is shown in Table 9. Observations which can be drawn from Table 9 are:

(1) The values of the frequencies of the ring breathing modes ω_2 and ω_{10} are progressively smaller from the 5- to the 7-membered ring, whereas the values of the force constants are progressively larger. This frequency depends to a large extent on G_{tt} which is dependent on the C—C—C angle. This angle changes from 108° for $(C_5H_5)^-$ to 120° for C_6H_6 to 128° for $(C_7H_7)^+$.

VOL. 10 1957/5

(2) The force constants for the CH stretching fundamentals agree quite well among the 3 ring systems indicating that the ferrocene *cyclo*pentadienyl CH bond is an aromatic type CH bond.

Table 11. G elements for D_{5h} C_5H_5 ring

Species	G elements
A_1'	$G_{ss} = g_s^1$
	$G_{tt} = g_t^1 + 2g_t^2$
	$G_{\alpha\alpha} = g_\alpha^1 + 2g_\alpha^2 + 2g_\alpha^3$
	$G_{st} = 2g_{st}^1$
	$G_{s\alpha} = g_{s\alpha}^1 + 2g_{s\alpha}^2$
	$G_{t\alpha} = 2g_{t\alpha}^1 + 2g_{t\alpha}^2$
A_2''	$G_{\gamma\gamma} = g_\gamma^1 + 2g_\gamma^2 + 3g_\gamma^3$
E_1'	$G_{ss} = g_s^1$
	$G_{tt} = \left[\frac{1}{1+\cos\phi}\right][(1+\cos\phi)\,g_t^1 + (\cos\phi + \cos 2\phi)g_t^2 + (1+\cos\phi)g_t^2]$
	$G_{\beta\beta} = \left[\frac{1}{1-\cos\phi}\right][(1-\cos 2\phi)g_\beta^3 + (\cos\phi - \cos 2\phi)g_\beta^3 + (\cos 2\phi - \cos\phi)g_\beta^2 + (\cos 2\phi - 1)g_\beta^1]$
	$G_{st} = [0{\cdot}3909/\sqrt{(2/5)}]\ 2(1+\cos\phi)\ g_{st}^1$
	$G_{s\beta} = [0{\cdot}3326/\sqrt{(2/5)}]\ 2(1-\cos 2\phi)g_{s\beta}^1$
	$G_{t\beta} = (0{\cdot}3326)/(0{\cdot}3909)\ (1+\cos\phi)[-(1-\cos 2\phi)g_{t\beta}^1 + (\cos\phi - \cos 2\phi)g_{t\beta}^2 - (\cos 2\phi - \cos\phi)g_{t\beta}^3 - (\cos 2\phi - 1)g_{t\beta}^2]$
E_1''	$G_{\gamma\gamma} = g_\gamma^1 + 2\cos\phi g_\gamma^2 + 2\cos 2\phi g_\gamma^3$
E_2'	$G_{ss} = g_s^1$
E_2'	$G_{tt} = \left[\frac{1}{1+\cos 2\phi}\right][(1+\cos 2\phi)g_t^1 + (\cos 2\phi - \cos\phi)g_t^2 + 2\cos\phi g_t^3 + (\cos 2\phi + \cos\phi)g_t^2 + (1+\cos 2\phi)g_t^2]$
	$G_{\beta\beta} = \left[\frac{1}{1-\cos\phi}\right][(1-\cos\phi)g_\beta^3 + (\cos 2\phi - \cos\phi)g_\beta^3 + (\cos\phi - \cos 2\phi)g_\beta^2 + (\cos\phi - 1)g_\beta^1]$
	$G_{\alpha\alpha} = g_\alpha^1 + 2\cos 2\phi g_\alpha^2 + 2\cos\phi g_\alpha^3$
	$G_{s\alpha} = g_s{}^1{}_\alpha + 2\cos 2\phi g_s{}^2{}_\alpha$
	$G_{s\beta} = [0{\cdot}538/\sqrt{(2/5)}]\ 2(1-\cos\phi)g_s{}^1{}_\beta$
	$G_{st} = [1{\cdot}023/\sqrt{(2/5)}]\ 2(1+\cos 2\phi)g_s{}^1{}_t$
	$G_{\alpha\beta} = [0{\cdot}538/\sqrt{(2/5)}][2(1-\cos\phi)g_\alpha{}^2{}_\beta + 2(\cos 2\phi - \cos\phi)g_\alpha{}^3{}_\beta]$
	$G_{t\alpha} = [\sqrt{(2/5)}/(1{\cdot}023)(1+\cos 2\phi)]\,[g_t{}^1{}_\alpha + \cos 2\phi_t{}^1{}_\alpha + \cos\phi g_t{}^2{}_\alpha + \cos\phi g_t{}^3{}_\alpha + \cos 2\phi g_t{}^2{}_\alpha]$
	$G_{t\beta} = [0{\cdot}538/(1{\cdot}023)(1+\cos 2\phi)][-(1-\cos\phi)g_t{}^1{}_\beta + (\cos 2\phi - \cos\phi)g_t{}^2{}_\beta - (\cos\phi - 1)_t g^2{}_\beta]$

$\phi = 72°$. Expressions for the g's are given by FATELEY.

(3) The force constants for the CC fundamentals agree reasonably well among the 3 ring systems indicating that the CC linkage in ferrocene *cyclo*pentadienyl rings is of aromatic nature.

(4) The $F_{\gamma\gamma}(C_5H_5)$ force constant does not agree well with those of C_6H_6 and $(C_7H_7^+)$ for species A_2''. The fundamental mode associated with this force constant is a CH bending ($\perp$), ω_2 and ω_9. It is to be noted also, that the frequency due to this mode is considerably higher than in C_6H_6 or $(C_7H_7)^+$. These differences might be explained by a pertubation of this mode of vibration due to the ring–metal bond in ferrocene.

Table 12. Calculated G elements for D_{5h} C_5H_5 ring

Species	Calculated G elements
A_1'	$G_{ss} = 1{\cdot}0747$ $G_{tt} = 0{\cdot}1151$ $G_{st} = -0{\cdot}09788$
A_2''	$G_{\gamma\gamma} = 0{\cdot}9219 \times 10^{16}$
E_1'	$G_{ss} = 1{\cdot}0747$ $G_{tt} = 0{\cdot}1506$ $G_{\beta\beta} = 1{\cdot}059 \times 10^{16}$ $G_{st} = -0{\cdot}0792$ $G_{s\beta} = 0{\cdot}0458 \times 10^{8}$ $G_{t\beta} = -0{\cdot}1605 \times 10^{8}$
E_1''	$G_{\gamma\gamma} = 1{\cdot}150 \times 10^{16}$
E_2'	$G_{ss} = 1{\cdot}0747$ $G_{tt} = 0{\cdot}2082$ $G_{\alpha\alpha} = 0{\cdot}3787 \times 10^{16}$ $G_{\beta\beta} = 0{\cdot}9464 \times 10^{16}$ $G_{st} = -0{\cdot}0302$ $G_{s\alpha} = 0{\cdot}1625 \times 10^{8}$ $G_{s\beta} = 0{\cdot}0288 \times 10^{8}$ $G_{t\alpha} = -0{\cdot}1265 \times 10^{8}$ $G_{t\beta} = -0{\cdot}1393 \times 10^{8}$ $G_{\alpha\beta} = 0{\cdot}1005 \times 10^{16}$

(5) The valence force symmetry constants of (C_5H_5) generally compare quite well with those of C_6H_6 and $(C_7H_7^+)$ indicating that the (C_5H_5) ferrocene ring is planar and aromatic.

Recalculated thermodynamic functions

Since the thermodynamic functions were published several of the frequency assignments have been changed [2]. New calculations were made at 298·16°K. The recalculated values do not differ significantly from the original values.

The ΔH_{f0}^0 reported previously was 57·5 kcal/mole for ferrocene and 79·6 kcal/mole for nickelocene. The latter value is in error and should be 85·9 kcal/mole.

References

[1] LIPPINCOTT E. R. and NELSON R. D. *J. Chem. Phys.* 1953 **21** 1307–308.
[2] LIPPINCOTT E. R. and NELSON R. D. *J. Amer. Chem. Soc.* 1955 **77** 4990–4993.

VOL. 10 1957/5

[3] KEALY T. J. and PAUSON P. L. *Nature, Lond.* 1951 **168** 1039–1040.
[4] SIDGWICK N. V. *Chemical Elements and Their Compounds.* Clarendon Press, Oxford 1950.
[5] LIPPINCOTT E. R. and O'REILLY E. J. *J. Chem. Phys.* 1955 **23** 238–244.
[6] KAPLAN L., KESTER W. L. and KATZ J. J. *J. Amer. Chem. Soc.* 1952 **74** 5531–5532.
[7] WILKINSON G. *J. Amer. Chem. Soc.* 1952 **74** 6146–6147.
[8] WILKINSON G., PAUSON P. L. and COTTON F. A. *J. Amer. Chem. Soc.* 1954 **76** 1970–1974.
[9] KING F. T. and LIPPINCOTT E. R. *J. Opt. Soc. Amer.* 1956 **46** 661.
[10] FISHER R. D. *Raman Spectra of Certain Colored Substances and the Existence of an Optimum Concentration for Maximum Intensity of Scattered Radiation.* Unpublished M.S. thesis, Kansas State College, Manhattan, Kansas 1954.
[11] HERZBERG G. *Infrared and Raman Spectra of Polyatomic Molecules.* Van Nostrand, New York 1945.
[12] YOUNG C. W., DUVALL R. B. and WRIGHT N. *Analyt. Chem.* 1951 **23** 709–714.
[13] DUNITZ J. D. and ORGEL L. E. *J. Chem. Phys.* 1955 **23** 954.
[14] MOFFITT W. *J. Amer. Chem. Soc.* 1954 **76** 3386.
[15] PALIK E. D. Ohio State University, Private Communication to Dr. Basil Curnutte, Physics Department, Kansas State College, January 16, 1956.
[16] WINTER W. K. *The Infrared Spectrum and Structure of Crystalline Ferrocene.* Unpublished Ph.D. thesis, Kansas State College, Manhattan, Kansas 1956.
[17] FATELEY W. G., CURNUTTE B. and LIPPINCOTT E. R. *J. Chem. Phys.* 1957 **26** 1471.
[18] WILSON E. B. JR., DECIUS J. C. and CROSS P. C. *Molecular Vibrations.* McGraw-Hill, New York 1955.
[19] NELSON R. D., FATELEY WM. G. and LIPPINCOTT E. R. *J. Amer. Chem. Soc.* 1956 **78** 4870.

OL.
10
7/58

Spectrochimica Acta, 1958, Vol. 10, pp. 330 to 334. Pergamon Press Ltd., London

REPORTS OF MEETINGS

Symposium on Applied Spectroscopy

THE Fourth Annual Symposium on Applied Spectroscopy, sponsored by the Canadian Association for Applied Spectroscopy was held at Ottawa from 11 to 13 September 1957. The following papers were presented:

1. Emission Spectrometric Analysis

Automatic analysis: GEORGE L. BUC, Fisher Scientific Co., Pittsburgh, Pennsylvania.

Chemical robots for a variety of purposes are in a sense not completely new, but have been produced for some years. As developments in materials, electronics and optics proceed, the degree increases to which fuller automation of laboratory techniques becomes possible both in the technical and economic senses. What the present status is and what may be expected will be discussed in the light of specific instruments, including older as well as quite recent developments in which human participation is minimized.

The use of the Hilger direct-reader in the spectrochemical analysis of aluminium alloys: ROBERT WERNER, R. D. Werner (Canada) Ltd., Oshawa, Ontario.

R. D. Werner Co. (Canada) Ltd. have installed a Hilger direct-reader for analytical control of aluminium extrusions. Alloys controlled are mainly 50S, 65S, 1S, 2S, and 3S. An extensive set of tests was run on installation which generally conformed to A.S.T.M. specifications. Results of tests are discussed. Details are presented regarding installation and ease of operation. One point of great significance is that the superintendent of the Remelt Department is able to run his own analysis for re-melt control.

New direct-reading attachment for 20 in. camera. Three meter concave grating spectrograph: ELIOT DUBOIS and L. O. EIKREM, Baird-Atomic Inc., Cambridge, Massachusetts.

This paper describes the newly developed direct-reading attachment for the Baird-Atomic 3-meter concave grating spectrograph. The standard 20 in. plateholder of the spectrograph is replaced by a "DR box", which is an assembly containing a focal curve, exit slits, and photomultiplier tubes. Provision is made for reasonably rapid setting of the exit slits on the spectrum lines of interest by use of a special electronic slit-setting attachment used in conjunction with an oscilloscope. A separate cabinet contains the high and low voltage supplies, the measuring circuitry, and the reading units consisting of clocks which may be calibrated to read directly the concentrations of eight different elements at one time. To set up a "DR box" on a completely new problem requires approximately 2–3 hr. After once having been set up a "DR box" may be removed and held in standby status while other work is pursued photographically on the spectrograph. To return to direct reading then requires approximately 10 min. An important contribution to the success of the "DR" attachment is the development by Baird-Atomic Inc., of a servo-monitoring device which automatically and continuously keeps the spectrum lines precisely aligned with the exit slits. This device also makes possible the use of the electronic slit setting attachment. Stability of optical alignment is essential to precise analysis, and the servo-monitor makes possible the fulfillment of this requirement. It is not necessary to control the temperature in the laboratory.

The Quantovac. A direct reading instrument for the analysis of carbon, phosphorus and sulphur: B. R. BOYD, Applied Research Laboratories, Glendale, California.

A direct reading polychromator is now in production for the vacuum region of the ultraviolet.

VOL. 10 1957/5

The wavelength coverage is 1600–3300 Å, which includes most sensitive lines of P, C, and S, as well as lines of other elements of interest in the metal analysis field. Data will be presented covering the analysis of these important elements in iron base materials.

The use of hydrogen as internal standard in analysis of additives and wear metals in lube oils by direct-reading methods: R. R. Thieme, Jarrell Ash Co., Newtonville, Massachusetts.

A method is developed using hydrogen line 4861 Å as internal standard in analysis of additives and wear metals in lube oils by direct reading methods. Elements determined are Ag, Al, B, Cr, Cu, Fe, Pb, Si, Sn, Ba, Ca, Zn, in a range dependent on element from 1 p.p.m. to 3000 p.p.m.

From spectrographic plate to permanent record in one simple operation: F. Dufour and D. R. Jackson, Canadian National Railways, Montreal, Quebec.

This paper describes the design of a calculator and record card. Using them it is possible to go directly from microphotometer reading to graphical record entry in one simple operation. The interpretation of a spectrographic analysis of used lubricating oil is simplified by graphical presentation of related analyses. This type of calculator and record card may be of value with other routine spectrographic methods, especially when the results are used for quality control. The calculator has 12 separate scales, one for each of the 12 spectra on the plate. Each scale handles 8 determinations. Each record card accommodates up to 52 analyses for 8 elements. Space is provided for written notes and comments. The use of this system of data handling necessitated some changes in the spectrographic technique which was described at the first Ottawa Symposium. These changes in the technique are described. The sources of error inherent in this system of record keeping are evaluated. The system saves clerical labour and eliminates mistakes due to numerical calculations and data transcriptions.

An arc method for sample transfer in spectrochemical analysis: C. J. Leistner, General Motors Corporation, Indianapolis, Indiana.

This paper will include a survey of foreign literature dealing with the sample transfer method for spectrochemical analysis. An emphasis will be made on its application at the Allison Spectrographic Laboratory for semi-quantitative evaluation of various jet engine components.

The spectrochemical analysis of inorganic fillers in G.R.S. rubber compounds: W. J. Bennett and E. M. Law, Northern Electric Co., Lachine, Quebec.

G.R.S. elastomer insulations for wire and cable usually contain a variety of inorganic fillers and activators to impart specific electrical and physical properties to the wire or cable. These are in addition to vulcanizing agents, vulcanization accelerators, colour of pigments, softeners, antioxidants, carbon black, etc. which may be compounded into the elastomer. Among the inorganic materials used are clays, calcium, carbonate, zinc oxide, magnesium oxide and lead oxides. The actual amounts of these materials in the compounded and vulcanized elastomer are critical. Spectrochemical methods for the analysis of these inorganic materials in the elastomer have been developed and will be described.

The spectrographic determination of fluorine in cracking catalyst and the use of the streaming-velocity arc: L. W. Gamble, Esso Research Laboratories, Baton Rouge, Louisiana.

In the past several years the petroleum industry has been interested in the analysis of fluorine, particularly in catalysis. A spectrochemical method employing a streaming-velocity electrode which has been developed offers a number of advantages; namely,—increased sensitivity, reduced fractional distillation, and improved arc stability. Due to the nature of the arc, an elemental line can be used as an internal standard. The standard deviation is 0·13 at the 1 per cent level.

Application of the spectrograph to agriculture. Molybdenum toxicity: W. M. Langille and K. S. MacLean, Nova Scotia Department of Agriculture and Research Foundation, Truro, Nova Scotia.

Methods of analysing soil acid plant samples for cobalt, molybdenum and zinc in trace quantities are described. Application of the method pertaining to a molybdenum toxicity

problem in cattle is presented. Data are given to show average values for molybdenum in plant tissue and soil samples from toxic and non-toxic areas. Values for the elements copper, cobalt, zinc, manganese and calcium are also included.

The determination of trace elements in high purity silica: E. S. Hodge and B. L. Milan, Mellon Institute, Pittsburgh, Pennsylvania.

The investigation of color centers in quartz is greatly aided by spectrographic analysis. Samples have been analyzed by using an addition procedure with Spex Standards to high purity fused silica. Some of the precautions found necessary are described. Typical results are shown which have permitted some interpretations of color center data. Some detection limits found are Cr, Fe, Li, Mg, Mn, Ag, Ti, 1 p.p.m.; Ba, Be, Ca, Ni, 3 p.p.m.; Al, B, Co, Na, 6 p.p.m.; Cd, Pb, and Hg, 60 p.p.m.

Spectrographic determination of carbon in sedimentary rocks, using direct current arc excitation: W. H. Dennen, Massachusetts Institute of Technology, Cambridge, Massachusetts.

Many molecular bands are excited in the usual spectrographic sources, and some permit the determination of "non-spectrographic elements". Encouraging preliminary results have been obtained in the use of OH3064A for water determination and CN3883A for nitrogen determinations. Carbon may be determined in its various compounds by direct-current arc emission spectrography. When samples are excited in copper electrodes, the carbon in the sample combines with atmospheric nitrogen to form cyanogen, and the bandhead CN3883A is measured. Cathode excitation at 6 A and 50 V provides the best sensitivity for graphitic carbon and carbonates. A coefficient of variation of 13 per cent is obtained. Marked differences of relative intensity are related to the nature of the carbon compound, to the excitation conditions, and to the presence of silica. These matrix variations are controlled by comparing unknown samples with chemically similar standards, maintaining uniform arcing conditions, and diluting samples with quartz. Separate determinations for different compounds of carbon are required.

VOL.
10
1957/5

A spectrochemical method for the determination of selenium: C. L. Waring, H. Worthing and K. W. Hazel, U.S. Geological Survey, Washington, D. C.

Selenium can be determined in pyrite, chalcocite, and marcasite by a spectrochemical method that is simple, rapid, and requires no complicated arrangement of spectrographic equipment or chemical pretreatment of samples. Advantage is taken of the new short wavelength radiation plates (Eastman) and the addition of copper oxide to enhance the selenium lines 2039·85 Å and 2063·78 Å. The possibility exists of determining many other elements on the same exposure of the sample. The method has application in the range of 0·0015 to 2 per cent selenium. Tests indicated an average difference from the chemical results of 0·07 per cent in the low per cent range, 0·03 per cent in the 0·1 per cent range, 0·005 per cent in the 0·01 per cent range. The relative accuracy of the entire range is about 7 per cent of the concentration.

Spectrochemical analysis of solutions in an a.c. discharge: N. Tomingas, Canadian Copper Refineries Ltd., Montreal East, Quebec.

A rapid and accurate procedure is described for the estimation of impurities in solutions, in particular copper refinery tank house electrolytes. The solutions are excited in an a.c. arc discharge on flat surface electrodes which have been treated to provide uniform porosity. Chromium as an external standard has been found satisfactory for the determination of impurities: arsenic, antimony, bismuth, iron, and nickel. The agreement with chemical analysis is excellent. Considerations governing the selection of the internal standard and the type of electrodes are discussed.

Determination of major constituents in alloy steels by spectrographic solution methods: C. A. Waggoner, Pacific Naval Laboratory, Esquimalt, B. C.

In spectrographic laboratories handling a wide variety of metal alloy sample forms, it is often impractical to standardize for each form by conventional spark-to-solid methods. Solution

techniques may provide a useful alternative if samples are readily soluble. Procedures utilizing porous cup and rotating disk techniques are described for determining major constituents in different types of alloy steel. Cobalt is used as internal standard, and a buffer is added to minimize inter-element effects. Solutions are excited by an oscillating spark-like discharge. Results of comparable precision and accuracy are obtained by the two techniques.

The spectrochemical analysis of arsenic in steels: J. E. Burgener, Technical Service Laboratories Toronto, Ontario.

A vapour-cup method using arc excitation was investigated. The development work and results are described.

A method for determination of trace impurities: L. R. Pittwell, Dominion Magnesium Ltd., Haley, Ontario.

A method for determining trace impurities by concentration and d.c. arc spectroscopy.

2. Infra-red Spectroscopy

The Hilger double-beam recording infra-red spectrometer: J. E. Burgener, Technical Service Laboratories, Toronto, Ontario.

Description, operation and performance of the instrument.

Infra-red Spectroscopy in an organic research laboratory: G. Papineau, Couture, Ayerst, McKenna & Harrison Ltd., Montreal, Quebec.

Infra-red spectroscopy is often the fastest and the most precise method of solving various problems encountered in synthetic organic chemistry. The practical use of group frequencies will be illustrated by various samples. Reference will be made to both qualitative and quantitative methods.

The effect of hyperconjugation on —CH_2 vibrations: G. Pouliot and C. Sandorfy, University of Montreal, Montreal, Quebec.

The infra-red spectra of various compounds containing one or two —CH_2— groups in a conjugated environment were measured. The CH_2— stretching and scissoring bands are shifted from their usual positions showing the effect of hyperconjugation. Theoretical implications and the use of this observation for analytical purposes are discussed.

Differential infra-red spectroscopy as a tool for qualitative as well as quantitative analysis: J. C. Bartlet, Food and Drug Directorate, Ottawa, Ontario.

Differential infra-red spectroscopy has found widespread use for the quantitative determination of small amounts of an impurity in another material. In principle, the method depends on using a sample of known purity in one beam of a spectrometer and a second sample of the same substance in the other beam. Any difference in the spectrum of the two samples due to impurities will register on the recorder. The use of this technique has now been extended to identification of edible oils and fats. These materials have very similar spectra making identification by normal spectroscopy impossible. By using one oil in the reference beam, other oils may be identified by minor differences in spectra which become apparent by this technique. It is also possible to detect one oil in the presence of another by these spectral differences. The instrumental requirements for this type of analysis are discussed in detail.

Infra-red techniques with polymers: R. M. B. Small, Polymer Corporation Limited, Sarnia, Ontario.

A review is presented of the quantitative, semi-quantitative, and some qualitative analyses that are performed by infra-red absorption spectroscopy. Techniques which are peculiar to the analysis or study of high polymers are described. These include (1) the use of solid films pressed

between plates of silver chloride or mica, (II) differential analysis with films, (III) pyrolysis of intractable materials, (IV) extraction of material containing carbon black and (V) the use of elevated temperatures with crystalline polymers.

Some applications and innovations in absorption spectroscopy: W. A. E. McBryde, University of Toronto, Toronto, Ontario.

The most familiar quantitative application of absorption spectroscopy is in photometric analysis of solutions. This paper will describe several applications of absorptiometry to special cases of interest in general or inorganic chemistry. First, modified analytical procedures will be described applicable to solutions of optical density higher or lower than ideal. Second, applications to the study of acid–base equilibria will be discussed. Then some discussion of the measurement of distribution coefficients between water and an immiscible solvent will be given. This leads to an account of the technique of reversion, which may be applied to advantage in some analyses utilizing extractions, e.g. with dithizone. Finally some procedures will be described which permit measurement of the identity and stability of complexions formed in aqueous solution.

3. X-ray Fluorescence Spectroscopy

Absorption phenomena and their influence on quantitative fluorescence analysis: Heinz Ruck, Pulp and Paper Research Institute of Canada, Montreal, Quebec.

The tabulated absorption coefficients are supposed to allow for the fluorescent and scattered radiation only, as holds true for single crystals. In the case of powders, however, several additional effects can enter into the absorption formula as coefficients. These are small angle scattering, primary and secondary extinction (which are related to crystal and grain size), degree of compaction and microabsorption. This calls for a complete revision of the commonly accepted picture of absorption. It requires a redistribution of the intensities allotted for the different phenomena, especially the fluorescent radiation whose angular dependency has been recently discovered by P. M. de Wolff. The conditions under which samples of equal chemical composition produce equal amounts of characteristic radiation are pointed out. Variations in sampling techniques are usually responsible for inconsistent results. Precautions to overcome these are given. Furthermore, the bearing of the matrix on the result must be considered.

A new method for the analysis of ores and metallurgical products by X-ray fluorescence: G. R. Lachance, Quebec Metallurgical Industries, Billings Bridge, Ontario.

A new method has been developed that enables the analysis of ores and metallurgical products to be done very rapidly. The finely ground sample is mixed with aluminum oxide and scanned. From the graph it is possible to calculate the percentage of the constituents detected using simple calculations. Examples of actual analyses are given.

Sample preparation for accurate X-ray fluorescence analysis: F. Claisse, Laboratories Branch, Department of Mines, Quebec.

The method consists in fusing the sample in a suitable glass, making disks out of it, and analysing these by X-ray fluorescence. When the glass has the following composition—1 part of sample, 10 parts of barium peroxide, 10 parts of barium sulfate and 100 parts of fused borax—it has been observed that the matrix effect is practically negligible. The line intensities (background included) are almost linearly related with percentages up to 100. With this method, only one reading per sample is needed to obtain a result of analysis with an accuracy of the order of 0·3 per cent absolute in less than 2 min. For concentrations below 3 to 5 per cent a better accuracy is obtained by fusing 1 part of sample with 20 parts of borax and using an internal standard. A simple technique for making the glass disks is described. The method can be used for ores and rocks (including sulfides), and possibly for metals and alloys.

The role of the X-ray spectrograph in the copper base alloy industry: G. L. Crumrine, North American Smelting Co., Wilmington, Delaware.

VOL.
10
1957/5

Conference on Industrial Application of X-ray Analysis

THE Sixth Annual X-ray Conference on Industrial Applications of X-ray Analysis was held at the University of Denver, from 7 to 9 August 1957. The following papers on X-ray fluorescence analysis were presented:

A new microemission X-ray spectrograph. Design and operation of the direct emission curved crystal instrument: ERWIN C. BUSCHMANN, The General Electric Company, Schenectady, New York.

The Microemission X-ray Spectrograph is the result of the consolidation of the fine focus electron optics employed in the X-ray microscope, and the spectrograph goniometer used in fluorescent X-ray analysis.

The electron beam, 5 μ in diameter, directly bombards the sample under study. The beam is focused using a three element electrostatic lens system.

Provisions are made for continuous sample viewing with light optics. Sample manipulation provides for complete coverage of a sample $\frac{1}{4}$ in. in diameter.

The characteristic X-rays generated at the sample are allowed to pass through a beryllium window and fall on the analyzing crystal.

The curved crystal diffracts the characteristic X-ray wavelengths and refocuses them at the bilateral slit ahead of the detector. The goniometer may either be hand operated or motor driven through the various 2θ angles. Electron-beam currents are regulated by controlling filament power oscillator output. Signals are fed through a preamplifier into a ratemeter and recorder or into a high speed scaler which may be set to count for accurate preset periods of time. Samples may be investigated either by complete spectrum analysis of a single point on the sample or by determining concentration changes of a particular element by moving the sample across the electron beam.

Application of the microemission X-ray spectrograph. Comparison of analyses from small areas by J. F. NORTON, The General Electric Company, Schenectady, New York.

Techniques of determining spot size and sensitivity of the instrument will be developed. Spot sizes of the order of 5 μ have been obtained with the possibility remaining for improvement. Preliminary sensitivity measurements indicate that micro-microgram quantities of some elements are sufficient to be detected. Difficulties involved in finding desired target areas will be discussed. The inhomogeneities of standard samples used for conventional fluorescence X-ray quantitative analyses precludes their use for microemission techniques at least in some cases. Possible ways of determining homogeneity will be discussed. Analyses which can be performed to advantage may be classed into several categories.

1. The changes in composition occurring in grain boundaries can be detected and compared with the base material.
2. An inclusion in a metallic material can be brought under the electron probe and analyzed independently of the base material.
3. Changes in composition across a boundary between solid phases can be measured.
4. Diffusion coefficients between solid phases may be determined.
5. Thickness of thin films and variations in film thickness can be measured.

Examples of the instrument's performance will be given in some of these categories.

The X-ray fluorescent analysis of powders by the method of mixtures: JACOB SHERMAN, The Philadelphia Naval Shipyard, Philadelphia, Pennsylvania.

By developing the equations for X-ray fluorescent intensity it is possible to derive simple relations that will enable one to make precise analyses for an element, regardless of the matrix, in powder samples by the method of dilution with active or inert materials.

The method is applicable to any element, using K-radiation, if one were to use a monochromatic spectrograph. It is applicable in many instances using the ordinary polychromatic spectrograph.

The theory is developed and confirmed by experimental results.

X-ray spectrographic determination of tantalum, columbium, iron and titanium oxide mixtures using simple arithmetic corrections for interelement effects: Betty J. Mitchell, The Electro Metallurgical Company, Niagara Falls, New York.

A method of specific arithmetic corrections for absorption and enhancement interelement effects has been developed, with particular reference to the quantitative determination of mixtures of tantalum, columbium, iron, and titanium oxides. The combined oxides of these elements are prepared chemically from liquid, powder, or metallic samples; weight percentages are determined by reference to calibration and intensity correction curves relating fluorescent intensity to concentration and sample matrix. Tantalum, columbium, iron, or titanium oxide from 0·01 to 100 per cent concentration can be determined with a reproducibility of 1 per cent of the amount present at the 50 per cent concentration and 10 per cent of the amount present at the 1 or 0·1 per cent level. X-ray instrumental time required averages less than 10 min per determination. The corrections which have been established are universally applicable to combinations of these four oxides which may be obtained by chemical treatment from such materials as columbite or tantalite ores, tantalum or columbium metals, and titanium alloys. The method of arithmetic corrections for interelement effects is general in nature and may be applied to the determination of other elements in complex matrices.

Determination of uranium dioxide in stainless steels by the X-ray fluorescence-solution method: William Houk, Louis Silverman and Lavada Moudy, Atomics International, Canoga Park California.

In the fabrication of fuel elements for an experimental reactor, uranium dioxide and powdered stainless steel are mixed and then pressed between stainless steel plates.

The amount of chromium, nickel and iron present created a problem in the analysis of uranium present in the finished fuel elements. This paper describes a rapid method for the determination of uranium dioxide in stainless steel by direct X-ray fluorescent analysis after chemical solution of the sample in perchloric acid. Strontium is used as an internal standard. X-ray fluorescent methods of analysis have many advantages over the commonly used chemical methods such as the colorimetric, gravimetric, and volumetric because elements which ordinarily interfere need not be separated before analysis. Working curves, results, standard deviation, and method will be presented.

Results obtained with the modified Norelco Autrometer: David C. Miller, Philips Electronics, Inc., Mount Vernon, New York.

During the past year the Norelco autrometer has been modified with respect to several details. Operation with the helium path and flow counter is now possible for work with the soft elements. Rotation in and out of the loading position is automatic so that all that an operator is required to do is to load the specimen holder. The sample or standard in the reading position can be rotated in its own plane for elimination of diffraction effects and other sample preparation problems. Other modifications in the electronics have increased the reliability and ease of maintenance in the production models. A description will be given of this latest unit and data will be presented on the results obtained both with respect to precision and analytical determinations.

X-ray spectrographic analysis of nickel containing alloys with varied sample forms: C. Manning Davis and George R. Clark, The International Nickel Company, Inc., Bayonne, New Jersey.

The quantitative determination of metallic elements above atomic number 21 by X-ray spectrography employing flat metal specimens as samples has become a well established practice in many industrial laboratories. However, in a research laboratory samples for analyses are received in a variety of forms (e.g. solid wafers, millings, drillings, wire, powders, solutions, etc.).

Efforts have been made in our laboratory to apply the internal standard technique to dried oxides of metallic samples as well as applying this technique to samples mounted as received with no chemical treatment.

VOL.
10
1957/5

The advantage of the dissolved sample-dried oxide technique is the possibility of preparing synthetic standards. When available, metal wafers from which millings have been taken and analyzed by the dried oxide technique can be subsequently used to establish working curves for analysis using flat metal samples. Alloys investigated thus far include S-816, N-155, Ni-Vee Bronze and an additional material, Nisiloy.

Various mounting techniques with their advantages and limitations will be discussed. The accuracy and precision of the various techniques will also be presented.

A non-dispersive X-ray fluorescence unit for the analysis of biological tissue sections: Theodore Hall, The Sloan-Kettering Institute for Cancer Research, New York.

An X-ray fluorescence analysis unit has been designed and built especially for the measurement of certain mineral elements in individual biological tissue sections. Such a section may contain in the neighborhood of 10^{-10} g of an element of interest, in a concentration in the range of 1–100 p.p.m.

The unit consists of a special high-power X-ray tube with a built-in interchangeable secondary radiator, which irradiates the specimen with the characteristic lines of the radiator element, and a proportional counter and pulse-height analyzer system, which provides analysis of the X-ray spectrum emitted by the specimen. Because the emitted spectrum is greatly simplified by the use of an appropriate radiator element, a diffracting crystal can be omitted, permitting a great increase in absolute sensitivity.

The system is feasible only because of two pecularities of our biological specimens: they are so thin that matrix effects are negligible, and they consist essentially of a few mineral elements in a light matrix.

Design considerations, calibration procedures, procedures for the analysis of the observed proportional counter pulse-height spectra and results to date will be discussed.

OL.
10
7/58

Rock analysis by X-ray fluorescence spectroscopy: Arthur A. Chodos, J. J. Branco and C. G. Engel, The California Institute of Technology, Pasadena, California.

Our laboratory has been interested in the use of the X-ray spectrograph for routine rock analysis within limited rock types. This paper is meant as a progress report and to indicate the direction of our work on amphibolites to others interested in the problem of rock analysis.

Even with the use of flow counters and pulse discriminators the intensities of the magnesium, aluminum and silicon peaks are quite low and most dilution techniques may not be used. The direct determination of major elements (except sodium) yields results directly comparable to the chemical results for potassium, manganese and titanium in the range from 0·1 to 3 per cent as the oxides. For iron (10–20 per cent), calcium (8–12 per cent) and silicon (45–52 per cent) the accuracy is 2–3 per cent but for each element occasional samples will be 5 per cent from the chemical values. Aluminum and magnesium yield erratic results.

The use of ratios between elements occurring in the samples yields slightly improved accuracies. The use of a strong absorber such as tungstic acid (40 per cent by weight) greatly improves the ratios for aluminum and magnesium, without appreciably affecting their intensities. By a combination of the direct and tungstic acid techniques it is possible to attain accuracies of 2–3 per cent with analysis time of 2 hr. At present we are attempting a combination with an internal standard method to yield greater accuracy.

Micro-analysis by X-ray absorption, fluorescence, emission and diffraction using ultra-fine X-ray sources: V. E. Cosslett, P. Duncumb, J. V. P. Long and W. C. Nixon, The University of Cambridge, Cambridge, England.

Fine focus X-ray tubes developed for projection X-ray microscopy can also be used for X-ray micro-analysis. Areas about 10 μ dia. of thin sections have been analysed by measuring differences in X-ray transmission, with particular reference to the determination of calcium in biological materials and in minerals. The high intensity of this X-ray point source has permitted micro-fluorescence analysis of similar small areas with high sensitivity and reasonable time. The same electron optical system has been used for micro-emission analysis of rock slices and

mineral grains. By scanning the electron beam over the specimen surface and recording either the scattered electrons or the emitted X-rays, a two-dimensional picture can be displayed of the physical features or of the distribution of a particular element respectively. The analysis of a selected volume of 1 μ^3 in the surface has been obtained by plotting the characteristic line emission spectrum with a crystal spectrometer and proportional counter. The sensitivity is 0·1 per cent or 10^{-14} g. Micro-beam X-ray diffraction has also been used with a stationary X-ray source both for transmission and back reflection with a 10 min exposure from a 10 μ dia. area.

Applications of the electron probe microanalyzer: L. S. Birks and E. J. Brooks, The U.S. Naval Research Laboratory, Washington, D.C.

Applications to nonmetallic specimens such as minerals will be shown and the special techniques required for such specimens described. These include coating the surface with a thin conducting layer and pre-photographing to map out the areas of interest. Specific examples of copper–iron minerals will be given. Other applications to metallic systems such as mass transfer studies in liquid metal cooling systems will also be shown.

Applications of X-ray spectrography to continuous analysis for process control: Robert A. McCune, William M. Mueller and Pauline J. Dunton, The Denver Research Institute, Denver, Colorado.

Studies have been made of the application of X-ray spectrography to continuous analysis for process control. To date the most widespread application of fluorescent X-ray spectrography to process control has been in measurement of plating thickness. Realising that many other processes could use a method of continuous analysis of moving materials, these studies were undertaken.

A modified "dog-house" was constructed so that material could be passed through the X-ray beam of a conventional X-ray spectrograph at various linear speeds. Detectability vs. material speeds were studied for a number of elements in various mediums.

Application of fluorescent X-ray spectrography as a continuous analytical tool looks very promising. Further studies on specific plant problems should provide useful and advantageous industrial applications of the basic information developed here.

Direct assay for molybdenum and ruthenium in uranium alloys by X-ray emission spectrometry: D. S. Flikkema and R. V. Schablaske, The Argonne National Laboratory, Lemont, Illinois.

It has been found possible to determine quickly the concentrations of molybdenum and ruthenium in non-radioactive alloys representative of high burn-up reactor fuels by the method of X-ray emission spectrometry. Preliminary steps of chemical dissolution and separation are not required. The alloys, essentially ternaries of molybdenum and ruthenium with uranium, are being studied because they are considered to typify the alloys which will result from cycling uranium fuel elements through the sequence of fabrication, use and pyrometallurgical processing.

The analytical procedure involves sampling of the ingot by slicing with a silicon carbide wheel at the plane of interest and reducing the surface to the flatness and finish obtained by a 5 min grinding and polishing operation. In the X-ray spectrograph the flat surface is examined for the intensities of its molybdenum and ruthenium K-emission lines, with counting times of 1–8 min. Calibration plots of intensity versus chemically determined wt. per cent are established and used for subsequent sets of analyses.

X-ray emission spectrographic analysis of bastnaesite rare earths: Farrell W. Lytle, James I. Botsford and H. Heller, The U.S. Bureau of Mines, Reno, Nevada.

An X-ray emission spectrographic method of analysis is presented for the determination of rare-earth elements in fractions obtained from bastnaesite ore. The method includes the determinations of yttrium, thorium, lanthanum, and the rare-earth elements in various complex mixtures. The method is based upon comparing the sample to synthetic standards approximating the composition of the samples. Working curves are plotted on an absolute intensity basis, with

VOL. 10 1957/5

no correction for background. Examples of working curves and the analyses of typical rare-earth concentrates are included. The selection of spectral lines for the various sample matrices is discussed. A special technique is used for samples in which rapid hydration and carbonation occurred.

By analyzing synthetic samples of known composition, the accuracy of the method was determined. The error of analysis was about 3 per cent of the amount present in the range from 5 to 100 per cent and about 7 per cent in the 0·5 to 4 per cent range. A maximum of about 40 samples per day may be analyzed for 7 elements each. The advantages and disadvantages of the method are discussed.

Principles and applications of proportional counters for X-ray spectrographs: Irwin I. Bessen, Philips Electronics, Inc., Mount Vernon, New York.

The two general uses of proportional counters in X-ray analysis are discussed in the light of advantages and limitations inherent in the type of counter construction. Some effects on spectrographic results and industrial gaging are cited.

Components for X-ray polychromators: J. L. Jones, K. W. Paschen and H. H. Swain, The Applied Research Laboratories of Glendale, California.

The use of the polychromator (multichannel spectrometer) for X-ray analysis allows choice of the optimum combination of slit width, crystal type, focussing circle radius and detector for each of the elements to be determined by the instrument.

Comparisons will be made of various curved and ground crystals such as quartz, lithium fluoride, sodium chloride and ADP used in a focussing spectrometer. The effect of the width of the entrance and exit slits upon resolution, line intensity and line-to-background ratios will be discussed. Gas filled detectors such as Multitrons, flow-proportional counters and Geiger counters will be discussed as to the effect of the filling upon efficiency and upon their use with counting or integrating techniques. Limits of detectibility for various elements with optimum combinations of the above components will be reported.

OL.
10
7/58

Papers to be published in future issues

A. K. Rusanov and V. G. Khitrov: Spectrographic analysis of ores by introducing the powder into the arc in a stream of air

L. H. Jones: Systematics in the vibrational spectra of uranyl complexes

R. A. Spurr and T. A. Chubb: Absorption coefficients of four organic fluorine compounds in the vacuum ultra-violet

L. Bovey: A tuneable microwave cavity for excitation at 2540 Mc/s of an optical spectroscopic source

G. A. Crosby and M. Kasha: Intramolecular energy transfer in ytterbium organic chelates

C. G. Cannon: The nature of hydrogen bonding

R. C. Taylor and A. R. Emery: The Raman spectra of four isotopic varieties of diborane in the gas phase

L. Bovey: Emission and absorption spectra of plutonium excited in a King furnace

F. González-Sánchez: Infra-red spectra of the benzene carboxylic acids

H. R. Linton and E. R. Nixon: Infra-red spectrum and force constants of silyl-*d*-iodide

A. N. Zaïdel: Spectral-isotopic method for the determination of hydrogen in metals

C. Rimington, S. F. Mason and O. Kennard: Porphin

L. B. Archibald and A. D. E. Pullin: Solvent effects in infra-red spectra of compounds containing the carbonyl group

A. Stojiljkovic and D. H. Whiffen: The vibration frequencies of unsymmetrical *para*-dihalogenobenzenes

A. Stojiljkovic and D. H. Whiffen: The vibration frequencies of the symmetrical *para*-dihalogenobenzenes

N. S. Ham and A. Walsh: Microwave-powered Raman sources

R. A. Ford and F. Parry: Electronic and vibrational states of carbonyl compounds—I. Electronic states of camphorquinone

E. Bright Wilson, Jr.: Determination of the order of atoms in a linear molecule

L. E. Owen and D. C. Manning: Mechanized arc-spark stand for emission spectrography

J. M. Martin, Jr., R. W. B. Johnston and M. J. O'Neal: Infra-red absorption of solid state *n*-paraffins-relationships to crystalline type

D. F. Smith: Infra-red spectra analysis for hydrogen fluoride

B. Stevens: A relationship between some bond properties of diatomic molecules and the ionization potentials of their constituent atoms

VOL.
10
1957/5

Spectrochimica Acta, 1958, Vol. 10, pp. 341 to 368. Pergamon Press Ltd., London

The nature of hydrogen bonding

A review of published work and discussion

C. G. Cannon
Research Department, British Nylon Spinners Ltd., Pontypool, Mon.

(*Received* 29 *August* 1957)

Abstract—Published work on spectroscopic and theoretical investigations of hydrogen bonding are reviewed (eighty references).

This evidence is discussed and the conclusion that the quantum contribution to hydrogen bonding is of major importance leads to three criteria for hydrogen bond formation.

(a) Partially ionic proton donor bond $-X^{-\delta}-H^{+\delta}$.
(b) Asymmetric lone pair orbitals on proton acceptor.
(c) X—H bond and lone pair orbital collinear.

The extreme broadening of the OH stretching vibration band has many possible contributory mechanisms, but proton transfer across the bond from the vibrationally excited —X—H may make the major contribution.

General introduction

Several interaction mechanisms may operate when molecules are close packed in the liquid and solid states although some molecules, where such forces are strong, are known to be associated in the vapour state as well. Assemblies of molecules behave differently mainly because of differences in the magnitude of the various contributions to the total intermolecular interaction energy. Dispersion forces, which are quantum mechanical in origin, are directional but transient at any instant and attain a spherical symmetry with time. Dispersion forces are thus on average non-directional and lead to the closest packing of molecules. Other secondary forces which can be treated by simple electrostatics include ion–ion, dipole–dipole, and dipole–induction interactions. These, since the ions or dipoles are related directly to the geometry of the molecule, will be directional forces and will lead to orientation-dependent interactions, i.e. they develop a maximum interaction energy for a specific relative orientation of the molecules. Such specific interactions impose orientation conditions on the molecular packing which may oppose the tendency of the dispersion forces to give the closest packing. Specific orientation-dependent interactions will occur if they are energetically favoured, and will be disturbed by collision processes, i.e. sensitive to temperature particularly in the liquid or vapour states.

Hydrogen bonding has long been recognized as a specific interaction between an —X—H bond of one molecule, described as the proton donor, and an atom Y of another molecule, described as the proton acceptor. Hydrogen bonds have been studied by four methods: chemical, crystallographic, spectroscopic, and theoretical. This review is mainly concerned with the last two, although both here and in the literature they are all closely linked together.

The chemical approach involves the study of the thermodynamic properties of

liquids or solutions from which the energies and entropies of interaction are derived and the type of association e.g. dimeric, trimeric, polymeric, is analysed. This has led to all observed interactions in which molecules with —X—H bonds (even C—H) are involved, being ascribed rather loosely and perhaps unjustifiably to "hydrogen bonding". For example, the heat of mixing of two liquids which is a maximum for a 50 : 50 per cent mixture is taken as proof of the formation of a 1 : 1 hydrogen-bonded complex [2].

Actually it is only necessary for the dispersion forces between the molecules to differ in the two liquids for the heat of mixing to be a maximum in the 50 : 50 mixture. At best the energy changes can be taken only as a guide to possible interaction mechanisms. HUNTER [3] has reviewed the chemical aspects of hydrogen bonding.

The crystallographic studies have shown for very strong hydrogen bonds of the type X—H – – – – Y in crystals, that the X – – – Y distance is appreciably smaller than the sum of the known van der Waals' radii. This proves the existence of an attractive force able to overcome to some extent the repulsive forces between atoms (or molecules). Once again, any interaction which leads to short X—H – – – Y distances is loosely described as "hydrogen bonding". X-ray diffraction results for crystals have been reviewed by DONAHUE, who refers particularly to polypeptide structures in relation to simpler crystals [4].

The spectroscopic effects and the more physical aspects of hydrogen bonds have been summarized by DAVIES [5], who subscribes to the view that hydrogen bonding is a particular case of electrostatic interactions whose strength is due to the small size of the proton allowing a close approach of the interacting dipoles. KELLNER has dealt more specifically with OH group interactions and reviews several empirical and theoretical treatments of the problem from the spectroscopy viewpoint [6].

Very recently COULSON [6a] has reviewed the present position of the theory of hydrogen bonding and has dealt in greater detail with some of the theoretical points reviewed here.

The spectroscopic approach

Introduction

Several effects have been observed in the spectra of hydrogen bonded molecules. In the infra-red or Raman spectra, where molecular

$$\begin{matrix} & f & & f' & \\ \text{R—X—H} & - & - & - & - & - \text{Y—R'} \end{matrix}$$

bond stretching and deformation (bending) vibrations are observed, the force constants controlling the frequencies for the X—H bond (f) are modified by the hydrogen bond forces (f') and frequency shifts result on association. Similarly, the frequencies of the Y-atom vibrations will also be modified. Further, the existence of the hydrogen bond force field (f') means that discrete intermolecular vibrations may occur at low frequencies (hydrogen bond stretching vibrations).

Finally, it has been recognized that lone pair non-bonding electrons on the Y-atom play an important part in hydrogen bond formation [1], and the influence

VOL. 10 1957/5

of hydrogen bonding on the electronic absorption spectra ($n \rightarrow \pi$ transitions) associated with these non-bonding electrons has been studied [7, 7a].

The spectroscopic observations are listed below.

1. Shift in X—H stretching frequency (infra-red, Raman).
2. Change in —X—H absorption intensity (infra-red, Raman).
3. Considerable broadening of —X—H absorption band (infra-red, Raman).
4. Shift in —X—H deformation frequencies (infra-red, Raman).
5. Intensity and breadth of X—H deformation bands (infra-red, Raman).
6. Shift in proton acceptor (Y) bond frequencies (infra-red, Raman).
7. Intensity and breadth of Y—R′ absorption bands (infra-red, Raman).
8. Fine structure of low-frequency bands (Raman).
9. Changes in electronic absorption spectra (ultra-violet).

Clearly, an adequate theory of hydrogen bonding has much to explain, but, before reviewing the various attempts that have been made in the literature, some of the factors influencing frequency, intensity, and breadth of vibrational absorption bands will be briefly discussed.

Since, apart from secondary effects of mechanical or electrical coupling in the molecule or crystal lattice, the vibration frequency of a bond is determined by its strength (force constant) and the masses of the vibrating atoms, any potential field which can modify the bond strength can be detected by a frequency shift. For example, the relatively weak dispersion forces between the non-polar, symmetrical molecules of methane produce easily detectable frequency shifts with change of state [8] as illustrated in Table 1.

Table 1

	Gas	Liquid	Solid
CH_4	2914 cm^{-1}	2909 cm^{-1}	2906 cm^{-1} (83°K)
HCl	2886 cm^{-1}	2785 cm^{-1}	2768 cm^{-1} (100°K)

Dispersion forces have been approximately calculated as a function of the polarizability α and ionization potential I of the molecules and their distance R by LONDON [9]:

$$\left(\text{Energy} = -\frac{3}{4} \cdot \frac{\alpha^2 I}{R^6}\right)$$

Thus, as α or I increases, the dispersion forces increase and, for example, in HCl approach 5 cal/mole for a close-packed structure [1] with an observed frequency shift from gas to liquid of 100 cm^{-1}.

A frequency shift on association therefore cannot identify the interaction mechanism, although the magnitude of the shift will be a guide to the interaction energy [9a].

The intensity of an absorption band in the infra-red is pictured classically as a

function of the rate of change of the electrostatic dipole moment with the amplitude of vibration. This is illustrated in Fig. 1. [8; p. 241] which relates the dipole moment of the bond μ with its length r, r_0 being the equilibrium distance. An intensity change $(\delta\mu/\delta r)$ may be due to a change in r_0, a change in magnitude of the polarity of the bond (μ), or both. However, the observed increase in intensity of up to tenfold on hydrogen bonding would imply a very great increase in bond polarity and some other contributory mechanisms may be involved. Analogously, in Raman spectra the line intensity is a function of the rate of change of polarizability $(\delta\alpha/\delta r)$.

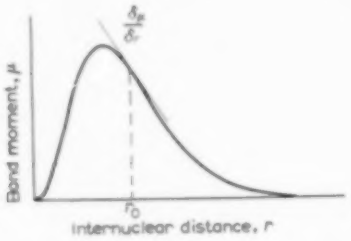

Fig. 1.

The band widths observed in hydrogen bonded molecules may be from 100 to 1000 cm^{-1} wide at the half-peak height. The natural line width, Doppler broadening, etc. will be negligible in comparison, so that the observed broadening must be due either to a transition involving equally diffuse energy levels for each molecule, or to the integral effect of a distribution of sharp energy transitions which vary in energy from molecule to molecule about a mean value (band peak).

In the liquid state the intermolecular distances will be distributed about a mean value because of the collisions due to translational energy. The width of the distribution will clearly be a function of the thermal energy (kT), and can be a contributory cause of the observed broadening of the absorption bands.

Review of Spectroscopic Work

Low-frequency spectra

The very low-frequency vibrations of hydrogen bonded molecules were first observed in the Raman spectrum of water and ice as long ago as 1936 by GROSS and VUKS [10], and CROSS, BURNHAM and LEIGHTON in 1937 published a detailed study of the Raman spectra of ice and water at a series of temperatures [11].

Recently, GROSS and VAL'KOV have reinvestigated these low-frequency Raman lines in ice, formic acid, and crystals of gypsum and magnesium chloride containing water of crystallization [12]. In the crystals of formic acid, gypsum and magnesium chloride a whole series of sharp closely spaced lines were observed around 200 cm^{-1} which GROSS assigns to intermolecular vibrations controlled by the hydrogen bond force constant.

The multiplicity of lines is ascribed to the very great anharmonicity of the potential function of the hydrogen bond due to the rather diffuse, shallow, potential well. Thus the vibrational levels will be close together, and at room temperature many levels will be populated by different molecules. The intensity

VOL.
10
1957/5

distribution in the various lines did not fit the expected population of the various energy levels however.

Such fine structure was observed in the Raman spectrum of ice at −4°C, the lines spreading from 160 to 300 cm^{-1} around the strong peak at 212 cm^{-1}, but was much more diffuse, perhaps due to the fact that the spectra were recorded very close to the melting point of ice. GROSS stresses his observation with these crystals of the sharp fine structure in the 200 cm^{-1} region while at the same time the OH stretching frequency 3500 to 3200 cm^{-1} was broad and diffuse, as in liquids.

The X—H *stretching frequency*

Examples of the investigation of the infra-red spectra of hydrogen bonded systems are far too numerous to list here and are covered by the reviews mentioned above [5, 6]. Experimental results of particular significance to the discussion of the theories of hydrogen bonding will be briefly reviewed. Studies of the overtones of the OH stretching frequency as well as the fundamental are described by MECKE [13], who also investigated the influence of the solvent medium on the association of phenol.

SHUBIN [14] has shown that the carboxylic acids (formic, acetic, propionic, *n*- and *iso*-butyric, and *iso*-valeric acids) exhibit OH absorption bands in the vapour phase as broad and complex as in the liquid state. The series of acids showed similar absorption bands of equal intensity both in vapour and liquid states, but the molar absorption coefficient of the liquid was about one and a half times the vapour value.

The breadth of OH bands in the liquid and solid (crystal) states has been discussed at some length [15]. KLETZ showed that in phenols the frequency shift was larger in the crystal than in the liquid, presumably due to the absence of thermal collisions in the solid state. The bands were still very broad in single crystals; only slightly sharper than in the liquid; so that collision perturbation only contributes a little to the breadth of the hydrogen bonded OH bands in liquids.

KETELAAR reported no change in the enormous breadth of the OH bands in crystals of KH_2PO_4 even at liquid-air temperatures far below the Curie point. He suggests the breadth may be due to coupling of the OH vibration with a continuum of low-frequency elastic oscillations or may result from the highly anharmonic potential function. MECKE suggested that the proton vibration may be highly damped by the strong attractive fields of the two oxygen atoms in an OH – – – O bond and therefore show a broad band. UBBELOHDE pointed out that, particularly in crystals, hydrogen bonding is a co-operative effect extending throughout the lattice, and is associated with anomalously large thermal expansions and by isotope effects on substituting deuterium for hydrogen (lattice expands).

The fine structure observed in the broad OH band of carboxylic acids and the NH peaks in the spectra of amides and polyamides [16, 17] have been analysed and interpreted as due to combinations of low-frequency intermolecular vibrations with the X—H stretching vibration. On this basis only difference tones are observed ($\nu_{OH} - \nu_{low}$) and no reason has been suggested for the complete absence

of sum tones ($\nu_{OH} + \nu_{low}$). SHEPPARD *et al.* [18], however, have shown for the carboxylic acids that there is no change in relative intensity of the components of the OH absorption band with temperature which would be expected if the fine structure were due to combination with low-frequency modes. No dependence of "ν_{low}", the apparent displacement of ν_{OH}, on the mass of the molecule was found, although any intermolecular vibration would be expected to vary in frequency between say propionic acid and palmitic acid. Furthermore, SHEPPARD [19] has shown that a quite different pattern of fine structure of the OD band is observed in the deutero acids as compared with the OH of the normal acids. He has very plausibly assigned each peak in both the OH and OD fine structure to overtones and combination frequencies of the —COOH or —COOD group (e.g. $\nu_{C=O} + \delta_{OH}$, etc.). These normally very weak bands are enhanced in intensity by Fermi resonance with a broad intense *structureless* OH (or OD) band or with CH or CH_2 bands. Eleven peaks in formic acid vapour spectrum, four in acetic acid, and the two principal peaks in benzoic acid were satisfactorily explained in this way.

In the case of the amide group the NH fine structure may be similarly assigned 3200 cm^{-1} to (amide-I + amide-II, 1650 + 1550 cm^{-1}) and 3080 cm^{-1} to (2 × amide-II). BADGER *et al.* [19a] have suggested similar assignments for the weak NH bands in urea and collagen.

The half-peak band widths of representative materials are given in Table 2, together with approximate frequency shifts ($\Delta\nu$ cm^{-1}).

Table 2

	Half-peak width	Band centre	$\Delta\nu$
Alcohols	350–450 cm^{-1}	3360 cm^{-1}	300 cm^{-1}
Phenols	350–450 cm^{-1}	3330 cm^{-1}	300 cm^{-1}
Carboxylic acids	600–1000 cm^{-1}	3000 cm^{-1}	600 cm^{-1}
$(FHF)^-$	c. 250 cm^{-1}	1450 cm^{-1}	2700 cm^{-1}

The integrated intensity of ν_{OH} for hydrogen-bonded alcohols was found by BARROW [19b] to increase with the frequency shift. The integrated intensity increased with the acidity of the alcohol and with the basicity of the proton acceptor.

BARROW concluded that the change in ionic character of X—H on hydrogen bonding contributes more to the intensity increase than alteration in hybridization of the X-atom.

HUGGINS and PIMENTEL [19c] also showed the correlation between integrated intensity and frequency shift for a given OH bond in different acceptor solvents. They demonstrated that the half-peak width varied linearly with frequency shift according to the equation $5\nu_{\frac{1}{2}} = 0{\cdot}72\ \Delta\nu + 2{\cdot}5$ cm^{-1}, and suggested that the presence of a variety of deviations from linear hydrogen bonds was responsible for the width.

VOL. 10 1957/5

The —X—H *deformation frequencies*

In the monomeric molecules, e.g. R—O—H alcohols, the deformation modes degenerate into free rotations of the —OH group around the R—O bond. With the restraints imposed by hydrogen bonding the in-plane $R\diagup O\diagdown H$, angle deformation ($\parallel\delta_{OH}$) and the out-of-plane deformation ($\perp\delta_{OH}$) are resolved. Similar modes exist for the carboxylic acid dimers. In the latter case HADZI and SHEPPARD [20] have assigned the band near 935 cm^{-1} to the out-of-plane deformation, but show, by the shifts produced by deuteration, that the in-plane mode couples with the C—O— stretching vibration to give two complex modes absorbing at or near 1420 and 1300 cm^{-1}. The half-peak band widths of these absorptions are listed in Table 3, taking the ranges covered in thirty spectra given by HADZI and SHEPPARD.

Table 3

Mode	Frequency	Width
$\perp\delta_{OH}$	935 cm^{-1}	50–100 cm^{-1}
$\parallel\delta_{OH}$	1300 cm^{-1}	25–50 cm^{-1}
ν_{C-O-}	1420 cm^{-1}	25–50 cm^{-1}

The situation is less clear in alcohols and phenols, since assignments of bands to the deformation modes cannot be made with certainty. The frequencies and band widths for liquid methanol recorded at British Nylon Spinners Ltd. (B.N.S.) are given here as an example in Table 4.

Table 4

Assignments	Frequency	Width
δ_{OH} ?	1410 cm^{-1}	80 cm^{-1}
	1110 cm^{-1}	40 cm^{-1}
ν_{C-O} ?	1025 cm^{-1}	40 cm^{-1}

STUART and SUTHERLAND have attempted to assign both in-plane and out-of-plane deformation frequencies of alcohols [67, 68] by studying the shifts due to association, and on substituting D- for H-atoms in the hydroxyl group. The out-of-plane frequency is found in liquid alcohols near 670 cm^{-1} (475 cm^{-1} for OD groups), but disappears on dilution or in the vapour [67]. In the later paper they discuss the in-plane deformation [68] for which several alternative assignments exist and several bands in the 1500–1000 cm^{-1} region shift both on dilution and deuteration, although the deutero alcohols only show a single frequency which shifts on dilution. Frequencies and band widths are summarized in Table 5.

Table 5

Mode	Associated		"Free"	
	Frequency	Width	Frequency	Width
$\parallel\delta_{OH}$	1410 / 1330 cm^{-1}	50–100 cm^{-1}	1250 cm^{-1}	sharp
$\parallel\delta_{OD}$	950 cm^{-1}	$\simeq$50 cm^{-1}	900 cm^{-1}	sharp
$\perp\delta_{OH}$	$\simeq$650 cm^{-1}	$\simeq$200 cm^{-1}	700–50 cm^{-1}	very diffuse

The broadness of the perpendicular deformation may well arise in part from the tendency to free rotation which is restricted by hydrogen bonding such that on association the band width in fact narrows.

HUGGINS and PIMENTEL [19c] have remarked on the lack of intensity change of bending modes on hydrogen bonding despite the increased intensity of the stretching mode. In water, for example, the intensity of δ_{OH} decreases.

The Y—R *frequency*

In the 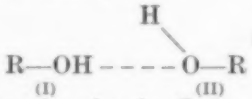 system the effects of the association on the OH frequencies of molecule (I) have been summarized above. The hydrogen bond to the oxygen atom of molecule (II) will have a second-order effect on the force constant of its free O—H bond and produce a very much smaller frequency shift. This may occur in dimeric association of alcohols or phenols or apply to the end molecule in polymeric association [21]. The R—O frequencies are shifted by association, but have not been studied in any detail.

Table 6

Substances and assignment	Frequency shift	Band width
Amide + phenol $\nu_{C=O}$	18 cm^{-1}	30 cm^{-1}
Carboxyl acids $\nu_{C=O}$	45 cm^{-1}	$\simeq$30 cm^{-1}

The situation is clearer in carboxylic acids, or in "mixed" hydrogen bonds formed between hydroxyl compounds and, for example, ketones, esters, or nitro compounds, etc. Such hydrogen bonds are of the type R—OH - - - O=C< and the >C=O frequencies are also lowered by the hydrogen-bond forces.

No fine structure has ever been reported, however, and the bands are not very broad. Illustrative examples taken from B.N.S. work are given in Table 6.

VOL. 10 1957/5

Correlation of frequency shifts with crystallographic data

The qualitative relations between the X—H stretching frequency shifts and the broadness of the band, and the energy of association and length of the hydrogen bond (X – – – – Y distance) have been recognized for a long time.

Recently, LORD and MERRIFIELD [22] and RUNDLE *et al.* [23] have established fairly precise correlations between X—H frequency shift and X – – – – Y distance for large numbers of crystals or vapours for which precise X-ray or electron

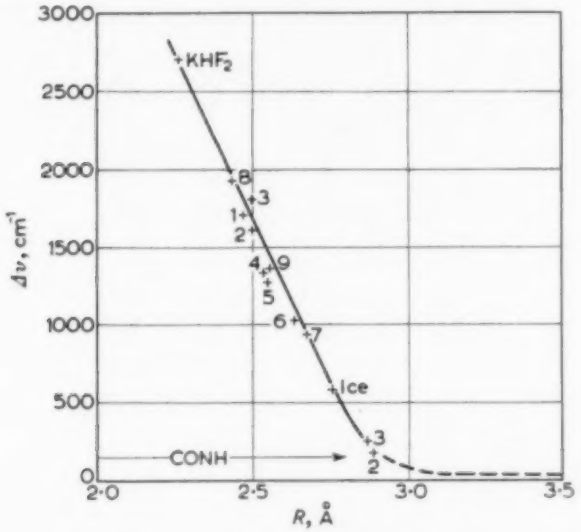

Fig. 2. Frequency shift ($\triangle\nu$) and X – – – Y distance (R).

diffraction data was available. LORD's graph is reproduced in Fig. 2. When the X – – – – Y distance becomes appreciably shorter than the sum of the van der Waals' radii of X—H and Y, the frequency shift increases linearly with decrease in XH – – – Y distance. The bifluoride ion $(F - - - H - - - F)^-$ with a frequency shift of 2700 cm^{-1}, an F – – – F distance of 2·24 Å, and interaction energy of 27 kcal/mole, represents the strongest and shortest hydrogen bond known. Measurements of heat capacities down to very low temperatures show no residual entropy at absolute zero, i.e. position of proton is unique and the ion must be symmetrical [24]. Analysis of the overtone bands of KHF_2 show from their anharmonicity coefficients that the potential function which controls the hydrogen vibration frequencies has a narrower well than a parabolic simple harmonic oscillator, which confirms the thermodynamic analysis that no double potential minimum exists [25]. Thus the symmetrical $(\overset{-e}{F}—\overset{+e}{H}—\overset{-e}{F})$ ion represents a limiting case of X—H – – – – Y interaction, but the formal charges on the atoms are an added complication in that both bonds in the ion should strictly be treated as partially covalent-partially ionic links.

These correlations have been extended by PIMENTEL and SEDERHOLM [25a], WELSH [25b] and MOULTON and KROMHOUT [25c].

Electronic spectra and hydrogen bonding

In comparison with infra-red and Raman data, there has been much less detailed work carried out on the effects of hydrogen bonding on ultra-violet absorption or emission spectra. Association band shifts are detectable; for example, NAGAKURA and GOUTERMAN [7b] have studied the association equilibria of α- and β-naphthols with three different proton acceptors in *n*-heptane solution. They conclude that hydrogen bonding is not solely electrostatic in mechanism and that a charge transfer (quantum mechanical delocalization) mechanism also contributes. The interpretation of the frequency shifts is still being developed and the papers of BREALEY and KASHA [7] and PIMENTEL [7a] summarize the present position. No great contribution to the theory of hydrogen bonding has resulted as yet from this field, although proton transfer across the hydrogen bond in the electronically excited state has been postulated [59a, see later, p. 343].

Theoretical approach

Earlier Work

The early electrostatic theories of BAUER and MAGAT have been critically compared by FREYMAN [26] with other elementary treatments involving resonance contributions from ionic structures. As early as 1936 GILLETTE *et al.* [27], assuming that the hydrogen bond in carboxylic acid dimers was covalent in character, postulated fourteen canonical forms and calculated values for the O - - - O distance and association energy which were in reasonable agreement with experiment.

CROSS, BURNHAM and LEIGHTON [11] worked out, by a simple perturbation method, the potential function for the hydrogen bond in ice crystals. They also assumed that the hydrogen bond had a covalent potential function and represented it by the O—H Morse function modified by a multiplying factor. By assuming ranges of values, they were able to get reasonable agreement between their observed Raman frequencies and calculated values when the factor was 0·25, i.e. the hydrogen bond was covalent and roughly a quarter of the strength of the —O—H bond.

On the other hand, DAVIES has given a detailed calculation of the association energy of acetic acid "dimers" based solely on electrostatic interactions but taking into account dipole–dipole, dipole–induction, and dispersion forces. He also gets a reasonable agreement with experiment [28].

Thus, right from the start there has been a conflict of opinion, backed up by plausible calculations from both sides, on hydrogen bonding being either solely an electrostatic interaction, or quantum mechanical in origin.

The electrostatic theories were all based on models in which the observed dipole moments of the molecules involved are represented as formal charges on the atoms, attributing ionic character to all bonds, e.g. $\overset{+\delta}{H}\!-\!\overset{-2\delta}{O}\!-\!\overset{+\delta}{H}$. This model was assumed in the wave mechanical treatment given by COGGESHALL [29]. He takes the Morse potential function for the OH bond modified by the electrostatic

VOL. 10 1957/5

field at the position of the proton due to the other atoms in the system and, solving the Schroedinger equation for the vibrational energy levels, calculated the frequency shifts and intensity changes, and the interaction energy. Reasonable values for the frequency shifts and energies were obtained, but calculated intensities were very much in error and have been severely criticized by FRANCIS [30].

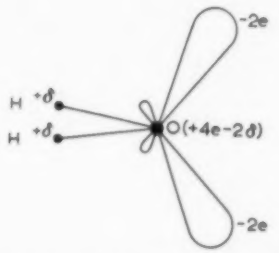

Fig. 3. Formal charge of water molecule (H—O—H ⊖ bonds and lone pair orbits tetrahedral).

The validity of this model for the electrostatic theories has been dealt a heavy blow by the L.C.A.O. M.O. calculations of COULSON [31] and LENNARD JONES and POPLE [32], who showed that in the water molecule, for example, the major contribution to the dipole moment of the molecule, comes from the lone pair electrons which occupy asymmetric hybrid orbitals (sp^3) of the oxygen atom. The OH bonds are thus much less ionic than the earlier workers supposed, and the formal charge distribution has to be modified (Fig. 3).

The tetrahedral structure of ice results from the complete co-ordination of the hydrogen atoms with the lone pair electrons, and the hydrogen bonds so formed have the O—H bonds colinear with the axis of the lone pair orbital. LENNARD JONES and POPLE still considered hydrogen bonding as an essentially electrostatic interaction but based their calculations on the refined formal point charge model below.

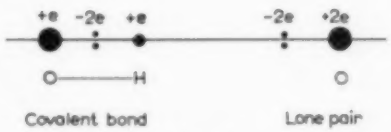

Fig. 4.

In the discussion of "lone pair interactions" they pointed out that for association to occur, the lone pair of electrons must occupy asymmetric hybrid orbits. In molecular nitrogen, (N_2), which shows no tendency to associate, the lone pairs occupy 2*s* atomic orbitals which are spherically symmetrical about the positive nucleus and have no resultant directional electric moment.

A refined calculation of orbital dipole moments in H_2O and NH_3 has been made by BURNELLE and COULSON [32a], who showed that the polarities of $\overset{-\delta}{O}—\overset{+\delta}{H}$

and $\overset{+\delta}{\text{N}}$—$\overset{-\delta}{\text{H}}$ bonds were in opposite senses. They also demonstrated a transverse bond moment which varies with bond angle and therefore contributes to the intensity of deformation vibrations in a different way from the longitudinal bond moment.

TORKINGTON [33] suggested that molecular orbital theory should be used to describe hydrogen bonding. The electrostatic theory fails to take into account the repulsion that would be expected in the absence of any specific interaction. He suggests that the σ-bonding electrons must be more localized between the X- and H-atoms, thus weakening the bond and allowing it to expand, so providing an attraction between the proton and the electron shell of the Y-atom. TORKINGTON suggests that this can only happen when both X- and Y-atoms have lone pairs of non-bonding electrons. He has not developed this brief qualitative picture further.

Many Russian workers have investigated hydrogen bonding both spectroscopically and theoretically. Three different theories have been put forward to account for experimental observations. These are the early fluctuation theory of LANDSBERG and BATUEV (perturbing effects of kT referred to above), the frequency modulation theory of BATUEV [34], and the predissociation theory of STEPANOV [35]. VOLKENSHTEIN, ELYASHEVICH and STEPANOV have attempted a critical evaluation of all three theories [36].

BATUEV has considered the problem in terms of classical mechanics and suggests that, since the XH bond will execute many cycles of oscillation while the hydrogen-bond stretching low-frequency mode executes one cycle, the overall effect will be a frequency modulation of the XH stretch by the X – – – Y oscillation. The unperturbed X—H frequency acts as the carrier wave and the modulation leads of course to side bands. This theory only restates in the descriptive language of radio-wave propagation the appearance of combination frequencies (sum and difference tones) of fundamental modes of vibration. BATUEV then considers that these combination bands become smeared out by thermal fluctuations into a broad featureless absorption band. In some cases residual fine structure is observed (e.g. carboxylic acids, see p. 333 below). The principal objection to this theory is the persistance of broad bands in dimers of the acids in the vapour state, and in crystals which simultaneously exhibit the low-frequency hydrogen-bond stretching frequencies as *sharp* lines. Any perturbation which smears out the fine structure of the high-energy X—H band must have a much greater effect on the low-energy transitions.

STEPANOV's predissociation theory is based on well-known effects observed in electronic emission or absorption spectra. If an energy transition occurs from a sharply defined ground state to a continuous band of energy levels, or to a state in which the molecule dissociates (or an atom ionizes), then a very broad absorption band results [72]. When dissociation occurs, quanta covering a frequency range can be absorbed and any excess energy appears as kinetic energy as the dissociating particles fly apart. Predissociation (or autoionization) describes the process where although both ground and excited states are sharply defined, and therefore only a discrete energy quantum can normally be absorbed (sharp spectral line), the lifetime of the excited state is extremely short. A virtually instantaneous transition to a third unstable state which promptly dissociates (or ionizes) takes place

VOL.
10
1957/5

(e.g. an anti-bonding electronic state for an atom, producing instantaneous ionization). Once again absorption of a frequency range becomes allowed as excess energy appears as kinetic energy. The contour of such absorption bands is usually asymmetric, being broadened on the high-energy side of the frequency at which a quantized transition would occur in the absence of dissociation (or ionization).

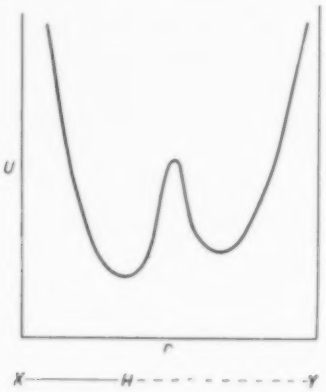

Fig. 5. Double well potential curve for proton.

OL.
10
7/58

STEPANOV *et al.* consider that because of the interaction between the XH stretching mode and the low-frequency intermolecular vibrations, the energy of the vibrationally excited X—H is transferred to the X - - - Y stretching mode and is sufficient to cause dissociation, i.e. to break the hydrogen bond. The short lifetime of the vibrationally excited X—H, and the accommodation of excess energy as kinetic energy when the hydrogen-bonded molecules dissociate, then explains the broad band observed.

A heated discussion between the exponents of the rival theories, and other prominent theoreticians, was recorded at a Russian conference on hydrogen bonding and makes very interesting reading [37]. The controversy raged, but was not settled conclusively in favour of any theory.

LANDSBERG made perhaps the most pertinent comment that the exponents were mainly disagreeing over the descriptive languages used to describe the same phenomenon (classical v. quantum).

KOVNER and CHUENKOV [38] at the same conference presented a detailed mathematical analysis of the effects to be expected from the distortion of the potential curve of the proton in an —X—H bond due to the close approach of atom Y. They adopt a potential function which is a simplified Morse function with a double potential minimum as sketched below and solve the Schroedinger equation for the vibrational levels of the proton assuming a fixed X - - - Y distance (i.e. neglecting intermolecular vibrations). This simplified but formal theory predicts a splitting of the vibrational energy levels and therefore a doubling of the absorption bands. (It is directly analogous to the inversion doubling of lines in the NH_3 spectrum.)

In relating this theory to experimental observations, the authors take the two principal peaks in the envelope of the diffuse structure observed in the spectra of carboxylic acid dimers as the "doublet" they predict. From this they estimate the height of the potential barrier to proton transfer from one minimum to the other.

The writer, in a brief qualitative discussion of the double well potential curve in hydrogen-bonded systems, suggested that the broad absorption band might result from proton transfer across the potential barrier causing the upper vibrational X—H levels to be rather indeterminate [39].

The quantum theory of hydrogen bonding was developed further by SOKOLOV [40], who treats the problem on an electron donor–acceptor model and stresses the contribution to the interaction energy due to the expansion and increased ionic character of the —X—H bond.

The Double Well Potential Function and Proton Transfer

KOVNER and KAPSHAL [41] have developed further the theory of the splitting of the XH frequency and the probability of proton transfer across hydrogen bonds by a tunnel effect (penetration of the potential barrier). The latter idea was used to explain ferroelectric properties of hydrated Rochelle salt, following the work of MASON [48]. They calculate that an activation energy for proton transfer of about 1 kcal/mole would result from a hydrogen-bond energy of about 20 kcal/mole. In Rochelle salt the O—H - - - O distance is short (2·54 Å) so a high energy is not unexpected (cf. $(FHF)^-$ energy 27 kcal/mole and F - - - F distance 2·27 Å).

Independent support for the postulate of proton transfer comes from a reaction rate study by GRAGEROV and BRODSKY [42].

They followed the proton exchange rate between d_4-hydroquinone and normal quinone and alternatively between the deuterium-labelled quinone and normal hydroquinone, e.g.

$$C_6D_4O_2 + C_6H_4(OH)_2 \rightleftharpoons C_6D_4(OH)_2 + C_6H_4O_2$$

approaching equilibrium exchange from both directions. The exchange took place in the *solid* quinhydrone formed between equimolar proportions of the components. From the kinetics of the reaction the activation energy for proton transfer was calculated to be 64 kcal/mole. Since no semi-quinone was found, they assume that proton transfer requires the simultaneous transfer of both protons from hydroquinone, as the semi-quinone structure would be unstable

Thus the activation energy per hydrogen bond

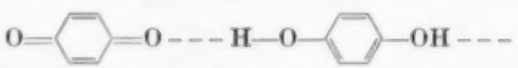

would be 32 kcal/mole. BATUEV has calculated the following values for the potential barrier: Water, 33 kcal/mole; fatty acid dimers, 24 kcal/mole; and crystalline β-oxalic acid, 4·8 kcal/mole [43].

VOL.
10
1957/5

Other experimental evidence for proton transfer has been based on electrical conductivity experiments. The subject has been treated mathematically by GIERER and WIRTZ [44], who have analysed the contribution of hydrogen or deuterium transfer across hydrogen bonds to the conductivity of water and heavy water. KAKIUTCHI, KOMATSU and KYOYA [45] have presented evidence for proton mobility in solid cetyl alcohol when a potential is applied across the sample. The conductivity cell was evacuated and connected to a discharge tube. When the potential was applied to the alcohol sample a weak discharge appeared in the tube above, which was proved spectroscopically to be due to hydrogen. On removal of the potential the discharge disappeared, which would disprove the possibility of electrolysis.

Several workers have discussed the contribution of proton mobility in hydrogen-bonded systems to electrical conductivity [45a, b, c].

DRYDEN and MEAKINS have attributed the dielectric absorption and d.c. conductivity of quinol to protont ransitions along the hydrogen-bonded chains [46].

More recent work on dielectric constant and dielectric loss of alcohols also supports the idea that proton transfer in hydrogen-bonded systems contributes to dielectric behaviour. GIACOMO and SMYTH find the dielectric effects present in alcohols and absent in thiols [74], while MEAKINS finds the effects absent in the so-called "hindered alcohols" like triphenyl carbinol, etc. [75], where hydrogen bonding is prevented by steric factors. HALL [47] from ultrasonic absorption experiments on water has suggested that every molecule continuously changes its state of association, and the mean lifetime of a given hydrogen bond would be about 10^{-11} sec.

WESTRUM and PITZER [24], in their work on KHF_2, also discuss the nature of the hydrogen bond in $(FHF)^-$. They consider briefly the effects to be expected as hydrogen bonds shorten and the potential barrier in the double well function decreases and finally disappears, as in $(FHF)^-$. With a double well the finite probability of proton transfer results in effectively an orientable dipole (sign of charge distribution changes when proton jumps the barrier) which should be both large and temperature dependent. WESTRUM and PITZER remark that indeed water, HF associated in gas and liquid states, and liquid formic acid all show a high dielectric constant which varies with temperature whereas KHF_2 has a low dielectric constant ($\varepsilon = 4{\cdot}1$) which is not temperature dependent.

WELLER has postulated proton transfer across hydrogen bonds in some electronically excited molecules [59a]. Salicylic acid and its methyl ester show an abnormally large Stokes shift of fluorescence compared with the corresponding methoxy compounds although their ultra-violet absorption spectra are the same. He concludes that the hydroxy molecules (OH intramolecularly hydrogen bonded to acid or ester C=O) must have some mechanism for energy change in the excited state. WELLER quotes the energies required for proton transfer as $\Delta H = +13$ kcal/mole in the ground state and $\Delta H^* = -1$ kcal/mole in the electronically excited state, although the calculations from which these are derived are not given. Thus if the proton transfers across the hydrogen bond in the excited state, the fluorescence emission will be at a frequency displaced from the absorption frequency

by approximately 14 kcal/mole ($\Delta H - \Delta H^*$), which agrees with the Stokes shift observed.

For many years UBBELOHDE *et al.* have studied the thermal expansions of crystals. They have found that in crystals in which fairly strong hydrogen bonding dominates the molecular packing, the substitution of deuterium for hydrogen causes an expansion of the lattice and alters the thermal expansion behaviour. Approaching the theory of hydrogen bonding from this viewpoint, UBBELOHDE and GALLAGHER [58] discuss hydrogen bonds almost entirely in terms of proton transfer as an acid–base effect, controlled by the dissociation constants even in a crystal. On this basis they consider three types of hydrogen bond:

(*a*) $AH - - - AH \rightleftharpoons A^+H_2 - - - A^-$ (e.g. carboxylic acids)

(*b*) $AH - - - B \rightleftharpoons A^- - - - B^+H$ (e.g. acid hydrates where $B = H_2O$)

(*c*) $AH - - - A^- \rightleftharpoons A^- - - - AH$ (e.g. acid salts, KH_2PO_4, etc.)

where basically there must be two alternative sites for the proton, on the unionized acid (A) or on the ionized base (B). These two sites would normally have different proton affinities. If the affinity (basicity) is very different, there is no appreciable overlap between the potential functions describing the two sites, i.e. hydrogen bonding is negligible. When the basicities become competitive for the proton, i.e. the two potential functions overlap, then the crystal may contain a proportion of what the authors describe as "proton transfer defect sites." That is, positions in the lattice where the proton occupies the alternative site. When the proportion of such transfer sites becomes sufficiently large, co-operative proton transfer effects must occur (e.g. the proton transfer reactions in quinhydrone above).

On this acid–base picture, crystalline NH_4Cl, for example, would be predominantly ionic because the basicity of the anion Cl^- will be low compared with NH_3. In ice the proton transfer defect sites correspond to $HO^- - - - HO^+H_2$.

When the number of defect sites is small they will behave independently, but may wander through the lattice by proton jumps. Co-operative interaction must occur when the potential barrier is not large compared with kT.

Ferroelectric transitions, lattice thermal expansions, and effects associated with isotope replacement (D for H) are all qualitatively explained by assuming a quantum mechanical contribution to hydrogen bonding leading to a finite probability of proton transfer. The shorter the hydrogen bond the greater the lattice expansion on replacing H- by D-atoms. The effective height of the potential barrier against proton transfer is measured from the vibrational ground state. With the heavier D-atoms the vibrational frequency is lower and therefore the absolute energy of the vibrational ground state is lower (lower zero-point energy) and the potential barrier is therefore higher for D- than H-atoms.

While UBBELOHDE's approach focuses attention on proton transfer effects, it is of course yet another descriptive language for the same phenomenon and no new concepts are introduced.

OSHIDA, OOSHIKA and MIYASAKA [59] also consider proton transfer effects in hydrogen bonds and give yet another variant of the wave mechanical analysis. They consider that the ground states and first excited vibration states for each well in the double minimum potential curve interact, leading to four linear

VOL. 10 1957/5

combinations of the single well (Morse) potential functions. No explanation of the broadened X—H bands is given, but low-frequency Raman lines are assigned to the intermolecular vibrations and 10^{-2} cm^{-1} and 1 cm^{-1} dielectric absorption is ascribed to proton transfer.

Experimental evidence against rapid transfer comes from nuclear magnetic resonance spectra of pure alcohols recorded by Ogg [69]. He has found that in alcohols from which all trace of electrolytic (i.e. ionizing) impurity is removed, the OH proton resonance line is split into a triplet by spin–spin interaction with the protons of the CH_2 group. For this to be observed, the —OH bond lifetime must be quite long. Richards [70] in a discussion of this point suggested a lifetime of at least 0·2 sec. This is very much at variance with the estimate of 10^{-11} sec made by Hall [47]. Ogg has demonstrated that in anhydrous (Na-dried) liquid ammonia the NH resonance peak is a triplet, as in the gas, but addition of a trace of water reduced the triplet to a singlet peak [71]. Ogg says that this means that in liquid ammonia in the absence of water the lifetime of the N^+H_3 molecule is long and no proton transfer occurs either by an ionic reaction ($NH_3 + NH_3 \rightleftharpoons N^-H_2 + N^+H_4$) or by hydrogen bonding. He considers that the trace of water added causes ultra-rapid proton exchange by ionic reactions ($H_2O + NH_3 \rightleftharpoons OH^- + N^+H_4$). Ogg concludes that the molecules in liquid-dry NH_3 associate only by dipole–dipole interaction. He has since studied the effect on the proton resonance spectrum of alcohol when pure (electrolyte-free) water was added [69]. This has no effect whatsoever, although Ogg added up to 10 per cent water. The triplet alcohol OH proton resonance remained unchanged and the separate singlet water OH appears as the water concentration increased. This evidence would certainly mean that the OH bond in hydrogen-bonded alcohol has a mean lifetime of a few tenths of a second or longer in its vibrational ground state; a lifetime in fact at least as long as the N—H in liquid-dry NH_3.

Very recently, Arnold [73] has reported a fairly detailed high-resolution proton magnetic resonance study of ethyl alcohol. He examined the effect of ionic impurities (HCl or NaOH), in minute amounts, on the OH proton triplet and calculates mean lifetimes. They vary from 0·24 sec in the pure alcohol to 10^{-2} sec for 10^{-5} N HCl or 6×10^{-3} sec for $1{\cdot}25 \times 10^{-4}$ N NaOH. He concludes that the H^+ or OH^- ions in ethanol catalyse the exchange of protons between hydroxyl groups, the exchange rates varying from 1/sec in the pure alcohol to about 100/sec with trace ionic impurities.

Other proton magnetic resonance studies of hydrogen bonding have given qualitative agreement with infra-red data [73a, 73b] on the degree of association in inert solvents, etc.

Conditions for the Formation of Hydrogen Bonds

Tsuboi [49] has reviewed the hydrogen-bond-forming powers of various atoms or groups and suggested that the proton-donor power of X—H will depend on the electron affinity of atom X. The hydrogen bond formed will in addition depend on the tendency of atom Y to attract electrons and acquire a negative charge. He has also suggested that π–π interaction may contribute to hydrogen bonding, but this seems a nebulous concept for, say, alcohols, but may be relevant to the association of aromatic molecules.

FYFE [50] has discussed in greater detail the conditions for the formation of hydrogen bonds. He poses the very relevant questions—Why are strong hydrogen bonds only formed with N, O, and F atoms? Why is H_2O strongly associated, and H_2S not? Why also does HF form strong hydrogen bonds even in the vapour and HCl remain unassociated in the liquid state?

Reference has been made above (pages 329–332) to the fact that dispersion forces and any directional interaction may be mutually exclusive when their energies are of the same order. FYFE shows that this explains the difference in behaviour of HF and HCl (HBr and HI), since going through the series HF, HCl, HBr, HI, the polarizability increases and therefore the dispersion forces increase in energy. In close-packed HCl they are of the order of 5 kcal/mole and, since HCl does not associate, this energy must exceed the (Cl—H - - - Cl—) hydrogen-bond energy. FYFE has attempted to generalize the molecular orbital calculations of LENNARD JONES and POPLE [32] for the water molecule to all types of hydrogen-bonding molecules. He suggests that the asymmetry of the lone pair orbit participating in a hydrogen bond is a necessary condition for its formation. FYFE calculates by POPLE's method the potential hydrogen-bond energy for H_2S as 1·8 kcal/mole, assuming a reasonable S—H - - - S distance of 3·7 Å. This energy is less than the normal dispersion forces and therefore no directional interaction takes place. FYFE further stresses that from the valence-bond angles (HOH $\simeq$ 105°, HSH $\simeq$ 90°) hybrid sp^3 bonds occur in water but practically pure "p" bonds occur in H_2S. Thus the oxygen atom has asymmetric lone pairs but the sulphur atom does not.

FYFE shows by calculation of overlap integrals that the bonding in the symmetrical $(FHF)^-$ ion has an appreciable covalent contribution, but this is a rather special case. He concludes that hydrogen-bond energies are the sum of the electrostatic interactions and the covalent contribution from the overlap of the X—H and lone pair orbitals.

SCHNEIDER [51], following FYFE, has considered in more detail the contribution of the lone pair electrons to the hydrogen-bond energy and from molecular orbital calculations of the lone pair orbital moments concludes that in order of proton acceptor power $sp > sp^2 > sp^3$ hybrids, and, for example, for sp^3 hybridization N > O > F. Lone pairs in a pure s orbit have no proton attraction at all. SCHNEIDER demonstrates by means of the point charge model (including orbital moments) that the maximum interaction energy occurs when the X—H bond is colinear with a lone pair orbital.

A clearer picture of a possible quantum mechanical contribution to hydrogen bonding was postulated by NUKASAWA, TANAKA and NAGAKURA [52]. They consider that even in the asymmetric hydrogen bond a weak covalent link is formed between H- and Y-atoms (cf. $(FHF)^-$ above). The bonding orbitals are pictorially represented below.

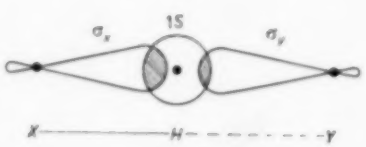

Fig. 6.

VOL. 10 1957/5

The —X—H bond forms by overlap of the σ_X atomic orbit with the hydrogen 1*s* orbit, and the hydrogen bond by overlap of the σ_Y lone pair orbital with the hydrogen 1*s* orbit. As a rigorous LCAO MO calculation, this model reduces to a three–orbital–four–electron problem, but the authors only attempt a simple perturbation treatment. Their preliminary calculations show that the possible covalent contribution to hydrogen-bond energy could amount to several kcal/mole, with the X – – – Y distances known to occur.

More Detailed Quantum Calculations

TSUBOMURA [53] enumerates four possible contributions to hydrogen bond energies:

(a) Electrostatic interaction.
(b) Dispersion forces.
(c) Exchange repulsion.
(d) Delocalization energy (electron transfer from Y to X—H).

He suggests that the success of the electrostatic model in predicting interaction energies is fortuitous, because the algebraic sum of (*b*), (*c*), and (*d*) may be roughly zero; it does not prove that (*b*), (*c*), or (*d*) are negligible in themselves. TSUBOMURA reports a calculation by atomic orbital methods of the delocalization energy for hydrogen-bonded water molecules, which is in reasonable agreement with experimental values. (See COULSON [6a] for more detailed discussion.)

In later papers, TSUBOMURA has presented detailed experimental and theoretical work on intensities [53a, 53b].

Calculations of a similar nature but rather more refined are reported by COULSON and DANIELSSON [54] with the object of discovering the significance of the covalent contribution to hydrogen bonding and its change with X – – –Y distance etc. They consider contributions from three wave functions only and restrict the calculation to the four electrons involved.

ψ_1, the valence-bond structure O_A——H O_B

ψ_2, the ionic structure O_A^- H^+ O_B

ψ_3, the fully covalent hydrogen bond O_A^- H—O_B^+

The weights of the contributions of ψ_1, ψ_2, or ψ_3 were shown to vary with O_A—H distance and with O_A – – – O_B distance. The covalent contribution to the hydrogen bond increases rapidly as the O_A—H bond lengthens. The energy of the hydrogen bond varies practically linearly with the weight of covalent contribution despite the fact that the calculations suggest that, in round figures, the hydrogen-bond energy of 10 kcal/mole should be represented as 84 per cent non-polar (ψ_1); 12 per cent ionic (ψ_2), and 4 per cent covalency in the hydrogen bond (ψ_3).

COULSON and DANIELSSON remark that a purely electrostatic model would appear from their calculations for a single isolated hydrogen bond, to be inadequate

to represent the true facts, particularly because extensive bonding between many molecules, e.g. in ice, will be a co-operative phenomenon where the charge displacements associated with the covalency of the hydrogen bonding may be "relayed" to adjacent bonds. In their tabulated calculations of the weights of the contributions of ψ_1, ψ_2, and ψ_3 for variations in O_A—H bond length and $O_A - - - O_B$ distance, and for pure p or sp^3 hybrid bonding orbitals on the oxygen atoms, the most striking thing is that although the ionic contribution varies but little from 10 to 13 per cent the weights of the ψ_1, ψ_3 contributions vary reciprocally, the "total covalency" remaining approximately constant. Thus as the covalency of the hydrogen bond increases, the covalency of O_A—H decreases.

This point is not discussed by COULSON and DANIELSSON, but it would support the quantum model postulated by NUKASAWA *et al.* [52] described above, from which of course such an effect would be predicted.

Other quantum calculations have been given in the literature. NORDMAN and LIPSCOMB [55] used Morse functions for X—H and H - - - Y to represent the potential function of the proton in the Schroedinger equation and solved for the proton vibrational energies. Similarly, KAKU [56] used superimposed Morse functions and calculated OH distances, force constants, and the height of the potential barrier for a linear OH - - - O bond. The variation of OH frequency with O - - - O distance was estimated by Baker [57] by a perturbation calculation, again using superimposed Morse functions. He, like the earlier Russian workers, predicts a splitting of the energy levels giving two bands of equal intensity. His predicted frequency shifts due to the hydrogen bonding were about 25 per cent too large.

All such treatments seem to be limited either by the assumption of the potential functions operating, or by the assumption of a limited number of possible structures which may contribute. In other words, to make the calculations manageable, drastic simplifications of one sort or another have to be made, and the deductions which can be drawn from such calculations are of necessity very limited.

By far the most elegant and most thorough treatment of hydrogen bonding to date is the analysis by LIPPINCOTT. Based on a quantum mechanical model, he has derived an internuclear potential function for diatomic molecules [60] which is more accurate than the older empirical Morse function. This function, which LIPPINCOTT and SCHROEDER demonstrate yields very accurate values for the dissociation energy and other bond properties of a wide variety of covalent diatomic molecules, has been applied by them to the hydrogen bond [61]. Although they only consider the simplified linear model $O^{(1)}$—H - - - $O^{(2)}$, they successfully predict the OH distance as a function of O - - - - O distance, the relation between OH frequency shift and O - - - O distance (cf. p. 337 above and references [22] and [23]), hydrogen-bond energy and O - - - O distance, and the O - - - O force constants and frequencies all in excellent agreement with experimental data (particularly on crystals). From their analysis the complete potential curve for the proton can be derived, from which the potential barrier to proton transfer can be found, and the potential curve for the intermolecular vibrations established.

Their complete potential function is made up of four terms:

$$V = V_1 + V_2 + V_3 + V_4$$

V_1 is the covalent potential for the OH bond, V_2 the covalent potential for the hydrogen bond, V_3 is the van der Waals' repulsion potential for the two oxygen atoms, and V_4 is an electrostatic term representing an *attraction* between the two oxygen atoms. The electrostatic attraction is more easily understood from the conventional resonance model which has the two contributing structures $\backslash O—H - - - O \backslash$ and $\backslash O^- \quad H——O^+ \backslash$. These correspond to the two "covalent" wave functions of COULSON's treatment (ψ_1 and ψ_3, p. 347). LIPPINCOTT does not introduce a contribution from the ionic structure assumed by COULSON (ψ_2), and the success of LIPPINCOTT's predictions of experimental data suggest that COULSON's supposition is at least unnecessary if not erroneous. Experimental support for LIPPINCOTT's assumption of an attractive potential can be found in the crystallographic data of JEFFREY and PARRY on oxalic acid [62], who present evidence for intramolecular attraction between the OH and C=O oxygen atoms. Although the central C—C bond is 1·54 Å, showing that the π–π conjugation between the carbonyl bonds is weak, the molecule is planar. The distance between adjacent oxygen atoms on the same side of the C—C bond is only 2·65 Å much smaller than the sum of the van der Waals' radii (*c.* 2·95 Å).

From the force constant derived from their model, LIPPINCOTT and SCHROEDER calculate the amplitude of the O - - - O intermolecular vibration, e.g. for the O - - - O distance in ice the amplitude is 0·12 Å. From the dependence of OH frequency on O - - - O distance this amplitude corresponds to a spread in OH frequency of 300 to 400 cm^{-1}. They suggest that this explains the broadening observed. While this would be true for a random statistical distribution of O - - - O distances, it is erroneous, since the hydrogen-bonded molecules execute quantized intermolecular vibrations. The only valid deduction is that a coupling of the two vibrations occurs to give combination frequencies—either on classical or quantum theories.

The authors conclude from the success of their covalent potential function in predicting hydrogen-bond properties, that the forces making the important contribution to hydrogen bonding are the same as those applicable to ordinary covalent bonds, i.e. of quantum mechanical origin.

Very recently, SHIGORIN and DOKUNIKHIN [63] [63a] have discussed the nature of hydrogen bonding and its effect on vibrational and electronic spectra, while SOKOLOV [64] has published a review (139 references) dealing with the inadequacy of electrostatic theories, various quantum treatments, and the possibilities of proton transitions.

Discussion and conclusions

The balance of the evidence presented above suggests that certainly strong hydrogen bonding must be represented as a combination of electrostatic and quantum mechanical interactions. The properties and energy of the hydrogen bond are determined more by the quantum contribution than by the electrostatic interaction. Clearly there is no reason to suppose that there will be any sharp division between the interactions which are solely electrostatic at long X - - - Y

distances and those where quantum effects contribute at shorter X - - - Y distances. There is, however, a maximum limit to the hydrogen-bond energy which can develop which will occur for the symmetrical X—H—Y system where the proton is central, and where the double minima in the potential energy curve coalesce into a single well potential function, e.g. $(F - - H - - F)^-$. Systems may well exist where directional electrostatic dipole–dipole interaction between molecules may reinforce or oppose any quantum interaction. The balance between all such possible contributions to interaction mechanisms, including dispersion forces, will be determined by both configurational and energy considerations.

When water molecules associate, the bond and lone pair orbital dipoles align so that the electrostatic interaction reinforces the hydrogen-bond quantum interaction.

In amides, on the other hand, the dipole–dipole interaction between the $^-OCN^+$ dipoles opposes the tendency for hydrogen-bond formation [65, 66]. A direct comparison of the relative strengths of the dipole interaction and the hydrogen bonding can be made from the crystal structure of formamide determined at −50°C by LADELL and POST [66a].

In the crystal the molecules are coplanar and are aligned in chains, with the $^-OCN^+$ dipoles approximately collinear, with an O - - - - N distance of 2·88 Å. These linearly associated chains of molecules then link together through the NH bond which is "*cis*" to the C=O in a structure analogous to cyclic dimers (i.e. with N—H - - - - O=C hydrogen bonds conforming to the criteria listed below). The "*cis*" N—H bond is collinear with an (sp^2) lone pair orbital of the carbonyl oxygen atom with an O - - - - N distance of 2·935 Å.

Thus in the direction of maximum dipole interaction the O - - - N distance is shorter than in the direction of maximum hydrogen-bond strength. In secondary amides, polyamides, and polypeptides, where the —CONH— group is in the "*trans*" form, the dipole interaction, being the stronger interaction, controls the association of the —CONH— groups.

It would be valuable to be able to decide from experimental observations which contribution dominates the interaction in order to predict further behaviour. In this sense true hydrogen bonding can now be more rigidly defined as a quantum interaction between the participating molecules. It is a matter of common observation that the lower the ionization potential of —X—H (i.e. higher acidity) and the higher the electron affinity of Y (i.e. higher basicity) the stronger is the hydrogen bond and the shorter the X - - - Y distance. This can be further amplified in terms of the quantum interaction and the properties of the lone pair electrons of Y.

From the review of the theoretical work the following criteria for the formation of hydrogen bonds may be listed [65, 66].

(*a*) The X—H bond must be partially ionic in character or, at least such that ionic character can be induced by polarization. The X-atom therefore must have a high electronegativity, leading to $-X^{-\delta} - - - - H^{+\delta}$ with the 1*S* orbit of the hydrogen atom not fully utilized in the formation of the covalent σ_{XH} bond and available for overlap with the lone pair orbital of Y.

(*b*) The Y-atom must have lone pair electrons in an asymmetric orbital—for example *sp* hybrid orbitals.

VOL. 10 1957/5

(*c*) For maximum quantum interaction, and therefore maximum hydrogen-bond energy, the X—H bond and the axis of the lone pair orbital must be collinear.

X—H frequency shifts and their relation to X – – – Y distance, the low-frequency intermolecular vibrations, and the expansion of the —X—H bond have been adequately explained by the quantum model. No serious attempt to estimate the intensity changes in the spectra have been made by quantum methods, (but see [53b]), nor has the extreme broadening of the X—H stretching frequency been explained satisfactorily.

Evidence for proton transfer has been reviewed in several hydrogen-bonded systems and penetration of the potential barrier seems both possible and probable.

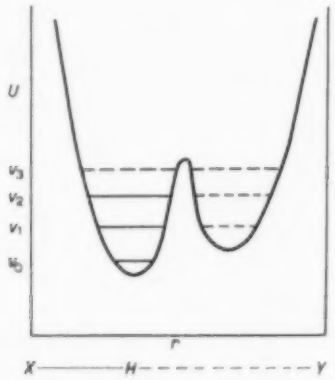

Fig. 7.

Proton transfer in fact can explain rapid hydrogen–deuterium exchange in hydrogen-bonded systems (although transient ionization is an alternative possibility) and can explain the high dielectric constant and ferroelectric behaviour of crystals with hydrogen bonds or bonded water of crystallization. The only evidence against proton transfer, or at least against rapid transfer in the vibrational ground state, comes from the proton magnetic resonance studies reviewed above.

The possibility still remains of more rapid proton transfer in the vibrationally excited states. Consideration of the proton potential curve shows that it is more probable, since the potential barrier is effectively less for excited states (Fig. 7).

On classical theory a damped oscillator would have a broad absorption or emission band (Fourier analysis of the wave form). In quantum theory, where each energy state is of *constant* amplitude, the concept of damping is replaced by the mean lifetime in an excited state, due to the probability of transition to another state. Once again a broad absorption or emission band results from a transition between energy states where either or both energy levels are diffuse due to a short lifetime. This broadening is a direct consequence of the Uncertainty Principle, where because the lifetime is short the energy is correspondingly indeterminate.

If band widths are assigned to this cause alone, then lifetimes can be calculated [72]

$$\text{Half-width (ergs) } b = \frac{h}{2\pi} \cdot \frac{1}{\tau}$$

where h = Planck's constant,

τ = lifetime,

or half-peak band width $\Delta\nu = \frac{1}{2\pi c} \cdot \frac{1}{\tau}$ (where c = velocity of light).

The values in Table 7 illustrate the excited-state lifetimes which have to be invoked to explain the breadth of X—H bands in hydrogen-bonded systems.

Table 7

$\Delta\nu$ cm^{-1}	τ sec
100	5×10^{-14}
200	$2{\cdot}5 \times 10^{-14}$
300	$1{\cdot}7 \times 10^{-14}$
500	1×10^{-14}
1000	5×10^{-15}

Thus, if the probability of the proton jumping the potential barrier is sufficiently great in the vibrationally excited states, the lifetime in these states will be short and the observed absorption band broad. As suggested previously [66], although the rigorous theory for a double potential minimum for an "isolated molecule" (OH – – – O) leads only to a splitting of the vibrational levels, hydrogen bonding is essentially a co-operative effect over two or more molecules and excess energy may be dissipated by kinetic processes, or by complex intermolecular oscillations involving many molecules.

This idea differs from STEPANOV's theory only in that he suggests that true dissociation of the hydrogen bond occurs from the vibrationally excited states, whereas here protons can transfer, if necessarily co-operatively over several molecules, across the potential barrier but without dissociating the hydrogen bonds.

It is difficult to imagine STEPANOV's postulate of dissociation of hydrogen bonds occurring in crystals, where the X—H bands are broader than in liquids. Furthermore, the stronger the hydrogen bond the broader is the X—H band, but the greater anharmonicity and lower stretching frequency means that the vibrational energy quantum gets *smaller*, i.e. the stronger the bond the lower is the energy available for STEPANOV's process.

The following facts are in favour of proton transfer from X—H stretching vibrationally excited states.

1. Only the X—H stretching frequencies are very broad, the X—H deformation bands and the Y—R stretching bands are much sharper, and their breadth can very plausibly be due to thermal or other perturbations.

VOL. 10 1957/5

2. The low-frequency X – – – – Y intermolecular vibrations are sharp in crystals but broadened by KT in liquids.
3. The transient dipole moment associated with the proton transfer may be responsible for the very great increase in the intensity of the X—H absorption (but see [53b]).

Against it is the fact that in $(FHF)^-$ with a symmetrical potential well the corresponding vibration band is broad, but clearly since no double minimum exists no proton transfer can take place.

The various energies and times involved in the X—H – – – Y system are tabulated below for comparison (Table 8).

Table 8

kT at 300°K $\equiv$ 200 cm^{-1} $\equiv$ 570 cal/mole Vibrational quantum (ν_{XH}) 3000 cm^{-1} $\equiv$ 8·6 kcal/mole
Potential barrier to proton transfer (calculated and experimental values, see above) (references [41] to [43]) 1 to 33 kcal/mole
Hydrogen-bond energies:—5 to 27 kcal/mole
(ν_{XH}) 3000 cm^{-1} $\equiv 9 \times 10^{13}$ c/s; period $\triangleq 10^{-14}$ sec
Excited state lifetime to account for broadening $\triangleq 10^{-14}$ sec
Proton exchange rate in pure ethanol—1/sec [74]

It is difficult to conceive of any other factors to account for the broadening if proton transfer (Cannon) or predissociation (Stepanov) are discounted. The great anharmonicity of the X—H potential function has been suggested [15] as a possible cause, but $(FHF)^-$ again rather discounts this as the anharmonicity is small and of opposite sign but the F—H—F stretching frequency is broad.

Of course, statistical perturbation must contribute in the liquid state, but kT at room temperature is only equivalent to about 0·5 kcal/mole, very much less than hydrogen-bond energies. In any case, bonded OH bands are still very broad in the vapour state (carboxylic acids), and in crystals at very low temperatures [15, 77].

The damping due to coupling of anharmonic vibrations may also contribute, but the calculations of Frisch and Vidale [78] for a typical hydrogen bond show that this mechanism can only account for a band width of 30 cm^{-1}.

Coulson (79) has pointed out that where hydrogen bonding extends over many molecules, the coupling between them would lead to splitting of energy levels, giving a band of closely spaced levels, which might well appear as a broad absorption band. Again, the broadness of the OH of carboxylic acid dimers in the vapour phase, and the appearance of sharp low-frequency transitions in Raman spectra of crystals where ν_{OH} is broad, shows that while coupling and splitting may contribute it is certainly not the major cause.

It is possible of course that yet another contributory factor exists, e.g. ionic bonding or partial ionic bonding leading to broadening can be suggested, since the bonding in $(FHF)^-$ is strongly ionic, but no obvious reason comes to mind.

The widths of the overtone bands of the X—H stretching mode should confirm the proton transfer theory and would repay further study. WILBUR KAYE has observed that there is a drastic reduction in the peak intensity of the first overtone of the bonded OH stretching frequency compared with the "free" OH, which is consistent with very considerable broadening [76].

Preliminary investigations of the widths of overtone bands of H_2O, HCOOH, $(CH_2)_2CHOH$, and $CH_3CONHC_2H_5$ show that the OH stretching vibration broadens very considerably in the higher overtones [80]. $4\nu_{OH}$ in formic acid at 12,000 cm^{-1} has a half-peak width of 2200 cm^{-1}; H_2O bands at 11,600 and 13,300 cm^{-1} have half widths of about 1350 cm^{-1}, whereas $4\nu_{NH}$ in N-ethyl acetamide is only about 200 cm^{-1} broad.

Examination of the widths of absorption bands in other systems may also be illuminating, e.g. charge transfer complexes, co-ordination complexes, etc.

Acknowledgements—The author is indebted to his colleagues in B.N.S. and elsewhere for many stimulating arguments and discussions, and to Mr. F. E. WALLWORK for his enthusiastic translation from the Russian journals of several papers containing highly complex mathematical treatments.

Thanks are due to Professor C. A. COULSON for his kindness in reading and commenting on the manuscript, and to British Nylon Spinners Ltd. for permission to publish.

VOL. 10 1957/5

References

[1] FYFE W. S. *J. Chem. Phys.* 1953 **21** 2–4.
[2] TAMRES M. *J. Amer. Chem. Soc.* 1952 **74** 3375.
[3] HUNTER L. *Rep. Progr. Chem.* 1946 **43** 141–155.
[4] DONAHUE J. *J. Phys. Chem.* 1952 **56** 502.
[5] DAVIES M. M. *Rep. Progr. Chem.* 1946 **43** 5–29.
[6] KELLNER L. *Rep. Progr. Phys.* 1952 **15** 1–23.
[6a] COULSON C. A. *Research* 1957 **10** 149–159.
[7] BREALEY G. J. and KASHA M. *J. Amer. Chem. Soc.* 1955 **77** 4462–8.
[7a] PIMENTEL G. C. *J. Amer. Chem. Soc.* 1957 **79** 3, 323.
[7b] NAGAKURA S. and M. GOUTERMAN *J. Chem. Phys.* 1957 **26** 881–6.
[8] HERZBERG G. *Infra-red and Raman spectra of polyatomic molecules* p. 535. Van Nostrand, New York 1945.
[9] LONDON F. *Z. Phys.* 1930 **63** 245.
[9a] BADGER R. M. *J. Chem. Phys.* 1940 **8** 288–9.
[10] GROSS E. and VUKS M. *J. Phys. Radium* 1936 **7** 113.
[11] CROSS P. C., BURNHAM J. and LEIGHTON P. A. *J. Amer. Chem. Soc.* 1937 **59** 1134–47.
[12] GROSS E. F. and VAL'KOV V. I. *Izv. Akad. Nauk SSSR (ser. fiz.)* 1950 **14** 426–8 B.N.S. translation No. T/58.
[13] MECKE R. *Disc. Farad. Soc.* 1950 No. 9, 151–177.
[14] SHUBIN A. A. *Izv. Akad. Nauk SSSR (ser. fiz.)* 1950 **14** 442–7. B.N.S. translation No. T/72.
[15] KLETZ T. A., KETELAAR J. A. A., TORKINGTON, P. MECKE R. and UBBELOHDE A. R. *Disc. Faraday Soc.* 1950 No. 9, 211–3.
[16] DAVIES M. M. and EVANS J. C. *J. Chem. Phys.* 1952 **20**, 342, and references therein.
[17] FUSON N. and JOSIEN M. L. *C. R. Acad. Sci., Paris* 1952 **235** 1025; *J. Opt. Soc. Amer.* 1953 **43** 1102.

[18] SHEPPARD N., HADZI D. and BRATOZ S. *Bull. Sci. Yugosl.* 1953 **1** 71.
[19] SHEPPARD N. Private communication, 1955; HADZI D. and SHEPPARD N. *Spectrochim. Acta* 1956 **8** 249–61.
[19a] BADGER R. M. and RUBALCAVA H. *Proc. Nat. Acad. Sci., Wash.* 1954 **40** 12–17. BADGER R. M. and WALDRON R. D. *J. Chem. Phys.* 1957 **26** 255–6; BADGER R. M. and PULLIN A. D. E. *Ibid.* 1954 **22** 1142.
[19b] BARROW G. M. *J. Phys. Chem.* 1955 **59** 1129–32.
[19c] HUGGINS C. M. and PIMENTEL G. C. *J. Phys. Chem.* 1956 **60** 1615–19.
[20] HADZI D. and SHEPPARD N. *Proc. Roy. Soc.* A 1953 **216** 247–66.
[21] SMITH F. A. and CREITZ E. C. *J. Res. Nat. Bur. Stand.* 1951 **46** 145–64.
[22] LORD R. C. and MERRIFIELD R. E. *J. Chem. Phys.* 1953 **21** 166–7.
[23] RUNDLE R. E. and PARASOL M. *J. Chem. Phys.* 1952 **20** 1487; NAKAMOTO K., MARGOSHES M. and RUNDLE R. E. *J. Amer. Chem. Soc.* 1955 **77** 6480–6.
[24] WESTRUM E. E. and PITZER K. S. *J. Amer. Chem. Soc.* 1949 **71** 1940–9.
[25] COTÉ G. L. and THOMPSON H. W. *Proc. Roy. Soc.* A 1951–2 **210** 206–16.
[25a] PIMENTEL G. C. and SEDERHOLM C. H. *J. Chem. Phys.* 1956 **24** 639–41.
[25b] WELSH H. K. *J. Chem. Phys.* 1957 **26** 710–1.
[26] FREYMANN R. *Spectre Infra-rouge et Structure Moleculaire* Chaps. VI, VII and VIII and references therein. Gauthier-Villars, Paris 1947.
[27] GILLETTE R. H. *et al.* *J. Amer. Soc.* 1936 **58** 1135, 1139–1143.
[28] DAVIES M. M. *Trans. Faraday Soc.* 1940 **36** 339.
[29] COGGESHALL N. G. *J. Chem. Phys.* 1950 **18** 978–83.
[30] FRANCIS S. A. *J. Chem. Phys.* 1951 **19** 505–6.
[31] COULSON C. A. *Valence* Section 8.10, pp. 207–11. Oxford 1952.
[32] JONES J. LENNARD and POPLE J. A. *Proc. Roy. Soc.* A 1950 **202** 166, 323; A 1951 **205** 151, 163. POPLE J. A. *J. Chem. Phys.* 1953 **21** 2234–5. DUNCAN A. B. F. and POPLE J. A. *Trans. Faraday Soc.* 1953 **49** 217.
[32a] BURNELLE L. and COULSON C. A. *Trans. Faraday Soc.* 1957 **53** 403–5.
[33] KLETZ T. A., KETELAAR J. A. A., TORKINGTON P., MECKE R. and UBBELOHDE A. R. *Disc. Faraday Soc.* 166, 323; 1950 No. 9, 212.
[34] BATUEV M. I. *Izv. Akad. Nauk SSSR* 1950 **14** 429–34. B.N.S. translation No. T/61.
[35] STEPANOV B. I. *Zh. fiz. khim.* 1945 **19** 507; 1946 **20** 407.
[36] VOLKENSHTEIN M. V., ELYASHEVICH M. A. and STEPANOV B. I. *Zh. fiz. khim.* 1950 **24** 1153–64. B.N.S. translation T/123.
[37] Discussion of papers on hydrogen bonding. *Izv. Akad. Nauk SSSR* 1950 **14** 4471–5. B.N.S. translation No. T/117.
[38] KOVNER M. A. and CHUENKOV V. A. *Ibid.* 435–441. B.N.S. translation No. T/50.
[39] CANNON C. G. *Angew. Chem.* 1951 **63** 440; *Research, Lond.* 1951 **4** 439.
[40] SOKOLOV N. D. *J. Exp. Theor. Phys.* 1952 **23** 392–403; 404–411 and references therein. B.N.S. translation No. T/215, 392–403.
[41] KOYNER M. A. and KAPSHTAL V. N. *Izv. Akad. Nauk SSSR* (*ser. fiz.*) 1953 **17** 561–6. B.N.S. translation T/291.
[42] GRAGEROV I. P. and BRODSKY A. I. *J. Gen. Chem., Moscow* 1953 **23** 1195. U.S.A. translation p. 1253.
[43] BATUEV M. I. *J. Phys. Chem., Moscow* 1949 **23** 1405.
[44] GIERER A. and WIRTZ K. *J. Phys. Chem.* 1952 **56** 914–7.
[45] KAKIUTCHI Y., KOMATSU H. and KYOYA S. *J. Chem. Phys.* 1951 **19** 132–3.
[45a] POLLOCK J. McC. and UBBELOHDE A. R. *Trans. Faraday Soc.* 1956 **52** 1112–17.
[45b] ZAROMB S. *J. Chem. Phys.* 1956 **25** 350.
[45c] BRADLEY R. S. *Trans. Faraday Soc.* 1957 **53** 687–91.
[46] DRYDEN J. S. and MEAKINS R. J. *Nature, Lond.* 1951 **168** 1121–2.
[47] HALL L. *Phys. Rev.* 1948 **73** 775.
[48] MASON W. P. *Phys. Rev.* 1947 **72** 854–65.
[49] TSUBOI M. *Bull. Chem. Soc. Japan* 1952 **25** 60, 385–92.
[50] FYFE W. S. *J. Chem. Phys.* 1953 **21** 2–4.

[51] SCHNEIDER W. G. *J. Chem. Phys.* 1955 **23** 26–30.
[52] NUKASAWA K., TANAKA J. and NAGAKURA S. *J. Phys. Soc. Japan* 1953 **8** 792–3.
[53] TSUBOMURA H. *Bull. Chem. Soc. Japan* 1954 **27** 445–50.
[53a] TSUBOMURA H. *J. Chem. Phys.* 1955 **23** 2130–3.
[53b] *Idem. Ibid.* 1956 **24** 927–31.
[54] COULSON C. A. and DANIELSSON V. *Ark. Fys.* 1954 **8** 239–255.
[55] NORDMAN C. E. and LIPSCOMB W. N. *J. Chem. Phys.* 1953 **21** 2077–8; *Ibid.* 1951 **19** 1422.
[56] KAKU K. *Kumamoto J. Sci.* Ser. A 1954 **1** 55–9.
[57] BAKER A. N. *J. Chem. Phys.* 1954 **22** 1625–6.
[58] UBBELOHDE A. R. and GALLAGHER K. J. *Acta Cryst. Camb.* 1955 **8** 71–83, and references therein.
[59] OSHIDA I., OOSHIKA Y. and MIFASAKA R. *J. Phys. Soc. Japan* 1955 **10** 849–59.
[59a] WELLER A. *Z. Elektrochem.* 1956 **60** 1144–7.
[60] LIPPINCOTT E. R. and SCHROEDER R. *J. Chem. Phys.* 1955 **23** 1131–41; LIPPINCOTT E. R. *Ibid.* 603.
[61] LIPPINCOTT E. R. and SCHROEDER R. *Ibid.* 1099–1106.
[62] JEFFREY G. A. and PARRY G. S. *Nature, Lond.* 1952 **169** 1105–6.
[63] SHIGORIN D. N. and DOKUNIKHIN N. S. *J. Phys. Chem., Moscow* 1955 **29** 1958–73.
[63a] SHIGORIN D. N. *et al.* *Dokl. Akad. Nauk SSSR* 1956 **108** 672–5.
[64] SOKOLOV N. D. *Adv. Phys. Sci., Moscow* 1955 **57** 204–78.
[65] CANNON C. G. *Mikrochem. Acta* 1955 Nos. 2–3, 555–588.
[66] CANNON C. G. *J. Chem. Phys.* 1956 **24** 491–2.
[66a] LADELL J. and POST B. *Acta Cryst.* 1954 **7** 559.
[67] STUART A. V. and SUTHERLAND G. B. B. M. *J. Chem. Phys.* 1952 **20** 1977.
[68] *Idem. J. Chem. Phys.* 1956 **24** 559–70.
[69] OGG R. A., Private communications, 1955. OGG R. A. *Helv. Phys. Acta* 1957 **30** 89–90.
[70] RICHARDS R. E. I.R.D.G. Meeting, Oxford, December 1955.
[71] OGG R. A. *Disc. Faraday Soc.* 1954 **17,** 215–220; *J. Chem. Phys.* 1954 **22** 560–1.
[72] HERZBERG G. *Spectra of Diatomic Molecules* (2nd Ed.) p. 407. Van Nostrand, New York.
[73] ARNOLD J. T. *Phys. Rev.* 1956 **102** 136–150.
[73a] COHEN A. D. and REID C. *J. Chem. Phys.* 1956 **25** 790–1.
[73b] HUGGINS C. M., PIMENTEL G. C. and SHOOLERY J. N. *J. Phys. Chem.* 1956 **60** 1311–14.
[74] SMYTH C. P. *Dielectric Behaviour and Structure* p. 163. McGraw Hill, New York 1955; DR. GIACOMO A. and SMYTH C. P. *J. Amer. Chem. Soc.* 1956 **78** 2032–5.
[75] MEAKINS R. J. *Trans. Faraday Soc.* 1956 **52** 320–7.
[76] KAYE WILBUR and THOMPSON A. paper presented at Ohio State University, Columbus, 1953 (Private communication).
[77] LORD R. C., QUINN RUTH S. and CANNON C. G. Unpublished work. M.I.T., 1953 (H_2O, D_2O and KHF_2 at liquid helium temperatures).
[78] FRISCH A. L. and VIDALE G. L. *J. Chem. Phys.* 1956 **25** 982–6.
[79] COULSON C. A. Private communication 1957.
[80] CANNON C. G. To be published.

VOL. 10 1957/5

Spectrochimica Acta, 1958, Vol. 10, pp. 369 to 376. Pergamon Press Ltd., London

Spectral-isotopic method for the determination of hydrogen in metals

A. N. ZAIDEL
Physical Institute, Leningrad State University, U.S.S.R.

(*Received* 11 *June* 1957)

IN RECENT years a number of papers have appeared on the development of spectrographic methods for the determination of hydrogen on metals [1, 2, 3]. An impulse discharge is generally used as a source of excitation, and the analysis is obtained from calibration curves constructed with standard samples. But the difficulty of obtaining reliable standards, and the effects of contaminated surfaces have hitherto made it impossible to obtain the requisite sensitivity and accuracy of analysis by this means.

This induced us to attempt to develop a method, which would not involve the use of standards, and enabling the determination of the total hydrogen in the sample and not only the part of it near the surface.

In selecting a method it was natural to decide on that of isotopic exchange; this does not require either the use of standards or the complete separation and purification of the hydrogen from the sample by heating and fusion *in vacuo*, as is necessary for other physico-chemical methods.

The method is particularly suitable in this case, because the isotopic composition of the gas to be analysed can easily be determined spectroscopically.

The work on the development of this method was carried out by PETROV, PETROV, ZAIDEL and VEINBERG [4, 5, 6, 7]. The present article gives a short account of this work. A fuller description is contained in reference [8].

1. Description of the method

A sample of metal weighing M g, and containing V_0 cm³ of hydrogen (measured at N.T.P.), is placed in a degassed quartz tube (the exchanger) of capacity V cm³. After evacuation, the exchanger is filled with deuterium at pressure P_D mm Hg. It is then disconnected from the vacuum system and heated until equilibrium concentrations of hydrogen and deuterium are established, as the result of isotopic exchange between the metal and the surrounding gas. The isotopic composition of a sample of the gas is then determined by spectroscopic analysis.

At isotopic equilibrium the ratio of the concentrations of hydrogen and deuterium is not, generally speaking, the same in the metal as in the surrounding gas phase. The distribution between the two phases depends on the difference in properties of the two hydrogen isotopes, and also on the experimental conditions, particularly on the temperature. Knowing the equilibrium constant of the exchange reaction and the concentrations of the isotopes in the gas phase, it is possible to calculate the ratio of the total numbers of hydrogen and deuterium atoms. Although for a number of metals, particularly for iron, the ratio of the solubilities of hydrogen and deuterium differs from unity by 6–8 per cent [9], yet

the corresponding analytical error is much less than this, because the solubilities of hydrogen and deuterium in iron are generally so small, that most of the hydrogen is concentrated in the gas, and not in solution. Calculation and experiment show that this error does not exceed 1–2 per cent of the hydrogen content. For other metals which have been investigated, this difference in solubility error is also considerably less than the errors due to other causes.

So, in all cases, it is possible to use the relationship—

$$(C_H/C_D)_{metal} = (C_H/C_D)_{gas} \tag{1}$$

But, of course, if a new metal is to be investigated, the magnitude of the error introduced in this way should be determined beforehand.

Let V_0' be the volume of hydrogen (at N.T.P.) taking part in the exchange, v the volume of the sample, V the capacity of the exchanger, P_D the pressure of deuterium, measured at temperature T, and P_0 the atmospheric pressure.

Then, it is easily shown that—

$$V_0' = \frac{C_H}{C_D}\frac{P_D}{P_0}\frac{273}{T}(V - v) \tag{2}$$

If the deuterium initially contains some hydrogen, whose concentration can be expressed by the ratio $(C_H/C_D)_0$, equation (2) must be replaced by the following—

$$V_0' = \left[C_H/C_D - C_H/C_D)_0\right]\frac{1}{1 + (C_H/C_D)_0}\frac{P_D}{P_0}\frac{273}{T}(V - v) \tag{3}$$

If the whole analytical procedure is performed without any metal in the exchanger, it is found that the walls always give off a certain amount of hydrogen whose volume V_0'' may be called the experimental blank. The hydrogen content of a sample is then obviously given by—

$$V_0 = V_0' - V_0'' \tag{4}$$

The value of the ratio C_H/C_D can be obtained from the ratios of the intensities of the Balmer lines of hydrogen and deuterium. This method has been used in a number of investigations. The simplest technique is that described by BROIDA and his collaborators [10, 11]. They excited the spectra using a high-frequency electrodeless discharge at low pressure. To reduce the effects of the hydrogen given off by the walls of the discharge tube, they passed the gas through in a continuous stream.

They investigated the dependence of the relative intensities of the lines of hydrogen and deuterium on the conditions of the discharge, but did not establish the cause of the variation.

They therefore proposed the use of calibration curves, obtained with standard hydrogen–deuterium mixtures, and the maintenance of constant conditions of discharge, particularly of the pressure in the discharge tube. VEINBERG, PETROV and ZAIDEL [12] modified BROIDA's apparatus and investigated the effects of different factors on the intensity ratio of the hydrogen and deuterium lines. As a result, they were able to establish that the most important factor affecting the intensity ratio was the separation of isotopes in the capillary tubes of the system.

VOL. 10 1957/5

It is easy to choose conditions of discharge such that, within the limits of experimental accuracy, the ratios of the intensities of the lines H_α/D_α and H_β/D_β are equal to the ratio of the concentrations of hydrogen and deuterium. Such conditions are: the discharge in water cooled quartz tube 1–2 mm in diameter, by the hydrogen pressure about 3–6 mm Hg; this is shown in Table 1.

Table 1. Measurements on standard mixtures

Made up standards	Determined from condition $\frac{T_H}{T_D} = \frac{C_H}{C_D}$
6·9 ± 0·3	7·3 ± 0·1
11·3 ± 0·3	11·4 ± 0·1
21·3 ± 0·3	21·2 ± 0·1
51·2 ± 0·4	51·0 ± 0 1
36·2 ± 0·3	36·2 ± 0·1
81·7 ± 0·3	81·8 ± 0·1
86·9 ± 0·4	86·5 ± 0·1
94·3 ± 0·3	94·1 ± 0·1

It is therefore possible to substitute the ratio of the line intensities I_H/I_D for the ratio of the concentrations C_H/C_D in equation (3), obtaining the equation—

$$V_0' = [I_H I_D - (C_H/C_D)_0] \frac{1}{1 + (C_H/C_D)_0} \frac{P_D}{P_0} \frac{T}{273} (V - v) \qquad (5)$$

The value of (I_H/I_D) is determined using a monochromator with a plane diffraction grating and a photo multiplier with recording equipment. A sample recording is shown in Fig. 1.

2. Experimental

The vacuum system is shown in Fig. 2 and 3. The exchanger, I, is a quartz tube with a ground connection cooled by running water. The length of the exchanger is 300–400 mm, its internal diameter 20–25 mm, and its capacity 100–200 cm³. The resistance furnace, 2, can easily be removed from the exchanger when necessary. The exchanger can be connected, through a system of tubes and taps, to the high vacuum pump, 3, the MacLeod gauge, 4, the manometer, 5, the deuterium reservoir, 6, and to the discharge tube, T, through a system of capillaries, A and B, for regulating the gas flow.

The previously degassed exchanger, with the sample of metal inside, is filled with deuterium at a pressure of about 10 mm Hg, carefully measured with the MacLeod gauge.

The exchanger is then isolated from the vacuum system, and heated to the temperature required by the metal under investigation. When isotopic equilibrium has been reached, the gas in the exchanger is passed through the system of capillaries A to the discharge tube T, and is pumped out through the system of capillaries B. The stream of gas through the discharge tube is regulated by changing the numbers of entrance and exit capillaries in use.

The diameters of the entrance and exit capillaries are chosen so that the gas flows at 1–2 cm³/min, and the pressure in the discharge tube is 2–5 mm of Hg.

Knowing the pressure and temperature of the deuterium, its original hydrogen content, the previously determined value of the blank, the volume of the exchanger and the intensity ratio I_H/I_D, the hydrogen content of the sample can be calculated from equation [5].

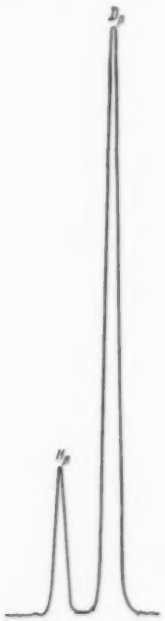

Fig. 1.

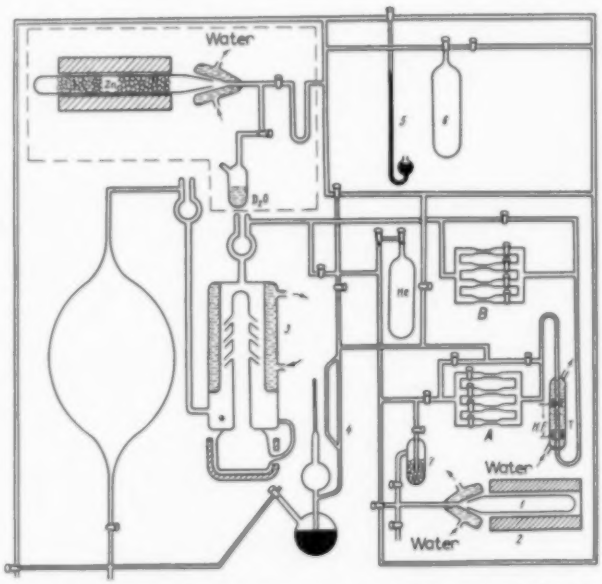

Fig. 2. Diagram of vacuum system. The part enclosed by the dotted line is for the liberation of deuterium from D_2O.

Sensitivity and accuracy of method

The method of analysis described has the following sources of error.

(a) *Error in the isotopic analysis of the equilibrium gas.* As discussed above, this error can easily be kept below 2 per cent and, consequently does not determine the total error of the method. This error might be increased if the metal contained large quantities of other gases together with the hydrogen. In this case the hydrogen could be purified, as for example, by passage through an active carbon trap.

In practice it has never been found necessary to use such purification. Relatively large quantities of foreign gases, such as carbon monoxide given off during the analysis of carbon steels, do not interfere with the isotopic analysis.

(b) *Errors due to incomplete attainment of isotopic equilibrium.* The time required to reach isotopic equilibrium depends on the temperature, the metal to be analysed and the weight and shape of the sample.

The time required by each metal must be determined previously by analysis of the gas during the approach to equilibrium. It is the time after which there is no

Fig. 3. Vacuum system.

VOL.
10
1957/5

further change in the composition of the gas phase. Typical curves representing the approach to equilibrium for zirconium and carbon steels are shown in Figs. 4 and 5. The time allowed in practice is always greater than the minimum necessary, so that the error due to non-attainment of equilibrium is always small enough to be neglected.

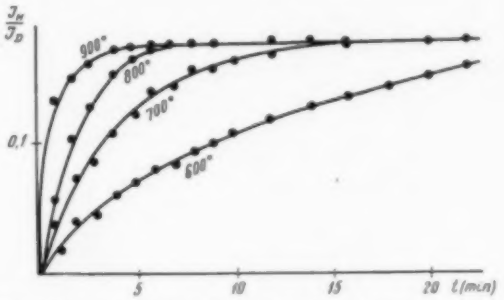

Fig. 4. Establishment of equilibrium for zirconium at different temperatures.

(c) *Error in blank correction.* When a blank experiment is performed the system always gives off some hydrogen. The value of this blank depends on the dimensions and composition of the exchanger, the tightness of the vacuum seal, etc.

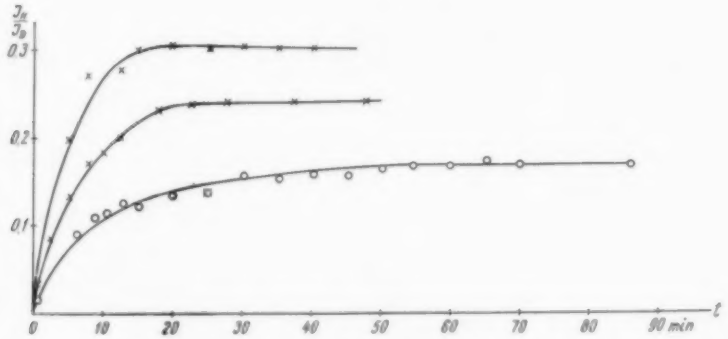

Fig. 5. Establishment of equilibrium for steel at 100°C.
○-chrome-nickel steel.
×-carbon steel.

Its value must be carefully determined for any given apparatus, and included in the calculations. However, in some cases the blank fluctuates between one experiment and another. For example, with one exchanger, the blank correction V_0'' of 0·126 cm³ showed a variation $\Delta V_0''$ of 0·015 cm³.

The value of $\Delta V_0''$ varies in a random way, and with small or moderate hydrogen contents in the metal, is an important source of error in the determinations; this is shown in Table 2.

It can be seen from Table 2 that, if an accuracy of 10 per cent is required with

a hydrogen content of 1 cm³/100 g, it is necessary to use not less than 10 g of sample.

(d) *Error due to contamination of the surface of the sample.* This error largely depends on the form and dimensions of the sample. It may be unacceptably large with finely divided powders and porous samples with highly developed surfaces. For compact samples, with minimum dimensions of a few mm this error is not significant down to hydrogen contents of 1/10 cm³/100 g of metal. Of course, before analysis, the surface of the sample should be carefully cleaned and degreased with carbon tetrachloride or ether.

Table 2. Error due to blank ($\Delta V_0'' = 0{\cdot}015$ cm³)

H_2 content in cm³/100 g	1	5	10
Weight of sample			
5	30%	7·5%	4%
10	7·5%	4%	2%
20	4%	2%	1%

It is the variation of the blank, rather than uncontrolled contamination of the surface, which limits the sensitivity of the method.

It is necessary that the quantity of hydrogen in the sample should excede three times the value of $\Delta V_0''$. With 20 g samples it was found possible to measure hydrogen contents in the region of 0·5 cm³/100 g with a standard error for a single determination of about 10 per cent.

The figure of 0·5 cm³/100 g is not the lower limit, but not much lower concentrations have been encountered.

The error arising from inhomogeneity of the sample is not discussed here, as this is not an error in the analysis.

Choice of conditions for the analysis of various metals

The weight of sample to be used is decided by the fact that the main analytical error is the variation of the blank. If the permissible relative error of the analysis is ε, then with C cm³ of hydrogen per 100 g, and a blank variation $\Delta V_0''$, the necessary weight of the sample is given by—

$$m = \Delta V_0''/\varepsilon C \qquad (6)$$

If the value of ε is set to be less than 4–5 per cent, then the main source of error will not be due to the variation of the blank, but to other causes. The pressure of deuterium in the exchanger should be chosen such that the amount of deuterium participating in the process is approximately equal to the hydrogen content of the sample. The error of the isotopic analysis is then a minimum. Table 3 shows the conditions for obtaining equilibrium with various metals.

There is a known difficulty to be considered in the analysis of those metals in which

VOL. 10 1957/5

the solubility of hydrogen is large at high temperatures, as, for example, Ti and Zr. The pressure of the equilibrium mixture round the metal may then be so low that it is difficult to induce a normal discharge, and there may be some separation

Table 3. Approximate conditions for the attainment of isotopic equilibrium

Metal	Temperature °C	Time in min	Remarks
Aluminium	900–1000	20–30	The sample is placed in a quartz boat
Iron	1000–1100	30–40	
Carbon steel	1000	20–30	
Chrome-nickel steel	1100	50–60	
20% Cr–80% Ni	1100	about 250	
Zinc	500–600	20–30	The sample is placed in a quartz boat
Titanium	1100	20–30	Addition helium after attainment of equilibrium.
Zirconium	800	15	,, ,, ,,
Degassing of exchanger.	1000	10	

of hydrogen isotopes in the capillaries of the system [12]. In this case, pure helium is introduced at a pressure of 10–15 mm Hg, after attainment of equilibrium in the exchanger.

Table 4. Analyses by different methods ($cm^3/100$ g)

Metal		Isotope spectra	Vacuum fusion	Saturated samples
Chrome-	1	2·07	2·60	
nickel	2	2·69	2·70	
steel	3	2·02	1·80	
	4	1·28	1·10	
	5	1·49	1·50	
Titanium	1	55 ± 1·5	58	
	2	41	42	
Zirconium	1	3·1	3·7	
	2	3·2	2·8	
	3	4·0	3·6	
	4	91·5	87	
	5	1067		1100
	6	539		550
	7	110		110

This introduction of helium does not affect the relative intensities of the hydrogen and deuterium lines. In a number of cases it was possible to check the results against those obtained for the same samples in other laboratories by the vacuum

fusion method, and also by the analysis of samples specially saturated with measured quantities of hydrogen.

Table 4 shows the results of such comparisons. Average figures are given for a number of analyses.

References

[1] SVENTITSKII N. S. and TAGANOV K. I. *Technical Information Bulletin of the Leningrad House of Scientific-technical Propaganda* 1955 No. 3 671.

[2] GERASIMOVA N. G., IVANOVA T. F. SVENTITSKII N. S., STARTSEV G. P., TAGANOV K. I. and TRENTOVIOUS M. E. *Bull. Acad. Sci. U.S.S.R.* 1955 **19** 2.

[3] SVENTITSKII L. S., SUKHENKO K. A., GOLONOV P. P., FAL'KOVA O. B., ALPATOV M. S. and TAGANOV K. I. *Zavod. Lab.* 1956 No. 6.

[4] ZAIDEL A. N. and PETROV A.A . *Zh. tekh. fiz., Mockba* 1955 **25** No. 14 2571.

[5] ZAIDEL A. N. and PETROV K. I. *Zavod. Lab.* 1956 No. 8.

[6] ZAIDEL A. N. *Bulletin of Leningrad State University* 1956 No. 16 29.

[7] ZAIDEL A. N. and A. A. PETROV *Bulletin of Leningrad State University* 1957 No. 10 40.

[8] ZAIDEL A. N., PETROV A. A. and VEINBERG G. V. *Spectral-isotopic Method for the Determination of Hydrogen in Metals* Press Leningrad State University 1957.

[9] BARRER R. M. *Diffusion in and through Solids.* Cambridge 1941.

[10] BROIDA H. P. and MOYER J. W. *J. Opt. Soc. Amer.* 1952 **42** 37.

[11] BROIDA H. P. and MORGAN G. *Analyt. Chem.* 1952 **24** 799.

[12] VEINBERG G. V., ZAIDEL A. N. and PETROV A. A. *Optika i Spectroskopia* 1956 **1** 972.

VOL.
10
1957/5

Spectrochimica Acta, 1958, Vol. 10, pp. 377 to 382. Pergamon Press Ltd., London

Intramolecular energy transfer in ytterbium organic chelates†

G. A. CROSBY‡ and M. KASHA
Department of Chemistry, Florida State University, Tallahassee, Florida

(*Received* 7 *August* 1957)

Abstract—The $^2F_{5/2} \rightarrow {}^2F_{7/2}$ intra-multiplet transition has been observed as a luminescence emission in the tris-dibenzoylmethane-Yb^{+++} chelate. A single strong luminescence line was recorded at 9710 ± 40 Å upon excitation of the broad π, π^* absorption band of the chelate with 3650 Å light. The transition frequency agrees well with earlier observations on the unique intra-multiplet transition of Yb^{+++}. The intramolecular energy transfer is unusual in that the apparent electronic energy difference between the initial and final states is over 10000 cm^{-1}. The importance of vibrational interaction in the mechanism of energy transfer is pointed out.

Introduction

INTRAMOLECULAR energy transfer, between the lowest π, π^* excited singlet state§ of rare-earth chelates and the electronic states of the rare-earth ion, was first observed by WEISSMAN [1] and investigated later by SEVCHENKO *et al.* [2]. Chelates of trivalent europium, samarium, and terbium were studied, using various ligands, such as dibenzoylmethane and benzoylacetone. Excitation of the broad, intense near-ultraviolet absorption band of such chelates with 3650 Å light yields a strong line-like luminescence emission, which is characteristic of the rare-earth ion. The discrete luminescence lines bear a close resemblance to the very weak sharp absorption bands observed for the trivalent ion in solution. These latter lines have been recognized generally as originating in the $4f$ orbitals of the lanthanide ion.

Since there is considerable interest in the mechanism of electronic energy transfer, and the previous observations had indicated a rather high efficiency for the intramolecular process in the rare-earth chelates, we have undertaken a general investigation of this problem. In this paper we report the intramolecular energy transfer for the rather exceptional case of trivalent ytterbium chelates, which had eluded detection previously [1].

For a description of the spectroscopic behavior of organic chelates of the trivalent lanthanide rare-earth ions, it is convenient to divide them into three general classes. Into *Class* I we place the ions (La^{+++} and Lu^{+++}) with the closed f-orbital configurations: $4f^0$ and $4f^{14}$, for which there are no electronic transitions in the visible and infrared regions. The ion Gd^{+++}, with an f-orbital configuration $4f^7$, also falls into this class. If dibenzoylmethane is used as a ligand in the chelate formation, the lowest excited singlet and triplet π, π^* states of the chelates lie at

† Work done under a contract between the Physics Branch Office of Naval Research, U.S. Navy, and the Florida State University.

‡ Present address: Department of Chemistry, University of New Mexico, Albuquerque, New Mexico.

§ We designate a π, π^* state as one having an electronic configuration in which the optical electron was promoted from a π-bonding to a π-antibonding orbital.

about 23500 and 20500 cm^{-1} above the ground state [3], respectively. Consequently, in the tris-dibenzoylmethane chelates of the ions of Class I, the intramolecular energy transfer is energetically impossible (see Fig. 1). Therefore, the main effect of the rare-earth ions on the spectroscopic properties of the chelates of this class is to enhance the singlet-triplet mixing in the π-electronic states of the chelate, as a spin-orbital, or magnetic, perturbing agent [3, 4]. Into *Class* II we place the remaining rare-earth trivalent ions which include a $4f^2$ to $4f^{12}$ configuration. In these cases, as indicated schematically in Fig. 1, energy transfer is feasible from the excited singlet or triplet π, π^* states of the chelate to the lower electronic

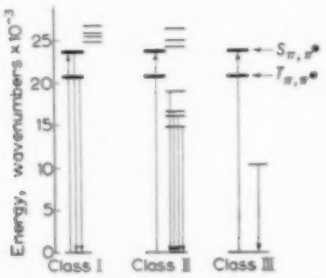

Fig. 1. Classification of rare-earth chelates. Electronic levels of the rare-earth ion on right of diagrams.

states of the chelated ion. However, as will be described later in another place [5], the efficiency of the energy transfer apparently depends on the electronic configuration of the rare-earth ion, efficient transfer correlating with the proximity of the f-orbital configuration to $4f^0$, $4f^7$ or $4f^{14}$. Into *Class* III we place the exceptional lanthanide ions with $4f^1$ and $4f^{13}$ f-orbital configurations, namely Ce^{+++} and Yb^{+++}. There is a single electronic transition which can take place within the f-orbital in these cases (see Discussion), and is observed in the infrared region. The corresponding energy diagram for Class III chelates (Yb^{+++} case) is given in Fig.1. Particular interest is attached to the efficiency of the energy transfer in this unusual situation. Moreover, the uniqueness of the rare-earth level in this case simplifies the energy transfer analysis. Although as we shall see, the Ce^{+++} chelate case was unamenable for study, the tris-dibenzoylmethane-Yb^{+++} chelate exhibited a remarkably efficient intramolecular energy transfer.

Experimental

The dibenzoylmethane used was Eastman, White Label grade, and was twice sublimed in a high vacuum. Piperidine used as a precipitating agent was a Matheson, Coleman, and Bell product, and was purified by distillations to give a colorless liquid. The Yb_2O_3 was* first converted to the chloride, then the chloride dissolved in alcohol and added to an equimolar solution of dibenzoylmethane and piperidine in alcohol. The precipitate was washed twice with absolute ethanol and dried in a vacuum desiccator. The samples were dissolved in absolute ethanol for the absorption curve determinations. For the low temperatures (77°K)

* Obtained from the Institute for Atomic Research, Iowa State College, Ames, Iowa.

VOL. 10 1957/5

luminescence studies, a 1 : 1 : 1 (volume parts) mixture of ethyl ether, *iso*pentane, absolute ethanol was used as a solvent. The dilute solutions of the chelate were frozen in a liquid-nitrogen bath to form transparent rigid glass solutions.

The luminescence spectra were recorded on Eastman I-M spectroscopic plates, hypersensitized in ammonia solution. The spectrograph used was a 3-prism Steinheil Universal GH, equipped with (approx. $f3{\cdot}5$) glass optics. A 1 kW 100 atmosphere AH-6 mercury arc was used for excitation, filtered by a $CuSO_4$ solution (5 cm, 100 g/l. of the pentahydrate) and a Corning Glass 5840 standard filter, yielding mainly 3650 Å light. The absorption spectra were determined on a Beckman DK-1 recording spectrophotometer.

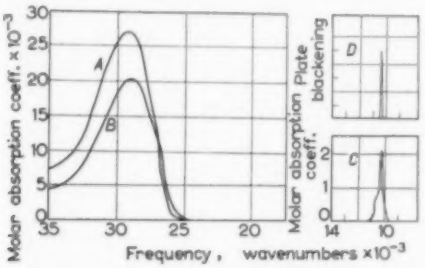

Fig. 2. Curve *A*, absorption spectrum of dibenzoylmethane in absolute ethanol at 293°K. Curve *B*, absorption spectrum of tris-dibenzoylmethane-Yb^{+++} in absolute ethanol at 293°K. Curve *C*, near infrared absorption spectrum of Yb^{+++} in aqueous solution at 293°K (after HOOGSCHAGEN). Curve *D*, the luminescence emission of tris-dibenzoylmethane-Yb^{+++} at 77°K in rigid glass solvent upon 3650 Å excitation, slit ~0·1 mm, exposure about 10 min. [See Experimental.]

Results and discussion

Rare-earth ions having f^1 and f^{13} inner orbital configurations may have a single intra-*f*-orbital transition, corresponding to the unique recoupling of L and S angular momenta (in the language of Russell–Saunders coupling). This leads to a single relatively sharp and characteristically weak line-like absorption in the spectrum of the aqueous ion. The fact that the two levels involved in the transition are doublet components, split by spin-orbital interaction, results in the occurrence of these lines relatively far in the infrared. Probably it is for this latter reason that in the literature [6, 7, 8] it is generally not recognized that the Ce^{+++} and Yb^{+++} ions have a sharp line absorption in addition to their relatively well-known nearly continuous ultraviolet absorption.

Ytterbium as a trivalent positive ion has a $^2F_{7/2}$ ground state, and a $^2F_{5/2}$ upper state for the intra-multiplet transition. The energy of this transition for the gaseous ion, which could be deduced from appropriate atomic term values, is unknown. In aqueous solution the corresponding sharp absorption band for Yb^{+++} was first observed by FREYMAN and TAKVORIAN [9] at 10270 cm^{-1} (9735 Å), and corroborated by GOBRECHT [10, 11], who assigned it as the $^2F_{7/2} \rightarrow {}^2F_{5/2}$ transition. The absorption band has been observed subsequently by other investigators [12, 13] and its intensity measured by HOOGSCHAGEN [14]. The molar absorption coefficient defined by $\epsilon = (1/cd) \log_{10} (I_0/I)$ with c in moles/l. and d in cm, is 2·08 at the band maximum (see Fig. 2). The corresponding oscillator

strength defined by $f = 4{\cdot}32 \times 10^{-9} \int \epsilon \, d\bar{\nu}$ is $3{\cdot}86 \times 10^{-6}$ [15]. The weakness and characteristic sharpness of this transition makes Gobrecht's assignment secure. Although the corresponding luminescence emission has not been reported for solutions or crystals of ytterbium salts, Brauer and Brauer [16] have observed a line emission at about 9700 Å for trivalent ytterbium oxide as an impurity in strontium and aluminium oxide phosphors, excited by 20 kV cathode rays.

For the intramolecular energy transfer study the chelate used was tris-dibenzoylmethane-Yb^{+++} (see Fig. 3). The lowest π, π^* allowed absorption band (see Fig. 2) of the chelate was excited by 3650 Å light with the sample in dilute rigid glass solution at 77°K (see Experimental). An intense luminescence emission

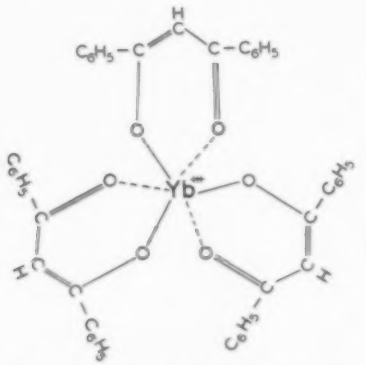

Fig. 3. Structural formula of tris-dibenzoylmethane-Yb^{+++}.

with λ_{max} at approximately 9710 ± 40 Å was observed (see Fig. 2) for the Yb^{+++} chelate, which must be the $^2F_{5/2} \rightarrow {}^2F_{7/2}$ emission for the chelated ion. The low dispersion of our spectrograph in this region prevented our obtaining a greater precision. The observed luminescence is remarkable for its absence of subsidiary structure and for its sharpness.

The quantum yield of the chelate luminescence was not determined absolutely, but a rough estimate from slit-width and exposure times and comparison with other efficient luminescence cases in this region leads to a probable value of quantum yield within the range 0·2–1. In other words, the intramolecular energy transfer is certainly efficient in this case. The only other emission from the Yb^{+++} chelate was a feeble blue fluorescence and a long-lived green luminescence, both of which are due probably to an organic impurity in the sample. The observed efficiency is all the more remarkable because the radiationless transition leading to the Yb^{+++} luminescence in the chelate requires an energy loss of 17,000 cm^{-1}, which must be dissipated thermally.

The differences in energy between the Yb^{+++} excited $^2F_{5/2}$ level and the zero-point π, π^* levels are of course somewhat less than the value quoted above, based on the exciting frequency. If the energy transfer is from the π, π^* singlet level of the chelate, an apparent energy difference of about 13,500 cm^{-1} would be involved; for the π, π^* triplet of the chelate, the corresponding difference would be 10,500 cm^{-1}. An efficient energy transfer between electronic states which are this far

VOL.
10
1957/5

apart would not seem to be plausible on a quantum mechanical basis, since levels so widely separated do not interact very strongly. Consequently, it seems necessary to assume that the mechanism of energy transfer involves interaction between (a) high vibrational levels of the chelate coupled with the $^2F_{5/2}$ excited state of the ytterbium ion and (b) the pure π, π^* electronic states of the chelate.

The requirement of vibrational interaction, for the energy transfer mechanism, is not ruled out by the absence of vibrational fine structure in the luminescence emission of the Yb^{+++} chelate. Optical transitions of the type $^2F_{5/2} \rightarrow {}^2F_{7/2}$ in the chelate undoubtedly are accompanied by insignificant molecular distortion, and as a consequence of the Franck-Condon principle, no vibrational fine structure should appear.

It is of interest to point out that the lowest π, π^* absorption band of dibenzoylmethane is significantly altered upon formation of the Yb^{+++} chelate (see Fig. 2). A shift of about 400 cm^{-1} in the band maximum is observed, accompanied by a considerable diminution in intensity (the absorption coefficient for the chelate being calculated *per mole of dibenzoylmethane*). It is probable that the 4*f* orbitals of Yb^{+++} are not directly involved in the chelate binding (since the chelate emission is so little displaced from the frequency of the analogous transition in the ion in solution). Nevertheless the possibility of strong vibrational coupling is suggested by the effect of chelation on the π, π^* absorption noted above.

The intra-multiplet transition should be observable in other rare earth ions, and the observations of BRAUER and BRAUER [16] give three examples in addition to the trivalent ytterbium. The case of Ce^{+++} is an interesting one to consider, even though direct observations are lacking for it. The ground state of Ce^{+++} is $^2F_{5/2}$, and for the gaseous ion the $^2F_{5/2} - {}^2F_{7/2}$ separation has been deduced by LANG [17] to be 2253·0 cm^{-1}; this assignment has been confirmed by a Zeeman pattern analysis [18]. Unfortunately, the study of electronic transitions near 5 μ is difficult, and we have not yet succeeded in observing this transition either in absorption (ion) or in emission (chelate). In the case of the *actinide* rare earths, with incompletely filled 5*f* orbitals, the hexavalent neptunium ion and the normally unstable pentavalent uranium ion should exhibit a unique intra-multiplet transition [19].

Acknowledgements—The authors are indebted to Prof. ROBERT E. CONNICK of the University of California, and Dr. C. J. RODDEN, now of the New Brunswick AEC Laboratory, for valuable communications on the spectra of rare earth ions.

It is a pleasure to acknowledge the co-operation of Prof. F. H. SPEDDING in helping us procure the ytterbium oxide sample.

References

[1] WEISSMAN S. I. *J. Chem. Phys.* 1942 **10** 214.
[2] SEVCHENKO A. N. and TROFIMOV A. K. *J. Exp. Theor. Phys.* 1951 **21** 220; SEVCHENKO A. N. and MORACHEVSKY A. G. *Izv. Akad. Nauk SSSR (ser. fiz.)* 1951 **15** 628.
[3] YUSTER P. and WEISSMAN S. I. *J. Chem. Phys.* 1949 **17** 1182.
[4] KASHA M. and MCGLYNN S. P. *Ann. Rev. Phys. Chem.* 1956 **7** 403.
[5] CROSBY G. A. To be published.
[6] VAN VLECK J. H. *J. Phys. Chem.* 1937 **41** 67.

[7] Yost D. M., Russell H., Jr. and Garner C. S. *The Rare Earth Elements and Their Compounds.* John Wiley, New York 1947.
[8] Kauzmann W. *Quantum Chemistry* p. 671. Academic Press, New York 1957.
[9] Freyman R. and Takvorian S. *C. R. Acad. Sci., Paris* 1932 **194** 963.
[10] Gobrecht H. *Z. Ges. Naturw.* 1937 **3** 351.
[11] Gobrecht H. *Ann. Physik* 1938 **31** 600 755.
[12] Rosenthal G. *Physik. Z.* 1939 **40** 508.
[13] Rodden C. J. *J. Res. Nat. Bur. Stand. Wash.* 1942 **28** 265.
[14] Hoogschagen J. *Physica* 1946 **11** 513.
[15] Hoogschagen J. and Gorter C. J. *Physica* 1948 **14** 197.
[16] Brauer E. and Brauer P. *Naturwissenschaften* 1947 **34** 120.
[17] Lang R. J. *Canad. J. Res.* 1935 **13** A 1; 1936 **14** A 127; *Phys. Rev.* 1936 **49** 552.
[18] van de Vliet H. J. Dissertation, Univ. Amsterdam, 1939; *Chem. Abstr.* 1939 **33** 2033.
[19] Connick R. E., Kasha M., McVey W. H. and Sheline G. E. *The Transuranium Elements* (Edited by Seaborg, Katz and Manning) Chap. 4.20. *National Nuclear Energy Series.* McGraw-Hill, New York 1949.

VOL.
10
1957/5

Spectrochimica Acta, 1958, Vol. 10, pp. 383 to 394. Pergamon Press Ltd., London

Emission and absorption spectra of plutonium excited in a King furnace

L. Bovey
Atomic Energy Research Establishment, Harwell, Didcot, Berks

(*Received* 22 *August* 1957)

Abstract—A list is given of wavelengths of plutonium absorption and emission lines excited in a King-type furnace and photographed in the second order of a 3 m grating instrument over the region 2791–6888 Å. The problems connected with measurement of such lines are briefly discussed and tentative conclusions reached from an attempt to find the energy levels are given.

Introduction

The successful assignment of the spectral lines of an element into a series of electronic levels depends fundamentally on accurate measurement of their wavelength. In addition, it is advantageous to have the spectrum excited by different methods so that groups of lines having common characteristics can be distinguished. As part of the study of plutonium, it was decided to examine first its emission and absorption spectra produced in a carbon furnace operating at 2500°C. An account of the design of the furnace has already been given [2]. Whilst the work was in progress a report was issued by Conway [1] on the emission spectrum. Since the furnace was then nearly complete and absorption data had not been obtained, it was decided to continue the work. Subsequently, it has been found that the wavelengths quoted by Conway are in error by as much as 0·5 Å, although the accuracy of measurement was stated to be 0·1 Å. An attempt has been made to increase the accuracy to 0·02 Å, but because of factors discussed below, an overall accuracy better than about 0·05 Å cannot be claimed, although stronger lines are probably in error by less than this figure.

Emission and absorption spectra

Emission spectra have the disadvantage that relatively long exposures are required up to a period of hours. For materials such as the rare earths this is not a serious disadvantage, but in the case of the metals, uranium and plutonium, such times have not been possible, because the tube or liner disintegrated too quickly. Absorption spectra can be given in a few seconds, but only a much smaller number of lines is recorded. It is difficult to measure the weak absorption lines against the continuous background. However, it is possible to photograph absorption lines at shorter wavelengths, since background sources emitting ultra-violet light can be used. The strength of emission lines partly controlled by the shape of the black body emissivity curve falls off considerably in the ultra-violet. It is advantageous to take for comparison both emission and absorption spectra where this is possible. The emission spectra were used for measurement, whenever both existed.

The theoretical significance of absorption spectra is that the lines appearing should arise from levels which can be excited thermally by temperatures of the furnace, say 2500°C. This corresponds approximately to levels below 10,000 cm^{-1}. Work on lutetium [3] shows that this assumption is generally true. Some lines

found in lutetium absorption spectra cannot be assigned to low-lying levels and absorption spectra on scandium, yttrium and lanthanum have also been taken with the object of both testing the King furnace and checking whether all absorption lines arise from levels below 10,000 cm^{-1}.

Wavelength measurement

It would be advantageous if wavelengths could be measured to at least 0·001 Å, since this would reduce the chance coincidence effect when significant differences are being looked for [4]. To obtain this accuracy calls for extreme care in both photographing and measuring the spectrum; 0·005 Å is probably a more practical figure, and even this figure can only be obtained by extremely careful work on high dispersion (e.g. 21 ft grating) instruments.

In the past, King furnace work has been used to distinguish stages of excitation and the lines themselves have not been measured accurately. Since so much effort has been put into obtaining the furnace spectra and reliable wavelengths were not available when this work was begun, it was felt desirable to measure the lines in the hope that the data could be used in term analysis.

A serious difficulty for accurate measurement has been the width of the iron arc lines, many of which are several times wider than the emission lines from the furnace. Although the error arising from the uncertainty in placing a cross-wire on such broad lines was compensated to some extent by the large number of iron lines measured, future work will make use of a source giving finer standard lines, e.g. an auxiliary small furnace or a "Dieke" hollow cathode [5].

Each spectrum has been measured twice on the comparator, being put upside down between each measurement so that the line passes under the cross-wire in a reverse direction. The difference of readings is used in the hope that this compensates for any bias of the observer caused by lack of symmetry in the line. Many of the lines have been measured on two or more plates.

Results

Wavelengths

A list of wavelengths found is shown in Table 2. In general, we are in excellent agreement with van den Berg and Klinkenberg [6] on the values of the wavelength. They used a hollow cathode source and their standard wavelengths were taken from the spectra of argon which was present in the source. The argon lines therefore appeared simultaneously with the plutonium spectra. Agreement with the wavelengths of Fred and Tomkins [7] is satisfactory, but since their spectra are almost entirely spark lines, the number of lines common to both lists is small. Marked differences were found in a comparison of the wavelengths with those of Dodgen, Chrisney and Rollefson [8].

Table 1 shows a comparison of a few lines measured by four observers (Russian [9], British, Dutch [6] and American [1]). The European measurements agree better with one another than with the other two.

Comparison of emission lines with those of Conway shows that wavelengths differ occasionally by as much as 0·5 Å. There are more lines at shorter wave-

VOL.
10
1957/5

lengths than in his list, but at longer wavelengths his list is bigger.* This difference may be caused by the spectrograph rather than conditions within the furnace. The grating in our Hilger-3m spectrograph appears to be very inefficient in reflecting power at longer wavelengths.

Intensities

These are relative values based on a visual estimate and are denoted by very very weak, very weak, weak, medium, strong, very strong.

Table 1. Comparison of some plutonium lines measured by four observers

Striganov [9]	Bovey	Klinkenberg [6]	Conway [1]
4140·10	40·01	40·01	—
4151·38	51.41	51·44	51·63
4159·87	59·93	59·93	59·89
4206·37	06·47	06·51	06·59
4472·70	72·75	72·79	73·11
4478·63	78·64	78·63	79·02
4506·56	06·63	06·65	06·95
4676·18	76·46	76·49	—
4798·93	99·06	99·06	99·16
4986·72	86·78	86·80	—
5044·53	44·57	44·65	44·37
5590·51	90·48	90·48	90·78
5630·48	30·46	30·44	30·45
6192·63	92·81	92·7	92·64

The values of intensities found from a microphotometer trace on one plate gave good agreement with these broad divisions, but it was not found possible to spend the large amount of time necessary to deal similarly with every plate. In any case, the intensity scale must vary from region to region and without a calibration technique any figures produced would still be of only a relative character.

Impurities

Impurities may be present in either the sample or the materials of the furnace—in particular the heated tube. The evidence is that the latter is responsible for most of the impurity lines. Titanium, iron and calcium are certainly present and there is strong evidence for the presence of cobalt, nickel and tantalum and possibly vanadium. No difficulty arises when strong lines of these elements are concerned. However, when there is agreement between the wavelength of a line in the spectrum and that of a *weak* arc line of a possible impurity, doubts arise. Many of these can be resolved by comparison with plutonium spectra taken under different conditions (e.g. in a hollow cathode) or by comparison with plates of other elements (e.g. uranium) taken under similar conditions (i.e. in the furnace).

* A detailed comparison was given in an earlier report [14]. Many of the lines also occur in previously unpublished work at the Oak Ridge Laboratory now summarized in a general report [15]. Examination for lines common to both reports was greatly helped by the courtesy of Dr. J. Rand McNally, of that laboratory, who sent the data already punched on Hollerith cards.

Table 2. A list of lines found in the furnace spectra

Wavelength Å	Strength Em	Strength Abs	Wavelength Å	Strength Em	Strength Abs	Wavelength Å	Strength Em	Strength Abs	Wavelength Å	Strength Em	Strength Abs
2791·42		w	2907·82		vw	2988·89		vw	3044·35		vw
2796·60*		w	2909·12*		vw	2990·50*		vw	3044·59		vw
2798·22		vw	2912·50		vw	2991·95*		vw	3045·28		vw
2798·75		vw	2913·06		vw	2993·52		vw	3045·38		vw
2806·08		vw	2917·38		vw	2994·05*		w	3046·15		vw
2806·81		vw	2918·82*		vw	2995·34		w	3046·74		w
2809·13*		vw	2919·58*		vw	3000·03		w	3047·43*		vw
2809·71		vw	2919·74		vw	3000·56*		w	3048·48*		vw
2811·44		vw	2920·72*		vw	3001·39		vw	3049·63*		w
2812·45		vw	2930·12		w	3001·60		vw	3051·54		vw
2816·94		vw	2930·64		w	3003·29		vw	3051·91*		vw
2825·35*		vw	2930·99*		vw	3003·49		vw	3052·43		vw
2833·04		vw	2932·21		vw	3003·82		vw	3054·32*		vw
2834·40*		vw	2932·51		vw	3005·80		vw	3054·62		vw
2838·07		w	2933·52*		vw	3009·04		w	3054·88		vw
2839·77		vw	2933·81		vw	3011·59		vw	3055·59		vw
2844·43*		vw	2933·94		vw	3011·73		vw	3058·76		vw
2847·24		vw	2934·40		vw	3012·55*		vw	3059·53		vw
2847·62		vw	2941·04*		vw	3012·86		vw	3059·77		vw
2848·79		vw	2941·39		vw	3014·05		vw	3060·34		vw
2850·78		vw	2941·66		vw	3014·30		vw	3060·74		vw
2851·67*		vw	2942·44*		vw	3015·41		vw	3061·54		vw
2852·13*		w	2945·89		vw	3018·45*		w	3066·34		w
2855·28		w	2950·09		w	3022·29*		vw	3067·60		vw
2857·30*		vw	2951·30		vw	3022·76		vw	3074·99		w
2857·52		vw	2951·80*		w	3023·20		vw	3075·34*		w
2859·09		vw	2954·42		vw	3023·83		vw	3077·12*		w
2859·97*		vw	2956·35		vw	3024·30*		vw	3078·41*		vw
2861·23		vw	2958·22		w	3024·54		vw	3081·56		vw
2861·73		vw	2958·76		w	3025·03		vw	3081·77*		vw
2862·57*		vw	2962·40		vw	3025·21*		vw	3082·20		vw
2863·66		vw	2963·44		vw	3029·65		vw	3082·38		vw
2864·32*		vw	2964·62		w	3029·88		vw	3082·95*		w
2866·47		vw	2965·07		vw	3030·27*		vw	3084·50*		vw
2867·78		vw	2968·74		vw	3030·57		vw	3085·27		vw
2869·03		vw	2968·92		vw	3032·10		vw	3086·53		w
2872·63		vw	2970·55*		vw	3032·59		vw	3087·48*		vw
2875·87		vw	2971·82		vw	3033·60		vw	3088·31*		vw
2879·95*		vw	2973·48		vw	3034·16*		vw	3088·53		vw
2880·25		vw	2975·53*		vw	3034·50*		vw	3088·75*		vw
2887·49		w	2976·62		vw	3036·82		w	3089·15*		vw
2892·27		vw	2976·92		vw	3037·05*		vw	3089·71*		w
2896·25		w	2978·51		vw	3038·31*		vw	3091·15*		vw
2903·17*		vw	2981·24*		vw	3038·93		vw	3091·34		vw
2903·41		vw	2983·13		vw	3039·41		vw	3092·52*		vw
2904·97		w	2985·84*		vw	3042·15		vw	3092·72*		vw
2905·82*		vw	2986·02		vw	3042·60*		vw	3097·21		vw
2906·11		vw	2986·44*		vw	3042·94		vw	3100·79		vw
2906·85		vw	2986·65		vw	3043·82		vw	3101·14		vw
2907·18		vw	2988·57*		w	3044·04*		vw	3101·47*		vw

VOL. 10 1957/5

Table 2—*continued*

Wavelength Å	Strength		Wavelength Å	Strength		Wavelength Å	Strength		Wavelength Å	Strength	
	Em	Abs		Em	Abs		Em	Abs		Em	Abs
3102·52*		vw	3761·41*		vw	3215·06		w	3271·26		vvw
3102·75		vw	3162·36*		vw	3215·53		vvw	3272·03		vvw
3104·31		vw	3165·50*		vw	3216·17		vw	3272·55		vvw
3105·44*		vw	3166·69		vw	3219·78		vw	3273·18*		vvw
3105·62*		vw	3168·62		vw	3220·42		vw	3273·63		vvw
3106·06		vw	3168·75		vw	3220·81		vw	3273·85*		vvw
3107·25*		vw	3169·17		w	3221·28*		vw	3274·53*		vvw
3107·44*		w	3171·39*		vw	3227·20		vw	3274·91*		vw
3108·67		w	3172·22		vvw	3228·36		vvw	3275·20		m
3110·79		vw	3172·41		vvw	3228·56		vvw	3275·61*		vvw
3112·81		vw	3174·72		vvw	3229·53		vw	3275·78		vvw
3113·93*		vw	3175·12		vw	3232·20		s	3276·65		vvw
3116·69		vw	3178·81		vw	3236·03		vvw	3276·89		vw
3117·46*		vw	3178·97*		w	3236·25		vvw	3279·95		vvw
3119·39		w	3179·61		w	3237·56		vvw	3280·12		w
3120·00*		vw	3180·92*		vvw	3238·73		vvw	3280·87		vw
3121·39*		vw	3181·51*		vvw	3239·05*		vw	3281·35		vw
3121·54*		vw	3184·30*		vw	2339·27		vw	3281·76		w
3124·88		w	3185·90*		vvw	3240·25		w	3282·33*		vw
3126·85		vw	3186·12		vvw	3241·18		vvw	3284·32*		vvw
3127·54		vw	3188·78*		vw	3241·42		vvw	3285·67		vvw
3130·60*		vw	3190·48		vvw	3242·31		vvw	3285·83		vvw
3130·78		vw	3193·54		vw	3244·12*		w	3286·40*		vvw
3133·15		vw	3194·46*		vvw	3245·17		vvw	3287·00*		m
3133·48		vw	3195·16*		vvw	3245·28*		vvw	3287·30*		vw
3134·73		w	3195·61*		vvw	3245·43		vw	3288·13*		vvw
3135·28		w	3195·75		vvw	3245·67		vw	3288·59		vw
3136·10		w	3195·99		vvw	3246·31		vvw	3289·67		vw
3136·54		vw	3196·62		vw	3247·52		vvw	3291·85*		vvw
3138·96*		w	3197·53*		vvw	3247·75		vvw	3292·49*		vw
3140·31		w	3197·71		vvw	3248·52*		vvw	3292·82		vvw
3140·52		w	3198·49		vvw	3249·92		vw	3293·26		vw
3141·08		w	3199·36*		vvw	3252·03		vw	3293·58		vw
3141·51*		vw	3199·49		vvw	3253·93*		vvw	3293·80*		vvw
3145·95		vw	3200·79*		vvw	3254·68		w	3294·07		vvw
3146·57		w	3201·83		vw	3257·89		vvw	3295·09		vvw
3148·81		vw	3202·85		vw	3258·30		vvw	3296·19		vvw
3149·67		vw	3202·98		vw	3259·46		w	3296·46		vvw
3150·09*		vw	3203·28		vvw	3260·51		vvw	3296·89		vvw
3153·24*		vw	3203·84*		vvw	3260·68		vvw	3297·72		vvw
3155·31*		vw	3204·50		vvw	3261·01		vvw	3297·84		w
3155·55		vw	3204·78		vvw	3262·31		vvw	3299·11*		vvw
3156·04		vw	3205·76		vvw	3262·47		vvw	3301·73		w
3157·57		vw	3206·55		w	3263·46		vvw	3302·59*		vw
3157·98*		vw	3207·91*		w	3264·19		vvw	3304·07*		vvw
3158·59		vvw	3209·10		vvw	3265·15		w	3304·71		vvw
3158·90*		vvw	3209·78		vvw	3268·76		vw	3305·01		vvw
3159·15		vvw	3210·66		w	3269·26		vvw	3306·27		vvw
3159·33		vvw	3211·35*		vw	3269·91		vvw	3306·55		w
3160·89		vvw	3214·30*		m	3270·68		vvw	3306·67		w

Table 2—*continued*

Wavelength Å	Strength		Wavelength Å	Strength		Wavelength Å	Strength		Wavelength Å	Strength	
	Em	Abs		Em	Abs		Em	Abs		Em	Abs
3307·64		vw	3338·64		vvw	3380·67•		vw	4319·56•		vvw
3307·80		vw	3338·94		s	3381·76		vw	3420·98		vw
3308·29		vw	3339·27		vvw	3382·67		vw	3421·19		vvw
3308·74		w	3343·84		vvw	3385·11		vw	3421·67		vw
3309·41		vvw	3344·02		vvw	3385·69•		vvw	3422·17		vw
3310·55		vw	3344·54•		vw	3386·40		vw	3422·71		vw
3310·80		vvw	3344·78		vvw	3386·95		vw	3422·98		vvw
3311·74		vw	3345·45		vvw	3387·36		vvw	3424·84		vw
3311·87•		vw	3346·08		vw	3387·78		vvw	3428·33		vvw
3312·29		vvw	3348·39		m	3387·97		vvw	3429·46		vvw
3312·64•		vvw	3349·64		m	3388·12•		vvw	3431·64•		vvw
3312·96•		vvw	3351·98		vvw	3389·83		m	3432·01		vvw
3315·34•		vvw	3352·12		vvw	3392·27		vw	3432·35		vvw
3315·76		vvw	3352·32		vvw	3392·80		vvw	3433·28		vvw
3316·93		vw	3354·12		vvw	3393·41		vvw	3433·68		vvw
3317·20•		vvw	3355·50		vw	3393·63		vw	3433·83		vvw
3317·61		vvw	3355·63		vvw	3394·24		w	3434·40		vw
3317·86		vvw	3356·44•		vvw	3395·56		vvw	3434·81		vw
3318·81•		vvw	3357·50		vw	3395·77		vvw	3435·37		vw
3319·01		vw	3358·25		vw	3396·06		vvw	3437·39		vvw
3320·01		vw	3358·44		vw	3396·69		vvw	3437·65•		vvw
3320·16		vvw	3359·85		vvw	3397·13		vvw	3438·05		vw
3320·56		w	3361·58•		vvw	3397·40		vvw	3438·31		vvw
3320·81		w	3362·33		vw	3397·82•		vvw	3438·57		vw
3321·79		vvw	3362·59		vw	3399·63		vvw	3439·14		vw
3322·11		vw	3363·38		vw	3401·07		w	3439·47		vw
3322·32•		vw	3363·89		vw	3402·64•		vw	3439·64		vvw
3323·47		w	3364·87		vvw	3403·52		vvw	3441·48•		vw
3324·05		vvw	3365·21		vw	3403·62		w	3441·90		vvw
3324·24		vvw	3365·59•		vw	3404·00		vvw	3442·22		vvw
3324·44		vvw	3366·30		vvw	3405·20•		vw	3442·56		vvw
3325·03		w	3366·59		vvw	3406·19		vw	3442·94•		vvw
3325·72•		vvw	3367·00		vvw	3407·10		vvw	3443·29		vw
3326·13		vw	3368·07		vvw	3407·60		vw	3444·07		vw
3326·67		vvw	3368·85		vw	3408·17		vvw	3446·29•		vw
3327·17		vw	3370·48•		vvw	3408·82		w	3446·95		vw
3327·75		vvw	3371·19		vw	3409·51•		vvw	3450·25		vw
3328·32		vw	3371·65		vvw	3410·88		vvw	3450·74		vvw
3330·07		vw	3372·42		vvw	3411·30		vvw	3452·24		vw
3331·37		vw	3372·66		vvw	3412·05		s	3452·55		vw
3331·54		vw	3372·94		vvw	3412·52•		vvw	3452·88•		vw
3331·79•		vvw	3373·18		vvw	3412·87		vvw	3453·42		m
3332·32		w	3375·79		vvw	3413·59		vvw	3454·16		vvw
3333·00		vw	3376·06•		vvw	3413·79		vvw	3454·49		vvw
3333·16		vw	3376·75		vvw	3415·00		vvw	3456·01	vvw	w
3333·89		vw	3377·21		vvw	3415·95		vvw	3457·27		vw
3334·79		vvw	3377·75		vvw	3417·79		w	3457·44		vw
3337·23		vvw	3379·47		vvw	3418·45		vvw	3459·04		vvw
3337·47		vvw	3379·59		vvw	3418·85		vvw	3459·38		vw
3338·39		vvw	3379·90		vw	3419·35		vvw	3459·99		vvw

VOL. 10 1957/5

Table 2—*continued*

Wavelength Å	Strength		Wavelength Å	Strength		Wavelength Å	Strength		Wavelength Å	Strength	
	Em	Abs		Em	Abs		Em	Abs		Em	Abs
3460·21		vvw	3488·99		vvw	3531·83•		vvw	3651·60		vvw
3460·44•		vvw	3489·32		vvw	3533·60	vvw	m	3652·29		vvw
3460·77		vvw	3489·60		vw	3534·99		vw	3652·87		vvw
3461·12		vvw	3490·02		vvw	3536·54		m	3654·26	vvw	vw
3461·42		vvw	3490·30		vvw	3538·48		w	3656·09		vvw
3462·23		vw	3491·70	vw	s	3540·78		m	3656·78		vvw
3462·64		vvw	3493·06•		vw	3541·70		vw	3660·35		vvw
3462·81•		vvw	3493·33		vvw	3549·41		m	3667·22	vvw	m
3463·23		vw	3493·63		vvw	3550·35		m	3670·59		vw
3463·93		vvw	3494·69		w	3553·09		vvw	3671·61	vw	s
3464·46		vvw	3495·24		vw	3555·65		w	3672·77		w
3466·06		w	3495·81		vw	3558·21		w	3674·75		vw
3466·37		vw	3496·38	vw	s	3561·22		vw	3675·82		vvw
3467·18		vw	3497·06		vvw	3567·63	vw	m	3676·85		vvw
3467·57•		vvw	3497·38		vvw	3570·88		vw	3677·53	vw	w
3467·81		vvw	3498·10		vvw	3571·11		vw	3678·50	vvw	vw
3468·47		vvw	3498·37		vvw	3573·67•		vvw	3679·93		m
3468·56		vvw	3498·62	vw	s	3575·58		vvw	3683·81	vw	m
3468·78		vw	3498·79		vvw	3577·02		vvw	3684·85		vw
3469·71		vw	3499·59	vw	m	3585·08		vw	3687·35		vw
3471·28		vw	3499·85		w	3585·90		vw	3688·30	vvw	vw
3472·14		vw	3501·82		vvw	3586·48		vw	3689·57		vw
3473·62•		vvw	3502·35•		vvw	3588·01•		vw	3695·19	vw	m
3473·84		vvw	3502·61		vvw	3590·64		vvw	3698·59	vvw	m
3474·09•		vw	3502·98		vvw	3591·19		vvw	3699·20	vvw	m
3474·73		vvw	3503·99•		vvw	3592·15		vvw	3701·83•		vvw
3474·95		vvw	3506·34•		vw	3593·94		vw	3705·56	vvw	m
3476·48	vw	w	3506·96		vvw	3604·59		w	3705·72	vw	w
3477·48		vw	3507·36		vvw	3605·34	w	va	3705·97		m
3477·88		vw	3508·83		w	3606·50		w	3706·41		m
3478·37		vw	3509·72		vw	3607·85		w	3707·83		m
3478·59	vw	w	3510·12		vw	3609·30•		vw	3709·61		vvw
3479·34		vvw	3510·52		vvw	3611·52		vw	3711·05		w
3479·77		vvw	3510·77		vvw	3611·97	vvw	w	3711·72		w
3480·17	vvw	m	3511·59		vw	3613·20		vw	3312·77	vvw	w
3481·75		vw	3511·78		vw	3614·41		vw	3713·50		vvw
3482·21		vvw	3512·62•		vvw	3615·04		vw	3713·86	vvw	w
3482·34		vw	3513·94•		vw	3616·68		vw	3714·24		vw
3483·18		vvw	3514·41	vvw	w	3619·15		vw	3714·69	vvw	m
3483·90		vvw	3514·87		vw	3620·97		w	3714·82	vvw	m
3484·47	vvw	vw	3515·58		w	3626·97	vw	s	3717·36	vvw	vvw
3484·67		vw	3516·52		vw	3631·31	vw	m	3718·56	vvw	w
3485·08		vw	3516·70		vw	3632·20		m	3718·99		w
3485·18		vw	3517·43		vw	3637·62		w	3720·23	vw	m
3485·77		vw	3518·13		vvw	3638·76		w	3720·56	vw	m
3486·99		vvw	3523·22		vw	3643·30		m	3721·33	vw	m
3487·18		vvw	3524·52	vvw	vw	3643·73		vw	3722·78	vw	w
3487·53•		vw	3526·61	vvw	vw	3644·54		vw	3723·01	vw	w
3487·80		vw	3530·59•		vw	3645·23		vw	3724·15		vw
3488·76		vw	3531·40		vw	3646·68		vvw	3725·98	vw	m

Table 2—*continued*

Wavelength Å	Strength		Wavelength Å	Strength		Wavelength Å	Strength		Wavelength Å	Strength	
	Em	Abs		Em	Abs		Em	Abs		Em	Abs
3728·49	vvw	w	3801·04	vw	m	3878·52	s	vs	3962·86	vw	vvw
3728·84	vw	w	3801·30	vvw	vw	3879·86	vvw	vvw	3964·26	vw	
3729·80	w	m	3802·13	vw	w	3881·16	vvw	vw	3964·95	w	m
3732·17	vw	m	3802·58	vvw	w	3881·67	vvw	vw	3967·28	vw	vw
3733·71			3805·91	w	s	3882·30	vvw	vw	3968·46	vvw	
3735·93	vvw	vw	3808·41	w	s	3886·12	vvw	s	3972·12		vvw
3737·70		w	3809·11	w	s	3888·59		vw	3974·02	vvw	vw
3740·70	vw	vw	3809·52	w	s	3889·35	vvw	vw	3976·90	vvw	vw
3741·05	w	vw	3811·38	w	s	3889·97	vw	m	3977·16	vvw	
3743·66		vw	3813·60	vw	s	3892·14	vvw	vw	3979·46	w	m
3744·77	w	vvw	3815·03	vw	s	3892·40		vw	3980·71	vvw	
3746·82		s	3816·32•	w	m	3895·65•		vw	3982·48	s	
3748·63	vw	w	3818·46	vw	m	3895·88	w	s	3983·02	vw	m
3748·80	vw	m	3819·34	w	w	3896·41	vw		3988·72	vw	w
3752·86	w	m	3820·92	vw	m	3898·04	vw		3989·75	s	m
3753·61•	s	s	3821·12	w	s	3898·26		vvw	3990·21	w	m
3754·12	w	w	3823·49•		m	3901·56	vvw	vw	3996·90		vvw
3755·08	vw	vw	3823·88•		vw	3902·83	w	m	3998·65	s	m
3755·91	w	s	3827·55	w	m	3907·94	vw	vvw	4006·21	vvw	
3757·58	vw	m	3829·03	vw	w	3910·47	vvw	vw	4008·92	vw	
3757·82	vw	w	3829·62	vw	w	3911·24	w	s	4010·07	vw	
3758·32	vw	w	3833·43		vw	3911·60	vvw	vw	4010·61	vw	vw
3758·89	vw	m	3835·00	vw	m	3913·41	vvw		4011·07		vw
3760·52		vw	3835·48	w	s	3914·33	vvw		4011·49	vw	vw
3761·08		vw	3835·86	vw	m	3916·34		vvw	4014·58	vw	
3764·59	vvw	vw	3836·92	vw	m	3918·17	vvw		4015·30	vw	
3765·14	vvw		3838·87	w	m	3918·51		vw	4017·38	vw	
3765·92	vw	m	3842·06	w	s	3918·71	w	m	4020·03	w	
3767·46	vw	m	3843·96	vw	w	3924·53	vw	vw	4024·23	m	vw
3768·19	vw	m	3844·07	vw	w	3925·71	vvw	vw	4024·57	s	s
3771·64	vvw		3845·99	vvw	w	3926·77	vvw	m	4026·18•	m	
3773·54		vw	3847·11	vw	m	3928·53	w	s	4027·07•	s	
3774·37	vw	m	3848·17		vw	3929·89	vw	vw	4031·75•	w	m
3776·67	vw	s	3848·81		vw	3933·64	vvw		4032·97	s	m
3776·78	vvw		3850·98	w	s	3936·32	w	m	4035·54•	s	s
3777·34	vvw	w	3851·70	vvw	w	3938·41	vvw	vvw	4036·28	m	w
3779·70	vvw	vw	3851·83	vw	m	3939·48	vw	m	4038·39	vw	
3784·32		w	3852·13		w	3940·55		vvw	4039·03	s	s
3784·56		vvw	3856·07	w	m	3941·49	vw	m	4041·30	s	w
3785·26	vvw		3859·09		vw	3942·91	vvw	vw	4041·79•	w	
3786·86		w	3860·76	w	vw	3944·00•	vvw	vw	4042·53	m	
3787·28	vvw	w	3862·29	vvw	m	3944·33	vvw	vw	4047·25	m	
3790·27		w	3864·42	vw	vvw	3947·43	vvw	w	4048·07	w	
3790·41	vw	w	3869·66		m	3947·76	vw	vw	4048·50	m	
3790·88		vw	3870·08	w	s	3948·68	w	m	4049·95	w	
3792·21	w	s	3873·92•	vvw		3953·18	vvw	vvw	4052·22	m	
3794·52	vw	w	3874·32	vvw	vvw	3955·88	vw	m	4052·57	m	vw
3798·23•	w		3874·78		vvw	3956·34	w	m	4055·10	s	s
3799·03	vw	w	3875·91	vvw	vw	3958·21	w	m	4055·62	m	w
3799·36	w	s	3876·36	vvw	vw	3960·44	vw	w	4059·57	s	

VOL. 10 1957/5

Table 2—*continued*

Wavelength Å	Strength		Wavelength Å	Strength		Wavelength Å	Strength		Wavelength Å	Strength	
	Em	Abs		Em	Abs		Em	Abs		Em	Abs
4061·91	w		4199·29	w		4366·98	w		4536·08*	s	
4062·80	w		4205·90	m	vw	4367·37	s	s	4536·15	s	
4063·24	w		4206·47	vs	vvs	4374·56	w		4553·45	s	s
4063·60*		w	4208·24	vs	vs	4379·22*	w		4554·02*	w	
4070·15	s	m	4211·66	w		4379·37	vw		4555·48	m	
4073·04	s	w	4221·87	s	m	4379·87	vw		4566·62*	w	
4075·20	m		4224·10	s	m	4380·96	vw		4570·50	vw	vw
4075·90	w		4232·33	m		4381·20	vw		4574·29*	m	
4079·56	m		4235·42	m		4384·69	vw		4582·08	m	
4082·37	m		4238·21	m	w	4385·30	vw		4590·82	vw	
4085·84	s	m	4239·02	w		4388·72	w		4594·50	m	
4086·18	w	w	4241·05	w		4392·09	m	m	4596·61	vw	
4088·79	w	w	4247·23	w		4399·31	w		4599·09	vw	
4090·58	w	w	4250·69	w		4400·75	vw		4599·95	vw	
4092·22	s	s	4253·67	w		4403·06	s	s	4600·75*	vw	
4095·27	w		4259·42	w		4404·90	s	vs	4601·13*	vw	
4095·62	w		4259·76	w		4406·81	w		4602·64	vw	
4097·12	m	s	4261·15	m	w	4407·03	vw		4602·90*	vw	
4101·92	s	s	4261·60*	w		4409·53	m	w	4604·38	vw	
4102·49	s	s	4261·88	s	s	4414·72	m	vw	4605·00*	w	
4106·61	w		4268·05	w		4417·53	vw		4605·82	w	
4111·05	m		4269·76	s	m	4425·01	m	vw	4607·02	s	
4112·35	w		4274·94	vs	s	4433·79	s	s	4607·32	w	
4112·73*	m		4280·28	w		4436·24	vw		4608·65	m	
4114·90	m	s	4281·18	s	m	4439·09	w	vw	4609·35	w	w
4119·78	m	s	4281·82	w		4447·12*	m		4610·66	w	
4128·10	m	m	4288·36	w		4453·15	s	s	4615·72	m	
4129·28	w		4288·72	w		4454·51	w		4616·12*	w	
4133·00	s	s	4294·93	vw		4455·92*	m	w	4616·96	vw	
4135·28	m	w	4300·82	m		4457·69	m		4619·48*	w	
4135·96	s	s	4302·33	w	vw	4461·21	w		4624·81	vs	m
4140·01	s	s	4310·30	m	m	4472·75*	w		4625·86	m	
4140·22	w		4310·70	s	m	4476·24	w		4626·17*	w	
4151·08	m	s	4311·67*	vw		4478·64	m		4627·46*	m	
4151·41	m	s	4312·15	vw		4482·15	vvw		4630·91	w	
4154·39	vw		4318·29	w		4484·38	m		4632·67	vw	
4154·71	vw		4329·83	vw		4498·39	w		4633·00*	vw	
4155·14	w		4330·48	vw		4504·92	m		4634·55	m	
4155·42	s	s	4336·06	vw		4506·63	s	s	4636·36	m	vw
4157·44	m	w	4336·38	vw		4508·04	w		4639·32*	vw	
4159·93	s	s	4337·18	w		4518·02*	m	vw	4640·90	vw	
4167·76	m	w	4338·71	vw		4520·70	m		4642·71	vw	
4170·93	s	s	4339·79*	vw		4524·34	w		4645·40	s	
4172·43	m	w	4351·78	vw		4527·71	vvw		4645·84	m	
4181·10	m	vw	4356·83	vw		4530·65*	w		4646·16*	m	
4182·53	s	s	4358·02	vw		4533·89	w		4646·62	s	m
4182·74	w		4362·10	w		4534·04	w		4650·03*	s	
4183·49	s	s	4362·60	w		4534·51	w		4651·27*	vw	
4192·23	w		4366·23	m		4535·58*	m	m	4652·17*	w	
4197·30	w		4366·57	vw		4535·93*	m	w	4657·42*	w	

Table 2—*continued*

Wavelength Å	Strength		Wavelength Å	Strength		Wavelength Å	Strength		Wavelength Å	Strength	
	Em	Abs		Em	Abs		Em	Abs		Em	Abs
4658·76•	w		4761·07	w		4954·64	vw		5272·59	vvw	
4662·15	vw		4762·80	vw		4955·63	vw		5289·48	vvw	
4664·21	w		4764·99	vw		4964·86	vw		5296·63	vvw	
4668·31	vw		4767·15•	m		4969·39	vw		5298·24•	vvw	
4669·11	vw		4770·37	vw		4969·75•	vw		5301·44	vvw	
4671·70•	vw		4771·61	vw		4984·50	vvw		5304·38	w	
4672·58	vw		4777·88•	w		4986·78	s	m	5304·72	vvw	
4673·40	s	w	4778·25•	vw		4997·30	vvw		5305·18	vvw	
4676·46	s	w	4779·40	vw		5004·40	m		5307·05	vvw	
4677·08	w		4780·95•	m		5008·26	vvw		5308·64	vvw	
4678·94	vw		4788·46	vw		5009·63	vvw		5309·81	vw	
4681·89•	vs		4798·56	vw		5026·45	vvw		5310·31	w	
4683·26	m		4799·06	w		5037·32•	vvw		5317·29	vw	
4683·82	w	w	4799·60	vw		5037·63•	vvw		5334·27	vvw	
4684·83•	vw		4801·19•	vw		5044·57	m		5345·81•	vvw	
4685·96	w		4804·11	vw		5051·20	vvw		5364·12	w	
4689·08	w		4806·07	vw		5058·91	vw		5370·40	vvw	
4689·56	s	s	4809·36	vw		5067·94•	vvw		5374·07	vvw	
4690·49	vw		4811·15	w		5078·93	w		5374·33	vvw	
4691·84•	vw		4812·75•	s		5089·95	vvw		5374·76	vvw	
4692·39	vw		4814·44	vs	m	5094·66	vvw	vw	5375·08	vvw	
4692·79	vw		4817·87•	w		5115·64	vvw		5375·54	vvw	
4693·14	vw		4823·32	vw		5118·95	vvw		5381·00	s	
4693·61	vw		4825·42•	vw		5136·46•	m		5389·29•	vvw	
4694·07	vw		4830·36	vw		5138·16	vvw		5393·00	vvw	
4695·23	s	m	4835·95	vw		5141·65•	vvw		5402·51•	w	
4701·29•	w		4841·48	vw		5142·15	vw		5408·58	vvw	
4706·29	w		4852·04	m		5148·99	vvw		5409·76•	vw	
4710·69	vw		4854·43	vw		5153·38•	vvw		5414·24	vvw	
4711·78	w		4860·21	vw		5156·42	vvw		5418·22	w	
4712·76	s		4861·42	vw		5163·65•	vvw		5421·49	vw	
4715·33•	vw		4861·78•	vw		5168·94	vvw		5427·82	vvw	
4715·71•	vw		4872·61	w		5178·97	vvw		5446·09	vvw	
4716·53	w		4881·14	vw		5182·03	vvw		5449·47	vvw	
4718·57	vw		4883·91•	vw		5183·84	vw		5459·30	vvw	
4720·72	s		4884·22	vw		5188·81•	vvw		5476·64•	w	
4721·42	vw		4888·17	vw		5193·68	vw		5479·61	vvw	
4722·85•	w		4894·41	m	s	5212·75•	vvw		5482·00	vw	
4725·29	s		4907·69•	m		5218·41•	vvw		5482·57	vvw	
4730·91	w		4908·31	vw		5221·39	vvw		5486·25	w	
4735·40	vs	vs	4911·74	m		5223·65•	vvw		5498·47	s	s
4738·55	w		4914·52	vw		5229·15	vvw		5510·65	w	
4739·35	vw		4914·92•	vw		5229·47	vvw		5517·97	vw	
4741·76	w		4916·98	vw		5231·22	vvw		5537·56	w	
4748·03	w		4921·20•	m		5233·09	vvw		5538·07	vw	
4748·83	w		4925·97•	vw		5252·14	vvw		5549·59	m	
4753·51	s	w	4926·75	vw		5257·34	vvw		5551·54	vvw	
4753·93•	s	m	4927·45	vw		5259·22	vw		5561·98	vs	s
4756·51•	s		4933·62	vw		5264·13•	vvw		5570·47	s	m
4758·64	w		4934·06•	vw		5269·82	vvw		5577·22	vw	

VOL. 10 1957/5

Table 2—*continued*

Wavelength Å	Strength		Wavelength Å	Strength		Wavelength Å	Strength		Wavelength Å	Strength	
	Em	Abs		Em	Abs		Em	Abs		Em	Abs
5590·48	vs	s	5712·42	s	s	5893·07	w		6044·65	w	
5592·29•	s	m	5727·10	vvw		5919·03•	vw		6045·33•	w	
5592·61	vvw		5733·15	m	w	5922·97	vw		6092·20	m	w
5593·33	vvw		5747·01	vw		5925·80	vw		6100·45	w	
5610·45	vvw		5748·39•	m	w	5926·93	vw		6105·30	w	
5613·46	vvw		5770·19	m		5937·13	vw		6138·76	w	
5613·80	vvw		5776·76•	w		5939·78•	vw		6192·81	s	s
5628·41	vw		5780·69•	w		5944·01•	m		6196·07	w	
5630·46	vs	s	5788·07•	vw		5945·08	m		6214·94	w	
5630·61	vvw		5807·15•	m	m	5952·34	vw		6256·62•	w	
5663·19	w		5811·09•	s		5983·25	s	s	6260·71	vw	
5664·85	w		5832·87	w		5993·04	vvw		6304·72	s	s
5667·50	w		5835·93	w		5993·76	vw		6486·75	w	w
5672·66	vvw		5839·04	s	m	5995·18	vw		6488·87	m	s
5672·87	vvw		5847·59	vvw		5997·24•	vvw		6535·26	w	
5674·10	vvw		5853·77•	m		5999·64•	vw		6609·11•	m	
5686·82	w		5860·89	vw		6000·57	vw		6880·18	m	
5694·96•	w		5864·88	vs	m	6012·73	vw		6887·60	s	m
5698·85	vw		5877·38•	w		6031·33	w				
5709·59	vw		5880·83	w		6032·35	w				

• Possibility of line being an impurity.

Intensity scale:—vvw very very weak
vw very weak
w weak
m medium
s strong
vs very strong
vvs very very strong

Classification of spectra

The furnace, having a low-voltage form of excitation, favours the production of spectra from the neutral atom. Nevertheless, lines from the ionized atom can arise, but since these will be weakened in such a source they must arise from strong transitions. Only two lines in the absorption spectra of lutetium have been assigned [10] to the ionized spectra and these arise from strong transitions involving the ground state. A preliminary division into I and II spectra has been made by VAN DEN BERG and KLINKENBERG [6] and STRIGANOV and KOROSTYLEVA [9], and in general there is agreement with the assignment of these authors. In the few cases where there is disagreement between these two groups of workers, the presence or absence of furnace lines has confirmed most of the former's assignments.

Term analysis

Plutonium has a position among the transuranic group analogous to that occupied by samarium among the rare earths. If this resemblance extended to the energy levels, a ^7F arising from the electronic configuration $(5f)^6(7s)^2$ would be expected as the lower multiplet. The ground state configurations of americium-I and americium-II have been shown to be f^7s^2 and f^7s respectively [11] and the

preliminary analysis of Pu-II gives f^6s as the lowest configuration [12]. Both of these results would suggest that f^6s^2 should be low in Pu-I.

However, the incomplete analysis of uranium-I [13] gave f^3ds^2 as the lowest configuration, and this result together with the fact that the binding of the $6d$ electron in the transuranics is comparable with that of the $5f$ indicates that such configurations as f^5ds^2, f^5d^2s and f^6ds may also be low in Pu-I. These configurations would give a complex series of multiplets of which the lowest expected might be ^7K, ^9L and ^9H respectively. A further possibility if the isoelectronic sequence from Am-II were followed is f^7s giving $^9S_4$ and $^7S_3$. If the f^6s^2 or f^7s configurations were lowest the spectrum would probably be dominated by transitions to them as in Sm-I and Am-II respectively.

The data obtained were examined for any sets of differences among both the emission and absorption lines. Promising differences of 307, 562, 896, 978, 2096, 2204 and 2606 cm^{-1} from the absorption data were obtained, but attempts to put the associated lines into a multiplet structure were not successful. The basic difficulty was the wide interval $\pm 0{\cdot}2$ cm^{-1} used in taking differences to allow for experimental error in the wavelengths, with the result that many coincidental differences were included. It is also probable that weaker lines excluded in order that the number of coincidental differences may be kept to a minimum are necessary even in the preliminary stages of analysis to show the multiplet structure.

It seems therefore that both the absence of outstandingly strong lines and the lack of any dominant multiplet among the absorption lines points to the presence of several electron configurations at low levels in the Pu-I spectrum. As has been stressed by several previous workers, further progress can only be made from more accurate wavelength data together with other techniques for classification of lines such as Zeeman and isotope effects.

VOL.
10
1957/5

Acknowledgements—The author would like to thank Mr. H. WISE for his assistance in measuring the plates, and Mr. C. W. NOTT of the National Physical Laboratory for his help in both the work on wavelength computations from the experimental data and the supply of various sorted lists.

References

[1] CONWAY J. G. *J. Opt. Soc. Amer.* 1954 **44** 276.
[2] BOVEY L. *J. Sci. Instrum.* 1955 **32** 376.
[3] BOVEY L. and GARTON W. *Proc. Phys. Soc.* 1954 **57** 291.
[4] BOVEY L. and NOTT C. W. *A.E.R.E. Report* 1952 C/R 1334.
[5] CROSSWHITE H. M., DIEKE G. H. and LEGAGNEUR C. S. *J. Opt. Soc. Amer.* 1955 **45**, 270.
[6] VAN DER BERG M. and KLINKENBERG P. F. A. *Physica* 1954 **XX** 461.
[7] TOMKINS F. S. and FRED M. *J. Opt. Soc. Amer.* 1949 **39** 357.
[8] DODGEN H. W., CHRISNEY J. and ROLLEFSON G. K. *U.S.A.E.C. Report* 1944 C.K. 2247.
[9] STRIGANOV A. R. and KOROSTYLEVA L. A. *Optika i Spectroskopia* 1956 **1** 957.
[10] BOVEY L. and PEARSE R. W. B. *A.E.R.E. Report* 1956 C/R 1976.
[11] TOMKINS F. S. and FRED M. *J. Opt. Soc. Amer.* 1957 **47** In press.
[12] GRIFFIN P. M. and MCNALLY J. R. *J. Opt. Soc. Amer.* 1955 **45** 63.
[13] KIESS C. C., HUMPHREYS C. J. and LAUN D. D. *J. Res. Nat. Bur. Stand.* 1946 **37** 57.
[14] BOVEY L. and WISE H. *A.E.R.E. Report* 1955 C/R 1763.
[15] MCNALLY J. R. *Oak Ridge National Laboratory Report* 1956 ORNL –2154 Physics.

Spectrochimica Acta, 1958, Vol. 10, pp. 395 to 403. Pergamon Press Ltd., London

Systematics in the vibrational spectra of uranyl complexes*

LLEWELLYN H. JONES
Los Alamos Scientific Laboratory, University of California, Los Alamos, New Mexico

(*Received* 15 *August* 1957)

Abstract—The calculation of U–O bond force constants for uranyl complexes from their infrared absorption spectra is discussed. The maximum error involved in treating the uranyl group as free UO_2^{++} for calculation of the U–O force constant is estimated to be less than 3 per cent. Approximate anharmonicity constants for general use for the uranyl vibrations are given. The application of Badger's rule relating U–O force constant to U–O bond distance is discussed.

Introduction

THE bare uranyl ion, UO_2^{++}, is in itself a strong complex of U(VI) with O(II). However, it probably never exists as a free triatomic ion but is always co-ordinated directly with from two to six other ions or molecules. Infrared and Raman spectra have been reported [1–10] on many of these uranyl compounds. Also extensive studies have been made of the fluorescence spectra and visible absorption spectra of many uranyl compounds. These are reported and discussed by DIEKE and DUNCAN [11] and by RABINOWITCH [12]. The latter author gives a rather complete bibliography up to 1952.

The above mentioned work shows that the uranyl group is almost surely linear and has three vibrational frequencies which vary considerably from one compound to another. There is a symmetric stretching frequency, ν_1, appearing between 800 and 900 cm^{-1}; an asymmetric stretching frequency, ν_3, appearing between 850 and 1000 cm^{-1}; and a bending frequency in the neighborhood of 200 cm^{-1}. We desire to have approximate relations from which the U–O bond force constant can be calculated for a given compound with reasonable accuracy. The U–O bond force constant should eventually serve as a fairly accurate measure of the U–O bond distance in a given compound.

ZACHARIASEN [13] discusses the crystal structures of many uranyl compounds and points out that in all cases known the uranyl group is collinear. ZACHARIASEN [13] also predicts that the uranyl U–O bond distance varies all the way from 1·60 Å in $NaUO_2(CH_3CO_2)_3$ to 1·92 Å in $MgUO_2O_2$. Such a large range of distances should produce a very large range of uranyl frequencies. The values he has measured are 1·76 ± 0·03 for $K_3UO_2F_5$, 1·92 ± 0·03 for $MgUO_2O_2$, and 1·91 ± 0·10 for $CaUO_2O_2$. CROMER and HARPER [14] report a U–O distance of 1·67 ± 0·09 Å in solid UO_2CO_3. From these values and analyses of the infrared spectra we hope in future publications to be able to report constants for use in a relation such as BADGER's rule [15] for determination of the U–O bond distance of a uranyl compound from its infrared spectrum. This can then be extended, with modification to the transuranyl compounds. In this paper we shall not treat any special cases but rather give a general treatment to show what information we can hope to obtain and to estimate the error involved in certain simplifying approximations.

* This work was sponsored by the U.S. Atomic Energy Commission.

Determination of force constants

For the free uranyl ion it would be quite simple to determine the U–O force constants from the two fundamental stretching frequencies. However, the uranyl ion is undoubtedly never "free", but considering the two uranyl oxygens as poles, it will have anywhere from 2 to 6 equatorial ligands bound to the uranium atoms. For example, ZACHARIASEN [16] has determined the crystal structures of $K_3UO_2F_5$ and finds $UO_2F_5^{-3}$ groups with the fluorine atoms approximately in a plane with the uranium and in nearly pentagonal symmetry about the uranyl axis. The U–F bonds (secondary bonds) have a distance of $2{\cdot}24 \pm 0{\cdot}02$ Å while

Table 1. Number of vibrations of various symmetry species for UO_2L_n of symmetry D_{nh}

D_{2h}	D_{3h}	D_{4h}	D_{5h}	D_{6h}
A_g 2	A_1' 2	A_{1g} 2	A_1' 2	A_{1g} 2
B_{1g} 1	A_2'' 2	A_{2u} 2	A_2'' 2	A_{2u} 2
B_{1u} 2	E' 3	B_{1g} 1	E_1' 3	B_{1u} 1
B_{2u} 2	E'' 1	B_{2g} 1	E_1'' 1	B_{2g} 1
B_{3u} 2		B_{2u} 1	E_2' 2	B_{2u} 1
		E_g 1	E_2'' 1	E_{1g} 1
		E_u 3		E_{1u} 3
				E_{2g} 2
				E_{2u} 1

the U–O (primary) bonds are $1{\cdot}76 \pm 0{\cdot}03$ Å. These secondary bonds will always be weaker than the primary U–O bonds but nevertheless they will have an effect on the uranyl vibrational frequencies. It is important to evaluate this effect and to show in what approximation it is justifiable to neglect it and treat the uranyl frequencies as arising from linear, triatomic O–U–O in order to determine the U–O bond force constant.

For simplicity we will first discuss the general case of n atoms arranged symmetrically in the equatorial plane about the uranium atom. This will give the free UO_2L_n ion (or molecule) the symmetry D_{nh}. L stands for the ligand atoms or groups in general. In this paper we will not attempt to discuss lattice interaction but will treat the complex uranyl ions as non-rotating, non-interacting entities. From the tables given by HERZBERG [17] we find that the number and representation of frequencies for symmetries D_{2h} through D_{6h} are as given in Table 1.

The frequencies of the top row (A_g, A_{1g} or A_1'') are the symmetric stretching frequencies involving symmetric stretching of the U–O bonds and of the U–L bonds. There are two vibrations in each of these representations. They will be called ν_1 and ν_2 and will be as depicted in Fig. 1a for D_{4h} as an example. The vibration ν_1 will involve mainly the stretching of U–O bonds while ν_2 involves mainly the stretching of the U–L bonds.

There will be one symmetry species in each case which involves asymmetric

VOL. 10 1957/5

stretching of the U–O bonds. These are B_{2u}, A_2'', A_{2u}, A_2'' and A_{2u}, respectively, for D_{2h}, D_{3h}, D_{4h}, D_{5h}, D_{6h}. Each of these representations will have two vibrations. For consistency we will call these two frequencies ν_3 and ν_4. The motions involved are shown in schematic in Fig. 1b (for D_{4h} as an example). Thus ν_3 is mainly an asymmetric U–O stretching vibration while ν_4 involves primarily the bending of the O–U–L angle.

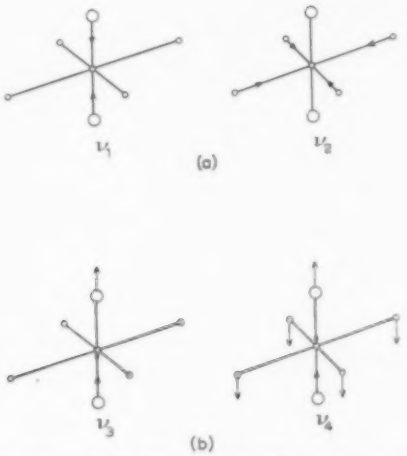

Fig. 1. Schematic form of vibrations of uranyl complexes of symmetry D_{4h}. Large circles represent uranyl oxygens.

Using a general quadratic valence force potential function we arrive at the following frequency relations.

$$\lambda_1 + \lambda_2 = \mu_O F^S_{UO} + \mu_L F^S_{UL} \tag{1}$$

$$\lambda_1\lambda_2 = \mu_O\mu_L[F^S_{UO}F^S_{UL} - (F^S_{UO,UL})^2] \tag{2}$$

$$\lambda_3 + \lambda_4 = (\mu_O + 2\mu_U)\, F^A_{UO} + (n\mu_U + \mu_L)\rho^2_{UL}F^A_\alpha - (8n)^{1/2}\mu_U\rho_{UL}F^A_{UO,\alpha} \tag{3}$$

$$\lambda_3\lambda_4 = (n\mu_O\mu_U + \mu_O\mu_L + 2\mu_L\mu_U)\, \rho^2_{UL}[F^A_{UO}F^A_\alpha - (F^A_{UO,\alpha})^2] \tag{4}$$

$$\mu_i = \frac{1}{M_i}\,,\ \rho_{ij} = \frac{1}{R_{ij}}$$

Superscript S refers to symmetric vibrations. Superscript A refers to asymmetric vibrations.

$$F^S_{UO} = F_{UO} + F_{UO,UO'} \tag{5}$$

$$F^S_{UL} = F_{UL} + (n-1)F_{UL,UL'} \tag{6}$$

$$F^S_{UO,UL} = (2n)^{1/2}F_{UO,UL} \tag{7}$$

$$F^A_{UO} = F_{UO} - F_{UO,UO'} \tag{8}$$

$$F^A_\alpha = F_\alpha + (n-1)F_{\alpha\alpha} \tag{9}$$

$$F^A_{UO,\alpha} = (8n)^{1/2}F_{UO,\alpha} \tag{10}$$

$\Delta\alpha$ = change in angle UL bond makes with the linear OUO axis.
F_{UO} = UO bond force constant.
F_{UL} = UL bond force constant.
F_{α} = force constant for $\Delta\alpha$.
$F_{UO,UO'}$ = constant for interaction of one UO bond with the other UO bond.
$F_{UL,UL'}$ = constant for interaction of one UL bond with any other UL bond (not necessarily neighbours).
$F_{UO,UL}$ = constant for interaction of either UO bond with any UL bond.
$F_{\alpha\alpha}$ = constant for interaction of one $\Delta\alpha$ with any other $\Delta\alpha$.
$F_{UO,\alpha}$ = constant for interaction of UO bond stretching with change in adjacent OUL angle.

A more specific potential function is that derived from a Urey–Bradley field—attributing interaction terms to mutual repulsion of the O and L atoms and also of the L atoms for each other. These repulsions appear in most cases to be approximated by the Leonard–Jones repulsive potential, aR^{-12}. Thus, we shall add two repulsion terms to the potential energy for repulsion of O for L and of L for L.

In using these repulsive potentials we also will retain the resonance interaction constant, $F_{UO,UO'}$. The frequency relations are the same as the set of equations (1)–(4) with the force constants defined as below.

$$F^S_{UO} = F_{UO} + 2A_1 nq^{-2}[R^2_{UO} - 0{\cdot}077r^2_{UL}] + F_{UO,UO'} \tag{11}$$

$$F^S_{UL} = F_{UL} + 4A_1 q^{-2}[r^2_{UL} - 0{\cdot}077R^2_{UO}] + 8A_2 \sin^2 \pi/n \tag{12}$$

$$F^S_{UO,UL} = (8n)^{1/2} A_1 q^{-2}(1{\cdot}077)R_{UO}r_{UL} \tag{13}$$

$$F^A_{UO} = F^S_{UO} - 2F_{UO,UO'} \tag{14}$$

$$F^A_{\alpha} = F_{\alpha} + 2{\cdot}154A_1 q^{-2}R^2_{UO}r^2_{UL} \tag{15}$$

$$F^A_{UO,\alpha} = (8n)^{1/2}(2A_1)q^{-2}[R^2_{UO}r_{UL} - 0{\cdot}077r^3_{UL}] \tag{16}$$

$q = (R_{OL})_O$

$A_1 = \frac{1}{2}\frac{d^2V_1}{dR^2}$ $\qquad V_1$ = O–L repulsion potential

$A_2 = \frac{1}{2}\frac{d^2V_2}{dR^2}$ $\qquad V_2$ = L–L repulsion potential

We have made qualitative studies of several uranyl complexes, and in most cases it is easy to observe and assign the fundamental frequency, ν_3, and the combination frequency, $\nu_1 + \nu_3$. Approximate anharmonic constants can be assigned (as discussed later in this paper) giving us the fundamental frequencies, ω_1 and ω_3. However, the rest of the spectrum is generally quite complex and it may not be possible to determine the remaining fundamental frequencies. For calculating the UO force constant and the UO,UO′ interaction constant, it would greatly simplify matters if we could essentially neglect the interaction of the UO bonds with the ligands, which amounts to saying

$$F^S_{UO} = M_O\lambda_1 \tag{17}$$

$$F^A_{UO} = \frac{M_O M_U}{M_U + 2M_O}\lambda_3 \tag{18}$$

VOL. 10 1957/5

or using a general quadratic function

$$F_{UO} = (M_O/2)(\lambda_1 + g\lambda_3) \tag{19}$$

$$F_{UO,UO'} = (M_O/2)(\lambda_1 - g\lambda_3) \tag{20}$$

M_i = mass of atom i

$g = M_U/(M_U + 2M_O)$

Thus, we wish to estimate the error involved in making this simplifying approximation.

Approximation for F^S_{UO}

From the frequency relations (1)–(4) for λ_1 and λ_2 we derive the following relation for per cent error involved by using the approximate relation of equation (17).

$$\% \text{ error} = 100\frac{(F^S_{UO})_O - (F^S_{UO})_T}{(F^S_{UO})_T} = \frac{100(F^S_{UO,UL})^2}{M_O\lambda_1(M_L\lambda_1 - F^S_{UL}) - (F^S_{UO,UL})^2} \tag{21}$$

in which $(F^S_{UO})_O$ is the force constant calculated with neglect of the ligands (from equation (17)) and $(F^S_{UO})_T$ is the true value of F^S_{UO}. Thus if the interaction constant $F^S_{UO,UL}$ is zero, the equation for λ_1 and λ_2 is separable and no error is involved in using equation (17). In order to estimate the error as a function of $F^S_{UO,UL}$ we must assign approximate values to the other constants of equation (21). As a typical example, for $K_3UO_2F_5$ it appears that $\nu_1 \approx 800$ cm^{-1} giving $(F^S_{UO})_O \approx 6$ m dyn/Å. Using the UF bond distance of 2·24 Å [16] and BADGDR's rule in combination with the UO bond distance of 1·76 Å [16], we calculate $F^S_{UF} \approx 1$ m dyn/Å. A good approximation of equation (21) is then

$$\% \text{ error} = 3(F^S_{UO,UL})^2 \tag{22}$$

with $F^S_{UO,UL}$ in m dyn/Å. There is really no reliable data to enable us to estimate $F^S_{UO,UL}$. In the case of UF_6, assuming a Urey–Bradley field, GAUNT [18] found a repulsion constant of 0·32 m dyn/Å. The F—F distance is believed to be about 2·86 Å [19]. In $K_3UO_2F_5$ the F–O distance is ~2·84 Å, so if the Urey–Bradley field were applicable we should expect a value of A_1 of ~0·3 m dyn/Å. Using this in equation (13), for $UO_2F_5^{=}$, we find $F^S_{UO,UF} \approx 1{\cdot}0$ m dyn/Å. However, as GAUNT has pointed out [18], the Urey–Bradley treatment of UF_6 gives much too large a value for the repulsion constant, A, especially considering that the F–F distance is somewhat greater than two times the normal van der Waal's radius of fluorine. Furthermore, in $UO_2F_5^{=}$, the F–O distance of 2·84 Å is considerably longer than the F–F distance of about 2·63 Å (calculated from reference [16]). Therefore, the F–O repulsion should be negligible compared to the F–F repulsion. Thus it appears that the Urey–Bradley field is not a satisfactory potential function for UF_6 or uranyl complexes, and a valence bond resonance interaction is likely to be more important than repulsion of O for L. Using a general quadratic valence bond potential function for UF_6 the constant for interaction of one UF bond with any other UF bond (except its opposite) is found to be about −0·07 cm^{-1}.* Using this for

* From calculations by the author using the frequencies of reference [18].

$F_{UO,UL}$ from equation (7) we calculate $F^S_{UO,UL} = -0{\cdot}24$ for D_{6h} to $-0{\cdot}14$ for D_{2h}. Due to the UO double bonds (increasing the chance for resonance) we might expect a somewhat larger interaction term in uranyl complexes. This approximate treatment has been for $UO_2F_5^{\equiv}$. In the other uranyl compounds discussed by ZACHARIASEN [13] the O–L distance is greater than in $K_3UO_2F_5$; thus we expect the UO,UL interaction to be smaller.

In view of the above discussion, we will place an upper limit of 1·0 m dyn/Å for $F^S_{UO,UL}$ with the expectation that it is probably considerably smaller. Then from equation (22) we see that the maximum per cent error in saying $F^S_{UO} = M_O\lambda_1$ is three per cent and the probable error is much less. Though 3 per cent error in F_{UO} at 800 cm^{-1} corresponds to an error of about 14 wave numbers, which is somewhat larger than the experimental error, it is not a large error in the force constant and corresponds to a very small change in bond distance ($\sim$0·005 Å).

Approximation for F^A_{UO}

In analysing the relations for λ_3 and λ_4 in equations (3) and (4), it turns out that the most important term to consider is $F^A_{UO,\alpha}$. Variations of F^A_α, M_L, and n within reasonable limits have only a small effect on the calculated value of F^A_{UO} for a given value of λ_3. However, the effect of $F^A_{UO,\alpha}$ is considerable.

Calculations show that if $\rho_{UL}F^A_{UO,\alpha}$ is between $-0{\cdot}05$ and $+0{\cdot}28$ m dyn/Å, the error arising in using equation (18) is less than 3 per cent if $F^A_{UO} = 4$ m dyn/Å. For larger values of F^A_{UO} (it appears usually to be between 6 and 8 m dyn/Å), the allowable spread of $\rho_{UL}F^A_{UO,\alpha}$ is even greater.

As discussed above, the only evidence in the literature for calculation of an approximate value of $\rho_{UL}F^A_{UO,\alpha}$ is the value of A of 0·32 m dyn/Å found by Gaunt [18] for UF_6. If we use this value for A_1 in equation (16), we find $\rho_{UL}F^A_{UO,\alpha} \approx 0{\cdot}23$ m dyn/Å if $N = 6$, $R_{UL} = 2{\cdot}2$ Å and $R_{UO} = 1{\cdot}8$ Å. The calculations mentioned in the footnote on p. 387 show that for UF_6 the most reasonable force constants are obtained if $F_{UF,\alpha}$ is ≈ 0. Also F_α is $\approx 0{\cdot}14$ cm^{-1} so we might expect $F_{UF,\alpha}$ to be $< 0{\cdot}1$ cm^{-1}. In the uranyl complexes under discussion the U–L bonds are considerably weaker than the U–F bonds in UF_6 (see reference [13]). Thus, we should expect smaller interaction constants (considerably less than 0·1 cm^{-1}).*

The above discussion gives us confidence that we can surely use equations (19) and (20) with a maximum error of 3 per cent in F_{UO} and a probable error of considerably less. Of course the true test will be a complete analysis of the spectrum of a few complexes, such as $K_3UO_2F_5$.

Lattice coupling of the vibrations will not be considered here. It undoubtedly will have a much smaller effect on the frequencies than the effects we have discussed here.

Anharmonicity constants

In order to calculate true Hooke's Law force constants one should use, if possible, the frequencies for infinitesimal vibrations. This requires a knowledge

* If we define the resonance interaction constant ($F_{UO,\alpha}$) as representing interaction between ΔR and $\Delta\alpha$ when $\Delta\alpha$ is the absolute value of the change in OUL angle from its equilibrium value of 90°, $F^A_{UO,\alpha}$ becomes zero with neglect of O–L repulsion.

VOL. 10 1957/5

of anharmonicity constants. DIEKE and DUNCAN [11] give a wealth of data on the fluorescence spectra and visible absorption spectra of uranium compounds. They report frequencies for several vibrational levels of these compounds. From their results it is possible to calculate several of the anharmonicity constants for the uranyl vibrations in these compounds.

Table 2. Anharmonicity constants X_{11} and X_{13} for several uranyl complexes in the solid state

Compound	X_{11}	X_{13}
$CsUO_2(NO_3)_3$	$-1{\cdot}23 \pm 0{\cdot}09$	$-4{\cdot}95 \pm 0{\cdot}19$
$RbUO_2(NO_3)_3$	$-1{\cdot}26 \pm 0{\cdot}26$	$-5{\cdot}58 \pm 0{\cdot}33$
$KUO_2(NO_3)_3$	$-1{\cdot}34 \pm 0{\cdot}10$	$-5{\cdot}07 \pm 0{\cdot}19$
$Rb_2UO_2(NO_3)_4$	$-1{\cdot}42 \pm 0{\cdot}18$	$-7{\cdot}20 \pm 0{\cdot}47$
$K_2UO_2(NO_3)_4$	$-1{\cdot}43 \pm 0{\cdot}10$	$-5{\cdot}92 \pm 0{\cdot}19$
$UO_2(NO_3)_2.3H_2O$	$-1{\cdot}91 \pm 0{\cdot}74$	$-4{\cdot}20 \pm 0{\cdot}35$
$Cs_2UO_2Cl_4$	$-1{\cdot}33 \pm 0{\cdot}05$	$-6{\cdot}01 \pm 0{\cdot}15$
Average	$-1{\cdot}42$	$-5{\cdot}62$

DL.
10
7/58

For the linear triatomic uranyl ion the observed frequencies should follow the energy expression

$$\nu_{v_1 v_2 v_a v_b} = \sum_i \omega_i v_i + \sum_{\substack{ij \\ j \geq i}} x_{ij}[v_1 v_j + \tfrac{1}{2}(v_i + v_j)]$$

v_1 = quantum number of symmetric stretching vibration.

v_3 = quantum number of asymmetric stretching vibration.

v_a = quantum number of one component of bending vibration.

v_b = quantum number of other component of bending vibration.

A least squares treatment of some of the fluorescence data of DIEKE and DUNCAN yielded the results given in Table 2.

The limits given are standard deviations. For several vibrational levels of $CsUO_2(NO_3)_3$ we find $X_{1a} \approx X_{1b} \approx -0{\cdot}14$ cm^{-1}. There is only one determination of X_{33} which $\approx -2{\cdot}4$ cm^{-1}. There are no observations of X_{3a} or X_{3b} but as X_{1a} and X_{1b} are so small we shall assume $X_{3a} \approx X_{3b} \approx$ zero.

From the data of Table 2 it appears that X_{11} is fairly constant for various uranyl complexes. X_{13} varies a little more but the variation appears to be within $\pm 1{\cdot}5$ cm^{-1}. Though we have only one determination of X_{33}, from the reasonable constancy of X_{11} and X_{13} we may presume that X_{33} is fairly constant for different uranyl complexes.

From the above discussion we will assign the values of Table 3 as appropriate anharmonicity corrections to apply to the observed frequencies to determine the zero-point fundamental U–O stretching frequencies.

Since we generally can observe the asymmetric stretching frequency (ν_1) and the combination of the symmetric and asymmetric stretching frequencies ($\nu_1 + \nu_3$), with the aid of the constants of Table 3 we can determine the fundamentals ω_1 and ω_3 from the relations

$$\omega_3 = \nu_3 + 7{\cdot}8 \text{ cm}^{-1}$$
$$\omega_1 = (\nu_1 + \nu_3) - \nu_3 + 11{\cdot}2 \text{ cm}^{-1}$$

Table 3. Anharmonicity constants for uranyl complexes

$$X_{11} = -1{\cdot}4 \pm 0{\cdot}2^a \text{ cm}^{-1}$$
$$X_{13} = -5{\cdot}6 \pm 0{\cdot}9^a \text{ cm}^{-1}$$
$$X_{33} = -2{\cdot}5 \pm 1{\cdot}5 \text{ cm}^{-1}$$
$$X_{3a} \approx X_{3b} \approx X_{1b} \approx X_{1c} \approx \text{zero} \pm 0{\cdot}5 \text{ cm}^{-1}$$

[a] These limits are 95 per cent confidence limits treating values of Table 2 as of equal certainty

It is difficult to estimate the uncertainty, but from the limits given in Table 2 it is probably less than 4 cm^{-1} for ω_3 and less than 10 cm^{-1} for ω_1.

Relation between force constant and bond distance

We hope to be able to determine the constants to use in BADGER's relation [15]

$$R_{UO} = \beta_{UO}(F_{UO})^{-1/3} + d_{UO}$$

Such a relation should hold quite well for bonds between atoms of the same pair of elements in different compounds. Assuming that $\beta_{UO} \approx 0{\cdot}5$ Å X(megadynes/cm)$^{1/3}$ as found by BADGER [15] for practically all pairs of atoms and that $F_{UO} \approx F_{UO}^4$ (see equation (1)–(4)) we can arrive at the relation

$$\Delta R \approx -5 \times 10^{-7} \nu_3 (\Delta \nu_3)$$

Thus, in the region of ν_3 (700–1000 cm^{-1}) a small change in U–O distance (+0·01 Å) should give a significant change in the asymmetric U–O stretching frequency, ν_3 (~20 cm^{-1} at 1000 cm^{-1} and ~28·5 cm^{-1} at 700 cm^{-1}). This means that the large range of predicted [13] U–O bond distances in various uranyl complexes (1·6 Å–1·9 Å) should lead to a very large range of values for ν_3.

We have started a program to determine the U–O force constant in various uranyl complexes in order to arrive at systematic data from which we can determine U–O bond distances fairly accurately from the two spectral observations, ν_3 and $(\nu_1 + \nu_3)$. The first step will be the determination of the U–O stretching force constants for the two uranyl complexes having fairly accurately known U–O distances, namely, $K_3UO_2F_5$ (1·76 ± 0·03 Å) and $MgUO_2O_2$ (1·92 ± 0·03 Å).

References

[1] PRINGSHEIM P. and YOST M. *Z. Physik.* 1929 **58** 1.
[2] CONN G. K. T. and WU C. K. *Trans. Faraday Soc.* 1938 **34** 1483.
[3] LECOMTE J. and FREYMANN R. *Bull. Soc. Chim.* 1941 **8** 622.
[4] SATYANARAYANA B. S. *Proc. Indian Acad. Sci.* 1942 A **15** 414.
[5] SEVCHENKO A. N. and STEPANOV B. I. *J. Exp. Theor. Phys.* 1949 **19** 1113.

VOL. 10 1957/5

[6] CRANDALL H. W. *J. Chem. Phys.* 1949 **17** 602.
[7] SUTTON J. *Nature, Lond.* 1952 **169** 235.
[8] JONES L. H. and PENNEMAN R. A. *J. Chem. Phys.* 1953 **21** 542.
[9] JONES L. H. *J. Chem. Phys.* 1955 **23** 2105.
[10] TRIDOT G. *Ann. Chim.* 1955 **10** 15.
[11] DIEKE G. H. and DUNCAN A. B. F. *Spectroscopic Properties of Uranium Compounds, NNES* III–2. McGraw-Hill, New York 1949.
[12] RABINOWITCH E. *ANL* 1953 5122, 5173.
[13] ZACHARIASEN W. H. *Acta Cryst.* 1954 **7** 795.
[14] CROMER D. T. and HARPER P. E. *Acta Cryst.* 1955 **8** 847.
[15] BADGER R. M. *J. Chem. Phys.* 1935 **3** 710.
[16] ZACHARIASEN W. H. *Acta Cryst.* 1954 **7** 783.
[17] HERZBERG G. *Infrared and Raman Spectra of Polyatomic Molecules* pp. 136–139. D. Van Nostrand, New York 1947.
[18] GAUNT J. *A.E.R.E, C/R*-1237; *Trans. Faraday Soc.* 1953 **49** 1122.
[19] GLAUBER and SCHOMAKER. *Phys. Rev.* 1953 **89** 667.

DL.
10
7/58

Spectrochimica Acta, 1958, Vol. 10, pp. 404 to 418. Pergamon Press Ltd., London

Spectrographic analysis of ores by introducing the powder into the arc in a stream of air

A. K. Rusanov and V. G. Khitrov
Institute of Applied Mineralogy U.S.S.R., Moscow

(*Received* 11 *June* 1957)

Abstract—A new method is presented for the spectrographic analysis of substances in powder form, using an alternating current arc, which is initiated by a high frequency discharge. The powder, carried in a stream of air, is introduced evenly into the discharge zone of a horizontal carbon or metallic arc. The air stream also stabilizes the arc.

The introduction of the material in a stream of air prevents reactions which normally occur on the electrodes, prevents the fractional evaporation of the different elements, and ensures their uniform entry into the discharge zone and uniform conditions of excitation. The excitation conditions depend very little on the compositions of the electrodes, and are mainly determined by the ionization potentials of the elements in the powder blown in.

This technique gives a significant increase in sensitivity and reproducibility, and reduces the time required for analysis. It offers great possibilities for direct photoelectric measurement of line intensities because the radiation remains constant.

VOL.
10
1957/5

Introduction

The arc discharge is widely used for the quantitative spectral analysis of rocks, ores minerals, slags, salts and other substances in powder form, but it does not always give results of requisite reproducibility.

To a large extent this is due to the fractional evaporation of the elements from the electrodes, which produces a marked variation in the concentrations of the elements in the atmosphere of the arc gap, and consequently a change in the intensities of the spectral lines with time. Such a change in composition usually affects the temperature conditions for the excitation of spectra, which again alters the intensities of the lines. Sometimes this change in composition is responsible for the re-absorption of lines in the atmosphere of the arc.

The line intensities vary in a regular way with the composition of the sample, but they also vary in a random manner as the flame moves over the surface of the electrode. This movement disturbs the conditions for the evaporation of the elements into the arc, and produces irregularities in the distributions of concentration and temperature in the zone of the discharge [1]. As a result, successive photographs may represent spectra of differently radiating regions of the atmosphere of the arc.

It therefore follows that an improvement in the reproducibility of spectral analysis in an arc should be obtained by doing away with the process of evaporating the sample from an electrode, by ensuring a constant rate of feed of sample into the discharge zone, and by stabilizing the position of the flame and the gap between the electrodes [2]. To a large extent these conditions are satisfied by the uniform introduction of the powder with air directly into the discharge zone of

the arc. With this method of excitation in an alternating current arc, initiated by a high frequency discharge the intensity of the air stream is of decisive importance for improving the reproducibility of the analyses. The air flowing over the electrodes, not only stabilizes the position of the flame, but strongly cools the ends of the electrodes; this reduces to a minimum the processes which occur at the electrodes when, either the sample is evaporated from a cavity in the carbon, or the powder is sprinkled in an uncontrolled manner and carried by convection into the flame of the arc, as in the method of NEDLER [3].

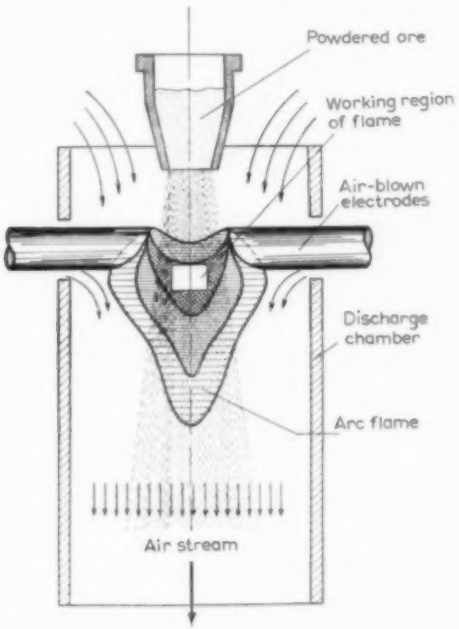

Fig. 1. Method of introducing powdered ore into the arc in a stream of air.

Apparatus and method for introducing powder into the arc discharge

The sample is ground to pass a 200 mesh sieve, and 0·05–0·5 g are introduced at a uniform rate into the discharge chamber. An air stream, with a speed of 2–10, usually 4–6 m per sec, is drawn through the chamber by a small fan, the rate being controlled by a throttle. This air stream carries the powder particles into the discharge zone of the arc. The radiation from the arc is directed through an opening in the front of the chamber on to the slit of the spectroscope, and the spectrum can be photographed or registered photoelectrically. The air stream deflects the flame downwards in the form of an inverted cone, and stabilizes it in this position.

Fig. 1 shows the method of introducing the powdered sample into the arc with the aid of an air stream, and the region of the flame used for analysis.

The arc is fed from a standard SVENTITSKII [4] generator for alternating current arcs, and is initiated by a high frequency discharge.

The electrodes are mostly of spectral pure carbon, of diameter 6 mm or copper electrodes 3–4 mm. The arc gap is usually 6–8 mm, and the current 14–18 A for carbon and 8–10 A for copper electrodes.

The ends of the electrodes are usually not preshaped, but they acquire a characteristic shape in use, which is maintained in successive uses. Carbon electrodes clean themselves in a short pre-arcing under normal operating conditions; copper electrodes are cleaned in hydrochloric acid.

Fig. 2(a) shows a general view of the apparatus with vibrating funnel for introducing the powdered sample into the arc.

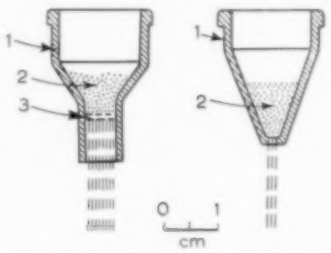

Fig. 3. Funnel for pouring in powder: 1—funnel; 2—powder; 3—sieve.

The stand (1), firmly mounted on the optical bench of the spectrograph, carries the following components: the arc discharge chamber (2), with the duct (3), for sucking air out of the chamber, connecting with the separately supported fan (4); the stand (5), for the electrode holders (6), with the necessary fittings for changing the electrodes (7); the stand (8), giving rigid support to the device (9) for adding powder to the discharge, consisting of an interchangeable conical funnel (10), with an opening or a sieve, which is given a reciprocating motion in a vertical plane by means of a finger sliding over the teeth of a ratchet wheel (11). The axle of the latter is rotated by the belt (12) from the electric motor (13).

The shapes of the funnels for introducing the powder in a wide or narrow stream are shown in Fig. 3.

For the analysis of substances of widely different moisture contents, instead of vibrating the funnel, use is made of the small conveyer, shown in Fig. 2(b). By means of the hinged former (14), the powder to be analysed is distributed in an even layer on the surface of the belt (15), which moves at a rate of one cm/sec, and spills down the chute (16), into the funnel above the flame. The chute and funnel are continuously vibrated by an electromagnetic vibrator. The chute corrects for irregularities in the feed of powder from the conveyer; its slope is adjusted in accordance with the dryness of the sample.

Conditions for the entry of elements into the region of the arc

When a powdered material is blown into the flame the particles do not always remain long enough in the arc to evaporate completely, and, to some extent, this favours the more volatile components which can evaporate from the fused particles. Because of the strongly oxidizing conditions, the appearance of the vapour of an element in the luminous zone of the arc will depend, not only on the volatility

VOL. 10 1957/5

VOL.
10
7/58

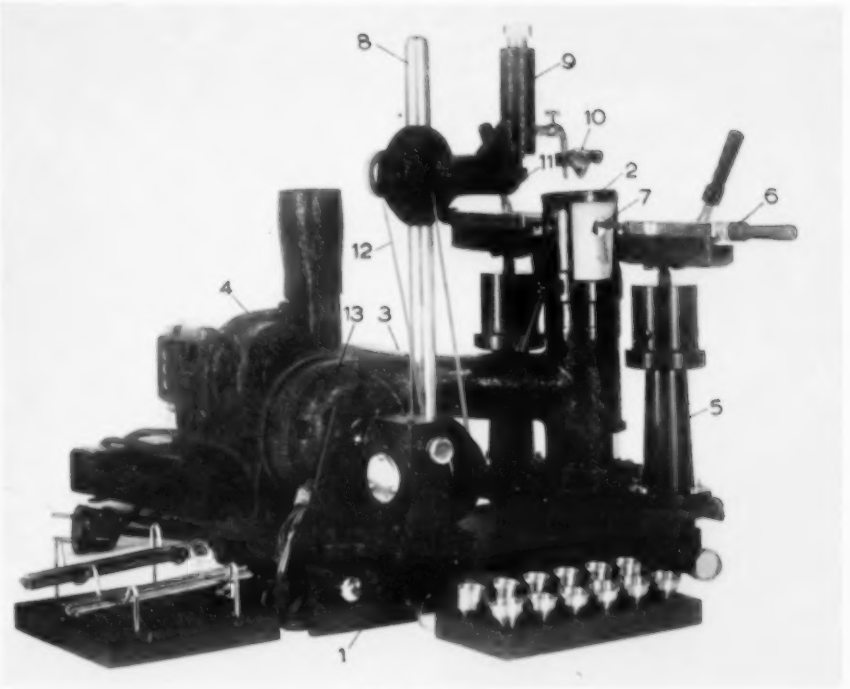

Fig. 2(a)

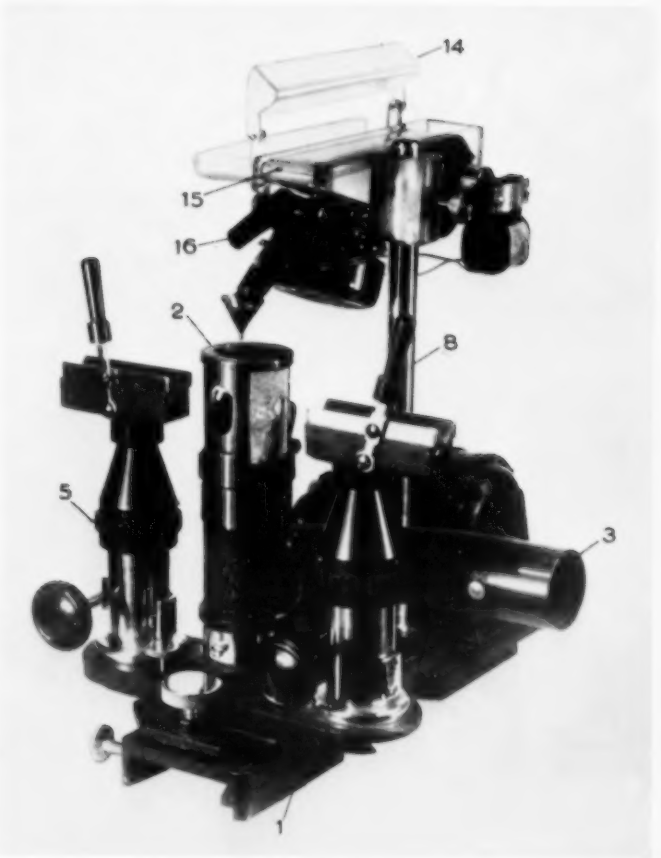

Fig. 2(b)

Fig. 2. Apparatuses for blowing powdered ore into discharge region of arc, (a) with vibrating funnel, (b) with the conveyer.

VOL.
10
1957/5

of the compound of the element initially present, but also on the volatility of the oxide, newly formed in the flame.

Thus the conditions for the evaporation of an element when the powder is blown into the flame are essentially different from those for evaporation from a crater in the carbon. In the latter the conditions are reducing, and free metals or carbides may gradually be formed; thus, in the early stages of the burning, the appearance of an element in the flame of the arc depends on the volatility of the compound originally present in the sample, but, in the later stages, it depends on the volatility of the substances newly formed in the crater of the electrode.

From this it follows that the order of the appearance of the vapours of different elements in the arc should depend on which method of evaporation is used. That this is so can be seen from previously published work [5, 6]. Sequences I to IV, give the successive appearances in the arc of elements, evaporated as their oxide or sulphide ores, by direct injection into the arc, or by evaporation from the crater of a carbon electrode.

Sequence I. Successive appearances of elements on the direct injection of their oxide ores into the flame of a carbon arc. [As, Hg, Tl, Sb, Mo, Pb, Cd, Bi, W, Zn, (K, Na, Li), B, In, Ga, Ge, Cu], [Fe, Co, Ni, Si], [Ba, Sr, Ca, Mg, Al, Be, Sc, rare earths, Hf, Zr, Th].

Sequence II. Successive appearances of elements on the evaporation of their oxide ores from the crater of a carbon electrode.

← Li, Na, K, Rb, Cs →

[Hg, As, Cd, Zn, Bi, Sb, B*, Pb, Tl, Mo*, Sn, W*, In, Ga, Ge], [Mn, Mg, Cu], [Fe, Co, Ni, Ba, Sr, Ca, Si, Cr, Al, V, Be, Ti, U], [Sc, Mo*, Zr, Hf, Th, Nb, Ta, W*, B*].

← rare earths →

The elements Li, Na, K, Rb, Cs stand somewhere between Bi and Ge, whereas rare-earth elements stand between Sc and Nb.

Sequence III. Successive appearances of elements on direct injection of their sulphide ores into the flame of a carbon arc. [As, Hg, Sb, Sn, Ge, Pb, Cd, Zn, Mo, Ag, Tl, In], [Cu, Fe, Co, Ni, Mn].

Sequence IV. Successive appearances of elements on the evaporation of their sulphide ores from the crater of a carbon electrode. Hg, As, Ge, Cd, Pb, Sb, Bi, Zn, Tl, Mo*, Re*, In, Ag, Cu, Ni, Co, Mn, Fe, Mo*, Re*.

The separate groups of elements in square brackets differ markedly from those in the other brackets in the conditions for their appearance in the flame. The asterisks mark elements which can appear in the flame, together with volatile components of the sample either as readily vapourizable oxides or sulphides; these elements gradually form nonvolatile metals and carbides.

It will now be understood that, when the powdered sample to be analysed is introduced, evenly, directly into the arc flame, then the position of an element in the volatility Sequences I and III is a measure of the completeness of evaporation of that element from a powder particle flying through the flame.

With the direct introduction of the powder into the flame, the preferential appearance of the more volatile compounds in the discharge zone can only take place due to incomplete evaporation of particles and it is less marked than with

the evaporation of material from an electrode cavity. Further the chemical reactions do not alter; the conditions of appearance of elements in the flame, as they were at the beginning of the arc burning; these conditions remain constant for any desired interval of time.

Distribution of intensity of the lines of elements and the conditions of excitation in the flame of the arc

The method of investigating the distribution of line intensity, in the flame of the arc, has been previously published by us [1]. We showed that the spatial distribution is of the type shown in Figs. 4 and 5, and that, both for arc lines and

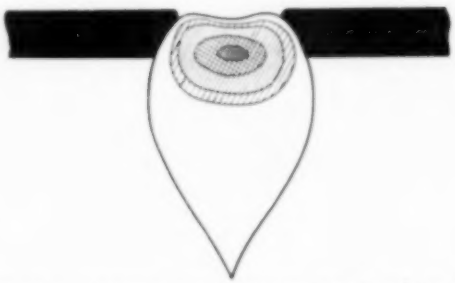

Fig. 4. Spatial distribution of intensity of the line Pb I 2873·3 Å, in the atmosphere of a horizontal carbon arc, when the powdered ore is blown into the discharge zone in a downward stream of air.

VOL. 10 1957/5

for spark lines in the atmosphere of the arc, it depends very little on the composition of the powder or on the properties of the elements (ionization potential, atomic weight, position in the volatility sequences). The greatest intensity is always shown by radiation from the central region of the flame, a few millimetres below the axis

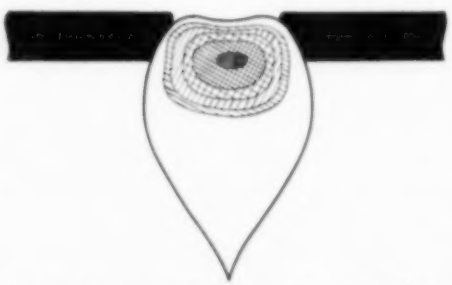

Fig. 5. Spatial distribution of intensity of the line Ti II 3078·6 Å, in the atmosphere of a horizontal carbon arc, when the powdered ore is blown into the discharge zone in a stream of air.

of the electrodes. For example, it can be seen from Figs. 4 and 5 that, both for the arc lines of the readily volatilizable lead and for the spark lines of the much less volatile titanium, there is a regular fall in intensity from the centre to the periphery of the flame. Figs. 4, 5, 7 show regions of equal intensity for the flame of a carbon arc; successive regions differ in the intensity of radiation by a factor of two.

This regularity of the distribution of line intensity is primarily dependent on the distribution of concentration of the elements in the atmosphere of the arc, and does not coincide with the distribution of excitation conditions.

This is evident from a comparison of Figs. 4 and 5 with Fig. 6. The latter shows the spatial distribution of relative intensity of the lines V II 3110·7 Å and V I 3185·4 Å; this ratio is strongly dependent on the conditions of excitation [7]. A study of the distribution of the relative intensity of the spark and arc lines of vanadium, tianium and other elements, shows that the hottest zone, favourable to the excitation of the spectra of ionized atoms, is always near the electrodes, whatever the composition of the powder which is introduced or the electrode material.

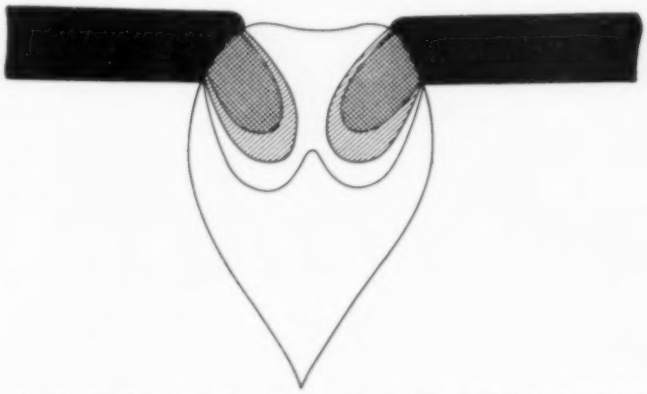

Fig. 6. Spatial distribution of relative intensity of the lines V II 3110·7 Å and V I 3185·4 Å in the atmosphere of a horizontal carbon arc.

A difference is always observed between the distribution of line intensities when the sample is evaporated from the crater in an electrode, and when the same sample is blown as a powder directly into the arc. This is evident from Fig.7, which shows the intensity distribution of the lines of boron, using carbon electrodes containing boron; similar distributions are observed for the cyanogen bands of a carbon arc in air, and for the copper lines between copper electrodes.

A similar distribution of regions of equal intensity in the flame, reminiscent of a torch deflected by a stream of air, is observed with a freely burning horizontal arc in air, but the conical point of the flame is directed upwards [1].

The increase in intensity near the electrodes, shown in Fig. 7, is observed for all lines, arc and spark, from the electrode material or from substances evaporated from the electrodes. It is obviously due primarily to the very high concentration of material in the region of the flame surrounding the electrodes.

This difference in the distribution of intensities of the lines of elements evaporated from the arc and of elements blown directly into the flame is of vital importance for analysis. It makes it possible to observe a region of the flame where the spectrum of the sample is very strong, but the interfering spectrum of the electrodes and the background are of low intensity.

Our experimental data show that, when a substance is injected directly into the flame of the arc in a stream of air, the excitation conditions depend on the ionization potentials of the elements present in the discharge zone (Fig. 8). Semenova [8] has previously shown that the same applies to substances evaporated into a carbon arc from a crater in an electrode.

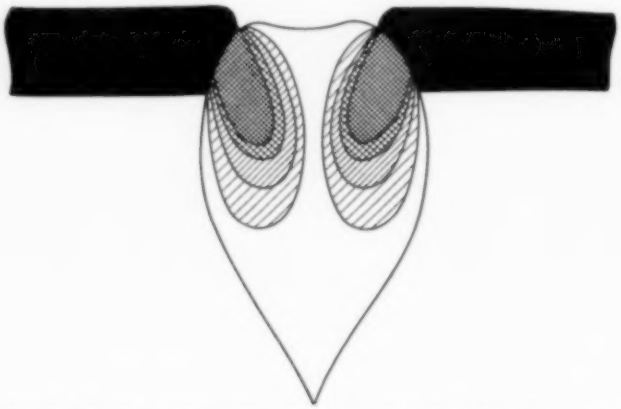

Fig. 7. Spatial distribution of intensity of the line B I 2497·7 in the atmosphere of a horizontal arc formed between carbon electrodes containing boron.

VOL. 10 1957/5

However, the conditions for excitation in the centre of the discharge zone, when the powder is blown directly into the arc, differ from those when an ordinary arc is used in the normal way, in that they depend very little on the composition of the electrode, but are determined by the composition of the powder blown

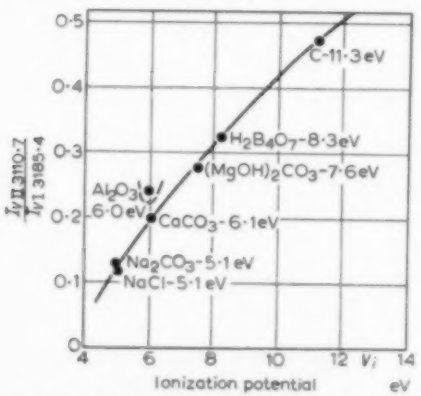

Fig. 8. Dependence of the relative intensities of the lines V II and V I on the ionization potentials of the elements entering the flame of a copper arc burning in a stream of air.

into the flame. This explains how the curve in Fig. 8, for an arc between copper electrodes, can extend above the ionization potential of copper (7·7 eV).

As can be seen in Fig. 8, a high value is obtained for the ratio of the intensities of the lines V II/V I in the presence of aluminium. This is evidently connected

with the fact that aluminium goes into the discharge zone in the form of the difficultly volatile oxide (Al_2O_3).

Fig. 9 shows the dependence of the ratio of intensities of the lines V II 3110·7 and V I 3185·4, for a copper arc, on the rate of entry into the discharge zone of elements with different ionization potentials—Na 5·1, Ca 6·1, Mg 7·6, B 8·3 and C 11·3 eV. These elements were added as powders of the following compounds: NaCl and Na_2CO_3, $CaCO_3$, $(MgOH)_2CO_3$, $H_2B_4O_7$ and graphite.

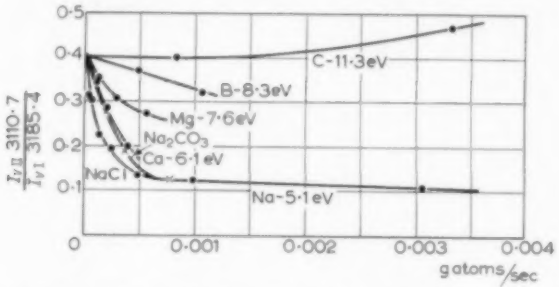

Fig. 9. Dependence of the relative intensities of lines on the number of g atoms of Na, Ca, Mg, B and C entering in unit time into the discharge zone of a horizontal copper arc burning in a stream of air.

It follows from Fig. 9 that, when powders of different composition are blown into the arc, excitation conditions can easily be stabilized by adding to the sample a sufficient quantity of a compound of an element of low ionization potential. It is evident, for instance, from Fig. 10, that the addition of about 30 per cent of

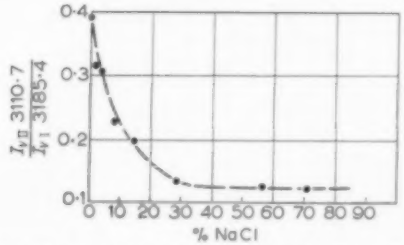

Fig. 10. Dependence of the relative intensities of the lines V II and V I on the content of NaCl in the powdered ore blown into a horizontal copper arc.

sodium chloride to a silicate ore satisfactorily stabilizes the excitation conditions in the flame of a copper arc. However, this also reduces the intensities of the arc and spark lines in the spectrum and increases the background, so that there is a loss in the sensitivity of the analysis.

The conditions for the excitation of spectra in the central region of the flame of a copper or carbon arc depend very little, however, on the value of the arc current. For instance, the ratio of intensities of the spark and arc lines V II 3110·7 and V I 3185·4 remains constant when the current is varied from 4 to 16 A in a copper arc. But it should be noted that an increase in the current between

carbon electrodes sometimes produces a slight change in conditions, favouring the excitation of spark lines.

Both with metallic and carbon electrodes, an increase in the arc current increases the intensity of the spectra of elements present in the flame. Particularly

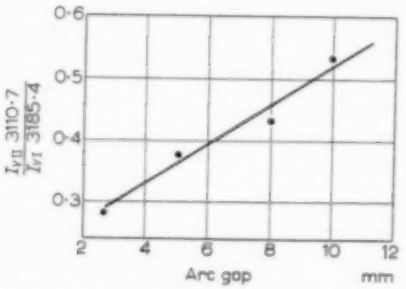

Fig. 11. Effect of the size of the arc gap on the relative intensities of the lines V II and V I when quartz, containing vanadium is blown into the flame of a copper arc. Current 8 A.

with the carbon arc, there is usually a relative increase in the intensity of lines compared with the background, which in many cases leads to a higher sensitivity of the analysis.

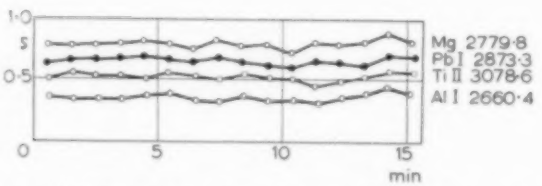

Fig. 12. Variation of the blackening of the lines of elements with the time of burning of the arc. Powdered ore is blown into a horizontal carbon arc.

It has been found that the excitation conditions in the centre of the flame depend on the size of the arc gap, so that the latter must be carefully controlled. It can been seen from Fig. 11, for instance, that, as the arc gap between copper

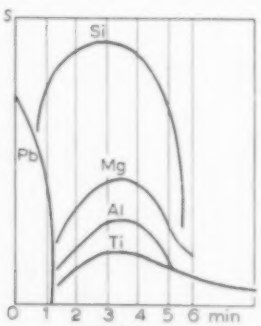

Fig. 13. Variation of the blackening of the lines of elements with the time of burning of the arc. Ores are evaporated from a crater in a carbon electrode. Mg 2779·8 Å; Pb I 2873·3 Å; Ti II 3078·6 Å and Al I 2660·4 Å.

VOL.
10
1957/5

electrodes is increased, the conditions become more favourable for the excitation of spark lines. With a carbon arc the effect of the size of the spark gap is more complicated. In some cases an increase in the arc gap may increase the sensitivity of an analysis by weakening the background and the electrode lines and strengthening the spectral lines of the sample blown in.

A special feature of the method of blowing the powder into the discharge zone is the simultaneous appearance in the spectrum of the lines of all the elements

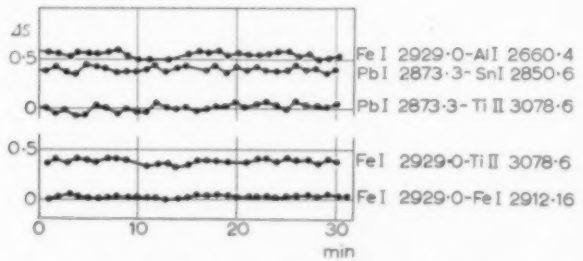

Fig. 14. Variation of the relative blackenings of lines with the time of burning of the arc. Powdered ore is blown into a horizontal carbon arc.

in the sample, uninfluenced by their volatilities, and the fact that the absolute intensities of the lines do not change significantly during the period of arcing. This is clearly seen from a comparison of Figs. 12 and 13, which show the changes in intensity with time of the lines of a few elements. Fig. 12 is for a siliceous ore, blown as a powder into the flame of a carbon arc, while Fig. 13 is for the same ore placed on the electrode in the usual way.

Very valuable features of the method of blowing in the powder are the independence of the relative intensities of lines on the time of arcing, and only a slight dependence on the quantity of powder introduced into the discharge zone, and the possibilities of using for analysis pairs of lines which are not homologous and lines of elements with very different volatilities.

Some idea of the constancy of the relative intensities of different pairs of lines with time can be obtained from Fig. 14.

This constancy of the relative intensities of spark and arc lines during the period of arcing shows that the conditions of excitation, controlled by the composition of the powder fed in, do not vary with the prolongation of the arcing time; whereas the conditions do vary when the sample is evaporated from a crater in an electrode. This can be seen from Fig. 15, which shows the changes in the relative densities of the lines Ti II 3078·6 and Ti I 2956·1, when a siliceous ore is blown into the flame of the arc, and when it is evaporated from an electrode cavity.

Sensitivity and reproducibility

The increased evaporation of materials, blown as a powder by air into the discharge zone of a horizontal arc, and the previously mentioned reduction of the background from the electrodes and intensification of the spectral lines of the

sample in the central region of the flame, make for a high sensitivity in the determination of elements.

This is evident from Table 1 which shows sensitivities for the determination of elements when 100 mg of quartz powder, mixed with oxides of the elements, are blown for 10–15 sec into the flames of carbon and copper arcs. The spectra were photographed with a quartz spectrograph of medium dispersion ISP–22.

The table shows that, for a large number of elements, the sensitivity for simultaneous determination is usually increased by one order magnitude, compared

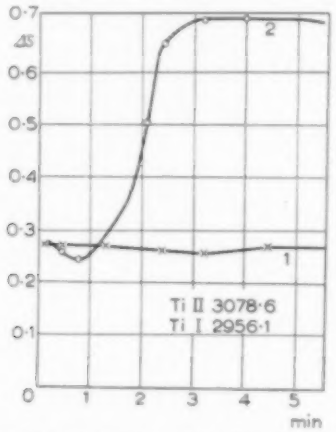

Fig. 15. Variation of the relative blackening of the lines Ti II 3078·6 Å and Ti I 2956·1 Å with the time of burning of a carbon arc.
1. The powdered ore is blown into the discharge zone. 2. The ore is evaporated from an electrode crater.

with the usual method of evaporation from an electrode cavity. It should be kept in mind that the sensitivity of the determination of elements depends upon the composition of the analysing powder.

The reproducibility of the method has been investigated by measuring the relative densities of pairs of lines. It is found that the arithmetic mean error of a single determination of the concentration of an element in an ore, using a calibration curve, expressed in terms of the parameters ΔS and $\log C$, does not normally exceed ± 5 per cent.

This is true, not only for homologous lines, but also for lines whose relative intensity varies when the excitation conditions are not kept constant (analytical pairs consisting of the arc and spark lines of elements).

As an example, Table 2 shows the arithmetic mean errors obtained from measurements on fifty photographs of the spectra of siliceous ores, containing iron, aluminium, magnesium, titanium and small admixtures of lead, tin, antimony and tungsten. The spectra were obtained, using both injection in a stream of air and evaporation of the ore in the usual way from a crater in a lower vertical reinforced carbon electrode, under comparable conditions. In the latter case the ore was mixed with an equal weight of carbon powder, and was inserted in a cavity 6 mm deep and 2 mm in diameter. The electrodes were both 3·5 mm in diameter.

VOL. 10 1957/5

Table 1. Sensitivity of the analysis of ores injected in a stream of air

Element	Analytical line A	Measurable concentration per cent		
		Injection in air		Evaporation from crater in carbon
		Carbon arc	Copper arc	
1	2	3	4	5
Mercury	2536·5 I	$1 . 10^{-3}$	$1 . 10^{-2}$	$5 . 10^{-2}$
Arsenic	2349·8 I	$4 . 10^{-3}$	$1 . 10^{-2}$	$1 . 10^{-2}$
Thallium	2767·9 I	$<1 . 10^{-3}$	$1 . 10^{-3}$	$1 . 10^{-2}$
Thallium	3775·7 I	—	$1 . 10^{-4}$	$1 . 10^{-3}$
Antimony	2598·1 I	$1 . 10^{-3}$	$4 . 10^{-3}$	$1 . 10^{-2}$
Molybdenum	3132·6 I	$1 . 10^{-4}$	$5 . 10^{-4}$	$1 . 10^{-3}$
Lead	2833·1 I	$1 . 10^{-3}$	$1 . 10^{-3}$	$3 . 10^{-3}$
Cadmium	3261·1 I	$1 . 10^{-3}$	$4 . 10^{-2}$	$3 . 10^{-3}$
Bismuth	3067·7 I	$5 . 10^{-4}$	$5 . 10^{-4}$	$1 . 10^{-3}$
Tungsten	2944·4 I	$1 . 10^{-3}$	$1 . 10^{-2}$	$1 . 10^{-2}$
Tin	3175·0 I	$5 . 10^{-4}$	$1 . 10^{-3}$	$1 . 10^{-3}$
Zinc	3345·0 I	$1 . 10^{-2}$	$1 . 10^{-2}$	$2 . 10^{-2}$
Boron	2497·7 I	$7 . 10^{-4}$	$7 . 10^{-4}$	—
Germanium	2651·2 I	$1 . 10^{-3}$	$1 . 10^{-3}$	$1 . 10^{-3}$
Indium	3256·1 I	$<1 . 10^{-4}$	—	$1 . 10^{-3}$
Copper	3274·0 I	$<1 . 10^{-4}$	—	$<1 . 10^{-3}$
Iron	3020·6 I	$5 . 10^{-4}$	$<1 . 10^{-3}$	$1 . 10^{-3}$
Cobalt	3453·5 I	$5 . 10^{-4}$	$4 . 10^{-3}$	$1 . 10^{-3}$
Nickel	3414·8 I	$<5 . 10^{-4}$	—	$1 . 10^{-3}$
Silver	3280·7 I	$\leqslant 1 . 10^{-4}$	—	$3 . 10^{-4}$
Calcium	3179·3 II	$1 . 10^{-2}$	—	$1 . 10^{-1}$
Calcium	3158·9 I	—	$1 . 10^{-2}$	$1 . 10^{-1}$
Strontium	4607·3 I	$<1 . 10^{-4}$	$1 . 10^{-4}$	$3 . 10^{-4}$
Barium	4554·0 II	—	$1 . 10^{-4}$	$3 . 10^{-4}$
Magnesium	2795·5 II	$<1 . 10^{-4}$	$1 . 10^{-4}$	$1 . 10^{-3}$
Manganese	2794·8	$<1 . 10^{-4}$	$1 . 10^{-4}$	$1 . 10^{-3}$
Beryllium	2348·6 I	$5 . 10^{-5}$	$7 . 10^{-4}$	$3 . 10^{-4}$
Vanadium	3185·4 I	$<1 . 10^{-4}$	$1 . 10^{-3}$	$1 . 10^{-3}$
Vanadium	3184·0 I	$1 . 10^{-4}$	$1 . 10^{-3}$	$3 . 10^{-3}$
Chromium	2843·2 II	$4 . 10^{-3}$	$1 . 10^{-2}$	$1 . 10^{-2}$
Titanium	3088·0 II	$<4 . 10^{-3}$	—	$3 . 10^{-3}$
Zirconium	3392·0 II	$5 . 10^{-4}$	—	$3 . 10^{-3}$
Zirconium	3438·2 II	$5 . 10^{-4}$	$1 . 10^{-2}$	$3 . 10^{-3}$
Yttrium	3710·3 II	—	$1 . 10^{-2}$	$3 . 10^{-3}$
Yttrium	4374·9 II	$3 . 10^{-3}$	—	$3 . 10^{-3}$
Lanthanum	3245·1 II	$1 . 10^{-2}$	—	$3 . 10^{-2}$
Lanthanum	3337·5 II	$1 . 10^{-2}$	$1 . 10^{-1}$	$1 . 10^{-2}$
Niobium	2927·8	$4 . 10^{-3}$	$4 . 10^{-2}$	$1 . 10^{-2}$
Niobium	3163·4 II	$1 . 10^{-3}$	$1 . 10^{-2}$	—
Tantalum	2685·1	$1 . 10^{-2}$	$1 . 10^{-1}$	$3 . 10^{-2}$
Uranium	2865·7 II	$3 . 10^{-2}$	$1 . 10^{-1}$	$1 . 10^{-1}$
Uranium	4090·1 II	—	$3 . 10^{-3}$	—
Thorium	2870·4	$1 . 10^{-2}$	$1 . 10^{-1}$	$1 . 10^{-2}$

Table 2. Comparison of the errors in the determination of the concentrations of elements by the methods of injection in air and of evaporation from a crater in a carbon electrode

No.	Analytical line pair Å	Ionization potentials of elements eV	Excitation potentials of lines eV	Difference in excitation potentials eV	Mean arithmetic error of single determination		Difference in volatility of elements
					Air evaporation %	Evaporation from crater %	
1.	Fe I 2929·0	7·9	6·4	0·0	2	—	none
	Fe I 2912·2	7·9	6·4				
2.	Fe I 2929·0	7·9	6·4	2·3	3	6	small
	Co I 3044·0	7·9	4·1				
3.	Sn I 2840·0	7·3	5·4	0·0	5	12	small
	Sb I 2877·9	8·6	5·4				
4.	Pb I 2873·3	7·4	5·6	0·2	4	—	small
	Sn I 2850·6	7·3	5·4				
5.	Fe I 2929·0	7·9	6·4	1·8	3	—	noticeable
	W I 2947·0	8·0	4·6				
6.	Fe I 2929·0	7·9	6·4	—	3	13	noticeable
	Mg I 2779·9	7·6	—				
7.	Fe I 2929·0	7·9	6·4	1·7	5	8	noticeable
	Al I 2660·4	6·0	4·7				
8.	Fe I 2929·0	7·9	6·4	4·5	3	26	noticeable
	Ti II 3078·6	6·8	10·9				
9.	Fe I 2779·1	7·9	5·5	0·1	5	—	large
	Pb I 2873·3	7·4	5·6				
10.	Pb I 2873·3	7·4	5·6	1·4	4	—	large
	Ti I 2956·1	6·8	4·2				
11.	Pb I 2873·3	7·4	5·6	5·3	5	—	large
	Ti II 3078·6	6·8	10·9				

It can be seen from Table 2 that the reproducibility of the determination of elements, by the method of blowing the powder into a stable arc, is very much better than that obtained, under favourable conditions, by evaporation of the ore from an electrode crater. For obviously non-homologous lines the reproducibility by the air injection method may be nine times as good as that by the method of evaporation from a cavity.

As we have noted in an earlier publication [2], when using the air injection method, there are fewer cases of shifts in the calibration curves due to variation in the composition of the sample, and, consequently, there is a reduction of the systematic error arising from analysing substances of variable composition.

Fig. 16 gives an idea of the shifts in calibration curves, obtained with samples

VOL. 10 1957/5

of varying composition, using the methods of air injection and evaporation from an electrode. The samples consisted of quartz mixed with an equal weight of magnesium oxide, iron oxide or calcium carbonate, together with a variable amount of cassiterite, a constant amount (1 per cent) of antimony oxide and 25 per cent of sodium chloride. The observed shifts in the relative densities of the lines Sn 2840·0 Å and Sb 2877·9 Å cannot be due to changes in the excitation conditions in the arc, as the relative intensities of the spark and arc lines of each element remain constant. These shifts are apparently associated with reactions

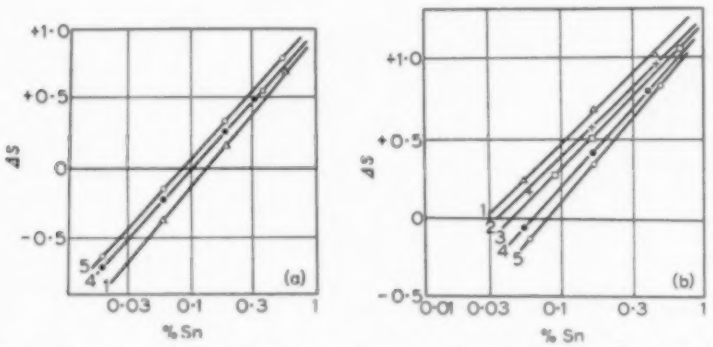

Fig. 16. Variation of the relative blackenings of the lines Sn I 2840·0 Å and Sb I 2877·9 Å with the tin content of the powder.
1. 50 per cent SiO_2, 50 per cent MgO. 2. 50 per cent SiO_2, 50 per cent Al_2O_3. 3. 100 per cent SiO_2. 4. 50 per cent SiO_2, 50 per cent Fe_2O_3. 5. 50 per cent SiO_2, 50 per cent $CaCO_3$. (a) Powder introduced into discharge zone in stream of air. (b) Powder evaporated from electrode crater.

in the outer part of the flame, leading to interaction of the tin and antimony with the "artificial ore" with the formation of new compounds.

Changes in the rate of appearance of elements, due to incomplete evaporation of the powder particles of variable composition during their passage through the flame, may be a cause of the shift of calibration curves.

The decrease in the systematic error, due to changes in the composition of the sample, and the excellent reproducibility (± 5 per cent), shown also in the data of NEDLER [9], indicate the value of the air injection method of analysis.

This considerable reduction in the effect of the gross composition on the analytical results can only be expected when there is complete evaporation of the particles of ore blown into the flame. Further research is being carried out on the creation of the optimum conditions for complete evaporation of ores in the discharge zone of the arc.

Conclusions

The horizontal a.c. arc, burning in a stream of air, is a valuable source for the excitation of spectra. When the powdered ore is blown into the discharge zone in a stream of air there is a marked increase in the sensitivity, reproducibility and speed of analysis, as compared with the usual method of evaporating the ore from a crater in an electrode.

References

[1] Rusanov A. K. and Alekseeva V. M. *J. Anal. Chem., Moscow* 1954 **9** 183.
[2] Rusanov A. K. and Tarasova T. I. *J. Anal. Chem., Moscow* 1955 **10** 267.
[3] Nedler V. V. *Fact. Lab., Moscow* 1936 **5** 1469.
[4] Sventitskii N. S. *The Steeloscope.* Union of State Publishing Houses, Moscow 1948.
[5] Rusanov A. K. *Spectral Analysis of Ores and Minerals.* State Geological Publishing House, Moscow 1948.
[6] Rusanov A. K. *Bull. Acad. Sci. U.R.S.S. (Phys. Series)* 1955 **19** 106.
[7] Shipitsin S. A. *Bull. Acad. Sci. U.R.S.S. (Phys. Series)* 1950 **14** 677.
[8] Semenova O. P. *Bull. Acad. Sci. U.R.S.S. (Phys. Series)* 1945 **9** 715.
[9] Nedler V. V. *Fact. Lab., Moscow* 1955 **21** 1056.

VOL.
10
1957/5

Spectrochimica Acta, 1958, Vol. 10, pp. 419 to 422. Pergamon Press Ltd., London

The Raman spectra of four isotopic varieties of diborane in the gas phase

R. C. Taylor and A. R. Emery
Department of Chemistry, University of Michigan, Ann Arbor, Michigan

(*Received* 13 *September* 1957)

Abstract—Raman spectra of the four isotopic species, $^{11}B_2H_6$, $^{11}B_2D_6$, $^{10}B_2H_6$, $^{10}B_2D_6$, in the gas phase have been obtained and interpreted in terms of the D_{2h} bridge model. The results are in agreement with previous interpretations in the literature based on the spectrum of the liquid.

The compounds $^{11}B_2H_6$, $^{11}B_2D_6$, $^{10}B_2H_6$ and $^{10}B_2D_6$ were prepared during the course of a spectroscopic investigation of the borohydride ion and aluminum borohydride. Since the Raman spectra of only the first and last of the above isotopic varieties have been reported in detail, and those only for the liquid state, it was deemed of interest to obtain the gaseous Raman spectra for the complete series.

Experimental

The starting material in the preparation of the compounds was the diethyl ether complex of BF_3. This was converted to the appropriate diborane by means of lithium aluminum hydride or deuteride essentially according to the method given by Shapiro *et al.* [1]. The boron-11 compounds contained approximately 81 per cent of the ^{11}B isotope, the normal isotopic abundance, while the boron-10 compounds* contained 96 per cent of the desired isotope. The hydrogen content of the deuterated compounds was estimated at less than 2 per cent from the spectral evidence. Purification was accomplished by repeated fractionation on the vacuum line until a constant and reproducible vapor pressure was reached. The values observed for ordinary diborane agreed with those in the literature. The use of BF_3 etherate as a starting material eliminates possible contamination with SiF_4, which is difficult to remove by fractionation.

The spectra were recorded photographically, using the spectrograph and light source described previously [2]. The Raman tubes had an outside diameter of 25 mm with an illuminated length of 150 mm and contained the gases at approximately 4 atmospheres pressure. Collimating baffles largely eliminated light scattered from the walls and window. Saturated sodium nitrite solution served as a filter for all exposures; an *iso*propyl alcohol solution of rhodamine 5 GDN Extra and paranitrotoluene was utilized as an additional filter for a few of the spectra. Exposure times varied from 12 to 72 hr with Eastman 103a-J plates. The resolution of the spectrograph was quite adequate to resolve clearly the isotopic triplet of ordinary diborane at about 800 cm^{-1}. Wave length measurements were made both on the plates and on enlarged tracings made by a Leeds and Northrup microphotometer. Estimated probable errors accompany the averaged values listed for the frequencies.

Results

Observed frequencies, estimated intensities, and assignments for the hydrogen and deuterium compounds, respectively, are shown in Tables 1 and 2. Tracings of typical spectra of the deuterated compounds are shown in Fig. 1. No difficulty was met in identifying the A_g fundamentals, since the characteristic sharp appearance of totally symmetric bands in the Raman spectrum of gaseous compounds is at

* Boron-10 was obtained as the $CaF_2 \cdot BF_3$ complex from Union Carbide and Carbon, Oak Ridge National Laboratory.

Table 1. Observed Raman frequencies of gaseous $^{11}B_2H_6$ and $^{10}B_2H_6$

$^{11}B_2H_6$		$^{10}B_2H_6$		Intensity	Shape	Symmetry	Assignment
Frequency (cm^{-1})	$\pm\delta$	Frequency (cm^{-1})	$\pm\delta$				
—	—	683	3	*vw*	*sh*	A_g	$\nu_9 - \nu_{10}$
—	—	786	2	*vw*	*br*		?
788	1	—	—	*s*	*sh*	A_g	ν_4 ($^{11}B - {}^{11}B$)
802	1	—	—	*m*	*sh*	A_g	ν_4 ($^{11}B - {}^{10}B$)
818	2	816	1	*s*	*sh*	A_g	ν_4 ($^{10}B - {}^{10}B$)
—	—	832	3	*vvw*	*sh*		?
1026	6	1025	5	*w*	*br*		ν_7?, ν_{15}?
1184	1	1186	1	*m*	*sh*	A_g	ν_3
1310	5	1318	2	*w–vw*	*sh*	A_g	$\nu_9 + \nu_{10}$
1755	5	1768	8	*w*	*br*	B_{1g}	ν_6
2011	2	—	—	*vw*	*sh*	A_g	$2\nu_{15}$?
2109	1	2110	1	*s*	*sh*	A_g	ν_2
—	—	2352	2	*w*	*sh*	A_g	$2\nu_3$, $2\nu_{18}$
2485	7	—	—	*vvw*		A_g	$\nu_4 + 2\nu_5$?
2532	1	2537	1	*vs*	*sh*	A_g	ν_1
(2600)	10	2640	10	*w*	*br*	B_{2g}	ν_{11}

δ = probable error; *s* = strong, *m* = medium, *w* = weak, *sh* = sharp, *br* = broad; frequencies enclosed in parentheses are estimated; assignments followed by a question mark are based on fundamental frequencies obtained indirectly [3]

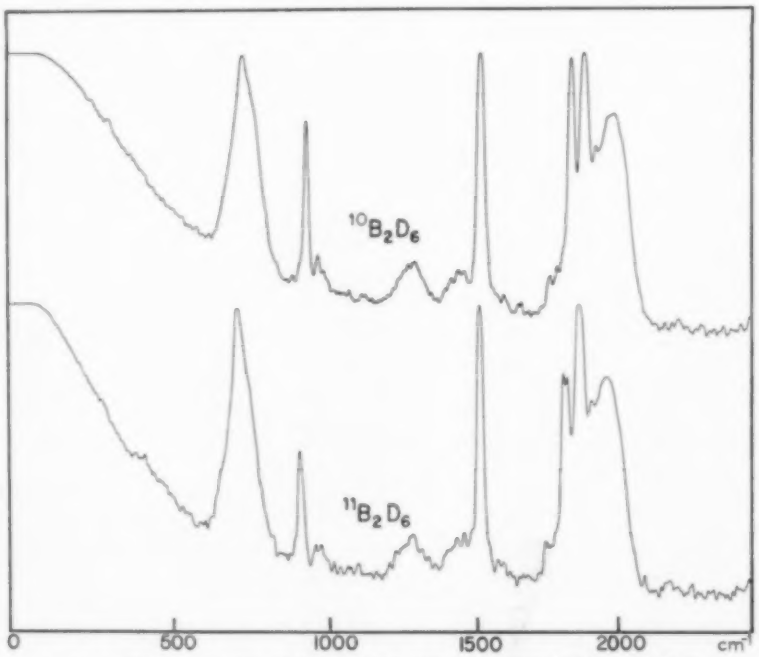

Fig. 1. Raman spectra of ^{10}B and ^{11}B deuteroboranes in the gas phase.

VOL. 10 1957/5

Table 2. Observed Raman frequencies of gaseous $^{11}B_2D_6$ and $^{10}B_2D_6$

$^{11}B_2D_6$		$^{10}B_2D_6$		Intensity	Shape	Symmetry	Assignment
Frequency (cm^{-1})	$\pm\delta$	Frequency (cm^{-1})	$\pm\delta$				
712	1	721	1	*s*	*sh*	A_g	ν_4
—	—	748	5	*w*	*br*		ν_7, ν_{12}, ν_{15}?
912	1	928	1	*m*	*sh*	A_g	ν_3
971	3	962	3	*vw*	*sh*	A_g	$\nu_{16} - \nu_{18}$?
1287	4	1285	5	*w*	*br*	B_{1g}	ν_6
1414	3	1446	3	*vw*	*sh*	A_g	$2\nu_4$
1438	3	—	—	*vw*	*sh*	A_g	$2\nu_{14}$
1459	3	—	—	*vw*	*sh*	A_g	$2\nu_7$, $2\nu_{12}$?
1488	4	—	—	*vw*	*sh*	A_g	$2\nu_{15}$?
1515	1	1515	1	*vs*	*sh*	A_g	ν_2
1748	2	1758	3	*vw*	*sh*	A_g	$2\nu_{18}$
1809	1	1836	1	*s*	*sh*	A_g	$2\nu_3$
1824	1	—	—	*m*	*sh*	A_g	$2\nu_3(^{11}B - {}^{10}B)$
1867	1	1883	1	*vs*	*sh*	A_g	ν_1
1912	2	1924	2	*w*	*sh*	A_g	$\nu_4 + 2\nu_5$
1968	2	1990	2	*m*	*br*	B_{2g}	ν_{11}

δ = estimated probable error; *s* = strong, *m* = medium, *w* = weak, *sh* = sharp, *br* = broad; assignments accompanied by a question mark are based on fundamental frequencies obtained indirectly [3].

least as conclusive as depolarization measurements. The other Raman-active fundamentals were typically broad and diffuse and lower in intensity so that frequently they could not be distinguished from the background. In some cases, they were obscured by A_g fundamentals or overtones. This appears to be the reason for the great breadth of the band near 700 cm^{-1} in the deuterated compounds.

Assignment of overtones and combination bands was made with the help of the infrared active fundamentals of the gas listed by LORD and NIELSEN [3]; where Raman-active fundamentals could not be identified from the present work, liquid values from the same paper were used. Frequently alternate possibilities existed for the assignment of weak bands. In such cases, the assignment with A_g symmetry, if one existed, was preferred on the grounds that bands of this class would likely be more intense in the Raman effect. Several cases in which the intensity of the overtone or combination was enhanced by Fermi resonance were noted, the most pronounced case occurring in the deuterated compounds and involving $2\nu_3$ and ν_1. The doublet appearing at the position of $2\nu_3$ in the spectrum of $^{11}B_2D_6$ is attributed to the presence of roughly 30 per cent of $^{11}B - {}^{10}B$ molecules. The unexpectedly high intensity of the isotopic satellite at 1824 cm^{-1} above that expected from the ratio of isotopic molecules arises from a closer resonance with the ν_1 fundamental in the lighter molecules.

The fundamentals derived from the present work are collected in Table 3. Since they agree quite well with those given by LORD and NIELSEN [3], who have considered all previous work, they will not be discussed in detail. It may be

pointed out that the general agreement found here supports the essential correctness of the assignments made by these authors.

The application of the Teller–Redlich product rule and also one of the isotopic sum rules to the frequencies of the A_g class is shown in Table 4. The data are satisfactory considering the lack of knowledge of the anharmonicities and the number of fundamentals involved in Fermi resonances.

Table 3. Raman active fundamentals of gaseous diboranes

		$^{11}B_2H_6$	$^{10}B_2H_6$	$^{11}B_2D_6$	$^{10}B_2D_6$
A_g	ν_1	2532	2537	(1860)	(1870)
	ν_2	2109	2110	(1512)	(1514)
	ν_3	1184	1186	(912)	(928)
	ν_4	788	816	712	721
B_{1g}	ν_6	1755	1768	1287	1285
	ν_7	—	—	—	—
B_{2g}	ν_{11}	2600	2640	1968	1990
	ν_{12}	—	—	—	—
B_{3g}	ν_{15}	—	—	—	—

Frequencies enclosed in parentheses are involved in Fermi resonances and have been corrected by an estimated shift.

Table 4. Product and sum rules for the A_g class frequencies of gaseous diboranes

Product ratio	Calc.	Theoret.
$(^{11}B_2H_6/^{11}B_2D_6)$	2·73	2·825
$(^{10}B_2H_6/^{10}B_2D_6)$	2·74	2·825
$(^{10}B_2H_6/^{11}B_2H_6)$	1·04	1·049
$(^{10}B_2D_6/^{11}B_2D_6)$	1·04	1·049
Sum difference $\Sigma[\nu_i^2\,(^{10}B_2H_6) - \nu_i^2\,(^{11}B_2H_6)]$	$= 7{\cdot}9 \times 10^4$	
$\Sigma[\nu_i^2\,(^{10}B_2D_6) - \nu_i^2\,(^{11}B_2D_6)]$	$= 8{\cdot}6 \times 10^4$	

Acknowledgements—This work was supported in part by the United States Air Force under Contract AF 33(616)–3343, the sponsoring agency being the Aeronautical Research Laboratory of the Wright Air Development Center, Air Research and Development Command.

References

[1] Shapiro I., Weiss H. G., Schmich M., Skolnik S. and Smith G. B. L. *J. Amer. Chem. Soc.* 1952 **74** 901.
[2] Vidale G. L. and Taylor R. C. *J. Amer. Chem. Soc.* 1956 **78** 294.
[3] Lord R. C. and Nielsen E. *J. Chem. Phys.* 1951 **19** 1.

VOL. 10 1957/5

Spectrochimica Acta, 1958, Vol. 10, pp. 423 to 430. Pergamon Press Ltd., London

RESEARCH NOTES

Infrared spectra of some deuterated carboxylic acids and alcohols

(*Received* 17 *August* 1957)

In connection with other work [1, 2] we have had occasion to examine the infrared spectra of various deuterated carboxylic acids and alcohols. Some features of these spectra seem worthy of record.

The acids examined were *iso*butyric acid, $(CH_3)_2CHCOOH$, its α-*d* analog, $(CH_3)_2CDCOOH$, and its α,O-d_2 analog, $(CH_3)_2CDCOOD$, *cyclo*hexanecarboxylic acid, $C_6H_{11}COOH$ and its α-*d* and α,O-d_2 analogs and *n*-butyric acid, $CH_3CH_2CH_2COOH$ and its α-*d* analog.

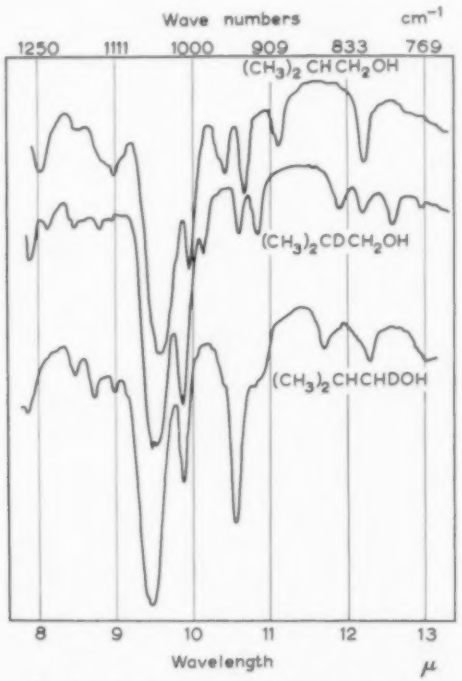

Fig. 1. Infrared spectra of *iso*butyl alcohols

The most striking feature in their spectra is the extreme weakness of the C–D band in the α-*d* acids. This band is so weak as to be barely distinguishable from noise in a 5 per cent chloroform solution or a thin capillary film, and even in a film so thick that the carbonyl band begins to broaden appreciably, the C–D band intensity is less than 10 scale divisions in a percentage plot. The weak bands lie at 2165 cm^{-1} in butyric acid-α-*d* and in *cyclo*hexanecarboxylic acid-α-*d* and at 2092 and 2169 cm^{-1} in *iso*butyric acid-α-*d*.

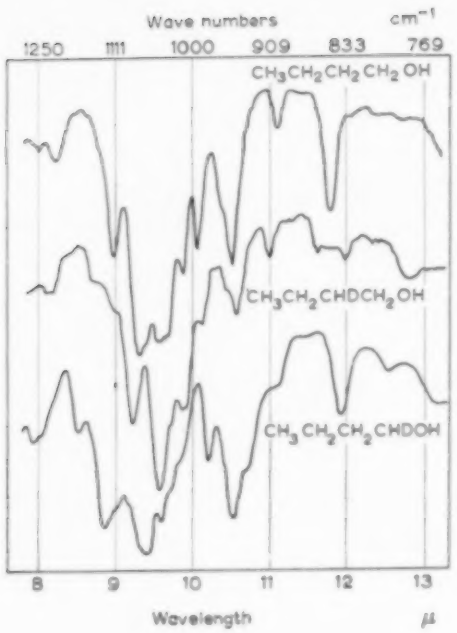

Fig. 2. Infrared spectra of *n*-butyl alcohols.

VOL.
10
1957/

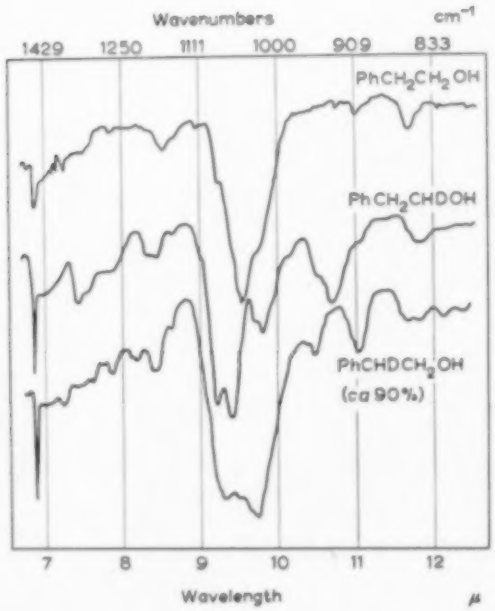

Fig. 3. Infrared spectra of 2-phenylethanols.

In contrast, the α,O-d_2 acids—whose spectra were measured under exactly the same experimental conditions (slit width, etc.) as those of the α-d acids—show both O–D and C–D bands of medium intensity (20 scale divisions or more in a thin film or 5 per cent solution) occurring at 2283 and 2101 cm^{-1} in *iso*butyric acid-α,O-d_2 and at 2268 and 2101 cm^{-1} in *cyclo*hexanecarboxylic acid-α,O-d_2. The *iso*butyric and *cyclo*hexanecarboxylic acids also show characteristic differences between the undeuterated, monodeuterated and dideuterated species in the 1100–1400 cm^{-1} region which are analytically useful [1]. The difference between the spectrum of *n*-butyric acid and that of its α-d analog is much less marked.

Recent interest in the assignment of the infrared bands of alcohols and their deuterated analogs [3, 4] prompts us to report the spectra of three such sets of the type $RR'CHCH_2OH$—$RR'CHCHDOH$—$RR'CDCH_2OH$ which are shown in Figs. 1–3 for the 8–13μ region. Deuteration changes the spectral bands in this region quite considerably. Only in the case of *iso*butyl alcohol can one clearly discern a broad band at about 1050–1060 cm^{-1} which is invariant with deuteration. The bands in this region undoubtedly arise from C–C stretching and C–H and O–H deformation as well as C–O stretching vibrations, or from the coupled motions of several of these vibrations.

Acknowledgements—This work is a contribution from the Radiation Project of the University of Notre Dame supported, in part, under Atomic Energy Commission contract AT(11-1)-38 and Navy loan equipment contract Nonr-06900. We are indebted to Prof. San-Ichiro Mizushima and Dr. G. B. B. M. Sutherland for their helpful advice and encouragement.

E. L. Eliel
C. C. Price*
R. J. Convery
T. J. Prosser

Department of Chemistry
University of Notre Dame
Notre Dame, Indiana.

OL.
10
7/58

References

[1] Eliel E. L. and Prosser T. J. *J. Amer. Chem. Soc.* 1956 **78** 4045.
[2] Price C. C., Eliel E. L. and Convery R. J. *J. Org. Chem.* 1957 **22** 347.
[3] Stuart A. V. and Sutherland G. B. B. M. *J. Chem. Phys.* 1956 **24** 559.
[4] Tarte P. and Deponthière R. *Bull. Soc. Chim. Belg.* 1957 **66** 525.

* Present address: Department of Chemistry, University of Pennsylvania.

The infra-red spectrum of NH_3 in carbon tetrachloride

(*Received* 29 *August* 1957)

Introduction

The spectra of NH_3 in various matrices at low temperatures have been briefly described by Becker and Pimentel [1]. Recently Vedder has reported an investigation of the $(NH_4)^+$ ion in solid solution in sodium chloride type lattices where rotation about one NH bond axis was detected but not free three-dimensional rotation [2].

Reding and Hornig have studied the Raman [3] and infra-red spectra [4] of solid NH_3 at low temperatures.

The spectrum of scrupulously dried NH_3 gas dissolved in dried carbon tetrachloride by bubbling the gas through the liquid has been determined. This note described the spectrum recorded in comparison with previous work.

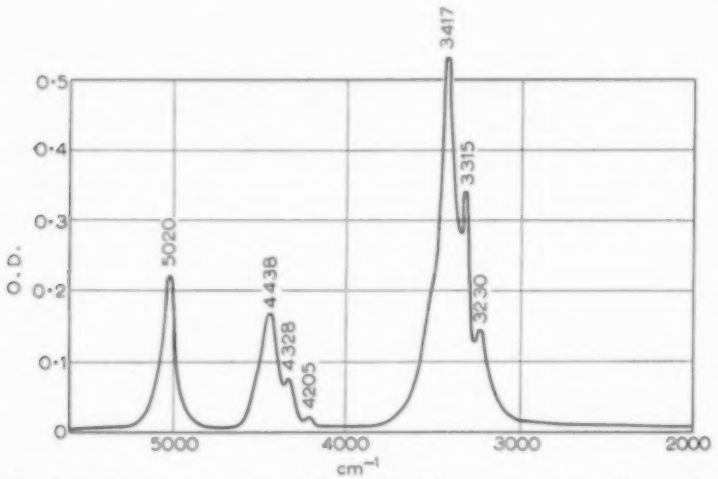

Fig. 1. LiF prism spectrum of NH_3 in CCl_4 0·2 per cent w/v (1 : 88 moles/mole) at 1 cm path.

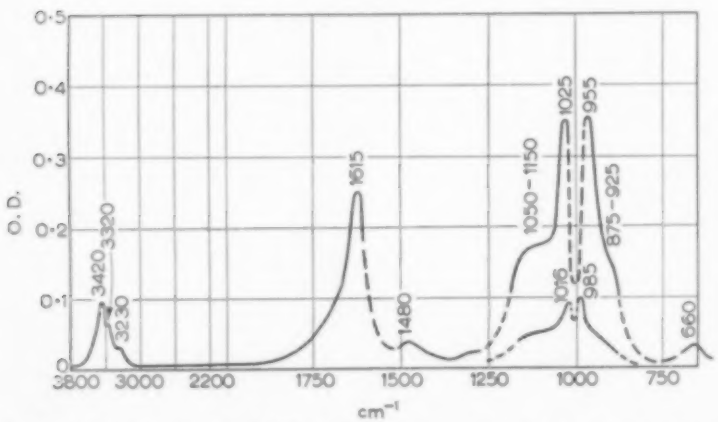

Fig. 2. NaCl prism spectrum of NH_3 in CCl_4 0·09 per cent w/v (1 : 396 moles/mole) at 4 mm path, upper trace; 1 mm path, lower trace.

Method and results

The high-frequency spectrum recorded for a solution of NH_3 in CCl_4 (0·2 per cent w/v, 1 cm path) with a Perkin–Elmer 12C spectrometer equipped with an LiF prism is shown in Fig. 1. The NaCl prism spectrum shown in Fig. 2 was recorded on a Perkin–Elmer Model 21 with pure solvent in the comparison beam for a 0·09 per cent w/v solution at 4 mm and 1 mm paths.

VOL.
10
1957/5

Table 1. Assignments and comparison of solid, solution and gas frequencies

NH_2 Assignment	Observed infra-red frequencies		
	Gas [6]	Dilute in CCl_4	Solid [4]
	cm^{-1}		
$\nu_2 + \nu_4$	5053	5020	4923
$\nu_2 + \nu_3$	4505 4433	4438	4397
$\nu_1 + \nu_2$	4302 4269	4328	
	cm^{-1}		
$\nu_2 + 2\nu_4$	4216 4176	4205	
ν_3 [7]	3444	3417	3378 (3450–3550 combinations of ν_1 or ν_3 with lattice modes)
ν_1	3335·9 3337·5	3315	3223
$2\nu_4$	3219	3230	3297
$3\nu_2$	2861		
$(\nu_3 - \nu_2)$ or $(\nu_2 + \nu_4)$	2472·6 2440·1		
$2\nu_2$	1922		1888 $(\nu_2 + \nu''_5)$
ν_4	1627·5	1615	1646
$\nu_2 + \nu_5$ [4]	—		1600
		1480	(1350–1600, ν_2 + lattice modes)
$\nu_2 + 3\nu_6$	—		1207
$\nu_2 + 2\nu_6$	—	(1150–1050 diffuse wing)	1151
	cm^{-1}		
$\nu_2 + \nu_6$	—		1100
ν_2	968 931·6	*(1025) (1016) (955) (985)	1060
$\nu_2 - \nu_6$	—	(925 to 875 diffuse wing)	995
$2\nu_2 - \nu_2$	629·3	660	(640–750, $2\nu'_5$)
ν_5 [4]	—		527
ν'_5 [4]	—		362
ν''_5 [4]	—		(250)
ν_6 [4]	—		53

* Exact positions varied with slit widths used—overlapped by strong CCl_4 absorptions at 982, 1006 cm^{-1}.

In the region of very strong solvent absorption, shown dotted, the slit control was switched from automatic to manual, the source current was turned up to maximum, and the scanning speed was reduced to a very slow rate. The gain settings and slit widths were adjusted so that even at the maximum absorption of the solvent the pen response time was reasonable for the scanning speed used. The spectrometer was stopped every 20 cm^{-1}

to check the pen response and adjust slit width and gain if necessary. In this way the complete spectrum was recorded in a single solvent. Of course in the dotted regions very wide slits were used with poorer resolution, and the intensities of absorption may be in error because of enhanced effects of stray radiation under conditions of high solvent absorption.

Although it would be desirable to record the spectrum in a second inert solvent to confirm the more doubtful regions, no alternative to CCl_4 has been found. NH_3 reacts with CS_2 and its solubility in hydrocarbons is too low. A specific interaction between NH_3 and $CHCl_3$ was detected [5].

The frequencies observed for NH_3 in dilute solution in CCl_4 are compared with those of the solid and gaseous forms in the table. The assignments are those of Reding and Hornig [4] and Herzberg [6] with the exception of ν_3, where the frequency for the gas phase given by Cumming and Welsh [7] is taken. Their frequency for liquid NH_3 was 3382 cm^{-1}, very close to the solid state value 3378 cm^{-1} observed by Reding and Hornig.

Discussion

The spectra in Figs. 1 and 2 are very similar to those given by Reding and Hornig except in the region 1600–1350 cm^{-1}, and in the contour of ν_2. Absorptions in the 1600–1350 cm^{-1} range were assigned to combinations with lattice modes in the solid which we would not expect to be present in dilute solution.

It is unfortunate that ν_2 is overlapped by the solvent bands but great care was taken to ensure that the compensation for solvent bands was exact. Repeat runs always reproduced the same contour. The observed splitting of ν_2 in dilute solution suggests that inversion doubling occurs as in the gas phase. Although ν_2 shows the most pronounced wings, ν_1 and ν_3 (which overlaps $2\nu_4$), and ν_4 both show shoulders or wings on both sides of the principal peaks. The overtone and combination bands also show slight wings. It is possible that these contours represent diffuse rotational wings and that perturbed free rotation as well as inversion doubling occurs in carbon tetrachloride solution.

The solution frequencies are, with the sole exception of ν_4, intermediate between the gas and solid states although they are very much closer to the gas phase values.

As expected from the change in intermolecular force fields, the stretching modes are at lower frequencies in solution and solid, while the bending mode ν_2 is higher in solution and solid than in the gas.

The anomalous ν_4 frequencies are even more puzzling because their first overtone ($2\nu_4$) frequencies occur in the expected order gas $<$ solution $<$ solid. In the solid and solution spectra $2\nu_4$ is very close to $2 \times \nu_4$ in frequency, suggesting very small anharmonicity for this mode. For the gas $2\nu_4$ (3219 cm^{-1}) is considerably less than $2 \times \nu_4$ (3255 cm^{-1}).

Since $2\nu_4 \div 2$ (1608 cm^{-1}) for the gas would be consistent with the solid and solution ν_4 frequencies it is possible that ν_4 has been misassigned in the gas spectrum, but this seems very unlikely in view of the high intensity of the 1627·5 cm^{-1} band in the gas phase.

Herzberg has discussed the possibilities of detecting rotations in the liquid state [6, pp. 531–534] and concluded that NH_3 and CH_4 were two of the very few molecules which might be expected to show rotational structure. Reding and Hornig [3, 4] concluded that the interactions between NH_3 molecules in the crystal were weak. The closeness of the observed frequencies in CCl_4 solution to the gas phase frequencies shows that interactions with the solvent are very weak indeed.

These facts, together with the large differences in size and mass of NH_3 and CCl_4 molecules, make the assignment of the observed structure in the spectrum to rotational wings fairly plausible.

VOL.
10
1957/5

Acknowledgements—The author is indebted to Prof. D. F. HORNIG for a discussion of these spectra, and to British Nylon Spinners Ltd., for permission to publish this work.

Research Dept., British Nylon Spinners Ltd. , C. G. CANNON
Pontypool, Mon., Wales

References

[1] BECKER E. D. and PIMENTEL G. C. *J. Chem. Phys.* 1956 **25** 224–28.
[2] VEDDER W. Paper presented at European Molecular Spectroscopy Meeting, Freiburg im Breisgau, July 1957.
[3] REDING F. P. and HORNIG D. F. *J. Chem. Phys.* 1954 **22** 1926–28.
[4] REDING F. P. and HORNIG D. F. *J. Chem. Phys.* 1951 **19** 594.
[5] CANNON C. G. *Spectrochim. Acta* 1958 **10** 417.
[6] HERZBERG G. *Infra-red and Raman Spectra of Polyatomic Molecules* pp. 295–97. D. van Nostrand, New York 1945.
[7] CUMMING C. and WELSH H. L. *J. Chem. Phys.* 1953 **21** 1119.

OL.
10
7/58

The interaction of NH_3 and $CHCl_3$ molecules in CCl_4 solution from infra-red spectra

(*Received* 29 *August* 1957)

Introduction

THE interactions of $CDCl_3$ with a variety of solvent molecules have been studied by LORD *et al.* [1] and HUGGINS and PIMENTEL [2] by recording frequency and intensity changes of the C–D stretching band in the infra-red spectra. GLICK has recorded the CH frequency shifts of haloforms interacting with triethylamine in tetrachlorethylene solutions [3]. This note records the C–H frequency shifts of chloroform on interaction with ammonia in dilute solution in carbon tetrachloride.

Results

The spectra were recorded with a Perkin–Elmer 12C equipped with LIF prism and slit drive [4]. The frequencies observed are collected in Table 1. The NH_3 concentrations were determined by titration (w/v) and the $CHCl_3$ concentrations were obtained by volumetric addition (v/v).

The ν_{CH} frequency of chloroform shows a lower frequency component in the presence of ammonia. At different relative molar concentrations of NH_3 and $CHCl_3$ (9 : 1 and 3 : 1 approx.) the relative intensities of these two frequencies change (optical densities, O.D., given in Table 1) showing that the lower frequency corresponds to the complex formed by the specific interaction of NH_3 and $CHCl_3$ molecules which produces a frequency shift of 31 cm^{-1}.

This shift can be compared with $\Delta\nu_{CD}$ of 36 cm^{-1} in pyridine (1) and $\Delta\nu_{CD}$ of 110 cm^{-1} with triethylamine [3]. Remembering the mass difference (H, D) these shifts are in the order of basicities of the nitrogen atoms.

No splitting or significant frequency shifts were detected for any of the NH_3 bands

Table 1. NH and CH frequencies of chloroform/ammonia mixtures in carbon tetrachloride

Assignments	Frequencies cm^{-1} in CCl_4 solutions			
	0·2% NH_3	0·13% NH_3 + 0·5% $CHCl_3$	0·13% NH_3 + 0·15% $CHCl_3$	0·5% $CHCl_3$
NH_3 $\nu_3 + \nu_4$	5025	5020		
$\nu_2 + \nu_3$	4438	4435		
$\nu_1 + \nu_2$	4330	4325		
$\nu_2 + 2\nu_4$	4205			
ν_3	3419	3417	3417	
ν_1	3315	3315	3315	
$2\nu_4$	3232	3228	3214	
$CHCl_3$		4217		4215
		O.D.	O.D.	
ν_{CH} "free"		3016 0·495	3017 0·145	3017 (O.D. 0·490)
ν_{CH} "associated"		2985 0·125	2985 0·025	—
CH frequency shift		= 31 cm^{-1}	= 32 cm^{-1}	
Molar ratio NH_3: CHCl		2·75 : 1	9·2 : 1	

observed, so the interaction must be solely between the lone pair electrons of the nitrogen and the CH bond of the chloroform.

Thanks are due to British Nylon Spinners Ltd., for permission to publish this note.

Research Dept., British Nylon Spinners Ltd. C. G. Cannon
Pontypool, Mon., Wales

References

[1] Lord R. C., Nolin B. and Stidham H. D. *J. Amer. Chem. Soc.* 1955 **77** 1365.
[2] Huggins C. M. and Pimentel G. C. *J. Chem. Phys.* 1955 **23** 896–98.
[3] Glick R. E. *Chem. & Ind. (Rev.)* 1956 No. 19 413.
[4] Cannon C. G. *J. Sci. Instrum.* 1952 **29** 50.

VOL. 10 1957/5

LETTERS TO THE EDITORS

Absorption coefficients of four organic fluorine compounds in the vacuum ultraviolet

(*Received* 15 *August* 1957)

In a study of absorption by organic fluorine compounds in the vacuum ultraviolet, absorption coefficients were measured in the region 1100–2000 Å for *iso*propyl methylphosphonofluoridate, dichlorotetrafluoroethane (Freon 114), dichlorodifluoromethane (Freon 12), and chlorodifluoromethane (Freon 22). The grating spectrometer used in these measurements has previously been described [1]. A windowless hydrogen arc operated at about 1370 V provided the source spectrum. Both monochromator slits were 0·1 mm wide. The absorption cells, which were provided

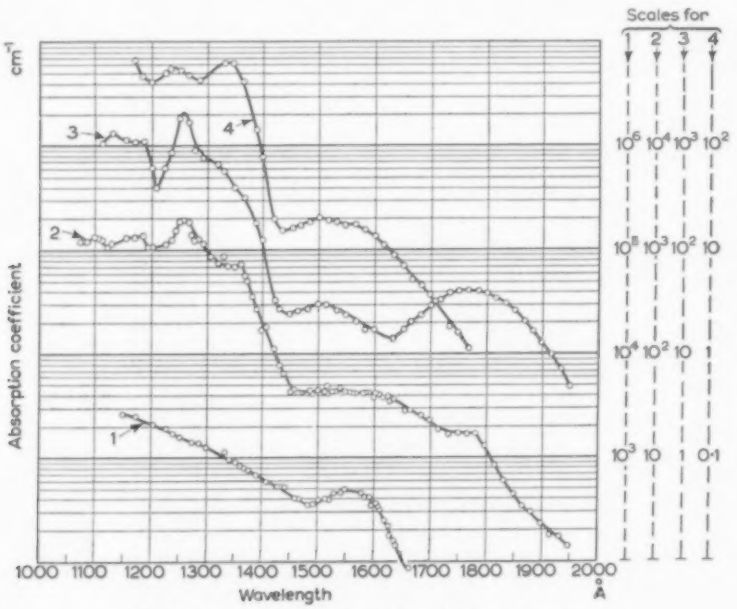

Fig. 1. Absorption spectra of fluorine compounds.
(1) $CH_3PF(O)OCH(CH_3)_2$ (2) $CClF_2CClF_2$
(3) CCl_2F_2 (4) $CHClF_2$

with lithium fluoride windows, had an absorption path length of 1 cm for *iso*propyl methylphosphonofluoridate and 2 mm for the other compounds. The response of a photomultiplier tube coated with sodium salicylate was registered on a strip-chart recorder. The wave length reading is accurate to about 3 Å. The *iso*propyl methylphosphonofluoridate was prepared at Army Chemical Center, Md., and redistilled before use. The other three compounds were reagent grade Matheson products more than 95 per cent pure. The spectra were measured in a region where the absorption coefficients are very high; hence appreciable interference by impurities is not to be expected.

Fig. 1 presents the absorption coefficients defined by the equation

$$k = \frac{760}{pd} \ln \frac{I_0}{I}$$

where I_0 and I are the incident and transmitted light intensities and d is the optical path length in cm in a gas at a pressure of p mm Hg. Coefficients determined at different gas pressures were consistent within a few per cent. The spectra of the three chlorofluoroparaffins exhibit similarities which are apparently of a generic nature. Dichlorodifluoromethane has a minimum at the Lyman alpha line and has proved useful in combination with O_2 as a filter to isolate this line in the hydrogen spectrum.

It has been pointed out to us by Dr. W. C. Price that the peaks in the region 1250–1350 Å for compounds 2, 3 and 4 probably arise from non-bonded p electrons of chloride. The absorption is shifted from the 1400 Å region, where methyl chloride [2] absorbs strongly, as a result of the inductive effect of fluorine. The peaks at 1250–1350 Å are not to be attributed to the electrons of fluorine atoms, since these are more tightly bound than the electrons on chlorine or oxygen atoms, which would therefore be preferentially excited.

Thanks are due to Mr. Charles Gelman of the Army Chemical Center for supplying the sample of *iso*propyl methylphosphonofluoridate, and to Mr. I. H. Blifford and Mr. G. Fielding for advice and assistance.

R. A. Spurr*
T. A. Chubb

U. S. Naval Research Laboratory
Washington, D.C.

References

[1] Tousey R., Johnson F. S., Richardson J. and Toran N. *J. Opt. Soc. Amer.* 1951 **41** 696.
[2] Price W. C. *J. Chem. Phys.* 1936 **4** 550.

* Now at Research Laboratories, Hughes Aircraft Company, Culver City, Calif.

VOL.
10
1957/5

A tuneable microwave cavity for excitation at 2425 Mc/s of an optical spectroscopic source

(*Received* 25 *July* 1957)

The use of electrodeless spectroscopic sources, excited by microwaves has increased in the past few years. The frequency 2425 Mc/s has been adopted because convenient magnetron generators are available from apparatus built for medical therapy. Considerable attention has been given to the actual preparation of the tubes [1, 2] and in most cases these have been excited by the director supplied with the generator. Some workers however have developed moderately complex circuits and resonance cavities for controlling the microwaves [3]. A compromise arrangement with some tuning on the supply of energy to the source gives a simpler construction.

The attached photograph shows the form of the cavity used with a Deutsche-Elektronik microwave generator. (The directors supplied with this equipment for medical therapy purposes did not spectroscopically excite the sources.) The microwaves are fed into a short section of waveguide through an adapter on the coaxial cable leading from the generator. The centre lead of this cable is joined to a piece of $\frac{1}{4}$ in. diameter brass tubing which extends through the waveguide into a concentric length of 1 in. diameter tubing. Two rods joined to a brass disc allow this disc to act as a short circuit tuning device between these inner and outer tubes. In the photograph this tuning plunger has been removed and lies in front of the optical bar. A similar

OL.
10
7/58

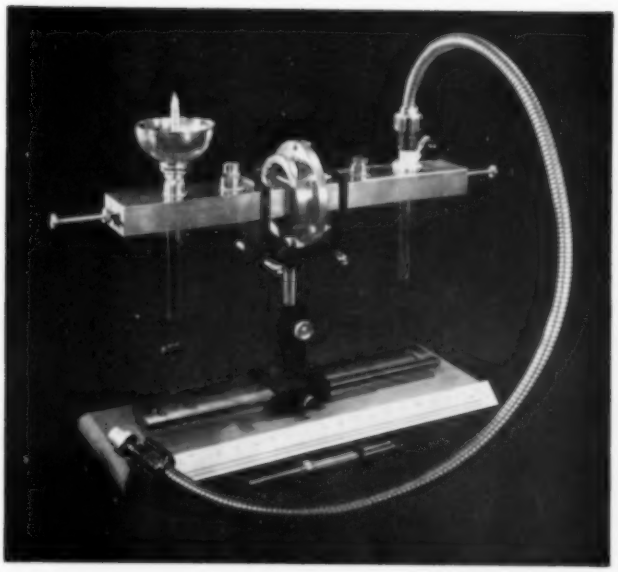

Fig. 1. Photograph of waveguide showing the fine and coarse tuning plungers with a part of the former lying in front. A source tube and the coaxial cable (normally connected to the microwave oscillator) are also in position.

VOL.
10
1957/5

tuning plunger arrangement is mounted at the other end of the waveguide. The central tube is joined to a socket on the other side of which is a spiral of wire. This both holds the tube and transfers energy into it. Coarse short circuit pistons are added at the ends of the waveguide. There are copper plates, at each end of the cavity, closely fitting the waveguide interior and connected to rods so that the plates could be clamped in any position. These horizontal rods can be seen in the photograph.

When originally built, the cavity was joined by conventional waveguide flanges so that it could be connected into test apparatus for examination of standing-wave ratios. Two additional sockets were provided for probes. It is found that these too can be used for small tuning corrections, but they are not essential.

The coarse end plungers are not usually changed when different source tubes are used. The positions of the tube plungers are adjusted until maximum source brightness is obtained. This is found to correspond to a minimum on the nominal power indicator of the Deutsche-Elektronik equipment. Some trouble has been caused by bad contact between the inner rod and the disc; a split collet construction for the disc has helped to eliminate this difficulty.

Although the preparation of the source is probably the most important factor in the successful use of this type of light excitation, the existence of this tuning device has been found to be advantageous.

Acknowledgement—The help given and interest shown by Mr. R. Bennett of the Engineering Services in the construction of the apparatus have been of great value.

L. Bovey

Atomic Energy Research Establishment
Harwell, Didcot, Berks.

OL.
10
7/58

References

[1] Corliss C. H., Bozman W. R. and Westfall F. O. *J. Opt. Soc. Amer.* 1953 **43** 398.
[2] Tomkins F. S. and Mark F. *J. Opt. Soc. Amer.* 1957. In press.
[3] Forrester A. T., Gudmundsen R. A. and Johnson P. O. *J. Opt. Soc. Amer.* 1956 **46** 339.

Spectrochimica Acta, 1958, Vol. 10, pp. 434. Pergamon Press Ltd., London

REPORT OF MEETING

THE Twelfth Annual Meeting of the Society for Applied Spectroscopy was held in New York on 7 and 8 November. The Annual Award of the Society was presented to Dr. Herbert Friedman, U.S. Naval Research Laboratories. The following papers were presented at the meeting:

Continuous analysis of refinery streams: C. W. SKARSTROM, Esso Research and Engineering Co., Linden, N.J.

Analysis of petroleum by mass spectrometry: E. J. LEVY, Atlantic Refining Company, Philadelphia, Pa.

Applications of high-resolution nuclear magnetic resonance spectrometry in the petroleum industry: N. F. CHAMBERLAIN, Humble Oil and Refining Co. Baytown, Texas.

Analysis of petroleum fractions by gas chromatography: W. A. DIETZ, Esso Research and Engineering Co., Linden, N.J.

Focal curve and performance of the plane grating spectrograph: ARNO ARRAK, Belmont Smelting and Refining Works Brooklyn, N.Y.

Perchlorylfluorine (ClO_3F), a new low background source for flame photometry: EARL J. SERFASS and GEORGE SCHMANCH, Lehigh University, Bethlehem, Penna.

New preparation for qualitive spectrochemical analysis: ARTHUR J. MITTELDORF, Spex Industries Hollis, N.Y.

Rapid scan spectroscopy: THOMAS F. FLYNN, Perkin–Elmer Corp., Norwalk, Conn.

Simplifying the infra-red analysis of high-molecular weight mixtures: WM. S. GALLOWAY and THERON JOHNS, Beckman Instruments, Fullerton, Calif.

Hydrogen bonding in aliphatic alcohols: JESSIE L. GOVE, American Cyanamid Co., Bound Brook, N.J.

Push-button, infra-red analysis of carbon and sulfur: GLENN SMITH, Baird-Atomic, Inc., Cambridge, Mass.

Improvement in the performance of model 21 I.R. spectrometer in the 15 to 30 micron region: ROBERT ANACREON, The Perkin–Elmer Corporation Norwalk, Conn.

Preparation of standards for use in X-ray fluorescence analyses: LOUIS MAGER, Alloyd Research Corp., Watertown, Mass.

X-ray spectrographic analysis of nickel-containing alloys with varied sample forms: C. MANNING DAVIS and GEORGE R. CLARK, International Nickel, Bayonne, N.J.

X-ray spectrographic analysis, using arithmetic corrections for interelement effects: MRS. B. MITCHELL, Electro Metallurgical Co. Niagara Falls, N.Y.

Techniques in X-ray spectrography and recent developments in X-ray spectrographic equipment: P. WILLIAM ZINGARO, Philips Electronics, Mt. Vernon, N.Y.

VOL.
10
1957/5

Book Review

PAUL DELAHAY: **Instrumental analysis.** Macmillan, New York, 1957. xi + 384 pp., $7.90, 55s.6d.

By the author's definition "instrumental analysis deals with the application of methods of physics and physical chemistry to chemical analysis". Instrumentation and automation have invaded the chemical laboratory as effectively as elsewhere and since all methods of analysis are basically physical methods there is little which can logically be excluded under this definition. The author is concerned only with the following topics: electrochemical methods (152 pp.) spectroscopic and other methods utilizing radiation (120 pp.), mass spectrometry (14 pp.) and nuclear radiation methods (30 pp.). Other subjects are excluded on the grounds that they are generally covered in courses on organic and physical chemistry.

The most complete section is that dealing with electrochemical methods, which begins with a chapter on electrode potentials followed by accounts of potentiometry, polarography and voltammetry, amperometric and voltammetric titrations, electrogravimetry, coulometry and conductometry. The principles of these methods are clearly described and the instrumentation is given in outline only. The other main section covers emission and absorption spectroscopy, fluorimetry, turbidimetry and nephelometry, Raman spectroscopy and X-ray methods. The main types of instrument are briefly mentioned and the accounts of such matters as the effect of finite line width and deviations from Beer's law will be particularly useful. The theory of spectra is not discussed apart from a brief qualitative introduction. The sections on X-ray methods, mass spectrometry and nuclear radiation methods are short accounts mainly for students with no previous knowledge of these subjects.

The book is presented as a lecture course for undergraduates and graduates, problems are given after each chapter and there is a final section of laboratory experiments, most of it dealing with electrochemical methods. The volume is well produced and clearly written, but students who have mastered the standard texts of physical chemistry will probably prefer to proceed directly to one of the more specialized monographs on each of the instrumental techniques, such as the author's own excellent account of instrumental methods in electrochemistry. Such students will nevertheless find the present work useful as a source book since full references to the original literature are given and each chapter is followed by a comprehensive bibliography.

G. PORTER

OL.
10
7/58

Editorial Note

The index to Volume X will be published in Vol. XI.

Papers to be published in future issues

E. G. McRae: Solvent effects on merocyanine spectra

D. W. Grant, D. E. Glanville and G. L. Strachan: A simple arrangement for the measurement of absorption spectra of aqueous systems at elevated temperatures

Brian Stevens: A relationship between some bond properties of diatomic molecules and the ionization potentials of their constituent atoms

D. F. Smith: Infrared spectra analysis for hydrogen fluoride

J. M. Martin, Jr., R. W. B. Johnston and M. J. O'Neal: Infra-red absorption of solid state *n*-paraffins-relationship to crystalline type

Louis E. Owen and David C. Manning: Mechanized arc-spark stand for emission spectrography

E. Bright Wilson, Jr.: Determination of the order of atoms in a linear molecule

R. A. Ford and F. Parry: Electronic and vibrational states of carbonyl compounds—I. Electronic states of camphorquinone

Norman S. Ham and A. Walsh: Microwave-powered Raman sources

A. Stojiljković and D. H. Whiffen: The vibration frequencies of the symmetrical *p*-dihalogenobenzenes

A. Stojiljković and D. H. Whiffen: The vibration frequencies of unsymmetrical *p*-dihalogenobenzenes

L. B. Archibald and A. D. E. Pullin: Solvent effects in infra-red spectra of compounds containing the carbonyl group

C. Rimington, S. F. Mason and O. Kennard: Porphin

H. Richard Linton and Eugène R. Nixon: Infra-red spectrum and force constants of silyl-d_3 iodide

Felipe González-Sánchez: Infra-red spectra of the benzene carboxylic acids

J. K. Hurwitz: Spectrographic analysis of segregates with a dynamic microvolume technique—II. Experimental verification of theory

M. Mach and N. Spielberg: Statistical factor in X-ray intensity measurements

Leo H. Spinar and John L. Margrave: Absorption spectra of gaseous alkali metal hydroxides

Masamichi Tsuboi, Takaharu Onishi, Ichiro Nakagawa, Takehiko Shimanonchi and San-Ichiro Mizushima: Assignments of the vibrational frequencies of glycine

D. P. Stevenson and H. M. McConnell: Ultraviolet criteria for monoaromaticity

Robert C. Hirt: Ultraviolet absorption vapor spectra of pyrazine and chloropyrazine

L. H. Sutcliffe: Rydberg term tables

M. N. Oganov and A. R. Stiganov: Quantitative analysis, by a spectrographic method, of the isotopic composition of hydrogen, deuterium and tritium mixtures

VOL.
10
1957/5

OL.
10
7/58